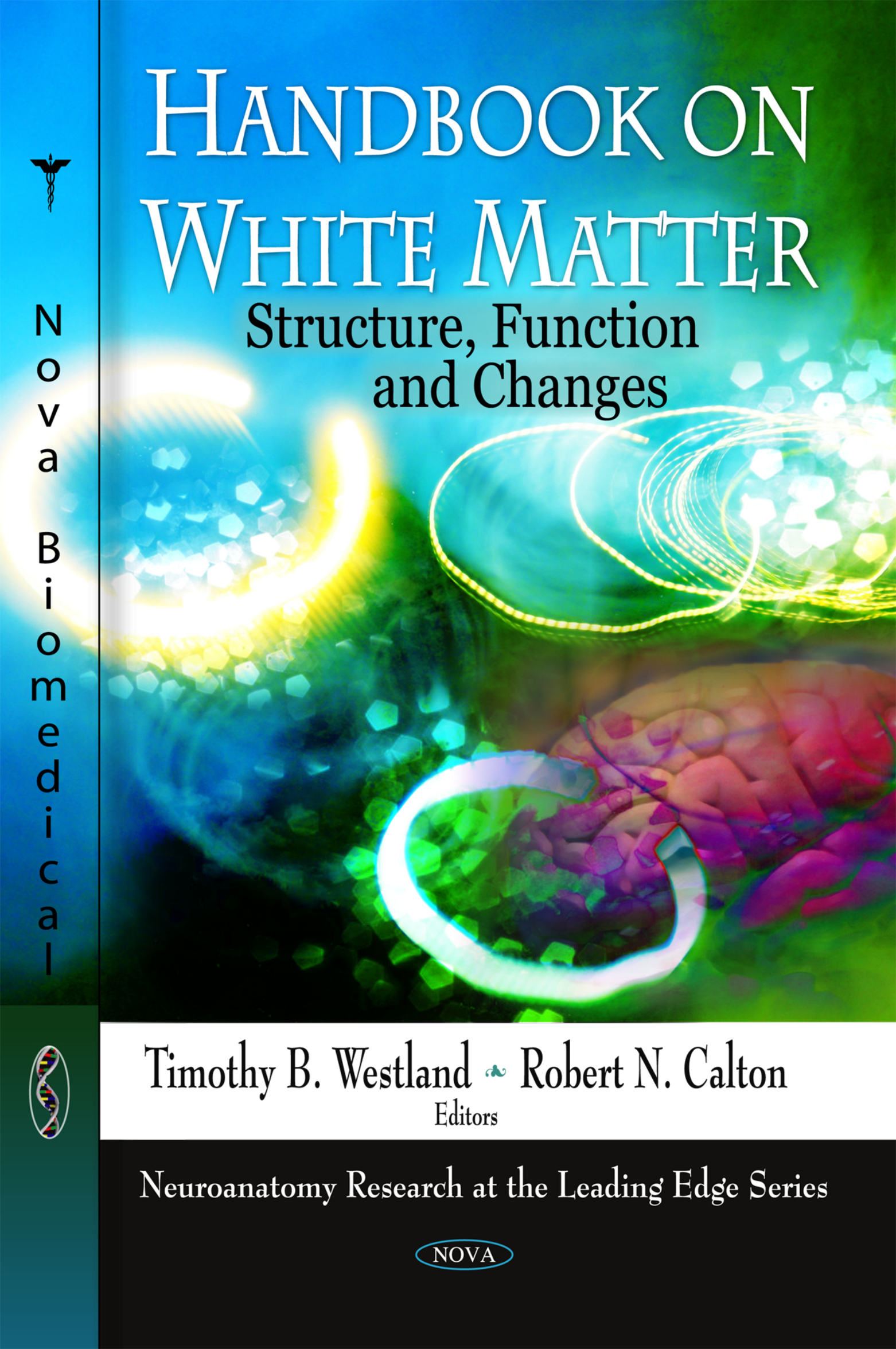
Nova Biomedical
HANDBOOK ON
WHITE MATTER
Structure, Function
and Changes
Timothy B. Westland
Robert N. Calton
Editors
Neuroanatomy Research at the Leading Edge Series
NOVA

Neuroanatomy Research at the Leading Edge

HANDBOOK ON WHITE MATTER: STRUCTURE, FUNCTION AND CHANGES

NEUROANATOMY RESEARCH AT THE LEADING EDGE

Handbook on White Matter: Structure, Function and Changes

Timothy B. Westland and Robert N. Calton

2009 ISBN: 978-1-60692-375-7

Neuroanatomy Research at the Leading Edge

HANDBOOK ON WHITE MATTER: STRUCTURE, FUNCTION AND CHANGES

TIMOTHY B. WESTLAND
AND
ROBERT N. CALTON
EDITORS

Nova Science Publishers, Inc.
New York

Library of Congress Cataloging-in-Publication Data

Handbook on white matter : structure, function, and changes / [edited by] Timothy B. Westland and Robert N. Calton.
p. ; cm.
Includes bibliographical references and index.
ISBN 978-1-61668-975-9 (E-Book)
1. Brain--Histology--Handbooks, manuals, etc. I. Westland, Timothy B. II. Calton, Robert N.
[DNLM: 1. Central Nervous System--physiopathology. 2. Central Nervous System--anatomy & histology. 3. Central Nervous System--physiology. 4. Nervous System Diseases--physiopathology. WL 300 H2366 2009]
QP376.H275 2009
612.8'2--dc22

2009000172

Published by Nova Science Publishers, Inc. ✦ New York

Contents

Preface

White matter is one of the three main solid components of the central nervous system. White matter tissue of the freshly cut brain appears white to the naked eye because of being composed largely of lipid. The other two components of the brain are gray matter and substantia nigra. This new handbook presents the latest research in the field.

Chapter I –The classical neurological notion of a dominant hemisphere responsible for language abilities and objective processing coupled with a non-dominant hemisphere prevailing for nonverbal, spatial, and intuitive tasks has been upheld by several studies, though this dichotomy is not seen with the brains of nonhuman mammals. Still, no matter how simple the task, no operation involves exclusively one hemisphere without the other; we are constantly switching between dominant and non-dominant functions, mandating an ample channel of communication between the two hemispheres. Along with the evolutionarily older anterior commissure, the corpus callosum has evolved to be one of the two major inter-hemispheric connectors in mammals.

Chapter II - White matter lesions are caused by cerebral small vessel disease, particularly by arteriolosclerosis. Arteriolosclerosis consists of a hyaline wall thickening with consequent narrowing of the arteriolar vessel lumen and tissue ischemia. Arteriolosclerosis relates to hypertension, and to other cerebral ischemic lesions (lacunar infarcts, symptomatic as well as asymptomatic). The instigating factors in the pathogenesis of arteriolosclerosis and therefore of white matter lesions, however, remain elusive. Most accepted of current theories is disruption of the blood brain barrier caused by endothelial dysfunction. New imaging modalities, like molecular imaging, and new insights in endothelial biology could therefore provide further insight into the pathogenesis of arteriolosclerosis. In the present chapter the authors will discuss these emerging issues, their potential pitfalls, and their possibility to eventually increase therapeutic options for the vascular pathology which underlies white matter lesions.

Chapter III - The widespread availability of highly active anti-retroviral therapy has lead to long-term survival for many individuals living with HIV infection. With advancing age, many older individuals living with HIV infection are beginning to develop aging-related changes in the brain structure, including white matter lesions. Given the known effect of white matter lesions in the general population, these lesions are also likely to have important effects in aging HIV-seropositive individuals as well. Aging related white matter lesions are

considered to be structural manifestations of brain small vessel vascular disease. These lesions, more predominant in older individuals, are typically related to vascular risk factors such as hypertension and diabetes. Furthermore, the presence of white matter lesions is a known risk factor for development of cognitive decline and dementia. For example, when compared to normal elderly individuals, those with lacunar infarcts score lower on cognitive tests and have approximately twice the risk of developing dementia in the future. Additionally, lacunar infarction in certain "strategic locations" such as the basal ganglia may result in profound cognitive deficits and even dementia. Multiple studies demonstrate that presence of leukoaraiosis is independently related to cognitive impairment in the elderly, and when present in patients with lacunar strokes, indicates increased severity of small vessel vascular disease and exacerbates adverse effects of these lesions on cognitive performance. In elderly individuals, cerebral manifestations of small vessel vascular disease are also important components of vascular dementia.

The relationship between white matter hyperintensities and cognitive performance in HIV infection is an active area of ongoing research. Links between presence of white matter hyperintensities and worse performance on tests of psychomotor speed and verbal memory have been established. Other studies show that dementia in HIV infection is associated with decreased white matter volumes, indicating that in this population the loss of white matter may contribute to cognitive decline. The authors' own research demonstrates that white matter lesion volume in HIV infection is correlated with degree of cortical atrophy, a potential underlying substrate for cognitive decline and dementia. Other studies, however, have reported no relation between white matter lesions and cognitive performance in HIV infection. This discrepancy has been partially resolved with the advent of newer neuroimaging techniques, which allow improved detection of white matter injury and provide further evidence for a connection between white matter damage and the severity of cognitive impairment in HIV-seropositive individuals. In conclusion, aging-related white matter hyperintensities likely contribute to development of cognitive decline and dementia in HIV infection, and physicians caring for HIV seropositive individuals should discuss the importance of treating vascular risk factors with their patients.

Chapter IV - White matter plays an important role by its involvement in a variety of pathological states. In HIV-1 infection of the brain, white matter is already affected at an early stage of the disease process. Whether white matter damage is a direct or indirect effect in drug addiction has yet to be elucidated.

Until now, systematic analyses of white matter in these disease states are lagging far behind. Much research is still to be done. In this endeavor, focus must be placed on assessing changes of the various myelin proteins, the fate and changes of oligodendrocytes, the role of astrocyte-oligodendrocyte cross-talk, and the changes in signal transduction cascades at work in the white matter. Systematic analyses using gene expression arrays, proteomics and metabolomics will provide new clues for elucidating the pathogenetic mechanisms leading to white matter changes.

Chapter V - In the United States alone, over 50,000 individuals are treated daily in intensive care units (ICUs). Approximately 50-80% of ICU patients develop delirium with over half of these cases leading to meaningful and permanent losses in brain functioning. This suggests that critical illness may lead to de novo long-term pathological changes in the

central nervous system. In the current chapter the authors review the evidence regarding links between white matter changes related to critical illness. In particular, they focus on both acute and distal alterations in white matter that may be caused by a number of factors including severe infection, glial cell atrophy, declines in axonal fractional anisotropy (FA) and global hypoperfusion. Evidence from several areas of the neurosciences (animal models, neuroimaging, case studies, etc.) suggests that delirium may be a hallmark of more permanent changes that are occurring in the CNS. Taken together, the current evidence suggests that critical illness may be linked to disruption of white matter tracts in the brain eventually leading to long-term deficits in cognitive functioning. The chapter concludes by highlighting several methodological challenges in investigating these hypotheses along with future directions within the field of delirium and critical illness neuroscience research.

Chapter VI - The frequency of inherited neuromuscular disorders in the human population is estimated to be approximately 1:3,500 worldwide. In some of these disorders there is an association of the neuromuscular and central nervous system (CNS) involvement. The explanation could be in a faulty process of expression of genetic information into the structure of vital proteins, which play a key role in both muscle and brain functions. In these multiorgan disorders a muscular dystrophy or peripheral neuropathy can be combined with the white matter lesion, or other structural abnormalities of the brain, eye, and other organs, and this combination can result in a spectrum of unusual clinical phenotypes.

The central nervous system involvement can be found especially in congenital muscular dystrophies (CMD, MDC), myotonic dystrophy types 1 and 2 (DM1, DM2), mitochondrial encephalomyopathies, and some variants of Charcot-Marie-Tooth disease (CMT).

The authors' research is focused on these important hereditary neuromuscular disorders with the white matter involvement in pediatric patients, especially children afflicted with various forms of congenital muscular dystrophies. They present most interesting and unusual case reports of our patients to demonstrate difficulties and pitfalls in the diagnostics of these rare disorders. The white matter lesion is a very important and valuable diagnostic sign, and also could have a serious impact on the management and prognosis of patients with neuromuscular disorders.

Chapter VII - Suicide is a major worldwide public health problem. Nearly one million lives are lost from suicide each year and between 3%-5% of adults make at least one suicide attempt at some point in their life. Despite intensive efforts, research has failed to find necessary and sufficient factors that indicate an increased likelihood for suicide, and effective prevention strategies have remained elusive, suggesting that our understanding of the interplay of factors that increase the risk of suicide remains incomplete. Furthermore, although a great deal of research has been published on socio-psychological factors affecting suicidal behaviour, the results lack sufficient specificity.

In recent years, studies have indicated that up to 43% of the variability in suicidal behaviour can be explained by genetics. Thus, combining independent clinical and biological predictors may provide improved predictive models.

A great deal of research analyzing the neurobiological basis of suicide has been published in the last few decades. For examples, many studies have identified abnormalities of the serotonergic system in suicidal individuals, particularly in the ventral prefrontal cortex, as well as several other possible abnormalities, such as reduction in messenger RNA and

protein levels of cyclic adenosine monophosphate response element binding, CRE-DNA binding activity, and basal and cyclic adenosine monophosphate–stimulated protein kinase A activityerations in the levels of endocannabinoid and in the density of the CB1 receptors, lower grey-matter cholesterol content, elevated cholecystokinin mRNA levels, expression of proteins involved in glial function, neurodegeneration and oxidative stress neuronal injury, and higher β-adrenergic receptor binding. In the last decade, researchers have pointed out how the brain's white matter is implicated in mental illnesses. The aim of the present chapter is to review research on the association among white matter hyperintensities (WMH) and suicide behaviour.

Chapter VIII - The objective of this study was to determine the degree of white matter pathology in the cerebral cortex in cases of variant Creutzfeldt-Jakob disease (vCJD) and to study the relationships between the white matter and grey matter pathologies. Hence, the pathological changes in cortical white matter were studied in individual gyri of the frontal, parietal, occipital, and temporal cortex in eleven cases of vCJD. Vacuolation ('spongiform change'), deposition of the disease form of prion protein (PrP^{sc}) in the form of discrete PrP deposits, and gliosis were observed in the white matter of virtually all cortical regions studied. Mean density of the vacuoles in the white matter was greater in the parietal lobe compared with the frontal, occipital, and temporal lobes but there were fewer glial cells in the occipital lobe compared with the other cortical regions. In the white matter of the frontal cortex, vacuole density was negatively correlated with the density of both glial cell nuclei and the PrP deposits. In addition, the densities of glial cells and PrP deposits were positively correlated in the frontal and parietal cortex. In the white matter of the frontal cortex and inferior temporal gyrus, there was a negative correlation between the densities of the vacuoles and the number of surviving neurons in laminae V/VI of the adjacent grey matter. In addition, in the frontal cortex, vacuole density in the white matter was negatively correlated with the density of the diffuse PrP deposits in laminae II/III and V/VI of the adjacent grey matter. The densities of PrP deposits in the white matter of the frontal cortex were positively correlated with the density of the diffuse PrP deposits in laminae II/III and V/V1 and with the number of surviving neurons in laminae V/V1. The data suggest that in the white matter in vCJD, gliosis is associated with the development of PrP deposits while the appearance of the vacuolation is a later development. In addition, neuronal loss and PrP deposition in the lower cortical laminae of the grey matter may be a consequence of axonal degeneration within the white matter.

Chapter IX - Progressive multifocal leukoencephalopathy (PML) is a rare demyelinating disease of the central nervous system. It is caused by opportunistic infection by the JC virus, a human polyomavirus. The primary infection is common and usually remains asymptomatic. The virus resides in the kidney in a latent form and can be reactivated when the immune system becomes compromised. B cells may transmit the virus to oligodendrocytes in the brain. Destruction of oligodendrocytes results in progressive and multifocal central nervous system symptoms and the outcome is usually fatal. PML has been increasingly detected in patients with AIDS and other secondary immunodeficiency conditions, and it might develop in exceptional cases with primary immunodeficiencies. Efficient therapies have not been established for patients with PML. Antiviral agents, highly active antiretroviral treatment in AIDS, and immunotherapies might be beneficial in acquired and iatrogenic

immunodeficiency. The associated conditions, assumed pathomechanism, clinical and neuropathological features and therapeutic possibilities are summarized.

Chapter X - Oligodendrocytes (OL) synthesize myelin sheaths that insulate axons, forming the main components of the central nervous system (CNS) white matter. The considerable importance of this structure is well underlined by the fact that its lesions occuring during Multiple Sclerosis (MS) result often in patients' severe disability. Permanent neurological deficit relies on axonal lesions that are associated with demyelination, and the remyelination process is impaired, for yet unknown reasons.

To get insight into these pathophysiological phenomenons the authors have analyzed the capability of OL to synthesize myelin in MS chronic lesions. A constant and pronounced decrease in the number of myelinated fibres per OL compared to the adjacent normal appearing white matter (NAWM) was observed (Fressinaud, 2007). This suggests that, at the cellular level, OL are incapable of synthesizing an appropriate number of myelin sheaths. Thus, restricted metabolic capacities of OL could result in their failure to remyelinate a sufficient number of damaged fibres, and might represent an important mechanism in MS, since conversely, the number of OL is less constantly decreased.

This hypothesis was supported by two sets of experimental data in vivo, and in vitro. In vivo, rat corpus callosum demyelination by lysophosphatidyl choline (LPC) stereotaxic microinjection is followed by spontaneous remyelination, and this process is significantly accelerated by treatment with either platelet-derived growth factor (PDGF) (Allamargot et al., 2001), or neurotrophin-3 (NT-3) (Jean et al., 2003). As expected, given the known proliferative effect of these growth factors on OL progenitors (Besnard et al., 1987; Barres et al., 1994), the number of OL increased by 20% in NT-3 remyelinated lesions compared to animals receiving LPC only, and, more interestingly, the number of myelinated fibres per cell increased far more, up to 100%, compared to spontaneous remyelination. Thus, these results strengthen the hypothesis that a more efficient remyelination relies not only on the availability of a sufficient pool of myelinating OL, but also, individually, on an increased capability of OL to synthesize myelin sheaths in large amounts, and that this ability too might be partly lost in MS.

Since MS often evolves on a remitting-relapsing pattern, the repetition of attacks could represent one of the main factors that account for the failure of OL to remyelinate adequately lesions; nevertheless, the consequences for OL of repeated insults were largely unknown. In order to mimic this schematically, the authors have constructed an in vitro paradigm in which OL from newborn rat brain, grown in pure cultures, were submitted to either a single exposure to LPC (2.10^{-5} M, 24 h) (Fressinaud and Vallat, 1994), or to several LPC exposures, although for shorter periods and at lower concentration ($0.5\ 10^{-5}$ M, 4 x 6 h). Indeed, OL were very susceptible to multiple attacks versus a single one (despite a similar total dose and duration of treatment), and in particular mature OL – which are the myelinating cells, and constitute the major part of the population of cells of the OL lineage in the adult CNS –. Mature OL might thus represent the principal target of relapses during MS (Fressinaud, 2005).

Taken together the authors' results converge, and suggest that cells of the OL lineage are particularly vulnerable to multiple insults, which lead both to the death of numerous cells and to restricted capability to synthesize myelin by surviving OL. This defect could constitute one

of the significant causes contributing to their failure to remyelinate axons in MS. Our data add to the accumulating scientific knowledge suggesting that early treatment and attempts to avoid relapses are needed for patients suffering from MS.

Chapter XI - The use of minimal invasive methods and edoscopic procedures for diagnosis and treatment of certain pathologic entities involving the spina canal expands permanently. The sacral spinal canal as a place of such interventions is for a long time known. Thecaloscopy is the endoscopy of lumbar subarachnoid space performed through different approaches by using flexible endoscopes.

The subject of this study was the measurement of certain anatomic diameters in the sacral spinal canal by using the lubosacral MRI studies of 25 patients.

Chapter XII – White matter fills nearly half of the brain, but receives disproportionately less scientific attention when compared to grey matter. For the past century, neuroscientists have demonstrated little interest in white matter, thought to be simply insulation for the more important axonal pathways contained within. The importance of white matter in learning tasks, mastering and executing mental and physical activities, as well as perfecting mental and social skills has become clearer over the recent decades. Much of this realization has developed from the study of diseases predominantly affecting white matter, and therefore disrupting intraneural communication, such as with multiple sclerosis and the leukodystrophies.

Two diseases that have reached epidemic status—diabetes and hypertension—also contribute to white matter disease. The mechanisms by which these two common disorders affect white matter remain under study and may share commonalities but also disparities. Interestingly, the human condition of white matter abnormalities in patients with diabetes and/or hypertension can be modeled in rodents, with the hope that this will lead to future understanding and management.

Chapter XIII - Brain tissue segmentation has important applications in studying the structure and function of the brain. A number of methods based on structural MRI data have been proposed for the segmentation problem. In this chapter, the authors present a robust method for automated brain tissue segmentation based on the multiple-channel fusion in DTI (diffusion tensor imaging) space. Our method can be employed to define accurate tissue maps when dealing with fused structural and diffusion MRI data. This enables us to study the gray matter diffusivity in neurodegenerative and neurological diseases. When fusing structural and diffusion information, the imperfect alignment of structural MRI data, e.g., SPGR (Spoiled Gradient Echo) image, with DTI data results in the problem of heterogeneous voxels when the anatomic information in the structural data is applied to the DTI data. Under the problem of heterogeneous voxels, the measurements of the GM (Gray Matter) diffusivity based on the anatomic information in the SPGR image may fail to reveal the real diffusion in the GM. Specifically, following non-rigid co-registration using the UCLA AIR tools, the GM boundaries of SPGR image are crossing CSF of ADC image. Consequently, the GM voxels in the SPGR image correspond to CSF (Cerebrospinal Fluid) voxels in the ADC (Apparent Diffusion Coefficient) image. Such a problem can occur for a variety of reasons, including geometric distortion in DTI imaging, partial volume effect, reslicing and interpolation of DTI data, and errors in co-registration.

Chapter XIV - Recent application of synchrotron radiation to high-resolution computed tomography has resolved three-dimensional structures at micrometer to submicrometer resolution, although little is known about the microstructure of soft tissues including white matter of human brain. This is because soft tissues are composed of light elements that give little contrast in a hard x-ray transmission image. In clinical diagnosis, luminal structures of a living body are visualized by using x-ray contrast media. These contrast media contain high atomic-number elements that absorb x-rays efficiently. The authors have recently shown that the neuronal structure of human brain can be visualized by contrasting neurons using the metal impregnation method. Here, the authors report x-ray microtomographic studies of human cerebral cortex stained with high atomic-number elements. Staining protocols were developed to visualize the three-dimensional microstructure of white and gray matter of human brain tissues. Methods for embedding and mounting soft tissues for the microtomographic analysis are also described. The obtained three-dimensional images revealed the microstructures of white and gray matter, which are responsible for human brain functions.

Chapter XV - Microglial cells are mononuclear phagocytes present ubiquitously in the developing brain. In the white matter, they first appear as round cells called the ameboid microglia which differentiate into ramified forms with maturation. The amoeboid microglial cells (AMC) are present in large numbers in the periventricular white matter (peripheral to the lateral ventricles) in the developing brain where they are known to exert other functions besides their primary phagocytic function. Although various theories have been proposed regarding the origin of these cells such as mesodermal, neuroectodermal and monocytic, their origin is still a matter of debate. The macrophagic nature of these cells has been demonstrated by different methods such as electron microscopy and immunohistochemistry. Expression of major histocompatibility complex class I and II antigens on them, induced by lipopolysaccharide or interferon-γ, supports their involvement in immune functions. They are also known to release cytokines and chemokines such as tumor-necrosis factor-α, interleukin-1β and monocyte chemoattractant protein-1 in inflammatory and hypoxic-ischemic injuries which may contribute to death of immature oligodendrocytes in such conditions. Recent investigations have reported that AMC also express potassium channels (Kv1.2) and release glutamate, nitric oxide and reactive oxygen species under hypoxic conditions. This chapter will review the origin and function of AMC in the periventricular white matter in the developing brain under normal conditions and the role of these cells in hypoxic/ischemic conditions.

Chapter XVI - *Objective***:** Susac's syndrome is characterized by the triad of hearing loss, branch retinal artery occlusions, and encephalopathy with predominantly cognitive and psychiatric symptoms. Focal ischemic lesions in the corpus callosum detectable by conventional magnetic resonance imaging (MRI) are a characteristic feature of Susac's syndrome. They do not, however, fully explain the type and severity of the neuropsychological deficits. In this study, the authors tested the hypothesis that widespread tissue damage of otherwise normal-appearing white matter (NAWM) can be detected in Susac's syndrome when using diffusion tensor imaging (DTI).

Methods: Three-dimensional fractional anisotropy (FA) maps were calculated from DTI data of five patients with Susac's syndrome and a group of 63 matched healthy controls.

Results: Voxel-based statistics of spatially normalized FA maps revealed highly significant widespread impairment of fiber integrity in all patients. Lesions were particularly located in the genu of the corpus callosum and in the frontotemporal connecting fascicles. Patients showed specifically reduced mean FA values in the region of interest outlining the genu. This was true even if the genu was not focally affected on conventional MRI.

Interpretation: The authors conclude that DTI is much more sensitive than conventional MRI in demonstrating WM abnormalities in Susac's syndrome. FA reductions in NAWM of the genu of the corpus callosum seem to be disease-specific. Psychiatric symptoms and cognitive deficits of these patients are most likely caused by the disruption of the anatomical connectivity of the frontal lobes.

Chapter XVII - The organisation of the myelinated central axon into discrete domains is key to the function of the central nervous system. While most of the axolemma is covered by lipid rich myelin, areas known as nodes of Ranvier are exposed to the extracellular space. These specialised regions are enriched with the Na^+ channels responsible for action potential conduction, which, due to the low capacitance of the internodal myelin sheath, can travel with remarkable speed along even the smallest of myelinated axons. Restricting current flow in this way also lessens the metabolic burden of electrical activity, permitting the development of extensive white matter tracts. Recent work has identified numerous other proteins present at nodes and adjacent areas. These include, for example, the scaffolding proteins $ankyrin_G$ and $^{\beta}$IV spectrin at the node and members of contactin associated protein family in the paranodal and juxtaparanodal regions. The exact mechanisms by which such proteins are recruited to the appropriate axonal domains remain elusive, although myelinating oligodendroglia appears to play an important role. This review will describe what is currently known about the organisation of Ranvier’s node and the myelinated central axon.

Chapter XVIII - The neural control of locomotion in vertebrates involves continuous interactions between various kinds of neural subsystems which are widely distributed throughout the central nervous system. Among these subsystems, the long descending reticulospinal pathways and their targets’ spinal lamina VIII commissural neurons with axons projecting across the midline to the contralateral side form a continuous, anatomical system that is involved in the generation and coordination of left-right reciprocal and bilateral locomotor activities. To advance understanding of locomotor roles of this brainstem-spinal cord system, the authors performed a series of neural tracing studies using anterograde neural tracers to characterize the axonal morphology of reticulospinal neurons and lamina VIII commissural neurons in the cat, with the goal of revealing some of the organizing principles of their projections along their rostrocaudal extent in the spinal cord, including: the number and frequency of their axon collaterals in the white matter, the patterns of their collateral arborizations in the gray matter, and the relationships between locations of the parent axons and their collateral termination areas. The reticulospinal pathways are morphologically heterogeneous, being composed of various types of in-parallel-descending axons, each of which has a commonality of the pattern of collateral termination along its rostrocaudal extent in the spinal cord. Commissural neurons can be classified into two major groups on the basis of their projections, viz. those that project primarily to laminae VIII-VII and those that project to the motor nuclei in lamina IX. These suggest that the reticulospinal pathways and their targets’ commissural neurons as a whole comprise varying types of functional subunits,

which may serve as the flexible optimal neural substrate essential for the generation and coordination of the bilateral locomotor rhythm in self-induced, goal-directed locomotion.

Short Communication - Among several techniques, single-shot echo-planar imaging has been a standard technique for diffusion-tensor MR imaging (DTI) of white matter because of its rapid acquisition time and high signal to noise ratio. However, inherent artifacts and distortions due to susceptibility often prevent the demonstration of normal structures and pathological changes in some situations.

Recently some studies have reported that line scan and single-shot fast spin-echo (ssfse) techniques (non echo-planar imaging techniques) have been used for DTI and their advantages. The line scan, simple spin-echo based one, can have benefits for brain stem and spinal cord imaging because of insensitivity of magnetic field inhomogeneity. Ssfse technique also avoids the artifacts and is useful for the region with geometric distortion (i.e., temporal lobe, metals after neurosurgical operation). However, these non echo-planar techniques have some disadvantages and therefore, are not commonly used in many institutions.

In this chapter, the authors review and illustrate the merits and limitations of non echo-planar imaging techniques for the DTI. Moreover, the authors discuss the current role and feasibility of the DTI for white matter studies in brain and spinal cord, i.e. quantitative analysis of apparent diffusion coefficient in patients with cervical myelopathy, including results from our experiments and clinical data.

Commentary - The use of minimal invasive methods and endoscopic procedures for diagnosis and treatment of certain pathologic entities involving the spinal canal expands permanently. The sacral spinal canal as a place of such interventions is for a long time known. Thecaloscopy is the endoscopy of lumbar subarachnoid space performed through different approaches by using flexible endoscopes.

The subject of this study was the measurement of certain anatomic diameters in the sacral spinal canal by using the lumbosacral MRI studies of 25 patients with unclear pain symptoms, in order to estimate, from the pure anatomic point of view, the capability to perform thecaloscopy in this anatomical region.

Since now anatomic morphometric data of the sacral region were delivered only from the cadaver specimens' sectioning performed in anatomic institutes during the 60's and 70's years.

The parameters measured were: 1. the inclination of the lumbosacral angle, 2. the duralsack's end, 3. the length of all the sacral spinal processes, 4. The length of the sacral spinal canal in its centre, and 5. The width of the sacral hiatus.

The results of the measurements were in detail presented and an evaluation of them concerning the applicability of flexible endoscopes in the sacral spinal canal was performed.

It was proven that the duralsack's end in 40% of the patients at the middle of the S2 vertebral body lies, an anatomical position, which through the sacral hiatus easy to access is. The length under the sacral spinal processes is smaller than the length of the sacral spinal canal in its centre, a fact that makes the manipulation of a flexible endoscope easier, if someone works straight under the spinal processes and has a smaller distance to run. Through the sacral hiatus the introduction of the flexible endoscope is by many patients possible because of its adequate width.

Research and Review Studies

In: Handbook on White Matter
Editors: T. B. Westland and R. N. Calton
ISBN: 978-1-60741-034-8

Chapter I

Interhemispheric Connectivity: The Evolution and Nature of the Corpus Callosum

Sarah B. Johnson and Manuel F. Casanova*
Department of Psychiatry; University of Louisville, KY, USA

Introduction

Though no one will doubt that animals have evolved into a shocking diversity of shapes and sizes, it is remarkable that the basic neurological layout of the vast majority of species, including at least all vertebrates and arthropods, remains preserved, with a pair of organs arranged about the longitudinal axis of the organism (Houzel and Milleret, 1999). Accordingly, Houzel and Milleret (1999) go on to suggest that this symmetric layout represents the manner in which we process and respond to our environment, with "our senses basically proceed[ing] by a balance between pairs of sensors, as our acts result from a dynamic equilibrium between pairs of effectors, and our decisions often follow[ing] judgements from contrasting points of view" (Houzel and Milleret, 1999). Though we perhaps perceive our surroundings in sensory pairs, it is imperative that the output efforts of our nervous system be united into a single, coherent, efficient response; as eloquently put by Charles Sherrington in 1906, "the resultant singleness of action from moment to moment is a keystone in the construction of the individual whose unity it is the specific office of the nervous system to perfect" (Sherrington, 1906). Based on this premise of a dichotomous receptive system requiring coherent processing and a coordinated response, "the brain must be seen as an ensemble of several multiply interconnected neuronal systems, each with its own functional specialization, and integration must be seen as the process of interactive

* Contact Information: Manuel F. Casanova, MD; Department of Psychiatry; University of Louisville; 500 South Preston Street, Building A, Room 217; Louisville, KY 40202; Email: m0casa02@louisville.edu; Tel: (502)852-4077 (O)

cooperation between these systems that allows efficient cognition and consistent behavioral control" (Berlucchi, 1999).

The classical neurological notion of a dominant hemisphere responsible for language abilities and objective processing coupled with a non-dominant hemisphere prevailing for nonverbal, spatial, and intuitive tasks has been upheld by several studies (Sperry, 1982), though this dichotomy is not seen with the brains of nonhuman mammals (Berlucchi, 1999). Still, no matter how simple the task, no operation involves exclusively one hemisphere without the other; we are constantly switching between dominant and non-dominant functions, mandating an ample channel of communication between the two hemispheres (Houzel and Milleret, 1999). Along with the evolutionarily older anterior commissure, the corpus callosum has evolved to be one of the two major inter-hemispheric connectors in mammals (Katz et al., 1983).

The corpus callosum, however, has not always been recognized as the critical cortico-cortical highway that it is. During the first half of the twentieth century, about the only importance attributed to this structure was the possibility that it facilitated the interhemispheric spread of generalizing seizure activity (Berlucchi, 1999); it was therefore frequently transected surgically as a cure for patients with epilepsy. This view was initially changed by an experiment by Sperry in 1953 in which the importance of the corpus callosum in interocular visual transfer was demonstrated by the fact that disrupting the optic chiasm did not hinder the ease with which visual pattern discriminations learned with one eye are transferred to the other eye, while disrupting both the optic chiasm and the corpus callosum certainly did (Sperry, 1961; Berlucchi, 1999). Since then, the importance of the corpus callosum in interhemispheric cooperation has been studied in increasing detail. Nonetheless, we still know strikingly little about the exact neuronal mechanisms of interhemispheric integration, a fact that Houzel and Milleret (1999) attribute to "the abundance of callosal fibers and to their manifold functions…, exist[ing] for sensory, motor, associative, frontal or limbic cortices, and… link[ing] heterologous as well as homologous areas" (Houzel and Milleret, 1999).

Before looking at the trends of corpus callosum evolution relative to brain evolution overall, it is interesting to consider just how the corpus callosum could have ever come to exist in the first place. Katz et al. (1983) offer one possible explanation based on ontophyletic analysis, which involves inferences about callosal evolution based on a comparison of developmental events in various organisms. Unlike the anterior commissure, which is believed to have evolved as new axons finding their way through a pre-established "substrate pathway," the corpus callosum, which is found only in placental mammals, appears to have appeared in the mammalian phylogeny with no apparent precursors (Katz et al., 1983). Katz et al. (1983) theorize the following chain of events in the evolutionary development of the corpus callosum: (1) the two cerebral hemispheres secondarily fused along the midline rostral to the lamina terminalis; (2) a small number of critical genomic mutations lead to the accumulation of a particular population of nonneuronal substrate cells, possibly a transient class of glia, on either side of this interhemispheric contact; (3) these glia migrated across the secondary interhemispheric fusion to form an interwoven cellular bridge, or "glial sling," between the two hemispheres; and (4) a portion of both new and existing axons eventually traversed this new passageway to ultimately form the corpus callosum (Katz et al., 1983).

Katz et al. go on to make what may be somewhat of an oversimplification in claiming, "further evolution of the corpus callosum occurred in a typical fashion for axon tracts: as the size of the neocortex increased, the size of the corpus callosum increased—with the additional axons following the preexisting callosal substrate" (Katz et al., 1983) They do add, however, that even with new axons the corpus callosum would not have the capacity to connect all cortical neurons directly (Katz et al., 1983).

This last concept foreshadows the results of a more recent study by Rilling and Insel (1999) to determine whether or not growth of the corpus callosum keeps pace with the growth of the forebrain in primate evolution. To accomplish this, whole brain MRI scans from 43 individuals spanning 11 primate species (human, bonobo, chimpanzee, gorilla, orangutan, gibbon, baboon, rhesus monkey, mangabey, cebus, and squirrel monkey) were analyzed for brain volume, gray/white ratio, corpus callosum area, and anterior commissure area. They hypothesized that "for cross-hemispheric communication via the corpus callosum to keep pace with brain growth, callosal projections must increase substantially in number and length" (Rilling and Insel, 1999), and going on the pre-established premises that (1) callosal fiber diameter changes only minimally and (2) callosal fiber density does not increase with increasing callosal area, they used the cross-sectional area of the corpus callosum as an estimate of the extent of callosal projections (Jerison, 1991; Rilling and Insel, 1999). Their results showed that corpus callosum size in fact does not keep pace with increased in brain volume, or, in other words, the ratio of corpus callosum area to brain volume decreased systematically with increasing brain size. In fact, in their sample the average human corpus callosum would have to be about one-third larger to match the ratio of corpus callosum area to neocortical surface area found in an average monkey. They also measured the anterior commissure in their samples to see if it could compensate for the reduction in callosal connectivity—however, they found an even greater reduction in connectivity via this commissure. Finally, they divided each corpus callosum into five equal parts and regressed each part individually on brain volume. In doing so, they found that the posterior fifth, corresponding roughly to the splenium, constitutes an increasing proportion of total callosal area with increasing brain size. The implications of all of these results when extrapolated to interhemispheric connectivity, which we define as "the number of callosal axons in the brain relative to the number of neocortical neurons" (Rilling and Insel, 1999), is concisely noted by another reviewer: "INTRAconnectivity [emphasis added] within each cerebral hemisphere, as expressed by the amount of white matter, was found to be larger in larger brains and to exceed in pace neocortical surface area. In contrast, INTERconnectivity [emphasis added] as expressed by surface area measurements of the corpus callosum was smaller in larger brains, like humans, than in smaller primate brains and seems not to keep pace with increasing brain size" (Semendeferi, 2001; Rilling and Insel, 1999). This reduction in interhemispheric connectivity likely parallels the functional lateralization that is thought to be an emergent property accompanying brain enlargement in primate evolution, and a possible reason for the relative sparing of the splenium amidst this reduction is the relative inability of the visual areas of the cortex (which project fibers to and receive fibers from the splenium) to tolerate as much of a reduction in interhemispheric connectivity as other cortical areas less dependent on rapid bi-hemispheric integration (Rilling and Insel, 1999).

As an interesting side note, Rilling and Insel (1999) in the course of their work found delphinid cretaceans (dolphins, for example) to have much smaller corpus callosa than anthropoid primates (controlling for brain volume), a result that echoes earlier research by Tarpley and Ridgway (1994) on corpus callosum size in delphinid cretaceans. The former group theorized "it may be that the scaling relationship between the corpus callosum and the brain is similar in [cetaceans and primates], but that the intercept is lower in cretaceans…, imply[ing] that a grade shift occurred with the evolution of cetaceans that involved a reduction in interhemispheric connectivity" (Rilling and Insel, 1999); the latter group drew similar conclusions, figuring that while humans developed a larger commissural link (relative to brain mass) to handle the elaborate interhemispheric coordination of functional asymmetry, evolutionary pressures favoring more hemispheric independence may have been at work on cetaceans (Tarpley and Ridgway, 1994).

So how do our relatively enlarged brains maintain the elaborate interhemispheric connections needed for integration and coordination of two dichotomous sides if the primary commissural projections between them have not expanded proportionally? An illuminating point raised by Buxhoeveden and Cassanova (2001) in their review of the minicolumn hypothesis is that "as brain evolution paralleled the increase in cell number, a reduction occurred in the sovereignty of individual neurons; fewer of them occupy critical positions. As a consequence, plasticity and redundancy have increased" (Buxhoeveden, 2001). This premise seems to make feasible a model where the corpus callosum could enlarge only moderately over time and still accommodate the necessary connections for a more profoundly expanding population of cortical neurons. Fortunately, an increasing number of studies on the number, caliber, chemical composition, architecture, path, and terminal arrangements of callosal fibers continue to reveal much about the nature of the intricate connective network between hemispheres that has evolved in the brains of higher mammals.

One of the earliest attempts to characterize callosal fibers came in 1954 with Tomasch's meticulous attempts to quantify the callosal fibers (count of all callosal fibers via Haeggquist's staining method, as well as count of myelinated fibers only via Weigert's staining method) in three postmortem human brains. The number of total callosal fibers for each of the three brains by his method was 177 million, 175 million, and 193 million, though he realized that very small fibers escaped staining (Tomasch, 1954). Still, even going by his highest figure of nearly 200 million callosal fibers, Tomasch concluded that "if one compares this number with the estimates of the total number of nerve-cells in the cerebral cortex [which was around 9.2 billion by an 1899 study using the estimation method of Hammarberg], it is but a small fraction" (Tomasch, 1954).

Fortunately, newer techniques have allowed for much keener characterization of the many properties of callosal fibers. As mentioned above, Houzel and Milleret (1999) rationalized that much of the trouble with adequately studying callosal fibers was their sheer number and abundance of overlapping and variable functions. To overcome this, several researchers have chosen to study a very specific population of callosal connections, namely those in the visual system of cats, where the corpus callosum is instrumental in effectively integrating "the visual world that is represented in two physically discontinuous cortical maps, split across the two hemispheres along the central vertical meridian of the visual field" (Houzel and Milleret, 1999). In doing so, many properties of callosal fibers have been

elucidated. First, using retrograde and anterograde tracing techniques, it has been demonstrated that while the visual cortical areas 17 and 18 were mostly free of interhemispheric projections, the common border of these areas (the 17/18 border) contained dense packings of cell bodies and axons of callosal neurons (Houzel and Milleret, 1999). Being that the 17/18 border in fact marks the cortical representation of the previously mentioned central vertical meridian of the visual field, this seems to indicate at least some degree of precise point-to-point connection between correspoding loci in the two hemispheres. Second, the technique of *in vivo* retrograde labeling followed by *in vitro* intracellular filling with lucifer yellow has allowed the identification of the cell types comprising callosal projections: while the vast majority are large pyramidal cells, up to one third appear to be other types, including spiny stellate, smooth stellate, and fusiform cells (Houzel and Milleret, 1999). Third, electron microscope studies in cats have revealed a considerable range in visual callosal axonal caliber (with two-thirds consisting of unmyelinated fibers between 0.08 and 0.40 □m and the remaining third consisting of myelinated fibers between 0.25 and 4.0 □m), which seems to indicate that "the callosal pathway actually comprises several channels with diverse morphological and physiological features" (Houzel and Milleret, 1999). Fourth, callosal axons were found to differ in the size of their terminal territories, with the majority of axons dividing extensively in the white matter and going on to terminate in sizable fields (mostly greater than 0.25 mm^2, and up to 9 mm^2). While the heaviest sites of termination were indeed at the homotopic contralateral site, the abundance of axons diverging to form heterotopic connections goes against a strict point-to-point mapping model between corresponding loci of the two hemispheres (Houzel and Milleret, 1999). Still, despite the variability in terminal territories of callosal fibers, individual callosal projections were found to terminate within distinct columnar and laminar compartments, the precise functionality of which could perhaps be determined by future research combining anatomical and functional analyses. Fifth, detailed inspection of branching points carried out for entire trees revealed a variety of architectures, ranging from 'parallel' arrangements to 'serial' arrangements to complex patterns evoking various combinations of both, and the application of conduction velocity measurements to these helped shape a theoretical model in which "synchronization might be achieved through equalization of conduction times in parallel arbors, or through appropriate modulation of calibers in serial axons; moreover, the degree of coactivation might be enhanced, or adjusted, by converging branches with fitting geometrical properties" (Houzel and Milleret, 1999). In attempting to sum up the functional significance of the various properties of callosal fibers reviewed above, Houzel and Milleret postulate that the ability of a callosal axon from a single area or column in one hemisphere to terminate on and thus cooactivate multiple target neurons in several columns of the other hemisphere provides a potential mechanism for the grouping of individual neurons or columns into a variety of functionally coherent assemblies. In further developing the role of callosal fibers in interhemispheric synchronization, they offer the following distinction between the roles of heterotopic and homotopic connections: "One can hypothesize that heterotopic callosal connections establish temporal relations essential to the integrate representation of sensory features, while homotopic connections allow accurate topographic correspondence between left and right maps and thereby

contribute to the generation of feature-selective receptive fields, such as in disparity-sensitive neurons" (Houzel and Milleret, 1999).

Other studies have provided additional fascinating details concerning callosal projections. Aggoun-Zouaoui et al. (1996) utilized anterograde tracing with biocytin followed by reconstruction from serial sections to describe the sequential development of callosal terminal arbors into the columnar distribution of preterminal branches and terminal boutons described in the cat visual cortex by Houzel et al. in 1994. The process involves the following sequential steps: (1) early growth of the developing callosal axons into the gray matter in column-like bundles; (2) exuberant growth of side branches; (3) formation of synapses in specific layers and columns; (4) reduction in the number of branches and synapses; (4) subsequent increase in the diameter or radially arranged boutons with age (Aggoun-Zouaoui et al., 1996; Buxhoeveden and Casanova, 2001). Ding and Elberger (2001) also studied the distribution and morphology of developing callosal axons, though in the rat visual and auditory cortices, and using the *in vivo* anterograde tracer biotinylated dextran amine (BDA). They found that most callosal axons from the visual cortex went to almost solely homotopic contralateral sites, while projections from the auditory cortex initially went extensively to both homotopic (contralateral auditory cortex) and heterotopic (contralateral visual cortex) sites, though the latter group proved transitory with most being eliminated by postnatal day 28. The homotopic callosal axons from the auditory cortex that persisted were noted to assume a distinct columnar organization (Ding and Elberger, 2001).

Yet another characteristic of callosal fibers being researched is their neurochemical profile, or neurotransmitters they utilize. Many researchers have used immunocytochemical techniques to detect neurotransmitters and modulatory peptides in callosal fibers in all stages of development, and the clearest conclusion seems to be that both developing and mature corpus callosum connections are neurochemically heterogenous (Conti et al., 1988; Ding and Elberger, 2000). In the adult, the majority of corpus callosum connections are immunopositive for excitatory amino acid neuro-transmitters such as glutamate and aspartate, with only a minority being immunopositive for the inhibitory transmitter gamma-aminobutyric acid (GABA) or modulatory peptides such as cholecystokinin, neuropeptide Y, or somatostatin.

What, then, can be said of the overall function of the corpus callosum, in terms of whether the primary nature of the fiber tract is excitatory or inhibitory? Several models of corpus callosum functioning have been presented, and for a while there was competition between a topographic, or homotopic, column-to-column excitatory theory and a diffuse, or regional, inhibitory theory. In 1984, Norman Cook took aspects of both of these models and attempted to fuse them into what he called a "topographic/homotopic inhibitory model." Though perhaps subsequently surpassed in technical complexity, his article remains a stimulating theoretical examination of the overall function of the corpus callosum. First off, Cook draws on previous estimates of callosal fiber number (between 180-200 million) and numbers of cortical columns (no more than 81 million, given a diameter of 50 □m) to validate the necessary premise of a homotopic column-to-column excitatory theory that there would in fact be ample callosal fibers to connect all homotopic columns at least twice (that is, one afferent and one efferent fiber). Next, he enlists what he feels are the relative strengths of the more popularly accepted diffuse inhibitory theory, which include this theory's ability to

better account for normal laterality in man (in other words, the asymmetry of hemispheric function in man), for the postoperative changes seen in split-brain patients, and for the cognitive abnormalities in individuals with callosal agenesis. He speculates that "where an excitatory model implies the corpus callosum functions to *reduce* hemispheric specializations, the inhibitory model implies that the specializations are themselves due primarily to callosal effects—and as such no recourse to lower level asymmetry is needed" (Cook, 1984).

With that introduction, Cook then presents his topographic inhibitory model, based on seven premises borrowed from either of the two former theories. These are: (1) approximate bilateral symmetry of the two cerebral hemispheres; (2) columnar organization of the neocortex; (3) predominantly homotopic callosal connections (at least 2 percolumn, as described above); (4) synaptic callosal inhibition of columnar activity; (5) unilateral cerebral dominance for speech production and understanding; (6) ipsilateral cortical surround inhibition among cortical columns; and (7) a bilaterally symmetrical subcortical mechanism for arousal and attention (Cook, 1984). Using these premises, he then weaves a theoretical example in which unilateral cortical activity, such as verbal processing in the left hemisphere, causes ipsilateral (left-sided) surround inhibition (as is rightly predicted by the diffuse inhibitory model), but no net decrease in the contralateral (right-sided) activity from effects of surround inhibition (as is rightly predicted by the homotopic excitatory model), thus allowing for a variety of interesting *complementary* (but not reduced) patterns of firing in the contralateral (right) hemisphere.

Finally, Cook attempts to apply his model to a real situation, i.e., cases of language deficits due to lesions of the right hemisphere. In such patients, the literal understanding and production of language remains intact, while the ability to appreciate and reproduce nuance, bizarreness, coherence (or lack thereof), and metaphor is lost. Cook refers to the "scaffolding" hypothesis posed by Wapner et al. (1981) that the right hemisphere provides the "contextual framework within which the literal understanding of the left hemisphere is normally placed" (Wapner et al., 1981; Cook, 1984). Cook then leads the following sophisticated theorization using the lateralization of language functions to support his homotopic inhibitory theory over the two previously mentioned models:

"The homotopic inhibitory theory… predicts that… in the process of activation of cortical columns in the left hemisphere during verbal processing, there would occur surround inhibition ipsilaterally and homotopic inhibition contralaterally. Since surround inhibition in the left hemisphere would prevent activation of the immediately surrounding columns with presumably their equally contiguous cognitive content, at least some portions of the peripheral linguistic meanings, connotations, and the conceptual context of the ongoing language would be suppressed. In the right hemisphere, on the other hand, *only* such peripheral columns would be activated—producing contextual but not literal understanding. Such asymmetry may therefore be the basis for literal capacities in the left—with much of the contextual framework missing, and equally high-level cognitive processing of the cognitive 'scaffolding' in the right—but with the immediate linguistic message itself inhibited by the verbally dominant left hemisphere."

Mishari (2006) explained the origin of the corpus callosum from a functional, developmental and genetic standpoint. From a functional standpoint, the corpus callosum is

key in numerous motor and sensory functions including binocular convergence and stereoscopic vision, midline fusion of two visual hemifields, bimanual coordination and sound localization. It also functions in developmental integration and learning processes. However, sectioning the corpus callosum does not appear to produce adverse effects aside from callosal disconnection syndrome. It has been suggested that the evolution of the corpus callosum stemmed from the necessity of integrating the two hemispheres across the midline. In nonplacental mammals, the anterior commisure and hippocampal commisure serve this purpose, but it is not practical for large-brained animals because of the distance that must be travelled to reach the contralateral hemisphere. Fossil records suggest that the corpus callosum likely developed between 100 and 130 million years ago, closely linked to the motor cortex.

Pathological Correlates

From a developmental standpoint, axons of the corpus callosum are closely linked to the hippocampal commisure and are able to cross the midline.

Human and animals studies suggest a genetic link in corpus callosum development because over 50 congenital syndromes are associated with agenesis of this structure. Many of these syndromes also are associated with other neurological deficits. No unique gene for corpus callosal development has been determined. This structure may have evolved partly due to changes in genes coding for molecules regulating axonal growth and guidance. (Mishari 2006)

Studying agenesis of the corpus callosum or hypogenesis can provide insight into the functional and structural evolution of this structure. The corpus callosum partially develops from pre-existing axon tracts. Neurons from the cingulated cortex and hippocampal cortex may provide a path for neocortical neurons to traverse the midline during cc development. Midline structures such as the glial wedge, zipper glia and indusium griseum glia also guide corpus callosum development**.** After callosal axon fibers cross the midline and project onto targets in the contralateral hemisphere, they are selectively pruned in cats and ferret models and this may also contribute to corpus callosum development in humans (Paul et al., 2006)

Paul (2006) also suggests that animal studies in mice with agenesis of the corpus callosum provide insight into genetic contribution to the development of the corpus callosum. Mice with agenesis of the corpus callosum were found to have inactivated Disc 1, the gene disrupted in schizopheneia. This may suggest a link between agenesis of the corpus callosum and schizophrenia. Agenesis of the corpus callosum, and thus development, in humans is thought to result from monogenetic, polygenetic and complex genetic interactions. Environmental factors also likely contribute to development of the CC, either by disrupting formation or the pruning process.

Studies of psychiatric patients with various conditions with known developmental, genetic and environmental influences may someday shed light on how the corpus callosum evolved because many affected individuals display marked differences in callosal morphology as evidenced by recent work.

Attention Deficit-Hyperactivity Disorder

Abnormalities have been found in the corpus callosum in many studies. Seidman et al. noted that although the methodologies of the body of evidence make comparison difficult, there is consistent evidence to implicate posterior regions of the corpus callosum linking the temporal and parietal brain regions (Seidman et al., 2005). Hutchinson and Mathias further investigated structural differences in ADHD individuals compared to controls with a meta-analytic review of imaging studies. There are several different methods of dividing the corpus callosum to measure differences in research studies. This meta-analysis took into consideration these divisions when calculating differences in the regions of the CC (Hutchinson and Mathias 2008).

The overlap ranged from 92% in the midbody between ADHD subjects and controls to 48% in region 4, an area anterior to the splenium. The differences in splenium size between ADHD subjects and controls was statistically significant. The effect size of -0.54 and half a standard deviation. The splenium has connections to the temporal lobes and may be involved with memory.

These differences are unclear. They found that fewer axons connecting the parietal regions could be the cause of smaller area. Another explanation is that the fibers may be more myelinated in controls. Either of these explanations could lead to decreased processing between hemispheres in affected individuals (Hutchinson and Mathias 2008).

Buchman and colleagues (2003) studied functional differences between ADHD subjects and controls. In this study, transcranial magnetic stimulation was used to measure differences in motor function in ADHD and control subjects. TMS causes a motor response contraleteral and a transient inhibition of voluntary muscle movement in the ipsilateral hand muscles. This ipsilateral inhibition is known as the ipsilateral silent period (iSP) and is thought to be mediated by the corpus callosum transcallosal fibers and the inhibitory interneurons affecting the motor area III contralateral to the stimulus, also the site of callosal fiber projection.

Several parameters were measured in control and active subjects and differences between. Resting motor threshold measures membrane properties and was similar between subjects and controls. MEP was also similar, supporting that motor-cortical hyperexcitability is not the cause of ADHD. cSP was also not significantly different between controls and subjects. It is composed of early and late corticospinal tracts and this suggests that the inhibitory tracts underlying these tracts is not the cause of hyperexcitability iSP latencies were prolonged in ADHD subjects compared to controls. Previous studies have demonstrated that the corpus callosum is smaller in ADHD subjects compared to controls this latency could be caused by defective myelination. Another explanation could be defective callosal output neurons that provide GABA inhibition to the contralateral side and generate the iSP (Buchman 2003).

In a 2007 study, Rusch at el. investigated corpus callosal size in women with Borderline Personality Disorder and comorbid ADHD. Smaller isthmus size was found, supporting theories of disturbed interhemispheric connectivity contributing to symptoms of psychiatric illness. The posterior location of these findings supports previous studies suggesting impaired connectivity in the parietal region. A thinner posterior callosal area was also found in individuals who had suffered childhood sexual trauma. Findings from this study are are

consistent with previous studies and suggest that similar callosal properties may be present in both Borderline Personality Disorder and ADHD. These two illnesses share some common symptoms such as distractability and affect regulation and this study supports that they may have similar underlying structural pathology.

Bipolar Disorder

In an MRI study, smaller white matter area was found in total callosal area, genu, posterior body and isthmus. This suggests reduced connectivity between prefrontal areas that are connected by the genu, inferior temporal and superior parietal lobes that are connected by the posterior body and posterior parietal and superior temporal that are connected by the genu. The frontal and temporal lobes are thought to be involved in regulating the cortical circuitry underlying mood disorders, including: the prefrontal cortex, amygdala and hippocampus. These results were consistent with the study by Coffman et al., in 1990. This study also found differences between relationships between callosal area and age varied inversely in normal controls, but not in bipolar subjects, suggesting that bipolar subjects may not have normal age related changes (Brambilla et al., 2003).

Prior studies found that bipolar subjects had smaller corpus callosa, but size was not found to differ in previous pediatric studies. This study evaluated Corpus Callosum signal intensity, a measure of myelination. In an adult study, CCSI was lower, suggesting abnormal myelination (Yaser 2006). Lower CCSI was found in bipolar subjects, consistent with adult studies. CCSi has been found to decrease in age in normal subjects. In this study, it did not vary with age which could indicate abnormal maturation (Caetano 2008).

Functional MRI studies have also found differences in myelination in a pediatric population with bipolar disorder. A decrease in free water due to myelination causes increased signal intensity on MRI. In this study, signal was measured in anterior body, posterior body, genu, isthmus and splenium in bipolar and unipolar depressed subjects. This study found reduced signal in bipolar but not unipolar subjects, which may be caused from decreased myelination (Brambilla 2004).

Schizophrenia

Crow (1997) suggests that schizophrenia develops independent of environmental factors, given the uniform distribution in populations, genetic contribution and that the onset coincides with the reproductive phase of life. It may represent a breakdown between cortical areas as some some circuits are autonomous and may have parasitic foci. This suggests genetic variation has been recently introduced. To determine exactly which systems are involved, it is important to consider which evolved latest, which are variable and which are sexually dimorphic.

The corpus callosum is variable between different individuals and sexes and may be this site of this breakdown between hemispheres. This variability of cortico-cortical connection in schizophrenia must be located in fiber pairs that connect areas of cortex that are

asymmetrically distributed between hemispheres and this could be related to the dysynchronous development of the two hemispheres. Presumably, the areas affected would be in the areas that are latest developing and differ between the sexes. Post mortem evidence suggests that failure of hemispheric differentiation occurs in schizophrenia (Crow 2007).

Barnett et al. (2005) studied lexical decision making tasks in schizophrenic subjects and normal controls to support the hypothesis that interference between hemispheric connections contributes to symptoms of schizophrenia. Words were presented to right and left hemispheres individually and both hemispheres simultaneously. Normal subjects responded faster and with greater accuracy when words were presented to both hemispheres, Schizophrenic subjects lacked this advantage, suggesting differences in interhemispheric connections.

Literature supports differences in corpus callosal shape differences and displacements appear consistently in the literature although there is conflicting data regarding size differences (Nar et al., 2002). This study examined discordant pairs of mono- and dizygotic twin pairs in which one twin was affected with schizophrenia compared with normal controls to better understand the effects of genetics and environment.

MRI studies using T1 weighted images demonstrate increased signal in all callosal regions in schizophrenic subjects versus controls, similar to MRI findings in other conditions discussed above. This indicates altered white matter and .supports the notion that the symptoms of schizophrenia may be partly due to alterations in white matter pathways (Diwadkar et al., 2004)

Recent advances have allowed for investigating differences at a neurochemical level between schizophrenic subjects and controls. The proton magnetic resonance spectroscopy used in this study allows for investigating neurochemical changes and thus the integrity of white matter in schizophrenia. This study investigated the metabolic integrity of the CC during the prodromal phase of the illness in an attempt to support the neurodevelopmental model of illness (Aydin et al., 2008).

In this study, levels of NAA, an amino acid synthesized from acetyl coenzyme A asparatate by D-aspartate N-acetyltransferase, were decreased in individuals during the prodromal phase of schizophrenia. Neuron and axonal dysfunction have been reported to cause decreases in NAA. These findings suggest that the pathologic processes that cause dysfunction in the corpus callosum occur before the onset of disease (Aydin et al., 2008).

A greater understanding of the factors influencing the development and evolution of the corpus callosum allows for a better understanding of the complex etiology of some psychiatric illnesses. It is clear that the corpus callosum is necessary for interhemispheric communication and aberrations in its function may explain language and communication symptoms. As our research tools and methods of investigating this structure at molecular and chemical levels improve, so will our understanding of the psychiatric disease process.

References

Aggoun-Zouaoui, D.; Kiper, D.C.; Innocenti, G.M. Growth of callosal terminal arbors in primary visual areas of the cat. *European Journal of Neuroscience,* 8:1132-1148; 1996

Aydin K et al., Altered metabolic integrity of corpus callosum among individuals at ultra high ridk of schizophrenia and first-episode patients. *Biological Psychiatry,* 2008.

Barnett et al., Bilateral disadvantage: Lack of interhemispheric cooperation in schizophrenia. *Consciousness and Cognition,* 16:436-44; 2007.

Berlucchi, G. Integration of brain activities: The roles of the diffusely projecting brainstem systems and the corpus callosum. *Brain Research Bulletin,* 50(5-6):389-390; 1999.

Brambilla P et al., Magnetic Resonance Imaging Study of Corpus Callosum Abnormalities in Patients with Bipolar Disorder. *Biological Psychiatry*, 54: 1294-7; 2003.

Brambilla P et al., Corpus callosum signal intensity in patients with bipolar and unipolar disorder. *Journal of Neurology, Neurosurgery and Psychiatry*, 75:221-5; 2004.

Buchmann J et al., Disturbed transcallosally mediated motor inhibition in children with attention deficit hyperactivity disorder (ADHD). *Clinical Neuropsychology*, 14: 2036-42; 2003.

Buxhoeveden, D.P.; Cassanova, M.F. The minicolumn hypothesis in neuroscience: A review; 2001.

Caetano et al., Abnormal corpus callosum myelination in pediatric bipolar patients. *Journal of Affetive Disorders,* 108:297-301; 2008.

Conti, F.; Fabri, M.; Manzoni, T. Glutamate-positive corticocortical neurons in the somatic sensory areas I and II of cats. *Journal of Neuroscience,* 8:2948-2960; 1988.

Cook, N.D. Homotopic callosal inhibition. *Brain and Language,* 23:116-125; 1984.

Crow T. Genetic Contributions to Altered Callosal Morphology in Schizophrenia. *Schizophrenia Research,* 30: 111-4; 1997.

Ding, S.L.; Elberger, A.J. Neuropeptide Y- and somatostatin-immunoreactive axons in the corpus callosum during postnatal development of the rat. *Developmental Brain Research,* 124:59-65; 2000.

Ding, S.L.; Elberger, A.J. Postnatal development of biotinylated dextran amine-labeled corpus callosum axons projecting form the visual and auditory cortices to the visual cortex of the rat. *Experimental Brain Research,* 136:179-193; 2001.

Diwadkar V et al., Abnormailities in MRI measured signal intensity in the corpus callosum in schizophrenia. *Schizophrenia Research,* 67:277-82; 2004.

Houzel, J.C.; Milleret, C.; Innocenti, G.M. Morphology of callosal axons interconnecting areas 17 and 18 of the cat. *European Journal of Neuroscience,* 6:898-917; 1994.

Houzel, J.C.; Milleret, C. Visual inter-hemispheric processing: Constraints and potentialities set by axonal morphology. *J. Phsiol. (Paris),* 93:271-284; 1999.

Hutchinson A and Maathias D. Corpus Callosum Morphology in Children and Adolescents With Attention Deficit Hyperactivity Disorder: A Meta-Analytic Review. *Neuropsychology* 22:341-9; 2008.

Jerison, H.J. *Brain Size and the Evolution of Mind*. New York: American Museum of Natural History; 1991.

Katz, M.J.; Lasek, R.J.; Silver, J. Ontophyletics of the nervous system: Development of the corpus callosum and evolution of axon tracts. *Proc. Natl. Acad. Sci. USA,* 80:5936-5940; 1983.

Mihrshahi R. The corpus calosum as an evolutionary innovation. *Journal of Experimental Zoology.* 306B: 8-17; 2006

Narr et al., Genetic contributions to altered callosal morphology in schizophrenia. *The Journal of Neuroscience,* 22: 3720-9; 2002.

Paul et al., Agenesis of the corpus callosum:genetic, developmental andfunctional aspects of connectivity. *Neuroscience.8:287-299*; 2007

Rilling, J.K.; Insel, T.R. Differential expansion of neural projection systems in primate brain evolution. *NeuroReport* , 10:1453-1459; 1999.

Rusch N et al., Corpus callosum abnormalities in women with borderline personality disorder and comorbid attention-deficit hyperactivity disorder. J*ournal of Psychiatry and Neuroscience*, 32:417-22; 2007.

Seidman et al., Structural brain imaging of attention-deficeit hyperactivity disorder. *Biological Psychiatry*, 57:1263-72; 2005.

Semendeferi, K. Advances in the study of homonoid brain evolution: magnetic resonance imaging (MRI) and 3-D reconstruction. *Evolutionary Anatomy of the Primate Cerebral Cortex*. Cambridge University Press:281-283; 2001.

Sherrington, C.S. *The integrative action of the nervous system*. New Haven: Yale University Press; 1906.

Sperry, R.W. Cerebral organization and behavior. *Science,* 133:1749-1757; 1961.

Sperry, R.W. Some effects of disconnecting the cerebral hemispheres. *Science,* 217:1223-1226; 1982.

Tarpley, R.J.; Ridgway, S.H. Corpus callosum size in delphinid cetaceans. *Brain Behav Evol,* 44:156-165; 1994.

Wapner, W.; Hamby, S.; and Gardner, H. The role of the right hemisphere in the apprehension of complex linguistic materials. *Brain and Language,* 14:15-33; 1981.

In: Handbook on White Matter
Editors: T. B. Westland and R. N. Calton
ISBN: 978-1-60741-034-8

Chapter II

White Matter Lesions: From Present to Future

R.P.W. Rouhl[1], R.J. van Oostenbrugge[1,2] and J. Lodder[1,2]
[1] Department of Neurology
[2] Cardiovascular Research Institute Maastricht (CARIM)
Maastricht University Medical Centre, AZ Maastricht, The Netherlands

Abstract

White matter lesions are caused by cerebral small vessel disease, particularly by arteriolosclerosis. Arteriolosclerosis consists of a hyaline wall thickening with consequent narrowing of the arteriolar vessel lumen and tissue ischemia. Arteriolosclerosis relates to hypertension, and to other cerebral ischemic lesions (lacunar infarcts, symptomatic as well as asymptomatic). The instigating factors in the pathogenesis of arteriolosclerosis and therefore of white matter lesions, however, remain elusive. Most accepted of current theories is disruption of the blood brain barrier caused by endothelial dysfunction. New imaging modalities, like molecular imaging, and new insights in endothelial biology could therefore provide further insight into the pathogenesis of arteriolosclerosis. In the present chapter we will discuss these emerging issues, their potential pitfalls, and their possibility to eventually increase therapeutic options for the vascular pathology which underlies white matter lesions.

Introduction

Ever since the advent of Computed Tomography (CT) and Magnetic Resonance Imaging (MRI), cerebral white matter lesions (WML) have been noted in the brain. Current reviews of the literature mainly emphasize epidemiological and clinical data concerning these lesions. However, the cause of these lesions, and therefore any therapeutic or preventive regimen, remains elusive. Therefore, in this chapter we will introduce possible new strategies to unravel the pathophysiology of WML.

Cerebral White Matter Lesions and Cerebral Small Vessel Disease

The pathogenesis of WML remains unclear, however, epidemiological data suggest a vascular pathophysiology. For example on imaging, WML relate to lacunar infarcts, and most strongly to multiple lacunar infarcts[3], and also to dilated perivascular spaces[48]. WML relate to vascular risk factors like increasing age[60, 72] and hypertension[3]. Clinically, WML relate to (recurrent) ischemic stroke[6], cognitive disturbance (mainly in the area of executive functioning[45, 58, 69]) and cognitive decline[18, 60], gait disturbances,[1] and urinary problems[42]. In lacunar stroke patients, WML relate to a worse prognosis (with regard to morbidity, stroke recurrence, and mortality)[6], also on the long term[53]. All these epidemiological data strongly suggest an ongoing (vascular) pathology in the brain.

In pathological studies, there is strong evidence that WML are caused by cerebral small vessel disease (CSVD). CSVD also causes lacunar infarcts, however, there are different pathological processes in the cerebral small vessels which could cause lacunar infarcts, WML or both. Fisher meticulously described the types of small vessel abnormalities which occur proximal to a lacunar infarct: one he called *microatheromatosis*[13] (which represents atherosclerosis on an arteriolar level, mostly in arterioles of more than 200 micrometer in diameter, and causes large, single lacunar infarcts[15]) and the other one was characterized by segmental wall disorganization[12] (or *fibrinoid necrosis* in the acute stage and *lipohyalinosis* in a healed stage; later called *complex cerebral small vessel disease*[28], which occurs in arterioles of a diameter smaller than 200 micrometer, and causes multiple small lacunar infarcts[15]). Both lead to microvascular occlusion, as can be demonstrated by imaging[66]. Fisher suggested that hypertension was the major risk factor for both these conditions[14, 16].

Extensive, diffuse WML, however, relate to a third microvascular abnormality[1]: *arteriolosclerosis*[61, 64]. Arteriolosclerosis consists of hyaline wall thickening with consequent narrowing of the arteriolar lumen, and a poor response to changes in cerebral blood flow[29, 57]. The presence of arteriolosclerosis in brain arterioles is associated with age, hypertension, and diabetes[29]. WML patients more often have hypertension than cerebrovascular patients without WML; however, hypertension is not a *conditio sine qua non* for the development of WML as the vascular abnormalities can also be found in brains of non-hypertensives[30]. The risk factor profile (mainly the association with hypertension) is similar in patients with multiple lacunar infarcts (complex small vessel disease) and WML patients (arteriolosclerosis)[26], however, whether arteriolosclerosis is a preliminary stage of complex small vessel disease (or the other way around) remains to be elucidated[28].

Cerebral lesions like WML and lacunar infarcts could also be caused other vascular diseases than this aforementioned cerebral small vessel disease. Lammie e.g. suggested from the pathological appearance of some lacunar infarcts (which he called incomplete), that also transient processes like temporary reduction of blood flow, multiple emboli, or small vessel

[1] Note that punctuate WML (in contrast to the abovementioned diffuse or large confluent areas of WML) are pathologically very heterogeneous. These punctuate foci can represent myelin pallor, local demyelination, as well as areas of gliosis and ischemia. The underlying vascular pathology is therefore equally heterogeneous and sometimes even absent.

spasms could lead to multiple lacunar infarcts[31], as he could not demonstrate any arteriolar abnormality in these cases. Others also argue, especially in case of multiple lacunar infarcts, for an embolic source (which may be the heart or a proximal larger artery)[37]. However, when all patients with potential embolic sources are excluded from these studies, there are still patients with multiple lacunar infarcts[48]; even more strikingly, lacunar stroke is much less strongly related to a cardiac embolic source than other stroke subtypes[32]. Therefore, it is unlikely that an embolic source accounts for all multiple lacunar infarct patient in these series. CSVD (with microatheromatosis, complex cerebral small vessel disease, and arteriolosclerosis as pathological hallmarks) therefore remains the most probable cause of lacunar stroke and WML.

Pathogenesis of Cerebral White Matter Lesions

One of the main theories at this moment for the development of arteriolosclerosis and complex small vessel disease (WML and multiple lacunar infarcts) is that an increased permeability of the blood-brain barrier (BBB)[65, 68] leads to white matter damage and lacunar stroke. This is suggested by:

- oedema related gliosis in WML and its similarity to the brain edema which is caused by BBB disruption in animal models[27]
- the relation of cerebral oedema formation with factors which increase BBB permeability, like liver failure, renal failure, pancreatitis, and alcoholism. All these factors also relate to lacunar infarcts[30]
- changes in BBB integrity which have been demonstrated using MRI with Gadolinium contrast enhancement in lacunar stroke patients (these changes are only present in a lesser extent in patients with other types of stroke)[67] and in patients with WML[54].
- leakage of specific proteins from blood to cerebrospinal fluid, which is only possible in case of a defective BBB, in patients with recurrent lacunar stroke[59]

In turn, the defective BBB is probably caused by endothelial dysfunction. Several authors demonstrated that markers of endothelial dysfunction, like E-selektin[10], ICAM[10, 23], P-selektin[7], and VCAM[7] are present in peripheral blood of WML patients. Also, patients with WML progression have higher levels of markers of endothelial dysfunction (ICAM)[34]. Furthermore, there are also relations between certain gene polymorphisms which are involved in endothelial function on one hand and WML on the other[33].

Current imaging techniques are insufficient to visualize this microscopic vascular pathology in a lacunar stroke and/or WML patient. The pathology of the cerebral small vessels can only be guessed from MRI/pathologic-correlational studies. Therefore, conclusions from all studies up till now have to be appreciated with some reserve.

To further elucidate the pathogenesis, molecular imaging and new insights into endothelial biology, such as the role played by endothelial progenitor cells, could be important. Molecular imaging could advance knowledge on pathogenesis by direct

visualization of the vascular pathology and endothelial activation and dysfunction, using probes targeted to cells with specific properties. Endothelial progenitor cells could advance knowledge on the endogenous repair mechanisms of endothelial damage, and the role of risk factors.

Molecular Imaging

MR Imaging has been used to rate WML severity, e.g. by the widely used semiquantitative Fazekas scale[11]. More advanced volumetric measurements led to an increased detail in the quantification of WML (even to exact quantification) and WML progression with increasing age or under the influence of hypertension. More sophisticated visual rating scales such as a new scale introduced by Prins et al., also measure change in WML load reliably over time[43]. Of course, none of these scales assesses the underlying vascular pathology. With regard to BBB imaging, recent studies with Gadolinium DTPA have shown that patients with lacunar stroke have changes in their BBB function as compared to cortical stroke patients[67]. However, an instigating event for the BBB dysfunction is not known.

Sofar, imaging studies do not confer new evidence for an underlying, vascular pathophysiological mechanism[38, 49]. From the starting point of an endothelial dysfunction and a resultant defective BBB causing WML and lacunar infarcts, molecular imaging holds great promise.

Molecular imaging uses MRI with specific contrast media. These contrast media are coupled with antibodies or peptides which bind to specific proteins present in vessels or brain. As such, molecular imaging can visualize molecular processes in vivo, though yet only in experimental settings.

Different contrast media are used:

1. Contrast media with gadolinium (Gd): Gd DTPA can be coupled to specific antibodies, which are targeted to surface molecules of specific cells (which does not require a functioning cell), or to a peptide which is internalized by cells which possess its receptor (this already poses its disadvantage: the requirement of a functional receptor (and a functional cellular metabolism))
2. Contrast media with iron: microparticles or ultrasmall superparamagnetic particles, which consist of an iron core of several nanometers in diameter (the larger the iron core, the larger the paramagnetic effect in MR imaging and therefore the contrast) and are covered with specific antibodies or peptides targeted to surface molecules of specific cells. These particles could be safely used in humans, when made biodegradable[35].

Barber et al. found contrast enhancement shortly after experimental stroke in mice using Gadolinium coupled to a peptide which is internalized by E-selektin (Gd-DTPA-sLe^x)[2]. Similarly, expression of E-selektin has been demonstrated with Gd-DTPA-sLe^x in murine striatum (after experimental induction)[51], as well as in liver (in a murine experimental hepatitis model)[4].

Using Iron contrast, in the form of ultrasmall superparamagnetic iron oxide (USPIO), which are nanoparticles coupled to specific antibodies, vascular E-selektin expression has been demonstrated in mice with contact hypersensitivity[46]. Iron contrast with larger particles (microparticles) coupled to antibodies to VCAM has been demonstrated in cerebral small vessels in a rodent model for multiple sclerosis (allergic encephalomyelitis)[36]. McAteer et al., found contrast enhancement in atheroscerlotic plaques in apo-E knockout mice, using microparticles both targeted to VCAM as well as P-selektin[35].

Some investigators coupled iron contrast to an engineered peptide[25] (which was optimized later[39]) which is internalized by VCAM, and in this way they demonstrated VCAM expression in atherosclerotic plaques in mice.

Thus, markers of endothelial dysfunction, as have been demonstrated in WML patients in peripheral blood, can be imaged in vivo in animal models of different diseases. Though promising at first sight, there are some caveats: 1) there are no data on the use of the contrast agents in humans. The half life of the immunologically labelled contrast agents is not known, and its biological effects are not clear, however, the use in rodents seems safe; and 2) MR field strengths used in animal studies is high. Therefore, it is unknown whether the use of lower field strengths will yield similar results (there are no comparative studies), though new 7 Tesla Imaging already is available for human imaging, and capable of demonstrating ultrastructural abnormalities in the smallest vessels[19]. Despite these uncertainties, progress in this field, with regard to contrast media and quality of imaging, will eventually lead to application in humans.

Other imaging modalities, like MR-spectroscopy[40] PET-CT imaging using FDG[73], and 7 Tesla MR imaging in itself, could also contribute to our understanding of the pathology which underlies WML. However, both three of these modalities only provide indirect data because they depend on secondary changes in function of the endothelial cells or on neuronal damage. Though, 7 Tesla Imaging could be useful for assessing the presence of microatheromatosis, because the vessels in which microatheromatosis is localized (diameter of around 300 micrometers) can be visualized with 7 Tesla imaging[19].

In conclusion, molecular imaging holds great promise, as the presumed endothelial dysfunction, which probably precedes BBB dysfunction in cerebral small vessel disease, can be visualized. Possibly, not all patients will have endothelial dysfunction, as not all patients will have the same underlying vascular pathology (not all patients will have arteriolosclerosis or complex small vessel disease). Thus, molecular imaging could help to unravel and demonstrate different vascular pathologies during life.

New Insights into Endothelial Biology

Endothelial progenitor cells (EPC) are *immature* endothelial cells which circulate in peripheral blood. EPC are presumed to be involved in the repair of damaged endothelium, because EPC offspring is present in restored endothelium[17, 21, 63, 70]. Circulating numbers of EPC can be lower, which probably reflects a higher consumption of EPC for restoration of the endothelial damage. Clinically, EPC numbers are found to be lower in patients with atherosclerotic risk factors[24], amongst others in hypertension patients[8, 41,

56, 62]. In these cases, EPC numbers probably are lower as a consequence of a higher consumption, and run relatively short on restoring the damaged endothelium with consequent atherosclerosis and cardiovascular events. Furthermore, EPC numbers relate to cardiovascular prognosis: in patients with coronary artery disease, EPC numbers at baseline are lower in patients who will suffer a cardiovascular event than in event free patients (after at least ten months of follow up[50, 71]). This association between lower EPC numbers and worse cardiovascular prognosis remained significant after correction for other known cardiovascular risk factors. Therefore, EPC may constitute a new risk marker for future cardiovascular events.

Neurovascular research on EPC is limited until now[47]. Studies show that: 1) EPC numbers were lower in stroke patients than in healthy controls[5, 20], 2) EPC numbers were higher in patients with cardioembolic stroke than in patients with large or small vessel stroke[5], 3) EPC numbers were higher in patients with good outcome than in those patients with a bad outcome[52], and 4) EPC numbers rise in the first 7 days after a stroke[55, 74]. All these findings point to a possible role of EPC in the acute pathophysiological process after ischemic stroke. Higher EPC numbers seem beneficial, however, these results do not allow conclusions with regard to processes of EPC recruitment, because the studies were observational in character.

Therefore, there is ample room for further studies on the role of EPC in cerebrovascular disease[47]; cerebral small vessel disease and WML in particular. In WML patients the EPC response could also be defective, because the underlying pathology, arteriolosclerosis, is instigated by endothelial dysfunction, which results in disruption of the BBB. To demonstrate this, EPC numbers, and also EPC function, will have to be quantified in a standardized manner[47]. There is some circumstantial evidence that suggests that EPC are involved in attenuating the progression of WML. Patients who took ACE-inhibitors, which are known to increase circulating EPC numbers, showed less progression of WML in the PROGRESS study[9]. Of course, this effect could also be due to a blood pressure lowering effect. Since EPC numbers were not measured in this study, we are uncertain what caused the effect on the progression. There are other methods to increase EPC numbers, like drugs (statins, ACE-inhibitors, Angiotensin Receptor Blockers and erythropoietin) or growth factors which stimulate EPC release from the bone marrow. In future WML research, effects of these drugs should be investigated alongside EPC number and function. Therefore, the finding of a lower EPC number, or a decreased EPC function could open new therapeutic avenues for the treatment of WML patients.

In this area, animal models would be welcome. EPC could also be labelled to be visualized with molecular imaging; however, animal models which are available up till today (a.o. the stroke-prone spontaneously hypertensive rat; the salt-sensitive rat, and the multiple emboli rat model[44]) only partially provide insight into the pathogenesis of the vascular abnormality[22]. Stroke-prone, spontaneously hypertensive rats only suffer strokes with excessively high blood pressure levels, and therefore represent a model of malignant hypertension and not of cerebral small vessel disease[29]. There is no animal model which covers the whole spectrum of human cerebral small vessel disease, with regard to risk factors, vascular pathology, and clinical features[22]. Though limited, therefore, trials in these animal

models with EPC in combination with molecular imaging could provide further insight in the microvascular restorative capacities of the EPC.

In conclusion, EPC research holds great promise, as the presumed endothelial dysfunction, which probably precedes BBB dysfunction in cerebral small vessel disease, could be causally related to EPC disturbance, whether in number or function. Therapeutical interventions will then be possible by EPC stimulating drugs[47].

Conclusion

Cerebral small vessel disease has multiple, heterogeneous, underlying vascular pathologies. WML strongly relate to arteriolosclerosis, whereas multiple lacunar infarcts relate to complex small vessel disease. Research with molecular imaging, as well as endothelial progenitor cells could provide new insights into the different underlying pathogenetic mechanism and distinguish groups of patients during life with different vascular pathologies.

References

[1] Baezner H, Blahak C, Poggesi A, Pantoni L, Inzitari D, Chabriat H, Erkinjuntti T, Fazekas F, Ferro JM, Langhorne P, O'Brien J, Scheltens P, Visser MC, Wahlund LO, Waldemar G, Wallin A, Hennerici MG (2008) Association of gait and balance disorders with age-related white matter changes: the LADIS study. *Neurology*. 70:935-942

[2] Barber PA, Foniok T, Kirk D, Buchan AM, Laurent S, Boutry S, Muller RN, Hoyte L, Tomanek B, Tuor UI (2004) MR molecular imaging of early endothelial activation in focal ischemia. *Ann. Neurol.* 56:116-120

[3] Boiten J, Lodder J, Kessels F (1993) Two clinically distinct lacunar infarct entities? A hypothesis. *Stroke.* 24:652-656

[4] Boutry S, Burtea C, Laurent S, Toubeau G, Vander Elst L, Muller RN (2005) Magnetic resonance imaging of inflammation with a specific selectin-targeted contrast agent. *Magn. Reson. Med.* 53:800-807

[5] Chu K, Jung KH, Lee ST, Park HK, Sinn DI, Kim JM, Kim DH, Kim JH, Kim SJ, Song EC, Kim M, Lee SK, Roh JK (2008) Circulating endothelial progenitor cells as a new marker of endothelial dysfunction or repair in acute stroke. *Stroke.* 39:1441-1447

[6] de Jong G, Kessels F, Lodder J (2002) Two types of lacunar infarcts: further arguments from a study on prognosis. *Stroke.* 33:2072-2076

[7] de Leeuw FE, de Kleine M, Frijns CJ, Fijnheer R, van Gijn J, Kappelle LJ (2002) Endothelial cell activation is associated with cerebral white matter lesions in patients with cerebrovascular disease. *Ann. N. Y. Acad. Sci.* 977:306-314

[8] Delva P, Degan M, Vallerio P, Arosio E, Minuz P, Amen G, Di Chio M, Lechi A (2007) Endothelial progenitor cells in patients with essential hypertension. *J. Hypertens.* 25:127-132

[9] Dufouil C, Chalmers J, Coskun O, Besancon V, Bousser MG, Guillon P, MacMahon S, Mazoyer B, Neal B, Woodward M, Tzourio-Mazoyer N, Tzourio C (2005) Effects of blood pressure lowering on cerebral white matter hyperintensities in patients with stroke: the PROGRESS (Perindopril Protection Against Recurrent Stroke Study) Magnetic Resonance Imaging Substudy. *Circulation.* 112:1644-1650

[10] Fassbender K, Bertsch T, Mielke O, Muhlhauser F, Hennerici M (1999) Adhesion molecules in cerebrovascular diseases. Evidence for an inflammatory endothelial activation in cerebral large- and small-vessel disease. *Stroke.* 30:1647-1650

[11] Fazekas F, Chawluk JB, Alavi A, Hurtig HI, Zimmerman RA (1987) MR signal abnormalities at 1.5 T in Alzheimer's dementia and normal aging. *AJR. Am. J. Roentgenol.* 149:351-356

[12] Fisher CM (1968) The arterial lesions underlying lacunes. *Acta Neuropathol.* 12:1-15

[13] Fisher CM (1979) Capsular infarcts: the underlying vascular lesions. *Arch. Neurol.* 36:65-73

[14] Fisher CM (2002) Commentary on Subcortical Strokes. In: Donnan G, Norrving B, Bamford J, Bogousslavsky J (eds) Subcortical Stroke. Oxford University Press, Oxford, pp 17-25

[15] Fisher CM (1982) Lacunar strokes and infarcts: a review. *Neurology.* 32:871-876

[16] Fisher CM (1965) Lacunes: Small, Deep Cerebral Infarcts. *Neurology.* 15:774-784

[17] Fujiyama S, Amano K, Uehira K, Yoshida M, Nishiwaki Y, Nozawa Y, Jin D, Takai S, Miyazaki M, Egashira K, Imada T, Iwasaka T, Matsubara H (2003) Bone marrow monocyte lineage cells adhere on injured endothelium in a monocyte chemoattractant protein-1-dependent manner and accelerate reendothelialization as endothelial progenitor cells. *Circ. Res.* 93:980-989

[18] Garde E, Lykke Mortensen E, Rostrup E, Paulson OB (2005) Decline in intelligence is associated with progression in white matter hyperintensity volume. *J. Neurol. Neurosurg. Psychiatry.* 76:1289-1291

[19] Ge Y, Zohrabian VM, Grossman RI (2008) Seven-Tesla magnetic resonance imaging: new vision of microvascular abnormalities in multiple sclerosis. *Arch. Neurol.* 65:812-816

[20] Ghani U, Shuaib A, Salam A, Nasir A, Shuaib U, Jeerakathil T, Sher F, O'Rourke F, Nasser AM, Schwindt B, Todd K (2005) Endothelial progenitor cells during cerebrovascular disease. *Stroke.* 36:151-153

[21] Griese DP, Ehsan A, Melo LG, Kong D, Zhang L, Mann MJ, Pratt RE, Mulligan RC, Dzau VJ (2003) Isolation and transplantation of autologous circulating endothelial cells into denuded vessels and prosthetic grafts: implications for cell-based vascular therapy. *Circulation.* 108:2710-2715

[22] Hainsworth AH, Markus HS (2008) Do in vivo experimental models reflect human cerebral small vessel disease? A systematic review. *J. Cereb. Blood Flow Metab.* doi: 10.1038/jcbfm.2008.91

[23] Hassan A, Hunt BJ, O'Sullivan M, Parmar K, Bamford JM, Briley D, Brown MM, Thomas DJ, Markus HS (2003) Markers of endothelial dysfunction in lacunar infarction and ischaemic leukoaraiosis. *Brain.* 126:424-432

[24] Hill JM, Zalos G, Halcox JP, Schenke WH, Waclawiw MA, Quyyumi AA, Finkel T (2003) Circulating endothelial progenitor cells, vascular function, and cardiovascular risk. *N. Engl. J. Med.* 348:593-600

[25] Kelly KA, Allport JR, Tsourkas A, Shinde-Patil VR, Josephson L, Weissleder R (2005) Detection of vascular adhesion molecule-1 expression using a novel multimodal nanoparticle. *Circ. Res.* 96:327-336

[26] Khan U, Porteous L, Hassan A, Markus HS (2007) Risk factor profile of cerebral small vessel disease and its subtypes. *J. Neurol. Neurosurg. Psychiatry.* 78:702-706

[27] Lammie A (1998) The role of oedema in lacune formation. *Cerebrovasc. Dis.* 8:246

[28] Lammie G (2002) Pathology of lacunar infarction. In: Donnan G, Norrving B, Bamford J, Bogousslavsky J (eds) *Subcortical Stroke.* Oxford University Press, Oxford, pp 37-46

[29] Lammie GA (2000) Pathology of small vessel stroke. *Br. Med. Bull.* 56:296-306

[30] Lammie GA, Brannan F, Slattery J, Warlow C (1997) Nonhypertensive cerebral small-vessel disease. An autopsy study. *Stroke.* 28:2222-2229

[31] Lammie GA, Brannan F, Wardlaw JM (1998) Incomplete lacunar infarction (Type Ib lacunes). *Acta Neuropathol.* 96:163-171

[32] Lodder J, Bamford JM, Sandercock PA, Jones LN, Warlow CP (1990) Are hypertension or cardiac embolism likely causes of lacunar infarction? *Stroke.* 21:375-381

[33] Markus HS (2008) Genes, endothelial function and cerebral small vessel disease in man. *Exp. Physiol.* 93:121-127

[34] Markus HS, Hunt B, Palmer K, Enzinger C, Schmidt H, Schmidt R (2005) Markers of endothelial and hemostatic activation and progression of cerebral white matter hyperintensities: longitudinal results of the Austrian Stroke Prevention Study. *Stroke.* 36:1410-1414

[35] McAteer MA, Schneider JE, Ali ZA, Warrick N, Bursill CA, von zur Muhlen C, Greaves DR, Neubauer S, Channon KM, Choudhury RP (2008) Magnetic resonance imaging of endothelial adhesion molecules in mouse atherosclerosis using dual-targeted microparticles of iron oxide. *Arterioscler. Thromb. Vasc. Biol.* 28:77-83

[36] McAteer MA, Sibson NR, von Zur Muhlen C, Schneider JE, Lowe AS, Warrick N, Channon KM, Anthony DC, Choudhury RP (2007) In vivo magnetic resonance imaging of acute brain inflammation using microparticles of iron oxide. *Nat. Med.* 13:1253-1258

[37] Millikan CH (2002) About Lacunes. In: Donnan G, Norrving B, Bamford J, Bogousslavsky J (eds) Subcortical Stroke. Oxford University Press, Oxford, pp 154-159

[38] Mills S, Cain J, Purandare N, Jackson A (2007) Biomarkers of cerebrovascular disease in dementia. *Br. J. Radiol.* 80 Spec No 2:S128-145

[39] Nahrendorf M, Jaffer FA, Kelly KA, Sosnovik DE, Aikawa E, Libby P, Weissleder R (2006) Noninvasive vascular cell adhesion molecule-1 imaging identifies inflammatory activation of cells in atherosclerosis. *Circulation*. 114:1504-1511

[40] Nitkunan A, Charlton RA, McIntyre DJ, Barrick TR, Howe FA, Markus HS (2008) Diffusion tensor imaging and MR spectroscopy in hypertension and presumed cerebral small vessel disease. *Magn. Reson. Med.* 59:528-534

[41] Oliveras A, Soler MJ, Martinez-Estrada OM, Vazquez S, Marco-Feliu D, Vila JS, Vilaro S, Lloveras J (2008) Endothelial progenitor cells are reduced in refractory hypertension. *J. Hum. Hypertens.* 22:183-190

[42] Poggesi A, Pracucci G, Chabriat H, Erkinjuntti T, Fazekas F, Verdelho A, Hennerici M, Langhorne P, O'Brien J, Scheltens P, Visser MC, Crisby M, Waldemar G, Wallin A, Inzitari D, Pantoni L (2008) Urinary Complaints in Nondisabled Elderly People with Age-Related White Matter Changes: The Leukoaraiosis And DISability (LADIS) Study. *J. Am. Geriatr. Soc.* 56:1638-1643

[43] Prins ND, van Straaten EC, van Dijk EJ, Simoni M, van Schijndel RA, Vrooman HA, Koudstaal PJ, Scheltens P, Breteler MM, Barkhof F (2004) Measuring progression of cerebral white matter lesions on MRI: visual rating and volumetrics. *Neurology.* 62:1533-1539

[44] Rapp JH, Hollenbeck K, Pan XM (2008) An experimental model of lacunar infarction: embolization of microthrombi. *J. Vasc. Surg.* 48:196-200

[45] Reed BR, Eberling JL, Mungas D, Weiner M, Kramer JH, Jagust WJ (2004) Effects of white matter lesions and lacunes on cortical function. *Arch. Neurol.* 61:1545-1550

[46] Reynolds PR, Larkman DJ, Haskard DO, Hajnal JV, Kennea NL, George AJ, Edwards AD (2006) Detection of vascular expression of E-selectin in vivo with MR imaging. *Radiology.* 241:469-476

[47] Rouhl RP, van Oostenbrugge RJ, Damoiseaux J, Cohen Tervaert JW, Lodder J (2008) Endothelial progenitor cell research in stroke: a potential shift in pathophysiological and therapeutical concepts. *Stroke.* 39:2158-2165

[48] Rouhl RP, van Oostenbrugge RJ, Knottnerus IL, Staals JE, Lodder J (2008) Virchow-Robin spaces relate to cerebral small vessel disease severity. *J. Neurol.* 255:692-696

[49] Schaller BJ (2008) Strategies for molecular imaging dementia and neurodegenerative diseases. *Neuropsychiatr. Dis. Treat.* 4:585-612

[50] Schmidt-Lucke C, Rossig L, Fichtlscherer S, Vasa M, Britten M, Kamper U, Dimmeler S, Zeiher AM (2005) Reduced number of circulating endothelial progenitor cells predicts future cardiovascular events: proof of concept for the clinical importance of endogenous vascular repair. *Circulation.* 111:2981-2987

[51] Sibson NR, Blamire AM, Bernades-Silva M, Laurent S, Boutry S, Muller RN, Styles P, Anthony DC (2004) MRI detection of early endothelial activation in brain inflammation. *Magn. Reson. Med.* 51:248-252

[52] Sobrino T, Hurtado O, Moro MA, Rodriguez-Yanez M, Castellanos M, Brea D, Moldes O, Blanco M, Arenillas JF, Leira R, Davalos A, Lizasoain I, Castillo J (2007) The increase of circulating endothelial progenitor cells after acute ischemic stroke is associated with good outcome. *Stroke.* 38:2759-2764

[53] Staals J, van Raak L, Hilton A, Lodder J (2007) Differences in Long-Term Survival in Two Lacunar Stroke Types: A 15-Year Follow-Up Study in 782 Cerebral Infarct Patients. *Cerebrovasc. Dis.* 25:26-31

[54] Starr JM, Wardlaw J, Ferguson K, MacLullich A, Deary IJ, Marshall I (2003) Increased blood-brain barrier permeability in type II diabetes demonstrated by gadolinium magnetic resonance imaging. *J. Neurol. Neurosurg. Psychiatry*. 74:70-76

[55] Taguchi A, Matsuyama T, Moriwaki H, Hayashi T, Hayashida K, Nagatsuka K, Todo K, Mori K, Stern DM, Soma T, Naritomi H (2004) Circulating CD34-positive cells provide an index of cerebrovascular function. *Circulation.* 109:2972-2975

[56] Tao J, Wang Y, Yang Z, Tu C, Xu MG, Wang JM (2006) Circulating endothelial progenitor cell deficiency contributes to impaired arterial elasticity in persons of advancing age. *J. Hum. Hypertens*. 20:490-495

[57] Tomura N, Sasaki K, Kidani H, Nishii T, Yasuda K, Ishiyama K, Otani T, Sakuma I, Takahashi S, Watarai J, Yanagisawa T, Mizoi K (2007) Reduced perfusion reserve in Leukoaraiosis demonstrated using acetazolamide challenge 123I-IMP SPECT. *J. Comput. Assist. Tomogr.* 31:884-887

[58] Tullberg M, Fletcher E, DeCarli C, Mungas D, Reed BR, Harvey DJ, Weiner MW, Chui HC, Jagust WJ (2004) White matter lesions impair frontal lobe function regardless of their location. *Neurology.* 63:246-253

[59] Tzvetanov P, Nicoloff G, Rousseff R, Christova P (2008) Increased levels of elastin-derived peptides in cerebrospinal fluid of patients with lacunar stroke. *Clin. Neurol. Neurosurg.* 110:239-244

[60] van Dijk EJ, Prins ND, Vrooman HA, Hofman A, Koudstaal PJ, Breteler MM (2008) Progression of Cerebral Small Vessel Disease in Relation to Risk Factors and Cognitive Consequences. *Rotterdam Scan. Study. Stroke.* 39:2712-2719

[61] van Swieten JC, van den Hout JH, van Ketel BA, Hijdra A, Wokke JH, van Gijn J (1991) Periventricular lesions in the white matter on magnetic resonance imaging in the elderly. A morphometric correlation with arteriolosclerosis and dilated perivascular spaces. *Brain.* 114 (Pt 2):761-774

[62] Vasa M, Fichtlscherer S, Aicher A, Adler K, Urbich C, Martin H, Zeiher AM, Dimmeler S (2001) Number and migratory activity of circulating endothelial progenitor cells inversely correlate with risk factors for coronary artery disease. *Circ. Res.* 89:E1-7

[63] Walter DH, Rittig K, Bahlmann FH, Kirchmair R, Silver M, Murayama T, Nishimura H, Losordo DW, Asahara T, Isner JM (2002) Statin therapy accelerates reendothelialization: a novel effect involving mobilization and incorporation of bone marrow-derived endothelial progenitor cells. *Circulation.* 105:3017-3024

[64] Ward NS, Brown MM (2002) Leukoaraiosis. In: Donnan G, Norrving B, Bamford J, Bogousslavsky J (eds) *Subcortical Stroke.* Oxford University Press, Oxford, pp 47-66

[65] Wardlaw JM (2005) What causes lacunar stroke? *J. Neurol. Neurosurg. Psychiatry.* 76:617-619

[66] Wardlaw JM, Dennis MS, Warlow CP, Sandercock PA (2001) Imaging appearance of the symptomatic perforating artery in patients with lacunar infarction: occlusion or other vascular pathology? *Ann. Neurol.* 50:208-215

[67] Wardlaw JM, Farrall A, Armitage PA, Carpenter T, Chappell F, Doubal F, Chowdhury D, Cvoro V, Dennis MS (2008) Changes in background blood-brain barrier integrity between lacunar and cortical ischemic stroke subtypes. *Stroke*. 39:1327-1332

[68] Wardlaw JM, Sandercock PA, Dennis MS, Starr J (2003) Is breakdown of the blood-brain barrier responsible for lacunar stroke, leukoaraiosis, and dementia? *Stroke.* 34:806-812

[69] Wen HM, Mok VC, Fan YH, Lam WW, Tang WK, Wong A, Huang RX, Wong KS (2004) Effect of white matter changes on cognitive impairment in patients with lacunar infarcts. *Stroke.* 35:1826-1830

[70] Werner N, Junk S, Laufs U, Link A, Walenta K, Bohm M, Nickenig G (2003) Intravenous transfusion of endothelial progenitor cells reduces neointima formation after vascular injury. *Circ. Res.* 93:e17-24

[71] Werner N, Kosiol S, Schiegl T, Ahlers P, Walenta K, Link A, Bohm M, Nickenig G (2005) Circulating endothelial progenitor cells and cardiovascular outcomes. *N. Engl. J. Med.* 353:999-1007

[72] Wiszniewska M, Devuyst G, Bogousslavsky J, Ghika J, van Melle G (2000) What is the significance of leukoaraiosis in patients with acute ischemic stroke? *Arch. Neurol.* 57:967-973

[73] Wu YW, Kao HL, Chen MF, Lee BC, Tseng WY, Jeng JS, Tzen KY, Yen RF, Huang PJ, Yang WS (2007) Characterization of plaques using 18F-FDG PET/CT in patients with carotid atherosclerosis and correlation with matrix metalloproteinase-1. *J. Nucl. Med*. 48:227-233

[74] Yip HK, Chang LT, Chang WN, Lu CH, Liou CW, Lan MY, Liu JS, Youssef AA, Chang HW (2008) Level and value of circulating endothelial progenitor cells in patients after acute ischemic stroke. *Stroke.* 39:69-74

In: Handbook on White Matter
Editors: T. B. Westland and R. N. Calton
ISBN: 978-1-60741-034-8

Chapter III

White Matter Lesions and Aging in HIV Infection: Implications for Development of Cognitive Decline and Dementia

Aaron M. McMurtray[1], Beau Nakamoto[1,2], Kalpana Kallianpur[1] and Erin P. Saito[3]
[1] Department of Medicine, Neurology Division,
John A. Burns School of Medicine, University of Hawaii, Honolulu, HI
[2] Department of Neurology, Straub Clinics and Hospital, Honolulu, HI
[3] Department of Native Hawaiian Health,
John A. Burns School of Medicine, University of Hawaii, Honolulu, HI

I. Abstract

The widespread availability of highly active anti-retroviral therapy has lead to long-term survival for many individuals living with HIV infection. With advancing age, many older individuals living with HIV infection are beginning to develop aging-related changes in the brain structure, including white matter lesions. Given the known effect of white matter lesions in the general population, these lesions are also likely to have important effects in aging HIV-seropositive individuals as well. Aging related white matter lesions are considered to be structural manifestations of brain small vessel vascular disease. These lesions, more predominant in older individuals, are typically related to vascular risk factors such as hypertension and diabetes. Furthermore, the presence of white matter lesions is a known risk factor for development of cognitive decline and dementia. For example, when compared to normal elderly individuals, those with lacunar infarcts score lower on cognitive tests and have approximately twice the risk of developing dementia in the future. Additionally, lacunar infarction in certain "strategic locations" such as the basal ganglia may result in profound cognitive deficits and even dementia. Multiple studies demonstrate that presence of leukoaraiosis is independently related to cognitive impairment in the elderly, and when present in patients with lacunar strokes, indicates increased severity of small vessel vascular disease and exacerbates

adverse effects of these lesions on cognitive performance. In elderly individuals, cerebral manifestations of small vessel vascular disease are also important components of vascular dementia.

The relationship between white matter hyperintensities and cognitive performance in HIV infection is an active area of ongoing research. Links between presence of white matter hyperintensities and worse performance on tests of psychomotor speed and verbal memory have been established. Other studies show that dementia in HIV infection is associated with decreased white matter volumes, indicating that in this population the loss of white matter may contribute to cognitive decline. Our own research demonstrates that white matter lesion volume in HIV infection is correlated with degree of cortical atrophy, a potential underlying substrate for cognitive decline and dementia. Other studies, however, have reported no relation between white matter lesions and cognitive performance in HIV infection. This discrepancy has been partially resolved with the advent of newer neuroimaging techniques, which allow improved detection of white matter injury and provide further evidence for a connection between white matter damage and the severity of cognitive impairment in HIV-seropositive individuals. In conclusion, aging-related white matter hyperintensities likely contribute to development of cognitive decline and dementia in HIV infection, and physicians caring for HIV seropositive individuals should discuss the importance of treating vascular risk factors with their patients.

II. Introduction

White matter hyperintensities are a typical finding in elderly individuals (aged over 65 years). However, these lesions are also a marker of brain damage due to vascular insufficiency, as exemplified by the association between aging related brain white matter hyperintensities and cortical atrophy. With the increasing availability of already widespread highly active antiretroviral therapy, a greater proportion of HIV-seropositive individuals live to reach middle and old age, and it is likely that they will develop typical aging related changes in brain structure such as white matter hyperintensities. The aim of this chapter is to discuss the relationship between presence of white matter hyperintensities in human immunodeficiency virus, type 1 (HIV) seropositive individuals and brain structural changes including reduction in cortical gray matter volume. The relevance of white matter hyperintensities to cognition will be discussed. Additionally, we will present and discuss findings from the Honolulu-Asia Aging Study, including voxel-based morphometry comparison of cortical gray matter volumes between HIV-seropositive participants with moderate and minimal brain white matter hyperintensities.

A. Changes in the Demographics of HIV Infection in the United States

The prevalence of infection with human immunodeficiency virus, type 1 (HIV) continues to increase in the United States and throughout the world [1]. This has become particularly apparent among older individuals, due in part to the development and widespread distribution of highly active antiretroviral therapy (HAART) which has increased duration of survival after infection and has resulted in a shift of the age distribution of prevalent HIV infection

towards the elderly. In the United States, it is estimated that there are currently between 60,000 to 90,000 older adults living with acquired immune deficiency syndrome (AIDS), and other studies indicate that the number of older people newly infected with HIV may be increasing as well [2-4]. The elderly may also be particularly at risk for developing newly acquired HIV infections, as the rate of these infections appears to be increasing fastest among this age group. Since the 1990's, the number of elderly persons newly diagnosed with AIDS has shown approximately twice the rate of increase as that of new AIDS cases among young and middle-aged individuals [2]. The disproportionate increase in infection rates among older adults has caused a significant shift in the demographics of HIV infection in the United States, with older individuals now accounting for almost 15% of the total cases of AIDS in the country [2]. Furthermore, the prevalence in older and elderly adults is expected to increase even more in the future [2].

B. The Relationship between White Matter Hyperintensities and HIV Infection

On gross pathological examination, it is possible to divide the brain structures into gray and white matter regions. The "gray matter" regions include nerve cell bodies while the "white matter" regions include primarily nerve axons and their surrounding myelin sheath, as well as glial cells. The glial cells are thought to primarily play a supporting role and maintain the extracellular environment in a state that allows the neurons to function. The color of the "white matter" regions is due to the lipid-rich myelin sheaths that surround the nerve cell axons, as well as a general lack of nerve cell bodies and synapses. The largest of the "gray matter" regions within the brain is the cerebral cortex. Additional gray matter regions include structures in the basal ganglia, midbrain and brainstem.

As more HIV-seropositive individuals live to reach older ages, our understanding of how HIV affects the brain is undergoing a change, with more emphasis being placed on determining the relationships and potential interactions between HIV infection and typical aging related diseases that affect brain structure and function, such as degenerative dementias and vascular lesions. Many studies now commonly report typical age-related brain changes in older patients with HIV infection [5-7], indicating the growing interest in these relationships as well as their likely clinical importance. This chapter will focus on one particular aging-related change in brain structure that is considered in the general population to be a cerebral manifestation of small vessel ischemic vascular disease: the appearance of white matter hyperintensities. White matter hyperintensities (WMH) are areas of hyperintense signal on magnetic resonance imaging (MRI), often located in deep white matter tracts as well as in the periventricular regions of the brain [5-7]. Although WMHs are best visualized on MRI, where they appear as areas of increased signal intensity on T2-weighted and fluid attenuated inversion recovery (FLAIR) images [8], the same lesions disrupting the white matter tracts can also be visualized on computer tomography (CT) where they are termed leukoaraiosis. Areas of the brain most frequently involved are the periventricular and deep white matter regions, in which the presence of WMHs has been linked in the general population with both advancing age and vascular risk factors.

III. Pathogenesis of White Matter Hyperintensities in HIV Infection

A. Central Nervous System Inflammation

HIV-encephalitis (HIVE) is the clinical term for the neuropathological changes that occur in HIV infection [9]. Monocytes, macrophages, and microglia are the major cell central nervous system (CNS) cell types infected by HIV [10-12]. Mononuclear phagocytes are currently thought to play a key role in the the pathogenesis of HIVE. It is believed that monocytes are infected in the bone marrow and subsequently become a reservoir and vehicle for the dissemination of HIV. Early after primary infection by HIV, peripheral activation of monocytes leads to up-regulation of adhesion molecules on the brain microvascular endothelial cells and transmigration of the infected monocytes across the blood-brain barrier [13]. HIV gains access to the CNS, a normally immunologically privileged site, via this "Trojan horse" mechanism [14].

HIV-related neurotoxicity is mediated via direct and indirect pathways. In the direct pathway, infected brain macrophages release viral proteins which can cause neuronal injury and dysfunction. The viral molecules which are particularly implicated are gp120 [15] and Tat [16]. It is the indirect pathway, however, that is more important in the pathogenesis of the inflammatory process which characterizes HIVE. In the indirect pathway, activated monocytes which migrated across the blood-barrier activate perivascular and parenchymal microglia, initiating the release of proinflammatory cytokines (in particular interleukin-1β and tumor necrosis factor-α [17], excitatory amino acids, glutamate receptor agonists, and quinolinic acid [18]. These neuroactive substances interact with glutamate receptors on neurons, leading to neuronal dysfunction or death [13, 19].

Microscopic changes of the direct and indirect pathways of neurotoxicity include evidence of inflammation with the presence of multinucleated giant cells, which are particularly prevalent in the deep cerebral white matter regions [20, 21]. Accompanying the presence of multinucleated giant cells is evidence of white matter degeneration, including myelin breakdown, the accumulation of lipid-filled macrophages presumably containing lipid from myelin breakdown, and in more severe injury, axonal damage and amyloid-beta precursor protein accumulations in axon bulbs [19, 22, 23]. On computer assisted tomography, the pathological changes in the brain white matter appear as relatively radiolucent areas that are termed HIV-leukoencephalopathy. On magnetic resonance images, these same areas of white matter degeneration display the T-2 hyperintensity appearance typical of white matter lesions.

B. Small Vessel Ischemic Vascular Disease

In the general population, WMHs are usually regarded as a manifestation of brain small vessel ischemic vascular disease [5-7, 24]. Lacunar strokes are another common manifestation of brain small vessel ischemic vascular disease that are sometimes included in discussions about WMHs or confused with WMHs. While possibly related to the same

underlying etiology as WMHs, lacunar strokes represent a different pathological substrate, with complete infarction of brain tissue and by definition, a diameter of less than 15 mm. Lacunar strokes can be confused with WMHs because these lesions are also visible on brain magnetic resonance imaging as T2-weighted hyperintensities; however, lacunar infarcts are easily identified and differentiated from WMHs on pathological examination at autopsy. Another possible reason for misidentification of lacunar infarcts as WMHs is that both types of lesions are most often found in deep cerebral white matter and in subcortical structures such as the thalamus, basal ganglia and brainstem. The primary difference between WMHs and lacunar infarcts may be the degree of vascular insufficiency. Lacunar strokes result from more severe focal ischemic insults that cause tissue loss and small areas of necrosis, whereas WMHs represent regions of infarction that is insufficient to cause cell death, tissue necrosis or cystic changes.

In general population studies of normal elderly subjects (age > 65 years), WMHs have been shown to occur in up to 20-30% of individuals [25]. The location of white matter hyperintensities is not random, as they most commonly occur in the deep cerebral white matter due to the higher susceptibility of these areas to disruption of small arteriolar blood supply, the primary conduit of blood to these regions [26]. Widespread stenosis of the small arterioles can be have many causes, including aging related changes such as arteriolosclerosis and amyloid angiopathy, that are commonly recognized to contribute to tissue hypoxemia [27], in addition to more standard risk factors for cerebrovascular disease such as hypertension and stroke [27]. The relationship between white matter hyperintensities and vascular risk factors strongly supports a vascular etiology for these lesions. The vascular etiology of WMHs is reasonably well accepted by experts, and the presence of these lesions is considered an important component of several clinical criteria for vascular dementia [28-32].

On pathological examination, WMHs are associated with progressive loss of the myelin sheath surrounding the nerve cell axons. With continued disease progression, axonal loss develops due to the prolonged effects of tissue ischemia [27]. Interestingly, the secondary effects of the vascular insufficiency leading to development of WMHs are not uniformly distributed throughout the brain, and several studies suggest that the frontal lobes are particularly vulnerable to this type of injury. Several population based studies of normal elderly (age > 65 years old) individuals have shown that the presence of WMHs is associated with structural changes and atrophy and that these effects are most prominent in the frontal lobes [25, 33-35]. Other studies have implicated frontal lobe involvement though selective deficits on neuropsychological testing, suggesting impairment of frontal lobe functions [33, 36-39]. Predominant frontal lobe degeneration, as measured by frontal lobe cortical volume loss, has been shown to be related to the presence of WMHs in Alzheimer's disease as well as in normal aging [25, 40]. Together, these findings suggest that the frontal lobes are particularly susceptible to the effects of the small vessel ischemic vascular disease that is suspected to underlie development of WMH in the elderly.

IV. Relationship between White Matter Hyperintensities and Brain Atrophy

The importance of WMHs has been shown in several studies using magnetic resonance imaging and positron emission tomography to demonstrate significant associations between brain WMHs and regional cortical atrophy [33, 41, 42]. WMHs are known to be associated with several markers of brain atrophy, including enlarged ventricles, reduced whole brain volumes and reduced cortical blood volumes [33, 43].

Although white matter lesions and cerebral atrophy typically accompany HIV-associated dementia, their presence in earlier stages of HIV infection is less certain. In a volumetric MRI study of neurologically symptomatic and asymptomatic HIV-seropositive individuals [44], a significant reduction of fractional brain parenchymal volume, indicating atrophy, was noted in symptomatic but not in asymptomatic patients when compared with healthy participants. Total white matter lesion volume did not correlate with fractional brain parenchymal volume in the combined symptomatic and asymptomatic group.

In HIV-seronegative subjects with leukoaraiosis, cerebral deep white matter lesions have been shown to have significantly decreased brain vascular density [45]. Autopsy and postmortem MRI have indicated that leukoaraiosis is also associated with capillary loss in normal-appearing and deep white matter and in the cortex, thus globally affecting the brain [46]. The situation in HIV-seropositive individuals may be more complex. Comparison of premortem MRI with postmortem evaluation of neurodegeneration [47] has shown a diagnosis of HIV encephalitis to be linked with higher volumes of abnormal white matter (defined as tissue with subtle elevation of signal as well as definite hyperintensities). The abnormal white matter volume was inversely correlated with neocortical dendritic density in subjects with HIV encephalitis; however, HIV-seropositive individuals without encephalitis exhibited equally profound dendritic tissue loss.

While all brain regions may be affected by the underlying vascular insufficiency causing WMHs, several studies have now implicated the frontal lobes as having the greatest cortical atrophy associated with presence of these lesions [25, 40, 43]. The frontal region may be affected even in normal-appearing white matter. In HIV-seropositive individuals who had normal MRI results except for mild atrophy, diffusion tensor imaging has detected neurodegeneration, measured by an abnormally elevated diffusion constant, within subcortical white matter and the corpus callosum [48]. Higher diffusion constants (i.e., compromised white matter tract integrity) correlated with more advanced HIV disease. Particularly affected were the frontal lobes and the parietooccipital regions, with frontal subcortical white matter generally showing greater damage.

In the following sections we will discuss results from the Hawaii Aging with HIV Cohort Study and potential etiologies of cortical atrophy associated with WMHs.

A. White Matter Hyperintensities and Cortical Atrophy

In the Hawai‘i Aging with HIV Cohort (HAHC) Study, we examined the relationship between brain cortical gray matter volumes and white matter hyperintensities in patients with

HIV infection [49]. The HAHC is an ongoing prospective study of aging HIV-seropositive individuals in Hawaii and is based out of the University of Hawaii's AIDS Clinical Research Program. Details of enrollment and clinical characterization are published elsewhere [50]. In brief, participants were enrolled from Oct. 1, 2001 into two groups, those with age ≥ 50 years old (older group) or those with ages between 20-39 years old (younger group). Because the main outcomes of interest all involved cognitive functioning and dementia, individuals with potentially confounding factors that might affect cognitive performance, such as head injury, learning disability, or major neurological, psychiatric or brain opportunistic disease, were excluded from participation. The study collected blood and cerebrospinal fluid specimens as well as information from neurological examinations, a general medical history that included demographic data, a risk behavior inventory, HIV-1 laboratory parameters (viral load, CD4 cell count, and lowest ever CD4 cell count), medication histories, and any co-morbid illnesses. A total of 62 HAHC study participants underwent brain MRI because they either met HIV-associated dementia criteria based on American Academy of Neurology 1991 criteria or had a CD4 total lymphocyte count of 200cells/dL or less [51].

As previously published, the brain MRI was conducted using a GE Sigma 1.5-Tesla scanner (General Electric Healthcare, Piscataway, New Jersey, United States of America) and for all participants axial T1, T2, and FLAIR weighted images with a slice thickness of 5mm were acquired [49]. The classification system from the Rotterdam Scan Study (RSS) was used to determine the severity and distribution of brain white matter hyperintensities [52, 53]. In the RSS scale, WMHs are divided into small punctate subcortical lesions and periventricular lesions. Raters estimate the volume of the punctate subcortical white matter hyperintensities by using the largest diameter measurement for the lesions and assuming the lesions are spherical in shape. The severity of periventricular white matter hyperintensities is then calculated by assigning a score ranging from zero to three independently for three different brain white matter regions: adjacent to the frontal horn of the lateral ventricles, adjacent to the lateral wall of the lateral ventricles, and adjacent to the occipital horn of the lateral ventricles. These scores are assigned for both hemispheres simultaneously, with the larger rating for either hemisphere used. A total score for severity of all brain periventricular white matter hyperintensities can then be calculated by summing the scores from all three regions. For the purpose of dividing the study participants into groups of moderate or minimal WMHs, we assigned subjects to the moderate group if punctate subcortical white matter lesions were present or if the severity of the periventricular white matter lesions was graded as 2 or higher in any of the three periventricular regions, and to the minimal group if no subcortical white matter lesions were present and if ratings for severity of periventricular white matter lesions were 1 or less.

We tested the hypothesis that presence of moderately severe white matter hyperintensities would be associated with reduced cortical gray matter volumes and that this difference would be particularly evident primarily in the frontal lobe regions bilaterally [49]. Using voxel-based morphometry we identified specific voxels that were different between the groups, with these areas representing decreased regional cortical volume in the participants with moderate WMHs compared to those with only minimal WMHs [49]. To determine the location of the differences, the voxels identified as significantly different between the groups were then overlaid on a series of three orthogonal mask images [49]. The overlay suggested

that the regions identified as different between the groups correspond to regions within the frontal lobes bilaterally [49].

While the findings of the study strongly suggested that the frontal lobes are particularly vulnerable to the effects of the small vessel ischemic vascular disease that underlie development of WMHs, the study does have significant limitations. The study used a visual quantification of WMHs, but more advanced computerized volumetric methods may provide more accurate measurements of lesion volumes. However, the use of visual scales rather than computerized methods may increase the usefulness of the study results for busy practicing physicians, who are more likely to employ visual methods for quantifying WMHs rather than more time-consuming computer-based approaches. Because white matter hyperintensity volumes are associated with the aging process, the study was unable to exclude the potentially confounding effect of aging on cortical gray matter volumes; consequently, further investigation, perhaps with age-matched controls, is necessary to confirm that the changes described above were due primarily to ischemic vascular disease and not aging.

B. Etiology of Cortical Atrophy Associated with White Matter Hyperintensities

There are several theories that may explain how underlying cortical gray matter atrophy may be caused either directly by the same factors causing the WMHs or as a secondary effect of these factors on the brain cortical gray matter regions. The first theory suggests that cortical gray matter loss or atrophy results primarily from Wallerian degeneration that occurs due to axonal damage from small vessel ischemic disease [25]. Wallerian degeneration is a descriptive term for a well known series of pathological changes that occur in sequence after severe axonal injuries that result in the isolation of a distal axonal segment from the nerve cell body [54]. First there is degeneration of the distal axonal segment since isolation from the cell body causes this part of the axon to no longer have access to the proteins and other materials necessary for maintaining the axon [54]. The nerve cell body then undergoes chromatolysis, which include swelling of the cell body, displacement of the nucleus from the center of the cell body and swelling of the nucleus, dispersion of the endoplasmic reticulum, and detachment of afferent synapses accompanied by swelling of nearby astrocytes and microglia [54]. Wallerian degeneration then leads directly to neuronal cell loss through apoptosis, or programmed cell death [54].

Axonal denervation is another possible mechanism explaining how cortical gray matter neuronal cell loss and atrophy could result from axonal damage in the white matter that occurs in WMHs [25]. Axonal denervation is another well characterized phenomenon that is related to Wallerian degeneration, but one in which the axon, while not directly damaged or severed from the nerve cell body, can no longer be maintained by it [54]. In contrast to Wallerian degeneration, in axonal degeneration it is the most distal segment of the axon that is affected first, with the remainder of the axon degenerating in a “dying back” fashion [54]. In axonal degeneration the axon and cell body are destroyed in an orderly process that is similar but not equivalent to apoptosis [54]. Histological changes characteristic of axonal denervation include swelling, myelin sheath breakdown, compartmentalization and finally

disorganization of the axon and sometimes the nerve cell body [54]. WMHs are believed to occur due to tissue hypoperfusion, and consequently may trigger axonal denervation when the ischemic environment overwhelms the ability of the nerve cell body to sustain the axon.

A third possibility is that WMH's do not directly cause cortical gray matter loss but serve instead as markers for ischemia, or reduced cerebral blood flow to the cortex. This hypothesis posits that rather than the WMHs, it is the gray matter tissue ischemia arising from the small vessel ischemic vascular disease that directly causes neuronal cell loss and cortical gray matter atrophy [25]. At present there is no way to determine which of these three hypotheses or other possible etiologies represents the true underlying cause of cortical atrophy associated with WMHs.

V. Cognitive Effects of White Matter Hyperintensities in HIV Infection

Cognitive deficits in HIV-seropositive patients have been correlated with diffuse damage to cerebral white matter, even in the absence of dementia [55, 56]. In several population-based studies [40-43], WMHs have been associated with worse performance on cognitive tasks and with increased risk for cognitive decline and development of dementia. Yet while the association between WMHs and cognitive decline or development of dementia in the general population is well recognized, the relationship is still somewhat controversial in HIV infection, since WMHs may be caused by inflammation due to HIV infection rather than to small vessel ischemic vascular disease.

Even in HIV-seropositive populations, associations between WMHs and poorer performance on tests of psychomotor speed and verbal memory have been reported [57], although other studies have not detected the same relationships [58-60]. Compared with asymptomatic HIV patients, T2-weighted white matter lesion volume was greater in HIV-seropositive individuals with mild cognitive decline [44], but this difference did not achieve statistical significance, perhaps because of the high variability of lesion volumes observed with conventional MRI. It has been suggested that the sensitivity of volumetric MRI can be increased by techniques such as magnetization transfer ratio histogram analysis, potentially allowing for very early detection of HIV-induced neurodegeneration and cognitive impairment [44].

VI. Conclusion

WMHs and other manifestations of cerebral small vessel ischemic vascular disease are likely to be increasingly important in the HIV-seropositive population as the demographics of prevalent HIV infection continue to shift to larger numbers of the middle-aged and elderly. The mean age of HIV-seropositive individuals in the developed world continues to rise, necessitating a better understanding of cerebral small vessel ischemic vascular disease and its effects on brain structure and function. Knowledge of the relationship between WMHs and small vessel ischemic vascular disease is likely to prove useful to clinicians caring for aging

HIV-seropositive individuals, and will provide a rationale for discussing prevention of vascular brain damage through risk factor modification. The aggressive treatment of vascular risk factors such as diabetes and hypertension is therefore an important clinical goal in the care of aging HIV-seropositive individuals.

References

[1] Goodkin K, Wilkie FL, Concha M, Hinkin CH, Symes S, Baldewicz TT, et al. Aging and neuro-AIDS conditions and the changing spectrum of HIV-1-associated morbidity and mortality. *J. Clin. Epidemiol.* 2001 Dec;54 Suppl 1:S35-43.

[2] Centers for Disease Control. HIV/AIDS Surveillance Report, 2005. Atlanta: US Department of Health and Human Services, Centers for Disease Control and Prevention. 2007.

[3] Mack KA, Ory MG. AIDS and older Americans at the end of the Twentieth Century. *J. Acquir. Immune Defic. Syndr.* 2003 Jun 1;33 Suppl 2:S68-75.

[4] Stoff DM, Khalsa JH, Monjan A, Portegies P. Introduction: HIV/AIDS and Aging. *AIDS.* 2004 Jan 1;18 Suppl 1:S1-2.

[5] Basile AM, Pantoni L, Pracucci G, Asplund K, Chabriat H, Erkinjuntti T, et al. Age, hypertension, and lacunar stroke are the major determinants of the severity of age-related white matter changes. The LADIS (Leukoaraiosis and Disability in the Elderly) Study. *Cerebrovasc. Dis.* 2006;21(5-6):315-22.

[6] Inzitari D. Leukoaraiosis: an independent risk factor for stroke? *Stroke.* 2003 Aug;34(8):2067-71.

[7] Ovbiagele B, Saver JL. Cerebral white matter hyperintensities on MRI: Current concepts and therapeutic implications. *Cerebrovasc. Dis.* 2006;22(2-3):83-90.

[8] Kalaria RN, Kenny RA, Ballard CG, Perry R, Ince P, Polvikoski T. Towards defining the neuropathological substrates of vascular dementia. *J. Neurol. Sci.* 2004 Nov 15;226(1-2):75-80.

[9] Gehrmann J, Kleihues P. Neuropathology of central nervous system human immunodeficiency virus infection. *Curr. Diag. Pathol*. 1994;1:121-30.

[10] Gendelman HE, Lipton SA, Tardieu M, Bukrinsky MI, Nottet HS. The neuropathogenesis of HIV-1 infection. *J. Leukoc. Biol.* 1994 Sep;56(3):389-98.

[11] Koenig S, Gendelman HE, Orenstein JM, Dal Canto MC, Pezeshkpour GH, Yungbluth M, et al. Detection of AIDS virus in macrophages in brain tissue from AIDS patients with encephalopathy. *Science.* 1986 Sep 5;233(4768):1089-93.

[12] Williams KC, Hickey WF. Central nervous system damage, monocytes and macrophages, and neurological disorders in AIDS. *Annu. Rev. Neurosci.* 2002;25:537-62.

[13] Persidsky Y, Gendelman HE. Mononuclear phagocyte immunity and the neuropathogenesis of HIV-1 infection. *J. Leukoc. Biol*. 2003 Nov;74(5):691-701.

[14] Peluso R, Haase A, Stowring L, Edwards M, Ventura P. A Trojan Horse mechanism for the spread of visna virus in monocytes. *Virology.* 1985 Nov;147(1):231-6.

[15] Brenneman DE, Westbrook GL, Fitzgerald SP, Ennist DL, Elkins KL, Ruff MR, et al. Neuronal cell killing by the envelope protein of HIV and its prevention by vasoactive intestinal peptide. *Nature.* 1988 Oct 13;335(6191):639-42.

[16] New DR, Ma M, Epstein LG, Nath A, Gelbard HA. Human immunodeficiency virus type 1 Tat protein induces death by apoptosis in primary human neuron cultures. *J. Neurovirol.* 1997 Apr;3(2):168-73.

[17] Wesselingh SL, Power C, Glass JD, Tyor WR, McArthur JC, Farber JM, et al. Intracerebral cytokine messenger RNA expression in acquired immunodeficiency syndrome dementia. *Ann. Neurol.* 1993 Jun;33(6):576-82.

[18] Heyes MP, Brew BJ, Martin A, Price RW, Salazar AM, Sidtis JJ, et al. Quinolinic acid in cerebrospinal fluid and serum in HIV-1 infection: relationship to clinical and neurological status. *Ann. Neurol.* 1991 Feb;29(2):202-9.

[19] Bell JE. An update on the neuropathology of HIV in the HAART era. *Histopathology.* 2004 Dec;45(6):549-59.

[20] Budka H. Multinucleated giant cells in brain: a hallmark of the acquired immune deficiency syndrome (AIDS). *Acta. Neuropathol.* 1986;69(3-4):253-8.

[21] Sharer LR, Cho ES, Epstein LG. Multinucleated giant cells and HTLV-III in AIDS encephalopathy. *Hum. Pathol.* 1985 Aug;16(8):760.

[22] Giometto B, An SF, Groves M, Scaravilli T, Geddes JF, Miller R, et al. Accumulation of beta-amyloid precursor protein in HIV encephalitis: relationship with neuropsychological abnormalities. *Ann. Neurol.* 1997 Jul;42(1):34-40.

[23] Bell JE. The neuropathology of adult HIV infection. *Rev. Neurol.* (Paris). 1998 Dec;154(12):816-29.

[24] Hachinski VC, Potter P, Merskey H. Leuko-araiosis. Arch Neurol. 1987 Jan;44(1):21-3.

[25] Rossi R, Boccardi M, Sabattoli F, Galluzzi S, Alaimo G, Testa C, et al. Topographic correspondence between white matter hyperintensities and brain atrophy. *J. Neurol.* 2006 Jul;253(7):919-27.

[26] Roman GC. Vascular dementia revisited: diagnosis, pathogenesis, treatment, and prevention. *Med. Clin. North Am.* 2002 May;86(3):477-99.

[27] O'Brien JT, Erkinjuntti T, Reisberg B, Roman G, Sawada T, Pantoni L, et al. Vascular cognitive impairment. *Lancet Neurol.* 2003 Feb;2(2):89-98.

[28] Chui HC, Victoroff JI, Margolin D, Jagust W, Shankle R, Katzman R. Criteria for the diagnosis of ischemic vascular dementia proposed by the State of California Alzheimer's Disease Diagnostic and Treatment Centers. *Neurology.* 1992 Mar;42(3 Pt 1):473-80.

[29] Hachinski VC, Lassen NA, Marshall J. Multi-infarct dementia. A cause of mental deterioration in the elderly. *Lancet.* 1974 Jul 27;2(7874):207-10.

[30] Roman GC, Erkinjuntti T, Wallin A, Pantoni L, Chui HC. Subcortical ischaemic vascular dementia. *Lancet Neurol*. 2002 Nov;1(7):426-36.

[31] Roman GC, Tatemichi TK, Erkinjuntti T, Cummings JL, Masdeu JC, Garcia JH, et al. Vascular dementia: diagnostic criteria for research studies. Report of the NINDS-AIREN International Workshop. *Neurology*. 1993 Feb;43(2):250-60.

[32] World Health Organization. International statistical classification of diseases and related health problems. Geneva: *World Health Organization*. 1989:311-88.

[33] DeCarli C, Murphy DG, Tranh M, Grady CL, Haxby JV, Gillette JA, et al. The effect of white matter hyperintensity volume on brain structure, cognitive performance, and cerebral metabolism of glucose in 51 healthy adults. *Neurology.* 1995 Nov;45 (11):2077-84.

[34] Mirsen TR, Lee DH, Wong CJ, Diaz JF, Fox AJ, Hachinski VC, et al. Clinical correlates of white-matter changes on magnetic resonance imaging scans of the brain. *Arch. Neurol.* 1991 Oct;48(10):1015-21.

[35] Ylikoski A, Erkinjuntti T, Raininko R, Sarna S, Sulkava R, Tilvis R. White matter hyperintensities on MRI in the neurologically nondiseased elderly. Analysis of cohorts of consecutive subjects aged 55 to 85 years living at home. *Stroke.* 1995 Jul;26(7):1171-7.

[36] Boone KB, Miller BL, Lesser IM, Mehringer CM, Hill-Gutierrez E, Goldberg MA, et al. Neuropsychological correlates of white-matter lesions in healthy elderly subjects. A threshold effect. *Arch. Neurol.* 1992 May;49(5):549-54.

[37] Longstreth WT, Jr., Bernick C, Manolio TA, Bryan N, Jungreis CA, Price TR. Lacunar infarcts defined by magnetic resonance imaging of 3660 elderly people: the Cardiovascular Health Study. *Arch. Neurol.* 1998 Sep;55(9):1217-25.

[38] Mendez MF, Cummings JL. Dementia: a clinical approach, 3rd edition. Philadelphia, PA: Elsevier Science Publishing Company; 2003.

[39] Vermeer SE, Den Heijer T, Koudstaal PJ, Oudkerk M, Hofman A, Breteler MM. Incidence and risk factors of silent brain infarcts in the population-based Rotterdam Scan Study. *Stroke.* 2003 Feb;34(2):392-6.

[40] Capizzano AA, Acion L, Bekinschtein T, Furman M, Gomila H, Martinez A, et al. White matter hyperintensities are significantly associated with cortical atrophy in Alzheimer's disease. *J. Neurol. Neurosurg. Psychiatry.* 2004 Jun;75(6):822-7.

[41] Sultzer DL, Mahler ME, Cummings JL, Van Gorp WG, Hinkin CH, Brown C. Cortical abnormalities associated with subcortical lesions in vascular dementia. Clinical and position emission tomographic findings. *Arch. Neurol.* 1995 Aug;52(8):773-80.

[42] Takahashi W, Takagi S, Ide M, Shohtsu A, Shinohara Y. Reduced cerebral glucose metabolism in subjects with incidental hyperintensities on magnetic resonance imaging. *J. Neurol. Sci.* 2000 May 1;176(1):21-7.

[43] Wen W, Sachdev P, Shnier R, Brodaty H. Effect of white matter hyperintensities on cortical cerebral blood volume using perfusion MRI. *Neuroimage.* 2004 Apr;21(4):1350-6.

[44] Ge Y, Kolson DL, Babb JS, Mannon LJ, Grossman RI. Whole brain imaging of HIV-infected patients: quantitative analysis of magnetization transfer ratio histogram and fractional brain volume. *AJNR Am. J. Neuroradiol.* 2003 Jan;24(1):82-7.

[45] Moody DM, Thore CR, Anstrom JA, Challa VR, Langefeld CD, Brown WR. Quantification of afferent vessels shows reduced brain vascular density in subjects with leukoaraiosis. *Radiology*. 2004 Dec;233(3):883-90.

[46] Brown WR, Moody DM, Thore CR, Challa VR, Anstrom JA. Vascular dementia in leukoaraiosis may be a consequence of capillary loss not only in the lesions, but in normal-appearing white matter and cortex as well. *J. Neurol. Sci.* 2007 Jun 15;257(1-2):62-6.

[47] Archibald SL, Masliah E, Fennema-Notestine C, Marcotte TD, Ellis RJ, McCutchan JA, et al. Correlation of in vivo neuroimaging abnormalities with postmortem human immunodeficiency virus encephalitis and dendritic loss. *Arch. Neurol.* 2004 Mar;61(3):369-76.

[48] Filippi CG, Ulug AM, Ryan E, Ferrando SJ, van Gorp W. Diffusion tensor imaging of patients with HIV and normal-appearing white matter on MR images of the brain. *AJNR Am. J. Neuroradiol*. 2001 Feb;22(2):277-83.

[49] McMurtray A, Nakamoto B, Shikuma C, Valcour V. Cortical atrophy and white matter hyperintensities in HIV: the Hawaii Aging with HIV Cohort Study. *J. Stroke Cerebrovasc. Dis.* 2008 Jul-Aug;17(4):212-7.

[50] Valcour V, Shikuma C, Shiramizu B, Watters M, Poff P, Selnes O, et al. Higher frequency of dementia in older HIV-1 individuals: the Hawaii Aging with HIV-1 Cohort. *Neurology*. 2004 Sep 14;63(5):822-7.

[51] Nomenclature and research case definitions for neurologic manifestations of human immunodeficiency virus-type 1 (HIV-1) infection. Report of a Working Group of the American Academy of Neurology AIDS Task Force. *Neurology.* 1991 Jun;41(6):778-85.

[52] De Leeuw FE, de Groot JC, Achten E, Oudkerk M, Ramos LM, Heijboer R, et al. Prevalence of cerebral white matter lesions in elderly people: a population based magnetic resonance imaging study. The Rotterdam Scan Study. *J. Neurol. Neurosurg. Psychiatry*. 2001 Jan;70(1):9-14.

[53] McMurtray A, Nakamoto B, Shikuma C, Valcour V. Small-vessel vascular disease in human immunodeficiency virus infection: the Hawaii aging with HIV cohort study. *Cerebrovasc. Dis.* 2007;24(2-3):236-41.

[54] Wang J, Zhai Q, Chen Y, Lin E, Gu W, McBurney MW, et al. A local mechanism mediates NAD-dependent protection of axon degeneration. *J. Cell Biol.* 2005 Aug 1;170(3):349-55.

[55] Aylward EH, Brettschneider PD, McArthur JC, Harris GJ, Schlaepfer TE, Henderer JD, et al. Magnetic resonance imaging measurement of gray matter volume reductions in HIV dementia. *Am. J. Psychiatry.* 1995 Jul;152(7):987-94.

[56] Hall M, Whaley R, Robertson K, Hamby S, Wilkins J, Hall C. The correlation between neuropsychological and neuroanatomic changes over time in asymptomatic and symptomatic HIV-1-infected individuals. *Neurology.* 1996 Jun;46(6):1697-702.

[57] Harrison MJ, Newman SP, Hall-Craggs MA, Fowler CJ, Miller R, Kendall BE, et al. Evidence of CNS impairment in HIV infection: clinical, neuropsychological, EEG, and MRI/MRS study. *J. Neurol. Neurosurg. Psychiatry.* 1998 Sep;65(3):301-7.

[58] Dooneief G, Bello J, Todak G, Mun IK, Marder K, Malouf R, et al. A prospective controlled study of magnetic resonance imaging of the brain in gay men and parenteral drug users with human immunodeficiency virus infection. *Arch. Neurol.* 1992 Jan;49(1):38-43.

[59] Levin HS, Williams DH, Borucki MJ, Hillman GR, Williams JB, Guinto FC, Jr., et al. Magnetic resonance imaging and neuropsychological findings in human immunodeficiency virus infection. *J. Acquir. Immune Defic. Syndr.* 1990;3(8):757-62.

[60] McArthur JC, Kumar AJ, Johnson DW, Selnes OA, Becker JT, Herman C, et al. Incidental white matter hyperintensities on magnetic resonance imaging in HIV-1 infection. Multicenter AIDS Cohort Study. *J. Acquir. Immune Defic. Syndr.* 1990;3(3):252-9.

In: Handbook on White Matter
Editors: T. B. Westland and R. N. Calton
ISBN: 978-1-60741-034-8

Chapter IV

White Matter Changes in Drug Abuse and in HIV-1 Infection

***Andreas Büttner*[a], *Jeremias Wohlschaeger*[b], *Ida C. Llenos*[c] *and Serge Weis*[c]**

[a] Institute of Forensic Pathology,
University of Rostock, Germany
[b] Institute of Pathology and Neuropathology,
University Duisburg-Essen, Essen, Germany
[c] Laboratory of Neuropathology, Department of Pathology and Neuropathology,
State Neuropsychiatric Hospital Wagner-Jauregg, Linz, Austria

Introduction

1. Gross-Anatomy of White Matter

White matter is composed of axons that arise from neurons located in the gray matter [Paxinos & Mai 2004]. The axons are wrapped by myelin sheaths that constitute extensions of oligodendroglial cell membranes. Due to the staining properties of the myelin sheaths, this region stains light on sections, hence the name "white matter". In addition, astrocytes, microglia and vessels are found in the white matter.

Due to its oval form on horizontal sections of the brain, the white matter of the telencephalon is called centrum semiovale. By blunt dissection, different fiber systems of the white matter become apparent. The fiber systems of the white matter are distinguished as follows: (1) projection fibers, (2) association fibers, and (3) commissural fibers.

1.1. Projection Fibers

Projection fibers conduct impulses from the cortex to centers located deep in the brain and vice versa. Projection fibers that project fan-like from inferior centers to the cortex are called corona radiata. At the rostral end of the brain stem, these fibers lie close together and form the internal capsule. The fibers that form the anterior limb of the internal capsule project horizontally, vertically, and laterally to the frontal lobe. Those fibers forming the posterior limb terminate in the parietal lobe. The fibers that project most posteriorly to the calcarine sulcus are called optic radiation. The thalamo-cortical fascicle is the fiber system that contains all fibers connecting the thalamus with nearly all cortical areas. Other fiber systems connecting cortical regions with deeply-located brain centers are the cortico-thalamic, cortico-pontine, cortico-bulbar, and cortico-spinal fascicles.

Internal Capsule

The area between the caudate nucleus and both the putamen and globus pallidus is called the internal capsule. The internal capsule contains all fiber systems that project from the cerebral cortex to deep brain centers as well as fibers that connect these deep brain centers with the cerebral cortex.

The internal capsule is made up of five parts that are best seen on horizontal sections:

1. The anterior limb of the internal capsule lies between the head of the caudate nucleus and both the putamen and globus pallidus.
2. The knee of the internal capsule lies between the anterior and the posterior limb.
3. The posterior limb of the internal capsule lies between the thalamus and both the putamen and globus pallidus.
4. The sublentiform part of the internal capsule lies below the putamen and the globus pallidus.
5. The retrolentiform part of the internal capsule lies behind the putamen and the globus pallidus.

1.2. Association Fibers

Association fibers connect cortical gyri within the same hemisphere. Short and long association fiber tracts are distinguished: (1) short association fibers connect adjacent gyri, but may sometimes skip one gyrus and (2) long association fibers connect distant gyri within the same hemisphere.

The following fascicles have been described:

1. The uncinate fascicle is composed of fibers connecting the limen insulae with orbital gyri of the frontal lobe, as well as fibers that connect the middle and inferior frontal gyri with the anterior parts of the temporal lobe.
2. The arcuate fascicle contains fibers that connect the middle and superior frontal gyri with the temporal lobe.

3. The superior longitudinal fascicle is composed of fibers that connect regions of the parietal lobe with regions of the occipital lobe.
4. The inferior longitudinal fascicle contains fiber tracts that run from the occipital lobe to the temporal lobe.
5. The cingulum is composed of fibers that are located in the cingulate gyrus. These fibers connect regions of the frontal lobe with the parahippocampal gyrus.

The external and extreme capsules also contain association fibers.

1.3. Commissural Fibers

Commissural fibers connect cortical regions of one hemisphere with the corresponding regions of the contralateral hemisphere as homotopic fibers, and non-corresponding regions of the contralateral hemisphere as heterotopic fibers.

Corpus Callosum

The corpus callosum is the largest commissural fiber system of the human brain. Four parts of the corpus callosum are distinguished from rostral towards the caudal end: (1) rostrum, (2) genu, (3) truncus, and (4) splenium. There exists no distinct boundary between these different parts. Callosal fibers also radiate fan-like to the telencephalon, called the radiatio corporis callosi.

The connections between the different cortical regions by callosal fibers are described as follows:

1. Rostrum—contains fibers from regions of the orbital surface of the frontal lobe and from deep layers of the extreme capsule.
2. Genu (knee) —fibers from other regions of the frontal lobe cross through the knee.
3. Truncus (trunk) —these fibers connect the middle frontal gyrus, opercular part of the inferior frontal gyrus, inferior parietal lobule, superior and inferior temporal gyri, insula, cingulate gyrus, precentral gyrus, paracentral lobule, and precuneus.
4. Splenium—fibers from the occipital lobe, precuneus, and cuneus cross here and run to the contralateral hemisphere.

Fibers that cross through the splenium and run occipitally to separate the posterior horn of the lateral ventricle from the optic radiation are called tapetum. On horizontal sections, the fibers that connect both frontal lobes and both occipital lobes are called anterior forceps and posterior forceps, respectively.

Anterior Commissure

The anterior commissure contains fibers that interconnect regions of the frontal lobes and mainly the middle and inferior temporal gyri with the corresponding regions of the contralateral hemisphere.

2. Microscopy of White Matter

2.1 Astrocytes

Two major types of astrocytes are distinguished, namely protoplasmic astrocytes, which are mainly found in the gray matter, and fibrous astrocytes, which are most numerous in the white matter [Compston et al., 1997]. Fibrous astrocytes have long processes (up to 300 µm); however, they are less elaborate than protoplasmic astrocytes. They establish several perivaskular or subpial endfeet. Fibrous astrocytes possess numerous extensions (perinodal processes) that contact axons at the nodes of Ranvier. The numerical density of fibrous astrocytes in the white matter is approximately 200,000/mm3.

Astrocytes fulfill trophic and reparatory functions. Through their processes, they bridge the gap between neurons and capillaries, thus allowing the diffusion of various nutritive substances from the blood stream to the nerve cells. Damaged neuronal tissue is replaced by a scar which is mainly formed by astrocytic processes containing glial fibrillary acidic protein (GFAP) [Norenberg 1994].

The functions of astrocytes are manifold and include (1) development (regulation of neuro- and gliogenesis, neural path finding, regulation of synaptogenesis), (2) structural (scaffold of the nervous system, continuous syncytium), (3) vascular (glial-vascular interface, regulation of cerebral microcirculation), (4) metabolic (providing energy substrates for neurons, collecting neuronal waste), (5) control of CNS environment (regulation of extracellular ion concentrations, regulation of extracellular pH, removal of transmitters, brain water homeostasis), and (6) signaling (modulation of synaptic transmission, release of neurotransmitter, long-range signaling within glial syncytium, integration of neuronal-glial network).

2.2. Oligodendrocytes

Oligodendrocytes which are found closely apposed to neuronal perikarya in the gray matter are known as the perineural satellite cells, while the interfascicular oligodendrocytes are those seen in the white matter [Compston et al., 1997, Paxinos & Mai 2004]. Oligodendrocytes form the myelin sheath of axons in the central nervous system. In the peripheral nervous system the cells fulfilling the same function are called Schwann cells.

Oligodendrocytes have round to oval nuclei, scant cytoplasm and small processes. They were first described in 1928 by Del Rio Hortega who classified them into four types:

- Type I have small round cell bodies and produce four to six primary processes which branch and myelinate 10 to 30 axons with a diameter of <2µm. They form a single internodal myelin segment of approximately 100-200 µm length. They are found in the forebrain, cerebellum and spinal cord.
- Type II are similar to type I; they have small round cell bodies and produce four to six primary processes which branch and myelinate 10 to 30 axons with a diameter of <2µm. They form a single internodal myelin segment of approximately 100-200 µm

length. They are found only in the white matter (e.g., corpus callosum, optic nerve, cerebellar white matter, etc.).

- Type III oligodendrocytes have larger cell bodies and several thick primary processes which myelinate up to five thick axons (4–15 μm in diameter). They produce myelin sheaths with approximately 200–500 μm internodal length. They are found in the cerebral and cerebellar peduncles, the medulla oblongata, and spinal cord.
- Type IV oligodendrocytes don't have processes. They form a single long myelin sheath up to 1000μm internodal length on the largest diameter axons. They are found around the entrances of the nerve roots into the CNS.

2.3. NG2 Cells

Using antibodies against chondroitin sulphate proteoglycan, this cell type was identified and named NG2 [Polito & Reynolds 2005, Wigley et al., 2007]. NG2 cells express many specific markers of oligodendrocytes progenitor cells (OPC), e.g., platelet-derived growth factor alpha receptors. They do not express markers for mature oligodendrocytes or astrocytes. NG2 cells have small somata and extending numerous thin, radially oriented processes. They are mitotically active. They generate oligodendrocytes during developmental remodeling of the CNS and following demyelination. NG2 cells might be multipotent adult neural stem cells.

2.4. The Axon

One axon usually originates from the cell body. The site of origin of the axon on the soma is called axon hillock. The axon hillock is characterized by the lack of Nissl substance. The length of the axon is highly variable and may amount between several μm up to 1.5 meters. Small processes, the axonal collaterals, originate from the axon and abut on other neurons. The axon ramifies at its distal part in axonal terminals. The roundly thickened ends of the axonal terminals are called boutons terminaux. They participate in the formation of synapses. At these sites the neuronal information is transmitted either to other neurons or to effector organs (i.e., glands, muscle). The axon forms the throughput zone of the neuron while the axonal collaterals and the axonal terminals constitute the output zone. The axoplasm contains various amounts of cell organelles as well as neurotubules and neurofilaments.

2.5. The Myelin Sheath

The axon is insulated by a fatty layer, i.e. the myelin sheath [Simons & Trotter 2007]. It enables the salutatory conduction of action potentials. The axon is wrapped by the myelin sheath forming concentric layer or lamellae. Myelin sheaths are separated from each other by

the nodes of Ranvier. Here the axon is devoid of myelin and constitutes the place where the action potentials are propagated. The internode denotes myelin sheath between two nodes of Ranvier. Myelin sheaths are continuations of the cell membrane. The apposing phospholipid bilayers are fused to form the lammellae of compacted myelin. The fusion of apposed cytoplasmic interfaces of the cell membrane forms the major dense lines, while the fusion of the outer interfaces of the cell membrane forms the minor dense line. Schmidt-Lantermann incisures constitute a ridge of cytoplasm around the edge of the compacted myelin sheath and isolated strands of cytoplasm with the compacted myelin. They play important roles for intracellular transport from the cell body to the myelin sheath.

3. Molecular Composition of White Matter Myelin

Myelin is mainly made of lipids (70% of its dry weight) and of proteins (30% of its dry weight). Lipids provide myelin with its insulating properties, while proteins serve to fuse and stabilize myelin lamellae and to mediate membrane-membrane interactions between myelin lamellae, and between the axon and myelin sheath [Paxinos & Mai 2004].

3.1. Lipids

The major component of myelin is cholesterol followed by phospholipids and glycolipids. Myelin lipids are rich in glycosphingolipids, particularly in galactocerebrosides (GalC) and their sulfated derivatives, sulphatides. Other galactolipids include fatty esters of cerebroside and a number of gangliosides. Galactolipids play an essential role in axon-glial interactions. Animals lacking GalC display abnormalities of internodal myelin spacing and complete absence of transverse bands at the paranodal axo-glial junction [Paxinos & Mai 2004].

3.2. Myelin Proteins

3.2.1. Myelin Basic Protein (MBP)

MBP is a family of proteins with many isoforms. The main function of MBP is in the fusion of the cytoplasm interface of the myelin lamellae and the formation of the major dense line. Multiple isoforms of MBP are differentially expressed in oligodendrocyte somata and myelin, indicating that they have multiple functions. The shiverer mutant mouse, resulting from a large deletion of the MBP, shows loss of the major dense line [Baumann & Pham-Dinh 2001, Campagnoni & Skoff 2001, Montague et al., 2006, Smith 1992].

3.2.2. Proteolipid Protein (PLP)

PLP makes up to 50% of the CNS myelin proteins, with two isoforms, namely PLP and DM20. PLP is important for fusing the extracellular face of the myelin lamellae and for forming the intraperiod line. Absence of PLP/DM20 results in axonal degeneration. Animals

with spontaneous mutations include the jimpy mouse, myelin deficient rat, and the shaking pup [Baumann & Pham-Dinh 2001, Campagnoni & Skoff 2001].

3.2.3. Myelin-Associated Glycoprotein (MAG)

MAG is a minor component of myelin but is the major glycoprotein. MAG is confined to the periaxonal cytoplasmic ridges of the myelin sheath in the CNS. Two isoforms are known: L(large)- MAG is expressed during early myelination and declines during development while S(small)-MAG is the predominant form in the adult. MAG plays a role in axon-myelin interactions. Its absence is associated with abnormal formation of the paranodal loops and periaxonal cytoplasmic ridge [Baumann & Pham-Dinh 2001, Quarles 2007].

3.2.4. Myelin Oligodendrocyte Glycoprotein (MOG)

MOG is specific to oligodendrocytes. It is located on the cell surface and outermost lamellae of compacted myelin in the CNS. The function of MOG is not clearly resolved. It might have similar adhesive and intracellular functions as MAG and myelin protein 0 (P0) [Baumann & Pham-Dinh 2001].

3.2.5. 2',3'-Cyclic Nucleotide 3'-Phosphodiesterase (CNP)

CNP function in myelin in unresolved. Two isoforms of CNP exists, i.e., CNP1 and CNP2. CNP is specific to oligodendrocytes in the CNS and Schwann cells in the PNS. CNP is localized to the cell body and processes. CNP might interact with the actin cytoskeleton and microtubule to regulate the outgrowth of processes [Baumann & Pham-Dinh 2001].

3.2.6. Myelin Oligodendrocyte Basic Protein (MOBP)

MOBP consist of several isoforms that are relatively abundant. They are located in the major dense line, where they play a similar role than MBP. MBP isoforms are differentially expressed within oligodendrocyte somata and myelin [Baumann & Pham-Dinh 2001].

3.2.7. Other CNS Myelin Proteins

Other proteins include P2, OMgp (paranodal area), Noga-A (oligodendrocyte cell bodies), MOSP (extracellular face of myelin), transferrin (iron transport glycoprotein in the oligodendrocyte cell body), carbonic anhydrase, OSp/claudin-11 (tight junctions of myelin sheaths), connexins (Cx32, Cx47) and tetraspan [Baumann & Pham-Dinh 2001, Bronstein et al., 1997].

4. White Matter in Drug and Alcohol Abuse

The cerebral white matter is vulnerable to a wide variety of toxins causing toxic leukoencephalopathy. Damage of the white matter has been described from cranial irradiation, cancer chemotherapeutic drugs, and from a number of other therapeutic agents, drugs of abuse, and environmental toxins [Filley & Kleinschmidt-DeMasters 2001].

The major illicit drugs of abuse are cannabis, opiates, cocaine, amphetamines, designer drugs, and solvents [Büttner & 2004, Karch 2008]. Although no brain lesion specific for drug

abuse exists, a broad spectrum of changes affecting the central nervous system (CNS) are seen in illicit drug abusers [Büttner & 2004, Karch 2008]. Furthermore, drugs of abuse lead to a variety of neurological and psychiatric signs and symptoms [Darke et al., 2000, Mintzer et al., 2005, Pakesch et al., 1992].

Alcohol abuse and dependence are serious medical and economic problems in the Western countries as the effects of alcohol on the CNS are wide ranging [Büttner & Weis 2008]. Direct toxicity of ethanol and its first metabolite acetaldehyde accounts for some of these effects by altering basic physiological and neurochemical functions [Zimatkin & Deitrich 1997], which ultimately result in structural damage.

4.1. Neuroimaging

(Poly)Drug Abuse

In the cerebral white matter of drug abusers, hyperintense areas have been observed on magnetic resonance imaging (MRI) [Bartzokis et al., 1999, De Roock et al., 2007, Lyoo et al., 2004, Volkow et al., 1988]. Other neuroimaging studies have shown that nearly all drugs of abuse lead to abnormalities of the white matter [Ernst et al., 2000, Lim et al., 2002, Schlaepfer et al., 2007, Strickland et al., 1993]. A specific pattern or a predominance of a specific brain region could not be determined. As possible morphological substrates for these alterations, ischemic lesions [Bartzokis et al., 1999, Lyoo et al., 2004, Volkow et al., 1988], glial activation [Ernst et al., 2000], a direct neurotoxic drug effect, or a pre-existing abnormality in the process of myelination during brain development [Schlaepfer et al., 2007] were proposed.

Solvent Abuse, Toxic Leukoencephalopathy

Chronic exposure to toluene and related substances (thinner, spray paints, glues) leads to dose-dependent impairment on myelin up to the production of dementia [Filley et al., 1990]. The clinical syndrome, toxic leukoencephalopathy, can be detected by a combination of characteristic symptoms and signs, detailed neurobehavioral evaluation, and brain magnetic resonance imaging [Filley et al., 2004]. Toluene preferentially affects the white matter and periventricular/subcortical regions. The lipid-dependent distribution and pharmacokinetic properties of toluene could explain the pattern of MRI abnormalities, as well as the clinical signs and symptoms of toluene encephalopathy [Yücel et al., 2008]. MRI in chronic toluene abusers show diffuse cerebral, cerebellar, and brainstem atrophy, loss of differentiation between the gray and white matter, and white matter hyperintensities in cerebrum, brain stem, and cerebellum on T2-weighted images, in some cases, with additional hypointensities in the corresponding T1-weighted images [Rosenberg et al 1988, Yamanouchi et al., 1995, Yücel et al., 2008]. It has been postulated that toluene-induced brain changes start in the periventricular white matter and progress through to subcortical and cortical white matter [Aydin et al., 2003].

Alcohol Abuse

The predominant neuroimaging finding in chronic alcohol abuse is cerebral atrophy which has been shown both on CT [Rosse et al., 1997, Wilkinson 1982] and MRI [Jernigan et al., 1991, Sullivan et al., 1996]. Using magnetic resonance diffusion tensor imaging alcoholics showed widespread white matter deficits [Pfefferbaum et al., 2006a, b].

Several studies demonstrated that the brain atrophy in alcoholics is not due to a loss of gray matter but rather due to a reduction in the volume of the white matter [Harper et al., 1985, Kril & Halliday 1999]. The disproportionate loss of cerebral white matter relative to cerebral cortex suggests that chronic alcohol consumption predominantly affects the white matter [Harper et al., 1985, Kril & Halliday 1999]. These abnormalities may be reversed by abstinence from alcohol [de la Monte 1988, Harper 1998, Harper & Kril 1990, Trabert et al., 1995].

4.2. Neuropathology

A systematic investigation of human polydrug abusers using histology, immunohistochemistry and morphometry revealed a significant neuronal loss and a reduction of GFAP-positive astrocytes [Büttner & Weis 2006]. In the white matter the numerical density of perivascular and parenchymal microglia was increased with concomitant widespread ß-APP deposits. The cerebral microvessels showed a prominent vascular hyalinosis, endothelial cell proliferation, and a loss of immunoreactivity for collagen type IV within the vascular basal lamina. These findings demonstrate that drugs of abuse initiate a cascade of interacting toxic, vascular and hypoxic factors which finally result in widespread disturbances within the complex network of CNS cell-cell interactions [Büttner & Weis 2006].

ß-Amyloid precursor protein (ß-APP) is a neuronal functional protein which is transported by fast anterograde transport in undamaged axons. After lesions of the axonal cytoskeleton, ß-APP accumulates proximal to the disrupted segment and the axon undergoes secondary axotomy [Dolinak et al., 2000, Giometto et al., 1997, Medana & Esiri 2003, Oehmichen et al., 1998]. Immunohistochemical staining for ß-APP is a sensitive marker for the detection of damaged axons [Oehmichen et al., 1998].

Using ß-APP, axonal damage has been described in 55% of 38 drug deaths in the rostral pons and parasagittal white matter [Niess et al., 2002]. According to the authors this axonal damage represents a secondary phenomenon resulting from global hypoxic brain damage in the course of respiratory depression. However, this study has been criticized by others due to inadequate sampling and the possible influence of raised intracranial pressure [Smith et al., 2003]. In a systematic morphological study of the white matter in polydrug abusers, with opiates as the most frequently abused substances, significant accumulations of ß-APP could be found (Figure 1), while no changes of myelin were noted [Büttner et al., 2006]. The fact that there was a significant microglial significant microglial activation selectively in the white matter in these cases [Büttner et al., 2006] indicates a chronic-progressive process of axonal damage, which might be initiated and supported by drugs of abuse, finally leading to retrograde neuronal degeneration. This in turn might result in neurological signs and

symptoms similar to the subcortical pattern of HIV-1 leukoencephalopathy [Büttner et al., 2006].

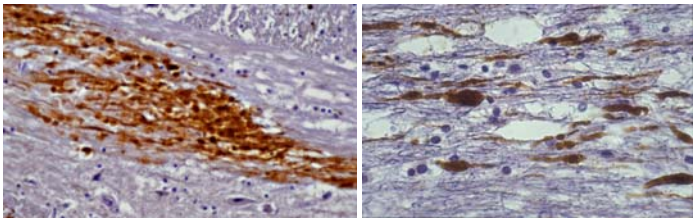

Figure 1. Immunohistochemistry demonstrating ß-APP-immunopositive bundles and ß-APP-immunopositive globular deposits in the white matter of polydrug abusers (a: pons, magnification x240; b: occiptal lobe, magnification x400; all counterstained with hematoxylin).

A distinct entity spongiform leukoencephalopathy has been described to occur almost exclusively after inhalation of pre-heated heroin ("chasing the dragon", "Chinese blowing") [Rizzuto et al., 1997, Strang, et al., 1997, Wolters et al., 1982]. The clinical picture consists of three distinct stages classified on the basis of the presence of key symptoms. The patients may remain in one stage or pass through two or all three stages. In the initial stage, motor restlessness, apathy, bradyphrenia, speech disturbances and cerebellar ataxia are observed. In the intermediate stage there is a rapid worsening of the cerebellar symptoms, with gait disturbances, hyperactive tendon reflexes, pathological reflexes, spastic hemi- or tetraparesis, tremor, myoclonic jerks or choreo-athetoid movements. The terminal stage is characterized by a vegetative dysregulation with spastic quadriparesis and profuse perspiration with central pyrexia. All patients entering the terminal stage died [Wolters et al., 1982]. A lipophilic toxin related to contaminants in conjunction with cerebral hypoxia is considered to be the cause, but a definite toxin has not yet been identified.

On computed tomography (CT) there are symmetrical non-enhancing hypodense areas in the cerebral and cerebellar white matter visible [Kriegstein et al., 1997].

On MRI-scans, the affected areas show decreased signal intensity on T1-weighted images and increased signal intensity on T2-weighted images [Kriegstein et al., 1997]. The neuroradiological findings are usually not correlated with the extent of the neurological deficit [Wolters et al., 1982].

On neuropathological examination, there is a diffuse spongiosis of the white matter with loss of oligodendrocytes, axonal reduction and astrogliosis; myelin breakdown products are not seen. The gray matter is usually unremarkable and the subcortical (U-)fibers, brainstem, spinal cord and peripheral nerves are spared [Kriegstein et al., 1997, Rizzuto et al., 1997, Wolters et al., 1982].

The absence of typical hypoxic lesions and the presence of spongiosis with massive astrogliosis distinguish these cases from those with delayed leukoencephalopathy following severe hypoxia [Rizzuto et al., 1997].

Gene expression profiling in the brains of human cocaine abusers revealed a substantial decrease of a group of myelin-related genes indicative of a possible dysregulation of myelin [Bannon et al., 2005].

Since drug fatalities usually have been polydrug abusers, it is hard to determine which substance might account for the observed alterations, however, opioids being the major substances are the most likely candidates.

The brain changes in chronic organic solvent vapor inhalation mainly consist of a demyelinating process with brain atrophy, thinning of the corpus callosum and ill-defined myelin pallor of the cerebral and cerebellar white matter [Filley et al., 2004, Kornfeld et al., 1994, Rosenberg et al., 1988].

Central pontine myelinolysis (CPM) is a demyelinating disease of the pons often associated with demyelination of other brain areas [Brown 2000, Kleinschmidt-DeMasters et al., 2006, Lampl & Yazdi 2002, Newell & Kleinschmidt-DeMasters 1996, Wright et al., 1979]. Besides a complication of alcohol abuse, CPM has been shown to occur most frequently in association with rapid correction of hyponatremia [Brown 2000, Norenberg 1982; Sterns et al., 1986].

On neuropathological examination, CPM predominantly presents as a single large symmetric focus of demyelination in the central part of the base of the pons, with sparing of axis cylinders (Figure 2). There are no inflammatory changes within the lesion and the blood vessels are not affected [Endo et al., 1981, Kleinschmidt-DeMasters et al., 2006, Newell & Kleinschmidt-DeMasters 1996]. The pathogenesis and etiology of the myelin loss is still unclear [Ashrafian & Davey 2001].

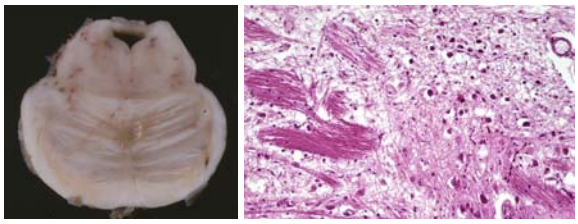

Figure 2. Central pontine myelinolysis in the pons: a) macroscopic view, b) demyelination (Stain: H&E, magnification x100).

Marchiafava-Bignami syndrome is an extremely rare neurological disorder associated with chronic alcoholism [Kohler et al., 2000]. There is a primary demyelination/necrosis and subsequent atrophy of the corpus callosum. The lesion is not only limited to the corpus callosum but also affects the cortico-cortical and cortico-subcortical projections due to disconnection, and causes frontal lobe syndromes and dementia.

On macroscopic examination, necrotizing, often cystic lesions of the corpus callosum are seen. Microscopically, there is prominent demyelination with relative sparing of the axons. There is a numerical reduction of oligodendrocytes and numerous lipid-laden macrophages. Astrocytes demonstrate only mild reactive changes. The blood vessels often show proliferation and hyalinization [Harper & Butterworth 2002].

5. White Matter in HIV-1 Infection

5.1. HIV-1 Related Neuropathology

The acquired immunodeficiency syndrome (AIDS) is caused by the infection with the human immunodeficiency virus 1 (HIV-1). As a matter of fact, up to 50% of AIDS patients develop neurological and psychiatric signs and symptoms during the course of the infection [Navia et al., 1986a]. Due to administration of highly active antiretroviral treatment (HAART), the number of patients with neurological complaints that can be attributed to HIV associated dementia (HIV-D) could be lowered by 40 to 50%. Moreover, the incidence of opportunistic brain infections and the overall AIDS related death rate could be significantly decreased [Anthony et al., 2005, Bell 2004, Brew 2004, Jellinger et al., 2000, Langford et al., 2002, Sotrel & Dal Canto 2000]. Neuropathological examination reveals damage to the central nervous system in up to 96% of all AIDS cases [Budka 1989, Büttner & Weis 2005, Weis et al., 1992]. Neuropathological changes are classified as primary and secondary changes. Primary neuropathological changes encompass HIV-1 encephalitis (HIVE) and HIV-1 leukoencephalopathy (HIVL) [Budka 1989, Budka et al., 1991]. In the pre-HAART period the annual incidence of HIV-D after AIDS was 7%, and the cumulative life-time risk of developing HIV-D was 5 to 20%. The incidence of HIV-D significantly declined soon after the introduction of combined antiretroviral treatment [Jellinger et al., 2000]. However, since the beginning of the 21st century, HIVE is increasing again, possibly due to virus resistance and/or treatment limitations due to toxicity or lack of compliance or as newly defined "burnt out forms" with glial scarring [Gray et al., 2003, Gray et al., 2005, Sacktor et al., 2001]. It is becoming apparent that patients of the HAART era suffer from protracted forms of HIVE/HIVL that might lead to more subtle forms of mental impairment rather than overt dementia [Cherner et al., 2002, Diesing et al., 2002].

Gray et al., (2003) described a new variant of HIVE in HAART-patients characterized by severe leukoencephalopathy with intense perivascular macrophage and lymphocytic infiltration, possibly due to an exaggerated response from a newly reconstituted immune system. Furthermore, they detected chronic "burnt out" forms of HIVE as well as varicella zoster virus encephalitis, toxoplasmosis and PML, possibly associated with prolonged survival, in which neither inflammation nor organisms could be detected.

Langford et al., (2003) suggested that the increasing resistance of HIV strains to antiretrovirals led to the resurgence in the frequency of HIVE and HIVL. HIVE and HIVL in AIDS patients failing HAART is characterized by massive infiltration of HIV infected monocytes/macrophages into the brain and extensive white matter destruction. This condition might be attributable to interactions of anti-retrovirals with cerebrovascular endothelium, astroglial cells and white matter of the brain. These interactions might lead to cerebral ischemia, increased blood-brain barrier permeability and demyelination. The authors postulate that potential mechanisms of such interactions include alterations in host cell signaling that may result in trophic factor dysregulation and mitochondrial injury [Langford et al., 2003].

Secondary changes include opportunistic infections as well as primary or secondary lymphoma [Gray et al., 1988].

Early studies proposed neuropathological changes to be mainly found in subcortical brain structures. These changes were initially thought to constitute the morphological substrate of the AIDS dementia complex (ADC), which was defined to be a subcortical dementia [Navia et al., 1986b]. However, it has been shown that the cerebral cortex is also involved in the course of the HIV-1 infection. Ketzler et al., (1990) and Weis et al., (1993) were the first to show, by morphometric investigations, loss of neurons in the fronto-orbital cortex (Area 11 after Brodmann), whereas the superior parietal cortex (Area 7 after Brodmann) was not affected. The loss of neurons did not correlate with the presence or absence of dementia [Weis et al., 1993].

HIV-1 encephalitis is histologically characterized by multiple disseminated foci composed of microglia, macrophages and multinucleated giant cells, which are predominantly located in the cortex, the deep gray matter and the white matter [Budka et al., 1991, Büttner & Weis 2005]. Aside from the presence of multiple disseminated foci composed of microglia, macrophages and multinucleated giant cells, HIVL-1 is characterized by diffuse damage of the white matter with myelin pallor and/or loss and reactive astrogliosis with few or no inflammatory infiltrates [Budka et al., 1991, Büttner & Weis 2005]. HIVL-1 represents a primary HIV-1 induced change of the white matter. Studies dealing with white matter damage in HIV-1 infected brains were rarely published.

5.2 Neuroradiology in HIV-1 Infection

Conventional neuroimaging of the brain has identified several abnormalities, typically occurring in symptomatic HIV-infected individuals and increasing with declining clinical and cognitive status [Broderick et al., 1993]. Nonspecific white matter hyperintensities (WMHI) may be present in HIV patients and the presence of large volumes of WMHI are predictive concerning survival.

Olson et al., (1988) described that from 365 patients with AIDS 31% had signal abnormalities confined to the white matter grouped into the following four patterns, were observed: (a) diffuse: widespread involvement of a large area; (b) patchy: localized involvement with ill-defined margins; (c) focal: well-defined areas of involvement; and (d) punctuate: small foci less than 1 cm in diameter. The diffuse pattern correlated with ADC.

Focal hyperintensities in the white matter were observed in 24% of the HIV-1 seronegatives, 26% of HIV-1 asymptomatic seropositives (CDC II/III), and 17% of those with ARC/AIDS. No significant associations were noted between the white matter hyperintensities and HIV-1 serostatus, neurological abnormalities, CD4 count, alcohol or drug use, hypertension, or smoking [McArthur et al., 1990]. The authors suggested that focal white matter hyperintensities identified on MR are not specific for HIV-1 infection and are probably incidental and of no clinical significance. Incidence of hyperintensities was low in all groups (243 HIV-positive and HIV-negative homosexual or bisexual men with no history of intravenous drug use), although slightly higher in patients with AIDS, and was not associated with neuropsychological performance [Bornstein et al., 1992].

The presence of these deep white matter abnormalities was not significantly different between groups with and without AIDS dementia ($p = .08$), although higher grades of deep

white matter abnormality were more likely to be associated with AIDS dementia complex [Bornstein et al., 1993].

A study by Wilkinson et al. (1998) on whether short echo-time proton magnetic resonance spectroscopy (H-MRS) could detect mobile lipid resonances attributable to myelin breakdown products in the deep cerebral white matter of patients with AIDS who have severe diffuse/patchy white matter hyperintensity on T2-weighted magnetic resonance imaging (MRI), suggested that mobile lipids are only rarely detected by H-MRS in patients with ADC and abnormalities on MRI and that their presence may be transitory.

Diffusion tensor imaging (DTI) is a magnetic resonance imaging (MRI) technique that is uniquely suited for the study of subtle white matter abnormalities. Abnormal fractional anisotropy was found in the white matter of the frontal lobes and internal capsules of the HIV-1patients, in the absence of group differences in mean diffusivity, computed proton density, and computed T2 [Pomara et al., 2001].

Calculating the diffusion constant and anisotropy in the subcortical white matter and corpus callosum in patients with HIV detected abnormalities despite normal-appearing white matter on MR images and nonfocal neurologic examinations [Filippi et al., 2001]. Patients with the highest diffusion constant elevations and largest anisotropy decreases had the most advanced HIV disease. Patients with the lowest viral load levels, who had normal anisotropy and diffusion constants, were receiving highly active antiretroviral therapy [Filippi et al., 2001]. The apparent diffusion coefficient was significantly increased in the HIV patients, primarily in the frontal white matter. Diffusivity correlated positively with the glial marker myo-inositol and negatively with cognitive performance. Thus, increased brain water diffusion may reflect increased glial activation or inflammation, which in turn, may contribute to the cognitive deficits in HIV patients [Cloak et al., 2004].

Pfefferbaum et al. (2007) observed a relationship between greater viral burden and more extensive WMHI in DTI studies. These hyperintense regions may reflect myelin pallor and rarefaction associated with the presence of multinucleated giant cells. However, results obtained by this methodology show considerable variability. Stebbins et al. (2007) found decreased white matter integrity in non-demented individuals as well as HIV-infected patients, indicating the enormous difficulties of assessing subtle diffuse white matter changes in the human brain [Pfefferbaum et al., 2007, Stebbins et al., 2007].

5.3. White Matter and HIV-1 Infection

Schmidbauer et al. (1992) delineated the following three distinct types of white matter lesion: (1) Vacuolar myelin damage in the hemispheric and interhemispheric white matter, in projection fiber tracts, and in intracerebral segments of cranial nerves III, VII, and VIII, (2) Angiocentric foci disseminated randomly in the white matter, and (3) HIV leukoencephalopathy, as previously defined, seen predominantly in the hemispheric white matter. Patients with advanced AIDS-dementia complex consistently show severe and combined white matter pathologies at autopsy.

Dambska et al. (1997) investigated the brains of six infants 14-34 months of age and with microencephaly (brain weight deficit 20–55.5%) which were vertically infected with HIV.

Within the periventricular white matter of four cases, evident lesions consisting of myelin pallor and concomitant gliosis were recognized as HIV-1 infection-related leukoencephalopathy. In all those cases, myelination delay was also noted. The authors suggest that in the majority of HIV infected infants changes resulting in the brain "too small for age" correlate with myelination delay coexisting with early-onset leukoencephalopathy.

Although diffuse damage to the cerebral white matter, demonstrable as pallor in sections stained for myelin, is a common autopsy finding in HIV infection [Anders et al., 1986, Budka et al., 1991, Price et al., 1988], some limiting factors with regard to staining and demonstrability of these changes must be considered. Raja et al. (1997) hypothesized that axonal ß-amyloid precursor protein (βAPP) immunoreactivity might be a more sensitive marker of white matter damage in HIV infection than myelin pallor. This is suggested by the fact that 26% of sections with normal myelin staining contained βAPP immunopositive axons and that, among the cases with no specific or no pathology, there were four cases that showed on sections normal myelin staining but which nevertheless contained foci of βAPP immunoreactivity. As shown in the present study, only the application of morphometric techniques, both at the gross-anatomical and ultrastructural level, revealed changes of the nerve fibers from brain tissue which, on myelin-stained histological sections, did not show any mild myelin pallor nor myelin loss.

Following some authors, diffuse damage to the cerebral white matter is more frequent in those subjects who show clinical features of encephalopathy than in those who are asymptomatic, with respect to the central nervous system (CNS) [Anders et al., 1986, Parmantier et al., 1995, Price et al., 1988]. Despite the published reports on severe neuronal loss occurring in the cerebral cortex, some authors still consider subcortical damage in the white matter and/or deep gray matter to play a more important role in mediating symptoms of the AIDS dementia complex [Esiri et al., 1991, Navia et al., 1986a,b, Parmantier et al., 1995, Peavy et al., 1994, Price et al., 1988, Sidtis et al., 1990]. Thus, following this line of thinking, HIV-1 leukoencephalopathy (HIVL-1), might partly represent the morphological substrate of the HIV-1 associated cognitive/motor complex. However, a clear-cut correlation between the presence of HIVL-1 and dementia was never drawn.

Using a non-isotopic PCR method, Sinclair & Scaravilli (1992) detected HIV proviral DNA in nine out of 15 cortical samples and in 10 out of 15 white matter samples, whilst HIV p24 antigen was localized to the cortex in three out of 15 and to the white matter in seven out of 15 cases.

Only a few investigations going beyond the routine histological examinations of white matter were performed until now.

Raja et al. (1997) examined brain sections from 55 autopsy cases of AIDS for the prevalence and severity of axonal damage, assessed using β-amyloid precursor protein (βAPP) immunoreactivity. Significantly, more foci containing βAPP+ axons were found in cases with HIV encephalitis with multinucleated giant cells (MGC) (80%) and in cases with other specific pathology (58%) than in those with nonspecific (30%) or no pathology (30%). The prevalence and abundance of βAPP+ axons generally paralleled the severity of pallor of myelin staining of the cerebral white matter in cases without other specific pathology. Foci of βAPP+ axons were found in subcortical and deep white matter but did not convincingly co-localize with foci of demonstrable HIV infection, as indicated by the presence of MGC and

HIV p24 immunoreactivity. In contrast, the authors showed an approximately perivascular distribution of βAPP at some sites in all of the disease categories studied.

Microtubule-associated protein-2 (MAP2e) is expressed transiently in developing oligodendrocytes during myelination, and in remyelinating oligodendrocytes in multiple sclerosis lesions. Cosenza et al. (2002) reported MAP2e+ cells to be significantly increased in HIVE compared to controls. MAP2e+ cells were negative for GFAP, CD68, LN3, RCA-1, von Willebrand factor and HIV-1 p24, but positive for MBP or Luxol-Fast Blue, supporting their oligodendroglial lineage. A topographical association between MAP2e and HIV-1 p24 expression was noted, but not between MAP2e and beta-APP, a marker of damaged axons.

Wohlschlaeger et al. (submitted) considered the corpus callosum to be a sensitive marker for damage of the cerebral white matter and investigated it by morphometry both at the macroscopic and electron microscopic level. In HIV-1 infected brains, a significant decrease of the profile area of the whole corpus callosum as well as of its different parts was noted. Furthermore, the absolute number of nerve fibers was significantly decreased with an emphasis on the frontal and occipital parts of the corpus callosum. Moreover, several morphometric parameters for nerve fibers, axons and myelin sheaths indicate in some areas a reduction of nerve fibers and axons, as well as a diminished myelin sheath thickness, whereas, in other regions, swelling of axons and myelin sheaths was observed. Wohlschlaeger et al., suggested that the observed changes must be considered to represent subtle changes affecting nerve fibers before histological evidence of HIVL, and might represent one aspect of the morphological substrates of the HIV-1 related cognitive/motor complex. The changes of nerve fibers in HIV-1 infected brains described in that study also encompass extensive swelling of myelin sheaths and axons, a finding that can be interpreted as an early stage of TNF-alpha-mediated cytotoxicity. These changes were mainly found in the frontal and occipital parts of the corpus callosum. In the middle sections, shrinkage of myelin sheaths and axons was observed, the latter probably representing a later stage of the changes, that possibly precede the complete degeneration of nerve fibers. The inconspicuous appearance of the tissue changes on myelin stains might indicate that subtle changes affect nerve fibers already early in the course of the disease.

Based on the morphometric results of the study by Wohlschlaeger et al. (submitted) showing obvious changes occurring in nerve fibers of the corpus callosum, several questions arise concerning the pathogenesis of these changes, especially with regard to potential mechanisms leading to the observed severe alterations. Any pathogenetic model for HIVL-1 has to take into consideration the selective localization of the virus on one hand, and the widespread areas of myelin loss, neuronal dropout [Everall et al., 1991, Ketzler et al., 1990, Weis et al., 1993, Wiley et al., 1991], alterations of neocortical dendritic spines [Masliah et al., 1992], reactive astrogliosis [Itoh et al., 1996, Weis et al., 1993], and reactive microgliosis [Weis et al., 1994] occurring in HIV-1 infected brains on the other hand.

Basically, the pathogenesis of white matter damage in HIV-1 infection is unclear. Myelin appears to be more affected than axons, though the myelin damage may be accompanied by patchy axonal swelling as shown in a case report [Giangaspero et al., 1988].

Oligodendrocytes show reactive changes but are not reduced in number [Esiri et al., 1991, Esiri & Morris 1996, Weis et al., 1994].

The direct effect of HIV-1 on the various cells making up the nervous system could result from infection of these cells. Until now, the only cells of the central nervous system shown to be productively infected by HIV-1 are macrophages, microglia and multinucleated giant cells [Pumarola-Sune et al., 1987, Sidtis et al., 1990, Sotrel & Dal Canto 2000].

Cell infection was reported by Albright et al. (1996) to occur in cultured oligodendrocytes via galactosylceramide (GalCer), an HIV-1 receptor other than CD4, which may lead to the loss of integrity of the myelin sheath. In addition, it was hypothesized that any infected oligodendrocyte could transmit new virions to many neurons [Kandel et al., 1991]. Furthermore, cultured oligodendrocytes containing HIV proteins or virions on their surface may be a target of lysis by microglia leading to further deterioration of myelin synthesis [Albright et al., 1996]. In the present study, immunohistochemical demonstration of HIV-1 specific proteins, i.e. gp41 and p24 did not show any positive cells in the examined region. Also, others could not demonstrate evidence of oligodendroglial infection with HIV [Esiri et al., 1991, Esiri & Morris 1996]. Therefore, direct virus-inflicted damage to oligodendrocytes is not a convincing explanation for the white matter damage. However, a recent study reported that Nef interferes with proper differentiation of oligodendrocytes and might be responsible for vacuolar myelopathy in some individuals [Radja et al., 2003].

Parmantier et al. (1995) investigated the binding of gp120 to rat oligodendrocytes in vitro and monitored changes in intracellular calcium. They showed that antibodies against galactosylceramide and sulfatide did bind to the cell membrane, but gp120 did not. The antibodies also led to increased intracellular free calcium levels in the oligodendrocytes, whereas gp120 did not. Following the authors, it seems highly improbable that the demyelination observed during HIV encephalopathy is a direct cytotoxic effect of gp120 on oligodendrocytes [Parmantier et al., 1995]. The binding of gp120 to various types of neural cells and its effects on myelination were examined in rat primary brain culture by Kimura-Kuroda et al. (1994). Seven days after the application, myelination in the culture was observed morphologically by staining with anti-myelin basic protein (MBP) antibody, and was found to be significantly inhibited by the addition of gp120. The processes of oligodendrocytes showed a reduction in length and arborization relative to the control, but MBP production by oligodendrocytes was unaffected. The data show that gp120 can cause a functional disorder of oligodendrocytes and, thus, could underlie the diffuse loss of myelin sheaths in HIV encephalopathy. Functional alterations in oligodendrocytes following binding of gp120 was reported by Bernardo et al. (1997). Indeed, the percentage of oligodendrocytes expressing myelin basic protein and the levels of all four MBP isoforms were substantially reduced after a 3-day treatment with 10nM gp120.

Alternatively, white matter damage might result from a breakdown of the blood-brain barrier and diffusion of myelinotoxic serum constituents into the CNS [Power et al., 1993, Smith et al., 1990]. Serum protein extravasation into deep cerebral white matter in subjects with AIDS was reported [Power et al., 1993, Smith et al., 1990]. Gisslen et al. (1996) showed that the sulfatide levels were associated with blood-brain barrier function, but not with intrathecal immunoglobulin production or with positive HIV isolation from CSF. Hence, signs of white matter changes, measured as increased CSF sulfatide concentration, could be found in some asymptomatic HIV-1 infected patients, but the highest levels were seen in patients with AIDS [Gisslen et al., 1996].

Following Raja et al. (1997), the location of βAPP+ axons may offer clues to the pathogenesis of deep white matter damage in HIV infection. Most of the foci and more scattered areas of damage detected by βAPP+ axons were found in subcortical and deep white matter. However, upon comparing the location of axonal βAPP immunoreactivity with that of HIV, the authors were not convinced of co-localization except in one instance. More striking was an approximately perivascular location of some βAPP+ axons. The affected axons did not always lie closely adjacent to the vessels around which they were grouped, and sometimes were some distance away from them. The vessel involved was usually a vein. The authors, therefore, believed that their findings tend to favor a role for systemic, vascular-related factors in the pathogenesis of HIV-related white matter damage.

Among the possible pathogenetic mechanisms proposed so far, one of the most widely accepted is the indirect nerve cell and myelin damage mediated by neurotoxins released by HIV-1 infected macrophages/microglia. Indirect mechanisms have been proposed, that possibly act by amplifying the effects of a persistent HIV-1 infection. Tyor et al. (1992) were able to show diffuse activation of the immune system in HIV-1 infected brains, in which only few cells expressed the HIV-1 antigen p24.

HIV-infected multinucleated macrophages and microglial cells occur, however, in cerebral white matter and this infection may provoke indirect damage to myelin by promoting local cytokine production or release of toxic HIV-encoded products, such as the envelope protein gp120 [Esiri & Morris 1996, Pulliam et al., 1991, Pumarola-Sune et al., 1987, Stanley et al., 1994]. Recent studies support these results and point to interactions between HIV-1 infected macrophages and astrocytes playing an important role in the generation of neuro- and myelotoxic agents [Giulian et al., 1990, Merrill et al., 1992, Pulliam et al., 1991]. Weis et al. (1993, 1994) and Itoh et al. (1996) investigated the reaction pattern of astrocytes and microglia in AIDS brains. They observed a significantly increased number of activated microglia both in the gray and white matter. The activation pattern was not influenced by the presence of HIV-1 antigens in the examined brain regions. The same reaction pattern was observed for astrocytes. These data show that microglia and astrocytes are activated in HIV-1 infected brains and might produce factors damaging or destroying neurons and myelin.

Cytokines seem to play a critical role in mediating neuro- and myelotoxic activity in HIV-1 infected brains [Genis et al., 1992]. Among these, Tumor-Necrosis-Factor alpha (TNF-alpha) and interleukin 1 (IL-1) are of special interest. TNF-alpha can damage oligodendrocytes and myelin [Robbins et al., 1987, Selmaj et al., 1988] and can also regulate HIV-1 gene expression [Vitkovic et al., 1990]. Bernardo et al. (1997) were able to show that exposure of oligodendrocytes to gp120 was followed by lowered expression of the myelin basic protein. Moreover, cytokines can activate HIV-1 expression in astrocytes [Tornatore et al., 1991], leading to a self-perpetuation of various pathogenetic mechanisms mentioned above.

TNF-alpha and IL-1 are associated with proliferation of glial cells, neurotoxicity and demyelination. These effects are prominent features of the HIVL; the latter is indicated by elevated levels of antibodies against sulfatide, the major acidic glycosphingolipid in myelin [Gisslen et al., 1996]. Selmaj et al. (1988) investigated whether recombinant human TNF-alpha (rhTNF-alpha) was toxic to mouse spinal cord cells. They observed a TNF-specific delayed swelling and dilatation of myelin sheaths and necrosis of oligodendrocytes. Some of

the nerve fibers were completely demyelinated after exposure to the TNF medium for 72 hours. The swelling of myelin sheaths was irreversible even after cultivation in normal TNF-free medium for three days following exposure to TNF. On light microscopy, the nerve fibers displayed local dilatations of their myelin sheaths, termed “bubbles” or “ballooning”. These TNF-associated changes did not show rapid onset, but evolved slowly with an 18 hours delay and proceeded gradually over time. After 48 hours, nearly 50% of the nerve fibers exhibited the changes described above. Swelling of myelin sheaths could be induced by TNF concentrations as low as 5•102 units/ml; higher concentrations caused the changes in a more severe form [Selmaj et al., 1988]. They postulated that the swelling, and/or the “bubbling” was due to an inflow of water into the dilated periaxonal spaces between the internodal segments. The exact mechanism, by which rhTNF mediates the changes described above, remains elusive up to now, although there is evidence that TNF might alter the function of the sodium/potassium ATPase.

Expansion of the lysosomal apparatus occurs in subcortical white matter in brains from persons with AIDS. Lysosomal hydrolase activity was assayed by Gelman et al. (2005) in 57 subjects who underwent neuropsychological testing within six months prior to autopsy. Increased beta-glucuronidase activity, a representative lysosomal glycosidase, was correlated with the amount of neurocognitive impairment. Significant correlation was present in five of seven functional testing domains, including some that draw upon frontal lobe output. The biochemical anomaly was negligible in cerebral cortex and cerebrospinal fluid and was not correlated with brain dysfunction in those compartments. These results support the suggestion that abnormal metabolism in white matter glial cells contributes to cognitive slowing in persons with HAD. Because membrane turnover is routed through the endosome-lysosome apparatus, these data are in agreement with brain spectroscopic data that have suggested that there is an increase in membrane turnover in white matter glia.

6. Conclusion

White matter plays an important role by its involvement in a variety of pathological states. In HIV-1 infection of the brain, white matter is already affected at an early stage of the disease process. Whether white matter damage is a direct or indirect effect in drug addiction has yet to be elucidated.

Until now, systematic analyses of white matter in these disease states are lagging far behind. Much research is still to be done. In this endeavor, focus must be placed on assessing changes of the various myelin proteins, the fate and changes of oligodendrocytes, the role of astrocyte-oligodendrocyte cross-talk, and the changes in signal transduction cascades at work in the white matter. Systematic analyses using gene expression arrays, proteomics and metabolomics will provide new clues for elucidating the pathogenetic mechanisms leading to white matter changes.

References

Albright, A.V.; Strizki, J.; Harouse, J.M.; Lavi, E.; O'Connor, M. & González-Scarano,F. (1996). HIV-1 infection of cultured human adult oligodendrocytes. *Virology, 217*, 211-219.

Anders, K.H.; Guerra, W.F. & Tomiyasu, U. (1986). The neuropathology of AIDS. UCLA experience and review. *Am J Pathol, 124*, 537-558.

Anthony, I.C.; Ramage, S.N.; Carnie, F.W.; Simmonds, P. & Bell, J.E. (2005). Influence of HAART on HIV-related CNS disease and neuroinflammation. *J Neuropathol Exp Neurol, 64*, 529-536.

Ashrafian, H. & Davey, P. (2001). A review of the causes of central pontine myelinosis: yet another apoptotic illness? *Eur J Neurol, 8*, 103-109.

Aydin, K.; Sencer, S.; Ogel, K.; Genchellac, H.; Demir T. & Minareci, O. (2003). Single-voxel proton MR spectroscopy in toluene abuse. *Magn Reson Imag, 21*, 777–785.

Bannon, M.; Kapatos, G. & Albertson, D. (2005). Gene expression profiling in the brains of human cocaine abusers. *Addict Biol*, 10, 119-126.

Bartzokis, G.; Goldstein, I.B.; Hance, D.B.; Beckson, M.; Shapiro, D.; Lu, P.H.; Edwards, N.; Mintz, J. & Bridge, P. (1999). The incidence of T2-weighted MR imaging signal abnormalities in the brain of cocaine-dependent patients is age-related and region-specific. *Am J Neuroradiol*, 20, 1628-1635.

Baumann, N. & Pham-Dinh, D. (2001). Biology of oligodendrocyte and myelin in the mammalian central nervous system. *Physiol Rev, 81*, 871-927.

Bell, J.E. (2004). An update on the neuropathology of HIV in the HAART era. *Histopathology, 45*, 549-559.

Bernardo, A.; Agresti, C. & Levi, G. (1997). HIV-gp 120 affects the functional activity of oligodendrocytes and their susceptibility to complement. *J Neurosci Res, 50*, 946-957.

Bornstein, R.A.; Chakeres, D.; Brogan, M.; Nasrallah, H.A.; Fass, R.J.; Para, M. & Whitacre, C. (1992). Magnetic resonance imaging of white matter lesions in HIV infection. *J Neuropsychiatry Clin Neurosci, 4*, 174-178.

Brew, B.J. (2004). Evidence for a change in AIDS dementia complex in the era of highly active antiretroviral therapy and the possibility of new forms of AIDS dementia complex. *AIDS, 18 (suppl. 1),* 75-78.

Broderick, D.F.; Wippold, F.J. 2nd; Clifford, D.B.; Kido, D. & Wilson, B.S. (1993). White matter lesions and cerebral atrophy on MR images in patients with and without AIDS dementia complex. *Am J Roentgenol, 161*, 177-181.

Bronstein, J.M.; Micevych, P.E. & Chen, K. (1997). Oligodendrocyte-specific protein (OSP) is a major component of CNS myelin. *J Neurosci Res, 50*, 713-720.

Brown, W.D. (2000). Osmotic demyelination disorders: central pontine and extrapontine myelinolysis. *Curr Opin Neurol, 13*, 691-697.

Budka, H. (1989). Human immunodeficiency virus (HIV)-induced disease of the central nervous system: pathology and implications for pathogenesis. *Acta Neuropathol, 77*, 225-236.

Budka, H.; Wiley, C. & Kleihues, P. (1991). HIV-1 associated disease of the nervous system: review of nomenclature and proposal for neuropathology-based terminology. *Brain Pathol, 1*, 143-152.

Büttner, A. & Weis, S (2008). Central Nervous System Alterations in Alcohol Abuse. In M. Tsokos (Ed.) *Forensic Pathology Reviews* Vol. 5, pp.69-90. Totowa, NJ: Humana Press Inc.

Büttner, A. & Weis, S. (2006). Neuropathological alterations in drug abusers: the involvement of neurons, glial, and vascular systems. *Forensic Sci Med Pathol, 2*, 115-126.

Büttner, A.; Rohrmoser, K.; Mall, G.; Penning, R. & Weis, S. (2006).Widespread axonal damage in the brain of drug abusers as evidenced by accumulation of b-amyloid precursor protein (b-APP): an immunohistochemical investigation. *Addiction, 101*, 1339-1346.

Büttner, A. & Weis, S. (2005). HIV-1 Infection of the Central Nervous System. In M. Tsokos (Ed.), *Forensic Pathology Reviews*, Vol. 3, pp.81-134. Totowa, NJ: Humana Press Inc.

Büttner, A. & Weis, S. (2004). Central Nervous System Alterations in Drug Abuse. In M. Tsokos (Ed.), *Forensic Pathology Reviews*, Vol. 1, pp.79-136. Totowa, NJ: Humana Press Inc.

Campagnoni, AT & Skoff, RP. (2001). The pathobiology of myelin mutants reveal novel biological functions of the MBP and PLP genes. *Brain Pathol, 11*, 74-91.

Cherner, M.; Masliah, E.; Ellis, R.J.; Marcotte, T.D.; Moore, D.J.; Grant, I. & Heaton, R.K. (2002). Neurocognitive dysfunction predicts postmortem findings of HIV encephalitis. *Neurology, 59*, 1563-1567.

Cloak, C.C.; Chang, L. & Ernst, T. (2004). Increased frontal white matter diffusion is associated with glial metabolites and psychomotor slowing in HIV. *J Neuroimmunol, 157*, 147-152.

Compston, A.; Zajicek, J.; Sussman, J.; Webb, A.; Hall, G.; Muir, D.; Shaw, C.; Wood, A. & Scolding, N. (1997). Glial lineages and myelination in the central nervous system. *J Anat, 190*, 161-200.

Cosenza, M.A.; Zhao, M.L.; Shankar, S.L.; Shafit-Zagardo, B. & Lee, S.C. (2002). Up-regulation of MAP2e-expressing oligodendrocytes in the white matter of patients with HIV-1 encephalitis. *Neuropathol Appl Neurobiol, 28*, 480-488.

Dambska, M.; Kozłowski, P.B.; Brudkowska, J.; Rao, C.; Anzil, A.P. & Laure-Kamionowska, M. (1997). The white matter changes in microencephalic HIV infected infants. A preliminary report. *Folia Neuropathol, 35*, 145-148.

Darke, S.; Sims, J.; McDonald, S. & Wickes, W. (2000). Cognitive impairment among methadone maintenance patients. *Addiction*, *95*, 687-695.

de la Monte, S.M. (1988). Disproportionate atrophy of cerebral white matter in chronic alcoholics. *Arch Neurol, 45*, 990-992.

De Roock, S.; Hantson, P.; Laterre, P.-F. & Duprez, T. (2007). Extensive pallidal and white matter injury following cocaine overdose. *Intensive Care Med, 33*, 2030-2031.

Diesing, T.S.; Swindells, S.; Gelbard, H. & Gendelman, H.E. (2002). HIV-1-associated dementia: a basic science and clinical perspective. *AIDS Read, 12*, 358-368.

Dolinak, D.; Smith, C. & Graham, D.I. (2000). Global hypoxia per se is an unusual cause of axonal injury. *Acta Neuropathol*, *100*, 553-560.

Endo, Y.; Oda, M. & Hara, M. (1981). Central pontine myelinolysis. A study of 37 cases in 1,000 consecutive autopsies. *Acta Neuropathol, 53*, 145-153.

Ernst, T.; Chang, L.; Oropilla, G.; Gustavson, A. & Speck, O. (2000). Cerebral perfusion abnormalities in abstinent cocaine abusers: a perfusion MRI and SPECT study. *Psychiatry Res*, *99*, 63-74.

Esiri, M.M.; Morris, C.S. & Millard, P.R. (1991). The fate of oligodendrocyte in HIV-1 infection. *AIDS, 5*, 1081-1088.

Esiri, M.M. & Morris, C.S. (1996). Cellular basis of HIV infection of the CNS and the AIDS dementia complex: oligodendrocyte. *J Neuro-AIDS, 1*, 133-160.

Everall, I.P.; Luthert, P.J. & Lantos, P.L. (1991). Neuronal loss in the frontal cortex in HIV infection. *Lancet, 337*, 1119-1121.

Filippi, C.G.; Ulug, A.M.; Ryan, E.; Ferrando, S.J. & van Gorp, W. (2001). Diffusion tensor imaging of patients with HIV and normal-appearing white matter on MR images of the brain. *Am J Neuroradiol, 22*, 277-283.

Filley, C.M. & Kleinschmidt-DeMasters, B.K. (2001). Toxic leukoencephalopathy. *N Engl J Med, 345*, 425-432.

Filley, C.M.; Halliday, W. & Kleinschmidt-DeMasters, B.K. (2004). The effects of toluene on the central nervous system. *J Neuropathol Exp Neurol, 63*, 1-12.

Filley, C.; Heaton, R.K. & Rosenberg, N.L. (1990). White matter dementia in chronic toluene abuse. *Neurology, 40*, 532–534.

Gelman, B.B.; Soukup, V.M.; Holzer, C.E. 3rd; Fabian, R.H.; Schuenke, K.W.; Keherly, M.J.; Richey, F.J. & Lahart, C.J. (2005). Potential role for white matter lysosome expansion in HIV-associated dementia. *J Acquir Immune Defic Syndr, 39*, 422-425.

Genis, P.; Jett, M.; Bernton, E.W.; Boyle, T.; Gelbard, H.A.; Dzenko, K.; Keane, R.W.; Resnick, L.; Mizrachi, Y.; Volsky, D.J.; Epstein, L.G. & Gendelman, H.E. (1992). Cytokines and arachidonic acid metabolites produced during HIV-infected macrophage-astroglial interactions: implications for the neuropathogenesis of HIV disease. *J Exp Med, 176*, 1703-1718.

Giangaspero, F. & Foschini, M.P. (1998). Diffuse axonal swellings in a case of acquired immunodeficiency syndrome. *Arch Pathol Lab Med, 112*, 1259-1262.

Giometto, B.; An, S.F.; Groves, M.; Scaravilli, T.; Geddes, J.F.; Miller, R.; Tavolato, B.; Beckett, A.A.J. & Scaravilli, F. (1997). Accumulation of ß-amyloid precursor protein in HIV encephalitis: relationship with neuropsychological abnormalities. *Ann Neurol*, *42*, 34-40.

Gisslen, M.; Fredman, P.; Norkrans, G. & Hagberg, L. (1996). Elevated cerebrospinal fluid sulfatide concentrations as a sign of increased metabolic turnover of myelin in HIV type 1 infection. *AIDS Res Hum Retroviruses, 12*, 149-155.

Giulian, D.; Vaca, N. & Noonan, C.A. (1990). Secretion of neurotoxins by mononuclear phagocytes infected with HIV-1. *Science, 250*, 1593-1596.

Gray, F.; Bazille, C.; Adle-Biassette, H.; Mikol, J.; Moulignier, A. & Scaravilli, F. (2005). Central nervous system immune reconstitution disease in acquired immunodeficiency

syndrome patients receiving highly active antiretroviral treatment. *J Neurovirol, 11(Suppl 3)*, 16-22.

Gray, F.; Chrétien, F.; Vallat-Decouvelaere, A.V. & Scaravilli, F. (2003). The changing pattern of HIV Neuropathology in the HAART era. *J Neuropathol Exp Neurol, 62*, 429-440.

Gray, F.; Gherardi, R. & Scaravilli, F. (1988). The neuropathology of the acquired immune deficiency syndrome (AIDS). A review. *Brain, 111*, 245-266.

Harper, C. (1998). The neuropathology of alcohol-specific brain damage, or does alcohol damage the brain? *J Neuropathol Exp Neurol, 57*, 101-110.

Harper, C. & Butterworth, R. (2002). Nutritional and metabolic disorders. In D.I. Graham & P.L. Lantos (Eds.) *Greenfield's Neuropathology*, 7th ed., pp. 607-652. London, Arnold Publishers.

Harper, C.G. & Kril, J.L. (1990). The neuropathology of alcoholism. *Alcohol Alcohol, 25*, 207-216.

Harper, C.G.; Kril, J.J. & Holloway, R.L. (1985). Brain shrinkage in chronic alcoholics: A pathological study. *Br Med J, 290*, 501-504.

Itoh, K.; Mehraein, P. & Weis, S. (1996). Astroglial reaction pattern in HIV-1 infected brains. *Neuropathology, 16*, 225-230.

Jellinger, K.; Setinek, U.; Drlicek, M.; Böhm, G.; Steurer, A. & Lintner, F. (2000). Neuropathology and general autopsy findings in AIDS during the last 15 years. *Acta Neuropathol, 100* ,213-220.

Jernigan, T.L.; Butters, N.; DiTraglia, G.; Schafer, K.; Smith, T.; Irwin, M.; Grant, I.; Schuckit, M. & Cermak, L.S. (1991). Reduced cerebral grey matter observed in alcoholics using magnetic resonance imaging. *Alcohol Clin Exp Res, 15*, 418-427.

Kandel, E.R.; Schwartz, J.H. & Jessel, T.M. (1991). *Principles of Neural Science* (3rd ed.) New York, Appleton and Lange.

Karch, S.B. (2008) *Karch's Pathology of Drug Abuse* (4th edn.) Boca Raton: CRC Press.

Ketzler, S.; Weis, S.; Haug, H. & Budka, H. (1990). Neuronal loss in the frontal cortex in AIDS brains. *Acta Neuropathol, 80*, 92-94.

Kimura-Kuroda, J.; Nagashima, K. & Yasui, K. (1994). Inhibition of myelin formation by HIV-1 gp120 in rat cerebral cortex culture. *Arch Virol, 137*, 81-99.

Kornfeld, M.; Moser, A.B.; Moser, H.W.; Kleinschmidt-DeMasters, B.K.; Nolte, K.B. & Phelps, A. (1994). Solvent vapor abuse leukoencephalopathy. Comparison to adrenoleukodystrophy. *J Neuropathol Exp Neurol, 53*, 389-398.

Kriegstein, A.R.; Armitage, B.A. & Kim, P.Y. (1997). Heroin inhalation and progressive spongiform leukoencephalopathy. *N Engl J Med, 336*, 589-590.

Kril, J.L. & Halliday, G.M. (1999). Brain shrinkage in alcoholics: a decade on and what have we learned? *Prog Neurobiol, 58*, 381-387.

Kleinschmidt-DeMasters, B.K.; Rojiani, A.M.; & Filley, C.M. (2006). Central and extrapontine myelinolysis: then ... and now. *J Neuropathol Exp Neurol, 65*, 1-11.

Kohler, C.G.; Ances, B.M.; Coleman, A.R.; Ragland, J.D.; Lazarev, M.; & Gur, R.C. (2000). Marchiafava-Bignami disease: literature review and case report. *Neuropsychiatry Neuropsychol Behav Neurol, 13*, 67-76.

Lampl C; Yazdi K (2002). Central pontine myelinolysis. *Eur Neurol, 47*, 3-10.

Langford, T.D.; Letendre, S.L.; Larrea, G.J. & Masliah, E. (2003). Changing pattern in the neuropathogenesis of HIV during the HAART era. *Brain Pathol, 13*, 195-210.

Lim, K.O.; Choi, S.J.; Pomara, N.; Wolkin, A. & Rotrosen, J.P. (2002). Reduced frontal white matter integrity in cocaine dependence: A controlled diffusion tensor imaging study. *Biol Psychiatry*, *51*, 890-895.

Lyoo, I.K.; Streeter, C.C.; Ahn, K.H.; Lee, H.K.; Pollack, M.H.; Silveri, M.M.; Nassar, L.E.; Levin, J.M.; Sarid-Segal, O.; Ciraulo, D.A.; Renshaw, P.F. & Kaufman,M.J. (2004). White matter hyperintensities in subjects with cocaine and opiate dependence and healthy comparison subjects. *Psychiatry Res: Neuroimag*, *131*, 135-145.

Masliah, E.; Ge, N.; Morey, M.; DeTeresa, R.; Terry, R. & Wiley, C.A. (1992). Cortical dendritic pathology in human immunodeficiency virus encephalitis. *Lab Invest, 66*, 285-291.

Medana, I.M. & Esiri, M.M. (2003). Axonal damage: a key predictor of outcome in human CNS diseases. *Brain*, *126*, 515-530.

McArthur, J.C.; Kumar, A.J.; Johnson, D.W.; Selnes, O.A.; Becker, J.T.; Herman, C.; Cohen, B.A. & Saah, A. (1990). Incidental white matter hyperintensities on magnetic resonance imaging in HIV-1 infection. Multicenter AIDS Cohort Study. *J Acquir Immune Defic Syndr, 3*, 252-259.

Merrill, J.E.; Koyanagi, Y.; Zack, J.; Thomas, L.; Martin, F. & Chen, I.S. (1992). Induction of Interleukin 1 and tumor necrosis factor alpha in brain cultures by human immunodeficiency virus type 1. *J Virol, 66*, 2217-2221.

Mintzer, M.Z.; Copersino, M.L. & Stitzer, M.L. (2005). Opioid abuse and cognitive performance. *Drug Alc Depend, 78*, 225-230.

Montague, P.; McCallion, A.S.; Davies, R.W. & Griffiths, I.R. (2006). Myelin-associated oligodendrocytic basic protein: a family of abundant CNS myelin proteins in search of a function. *Dev Neurosci, 28*, 479-487.

Navia, B.A; Jordan, B.D. & Price, R.W. (1986). The AIDS dementia complex: I. Clinical features. *Ann Neurol, 19*, 517-524.

Navia, B.A.; Cho, E.S.; Petito, C.K. & Price, R.W. (1986). The AIDS dementia complex: II. Neuropathology. *Ann Neurol, 19*, 525-535.

Newell, K.L. & Kleinschmidt-DeMasters, B.K. (1996). Central pontine myelinolysis at autopsy: a twelve year retrospective analysis. *J Neurol Sci, 142*, 134-139.

Niess, C.; Grauel, U.; Toennes, S.W. & Bratzke, H. (2002). Incidence of axonal injury in human brain tissue. *Acta Neuropathol*, *104*, 79-84.

Norenberg, M.D. (1994). Astrocyte responses to CNS injury. *J Neuropathol Exp Neurol, 53*, 213-220.

Norenberg, M.D.; Leslie, K.O. & Robertson, A.S. (1982). Association between rise in serum sodium and central pontine myelinolysis. *Ann Neurol, 11*, 128-135.

Oehmichen, M.; Meißner, C.; Schmidt, V.; Pedal, I.; König, H.G. & Saternus, K.-S. (1998). Axonal injury: a diagnostic tool in forensic neuropathology? *Forensic Sci Int*, *95*, 67-83.

Olsen, W.L.; Longo, F.M.; Mills, C.M. & Norman, D. (1988). White matter disease in AIDS: findings at MR imaging. *Radiology, 169*, 445-448.

Pakesch, G.; Loimer, N.; Grünberger, J.; Pfersmann, D.; Linzmayr, L. & Mayerhofer, S. (1992). Neuropsychological findings and psychiatric symptoms in HIV-1 infected and noninfected drug users. *Psychiatry Res*, *41*, 163-177.

Parmantier, E.; Monge, M.; Yagello, M.; Cabon, F.; Demerens, C.; Gluckman, J.C. & Zalc, B. (1995). HIV-1 envelope glycoprotein gp120 does not bind to galactosylceramide-expressing rat oligodendrocytes. *Virology, 206*, 1084-1091.

Paxinos, G. & Mai, J.K.(2004) *The Human Nervous System* (2nd Ed.). San Diego, Academic Press/Elsevier.

Peavy, G.; Jacobs, D.; Salmon, D.P.; Butters, N.; Delis, D.C.; Taylor, M.; Massman, P.; Stout, J.C.; Heindel, W.C.; Kirson, D.; Atkinson, J.H.; Chandler, J.L.; Grant, I. (1994). Verbal memory performance of patients with human immunodeficiency virus infection: evidence of subcortical dysfunction. *J Clin Exp Neuropsychol, 16*, 508-523.

Pfefferbaum, A.; Rosenbloom, M.J.; Adalsteinsson, E. & Sullivan, E.V. (2007). Diffusion tensor imaging with quantitative fibre tracking in HIV infection and alcoholism comorbidity: synergistic white matter damage. *Brain, 130*, 48-64.

Pfefferbaum, A.; Adalsteinsson, E. & Sullivan, E.V. (2006a). Supratentorial profile of white matter microstructural integrity in recovering alcoholic men and women. *Biol Psychiatry, 59*, 364-372.

Pfefferbaum, A.; Adalsteinsson, E. & Sullivan, E.V. (2006b). Dysmorphology and microstructural degradation of the corpus callosum: Interaction of age and alcoholism. *Neurobiol Aging, 27*, 994-1009.

Polito, A. & Reynolds, R. (2005). NG2-expressing cells as oligodendrocyte progenitors in the normal and demyelinated adult central nervous system. *J Anat, 207*, 707-716.

Pomara, N.; Crandall, D.T.; Choi, S.J.; Johnson, G. & Lim, K.O. (2001). White matter abnormalities in HIV-1 infection: a diffusion tensor imaging study. *Psychiatry Res, 106*, 15-24.

Power, C.; Kong, P.A.; Crawford, T.O.; Wesselingh, S.; Glass, J.D.; McArthur, J.C. & Trapp, B. (1993). Cerebral white matter changes in acquired immunodeficiency syndrome dementia: alterations of the blood-brain-barrier. *Ann Neurol, 34*, 339-350.

Price, R.W.; Brew, B.J.; Sidtis, J.; Rosenblum, M.; Scheck, A.C. & Cleary, P. (1988). The brain in AIDS: central nervous system HIV-1 infection and AIDS dementia complex. *Science, 239*, 586-592.

Pulliam, L.; Herndier, B.G.; Tang, N.M. & McGrath, M.S. (1991). Human immunodeficiency virus-infected macrophages produce soluble factors that cause histological and neurochemical alterations in cultured human brains. *J Clin Invest, 87*, 503-512.

Pumarola-Sune, T.; Navia, B.A.; Cordon-Cardo, C, Cho, E.-K. & Price, R.W. (1987). HIV-antigen in the brain of patients with AIDS dementia complex. *Ann Neurol, 21*, 490-496.

Quarles, R.H. (2007). Myelin-associated glycoprotein (MAG): past, present and beyond. *J Neurochem, 100*, 1431-1448.

Radja, F.; Kay, D.G.; Albrecht, S. & Jolicoeur, P. (2003). Oligodendrocyte-specific expression of human immunodeficiency virus type 1 Nef in transgenic mice leads to vacuolar myelopathy and alters oligodendrocyte phenotype in vitro. *J Virol, 77*, 11745-11753.

Raja, F.; Sherriff, F.E.; Morris, C.S.; Bridges, L.R. & Esiri, M.M. (1997). Cerebral white matter damage in HIV infection demonstrated using APP-amyloid precursor protein immunoreactivity. *Acta Neuropathol, 93*, 184-189.

Rizzuto, N.; Morbin, M.; Ferrari, S.; Cavallaro, T.; Sparaco, M.; Boso, G. & Gaetti, L. (1997). Delayed spongiform leukoencephalopathy after heroin abuse. *Acta Neuropathol*, *94*, 87-90.

Robbins, D.S.; Shirzai, Y.; Drysdale, B.; Lieberman, A., Shin, H.S. & Shin, M.L. (1987). Production of cytotoxic factors for oligodendrocytes by stimulated astrocytes. *J Immunol, 139*, 2593-2597.

Rosenberg, N.L.; Kleinschmidt-DeMasters, B.K.; Davis, K.A.; Dreisbach, J.N.; Hormes, J.T. & Filley, C.M. (1988). Toluene abuse causes diffuse central nervous system white matter changes. *Ann Neurol, 23*, 611-614.

Rosse, R.B.; Riggs, R.L.; Dietrich, A.M.; Schwartz, B.L. & Deutsch, S.I. (1997). Frontal cortical atrophy and negative symptoms in patients with chronic alcohol dependence. J Neuropsychiatry *Clin Neurosci, 9*, 280-282.

Sacktor, N.; Lyles, R.H.; Skolasky, R.; Kleeberger, C.; Selnes, O.A.; Miller, E.N.; Becker, J.T. & McArthur, J.C. (2001). HIV-associated neurologic disease incidence changes: multicenter AIDS cohort study, 1990-1998. *Neurology, 56*, 257-260.

Scaravilli, F.; Gray, F.; Mikol, J. & Sinclair, E. (1993). Pathology of the central nervous system. In F. Scaravilli (Ed.), *The Neuropathology of HIV Infection*. pp. 99-170. Berlin: Springer Verlag.

Schlaepfer, T.E.; Lancaster, E.; Heidbreder, R.; Strain, E.C.; Kosel, M.; Fisch, H.-U. & Pearlson, G.D. (2007). Decreased frontal white-matter volume in chronic substance abuse. *Int J Neuropsychopharmacol, 9*, 147-153.

Schmidbauer, M.; Huemer, M.; Cristina, S.; Trabattoni, G.R. & Budka, H. (1992). Morphological spectrum, distribution and clinical correlation of white matter lesions in AIDS brains. *Neuropathol Appl Neurobiol, 18*, 489-501.

Selmaj, K.W. & Raine, C.S. (1988). Tumor necrosis factor mediates myelin and oligodendrocyte damage in vitro. *Ann Neurol, 23*, 339-346.

Sidtis, J.J.; Price, R.W. (1990). Early HIV-1 infection and the AIDS dementia complex. *Neurology, 40*, 323-326.

Simons, M. & Trotter, J. (2007). Wrapping it up: the cell biology of myelination. *Curr Opin Neurobiol, 17*, 533-540.

Sinclair, E. & Scaravilli, F. (1992). Detection of HIV proviral DNA in cortex and white matter of AIDS brains by non-isotopic polymerase chain reaction: correlation with diffuse poliodystrophy. *AIDS, 6*, 925-932.

Smith, R. (1992). The basic protein of CNS myelin: its structure and ligand binding. *J Neurochem, 59*, 1589-1608.

Smith, C.; Graham, D.I.; Geddes, J.F. & Whitwell, H.L. (2003). The interpretation of ß-APP immunoreactivity. *Acta Neuropathol*, *106*, 97-98.

Smith, T.W.; De Girolami, U.; Hénin, D.; Bolgert, F. & Hauw, JJ. (1990). Human immunodeficiency virus leucoencephalopathy and the microcirculation. *J Neuropathol Exp Neurol, 49*, 357-370.

Sotrel, A. & Dal Canto, M.C. (2000). HIV-1 and its causal relationship to immunosuppression and nervous system disease in AIDS: a review. *Hum Pathol, 31*, 1274-1298.

Stanley, L.C.; Mrak, R.E.; Woody, R.C.; Perrot, L.J.; Zhang, S.; Marshak, D.R.; Nelson, S.J.; Griffin, S.T. (1994). Glial cytokines as neuropathogenic factors in HIV infection: pathogenic similarities to Alzheimer's disease. *J Neuropathol Exp Neurol, 53*, 231-238.

Stebbins, G.T.; Smith, C.A.; Bartt, R.E.; Kessler, H.A.; Adeyemi, O.M.; Martin, E.; Cox, J.L.; Bammer, R. & Moseley, M.E. (2007). HIV-associated alterations in normal-appearing white matter: a voxel-wise diffusion tensor imaging study. *J Acquir Immune Defic Syndr, 46*, 564-573.

Sterns, R.H.; Riggs, J.E. & Schochet, S.S. (1986). Osmotic demyelination syndrome following correction of hyponatremia. *N Engl J Med, 314*, 1535-1542.

Strang, J.; Griffiths, P. & Gossop, M. (1997). Heroin smoking by 'chasing the dragon': origins and history. *Addiction, 92*, 673-683.

Strickland, T.L.; Mena, I.; Villanueva-Meyer, J.; Miller, B.L.; Cummings, J.; Mehringer, C.M.; Satz, P. & Myers,H. (1993). Cerebral perfusion and neuropsychological consequences of chronic cocaine use. *J Neuropsychiatry Clin Neurosci*, *5*, 419-427.

Tornatore, C.; Nath, A.; Amamiya, K. & Major, E.O. (1991). Persistent HIV-1 infection in human fetal glial cells reactivated by T-cell factor(s) or by cytokines tumor necrosis factor and interleukin 1 beta. *J Virol, 65*, 6094-6100.

Sullivan, E.V.; Marsh, L.; Mathalon, D.H.; Lim, K.O. & Pfefferbaum, A. (1996). Relationship between alcohol withdrawal seizures and temporal lobe white matter volume deficits. *Alcoholism Clin Exp Res, 20*, 348-354.

Trabert, W.; Betz, T.; Niewald, M. & Huber, G. (1995). Significant reversibility of alcoholic brain shrinkage within 3 weeks of abstinence. *Acta Psychiatr Scand, 92*, 87-90.

Tyor, W.R.; Glass, J.D.; Griffin, J.W.; Becker, P.S.; McArthur, .C.; Bezman, L.; Griffin,D.E. (1992). Cytokine expression in the brain during the aquired immunodeficiency syndrome. *Ann Neurol, 31*, 349-360.

Vitkovic, L.; Kalebic, T.; De Cunha, A. & Fauci, A.S. (1990). Astrocyte conditioned medium stimulates HIV-1 expression in a chronically infected promonocyte clone. *J Immunol, 30*, 153-160.

Volkow, N.D.; Valentine, A. & Kulkarni, M. (1988). Radiological and neurological changes in the drug abuse patient: a study with MRI. *J Neuroradiol*, *15*, 288-293.

Weis, S.; Neuhaus, B. & Mehraein, P. (1994). Activation of microglia in HIV-1 infected brains is not dependent on the presence of HIV-1 antigens. *NeuroReport, 5*, 1514-1516.

Weis, S.; Haug, H. & Budka, H. (1993). Astroglial changes in the cerebral cortex of AIDS brains: a morphometric and immunohistochemical investigation. *Neuropathol Appl Neurobiol, 19*, 329-225.

Weis, S.; Haug, H. & Budka, H. (1993). Neuronal damage of the cerebral cortex in AIDS. *Acta Neuropathol, 85*, 185-189.

Weis, S.; Bise, K.; Llenos, I.C. & Mehraein, P. (1992). Neuropathologic features of the brain in HIV-1 infection. In S. Weis & H. Hippius (Eds.), *HIV-1 Infection of the Central Nervous System. Clinical, Pathologic and Molecular Aspects.* pp. 159-190. Seattle: Hogrefe & Huber Publishers.

Wigley, R.; Hamilton, N.; Nishiyama, A.; Kirchhoff, F. & Butt, A.M. (2007). Morphological and physiological interactions of NG2-glia with astrocytes and neurons. *J Anat, 210*, 661-670.

Wiley, C.A.; Masliah, E.; Morey, M.; Lemere, C.; DeTeresa, R. Grafe, M.; Hansen, L. & Terry, R. (1991). Neocortical damage during HIV infection. *Ann Neurol, 29*, 651-657.

Wilkinson, I.D.; Miller, R.F.; Hall-Craggs, M.A.; Paley, M.N. & Harrison, M.J. (1998). Short echo-time proton magnetic resonance spectroscopy in regions of severe HIV-related diffuse white matter abnormality on MRI. *J NeuroAIDS, 2*, 55-67.

Wilkinson, D.A. (1982). Examination of alcoholics by computed tomographic (CT) scans. A critical reviews. *Alcohol Clin Exp Res, 6*, 31-45.

Wolters, E.C.; Stam, F.C.; Lousberg, R.J.; van Wijngaarden, G.K.; Rengelink, H.; Schipper, M.E.I. & Verbeeten, B. (1982). Leucoencephalopathy after inhaling "heroin" pyrolysate. *Lancet, 2*, 1233-1237.

Wright, D.G.; Laureno, R. & Victor, M. (1979). Pontine and extrapontine myelinolysis. *Brain, 102*, 361-385.

Yamanouchi, N.; Okada, S.-I.; Kodama, K.; Hirai, S.; Sekine, H.; Murakami, A.; Komatsu, N.; Sakamoto, T. & Sato, T. (1995). White matter changes caused by chronic solvent abuse. *Am J Neuroradiol, 16,* 1643-1649.

Yücel, M.; Takagi, M.; Walterfang, M. & Lubman, D.I. (2008). Toluene misuse and long-term harms: A systematic review of the neuropsychological and neuroimaging literature. *Neurosci Biobehav Rev, 32*, 910-926.

Zimatkin SM; Deitrich RA (1997). Ethanol metabolism in the brain. *Addiction Biol, 2*, 387-399.

In: Handbook on White Matter
Editors: T. B. Westland and R. N. Calton
ISBN: 978-1-60741-034-8

Chapter V

White Matter Changes in Critical Illness and Delirium

Max L. Gunther [*1, 2, 3], ***Carlos Faraco*** [4, 5] ***and Alessandro Morandi*** [1, 6, 7]

[1] Vanderbilt University Medical Center – Center for Health Services Research
[2] Vanderbilt University – Department of Radiological Sciences, Nashville, TN
[3] Vanderbilt University Medical Center – VUIIS,
Vanderbilt Institute of Imaging Sciences
[4] Paul D. Coverdell Neuroimaging Center – University of Georgia
[5] University of Georgia Department of Psychology
[6] Department of Internal Medicine and Geriatrics,
Poliambulanza Hospital, Via Bissolati - 57, Brescia, 25100 Italy
[7] Geriatric Research Group, Via Romanino 1, Brescia, 25122 Italy

Abstract

In the United States alone, over 50,000 individuals are treated daily in intensive care units (ICUs). Approximately 50-80% of ICU patients develop delirium with over half of these cases leading to meaningful and permanent losses in brain functioning. This suggests that critical illness may lead to de novo long-term pathological changes in the central nervous system. In the current chapter we review the evidence regarding links between white matter changes related to critical illness. In particular, we focus on both acute and distal alterations in white matter that may be caused by a number of factors including severe infection, glial cell atrophy, declines in axonal fractional anisotropy (FA) and global hypoperfusion. Evidence from several areas of the neurosciences (animal models, neuroimaging, case studies, etc.) suggest that delirium may be a hallmark of more permanent changes that are occurring in the CNS. Taken together, the current evidence suggests that critical illness may be linked to disruption of white matter

All correspondence and reprint requests should be sent to: Max L. Gunther, PhD; Center for Health Services Research; 6100 Medical Center East; Nashville, TN 37232-8300; Phone: 615-936-1010; Fax: 615-936-1269; Email: Max.Gunther@Vanderbilt.Edu; Web: www.ICUdelirium.org

tracts in the brain eventually leading to long-term deficits in cognitive functioning. The chapter concludes by highlighting several methodological challenges in investigating these hypotheses along with future directions within the field of delirium and critical illness neuroscience research.

Introduction

Approximately 50-80% of intensive care unit (ICU) patients develop delirium [1-3], a life threatening acute brain dysfunction that is associated with brain damage [4] and higher rates of death [5]. The Diagnostic and Statistical Manual of Mental Disorders (DSM IV) defines delirium as an acute change or fluctuation in mental status, inattention, and disorganized thinking or an altered level of consciousness [6]. In the United States alone, over 50,000 individuals are treated daily in the ICU with more than half of these cases experiencing meaningful losses in brain function, quality of life and the ability to live independently [4, 7-13]. Moreover an increasing number of older patients are being admitted to ICUs, and currently account for 42-52% of ICU admission and ~60% of all ICU days [14]. ICU delirium predicts a 3- to 11-fold increased risk of death at 6 months, even after controlling for relevant covariates such as severity of illness [5, 15].

Here we review the evidence linking delirium and critical illness with changes in white matter. Research indicates both acute and distal alterations in white matter during critical illness and delirium may be caused by a number of factors including degradation of blood brain barrier (BBB) integrity, disruption of myelin sheathing, severe infection, glial cell atrophy, declines in axonal fractional anisotropy (FA) and global brain hypoperfusion. Evidence from multiple lines of investigation in clinical fields and the neurosciences suggest that delirium may be a hallmark of more permanent changes occurring in the CNS. ICU patients might suffer from disruption of white matter tracts in the brain, eventually leading to long-term deficits in cognitive functioning. The impact of delirium on the development of white matter changes, especially when associated with critical illness, might be even more striking in elderly populations, who often have high comorbidity, baseline functional impairment and physiological changes that can hinder recovery from critical illness.

Although a firm understanding of the pathophysiological mechanisms of ICU delirium remains elusive, several theories have been proposed [13, 16-24] to explain the syndrome (see figures 1 and 2). Here we focus on factors linked to white matter changes in the brain during critical illness.

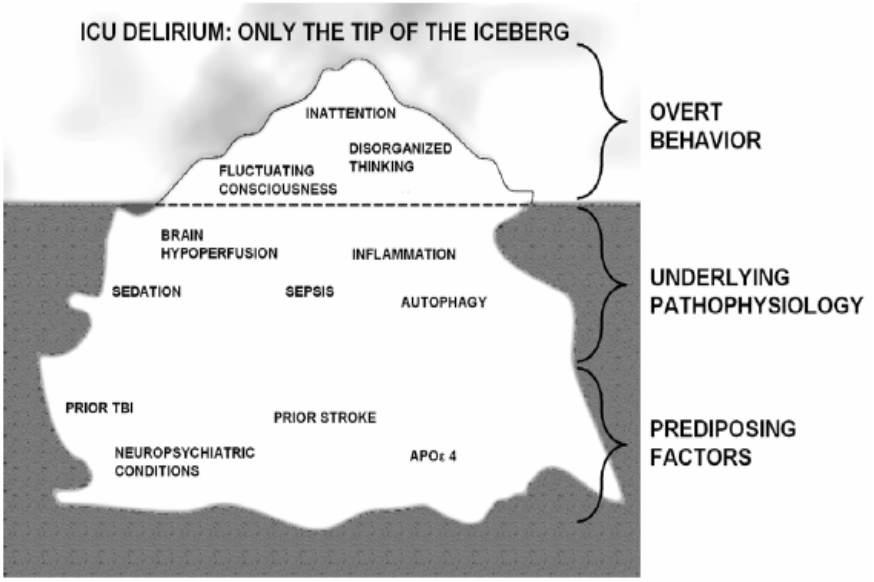

Figure 1. ICU delirium may only represent the behavioral "tip of the iceberg" related to massive underlying pathophysiological changes occurring in critically ill patients.

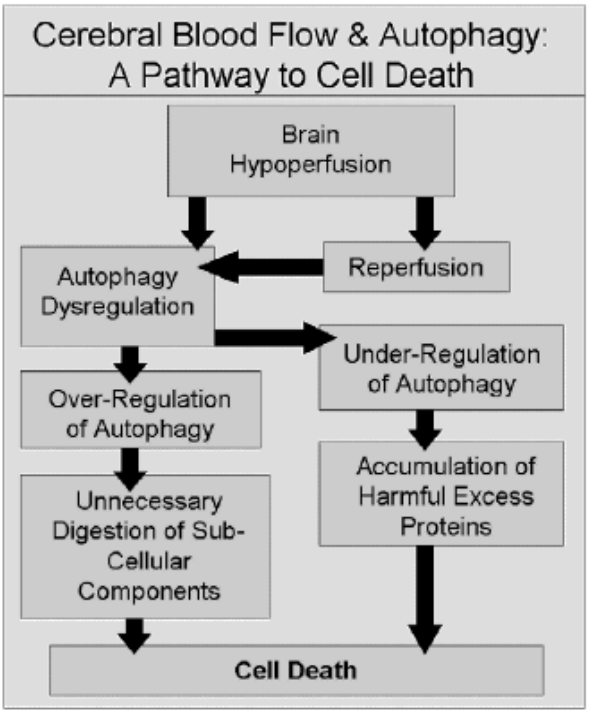

Figure 2. Brain hypoperfusion and reperfusion may lead to cell death by dysregulation of autophagic pathways.

The Role of White Matter in Healthy Cognitive Functioning

Before delving into ICU delirium linked white matter pathology, it may be useful to review our current understanding of the role of white matter in healthy individuals. White matter lesions (WML) are frequently seen on MRI studies of healthy elderly individuals [25]. MRI lesion prevalence rates in community-dwelling elderly samples are reported to range from 5.3% to 100% depending on study design, study population and assessment method [26, 27]. Destruction of white matter might be especially critical in late life, since white matter volume might decline with age more than gray matter volume [28]. WML have been reported and specifically linked to cognitive functions and physical performance in healthy elderly persons [29, 30]. In particular, periventricular and subcortical WML have been associated with decreased gait performance and memory decline respectively. Myelination of axons has increasingly been shown to be critical for healthy brain functioning [31] and predicts a wide range of neurocognitive abilities including working memory [32, 33] reading ability [33-35] and full scale IQ [36, 37]. Therefore WML may disrupt higher cortical functions involved in attention, memory, language, visuospatial ability, complex cognition, and emotion. The transmission speed of an action potential is dependent on myelin and because of this it is becoming increasingly clear that white matter integrity is critical for optimal cognitive functioning. A small revolution is currently underway in neuroscience whereby efforts are being refocused to answer key questions regarding the role of white matter for both normal and pathological behavior. Driving much of this has been the recent evidence that myelination is likely involved in key facets of brain plasticity, recovery from injury, as well as learning [33, 36, 38-40]. Previously, each of these roles had been primarily prescribed to grey matter function, where still most of the funding and research is conducted in neuroscience [39, 41]. For all of these reasons, the study of glial cells and oligodendrocytes has become a major focus of neuroscience and health services research [41]. As more data emerge linking various ailments to cognitive functioning, white matter integrity is likely to reveal new insights regarding the understanding and treatment of a wide range of brain related abilities.

Neuroimaging of Delirium

To expand our understanding of the role of white matter in delirium, it is necessary to explain this syndrome at multiple levels. Recent advances in magnetic resonance imaging (MRI), such as diffusion tensor imaging (DTI), have allowed researchers to answer important questions regarding the nature of ICU delirium. However, the initial links in the involvement of white matter and delirium came from more traditional anatomical images. We will begin by reviewing these [17, 42-53].

Several reports have documented long-term cognitive and behavioral sequelae of delirium, i.e. declines in intellectual functioning [4, 54, 55]. These are presumably attributable to underlying cellular changes in the brain. A number of studies have used CT or MRI to examine lesions or other structural abnormalities associated with delirium [17, 42-

53]. Frank hemorrhage or ischemia may cause delirium. In this scenario, [44-53], delirium is more likely to have been an effect rather than a result of stroke. Other studies, however, suggest that structural changes may have been caused by delirium [17, 42, 43]. An early CT study reported atrophy in the internal capsule in elderly psychiatric patients experiencing delirium compared to matched controls [56]. Furthermore, the degree of atrophy was related to patients' Mini Mental-State Examination (MMSE) scores. Patients in this study [56] also displayed cerebral infarctions and hemorrhages in frontal and parietal tracts. Some reports [53] have found little or no association between delirium and white matter neuropathology, yet others [17, 42] have suggested that major neuroanatomical changes may indeed occur in patients suffering from prolonged delirium. For example, CT scans revealed that 61% of critically ill patients were found to have either gross white matter atrophy, lesions or hyperintensities [42]. Another study [43] that examined the effects of electroconvulsive shock therapy (ECT) in delirious patients found white matter abnormalities and lesions in the basal ganglia. These reports have provided essential descriptions for potential links between myelin abnormalities and delirium [17, 42]. Future studies should address the presence and the consequences of white matter changes on cognition and physical functions in critically ill young and healthy elderly persons.

Critically ill patients facing an acute illness could also progressively develop a myoneuropathy caused by hypomobility and the presence of high levels of inflammation due to a septic process. Therefore, it should be also evaluated if white matter changes develop as a consequence of an acute brain dysfunction, These could act synergically with an acute myoneuropathy on the development of physical dysfunction following critical illness. In particular, elderly patients often present multiple comorbidities, malnutrition, immunosenescence and poor baseline functional status. Moreover they have physiological changes (i.e. cardiac, pulmonary, metabolic, renal and neurologic functions) that can foster a decline after an acute critical illness. It is even more important to avoid the occurrence of delirium and the potential development of white matter changes in a population already at high risk to develop cognitive and physical disabilities.

The studies described above highlight the links between white matter changes and acute delirium. It follows then that any changes to white matter that may occur during critical illness, even minor ones, have the potential to disrupt communication between neurons. Consider the following scenario. Two presynaptic neurons may have different distances from a given post-synaptic neuron. The propagation of a new action potential is dependent on the summation of the charges arriving. In order for the next action potential to be generated, both electrical signals must reach the soma of the neuron within milliseconds of each other [57]. Often this is not achieved by the change in resting potential via the input from a single dendrite; however, two signals that arrive simultaneously have more potential to create a large enough voltage response to trigger an action potential. If these input signals are coming from different distances, it is crucial that they arrive at the same time, or no new action potential will be generated. New evidence strongly suggests that myelination, which controls the speed of neuronal transmission in mammals, is the key element in the synchronization of these input signals [58]. Minor disruptions in the myelin sheath, either molecular or anatomical, may throw off the synchronicity of signals enough to disrupt normal central nervous system functioning to cause meaningful changes in cognition.

Conduction velocity is also regulated by an axon's thickness, its diameter, as well as the configuration of nodes of Ranvier all of which are influenced by myelination. As many of these factors are thought to be affected by conditions induced during critical illness (e.g. inflammation, and degradation of the blood brain barrier), asynchronous neuronal activity may result. Below we continue by examining how changes at the cellular and molecular levels during critical illness in white matter could impact cognitive functioning.

Sepsis

Sepsis is defined as a systemic inflammatory state caused by infection by acute gram negative bacteria and currently represents the most common causal factor for ICU delirium [59-61]. Multiple lines of investigation propose that sepsis is a gateway to acute delirium and brain damage via degradation of the blood brain barrier [62-76] that undoubtedly has a deleterious effect on both astrocytes and oligodendrocytes. The prevalence of delirium during sepsis ranges from 9% to 71% depending on diagnostic definitions [62, 63, 77]. A septic inflammatory cascade has the potential to decrease essential oxygen and nutrient delivery to cells by impairing capillary blood flow [73-75]. Elevated levels of tumor necrosis factor-alpha (TNF-α), interleukin-1 (IL-1) and other cytokines and chemokines that are released in response to lipopolysaccharide (LPS) can result in disseminated intravascular coagulation and promote leukocyte–vascular endothelium adhesion and induce endothelial damage [75, 78]. Therefore the brain damages caused by sepsis are related not only to a massive inflammatory cascade but also to a hypercoagulability status. The body's endogenous antithrombotic mechanism (i.e. protein C, protein S, tissue factor inhibitor, antithrombin) become impaired in septic patients. The presence of clots in the brain vessels could be seen as an explanation of development of WML. In particular, some reports have found that WML could be caused by cerebrovascular and cardiovascular diseases [79]. Therefore the process subtending these brain changes is likely due to cerebral hypoperfusion and ischemic lesions. Similarly, the septic cascade ultimately leads to hypotension and clot formations that can potentially be involved in the development of WML and delirium. Sharshar et al. [67] indeed have suggested that sepsis-induced encephalopathy may result from degradation of the blood brain barrier, leading to increased permeability, and recently reported that individuals who suffered from septic shock exhibited abnormal MRIs with varying degrees of encephalopathy and damage to white matter tracts [67]. Moreover, in sepsis the prolonged exposure to LPS may impair the axonal transport and therefore vital synaptic transmission [80]. Unfortunately, to date few studies have specifically examined the role of sepsis in delirium [42, 60, 63, 64, 67, 68, 72, 81, 82] with even fewer of these studies focusing on glial specific pathologies [42, 67, 82]. More basic lines of neuroscience, molecular and cell biology research suggest other pathways by which acute infections could lead to the disruption of white matter during critical illness [83].

Diffusion Imaging

Although traditional imaging studies of white matter in ICU patients using CT or typical MRI scanning parameters are useful, newer techniques are on the horizon that hold potential to greatly expand the understanding of both acute delirium and its long-term consequences. In the following section we briefly describe the basic methodological underpinnings of these new techniques (e.g. diffusion tensor imaging or DTI) and then report the findings related to white matter, critical illness and cognitive function. To date, no published studies that we are aware have used DTI to examine white matter changes in delirious individuals; however, a number of other investigations have provided clues for what one might expect by extrapolating DTI findings from similar cognitive conditions (e.g. schizophrenia, Alzheimer's disease, etc.).

MRI images typically come in two variations: images whose contrast is better able to define anatomy (T1-weighted) and images in which the contrast is better suited to examine pathology (T2-weighted). However, given that imaging parameters can be changed as needed, MRI is able to produce a wide variety of images that can be tailored to the nature of the specific question at hand. Recent advances in the field of MRI have led to what has been termed diffusion weighted imaging (DWI), which as the name implies, is used to detect the diffusion of water in a particular tissue of interest. In conditions where the diffusion of water may be impeded (e.g. an ischemic event) DWI can quantitatively record where these changes have occurred [84]. It is important to note that often these changes in water diffusion may not be evident using standard T1-weighted MRI or CT. Additionally, these changes are detectable within minutes of their occurrence [34, 85-90]. This is of particular importance for experimental animal models of delirium and brain changes, in that researchers could use small animal magnets to attempt to document the time course of changes in white matter diffusion following either experimentally induced delirium and or sepsis.

Although several types of magnetic resonance diffusion imaging exist, DWIs are the typical diffusion scans in a clinical setting. For this modality, the overall diffusion of water in 3D space is quantified by a scalar value known as the apparent diffusion coefficient (ADC); the ADC is easily calculated and provides enough information for differential diagnosis of many white matter pathologies. When diffusion is examined in 6 directions or more, the diffusion properties of the tissue at a particular image location (a voxel) can be more accurately described by a tensor. A tensor is a mathematical construct depicted as an ellipsoid (an elongated sphere) which is used to represent a vector field; in this case the vectors represent the three principal axes of diffusion. The diffusion axes are eigenvectors of the tensor, denoted v_1, v_2, and v_3. The strength of diffusion along diffusion axes are quantified by their corresponding eigenvalues, denoted λ_1, λ_2, and λ_3. The use of a tensor to describe diffusion characteristics acquired through MRI has become known as diffusion tensor imaging (DTI) and is becoming widely used in several clinical research applications.

A large amount of quantitative information is acquired during DTI scans. Therefore, the data is capable of providing much more than a simplistic (scalar) representation of the diffusion characteristics within a tissue. As just mentioned above, the eigenvectors composing the tensor indicate the three principal axes of diffusion. Using the corresponding eigenvalues, it is possible to calculate several measures of the diffusion properties of a tissue

of interest within a given voxel. The most commonly used measure is fractional anisotropy (FA), which describes how "anisotropic" diffusion is within a voxel; in other words, FA represents a measure of diffusion non-uniformity within a voxel. FA is calculated using the following equation:

$$FA = \sqrt{\frac{3}{2}} \sqrt{\frac{(\lambda_1 - \langle\lambda\rangle)^2 + (\lambda_2 - \langle\lambda\rangle)^2 + (\lambda_3 - \langle\lambda\rangle)^2}{\lambda_1^2 + \lambda_2^2 + \lambda_2^3}}$$

where $\langle\lambda\rangle$ represents the mean of the eigenvalues. In white matter, where factors such as intra-axonal organization, myelination, fiber diameter, and fiber orientation significantly constrict diffusion direction [91], v_1, the dominant axis of diffusion, will likely be of significantly greater magnitude than v_2 and v_3. As per the above equation, this will greatly influence FA values. The result is that voxels with v_1 of high magnitude will not only have high FA values but v_1 will also closely follow the orientation of the fiber pathway. An example of this can be seen in figure 3 where voxels running along the corpus callosum, a major white matter tract with high FA values, have tensors whose main eigenvector (v_1) is close to parallel to the orientation of the fibers . In contrast, voxels containing cerebrospinal fluid will have eigenvectors of similar magnitudes and adjacent voxels will have tensors that are likely in dissimilar orientations indicating no preferred direction of diffusion.

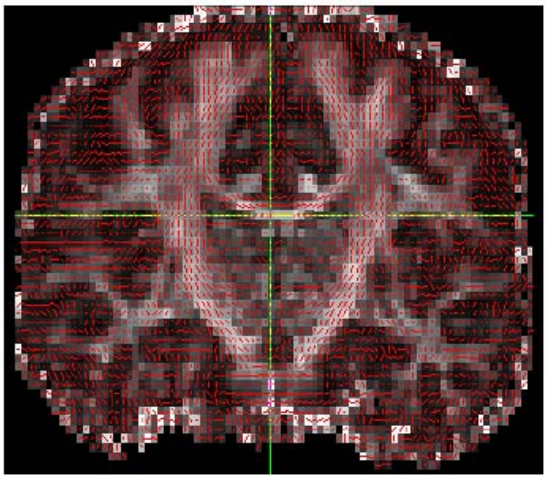

Figure 3. Coronal slice of FA map of the brain with the principal eigenvector (red lines) for each voxel overlaid on the image.

With the information provided by the tensors, it is also possible to track fiber pathways between different regions of interest, a method that has become known as tractography. It is important to note that tractography is usually performed in areas of white matter, where axons typically form cohesive fiber tracts, unlike in grey matter where axons are intermixed with the soma and do not form defined tracts. However, as diffusion imaging acquisition and tractography methods are becoming more advanced, tracking from or into the gray matter is becoming more common.

There are several ways that tractography may be performed; however, the most common method compares the orientation of the main eigenvectors within adjacent voxels. Voxels having similarly oriented eigenvectors are usually considered part of the same fiber tract. Tracking is terminated when the angle of curvature between the main eigenvectors in adjacent voxels is more acute than that specified by the user. Additionally, FA information can be employed to supplement fiber tracking; if a specific region has low FA values, it is likely that axons in that area do not constitute a cohesive tract of fibers. One of the major limitations with DTI tractography is that tensor data cannot distinguish between crossing fibers; that is, if fibers either cross or even touch briefly, DTI data is usually not acquired in sufficient directions to distinguish between the two, resulting in inaccurate fiber tracking.

Nonetheless, measures such as FA are also useful for group comparisons and could be used in determining whether ICU delirium causes immediate white matter changes in patients. For example, several studies have found FA values related to white matter degradation in schizophrenia. Although the etiology and course of ICU delirium may be very different from schizophrenia, there is a great deal of overlap in the acute presentation of these two syndromes [6, 23, 92-94]. Indeed, it may be possible to extract important information regarding ICU delirium from DTI studies in schizophrenics. Kanaan et al. reviewed [95] nineteen studies examining FA differences between schizophrenic patients and controls. They reported that schizophrenic patients were much more likely to exhibit reduced FA in the corpus callosum and the anterior cingulum; this is thought to indicate reduced white matter integrity in these areas. Other studies have shown decreased FA or inter-voxel coherence, a measure similar to FA, in the entorhinal cortex for schizophrenics compared to controls [96, 97]. Furthermore, multiple investigations have reported reduced FA values in the uncinate fasciculus, a section of the external capsule that connects frontal and temporal regions, key areas for the integration of sensory information that appears to be highly disrupted for patients with psychotic symptoms [98, 99]. In summary, DTI studies of schizophrenia provide several white matter regions of interest that could help to guide hypotheses regarding the disruption of cognitive processes in the critically ill.

DTI has also been used extensively to investigate dementia. Once again, although the etiology and course of the various types of dementia likely differ in important ways from ICU delirium, there are several similar neurocognitive and anatomical abnormalities that will likely offer insights to long-term cognitive impairment (LTCI) and acute brain dysfunction in ICU populations. Additionally, it appears that many of the areas found to have decreased FA in schizophrenia overlap with those in Alzheimer's Disease (AD). It is likely that these regions of common overlap are related to key cognitive processing regions that may also be implicated in ICU delirium and its associated LTCI. Medina et al. [100] stated that the most consistent finding across DTI studies of AD patients has been reduced FA in the corpus callosum, the temporal lobe, the parietal lobe, and the cingulum. These key cortical structures are thought to be some of the first to degrade in normal aging as well [101]. Medina et al, reported decreased FA mostly in posterior regions, which included structures such as the superior longitudinal fasciculus, arcuate fibers, and the posterior cingulum bundle. Because these regions tend to be more sensitive than most, they are likely to manifest the greatest impact when challenged during critical illness [101]. These areas have also been implicated in mild cognitive impairment (usually thought to be predictive of possible future dementia),

with decreased FA values only being more significant in the posterior cingulate sub-gyral white matter for the AD group. Yasmin et al. [102] performed a study in which they restricted DTI analysis to the uncinate fasciculus of AD patients and controls. Tractography was performed using seeding and tracking points to identify the axon pathway of interest. Results indicated significantly reduced FA values in the AD group. A study by Chen et al [103] found that AD patients with cerebrovascular lesions exhibited increased mean diffusivity (a scalar quantity representing the mean motion of water in all directions) compared to pure AD patients, in areas such as the dorsal medial thalamus, anterior thalamus, and the anterior and middle cingulate gyrus. It is important to note that areas identified as being affected by primary infarcts or lacunae were excluded when examining mean diffusivity values. As Chen et al. point out [103], this finding could be attributed to the fact that infarcts and the resulting lacunae could lead to demyelination as a result of anterograde degeneration, whereby atrophic processes occur to the post-synaptic neuron as a result of pre-synaptic neuronal cell death [104]. Similar processes may affect the critically ill as well. Taken together, these DTI investigations of AD have highlighted several white matter regions that may be especially sensitive to injury during critical illness, in particular for elderly populations.

DTI is extremely sensitive to neuroanatomical changes occurring in white matter regions and thus may represent a useful technique to pursue for both clinical and research investigations of ICU delirium. Since delirium is related to global brain hypoperfusion [69, 105, 106] it is possible that apoptotic or autophagic cell death is triggered as a result of lack of blood supply and or nutrients [107-111]. Furthermore, some of the same brain regions that have been shown to atrophy in normal aging, such as the medial prefrontal cortex and the hippocampus, are also more sensitive to hypoperfusion and may be sites of significant cell death during critical illness. Further progressive cognitive decline leading to LTCI may be caused by apoptotic cell death of neuroglia or astrocytes having been left in vulnerable states after hypoperfusion; this may cause microglia to release toxic amounts of glutamate causing surrounding neurons to fire excessively, initiating an excitotoxic anterograde cascade.

At present, no published studies that we are aware have employed DTI specifically to investigate ICU delirium and LTCI. For future studies examining this population, patients would ideally be scanned longitudinally, with one of the acquisitions occurring shortly after the delirious state. Such a data set would be able to better illuminate the deteriorative process that occurs with LTCI onset due to delirium by locating regions of reduced anisotropy. Given that LTCI is in the spectrum of dementing disorders, findings may be similar to those in AD patients, with fiber pathways such as the arcuate and uncinate fasciculus, cingulum bundle, and corpus callosum exhibiting reduced FA values.

Genetics

On the horizon, several molecular techniques appear to offer promising new means to investigate the relationships between delirium, LTCI, critical illness and white matter integrity. Recent advances in molecular genetics have begun to bridge gaps between bench science and bedside care. Dubbed, personalized medicine, the goal is to eventually be able to tailor healthcare to an individual's needs based on a patients' specific genotype and

phenotype. Genetic approaches may offer several opportunities to realize this goal and may also shed light on underlying metabolic and molecular mechanisms of acute brain dysfunction. One of the first genes that drew researcher's attention was the apoliprotein E (APOE) [112]. Because of delirium's links to dementia, this gene, which has been well studied in Alzheimer's disease patients, may provide clues regarding how individuals at risk for the development of early onset Alzheimer's disease could also be prone to delirium and LTCI. APOE is a 299 amino acid lipid binding protein with three common human isoforms (APOE 2, 3 and 4). In particular, the APOE4 variant is known to be associated with higher susceptibility for Alzheimer's disease [113] and has recently been implicated in increased duration of delirium for ICU patients [114]. These findings however remain somewhat controversial, c.f. Van Munster et al. [115]. Varying methodologies and patient populations may yield different results and larger more definitive investigations are warranted. Additionally, the individual contribution for each of these genetic influences requires more research. This line of investigation may eventually be able to aide in the implementation of personalized medicine in the ICU. A more refined understanding of genetic mechanisms of action will likely expand our understanding of delirium, its related long-term consequences and the development of preventive protocols.

References

[1] Halpern NA, Pastores SM, Greenstein RJ. Critical care medicine in the United States 1985-2000: an analysis of bed numbers, use, and costs. *Crit. Care Med.* 2004;32:1254-9.

[2] Pandharipande P, Costabile S, Cotton B, Morris J, Frizzell J, Fraley M, et al. Prevalence of delirium in surgical ICU patients. *Crit. Care Med.* 2005;33(12):A45.

[3] Pandharipande PP, Pun BT, Herr DL, Maze M, Girard TD, Miller RR, et al. Effect of Sedation With Dexmedetomidine vs Lorazepam on Acute Brain Dysfunction in Mechanically Ventilated Patients: The MENDS Randomized Controlled Trial. *JAMA*. 2007 December 12, 2007;298(22):2644-53.

[4] Jackson JC, Hart RP, Gordon SM, Shintani A, Truman B, May L, et al. Six-month neuropsychological outcome of medical intensive care unit patients. *Crit. Care Med.* 2003;31(4):1226-34.

[5] Ely EW, Shintani A, Truman B, Speroff T, Gordon SM, Harrell FE, Jr., et al. Delirium as a predictor of mortality in mechanically ventilated patients in the intensive care unit. *JAMA*. 2004;291(14):1753-62.

[6] APA. Diagnostic and Statistical Manual of Mental Disorders.; 1994.

[7] Ely EW, Evans GW, Haponik EF. Mechanical ventilation in a cohort of elderly patients admitted to an intensive care unit. *Ann. Intern. Med.* 1999;131(2):96-104.

[8] Ely EW, Inouye SK, Bernard GR, Gordon S, Francis J, May L, et al. Delirium in mechanically ventilated patients: validity and reliability of the confusion assessment method for the intensive care unit (CAM-ICU). *JAMA*. 2001;286(21):2703-10.

[9] Ely EW, Margolin R, Francis J, May L, Truman B, Dittus R. Evaluation of delirium in critically ill patients: validation of the Confusion Assessment Method for the Intensive Care Unit (CAM-ICU). *Crit. Care Med*. 2001;29:1370-9.

[10] Hopkins RO, Gale SD, Pope D, Weaver LK, Bigler ED. Ventricular enlargement in patients with acute respiratory distress syndrome. *Journal of the International Neuropsychological Society*. 2000;6:229-.

[11] Hopkins RO, Jackson JC. Long-term neurocognitive function after critical illness. *Chest.* 2006;130(3 (Print)):869-78.

[12] Gunther ML, Jackson JC, Ely EW. The Cognitive Consequences of Critical Illness: Practical Recommendations for Screening and Assessment. *Critical Care Clinics.* 2007;23:491–506.

[13] Gunther ML, Morandi A, Ely EW. Pathophysiology of Delirium in the Intensive Care Unit. *Critical Care Clinics.* 2008;24:45-65.

[14] Angus DC, Kelley MA, Schmitz RJ, White A, Popovich J, Jr. Caring for the critically ill patient. Current and projected workforce requirements for care of the critically ill and patients with pulmonary disease: can we meet the requirements of an aging population? *JAMA*. 2000;284(21):2762-70.

[15] Lin SM, Liu CY, Wang CH, Lin HC, Huang CD, Huang PY, et al. The impact of delirium on the survival of mechanically ventilated patients. *Crit. Care Med.* 2004;32(11):2254-9.

[16] Gunther ML, Jackson JC, Ely EW. Loss of IQ in the ICU: Brain Injury without the Insult. *Medical Hypotheses.* 2007(69):1179–82.

[17] Alsop DC, Fearing MA, Johnson K, Sperling R, Fong TG, Inouye SK. Interrelationship Between Delirium and Dementia. The role of neuroimaging in elucidating delirium pathophysiology. *J. Gerontol. A Biol. Sci. Med. Sci.* 2006;61A:1287-93.

[18] Marcantonio ER, Rudolph JL, Culley D, Crosby G, Alsop DC, Inouye SK. Interrelationship Between Delirium and Dementia. Serum biomarkers for delirium. *J. Gerontol. A Biol. Sci. Med. Sci.* 2006;61A:1281-6.

[19] Inouye SK, Ferrucci L. Elucidating the Pathophysiology of Delirium and the Interrelationship of Delirium and Dementia. Journals of Gerontology: Series A: *Biological Sciences and Medical Sciences.* 2006;61(12):1277-80.

[20] Van Der Mast RC, Fekkes D. Serotonin and amino acids: partners in delirium pathophysiology? *Semin. Clin. Neuropsychiatry*. 2000;5(2):125-31.

[21] Van Der Mast RC. Pathophysiology of delirium. *J. Geriatr. Psychiatry Neurol.* 1998;11:138-45.

[22] Trzepacz PT. Delirium. Advances in diagnosis, pathophysiology, and treatment. *Psychiatr. Clin. North Am.* 1996;19(3):429-48.

[23] Gupta N, de Jonghe J, Schieveld J, Leonard M, Meagher D. Delirium phenomenology: What can we learn from the symptoms of delirium? *Journal of Psychosomatic Research.* 2008;65(3):215-22.

[24] Gaudreau JD, Gagnon P, Roy MA, Harel F, Tremblay A. Association between psychoactive medications and delirium in hospitalized patients: a critical review. *Psychosomatics.* 2005;46(4):302-16.

[25] Ylikoski A, Erkinjuntti T, Raininko R, Sarna S, Sulkava R, Tilvis R. White Matter Hyperintensities on MRI in the Neurologically Nondiseased Elderly : Analysis of Cohorts of Consecutive Subjects Aged 55 to 85 Years Living at Home. *Stroke.* 1995 July 1, 1995;26(7):1171-7.

[26] de Leeuw FE, de Groot JC, Achten E, Oudkerk M, Ramos LMP, Heijboer R, et al. Prevalence of cerebral white matter lesions in elderly people: a population based magnetic resonance imaging study. The Rotterdam Scan Study. *J. Neurol. Neurosurg. Psychiatry.* 2001 January 1, 2001;70(1):9-14.

[27] Wen W, Sachdev P. The topography of white matter hyperintensities on brain MRI in healthy 60- to 64-year-old individuals. *Neuroimage.* 2004;22(1):144-54.

[28] Double KL, Halliday GM, Krill JJ, Harasty JA, Cullen K, Brooks WS, et al. Topography of brain atrophy during normal aging and alzheimer's disease. *Neurobiol. Aging.* 1996;17(4):513-21.

[29] Reinhold Schmidt SRCEKPSSHSPMMFF. White matter lesion progression, brain atrophy, and cognitive decline: The Austrian stroke prevention study. *Annals of Neurology.* 2005;58(4):610-6.

[30] GT W, T T, A L, RW B. A prospective study of cerebral white matter abnormalities in older people with gait dysfunction. . *Neurology.* 2001;57:990-4.

[31] Mabbott DJ, Noseworthy M, Bouffet E, Laughlin S, Rockel C. White matter growth as a mechanism of cognitive development in children. *Neuroimage.* 2006;33(3):936-46.

[32] Nestor PG, Kubicki M, Kuroki N, Gurrera RJ, Niznikiewicz M, Shenton ME, et al. Episodic memory and neuroimaging of hippocampus and fornix in chronic schizophrenia. *Psychiatry Research: Neuroimaging.* 2007;155(1):21-8.

[33] Gold BT, Powell DK, Xuan L, Jiang Y, Hardy PA. Speed of lexical decision correlates with diffusion anisotropy in left parietal and frontal white matter: Evidence from diffusion tensor imaging. *Neuropsychologia.* 2007;45(11):2439-46.

[34] Klingberg T, Hedehus M, Temple E, Salz T, Gabrieli JD, Moseley ME, et al. Microstructure of temporo-parietal white matter as a basis for reading ability: evidence from diffusion tensor magnetic resonance imaging. *Neuron.* 2000;25(2):493-500.

[35] Niogi SN, McCandliss BD. Left lateralized white matter microstructure accounts for individual differences in reading ability and disability. *Neuropsychologia.* 2006;44(11):2178-88.

[36] Schmithorst VJ, Wilke M, Dardzinski BJ, Holland SK. Cognitive functions correlate with white matter architecture in a normal pediatric population: a diffusion tensor MRI study. *Human Brain Mapping.* 2005;26(2):139-47.

[37] Miller EM. Intelligence and brain myelination: A hypothesis. *Personality and Individual Differences.* 1994;17(6):803-32.

[38] Yoshiura T, Mihara F, Ogomori K, Tanaka A, Kaneko K, Masuda K. Diffusion tensor in posterior cingulate gyrus: correlation with cognitive decline in Alzheimer's disease. *Neuroreport: For Rapid Communication of Neuroscience Research.* 2002;13(17):2299-302.

[39] Fields RD. White matter in learning, cognition and psychiatric disorders. *Trends Neurosci.* 2008;31(7):361-70.

[40] Fields RD, Stevens-Graham B. New insights into neuron-glia communication. *Science.* (New York, NY). 2002;298(5593):556-62.
[41] Fields RD. White matter matters. *Sci Am.* 2008;298(3):42-9.
[42] Hopkins RO, Gale SD, Weaver LK. Brain atrophy and cognitive impairment in survivors of acute respiratory distress syndrome. *Brain Inj.* 2006;20(3):263-71.
[43] Figiel GS, Coffey CE, Djang WT, Hoffman G, Jr., Doraiswamy PM. Brain magnetic resonance imaging findings in ECT-induced delirium. *The Journal Of Neuropsychiatry and Clinical Neurosciences.* 1990 Winter;2(1 (Print)):53-8.
[44] Vatsavayi V, Malhotra S, Franco K. Agitated delirium with posterior cerebral artery infarction. *J. Emerg. Med.* 2003;24:263-6.
[45] Castellanos-Pinedo F, Galindo R, Adeva-Bartolome MT, Zurdo M. A relapse of multiple sclerosis manifesting as acute delirium. *Neurologia.* 2004;19:323-5.
[46] Bogousslavsky J, Ferrazzini M, Regli F, Assal G, Tanabe H, Delaloye-Bischof A. Manic delirium and frontal-like syndrome with paramedian infarction of the right thalamus. *J. Neurol. Neurosurg. Psychiatry.* 1988;51:116-9.
[47] Ogasawara K, Komoribayashi N, Kobayashi M. Neural damage caused by cerebral hyperperfusion after arterial bypass surgery in a patient with moyamoya disease: case report. *Neurosurgery.* 2005;56:E1380.
[48] Takanashi J, Barkovich AJ, Shiihara T. Widening spectrum of a reversible splenial lesion with transiently reduced diffusion. *AJNR Am. J. Neuroradiol.* 2006;27:836-8.
[49] Tada H, Takanashi J, Barkovich AJ. Clinically mild encephalitis/encephalopathy with a reversible splenial lesion. *Neurology.* 2004;63:1854-8.
[50] Doherty MJ, Jayadev S, Watson NF, Konchada RS, Hallam DK. Clinical implications of splenium magnetic resonance imaging signal changes. *Arch. Neurol.* 2005;62:433-7.
[51] Roach RC, Hackett PH. Frontiers of hypoxia research: acute mountain sickness. *J. Exp. Biol.* 2001;204:3161-70.
[52] Naughton BJ, Moran M, Ghaly Y, Michalakes C. Computed tomography scanning and delirium in elder patients. *Acad. Emerg. Med.* 1997;4:1107-10.
[53] Kishi Y, Iwasaki Y, Takezawa K, Kurosawa H, Endo S. Delirium in critical care unit patients admitted through an emergency room. *Gen. Hosp. Psychiatry.* 1995;17(5):371-9.
[54] Hopkins RO, Weaver LK, Collingridge D, Parkinson RB, Chan KJ, Orme JF, Jr. Two-Year Cognitive, Emotional, and Quality-of-Life Outcomes in Acute Respiratory Distress Syndrome. *Am. J. Respir. Crit. Care Med.* 2005;171(4):340-7.
[55] Wacker P, Nunes PV, Cabrita H, Forlenza OV. Post-operative delirium is associated with poor cognitive outcome and dementia. *Dement. Geriat. Cogn. Disord.* 2006;21 221-7.
[56] Koponen H, Hurri L, StenbÃ¤ck U, Mattila E, Soininen H, Riekkinen PJ. Computed tomography findings in delirium. *The Journal Of Nervous And Mental Disease.* 1989;177(4 (Print)):226-31.
[57] Kandel ERS, J. H.; Jessell, T. M. *Principles of Neural Science.* 1991.
[58] Lang EJ, Rosenbluth J. Role of myelination in the development of a uniform olivocerebellar conduction time. *J. Neurophysiol.* 2003;89(4):2259-70.

[59] Girard TD, Ely EW. Bacteremia and sepsis in older adults. *Clinics In Geriatric Medicine.* 2007;23(3):633-47.

[60] Girard TD, Opal SM, Ely EW. Insights into severe sepsis in older patients: from epidemiology to evidence-based management. *Clinical Infectious Diseases: An Official Publication Of The Infectious Diseases Society Of America.* 2005;40(5):719-27.

[61] Girard TD, Shintani A, Pun BT, Miller RR, Ely EW. The effect of delirium on mortality appears greater in severe sepsis than in non-infectious critical illness. *Proc. Am. Thorac. Soc.* 2006;3:A501.

[62] Zauner C, Gendo A, Kramer L, Funk GC, Bauer E, Schenk P, et al. Impaired subcortical and cortical sensory evoked potential pathways in septic patients. *Critical Care Medicine*. 2002;30:1136-9.

[63] Bello JHSM, Park M. Sepsis-associated encephalopathy as a differential diagnosis with motor deficit plus altered mental status. *Clinics.* 2007;62:199-202.

[64] Ebersoldt M, Sharshar T, Annane D. Sepsis-associated delirium. *Intensive Care Medicine.* 2007;33(6):941-50.

[65] Freund HR, Muggia-Sullam M, Peiser J, Melamed E. Brain neurotransmitter profile is deranged during sepsis and septic encephalopathy in the rat. *J. Surg. Res.* 1985;38(3):267-71.

[66] Jeppsson B, Freund HR, Gimmon Z, James JH, von Meyenfeldt MF, Fischer JE. Blood-brain barrier derangement in sepsis: cause of septic encephalopathy? *Am. J. Surg.* 1981;141(1):136-42.

[67] Sharshar T, Carlier R, Bernard F, Guidoux C, Brouland JP, Nardi O, et al. Brain lesions in septic shock: a magnetic resonance imaging study. *Intensive Care Med.* 2007;33:798-806.

[68] Guidoux C, Sharshar T, Annane D. Sepsis-Induced Brain Dysfunction. *Mechanisms of Sepsis-Induced Organ Dysfunction and Recovery*; 2007. p. 407-14.

[69] Bowton DL, Bertels NH, Prough DS, Stump DA. Cerebral blood flow is reduced in patients with sepsis syndrome. *Crit. Care Med.* 1989;17(5):399-403.

[70] Sharshar T, Annane D, Gradmaison GL, Brouland JP, Hopkinson NS, Gray F. *The Neuropathology of Septic Shock. Brain Pathology*. 2004;14(1):21-33.

[71] Gray F, Sharshar T, Lorin de La Grandmaison G, Annane D. Neuropathology of septic shock. *Neuropathology and Applied Neurobiology.* 2002;28:159.

[72] Sprung CL, Peduzzi PN, Shatney CH, Schein RM, Wilson MF, Sheagren JN, et al. Impact of encephalopathy on mortality in the sepsis syndrome. *Crit. Care Med.* 1990;18(8):801-6.

[73] Opal SM, Esmon CT. Bench-to-bedside review: functional relationships between coagulation and the innate immune response and their respective roles in the pathogenesis of sepsis**.** *Crit. Care.* 2003;7(1):23-38.

[74] Terborg C, Schummer W, Albrecht M, Reinhart K, Weiller C, Röther J. Dysfunction of vasomotor reactivity in severe sepsis and septic shock. *Intensive Care Medicine.* 2001;27(7):1231-4.

[75] Goyette RE, Key NS, Ely EW. Hematologic changes in sepsis and their therapeutic implications. *Sem. Respir. Crit. Care Med*. 2004;25:645-59.

[76] Wheeler AP, Bernard GR. Treating patients with severe sepsis. *N. Engl. J. Med.* 1999;340(3):207-14.

[77] Young GB, Bolton CF, Austin TW, Archibald YM, Gonder J, Wells GA. The encephalopathy associated with septic illness. *Clin. Invest. Med.* 1990;13(6):297-304.

[78] Wheeler AP, Bernard GR. Treating patients with severe sepsis. *The New England Journal of Medicine.* 1999;340(3):207-14.

[79] Breteler MMB, van Swieten JC, Bots ML, Grobbee DE, Claus JJ, van der Hout JHW, et al. Cerebral white matter lesions, vascular risk factors, and cognitive function in a population-based study: the Rotterdam study. *Neurology.* 1994;44:1246–52.

[80] Ian C. Hellstrom MDGNLSW. Chronic LPS exposure produces changes in intrinsic membrane properties and a sustained IL-?-dependent increase in GABAergic inhibition in hippocampal CA1 pyramidal neurons. *Hippocampus.* 2005;15(5):656-64.

[81] Jeppson B, Freund H, Gimmon Z. Blood-brain barrier derangement in sepsis: cause of septic encephalopathy? *Am. J. Surg.* 1981;141:136-42.

[82] Sharshar T, Hopkinson NS, Orlikowski D, Annane D. Science review: the brain in sepsis - culprit and victim. *Critical Care Forum.* 2004;8 Published online.

[83] Uchikado H, Akiyama H, Kondo H, Ikeda K, Tsuchiya K, Kato M, et al. Activation of vascular endothelial cells and perivascular cells by systemic inflammation-an immunohistochemical study of postmortem human brain tissues. *Acta Neuropathol.* (Berl). 2004;107(4):341-51.

[84] J. Pfeuffer WD, E. Sykova, D. Leibfritz,. Water signal attenuation in diffusion-weighted 1H NMR experiments during cerebral ischemia: influence of intracellular restrictions, extracellular tortuosity, and exchange. *Magn. Reson. Imaging.* 1998;16:1023-32.

[85] Wang C, Stebbins GT, Nyenhuis DL, deToledo-Morrell L, Freels S, Gencheva E, et al. Longitudinal changes in white matter following ischemic stroke: A three-year follow-up study. *Neurobiol. Aging.* 2006;27(12):1827-33.

[86] Bammer R, Acar B, Moseley ME. In vivo MR tractography using diffusion imaging. *Eur. J. Radiol.* 2003;45(3):223-34.

[87] Moseley M, Bammer R, Illes J. Diffusion-tensor imaging of cognitive performance. *Brain and Cognition.* 2002;50(3):396-413.

[88] Skare S, Hedehus M, Moseley ME, Li T-Q. Condition Number as a Measure of Noise Performance of Diffusion Tensor Data Acquisition Schemes with MRI. *J. Magn. Reson.* 2000;147(2):340-52.

[89] Lim KO, Hedehus M, Moseley M, de Crespigny A, Sullivan EV, Pfefferbaum A. Compromised white matter tract integrity in schizophrenia inferred from diffusion tensor imaging. *Arch. Gen. Psychiatr.* 1999;56:367.

[90] Moseley ME, Kucharczyk J, Mintorovitch J. Diffusion-weighted MR imaging of acute stroke: correlation with T2-weighted and magnetic susceptibility-enhanced MR imaging in cats. *AJNR Am. J. Neuroradiol.* 1990;11:423-9.

[91] Pierpaoli C, Jezzard P, Basser PJ, Barnett A, Di Chiro G. Diffusion tensor MR imaging of the human brain. *Radiology.* 1996 December 1, 1996;201(3):637-48.

[92] Meagher DJ, MacLullich AMJ, Laurila JV. Defining delirium for the International Classification of Diseases, 11th Revision. *J. Psychosom. Res.* 2008;65(3):207-14.

[93] O'Malley G, Leonard M, Meagher D, O'Keeffe ST. The delirium experience: A review. *J. Psychosom. Res.* 2008;65(3):223-8.

[94] Kean J, Ryan K. Delirium detection in clinical practice and research: Critique of current tools and suggestions for future development. *J. Psychosom. Res.* 2008;65(3):255-9.

[95] Kanaan RAA, Kim J-S, Kaufmann WE, Pearlson GD, Barker GJ, McGuire PK. Diffusion Tensor Imaging in Schizophrenia. *Biological Psychiatry.* 2005;58(12):921-9.

[96] Schlösser RGM, Nenadic I, Wagner G, Güllmar D, von Consbruch K, Köhler S, et al. White matter abnormalities and brain activation in schizophrenia: A combined DTI and fMRI study. *Schizophr. Res.* 2007;89(1-3):1-11.

[97] Schmierer K, Wheeler-Kingshott CAM, Boulby PA, Scaravilli F, Altmann DR, Barker GJ, et al. Diffusion tensor imaging of post mortem multiple sclerosis brain. *Neuroimage.* 2007;35(2):467-77.

[98] Seal ML, Yücel M, Fornito A, Wood SJ, Harrison BJ, Walterfang M, et al. Abnormal white matter microstructure in schizophrenia: A voxelwise analysis of axial and radial diffusivity. *Schizophr. Res.* 2008;101(1-3):106-10.

[99] Mori T, Ohnishi T, Hashimoto R, Nemoto K, Moriguchi Y, Noguchi H, et al. Progressive changes of white matter integrity in schizophrenia revealed by diffusion tensor imaging. *Psychiatry Research: Neuroimaging.* 2007;154(2):133-45.

[100] Medina D, deToledo-Morrell L, Urresta F, Gabrieli JDE, Moseley M, Fleischman D, et al. White matter changes in mild cognitive impairment and AD: A diffusion tensor imaging study. *Neurobiol. Aging.* 2006;27(5):663-72.

[101] Buckner RL, Snyder AZ, Shannon BJ, LaRossa G, Sachs R, Fotenos AF, et al. Molecular, Structural, and Functional Characterization of Alzheimer's Disease: Evidence for a Relationship between Default Activity, Amyloid, and Memory. *J. Neurosci.* 2005 August 24, 2005;25(34):7709-17.

[102] Yasmin H, Nakata Y, Aoki S, Abe O, Sato N, Nemoto K, et al. Diffusion abnormalities of the uncinate fasciculus in Alzheimer's disease: diffusion tensor tract-specific analysis using a new method to measure the core of the tract. *Neuroradiology.* 2008;50(4):293-9.

[103] Chen S, Kang Z, Hu X, Zou Y. Diffusion tensor imaging of the brain in patients with Alzheimer's disease and cerebrovascular lesions. *Journal of Zhejiang University.* 2007;8(4):242-7.

[104] Gold G, Kovari E, Herrmann FR, Canuto A, Hof PR, Michel JP, et al. Cognitive consequences of thalamic, basal ganglia, and deep white matter lacunes in brain aging and dementia. *Stroke.* 2005;36(6):1184-8.

[105] Fong TG, Bogardus ST, Daftary A. Interrelationship Between Delirium and Dementia. Cerebral perfusion changes in older delirious patients using 99mTc HMPAO SPECT. *J. Gerontol. A Biol. Sci. Med. Sci.* 2006;61A:1294-9.

[106] Yokota H, Ogawa S, Kurokawa A, Yamamoto Y. Regional cerebral blood flow in delirium patients. *J. Psychiatry Clin. Neurosci.* 2003;57:337-9.

[107] Mizushima N, Levine B, Cuervo AM, Klionsky DJ. Autophagy fights disease through cellular self-digestion. *Nature*. 2008;451(7182):1069-75.

[108] Adhami F, Schloemer A, Kuan C-Y. The roles of autophagy in cerebral ischemia. *Autophagy*. 2007 01/18/2007 Jan-Feb;3(1):42-4.

[109] Adhami F, Liao G, Morozov YM, Schloemer A, Schmithorst VJ, Lorenz JN, et al. Cerebral ischemia-hypoxia induces intravascular coagulation and autophagy. *The American Journal of Pathology*. 2006 08;169(2):566-83.

[110] Chang RC-C, Yu M-S, Lai CS-W. Significance of molecular signaling for protein translation control in neurodegenerative diseases. *Neuro-Signals*. 2006 05/10/2006-2007;15(5):249-58.

[111] Yorimitsu T, Klionsky DJ. Autophagy: molecular machinery for self-eating. *Cell Death Differ*.12(S2):1542-52.

[112] Hixson JE, Vernier DT. Restriction isotyping of human apolipoprotein E by gene amplification and cleavage with HhaI. *J. Lipid Res.* 1990;31(3):545-8.

[113] Corder EH, Saunders AM, Strittmatter WJ, Schmechel DE, Gaskell PC, Small GW, et al. Gene dose of apolipoprotein E type 4 allele and the risk of Alzheimer's disease in late onset families. *Science.* 1993;261(5123):921-3.

[114] Ely EW, Girard TD, Shintani AK, Jackson JC, Gordon SM, Thomason JWW, et al. Apolipoprotein E4 polymorphism as a genetic predisposition to delirium in critically ill patients. *Critical Care Medicine.* 2007;35(1):112-7.

[115] Van Munster BC, Korevaar JC, de Rooij SE, Levi M, Zwinderman AH. The association between delirium and the apolipoprotein E4 allele in the elderly. *Psychiatric Genetics.* 2007;17(5):261-6.

In: Handbook on White Matter
Editors: T. B. Westland and R. N. Calton
ISBN: 978-1-60741-034-8

Chapter VI

White Matter Involvement in Neuromuscular Disorders

Petr Vondracek[1], Marketa Hermanova[2], Kristina Vodickova[*3], Lenka Fajkusova [4], Eva Brichtová[5] and Jarmila Skotakova[6]

[1] Department of Pediatric Neurology, University Hospital and Masaryk University, Brno, Czech Republic
[2] Department of Pathology, St.Anne´s Hospital and Masaryk University, Brno, Czech Republic
[3] Department of Pediatric Ophthalmology, University Hospital and Masaryk University, Brno, Czech Republic
[4] Center of Molecular Biology and Gene Therapy, University Hospital, Brno, Czech Republic
[5] Department of Pediatric Neurosurgery, University Hospital and Masaryk University, Brno, Czech Republic
[6] Department of Pediatric Radiology, University Hospital and Masaryk University, Brno, Czech Republic

Abstract

The frequency of inherited neuromuscular disorders in the human population is estimated to be approximately 1:3,500 worldwide. In some of these disorders there is an association of the neuromuscular and central nervous system (CNS) involvement. The explanation could be in a faulty process of expression of genetic information into the structure of vital proteins, which play a key role in both muscle and brain functions. In these multiorgan disorders a muscular dystrophy or peripheral neuropathy can be combined with the white matter lesion, or other structural abnormalities of the brain, eye, and other organs, and this combination can result in a spectrum of unusual clinical phenotypes.

[*] Correspondence to: P. Vondracek, MD, PhD, Department of Pediatric Neurology, University Hospital, Cernopolni 9, 625 00 Brno, Czech Republic. tel.: +420-5-3223 4934, e-mail: pvondracek@fnbrno.cz

The central nervous system involvement can be found especially in congenital muscular dystrophies (CMD, MDC), myotonic dystrophy types 1 and 2 (DM1, DM2), mitochondrial encephalomyopathies, and some variants of Charcot-Marie-Tooth disease (CMT).

Our research is focused on these important hereditary neuromuscular disorders with the white matter involvement in pediatric patients, especially children afflicted with various forms of congenital muscular dystrophies. We present most interesting and unusual case reports of our patients to demonstrate difficulties and pitfalls in the diagnostics of these rare disorders. The white matter lesion is a very important and valuable diagnostic sign, and also could have a serious impact on the management and prognosis of patients with neuromuscular disorders.

Keywords: congenital muscular dystrophy; MDC1A; mitochondrial encephalomyopathy; myotonic dystrophy; merosin; α-dystroglycan; X-linked Charcot-Marie-Tooth disease; CMTX1; connexin 32; CMT4D

1. Introduction

Inherited neuromuscular disorders are relatively frequent and often devastating diseases in both pediatric and adult patients, presenting not only medical but also a very serious social and economic problem of the modern world. The frequency of these disorders in the human population is estimated to be 1:3,500 worldwide (Emery, 1991). There are approximately 200,000 people affected in Europe (http://www.treat-nmd.eu). The United States, European Union, Japan and other developed countries provide enormous financial and material support to promote a scientific research of these diseases on the ground of sofisticated molecular genetic methods (http://www.treat-nmd.eu). Many recent advances have already been made in understanding mechanisms by which gene mutations cause degeneration of neurons, peripheral nerves and muscles. This progress of research in the field of inherited neuromuscular disorders holds great promise for the development of novel therapeutic strategie in the near future.

There is a very interesting and often surprising association of the neuromuscular and central nervous system (CNS) involvement in some of these disorders. The explanation could be in a faulty process of expression of genetic information into the structure of vital proteins, which play a key role in both muscle and brain functions. In these multiorgan disorders a muscular dystrophy or peripheral neuropathy can be combined with the white matter lesion, or other structural abnormalities of the brain, eye, and this combination can result in a spectrum of unusual clinical phenotypes.

White matter is the brain region underlying the gray matter cortex, composed of neuronal fibers coated with electrical insulation called myelin. Previously of interest in demyelinating diseases such as multiple sclerosis, myelin is attracting new interest as an unexpected contributor to a wide range of psychiatric disorders, including depression and schizophrenia (Fields RD, 2008). The white matter changes on the brain MRI were originally descibed in patients with merosin–deficient CMD with primary laminin α2 deficiency and concomitant reduction of α-dystroglycan (MDC1A) (Philpot, 1995; Philpot, 1999; Mercuri,

1995). The central nervous system involvement including white matter changes can be found especially in the following groups of neuromuscular disorders:

1. Congenital muscular dystrophies (CMD, MDC)
2. Myotonic dystrophy types 1 and 2 (DM1, DM2)
3. Mitochondrial encephalomyopathies
4. Charcot-Marie-Tooth disease (CMT) and related disorders (Congenital Cataracts Facial Dysmorphism Neuropathy syndrome and Marinesco-Sjögren syndrome (CCFDN, MSS)

In a large portion of patients with Duchenne muscular dystrophy (DMD) a cognitive impairment due to a deficient expression of dystrophin in the brain can be found, but no structural changes of the white matter were demostrated on the brain MRI. The recent findings on the role of dystrophin in the CNS have implications for the clinical management of boys with DMD (Anderson, 2002).

Our research is mainly focused on those interesting hereditary neuromuscular disorders with the white matter involvement in pediatric patients, especially children afflicted with various forms of congenital muscular dystrophies. We present most interesting and unusual case reports of our patients to demonstrate difficulties and pitfalls in the diagnostics of these rare disorders.

1.1. Congenital Muscular Dystrophies

The congenital muscular dystrophies (CMD, MDC) are a large group of clinically and genetically heterogenous disorders with autosomal recessive inheritance. A classification of CMD variants is based on clinical features and the primary or secondary protein defect due to mutations in responsible genes (Muntoni, 2004). Eleven genes causing specific CMD phenotypes have so far been identified (Jimenez-Mallebrera, 2005). Other clinically and genetically different forms of CMD have also been described. Is is therefore supposed, that at least 20 causal genes responsible for various CMD phenotypes will eventually be identified (Muntoni, 2004).

The central nervous system involvement is typically seen in merosin–deficient CMD with primary laminin α2 deficiency and concomitant reduction of α-dystroglycan (MDC1A). Brain magnetic resonance imaging (MRI) studies reveal white matter changes in all affected individuals. Brain and eye are severely involved in α-dystroglycanopathies – Fukuyama CMD (FCMD), Walker Warburg syndrome (WWS), Muscle-eye-brain disease (MEB), some cases of MDC1C, and MDC1D (Muntoni, 2004).

In patients with **MDC1A** brain MRI studies invariably show white matter changes after the age of 6 months. These changes can be demonstrated as increased signal intensity of white matter on T2-weighted MRI and are diffuse, although sparing the internal capsule, corpus callosum, basal ganglia, thalami, and cerebellum. Using fast-spin echo MRI sequence, these changes can be revealed already at birth. All patients with proven mutation in the *LAMA2* gene on chromosome 6q22 responsible for a complete laminin α2 deficiency were reported to have white matter changes after the age of 6 months (Muntoni, 2004). In addition

to the white matter lesion, structural abnormalities of the brain, such as polymicrogyria, agyria, hypoplasia of pons and cerebellum, have been reported in some patients with complete or mutation-proven partial laminin α2 deficiency (Philpot, 1999).

The cognitive functions are normal in MDC1A patients, however occipital agyria is associated with mental retardation. Epilepsy is a frequent complication of MDC1A and can affect up to 30% of cases (Muntoni, 2004). Visual (VEPs) and somatosensory (SEPs) evoked potentials are usually abnormal and demonstrate the impairment of central nervous pathways (Mercuri, 1995). Nerve conduction studies reveal a motor or sensory motor demyelinating neuropathy. In addition to muscular dystrophy, the lesion of both central and peripheral myelin can be demonstrated in MDC1A patients. MDC1A is the most frequent CMD variant in western countries and represents approximately 40% of cases.

The pathophysiology of white matter changes in MDC1A is not quite clear. Laminin α2 is expressed in various structures of the human brain. It was found in the basement membrane of blood vessels including the capillaries that form the blood-brain barrier, and also along developing axon tracts, where it might have a role in myelin membrane formation in oligodendocytes (Buttery PC, 1999). The quantitative proton magnetic resonance spectroscopy (MRS) of cerebral metabolites revealed a consistent pattern in the affected white matter. Reduced concentrations of N-acetylaspartate and N-acetylaspartylglutamate, creatine, and phosphocreatine, and to a milder degree of choline-containing compounds were detected. In contrast, concentrations of myo-inositol were in the normal range. Spectra of cortical and subcortical grey matter were normal. The observed metabolite profile is consistent with the white matter edema, that is reduced cellular density, and relative astrocytosis. This interpretation is in line with the hypothesis that laminin α2 deficiency results in leakage of fluids across the blood-brain barrier and a histopathological report of astrocytic proliferation (Brockmann K, 2007).

There is a severe brain involvement in other CMD variants collectively referred to as α-dystroglycanopathies – Fukuyama CMD (FCMD), Walker Warburg syndrome (WWS), Muscle-eye-brain disease (MEB), some cases of MDC1C, and MDC1D (Muntoni, 2004). In these disorders mutations in various genes involved in the process of glycosylation of α-dystroglycan result in a severe muscle and brain pathology. These brain abnormalities are recognised as part of the type II lissencephaly spectrum which encompasses the „cobblestone“ polymicrogyria-pachygyria or the complete agyria. The regular layering of the cerebral cortex is lost, and overmigration of neurons beyond the glia limitans into the leptomeninges develops during early fetal life. The brainstem is flattened, cerebellar cysts are present, and the cortical folding in the frontal and parietal areas is abnormal because of thickened cortex. In addition brain MRI typically shows a transient delay of myelination that tends to gradually diminish with age.

FCMD is caused by mutations of the *fukutin* gene on chromosome 9q31 and is particularly frequent in Japan where it represents the second most common form of muscular dystrophy after Duchenne dystrophy. The clinical features of FCMD are early manifestation of generalized muscle weakness, severe brain involvement with mental retardation, frequent occurrence of seizures and abnormal eye function.

MEB is a CMD variant of similar severity to FCMD, but the eye involvement is more profound and includes congenital myopia, glaucoma and retinal hypoplasia. Typically, MEB

patients present in the neonatal period with muscle hypotonia, and poor visual alertness. Patients with a severe form of the disease remain bedridden, never achieve sitting, head control, and visual contact. These patients may die during first years of life. Mental retardation is present and epilepsy is a common complication of MEB. Mutations in the *POMGnT1* gene are responsible for the MEB phenotype.

WWS represents the most severe CMD variant with a life expectancy of less than 3 years. Obstructive hydrocephalus is a common feature. An excessive weakness in WWS patients is caused by the combination of muscular dystrophy and brain involvement with virtual absence of the pyramidal tracts. The brain MRI shows a complete or near complete absence of gyration and widespread, confluent white matter changes. The corpus callosum is usually absent and partial fusion of cerebral hemispheres is common. The „cobblestone" type of lissencephaly and a complete loss of cortical layering are present. The WWS phenotype represents the severe phenotypic spectrum of mutations affecting genes that are involved in the process of α-dystroglycan glycosylation (Muntoni, 2004). These genes are *POMT1*, *fukutin*, *FKRP (fukutin-related protein)*, and *LARGE (like-glycosyltransferase)*.

MDC1C represents the severe end of the spectrum of *FKRP*-related myopathies. MDC1C patients with structural brain involvement, similar to MEB and WWS have been described (Topaloglu H, 2003; Beltrán VBD, 2004). The only case of **MDC1D** with a causal mutation in the *LARGE* gene has been described in humans. This 17-year-old girl presented with CMD, profound mental retardation, white matter changes and subtle structural abnormalities on brain MRI (Longman C, 2003).

1.2. Myotonic Dystrophy Types 1 and 2 (DM1, DM2)

Myotonic dystrophy type 1 (Steinert´s disease) (DM1) is a multisystem disorder involving muscle (muscular weakness and wasting, myotonia - slow and difficult relaxation of muscles after voluntary contraction), heart (cardiomyopathy), brain (mental retardation), eye (cataracts, ptosis), pancreas (insulin resistence), testes (hypogonadism, testicular atrophy), and peripheral nerves (neuropathy). The needle electromyography (EMG) examination shows a myopathic pattern with myotonic discharges. The incidency is estimated to be about 1:8,000 births but is probably underestimated. The causal mutation consists of an unstable CTG repeat expansion in the *DMPK* gene on chromosome 19q13.3 that encodes a protein with serine-threonine kinase activity. Normal number of CTG repeats in healthy subjects is 5-35, severely afflicted patients have hundreds or thousands. Transmission is autosomal dominant with an anticipation phenomenon (Harley HG, 1993; Angeard N, 2007). Four clinical forms of DM1 are distinguished, including a classical adult form, a late-onset form and two pediatric forms – a congenital form which almost always displays maternal transmission and a childhood form with maternal or paternal transmission (Angeard N, 2007).

Myotonic dystrophy type 2 (DM2) is caused by expansion of a CCTG repeat in the zinc finger protein 9 (*ZNF9*) gene on chromosome 3q21. DM1 and DM2 have very similar clinical presentations and the diagnosis of these two disorders needs to be confirmed by molecular genetic analysis (Huang CC, 2005). **Myotonic dystrophy type 3 (DM3)** has also been

described as a multisystem myotonic disorder with frontotemporal dementia, and a linkage to chromosome 15q21-24 (Le Ber I, 2004).

There is a frequent CNS involvement in both DM1 and DM2. In DM1 it ranges from mental retardation, which is characteristic in congenital forms to selective cognitive, executive, visual-spatial, and personality impairment in the classical form of adults (Angeard N, 2007). The brain MRI in DM1 and DM2 patients usually demonstrate white matter lesions in T2-weighted images, in addition to ventricular dilatation and brain atrophy. The brain MRI spectroscopy (MRS) showed different patters of neurochemical alterations involving gray and white matter in DM1 a DM2 patients. These results suggest that the diseases differ in their neurocellular pathology (Vielhaber S, 2006).

No association between white matter lesions and the CTG repeat size was proven (Di Costanzo 2008). Anterior temporal white matter lesions were exclusively seen in DM1 patients (Kornblum C, 2004). Differences in the distribution of white matter lesions between the congenital and classic adult forms of DM1 were also reported (Kuo HC, 2005; Di Costanzo 1 and 2, 2002; Di Costanzo 2008). The origin of white matter pathology seems to be mainly developmental in the congenital form, and mainly degenerative in the adult form of DM1 (Di Costanzo 1, 2002). Neuropsychological studies suggest that subcortical white matter lesions are correlated with focal dementia, while temporal and insular lesions may be responsible for the global intellectual dysfunction in patients with the classic adult form of DM1 (Kuo HC, 2008).

1.3. Mitochondrial Encephalomyopathies

Mitochondrial diseases represent a group of disorders related to respiratory chain dysfunction. Clinical features are usually extremely heterogeneous because mitochondrial pathology may involve several tissues with different degrees of severity. Muscle, brain, heart, and kidney are mostly affected, because of their high dependence on oxidative metabolism. Muscle can be the only affected tissue or involved as a part of a multisystem disorder. There are „ragged- red fibers“, accumulation of structurally altered mitochondria and cytochrome-c-oxidase (COX) negative fibers as the main pathological features in affected muscles (Filosto M, 2007). Clumps of diseased mitochondria accumulate in the subsarcolemmal region of the muscle fiber and appear as "ragged-red fibers" when muscle is stained with modified Gomori trichrome stain.

Mitochondrial encephalomyopathies may be caused by defects of either the mitochondrial or nuclear genome and may present at any age (Zeviani M, 2004; Taylor RW, 2004). The impaired intergenomic signaling, defects of mitochondrial motility, fission, and fusion may also lead to specific neuromuscular syndromes (DiMauro S, 2005). Mitochondrial diseases are usually transmitted by maternal inheritance and are heteroplasmic with mutant and wild-type mitochondrial DNA (mtDNA) coexisting in tissues in various proportions. Since 1988, more than 150 point mutations in mtDNA have been associated with human diseases, many involving mitochondrial tRNA genes and thus impairing mtDNA translation (DiMauro S, 2005; Scuderi C, 2007). Diseases such as Kearns-Sayre syndrome, Pearson's syndrome, and progressive external ophthalmoplegia are thought to be due to large-scale

mtDNA rearrangements, whereas other diseases such as MELAS syndrome, Leber´s hereditary optic neuropathy, myoclonic epilepsy with ragged-red fibers (MERRF), and others are due to point mutations in mtDNA.

In mitochondrial encephalomyopathies, CNS structures are affected according to different patterns of distribution and severity. Characteristic lesions are neuronal loss, vasculo-necrotic changes, gliosis, demyelination and spongy degeneration. In accordance with either grey matter or white matter involvement two main groups of diseases may be distinguished. Neuronal loss and vasculo-necrotic multifocal lesions are the common features of grey matter involvement, while demyelination and spongy degeneration occur when white matter is affected, often associated with less severe lesions of the grey structures. Grey matter lesions are prevalent in MERRF, MELAS, Alpers and Leigh syndromes. White matter involvement and alteration in the basal ganglia and brainstem are mostly seen in Kearns-Sayre syndrome, Leigh syndrome, and MELAS syndrome. White matter changes were also described in mtDNA depletion syndrome linked to dGK mutations and in the rare conditions associated with complex I and II deficiency (Filosto M, 2007; de Lonlay-Debeney P, 2000).

MELAS (mitochondrial encephalomyopathy, lactic acidosis and stroke-like episodes) is a typical example of mitochondrial cytopathy that affects particularly the brain and muscles. In most cases, the signs and symptoms of this disorder appear in childhood following a period of normal development. Early symptoms may include muscle weakness and pain, recurrent headaches, loss of appetite, vomiting, and seizures. Most affected individuals experience stroke-like episodes beginning before 40 years of age. These episodes often involve temporary muscle weakness on one side of the body (hemiparesis), altered consciousness, vision abnormalities, seizures, and severe headaches resembling migraines. Repeated stroke-like episodes can progressively damage the brain, leading to vision loss, problems with movement, and a loss of intellectual functions (dementia). Most patients with MELAS develop lacitic acidosis. Increased acidity in the blood can lead to vomiting, abdominal pain, extreme tiredness (fatigue), muscle weakness, and difficult breathing. Less commonly, people with MELAS may experience involuntary muscle spasms (myoclonus), impaired muscle coordination (ataxia), hearing loss, heart and kidney problems, diabetes, and hormonal imbalances. The brain MRI can show infarctlike lesions that did not correspond to the vascular territories (Valanne L, 1998).

MERRF (Myoclonic epilepsy associated with ragged-red fibers) is one of the major mitochondrial encephalomyopathies, and is caused by a maternally-inherited mitochondrial A8344G DNA mutation. This point mutation disrupts the mitochondrial gene for tRNA-Lys and thus disrupts synthesis of proteins essential for oxidative phosphorylation. The main clinical features are myoclonic epilepsy, cerebellar ataxia, and myopathy with ragged-red fibers. The brain MRI demonstrates bilateral symmetric lesions of the basal ganglia with putaminal necrosis (Orcesi S, 2006).

Kearns-Sayre syndrome is a disease caused by a 5,000 base deletion in the mtDNA. Unlike most mitochondrial diseases it is not maternally inherited. Rather, it occurs sporadically. Kearns-Sayre syndrome starts before the age of 20. Its expression is systemic, but many of the most common expressions are in the eyes, with ophthalmoplegia and retinal degeneration, especially retinitis pigmentosa, as common features. Other characteristic

features are dysphagia, proximal weakness, hearing loss, cerebellar ataxia, and cardiac conduction defects. White matter lesions are also usually seen.

Leigh syndrome is a heterogenous neurologic disease characterized by seizures, developmental delay, muscle weakness, respiratory abnormalities, optic abnormalities, including atrophy and ophthalmoplegia, and progressive cranial nerve degeneration with early onset in infants and children. Diagnosis of this encephalomyelopathy can be confirmed by characteristic pathologic findings of necrosis in the basal ganglia, thalamus, and brainstem. Symmetric brainstem and/or basal ganglia lesions on T2-weighted MRI are consistent with Leigh syndrome. Severe dysfunction of mitochondrial energy metabolism is generally present and involved in the etiology of this degenerative central nervous system disease. At the molecular level, a number of point mutations have been located in mitochondrial DNA genes, including ATPase6 and tRNA(Lys) genes, and in nuclear genes encoding subunits of oxidative enzymes, such as pyruvate dehydrogenase. Biochemically these mutations are responsible for enzymatic defects in either respiratory complexes (I, IV, or V) or pyruvate dehydrogenase (Filiano JJ, 2002; Absalon MJ, 2001).

NARP (neurogenic muscle weakness, ataxia, and retinitis pigmentosa) is a similar syndrome characterized by sensorimotor axonal polyneuropathy, cerebellar ataxia with MRI findings of cerebral and cerebellar atrophy and retinitis pigmentosa or optic atrophy. In addition, seizures, and learning difficulties are usually present.

1.4. Hereditary Neuropathies Charcot-Marie-Tooth

There are few relatively rare variants of hereditary neuropathy Charcot-Marie-Tooth (CMT disease) with cerebral white matter involvement sometimes mimicking multiple sclerosis, especially X-linked dominant CMT disease (CMTX1) and CMT4D.

X-linked dominant Charcot-Marie-Tooth disease (CMTX1) is an inherited motor and sensory neuropathy, caused by mutations affecting the *GJB1* gene coding for the gap junction protein beta 1 (connexin 32, Cx32), which is located within the Xq13 region. Over 250 different mutations in the *GJB1 (Cx32)* gene associated with the CMTX1 phenotype have been identified as yet. Mutations in this gene are the second most frequently identified molecular defect in CMT patients after CMT1A duplication. CMTX1 accounts for approximately 10-20% of all hereditary demyelinating neuropathies (Birouk N, 1998; Lewis RA, 2000). Mutations in the *GJB1 (Cx32)* gene cause a primary Schwann cell dysfunction leading to impaired Schwann cell–axon interactions (Lewis RA, 1999).

Clinical manifestations of CMTX1, as in other forms of CMT, are mainly distal muscle wasting and weakness, hyporeflexia, distal sensory disturbance and foot deformities. Males are usually more severely affected and the onset of a motor deficit is earlier than in females. In the pedigree the affliction is never transmitted from father to son.

Motor nerve conduction velocity (NCV) is intermediately slowed in the typical range of 30-38 m/s, but in some female patients NCV may be near-normal (Lewis RA, 1999; Lewis RA, 2000). Conduction velocities in the 20 m/s range are extremely rare in CMTX1 patients and can electrophysiologicaly distinguish CMTX1 from the more frequent CMT type 1A.

Markedly slow NCVs in this range can also be associated with double mutations involving *GJB1* and other myelin genes such as myelin protein zero *(MPZ)* (Lewis RA, 2000).

Connexin 32 is expressed in Schwann cells and oligodendrocytes in the peripheral and the central nervous systems respectively. Subclinical CNS involvement indicated by changes in visual evoked potentials (VEPs) or brainstem auditory evoked potentials (BAEPs) have been described (Lewis RA, 2000; Kuntzer T, 2003). However, it is quite unusual to detect CNS clinical manifestations in addition to the peripheral neuropathy in CMTX1 patients.

Transient and reversible white matter lesions on the MRI scans, correlating with only mild and transient CNS clinical symptoms have been occasionally reported (Bahr M, 1999; Gutierrez A, 2000; Lewis RA, 2000; Kuntzer T, 2003; Taylor RA, 2003; Hanemann, 2003). Two male patients with CMTX1 who developed reversible CNS involvement after a stay at high altitudes have also been described (Taylor RA, 2003). It remains unclear, why is not there more CNS involvement in CMTX1 patients. BAEPs with abnormal central conduction slowing can be used to distinguish CMTX1 from CMT1A and therefore assist in the selection of appropriate patients for the *GJB1 (Cx32)* gene mutation analysis.

Charcot-Marie-Tooth disease type 4D (CMT4D) (hereditary motor and sensory neuropathy – Lom) is an autosomal recessive demyelinating polyneuropathy, associated with deafness almost exclusively found in Gypsies and resulting from a homozygous R148X mutation in the N-myc downstream-regulated gene 1 *(NDRG1*). Only few case reports of patients with CMT4D without Gypsy ancestry have been descibed as yet. Two affected non-Gypsy brothers presented with severe demyelinating polyneuropathy, deafness, subcortical white matter abnormalities on the brain MRI studies, and the R148X mutation in the *NDRG1* gene (Echaniz-Laguna A, 2007).

There are other neuromuscular syndromes in which the brain MRI scans sometimes demonstrate white matter lesions, for example Congenital Cataracts Facial Dysmorphism Neuropathy (CCFDN) syndrome, and Marinesco-Sjögren syndrome (MSS). There is a significant phenotypic and genotypic overlap between these two conditions (Merlini L, 2008).

CCFDN is a complex developmental disorder of autosomal recessive inheritance, which has been found to occur exclusively in patients of Gypsy ethnicity. The syndrome includes congenital cataracts and microcornea, primary hypomyelination of the peripheral nervous system, impaired physical growth, delayed early motor and intellectual development, mild facial dysmorphism and hypogonadism. Rhabdomyolysis occuring during febrile conditions is a serious complication reported in an increasing number of patients. During general anaesthesia, patients with CCFDN require careful monitoring as they have an elevated risk of complications. The neuromuscular and CNS impairment is relatively mild and patients survive well into adulthood. CCFDN is a genetically homogeneous condition in which all patients are homozygous for the same ancestral mutation in the *CTDP1* gene, which maps to 18qter and encodes a protein phosphatase whose only known substrate is the phosphorylated serine residues of the carboxy-terminal domain of the largest subunit of RNA polymerase II, indicating that CCFDN affects basic cellular processes of gene expression and developmental regulation (Kalaydjieva L, 2006).

Marinesco-Sjögren syndrome (MSS) is a condition similar to CCFDN with an autosomal recessive pattern of inheritance. This condition is characterised by somatic and mental

retardation, congenital cataracts and cerebellar ataxia. Progressive myopathy was later reported to be also a cardinal sign of MSS, with myopathic changes on muscle biopsy. Additional features can be found in some patients, e.g peripheral neuropathy, optic atrophy, microcornea, hearing impairment, seizures, diabetes mellitus, cerebral atrophy and white matter lesions. Using homozygosity mapping strategy the MSS locus was identified on chromosome 5q31 (Lagier-Tourenne C, 2003).

2. Case Reports

2.1. Congenital Muscular Dystrophy Merosin-Deficient (MDC1A)

Our patient is a 13-year-old girl with a negative family history of any neurological or neuromuscular problem. Parents are healthy and non-consanguineous. She has no siblings. She presented with an early manifestation of peripheral hypotonia in infancy. Profound proximal muscle wasting and weakness developed. She was able to sit and crawl at 1 year of age, and never stand and walk unsupported. The electromyography (EMG) performed at age 2 revealed a profound myopathic pattern. A muscle biopsy showed dystrophic changes and deficient merosin immunostaining. The brain MRI studies demonstrated diffuse white matter changes. The diagnosis of merosin-deficient congenital muscular dystrophy (MDC1A) was established.

Ten years later the patient´s mother was pregnant for the second time and requested a prenatal genetic diagnostic testing. That is why the patient was reevaluated at 12 years of age. She displayed scoliosis, profound proximal muscle wasting and weakness and was wheel-chair bound. The serum creatinekinase (CK) level was 10 fold elevated above the upper normal limit. In addition to a profound myopathic pattern revealed by the EMG, nerve conduction studies demonstrated signs of demyelinating sensorimotor neuropathy with conduction velocities in the range of 30-34 m/s. A new MRI of the brain showed diffuse white matter changes (figures 1 and 2).

In the proband and both her parents genomic DNA was extracted from leukocytes using a standard method upon informed consent. Fetal DNA was extracted from cultivated amniocytes. The direct sequencing of all 64 exons and adjacent intron sequences of the *LAMA2* gene on chromosome 6q22 revealed that the proband was a compound heterozygot for paternal mutation c.6466C>T(p.Arg.2156Stop) and maternal mutation IVS60-1G >C. None of these two mutations were detected in the fetus and a healthy boy has been later born.

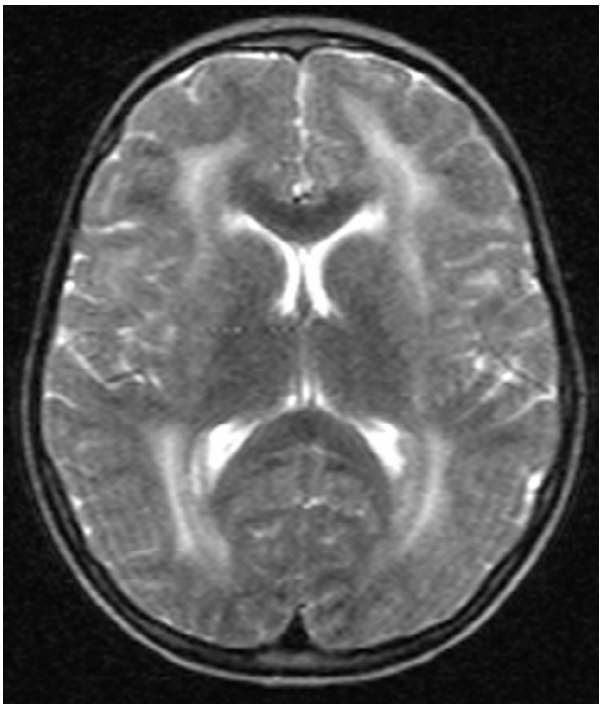

Figure 1.

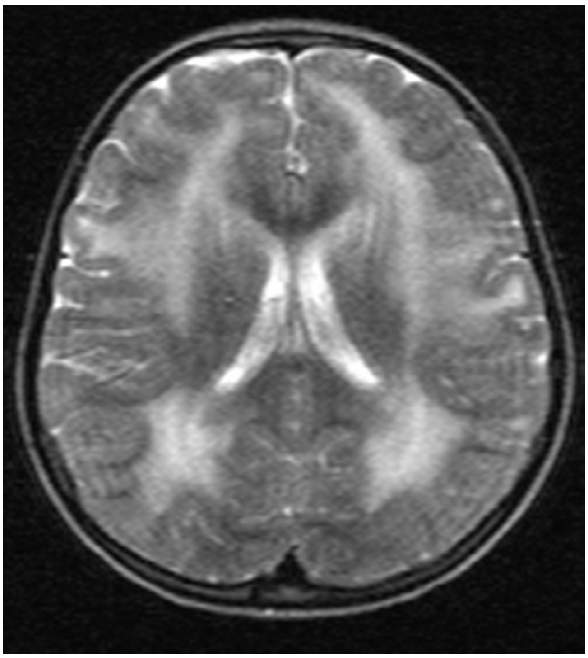

Figure 2.

Figures 1 and 2. Diffuse increased signal intensity of white matter on T2-weighted MRI of the brain in patient with merosin-deficient congenital muscular dystrophy (MDC1A).

2.2. Congenital Muscular Dystrophy with Normal Merosin and A-Dystroglycan

A female child was born at full term of unrelated healthy parents. She had a healthy brother and no one else in the family had neuromuscular problems. She was floppy from birth and breast-feeding was difficult due to facial muscle weakness. Talipes equinovarus in the left was reported.

On examination at 13 years of age she displayed profound proximal muscle weakness and hypotonia, severe arthrogryposis and lymphedema in the lower extremities (figure 3), bulbar syndrome, mild bilateral ptosis and chronic progressive external ophthalmoplegia (CPEO) but no pigmentary retinopathy. There was no rigid spine and no joints with hyperlaxity. The patient was alert, intelligent and cooperative. No seizures were reported. There were no clinical signs of CNS involvement. The electrocardiogram was unremarkable. She has been wheel-chair bound since 7 years of age.

Figure 3. Patient with congenital muscular dystrophy with normal merosin and α-dystroglycan. Severe arthrogryposis and lymphedema are seen in the lower extremities.

The EMG showed a typical myopathic pattern. Motor and sensory nerve conduction studies, visual and brainstem auditory evoked potentials (VEPs and BAEPs) were normal. Laboratory investigations showed normal serum creatine kinase (CK 103 units/l), lactate and transaminases levels. The brain MRI revealed increased signal intensity of white matter on T2-weighted sequences. These changes were multifocal confluent lesions located in paraventricular white matter of the frontal lobes (figure 4).

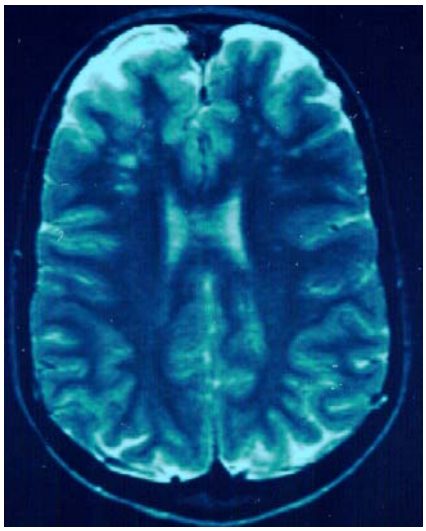

Figure 4. MRI of the brain in the patient with congenital muscular dystrophy with normal merosin and α-dystroglycan. Increased signal intensity of paraventricular white matter of the frontal lobes on T2-weighted sequences.

An open muscle biopsy from the right quadriceps femoris was performed at the age of 13 years. The biopsy displayed a myopathic pattern with evidence of fiber necrosis and regeneration, with significant variation of fiber size with type 2 fibers predominance ranging from 55-65 %, mild to moderate endomysial fibrosis, splitting and centrally nucleated fibers. A prominent multifocal endomysial lymphocytic infiltrate with both B (CD20+) and T (CD4+, CD8+) cells mimicking inflammatory myopathy was found (figure 5A). Immunohistochemistry revealed an overexpression of HLA I in sarcolemmal localisation. There were neither ragged-red fibres (RRF), nemaline bodies nor rimmed vacuoles. Cytochrome *c* oxidase (COX) deficient fibres were not found. High enzyme activities for NADH-tetrazolium reductase (NADH-TR) and succinyldehydrogenase (SDH) were revealed at the periphery of muscle fibers of both types suggesting the subsarcolemmal accumulation of mitochondria (figure 5B).

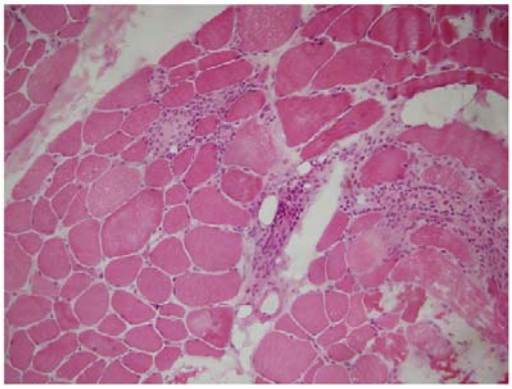

Figure 5A. Muscle biopsy: hematoxylin eosin, original magnification x200, abnormal variation in fiber size, regressive changes of muscle fibers, interstitial inflammatory infiltration.

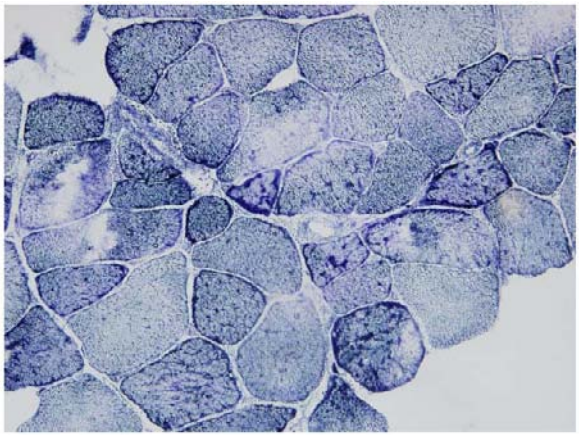

Figure 5B. Enzyme histochemistry for NADH-tetrazolium reductase (NADH-TR) activity, original magnification x400. High enzyme activity at the periphery of muscle fibers, preferentially type I, suggesting an accumulation of mitochondria.

Immunostaining showed normal expression of merosin, α and β-dystroglycans and other proteins except partial deficiency of dysferlin in 20% of muscle fibers. Western blot analysis of calpain3 was normal. No mutations in calpain3 *(CAPN3)* and dysferlin genes were found by analysing mRNA isolated from muscle tissue. Selenoprotein N gene *(SEPN1)* mutation analysis was also performed. Only common polymorphisms were found.

Electron microscopy revealed the accumulation of mitochondria located under the sarcolemma while in the deep sarcoplasm the number of mitochondria was decreased. No cores or other structural abnormalities were revealed.

These findings prompted us to obtain another muscle sample by a needle biopsy. The activities of respiratory chain complexes I, II, III and IV were all within normal ranges. Total DNA was extracted from skeletal muscle by standard procedures. Mitochondrial DNA rearrangements were excluded by long-range PCR, whilst a quantitative real-time PCR assay demonstrated no marked abnormality in mtDNA copy number in this tissue. The entire mitochondrial genome was sequenced. No potential pathogenic mtDNA mutation was found in our patient, all sequence variants detected were well-recognised polymorphic changes.

2.3. X-Linked Dominant Charcot-Marie-Tooth Disease (CMTX1)

We studied a three-generation family with one affected member in each generation. Peripheral neuropathy was found to be a familial trait on the maternal side of the pedigree (figure 6). Two healthy siblings from two generations were also studied (individuals 4 and 5). Clinical presentations were very similar in all affected members: the proband, a 13-year-old boy (patient 1), his mother (age 32; patient 2), and maternal grandmother (age 56; patient 3). They displayed distal muscle weakness, peroneal muscle atrophy, inability to walk on the heels, areflexia, and discrete distal sensory disturbance. The women were mildly affected and had no foot deformities. The boy had more severe weakness and pes equinovarus. He had an early onset of walking difficulties in infancy, whereas clinical symptoms in his mother and

grandmother did not develop until the end of the second decade. None of them had any clinical signs of the CNS involvement or hearing loss.

All three affected and the two unaffected family members were examined both clinically and electrophysiologically. Motor and sensory nerve conduction studies and needle electromyography of the first dorsal interosseous, tibialis anterior, and vastus lateralis muscles were performed. The nerve conduction studies revealed intermediately slowed velocities in the typical range of 30-38 m/s. Needle EMG revealed a profound chronic axonopathy with sporadic fibrillation potentials and long duration polyphasic motor unit potentials, corresponding to a reinnervation process. These findings were prevalent in peroneal muscles and considerably more severe in both older female patients than in the young boy. In clinically unaffected relatives all conduction and EMG parameters were normal.

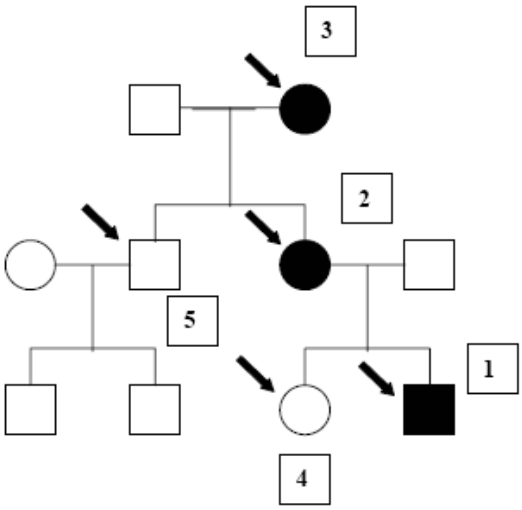

Empty circles indicate unaffected females; empty squares, unaffected males; filled circles, affected females; filled squares, affected males; DNA analysis was performed for patients marked with arrows.

Figure 6. CMTX1 family pedigree.

VEPs were normal in all of the tested individuals. BAEPs showed normal values in the unaffected brother of patient 2, while findings in the proband and both affected female patients were abnormal. In patient 2 delayed III–V interpeak intervals (2.73 ms left, 2.79 ms right, upper normal limit 2.4 ms) and I-V interpeak intervals (4.92 ms left, 4.89 ms right, upper normal limit 4.5 ms) were recorded. In patient 3 the recorded data were similar. These findings reflect abnormal central conduction delays in the brainstem. The brain MRI in patient 2 showed normal findings.

Molecular genetic studies were performed on all family members. DNA was extracted from leukocytes using a standard method after informed consent had been obtained. Initially, the CMT1A duplication on chromosome 17p11.2 was excluded with a set of 15 polymorphic microsatellite markers. Testing for deletions in the *SMN1* gene was negative and excluded spinal muscular atrophy (SMA). Direct sequencing of the *GJB1 (Cx32)* gene then showed a

homozygous T to G missence mutation at nucleotide position 380 in exon 2, resulting in the substitution of isoleucine at position 127 with serine (Ile127Ser) in the male patient 1. The same mutation, but in heterozygous state was detected in affected females of the family (patient´s mother 2 and maternal grandmother 3) (figure 7). This base change consegregated with all affected members of the family and was not present in unaffected members of the family, nor in 50 normal female control DNA samples. To the best of our knowledge, this mutation had not been previously reported.

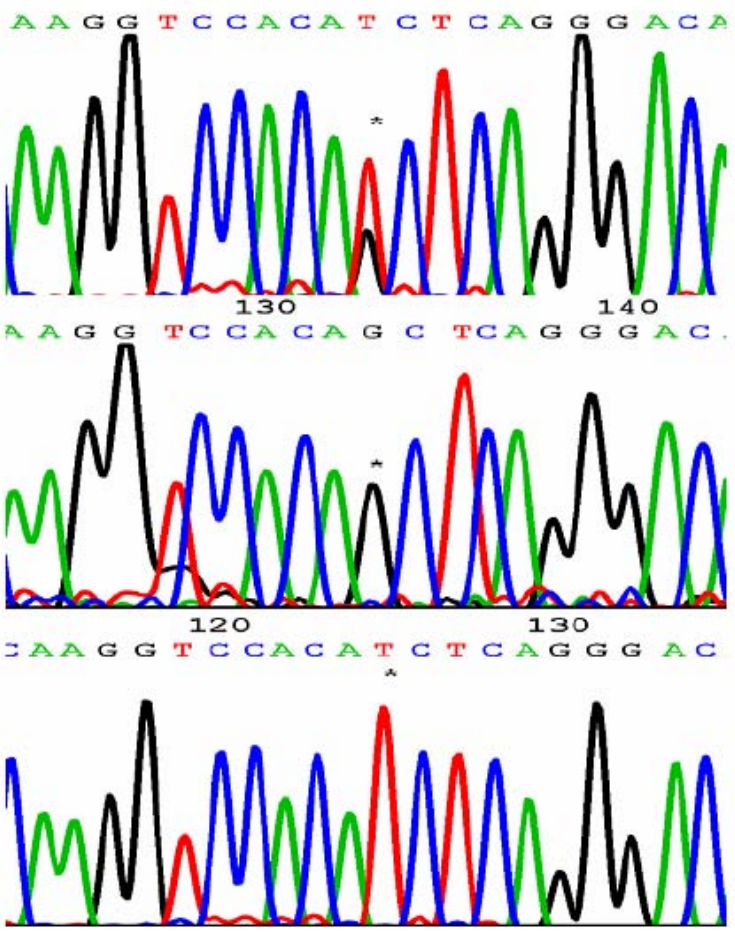

Figure 7. Results from sequencing analysis of the *GJB1* (*Cx32*) gene showing the site of the c.380 T to G (Ile127Ser) mutation (marked by asterisk). Upper line: patient 3- affected maternal grand-mother, carrying a heterozygous signal G/T at position 380, middle line: male patient 1, carrying a homozygous (hemizygous) signal G, bottom line: normal control with a wild type T signal, the same result – homozygous T, was also detected in the unaffected individuals 4 and 5.

A sural nerve biopsy in patient 2 showed a marked loss of myelinated fibres and few clusters of regenerating axons. The main histopathological feature was the presence of onion-bulb formations. An axonal atrophy, degeneration and loss of myelinated nerve fibres were revealed (figure 8). These findings suggested that both a demyelination and an axonal loss were present in this patient. There was a pronounced thickening of the perineurium and no

inflammatory infiltration. These findings are consistent with an inherited, predominantly demyelinating neuropathy.

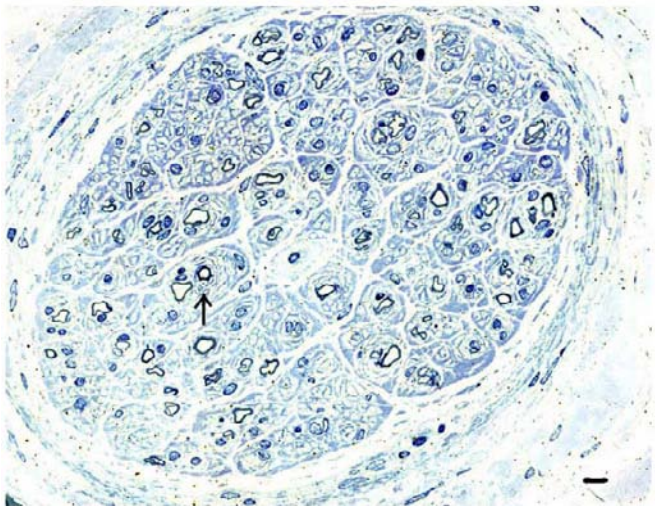

Figure 8. Sural nerve biopsy in patient with X-linked dominant Charcot-Marie-Tooth disease (CMTX1). (patient 2). Transverse section. Loss of myelinated fibers and onion-bulb formations (arrow) around almost all myelinated and unmyelinated fibers are seen. Semi-thin section stained with methylene blue-azure II-basic fuchsin. (original magnification x 1000, Bar = 10 μm).

3. Conclusion

Our first case report of the patient with MDC1A illustrates the importance of detailed and careful clinical, electrophysiological, neuroimaging, and molecular genetic examination for the prenatal diagnostics in families with the onset of serious genetic defects. Our patient displayed a typical MDC1A phenotype with an early onset of muscular dystrophy, demyelinating neuropathy and white matter changes. A healthy boy - patient´s brother, who is not a heterozygot for the *LAMA2* gene mutation has been recently born to happy parents.

In the second case report we present a sporadic case of inherited muscular disorder clinically and histopathologically consistent with CMD. The combination of severe arthrogryposis, bulbar syndrome, ptosis and CPEO is unusual. Brain MRI studies revealed the white matter changes similar to those seen in MDC1A and α-dystroglycanopathies, but the expression of merosin, α and β-dystroglycans was normal in our patient. Partial deficiency of dysferlin was probably secondary and unspecific. Serum CK level was surprisingly within normal limits. Patients with MDC1A have a demyelinating neuropathy. There were no signs of peripheral neuropathy in our patient.

The clinical phenotype with ptosis and CPEO was suggestive of mitochondrial muscle disease, but the activities of respiratory chain complexes were normal, and all mitochondrial genetic analyses including screens for mtDNA depletion, mtDNA rearrangements and mtDNA point mutations were negative. Mitochondrial abnormalities were probably secondary and unspecific in our patient.

In the differential diagnosis CMDs with normal merosin and normal CK should be excluded, especially *SEPN1* and *COL6*-related disorders. *SEPN1* gene sequencing was negative. *COL6* analysis can only be performed by RT-PCR on fresh muscle tissue which we are no more able to obtain. Anyway, our patient showed no signs of hyperlaxity of distal joints or other symptoms related to Bethlem/Ullrich myopathy. Another important differential diagnosis is RYR1-related myopathies but no cores were found on electron microscopy.

Phenotypic presentation is very unusual in our patient with combination of CMD and central nervous system involvement, differs considerably from all cases described so far, and may represent a novel CMD variant. The differential diagnosis of CMDs and inflammatory myopathies is very important for the clinical management of pediatric patients with muscular diseases.In the third case report the CMTX1 family with a novel Ile127Ser mutation in the *GJB1 (Cx32)* gene is described. The affected young male had an earlier onset of clinical symptoms and a more severe phenotype than his female relatives. Our electrophysiological findings showed intermediately slowed motor NCVs. CMAP amplitudes were significantly lower in the older females than in the young boy, which suggested an age-related loss of motor axons. In addition to nerve conduction studies we performed needle EMG, which revealed signs of a severe chronic axonopathy with reinnervation changes. In summary, the electrophysiological abnormalities in the young male were consistent with a diffuse motor and sensory demyelinating neuropathy, while in the older females a profound chronic axonopathy prevailed and apparently masked the underlying defect of myelin.

The sural nerve biopsy in our patient with Ile127Ser mutation showed a marked axonal loss and numerous onion-bulb formations as the sign of Schwann cell pathology. Findings in our family with the novel *GJB1 (Cx32)* mutation are consistent with the hypothesis that phenotypic features of CMTX1 are mainly caused by an age-related loss of large myelinated axons.

Our impression is that CMTX1 patients initially develop a demyelinating neuropathy, which is followed by a slowly progressive axonopathy. The disease is primarily caused by Schwann cell pathology which ultimately lead to axonal damage. Our clinical results give the evidence that conduction is first slowed then the axon degenerates, and as such it is likely that the mutation affects myelin prior to secondary axonal degeneration. Although this has been alluded to in previous studies, our electrophysiological and histopathological findings support this model of disease progression.

All patients, with the CMT phenotype and intermediate slowing of conduction velocities who are negative for CMT1A duplication/HNPP deletion and whose family shows a dominant trait without male-to-male transmission, should be screened for mutations in the *GJB1 (Cx32)* gene. Although our patient with CMTX1 had normal brain MRI, abnormal BAEPs with central conduction delays suggest a subclinical CNS involvement. It is therefore likely, that mutations in the *GJB1* gene impair a structure and function of both peripheral and central myelin.

White matter changes are not only a very important and valuable diagnostic sign, but could have a serious impact on the management and prognosis of patients with neuromuscular disorders.

Acknowledgments

The study was supported with grant NR 9517-3 (Internal Grant Agency of the Ministry of Health of the Czech Republic).

References

Emery AE. Population frequencies of inherited neuromuscular diseases - a world survey *Neuromuscul. Disord.* 1991; 1: 19-29.

http://www.treat-nmd.eu

Fields RD. White matter in learning, cognition and psychiatric disorders. *Trends Neurosci.* 2008 ; 7: 361-70.

Philpot J, Topaloglu H, Pennock J, Dubowitz V. Familial concordance of brain magnetic resonance imaging changes in congenital muscular dystrophy. *Neuromuscul. Disord.* 1995; 3: 227-31.

Philpot J, Cowan F, Pennock J, Sewry C, Dubowitz V, Bydder G, Muntoni F. Merosin-deficient congenital muscular dystrophy: the spectrum of brain involvement on magnetic resonance imaging. *Neuromuscul. Disord.* 1999; 2: 81-5.

Mercuri E, Muntoni F, Berardinelli A, Pennock J, Sewry C, Philpot J, Dubowitz V. Somatosensory and visual evoked potentials in congenital muscular dystrophy: correlation with MRI changes and muscle merosin status. *Neuropediatrics.* 1995; 26: 3-7.

Anderson JL, Head SI, Rae C, Morley JW. Brain function in Duchenne muscular dystrophy. *Brain*. 2002; 1: 4-13.

Muntoni F, Voit T. The congenital muscular dystrophies in 2004: a century of exciting progress. *Neuromuscul. Disord.* 2004; 14: 635-649.

Jimenez-Mallebrera C, Brown SC, Sewry CA, Muntoni F. Congenital muscular dystrophy: molecular and cellular aspects. *Cell Mol. Life Sci.* 2005; 62: 809-823.

Buttery PC, Ffrench-Constant C. Laminin-2/integrin interactions enhance myelin membrane formation by oligodendrocytes. *Mol. Cell. Neurosci.* 1999; 14: 199-212.

Brockmann K, Dechent P, Bonnemann C, Schreiber G, Frahm J, Hanefeld F. Quantitative proton MRS of cerebral metabolites in laminin alpha2 chain deficiency. *Brain Dev.* 2007; 6: 357-64

Topaloglu H, Brockington M, Yuva Y, et al. FKRP gene mutations cause congenital muscular dystrophy, mental retardation, and cerebellar cysts. *Neurology*. 2003; 60: 988-92.

Beltrán VBD, Voit T, Longman C, et al. Mutations in the FKRP gene can cause Muscle-Eye-Brain disease and Walker-Warburg syndrome. *J. Med. Genet.* 2004; 41: 61-6.

Longman C, Brockington M, Torelli S, et al. Mutations in the human LARGE gene cause MDC1D, a novel form of congenital muscular dystrophy with severe mental retardation and abnormal glycosylation of alpha-dystroglycan. *Hum. Mol. Genet*. 2003; 21: 2853-61.

Harley HG, Rundle SA, MacMillan JC, et al. Size of the unstable CTG repeat sequence in relation to phenotype and parental transmission in myotonic dystrophy. *Am. J. Hum. Genet.* 1993; 6: 1164-74.

Angeard N, Gargiulo M, Jacquette A, et al. Cognitive profile in childhood myotonic dystrophy type 1: is there a global impairment? *Neuromuscul. Disord.* 2007; 6: 451-8.

Huang CC, Kuo HC. Myotonic dystrophies. *Chang. Gung. Med. J.* 2005; 8: 517-26.

Le Ber I, Martinez M, Campion D, et al. A non-DM1, non-DM2 multisystem myotonic disorder with frontotemporal dementia: phenotype and suggestive mapping of the DM3 locus to chromosome 15q21-24. *Brain.* 2004; 9: 1979-92.

Vielhaber S, Jakubiczka S, Gaul C, et al. Brain 1H magnetic resonance spectroscopic differences in myotonic dystrophy type 2 and type 1. *Muscle Nerve.* 2006; 2: 145-52.

Di Costanzo A, Santoro L, de Cristofaro M, et al. Familial aggregation of white matter lesions in myotonic dystrophy type 1. *Neuromuscul. Disord.* 2008; 4: 299-305.

Kuo HC, Hsiao KM, Chen CJ, Hsieh YC, Huang CC. Brain magnetic resonance image changes in a family with congenital and classic myotonic dystrophy. *Brain Dev.* 2005; 4: 291-6.

Di Costanzo A, Di Salle F, Santoro L, Tessitore A, Bonavita V, Tedeschi G. Pattern and significance of white matter abnormalities in myotonic dystrophy type 1: an MRI study. *J. Neurol.* 2002; 9: 1175-82.

Di Costanzo A, Di Salle F, Santoro L, Bonavita V, Tedeschi G. Brain MRI features of congenital- and adult-form myotonic dystrophy type 1: case-control study. *Neuromuscul. Disord.* 2002 ; 5: 476-83.

Kuo HC, Hsieh YC, Wang HM, Chuang WL, Huang CC. Correlation among subcortical white matter lesions, intelligence and CTG repeat expansion in classic myotonic dystrophy type 1. *Acta Neurol. Scand.* 2008; 2:101-7.

Kornblum C, Reul J, Kress W, Grothe C, Amanatidis N, Klockgether T, Schröder R. Cranial magnetic resonance imaging in genetically proven myotonic dystrophy type 1 and 2. *J. Neurol.* 2004; 6: 710-4.

Filosto M, Tomelleri G, Tonin P, et al. Neuropathology of mitochondrial diseases. *Biosci. Rep.* 2007; 1-3: 23-30.

Zeviani M, Di Donato S. Mitochondrial disorders. *Brain*. 2004; 127: 2153-2172.

Taylor RW, Schaefer AM, Barron MJ, McFarland R, Turnbull DM. The diagnosis of mitochondrial muscle disease. *Neuromuscul. Disord.* 2004; 14: 237-245.

DiMauro S, Hirano M. Mitochondrial encephalomyopathies: an update. *Neuromuscul. Disord.* 2005; 15: 276-286.

Scuderi C, Borgione E, Musumeci S, et al. Severe encephalomyopathy in a patient with homoplasmic A5814G point mutation in mitochondrial tRNACys gene. *Neuromuscul. Disord.* 2007; 3: 258-61.

de Lonlay-Debeney P, von Kleist-Retzow JC, Hertz-Pannier L. Cerebral white matter disease in children may be caused by mitochondrial respiratory chain deficiency. *J. Pediatr.* 2000; 2: 209-14.

Valanne L, Ketonen L, Majander A, Suomalainen A, Pihko H. Neuroradiologic findings in children with mitochondrial disorders. *AJNR Am. J. Neuroradiol*. 1998; 2: 369-77.

Orcesi S, Gorni K, Termine C, et al. Bilateral putaminal necrosis associated with the mitochondrial DNA A8344G myoclonus epilepsy with ragged red fibers (MERRF) mutation: an infantile case. *J. Child Neurol.* 2006; 1: 79-82.

Filiano JJ, Goldenthal MJ, Mamourian AC, Hall CC, Marín-García J. Mitochondrial DNA depletion in Leigh syndrome. *Pediatr. Neurol.* 2002; 3: 239-42.

Absalon MJ, Harding CO, Fain DR, Li L, Mack KJ. Leigh syndrome in an infant resulting from mitochondrial DNA depletion. *Pediatr. Neurol*. 2001; 1: 60-3.

Birouk N, Le Guern E, Maisonobe T, et al. X-linked Charcot-Marie-Tooth disease with connexin 32 mutations. *Neurology.* 1998; 50: 1074–1082.

Lewis RA, Shy ME. Electrodiagnostic findings in CMTX: a disorder of the Schwann cell and peripheral nerve myelin. *Ann. N.Y .Acad. Sci.* 1999; 883: 504-507.

Lewis RA, Sumner AJ, Shy ME. Electrophysiological features of inherited demyelinating neuropathies: A reappraisal in the era of molecular diagnosis. *Muscle Nerve.* 2000; 23: 1472-1487.

Gutierrez A, England JD, Sumner AJ, Ferer S, Warner LE, Lupski JR, Garcia CA. Unusual electrophysiological findings in X-linked dominant Charcot-Marie-Tooth disease. *Muscle Nerve.* 2000; 23: 182–188.

Kuntzer T, Dunand M, Schorderet DF, Vallat JM, Hahn AF, Bogousslavsky J. Phenotypic expression of a Pro 87 to Leu mutation in the connexin 32 gene in a large Swiss family with Charcot-Marie-Tooth neuropathy. *J. Neurol. Sci.* 2003; 207: 77-86.

Bahr M, Andres F, Timmerman V, Nelis ME, Van Broeckhoven C, Dichgans J. Central visual, acoustic, and motor pathway involvement in a Charcot-Marie-Tooth family with an Asn205Ser mutation in the connexin 32 gene. *J. Neurol. Neurosurg. Psychiatry.* 1999; 66: 202-206.

Taylor RA, Simon EM, Marks HG, Scherer SS. The CNS phenotype of X-linked Charcot-Marie-Tooth disease: More than a peripheral problem. *Neurology.* 2003; 61: 1475-1478.

Hanemann CO, Bergmann C, Senderek J, Zerres K, Sperfeld AD. Transient, recurrent, white matter lesions in X-linked Charcot-Marie-Tooth disease with novel connexin 32 mutation. *Arch. Neurol.* 2003; 4: 605-9.

Echaniz-Laguna A, Degos B, Bonnet C, et al. NDRG1-linked Charcot-Marie-Tooth disease (CMT4D) with central nervous system involvement. *Neuromuscul. Disord.* 2007; 2: 163-8.

Merlini L. Marinesco-Sjogren syndrome, fanfare, and more. *Neuromuscul. Disord.* 2008; 2: 185-8.

Kalaydjieva L. Congenital cataracts-facial dysmorphism-neuropathy. *Orphanet J. Rare Dis*. 2006; 1: 32.

Lagier-Tourenne C, Tranebaerg L, et al. Homozygosity mapping of Marinesco-Sjögren syndrome to 5q31. *Eur. J. Hum. Genet.* 2003; 10: 770-8.

In: Handbook on White Matter
Editors: T. B. Westland and R. N. Calton
ISBN: 978-1-60741-034-8

Chapter VII

White Matter Hyperintensities in Psychiatric Disorders and Their Association with Suicide Risk

Maurizio Pompili[a,b], Gianluca Serafini, [a] Silvia Rigucci[a], Andrea Romano[c], Marco Innamorati[d], Antonio Del Casale[a], Daniela Di Cosimo[a], Roberto Tatarelli[a] and David Lester[e]

[a] Department of Psychiatry, Sant'Andrea Hospital,
Sapienza University of Rome, Italy
[b] McLean Hospital – Harvard Medical School, USA
[c] Department of Neuroscience, Division of Neuroradiology,
Sant'Andrea Hospital, Sapienza University of Rome, Italy
[d] Università Europea di Roma, Italy
[e] The Richard Stockton College of New Jersey, USA

Introduction

Suicide is a major worldwide public health problem. Nearly one million lives are lost from suicide each year and between 3%-5% of adults make at least one suicide attempt at some point in their life (Kessler, Borges and Walters, 1999; Szadoczky, Vitrai, Rihmer, et al., 2000; Weissman, Bland, Canino, et al., 1999). Despite intensive efforts, research has failed to find necessary and sufficient factors that indicate an increased likelihood for suicide, and effective prevention strategies have remained elusive, suggesting that our understanding of the interplay of factors that increase the risk of suicide remains incomplete. Furthermore, although a great deal of research has been published on socio-psychological factors affecting suicidal behaviour, the results lack sufficient specificity.

In recent years, studies have indicated that up to 43% of the variability in suicidal behaviour can be explained by genetics (Brent and Mann, 2005; McGuffin, Marusic and Farmer, 2001). Thus, combining independent clinical and biological predictors may provide improved predictive models (Mann, Currier, Stanley, et al., 2006).

A great deal of research analyzing the neurobiological basis of suicide has been published in the last few decades. For examples, many studies have identified abnormalities of the serotonergic system in suicidal individuals, particularly in the ventral prefrontal cortex (Arango, Underwood, Gubbi, et al., 1995; Mann and Arango, 2001; Stanley and Mann, 1983; Stanley, Virgilio and Gershon, 1982), as well as several other possible abnormalities, such as reduction in messenger RNA and protein levels of cyclic adenosine monophosphate response element binding, CRE-DNA binding activity, and basal and cyclic adenosine monophosphate–stimulated protein kinase A activity (Dwivedi, Rao, Rizavi, et al., 2003), noradrenergic overactivity (Arango, Ernsberger, Sved, et al., 1993), alterations in the levels of endocannabinoid and in the density of the CB1 receptors (Vinod and Hungund, 2006), lower grey-matter cholesterol content (Lalovic, Levy, Luheshi, et al., 2007), elevated cholecystokinin mRNA levels (Bachus, Hyde, Herman, et al., 1997), expression of proteins involved in glial function, neurodegeneration and oxidative stress neuronal injury (Schlicht, Buttner, Siedler, et al., 2007), and higher β-adrenergic receptor binding (Mann, Stanley, McBride, et al., 1986). In the last decade, researchers have pointed out how the brain's white matter is implicated in mental illnesses. The aim of the present chapter is to review research on the association among white matter hyperintensities (WMH) and suicide behaviour.

The Contribution of Neuroimaging Techniques

The ability to study white matter injury non-invasively and over time has tremendous implications for understanding neurodevelopment, neuroinflammation and neurodegeneration. While advanced magnetic resonance imaging (MRI) methods to study white matter offer great promise, interpretation of the results are often complicated by biological, biochemical and pathological features of healthy and diseased tissue for which MRI characteristics are not clearly defined or even known. The most commonly used MRI sequences for the evaluation of white matter lesions are T2-weighted spin echo, proton density and fluid attenuation inversion recovery, (FLAIR). FLAIR acquisitions help in lesion visualization by suppressing the water signal and increasing the contrast from the gray matter. Newer techniques such as magnetic transfer imaging, diffusion-weighted imaging and diffusion tensor imaging have been developed to further evaluate white matter. Diffusion tensor imaging is a new MRI-based technique that allows the visualization of the location, the orientation and the anisotropy of the brain white matter tracts in three dimensions. The architecture of the axons in parallel bundles and their myelin shield facilitates the diffusion of the water molecules along their main directions. If it is applied to diffusion gradients in at least 6 directions, it is possible to calculate, for each pixel, a tensor (i.e., a 3*3 matrix) that describes this diffusion anisotropy. The fiber directions are indicated by the tensor main eigenvector. This vector can be color-coded, yielding a carthography of the tracts' position and direction (red for left-right, blue for superior-inferior and green for anterior-posterior). The brightness is weighted by the tracts' anisotropy (Mori and Van Zijl, 2002). The newer techniques may detect abnormalities in white matter that is normal-appearing on FLAIR and T2-weighted spin echo.

It is very important for researchers to use a quantitative method for white matter evaluation, such as the Fazekas scale (modified by Coffey) which is a quantitative four-point rating scale that provides standardized information.

White Matter Hyperintensities

Although scientists have long regarded the brain's white matter as a passive infrastructure, new research shows that it actively affects learning and mental illness. White matter hyperintensities on T2-weighted magnetic resonance imaging are frequent incidental findings in the brains of elderly individuals. WMH are bright lesions seen in T2-weighted MRI images that result from localized changes in cerebral tissue composition. A customary subdivision of WMH into periventricular WMH and deep WMH exists depending upon whether they are adjacent to the wall of the lateral ventricle or whether there is normal-appearing white matter between the lesions and the ventricular wall. While there is considerable overlap in the recognized etiological factors for the two subtypes, periventricular WMH are more influenced by hemodynamic factors. This might be explained by the differences in the blood supply of the two regions. The periventricular region is supplied by vessels arising from subependymal arteries, originating from either the choroidal arteries or the terminal branches of the rami striate.

The deep white matter, including the centrum semiovale, is supplied by centripetal medullary arteries from the cortical branches of the cerebral arteries, which are more prone to the effects of arteriosclerosis. While cerebrovascular risk factors, such as hypertension, diabetes, high homocysteine, and so forth, are known risk factors for white matter hyperintensities, a significant proportion of the variance remains unexplained. Genetic factors, alone or in interaction with environmental factors, appear to be important. WMH are known to be associated with neuropsychological deficits and various neuropsychiatric disorders.

Periventricular White Matter Hyperintensities

Between one third and eighty percent of MRI scans done in persons over the age of 65 have changes in their cerebral white matter (figure 1) (Wong et al., 2002).

MRI studies of older persons with disequilibrium and gait disturbances of unknown cause often show frontal atrophy and subcortical white matter T2 hyperintense foci (Kerber et al., 1998). Pathological studies, although scanty, suggest frontal atrophy, ventriculomegaly, reactive astrocytes in the frontal periventricular white matter, and increased arteriolar wall thickness (Whitman et al., 1999).

Causes of periventricular white matter (PWM) lesions include normal senescent changes (which are called UBO's, for "unidentified bright objects"), small strokes, and disorders related to multiple sclerosis (MS). PWM are correlated with vitamin B6 (pyridoxine) deficiency. Age is certainly the single most common cause of PWM and is presumably a "wear and tear" phenomenon.

Regarding small strokes, a period of hypertension is a common cause. In the authors' experience, just a few days of extreme hypertension may be enough. This might suggest that small amounts of bleeding are the cause in some cases. Clinical studies also show an association with diabetes, but not consistently with atherosclerosis. PWM are often an accompaniment of migraine, occurring in roughly 20% of persons with migraine. Since about 10% of the population has migraine, this means that about 2% of the population has white matter lesions due to migraine.

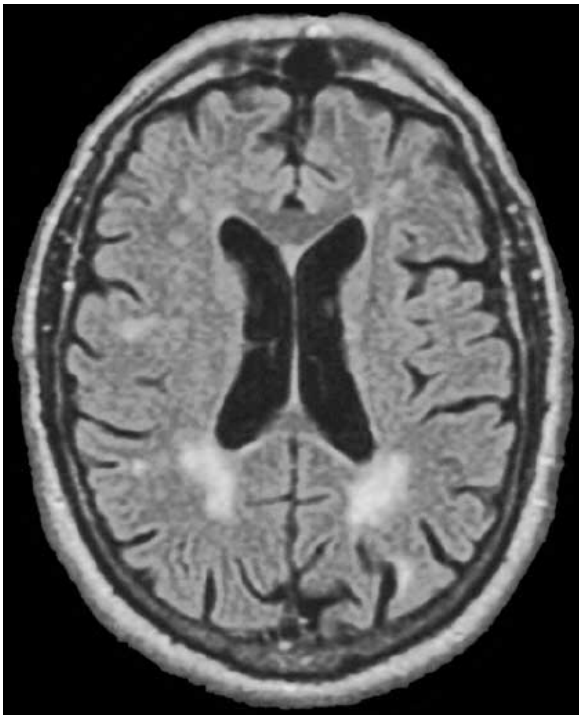

Source: Timothy C. Hain, MD. http://www.dizziness-and-balance.com/disorders/central/pvm.htm

Figure 1. MRI of the brain. This is section is in the horizontal plane, just above the ears. Mild periventricular white matter lesions can be seen (the white spots towards the bottom).

White matter lesions are associated with retinal microvascular abnormalities. Persons with both white matter lesions and retinopathy have a much higher risk of clinical stroke (20% vs 1.4%) (Wong et al., 2002). Demyelinating disorders, such as multiple sclerosis, can cause PWM. The consequences of periventricular white matter lesions may be serious. White matter lesions strongly correlate with reduced gait speed as well as reduced mental ability (Starr et al., 2003; Guttman et al., 2000; Whitman et al., 2001; Bazner et al., 2008). Periventricular location of white matter lesions seems to cause the most serious consequences. Individuals with PVM lesions perform nearly one standard deviation below average on tasks involving psychomotor speed.

Pathologically, PWM correspond to areas of myelin thinning and gliosis, and are often accompanied by lacunar (small holes) infarctions and small vessel atherosclerotic disease. Practically, PWM seem to be associated with severe consequences. Once a patient has them, they are present for life, and prevention is the main goal of treatment.

We advocate attention to reducing vascular risk factors, and especially controlling labile hypertension. Reducing elevated cholesterol and strict control of diabetes are probably helpful too. Small amounts of vitamin b6 (pyridoxine) supplementation also seem reasonable (i.e., 2 mg/day). It is not clear if daily aspirin intake is useful or harmful in persons with PWM. Beta-blockers such as propranolol and related medications may be especially suitable for preventing spikes in blood pressure. These drugs are also cardioprotective. In persons with migraine, a prophylactic regimen is recommended, such as a combination of low-dose aspirin and a migraine prevention agent such as verapamil, but it is not known whether this treatment regimen is effective. Beta-blockers would also seem reasonable.

Treatment of the demyelinating diseases may be possible. With respect to the common symptom of unsteadiness, treatments such as physical therapy may be useful. While medications are not, in general, helpful in situations where fiber tracts or neurons have died, trials of medications such as antidepressants or anti-Parkinsonian drugs may be helpful for some patients.

White Matter Hyperintensities in Neurological Disorders

White matter abnormalities are common in several neurological disorders, such as multiple sclerosis (MS), which is predominantly a disease of the white matter in the central nervous system. About 95% of all lesions associated with multiple sclerosis occur in the white matter. In fact, MS is one of the most common diseases affecting white matter. In MS lesions, the myelin shield around the axons has been destroyed by inflammation.

Vanishing White Matter Disease (VWM) is a type of leukodystrophy inherited in an autosomal recessive manner. Symptoms generally appear in young children who may seem to have been developing fairly normally. However, it has been shown recently that VWM can begin at or shortly after birth, as well as in adulthood. A striking feature of the disease is that the symptoms get worse slowly for the most part, but there are episodes of rapid deterioration that follow an infection or head trauma. The patient may have a partial recovery following these episodes, or the episode may lead to coma and death. VWM is caused by mutations in one of the five genes that are collectively called eIF2B (eukaryotic initiation factor 2B). This gene is necessary to make proteins in the body properly. VWM is caused by changes in these genes that reduce the function of eIF2B. This reduction in function becomes a particular problem during episodes of fever, infection, or head traumas, and deterioration accelerates after such episodes. Generally, symptoms such as neurological deterioration; febrile episodes, episodes of fever, drowsiness or coma, spasticity, lethargy, abnormal drowsiness and indifference to environmental stimuli may appear beginning in late infancy or early childhood and delay psychomotor development. The disease includes ovary dysgenesis, (defective development of the ovaries), cerebellar ataxia (loss of muscle coordination, a result of abnormal functioning of the cerebellum), optic atrophy (that includes abnormalities of the eyes), and seizures. Mental impairment may be present, although generally this is less severe than the motor dysfunction. The motor difficulties of VWM are progressive, but the progression is often stepwise and associated with fever or injuries.

In the brain, the white matter is irrigated by tiny blood vessels, which are the first to be affected by atherosclerosis and other diseases of the blood vessels. White matter disease purely refers to MRI or CT findings, which show that the white matter of the brain has been affected by certain disease processes, usually chronic in nature, such as high blood pressure, diabetes, high cholesterol, and the like. A small amount of these changes is expected to appear with age, but large amounts of them are associated with specific diseases such as multiple sclerosis, Wilson's disease, and even Alzheimer's disease. Changes in white matter known as amyloid plaques are associated with Alzheimer's disease and other neurodegenerative diseases. White matter injuries ("axonal shearing") may be reversible, while gray matter regeneration is less likely. People with high stroke risk factors are known to have a higher burden of white matter disease.

The white matter of the brain is involved in some neurological disorders in childhood. These are called "the white matter disorders". The diagnosis is usually made on the basis of MRI findings. White matter abnormalities on MRI can have different bases at the tissue level. It may be that there is a lack of myelin because the myelin was never made in sufficient amounts. It may be that the myelin was formed appropriately, but is now broken down and lost. It may be that innumerable vacuoles are formed within the myelin sheath. It may be that scar tissue is formed within the white matter. There may be increased amounts of water between the myelinated fibers. Nerve fibers may be lost as well. It is clear that the term "white matter disorder" comprises many different disorders which have different consequences for brain function. For instance, loss of myelin is worse for brain function than an increase in water content or the formation of scar tissue between nerve fibers. It is, therefore, clear that the resulting handicap for the child with a white matter disorder is highly variable depending on what is happening at brain tissue level. White matter disorders are usually progressive, the children affected are going to have increasing neurological handicaps and death may result.

White Matter in Psychiatric Diseases

White matter, long thought to be passive tissue, actively affects how the brain learns and dysfunctions. The timing of the growth and degree of completion can affect learning, self-control (and why teenagers may lack it), and mental illnesses such as schizophrenia, autism and even pathological lying. The prevalence and significance of WMH on brain MRI has been studied in patients with a number of psychiatric illnesses including substance abuse/dependence, depression, schizophrenia, obsessive-compulsive disorder, panic disorder, and several childhood psychiatric disorders.

Recently, the Toronto-based Centre for Addiction and Mental Health published a study showing that child molesters with pedophilia suffer from a "significant lack of white matter connecting six different areas of the brain all known to play a role in sexual arousal." (Brain wiring link to paedophilia; Pedophiles have less brain white matter: Toronto study).

White Matter Hyperintensities in Mood Disorders

WMH and Major Depressive Disorder

A large number of studies have found a higher rate and severity of white matter hyperintensities in individuals with late-life depression compared with healthy elderly controls (Iidaka et al., 1996; Tupler et al., 2002; Taylor et al., 2005; Coffey et al., 1993). Individuals with early onset depression (EOD), who by definition have experienced a longer duration of illness, should then demonstrate more severe white matter hyperintensities than individuals with late onset depression (LOD). The main hypothesis is that white matter hyperintensities in a subgroup of patients affected by depression may reflect an underlying condition (i.e., cerebrovascular disease) that predisposes individuals to the development of depression (Krishnan et al., 1997; Alexopoulos et al., 1997) by disrupting fiber tracts connecting cortical and subcortical structures (particularly frontostriatal circuits). Consistent with this hypothesis, LOD is also associated with pronounced deficits in processing speed and executive functions (Herrmann et al., 2007). Takahashi et al. (2007) suggested that, regarding deep white matter hyperintensities, patients affected by LOD exhibited a higher rating than EOD, particularly in the bilateral frontal areas and in the left parietooccipital area. LOD, but not EOD, is associated with more severe pathological changes, and there was a significant difference in the severity of changes in the right frontal areas. The frontal lobes have mutual fiber communications with subcortical nuclei, such as the thalamus, basal ganglia, and amygdala, with five independent parallel circuits proven, which Tekin and Cummings (2002) organized and classified into two groups: (1) the dorsolateral prefrontal and lateral orbitofrontal subcortical circuits and (2) the medial orbitofrontal and anterior cingulate circuits. Projections from the mesencephalon or the subcortical gray matter to the frontal lobes are related to the emotional processing of information and the maintenance of emotional states, and some investigators postulate that these neural networks may be disturbed in depression (Brody et al.., 2001). Therefore, it is possible that functional deficits in the frontal lobes are caused by subcortical lesions within these circuits, resulting in secondary functional deficits in the frontal areas that trigger mood disorders. Probably, in mood disorder patients, the time since the onset of disorder does not affect the development of white matter lesions, but white matter lesions are associated with late-onset mood disorders. As for brain regions, it has also been proposed that the frontal areas and the left parieto-occipital areas are important for the development of late-onset depression.

Regarding deep white matter hyperintensities (DWMH), there are many reports that suggest DWMH are more severe in late-onset depression than in normal controls (Greenwald et al., 1996; Kumar et al., 1997; Tupler et al., 2002). Salloway et al. (1996) reported that DWMH as well as PWH were significantly more severe in the late-onset depression group than in the early-onset depression group. These findings support the cerebrovascular hypothesis, reinforced by other findings, that in both depressed and non-depressed individuals, white matter hyperintensities are highly associated with cerebrovascular risk factors, in particular hypertension (Kumar et al., 1997; Awad et al., 1986; Taylor et al., 2005; Greenwald et al., 2001; Lesser et al., 2001) but also diabetes, a history of myocardial infarction or coronary artery disease, and smoking (Kumar et al., 1997; Fazekas et al., 1988).

Moreover, neuropathological studies show that white matter hyperintensities are characterized by arteriosclerosis, perivascular demyelination, dilated periventricular spaces, vascular ecstasia, ischaemia, incomplete infarction and infarction with necrosis (Chimowitz et al., 1999; Thomas et al., 2002). Increased severity of hyperintense lesions is related to a more chronic course of depression (Heiden et al., 2005; Hickie et al., 1997; O'Brien et al., 1998), poorer response to antidepressant medication (Hickie et al., 1995; Simpson et al., 1997; Taylor et al., 2003) and long-term disability (Hickie et al., 1997).

In addition, some authors have reported that WMH are related to cognitive decline in various domains, particularly executive skills, attention and mental speed (Lesser et al., 1994; Hickie et al., 1995; Kramer-Ginsberg et al., 1999; Murata et al., 2001), while several studies have failed to find an association of WMH with cognition (Harrel et al., 1991). It is possible that white matter hyperintensities are also of clinical significance in LOD. Consistent with the natural history of cerebrovascular disease, the vascular depression hypothesis predicts a late age of onset (Taylor et al., 2003). However, considering that there are various studies that have failed to show a difference between patients with LOD and EOD in the rate and severity of white matter hyperintensities (Kumar et al., 1995; Krishnan et al., 1993; Churchill et al., 1991; Miller et al., 1994; Ebmeier et al., 1997; Lloyd et al., 2004), Herrmann et al. (2008) suggested that the nature of confounding factors related to the presence or absence of WMH in LOD is still unclear, and further studies are needed to evaluate the nature of this association.

White Matter Hyperintensities and Bipolar Disorders

The severity and prevalence of WMH on T2-weighted magnetic resonance imaging in subjects with bipolar disorder have been studied. Meta-analyses have estimated that the common odds ratios for having WMH are 3.2–3.3 in bipolar patients, although some studies do not support this hypothesis. Magnetic resonance imaging (MRI) studies in adults with bipolar disorder (BD) have suggested the presence of assorted global cortical abnormalities, including differences in total brain volume, lobar volume, gray/white matter ratios, ventricular size, and number of white matter hyperintensities (WMH) (reviewed in Strakowski et al., 2000). These findings have not been replicated consistently, but the most consistent structural finding in adult BD has been the presence of increased numbers of WMH (Dupont et al., 1987, 1990; Figiel et al., 1991; Stoll et al., 2000; Swayze et al. 1990), areas of abnormally high signal intensity on T2 images compared with surrounding tissue. White matter hyperintensities might represent dilated perivascular spaces, areas of micro-infarcts or hemorrhage, or an as yet undiscovered neuropathologic entity.

By contrast, some studies, including one of first-hospitalization BD patients, failed to detect increased WMH in BD (Altshuler et al., 1995; Brown et al., 1992; Krabbendam et al 2000; Sassi et al., 2003; Strakowski et al., 1993b). Therefore, although there have been varying reports of morphologic brain abnormalities in BD and it is unclear whether WMH are causal to or the result of bipolar illness, overall patterns from the literature suggest that adults with BD might have prefrontal, temporal, ventricular, and white matter abnormalities.

In a recent trial, Zanetti et al. (2008) reported that there were no significantly increased rates or severity indices of white-matter hyperintensities in one of the separate psychosis subgroups relative to the control group (unipolar depression subgroup), a result that was consistent with the most recent MRI studies carried out with samples of non-elderly adults with major depression (Sassi et al., 2003; Iosifescu et al., 2006). Regarding the bipolar disorder subgroup, there seemed to be a low prevalence of white-matter hyperintensities.

Findings of increased rates in bipolar disorder have been previously reported. Two meta-analyses have found that the risk of individuals with bipolar disorder presenting with white-matter hyperintensities is over three times higher than that for healthy controls (Altshuler et al., 1995; Videbech, 1997). On the other hand, several studies suggested there was not an increased rate of white matter hyperintensities associated with bipolar disorder (Sassi et al., 2003; Brown et al., 1992; Krabbendam et al., 2000; Chang et al., 2005). Strakowski et al. (1993), in the only study to evaluate the frequency of white matter hyperintensities in first-episode mania, reported a nonsignificant increased rate of subcortical white matter hyperintensities in the bipolar disorder group. Also, there is relevant heterogeneity in previous reports regarding the prevalence rates in both those with bipolar disorder and control samples, with frequencies of total hyperintensities ranging, respectively, from approximately 5% to 66% and 0% to 58% among studies that evaluated young or adult individuals (Sassi et al., 2003; Krabbendam et al., 2000; Videbech, 1997; Chang et al., 2005; Lyoo et al., 2005; Ahn et al., 2004).

The main location of white matter lesions is controversial. Some studies report higher rates of white-matter hyperintensities in periventricular regions in bipolar disorder samples (Altshuler et al., 1995), while others suggest increased deep white-matter hyperintensity ratings associated with bipolar disorder (Videbech, 1997; Lyoo et al., 2002; McDonald et al., 1999). The only quantitative analysis of white matter lesions in individuals affected by psychiatric diseases reported increased volumes of white-matter hyperintensity in anterior brain regions of individuals with bipolar disorder compared with those with unipolar depression and healthy controls (Dupont et al., 1995). Several authors have reported frontal (Lyoo et al., 2002; Dupont et al., 1995) and frontoparietal (Figiel et al., 1991; Aylward et al., 1994) location of white-matter lesions in association with bipolar disorder. Only one recent study (de Asis et al., 2006) directly compared frontal deep white-matter hyperintensities in an elderly population of individuals with bipolar disorder and controls and found increased left frontal scores in the bipolar disorder group. Most of these studies have not systematically assessed vascular risk factors and history of substance abuse or dependence in the individuals recruited, and the majority of the studies have been conducted with small and heterogeneous samples, poorly controlled for several variables such as clinical disease course, age, gender and comorbidities. All these factors, together with methodological differences among studies, are likely to have contributed to the lack of consistency in the findings.

Recent MRI studies using diffusion tensor imaging in people with bipolar disorder (Haznedar et al., 2005; Beyer et al., 2005), but including again modest samples, revealed structural white matter abnormalities located in the frontal lobe and adjacently to the striatum and thalamus. Such findings suggest that diffusion tensor imaging techniques may be more sensitive for finding white matter abnormalities in association with bipolar disorder. In support of this possibility, a study combining diffusion tensor imaging and white-matter

hyperintensity measurements in healthy elderly individuals detected structural damage indicated by increased diffusion coefficients in areas of normally appearing white matter surrounding the foci of white-matter hyperintensities (Firbank et al., 2003). However, different mechanisms may be involved in the emergence of white-matter hyperintensities in the elderly. Rates of white-matter hyperintensities in the elderly population in fact increased in direct proportion to the presence of cardiovascular risk factors (Zanetti et al., 2007).

Another question is whether the use of psychotropic medication could influence the presence of white matter lesions. Though data regarding the possible influence of antipsychotic drugs is scarce, there is no evidence that the use of lithium, tricyclic antidepressants or antiepileptic drugs is linked to increased rates of white-matter hyperintensities (Sassi et al., 2003; Persaud et al., 1997; Altshuler at al, 1995; Videbech et al., 1997). An interesting perspective is that white matter lesions could simply represent the 'tip of the iceberg' in terms of structural white matter lesions and the techniques available are not powerful enough to detect the deep underlying alterations (Zanetti et al., 2008). The presence and severity of white-matter hyperintensities associated with bipolar disorder might be understood as an extreme consequence of underlying microstructural processes that affect brain connectivity and which may be more specifically investigated using diffusion tensor imaging methods.

White Matter Hyperintensities and Schizophrenia

Schizophrenia has been hypothesized to be a neurodevelopmental disorder in which genetic vulnerabilities combine with a variety of central nervous system insults to provoke the manifestation of symptoms. Some neuroimaging abnormalities in schizophrenia are evident before the onset of the disorder. People with prodromal symptoms who have a high risk of developing schizophrenia show abnormalities of prefrontal and anterior cingulate function and increased striatal dopamine levels that are qualitatively similar to the changes seen in established schizophrenia. These findings raise the possibility that neuroimaging could be used to detect pathophysiological changes associated with the disorder before the onset of frank illness. This is of particular clinical interest because only a proportion of people with prodromal symptoms go on to develop schizophrenia, and neuroimaging might facilitate the targeting of novel preventive treatments.

There have been conflicting findings regarding the frequency of white-matter hyperintensities in schizophrenia. Most studies of white-matter hyperintensities have been conducted with small and heterogeneous samples, and this might account for the inconsistencies.

Most studies suggest that the presence and extension of white-matter hyperintensities are not associated with vulnerability to psychotic symptoms in adult populations. The absence of significant correlations between white-matter hyperintensity scores and clinical variables related to psychotic features – duration of illness, duration of untreated psychosis and severity of psychotic symptomatology – corroborates this conclusion. It is important, however, to raise the possibility that white-matter hyperintensities could be a feature related to illness chronicity. Neuroimaging techniques have been applied to study late-onset

schizophrenia (LOS) in many published studies. Some magnetic resonance imaging (MRI) studies have suggested an excess of white matter lesions in subjects with late-onset schizophrenia in relation to normal comparison subjects, especially on T2-weighted imaging (Sachdev et al., 1999), but more recent systematic studies have not been supportive of this. The significance of increased periventricular hyperintensities in late-onset schizophrenia remains somewhat uncertain. Mild severity periventricular white matter hyperintensities are often not indicative of brain disease because they are found in healthy individuals with no evidence of neuropsychological impairment. While high severity periventricular hyperintensities are usually associated with intracerebral pathology, these findings are aspecific (Rivkin et al., 2000). The major mechanism for their development is considered to be trans-ependymal absorption of cerebrospinal fluid, usually associated with normal pressure hydrocephalus, subcortical arteriosclerotic encephalopathy, perivascular atrophy and cerebrovascular diseases.

Many studies have replicated the finding of higher signal hyperintensities in the thalami of subjects with late-onset schizophrenia, and this is noteworthy in light of the reports of thalamic abnormality in schizophrenia.

Decreased thalamic size has been consistently reported in the early-onset schizophrenia literature, both from neuroimaging and neuropathological studies. The presence of a subset of LOS subjects with notably large WMH volume suggests that white matter pathology might be at least a contributing factor to the development of schizophrenia late in life. One plausible scenario consistent with this is that a subset of subjects vulnerable to developing schizophrenia develops hypertension or other risk factors. These risk factors in turn provoke degenerative tissue changes that increase the probability of the development of WMH and symptomatic schizophrenia.

The correlation between signal hyperintensities and neuropsychological impairment has been investigated in many studies. Whereas consistent results have not emerged, most studies, but not all, have demonstrated a relationship between the extent of signal hyperintensities and neuropsychological dysfunction.

White Matter Hyperintensities and Their Association with Suicidality

A large body of evidence suggests that predisposition to suicide is certainly mediated by biological factors and that suicidal behavior has strong neurobiological determinants. Considering that suicide is a great healthy problem worldwide, understanding the neurobiology of suicide will ultimately yield clinical tools to treat suicidal behavior and prevent deaths (Mann et al., 1999). In recent decades, several research teams have tried to detect a biological basis for suicidality. As imaging techniques offer a unique possibility to investigate brain during psychiatric disturbances, they could be a useful tool for screening for biological markers for suicidal behavior.

The application of neuroimaging to the study of suicide attempts has been limited. Postmortem studies have suggested a reduction in the parahippocampal cortex. Neuronal density was increased in the prefrontal cortex of schizophrenic patients who committed

suicide but was unchanged in bipolar disorder suicide victims. Suicide attempters and victims have a variety of abnormalities in the serotoninergic system such as low cerebrospinal fluid (CSF) 5-Hydroxyindoleacetic acid (5-HIAA) levels, fewer serotonin transporter sites in the prefrontal cortex and upregulated postsynaptic 5-HT1A and 5-HT2A receptors (Mann, 2003). Two-thirds of the attempters had low levels of CSF 5-HIAA compared with the non-attempters of whom only one-third had low levels of CSF 5-HIAA. In an adolescent psychiatric population with major depression who have undergone appropriate treatments, it has been suggested that the more lethal is the attempt, the more likely there are to be lower levels of CSF 5-HIAA (Greenhill L, Shaffer D, Mann JJ, unpublished data, 1998; Mann et al., 1997). Low CSF 5-HIAA is also been found in suicide attempters with schizophrenia (Ninan et al., 1984; van Praag et al., 1983) and personality disorders (Gardner et al., 1990) compared with patients with the same diagnoses but with no history of suicide attempts. Probably the relationship between lower levels of CSF 5HIAA and suicide attempts could be regarded as an independent marker in understanding the neurobiology of specific psychiatric disorders (Mann et al., 1999).

A similar relationship may be observed between CSF 5-HIAA and severity of lifetime aggression (Goodwin 1986; Brown, 1982a; 1982b; 1986) - lower levels of CSF 5HIAA are correlated with an elevated severity of lifetime aggression. Considering that this relationship has been widely reported, CSF 5-HIAA levels may be a biological variable related to lifetime patterns of behavior and also predictive of future behavior, specifically a higher risk of future suicide attempts. In fact, patients who had lower levels of CSF 5-HIAA had a higher rate of completed suicide during the 12 months after hospital discharge (Nordström et al., 1994). Factors that influence serotonergic activity may be relevant for suicidal behavior. For example, blunted prolactin response to fenfluramine and abnormal serotonin responsivity correlates with past and future aggression and suicidal acts.

Finally by using the Positron Emission Tomography technique (P.E.T.), an increase in metabolic activity in the ventral prefrontal cortex (VPFC) in response to fenfluramine challenge has been found. These data are in keeping with those of structural and functional postmortem brain studies of suicidal victims regarding abnormalities in this specific cortical area (Mann et al., 1996).

Recent studies on young adults and elderly depressed women have demonstrated a significant association between MRI white matter hyperintensities and suicide attempts (Ahearn et al., 2001; Ehrlich et al., 2004; 2005). Depressed or bipolar patients, in comparison with healthy control subjects, have been shown to have a greater prevalence of white matter hyperintensities. A landmark study on neuroimaging in suicidal behavior by Ahearn and colleagues (2001) compared MRI findings in unipolar patients with and without a history of a suicide attempt. Their results demonstrated significant subcortical gray matter hyperintensities in unipolar patients with a history of a suicide attempt as compared to patients without such a clinical history. There was also a trend toward more periventricular white matter hyperintensities in patients with a suicide attempt using the Coffey classification system.

Previously, Ehrlich et al. (2003), in a sample of 153 child and adolescent psychiatric inpatients, reported a correlation between right parietal lobe DWMH with a high risk for a history of suicide attempt. The posterior parietal lobe is considered to be critical for spatial

cognition, attention, task switching and consciousness (Taylor, 2001), and abnormalities in the parietal lobe are associated with neglect, not only in unipolar, but also in bipolar disorders (Biver et al., 1994; Berns et al., 2002). Recently, Ehrlich (2004; 2005) and colleagues demonstrated a significantly increased prevalence of PWH but not DWMH in young adults with major depressive disorder and a history of suicide attempt as compared to depressed young adults without such a history. WMH lesions probably reflect disruptions of neuroanatomic pathways essential for the maintenance of normal mood (Steffens and Krishnan, 1998), and so their exact location is of great interest.

More recent studies have shown a significantly increased prevalence of periventricular white matter hyperintensities (PWH) but not deep white matter hyperintensities (DWMH) in adults with major affective disorders and a history of suicide attempt as compared to a psychiatric population without suicidal behavior. Unfortunately, WMH are also commonly associated with older age and several cardiovascular factors such as hypertension and diabetes (Videbech P, 1997; Steffens and Krishnan, 1998; Ovbiagele and Saver, 2006). There has been particular clinical interest in the association between WMH lesions and symptoms of depression (O'Brien et al., 1996; Schmidt et al., 1997), cognitive dysfunctions (Nebes et al., 2002; Steffens et al., 2001; 2002), adverse effects and treatment response to antidepressant medication (Coffey et al., 1989; Fujikawa et al., 1996; Hickie et al., 1995; Schmidt et al., 1997; Simpson et al., 2000).

After controlling for cardiovascular risk factors, many reports have suggested that the population of patients with WMH includes cases with silent cerebral infarction, seen as low signals intensity in T1-weighted images. As suggested by Ylikoski et al. (2000), WMH lesions particularly in elderly subjects without neurological diseases were strongly related to age, silent infarct, atrophy and some vascular risk factors, such as diabetes and cardiac arrhythmia. Komaki and colleagues (2008) concluded that there is no evidence that cerebrovascular disease is related directly to formation of WMH lesions, but aging itself is an important risk factor for WMH lesions. WMH lesions contribute to the initial onset of depression in the form of some organic factor, and the severity of illness is greater in subjects with WMH lesions. Subjects affected by WMH lesions and lacunar infarction are at high risk of suicide compared with patients with WMH and no lacunar infarction.

Pompili et al. (2007) found increased incidence of WMH in patients with major affective disorders and a history of suicide attempt, supporting the association previously observed between WMH and suicidality. Although WMH in patients with major affective disorders did not distinguish between non-suicidal and suicidal individuals, as suggested by other authors (Ehrlich et al., 2004; 2005), WMH, independently from other factors, may be considered to be a marker for suicide attempts, not only in patients with major affective disorders but also in patients with bipolar disorders. There is also a strong relationship between WMH and symptom severity. Higher rates of WMH were associated with multiple psychiatric admissions, higher rates of relapse and poor long-term outcome (O'Brien et al., 1998; Silverstone et al., 2003; Yanai et al., 1998). Also, Pompili et al. (2008) demonstrated that the MRI T2 FLAIR scans of attempters with major affective disorder and non attempters differed only in the presence of periventricular white matter hyperintensities (PWH). In their sample, attempters and nonattempters did not differ in the main cardiovascular risk factors such as

hypertension, hypertriglyceridemia, or hyperglycemia. The presence of PWH makes the risk of suicide behavior 8 times higher than the absence of any periventricular lesion.

Interestingly, PWH are less likely to be associated with confounding variables such as demographic and cardiovascular factors. In accordance with previous studies, it could be argued that patients with WMH (especially PWH) may be at higher risk for suicide attempts because of possible disruption of neuroanatomic pathways. A neuroanatomic model of mood regulation including the prefrontal cortex, amygdala–hippocampus complex, thalamus, basal ganglia and the extensive connections between these areas has been proposed. Lesions in one specific part or disruption of interconnections among areas regulating mood could trigger the onset of mood disorders and confer a biological vulnerability. MRI-detected hyperintensities may lead to mood disorders by disrupting vital pathways controlling mood regulation, and these alterations in combination with environmental stressors may result in suicidal behavior.

Age appeared to be positively associated with the frequency of WMH (Pompili et al., 2007). This finding may be explained considering the association between cardiovascular risk factors and DWMH as suggested by Ehrlich et al. (2004; 2005). WMH correlated with suicidality are probably different from WMH correlated with cardiovascular risk factors (Dufouil et al., 2001). The etiology of WMH with respect to suicidality could be hypoxic-ischemic insults during birth which are especially common in preterm infants. Perinatal white matters lesions represent damage of association-commissural and projection fibers and may lead to abnormalities in the organization and use of neural systems (Judas et al., 2005; Peterson, 2003). Neonatal cranial ultrasound diseases suggestive of white matter injury, probably triggering malfunctions in areas involving in the emotional regulatory circuit, could confer a biological vulnerability (Soares and Mann, 1997), increasing the risk of psychiatric disorders in adults (Whitaker et al., 1997). Cerebral white matter injury, characterized by loss of premyelinating oligodendrocytes, is the most common form of injury to the preterm brain and is associated with a high risk of neurodevelopmental impairment that significantly increases the risk for psychiatric symptoms.

In conclusion, patients with affective disorders and periventricular hyperintensities are more likely to have a history of suicide attempts even after controlling for potential confounding variables such as cardiovascular risk factors and age. However, PWH were able to explain only a small part of the variability of suicide attempt risk, indicating that one single variable is not sufficient to predict suicidality. Several clinical, personality and biological predictors need to be considered in order to make effective and specific predictions of the risk of attempted suicide. Combining clinical and biological predictors that are independent may provide an improved predictive model (Mann et al., 2006).

References

[1] Ahearn EP, Jamison KR, Steffens DC et al. MRI correlates of suicide attempt history in unipolar depression. *Biol. Psychiatry.* 2001; 50: 266-270.

[2] Ahn KH, Lyoo IK, Lee HK, et al. White matter hyperintensities in subjects with bipolar disorder. *Psychiatry Clin. Neurosci.* 2004;58:516–21.

[3] Alexopoulos GS, Meyers BS, Young RC, et al. 'Vascular depression' hypothesis. *Arch. Gen. Psychiatry.* 1997;54:915–22.

[4] Altshuler LL, Curran JG, Hauser P, et al. T2 hyperintensities in bipolar disorder: magnetic resonance imaging comparison and literature meta-analysis. *Am. J. Psychiatry.* 1995;152:1139–44.

[5] Arango V, Ernsberger P, Sved AF, Mann JJ. Quantitative autoradiography of alpha 1- and alpha 2-adrenergic receptors in the cerebral cortex of controls and suicide victims. *Brain Res.* 1993;630:271-82.

[6] Arango V, Underwood MD, Gubbi AV, Mann JJ. Localized alterations in pre- and postsynaptic serotonin binding sites in the ventrolateral prefrontal cortex of suicide victims. *Brain Res.* 1995;688:121-33.

[7] Assaf Y, Pasternak O: Diffusion tensor imaging (DTI)-based white matter mapping in brain research: a review. *J. Mol. Neurosci.* 2008;34(1):51–61.

[8] Awad IA, Spetzler RF, Hodak JA, et al.: Incidental subcortical lesions identified on magnetic resonance imaging in the elderly. I. Correlation with age and cerebrovascular risk factors. *Stroke.* 1986;17:1084–9.

[9] Aylward EH, Roberts-Twillie JV, Barta PE, et al.: Basal ganglia volumes and white matter hyperintensities in patients with bipolar disorder. *Am. J. Psychiatry*. 1994;151:687–93.

[10] Bachus SE, Hyde TM, Herman MM, Egan MF, Kleinman JE: Abnormal cholecystokinin mRNA levels in entorhinal cortex of schizophrenics. *J. Psychiatr. Res.* 1997;31:233-56.

[11] Baloh RW, Sloane PD, Honrubia V: Quantitative vestibular function testing in elderly patients with dizziness. *Ear, Nose and Throat.* 1989;68:935-9.

[12] Baszner H, Blahak C, Poggesi A, et al.:: Association of gait and balance disorders with age-related white matter changes. The LADIS study. *Neurology.* 2008:70:935-42.

[13] Belal A, Glorig A: Disequilibrium of aging (presbyastasis). *J. Laryngol. Otol.* 1986;100:1037-41.

[14] Berns GS, Martin M, Proper SM. Limbic hyperreactivity in bipolar II disorder. *Am. J. Psychiatry.* 2002; 159: 304-306

[15] Beyer JL, Taylor WD, MacFall JR, et al.: Cortical white matter microstructural abnormalities in bipolar disorder. *Neuropsychopharmacology.* 2005;30:2225–9.

[16] Biver F et al. Frontal and parietal metabolic disturbances in unipolar depression. *Biol. Psychiatry.* 1994; 36: 381-388

[17] Brain wiring link to paedophilia. Retrieved on September 19 2008. http://news.bbc.co.uk/2/hi/health/7116506.stm.

[18] Brent DA, Mann JJ: Family genetic studies, suicide, and suicidal behavior. *Am. J. Med. Genet. C Semin. Med. Genet.* 2005;133:13-24.

[19] Brown GL, Ebert MH, Goyer PF, et al. Aggression, suicide and serotonin: relations to CSF amine metabolise. *Am. J. Psychiatry.* 1982; 139: 741-746

[20] Brown GL, Goodwin FK, Bunney WE, Jr. Human aggression and suicide: their relationship to neuropsychiatric diagnoses and serotonin metabolism. *Adv. Biochem. Psychopharmacol.* 1982; 34: 287-307.

[21] Brown GL, Goodwin FK. Cerebrospinal fluid correlates of suicide attempts and aggression. *Ann. N. Y. Acad. Sci.* 1986; 487: 175-188.

[22] Brown FW, Lewine RJ, Hudgins PA, Risch SC: White matter hyperintensity signals in psychiatric and nonpsychiatric subjects. *Am. J. Psychiatry.* 1992;149:620–5.

[23] Chang K, Barnea-Goraly N, Karchemskiy A, et al.: Cortical magnetic resonance imaging findings in familial pediatric bipolar disorder. *Biol. Psychiatry.* 2005;58:197–203.

[24] Chimowitz MI, Awad IA, Furlan AJ: Periventricular lesions on MRI. Facts and theories. *Stroke.* 1989;20:963–7.

[25] Churchill CM, Priolo CV, Nemeroff CB, et al.: Occult subcortical magnetic resonance findings in elderly depressives. *Int. J. Geriatr. Psychiatry.* 1991;6:213–6.

[26] Coffey CE, Figiel GS, Djang WT, Saunders WB, Weiner RD, White matter hyperintensity on magnetic resonance imaging: clinical and neuroanatomic correlates in the depressed elderly. *J. Neuropsychiatry Clin. Neurosci.* 1989; 1: 135-144

[27] Coffey CE, Wilkinson WE, Weiner RD, et al.: Quantitative cerebral anatomy in depression. A controlled magnetic resonance imaging study. *Arch. Gen. Psychiatry.* 1993;50:7–16.

[28] de Asis JM, Greenwald BS, Alexopoulos GS, et al.: Frontal signal hyperintensities in mania in old age. *Am. J. Geriatr. Psychiatry.* 2006;14:598–604.

[29] De Groot, de Leeuw FE, Oudkerk M, et al.: Cerebral white matter lesions and cognitive function: the Rotterdam Scan study. *Ann. Neurol.* 2000:47:145-51.

[30] Dufouil C, de Kersaint-Gilly A, Besancon V. Longitudinal study of blood pressure and white matter hyperintensities: the EVA MRI Cohort*: Neurology.* 2001; 56: 921-926.

[31] Dupont RM, Jernigan TL, Butters N, et al.: Subcortical abnormalities detected in bipolar affective disorder using magnetic resonance imaging. Clinical and neuropsychological significance. *Arch. Gen. Psychiatry.* 1990;47:55–9.

[32] Dupont RM, Jernigan TL, Gillin JC, et al.: Subcortical signal hyperintensities in bipolar patients detected by MRI. *Psychiatry Res.* 1987;21:357–8.

[33] Dupont RM, Jernigan TL, Heindel W, et al.: Magnetic resonance imaging and mood disorders. Localization of white matter and other subcortical abnormalities. *Arch. Gen. Psychiatry.* 1995;52:747–55.

[34] Dwivedi Y, Rao JS, Rizavi HS, et al.: Abnormal expression and functional characteristics of cyclic adenosine monophosphate response element binding protein in postmortem brain of suicide subjects. *Arch. Gen. Psychiatry.* 2003;60:273-82.

[35] Ebmeier KP, Prentice N, Ryman A, et al.: Temporal lobe abnormalities in dementia and depression: a study using high resolution single photon emission tomography and magnetic resonance imaging. *J. Neurol. Neurosurg. Psychiatry.* 1997;63:597–604.

[36] Ehrlich S, Breeze JL, Hesdorffer DC et al. White matter hyperintensities and their associations with suicidality in depressed young adults. *J. Affect. Disord.* 2005; 86: 281-287.

[37] Ehrlich S, Noam GG, Lyoo IK, Kwon BJ, Clark MA, Renshaw PF. White matter hyperintensities and their associations with suicidality in psychiatrically hospitalized children and adolescents. *J. Am. Acad. Child Adolesc. Psychiatry.* 2004; 43: 770-776

[38] Fife TD, Baloh RW: Disequilibrium of unknown causes in older people. *Ann. Neurol.* 1993;34:594-702.

[39] Figiel GS, Krishnan KR, Rao VP, et al.: Subcortical hyperintensities on brain magnetic resonance imaging: a comparison of normal and bipolar subjects. *J. Neuropsychiatry. Clin. Neurosci.* 1991;3:18–22.

[40] Fujikawa T,Yokota N, Muraoka M, Yamawaki S. Response of patients with major depression and silent cerebral infarction to antidepressant drug therapy, with emphasis on central nervous system adverse reactions. *Stroke.* 1996; 27: 2040-2042

[41] Goodwin FK. Suicide, aggression and depression: a theoretical framework for future research. *Ann. N. Y. Acad. Sci.* 1986; 487: 351-355.

[42] Gardner DL, Lucas PB, Cowdry RW. CSF metabolites in borderline personality disorder compared with normal controls. *Biol. Psychiatry.* 1990; 28: 247-254.

[43] Greenwald BS, Kramer-Ginsberg E, Krishnan KRR, et al.: A controlled study of MRI signal hyperintensities in older depressed patients with and without hypertension. *J. Am. Geriatr. Soc.* 2001;49:1218–25.

[44] Greenwald BS, Kramer-Ginsberg E, Krishnan KRR, et al.: MRI signal hyperintensities in geriatric depression. *American Journal of Psychiatry.* 1996;153:1212–5.

[45] Guttmann CRG, Benson R, Warfield SK, et al.: White matter abnormalities in mobility impaired older persons. *Neurology.* 2000;54:1277-83.

[46] Harrell LE, Duvall E, Folks DG, et al.: The relationship of high-intensity signals on magnetic resonance images to cognitive and psychiatric state in Alzheimer's disease. *Arch. Neurol.* 1991;48:1136–40.

[47] Haznedar MM, Roversi F, Pallanti S, et al.: Fronto-thalamo-striatal gray and white matter volumes and anisotropy of their connections in bipolar spectrum illnesses. *Biol. Psychiatry.* 2005;57:733–42.

[48] Heiden A, Kettenbach J, Fischer P, et al.: White matter hyperintensities and chronicity of depression. *J. Psychiatr. Res.* 2005;39:285–93.

[49] Herrmann LL, Goodwin GM, Ebmeier KP: The cognitive neuropsychology of depression in the elderly. *Psychol. Med.* 2007;37:1693–702.

[50] Herrmann LL, Le Masurier M, Ebmeier KP: White matter hyperintensities in late life depression: a systematic review. *J. Neurol. Neurosurg. Psychiatry.* 2008;79:619-24.

[51] Hickie I, Scott E, Mitchell P, et al.: Subcortical hyperintensities on magnetic resonance imaging: Clinical correlates and prognostic significance in patients with severe depression. *Biol. Psychiatry.* 1995;37:151–60.

[52] Hickie I, Scott E, Mitchell P, Wilheim K, Austin MP, Bennet B. Subcortical hyperintensities on magnetic resonance imaging : clinical correlates and prognostic significance in patients with severe depression. *Biol. Psychiatry.* 1995; 37: 151-160

[53] Hickie I, Scott E, Wilhelm K, et al.: Subcortical hyperintensities on magnetic resonance imaging in patients with severe depression—A longitudinal evaluation. *Biol. Psychiatry.* 1997;42:367–74.

[54] Iidaka T, Nakajima T, Kawamoto K, et al.: Signal hyperintensities on brain magnetic resonance imaging in elderly depressed patients. *Eur. Neurol.* 1996;36:293–9.

[55] Inzitari D: Age-related white matter changes and cognitive impairment (Editorial). *Ann. Neurol.* 2000;47:141-2.

[56] Iosifescu DV, Renshaw PF, Lyoo IK, et al.: Brain white-matter hyperintensities and treatment outcome in major depressive disorder. *Br. J. Psychiatry.* 2006;188:180–5.

[57] Judas M, Rados M, Jovanov-Milosevic N, Hrabac P, Stern-Padovan R, Kostovic I. Structural, immunocytochemical, and md imaging properties of periventricoular crossroads of growing cortical pathways in preterm infants. *AJNR Am. J. Neuroradiol.* 2005; 26: 2671-2684.

[58] Kerber KA, Enrietto JA, Jacobson BA, Baloh RW: Disequilibrium in older people. A prospective study. *Neurology.* 1998:51:574-80.

[59] Kessler RC, Borges G, Walters EE: Prevalence of and risk factors for lifetime suicide attempts in the National Comorbidity Survey. *Arch. Gen. Psychiatry.* 1999;56:617-26.

[60] Komaki S, Nagayama H, Ohgami H, Takaki H, Mori H, Akiyosci J. prospective study of major depressive disorder with white matter hyperintensity. Comparison of patients with and without lacunar infarction. *Eur. Arch. Clin. Neurosci.* 2008; 258: 160-164

[61] Krabbendam L, Honig A, Wiersma J, et al.: Cognitive dysfunctions and white matter lesions in patients with bipolar disorder in remission. *Acta Psychiatr. Scand.* 2000;101:274–80.

[62] Kramer-Ginsberg E, Greenwald BS, Krishnan KRR, et al.: Neuropsychological functioning and MRI signal hyperintensities in geriatric depression. *Am. J. Psychiatry.* 1999;156:438–44.

[63] Krishnan KR, Hays JC, Blazer DG: MRI-defined vascular depression. *Am. J. Psychiatry.* 1997;154:497–501.

[64] Krishnan KR, McDonald WM, Doraiswamy PM, et al.: Neuroanatomical substrates of depression in the elderly. *Eur. Arch. Psychiatry.* 1993;243:41–6.

[65] Kumar A, Bilker W, Jin Z, et al.: Age of onset of depression and quantitative neuroanatomic measures: absence of specific correlates. *Psychiatry Res.* 1999;91:101–10.

[66] Kumar A, Miller D, Ewbank D, et al.: Quantitative anatomic measures and comorbid medical illness in late-life major depression. *Am. J. Geriatr. Psychiatry.* 1997;5:15–25.

[67] Kumar A, Miller D, Ewbank D, et al.: Quantitative anatomical measures and comorbid medical illness in late-life depression. *Am. J. Ger. Psychiatry.* 1997;5:15–25.

[68] Lalovic A, Levy E, Luheshi G, et al.: Cholesterol content in brains of suicide completers. *Int. J. Neuropsychopharmacol.* 2007;10:159-66.

[69] Lesser IM, Boone KB, Mehringer CM, et al.: Cognition and white matter hyperintensities in older depressed patients. *Am. J. Psychiatry.* 1996;153:1280–7.

[70] Lloyd AJ, Ferrier IN, Barber R, et al.: Hippocampal volume change in depression: late and early-onset illness compared. *Br. J. Psychiatry.* 2004;184:488–95.

[71] Lyoo IK, Lee HK, Jung JH, Noam GG, Renshaw PF: White matter hyperintensities on magnetic resonance imaging of the brain in children with psychiatric disorders. *Compr. Psychiatry.* 2002;43:361–8.

[72] Malone KM, Corbitt EM, Li S, et al. prolactin response to fenfluramine and suicide attempt lethality in major depression. *Br. J. Psychiatry.* 1996; 168: 324-329.

[73] Mann JJ, McBride PA, Malone KM, et al. Blunted serotonergic responsivity in depressed patients. *Neuropsychopharmacology.* 1995; 13: 53-64

[74] Mann JJ, Malone KM, Diehl JD, et al. Positron emission tomographic imaging of serotonin activation effects on prefrontal cortex in healthy volunteers. *J. Cereb. Blood. Metab.* 1996; 16: 418-426.

[75] Mann JJ, Malone KM. Cerebrospinal fluid amines and higher lethality suicide attempts in depressed inpatients. *Biol. Psychiatry.* 1997; 41: 162-171.

[76] Mann JJ, Arango V: Neurobiology of suicidal behavior. In: Wasserman D, ed. Suicide: an Unnecessary Death. London: Martin Dunitz; 2001:29–34.

[77] Mann JJ, Currier D, Stanley B, Amsel LV, Ellis SP. Can biological tests assist prediction of suicide in mood disorders? *Int. J. Neuropsychopharmacol.* 2006;9:465-74.

[78] Mann JJ, Stanley M, McBride PA, McEwen BS: Increased serotonin2 and beta-adrenergic receptor binding in the frontal cortices of suicide victims. *Arch. Gen. Psychiatry.* 1986;43:954-9.

[79] Mann JJ: Neurobiology of suicidal behaviour. *Nat. Rev. Neurosci.* 2003; 4:819-828

[80] McDonald WM, Tupler LA, Marsteller FA, et al.: Hyperintense lesions on magnetic resonance images in bipolar disorder. *Biol. Psychiatry.* 1999;45:965–71.

[81] McGuffin P, Marusic A, Farmer A: What can psychiatric genetics offer suicidology? *Crisis.* 2001;22:61-5.

[82] Miller DS, Kumar A, Yousem D, et al.: MRI high-intensity signals in depression and Alzheimer's disease: a comparison of subjects without major vascular risk factors. *Am. J. Geriatr. Psychiatry.* 1994;2:332–7.

[83] Miller JW, Green R, Mungas DM, et al.: Homocysteine, vitamin B6, and vascular disease in AD patients. *Neurology.* 2002;58:1471-5.

[84] Mori S, Van Zijl PC: Fiber tracking: principles and strategies. A technical review. *NMR Biomed.* 2002;15:468-80.

[85] Murata T, Kimura H, Omori M, et al.: MRI white matter hyperintensities, (1)H-MR spectroscopy and cognitive function in geriatric depression: a comparison of earlyand late-onset cases. *Int. J. Geriatr. Psychiatry.* 2001;16:1129–35.

[86] Nebes RD, Reynolds CF III, Boada F, Meltzer CC, Fukui MB, Saxton J, Halligan EM, DeKosky ST. Longitudinal in the volume of white matter hyperintensities in late-onset depression. *Int. J. Geriatr. Psychiatry*. 2002; 17: 526-530

[87] Ninan PT, van Kammen DP, Scheinin M et al. CSF 5-hydroxyindoleacetic acid levels in suicidal schizophrenic patients. *Am. J. Psychiatry.* 1984; 141: 566-569

[88] Nordström P, Samuelsson M, Asberg M, et al. CSF 5-HIAA predicts suicide risk after attemted suicide. *Suicide Life Threat Behav.* 1994; 24: 1-9.

[89] O'Brien J, Ames D, Chiu E, et al.: Severe deep white matter lesions and outcome in elderly patients with major depressive disorder: follow up study. *BMJ.* 1998;317:982–4.

[90] O'Brien J, Perry R, Barber R, Gholkar A, Thomas A. The associations between white matter lesions on magnetic resonance imaging and non cognitive symptoms. *Ann. N.Y. Acad. Sci.* 2000; 903: 482-489

[91] Ovbiagele B, Saver JL. Cerebral white matter hyperintensities on MRI: current concepts and therapeutic implications. *Cerebrovasc. Dis.* 2006; 22: 83-90.

[92] Pedophiles have less brain white matter: Toronto study. Retrieved on December 10 2007. http://www.cbc.ca/story/health/national/2007/11/28/pedophiles-study.html.

[93] Peterson BS. Brain imaging studies of the anatomical and functional consequences of preterm birth for human brain development. *Ann. N. Y. Acad. Sci.* 2003; 1008: 219-237.

[94] Pompili M, Ehrlich S, De Pisa E, Mann JJ, Innamorati M, Cittadini A, Montagna B, Iliceto P, Romano A, Amore M, Tatarelli R, Girardi P. White matter hyperintensities and their associations with suicidality in patients with major affective disorders. *Eur. Arch. Psychiatry Clin. Neurosci*. 2007; 257: 494-499

[95] Pompili M, Innamorati M, Mann JJ et al.: Periventricular white matter hyperintensities as predictors of suicide attempts in bipolar disorders and unipolar depression. *Progress in Neuro-sychopharmacology and Biological Psychiatry*. 32 (2008) 1501–1507.

[96] Raff MC, Abney ER, Cohen J, Lindsay R, Noble M: Two types of astrocytes in cultures of developing rat white matter: differences in morphology, surface gangliosides, and growth characteristics. *J. Neurosci.* 1983;3:1289–300.

[97] Sachdev P, Brodaty H: Quantitative Study of Signal Hyperintensities on T2-Weighted Magnetic Resonance Imaging in Late-Onset Schizophrenia. *Am. J. Psych.* 1999;156:1958-67

[98] Salloway S, Malloy P, Kohn R, et al.: MRI and neuropsychological differences in early- and late-life-onset geriatric depression. *Neurology.* 1996;46:1567–74.

[99] Sassi RB, Brambilla P, Nicoletti M, et al.: White matter hyperintensities in bipolar and unipolar patients with relatively mild-to-moderate illness severity. *J. Affect Disord.* 2003;77:237–45.

[100] Schlicht K, Buttner A, Siedler F, et al.: Comparative proteomic analysis with postmortem prefrontal cortex tissues of suicide victims versus controls. *J. Psychiatr. Res.* 2007;41:493-501.

[101] Schmidt R, Fazekas F, Hayn M, Schmidt H, kapeller P, Roob G, Offenbacher H, Shumaker M, Eber B, Weinrauch V, Kostner GM, Esterbauer H. Risk factors for microangiopathy-related cerebral damage in the Austrian stroke prevention study. *J. Neurol. Sci.* 1997; 152: 15-21

[102] Silverstone T, McPherson H, Li Q, Doyle T. Deep white matter hyperintensities in patients with bipolar depression, unipolar depression and age-matched control subjects. *Bipola Disord.* 2003; 5: 53-57.

[103] Simpson SW, Jackson A, Baldwin RC, et al.: IPA/Bayer Research Awards in Psychogeriatrics. Subcortical hyperintensities in late-life depression: acute response to treatment and neuropsychological impairment. *Int. Psychogeriatr.* 1997;9:257–75.

[104] Simpson S, Baldwin RC, Jackson A, Burns A, Thomas P. Is the clinical expression of late-life depression influenced by brain changes? MRI subscortical neuroanatomical correlates of depressive symptoms. *Int. Psychogeriatr.* 2000; 12: 425-434

[105] Soares JC, Mann JJ. The anatomy of mood disorder-review of structural neuroimaging studies. *Biol. Psychiatry.* 1997; 43: 705-712.

[106] Stanley M, Mann JJ: Increased serotonin-2 binding sites in frontal cortex of suicide victims. *Lancet.* 1983;1:214-6.

[107] Stanley M, Virgilio J, Gershon S: Tritiated imipramine binding sites are decreased in the frontal cortex of suicides. *Science.* 1982;216:1337-9.

[108] Starr JM, Leaper SA, Murray AD, et al.: Brain white matter lesions detected by magnetic resonance imaging are associated with balance and gait speed. *J. Neurol. Neurosurg. Psychiatry.* 2003;74:94-8.

[109] Stefan ET, Janis L. Breeze, Dale C. Hesdorffer et al.: MRI Correlates of Suicide Attempt History in Unipolar Depression. *Biol. Psychiatry.* 2001;50:266–270

[110] Steffens DC, Krishnan KR. Structural neuroimaging and mood disorders: recent findings, implications for classification and future directions. *Biol. Psychiatry.* 1998; 43: 705-712.

[111] Steffens DC, Bosworth HB, Provenzale JM, MacFall JR. Subcortical white matter lesions and functional impairment in geriatric depression. *Depress Anxiety.* 2002; 15: 23-28

[112] Steffens DC, Conway CR, Dombeck CB, Wagner HR, Tupler LA, Weiner RD. Severity of subcortical gray matter hyperintensity predicts ECT response in geriatric depression. *J. ECT.* 2001; 17: 45-49

[113] Stoll AL, Renshaw PF, Yurgelun-Todd DA, Cohen BM: Neuroimaging in bipolar disorder: What have we learned? *Biol. Psychiatry.* 2000;48:505–17.

[114] Strakowski SM, DelBello MP, Adler C, Cecil DM, SaxKW: Neuroimaging in bipolar disorder. *Bipolar Disord.* 2000;2:148–64.

[115] Strakowski SM, Woods BT, Tohen M, et al.: MRI subcortical signal hyperintensities in mania at first hospitalization. *Biol. Psychiatry.* 1993;33:204–6.

[116] Swayze VW 2nd, Andreasen NC, Alliger RJ, Ehrhardt JC, Yuh WT: Structural brain abnormalities in bipolar affective disorder. Ventricular enlargement and focal signal hyperintensities. *Arch. Gen. Psychiatry.* 1990;47:1054–9.

[117] Szadoczky E, Vitrai J, Rihmer Z, Furedi J: Suicide attempts in the Hungarian adult population. Their relation with DIS/DSM-III-R affective and anxiety disorders. *Eur. Psychiatry.* 2000;15:343-7.

[118] Takahashi K, Oshima A, Ida I, et al.: Relationship between age at onset and magnetic resonance image-defined hyperintensities in mood disorders. *J. Psychiat. Res.* 2008;42:443-50.

[119] Taylor JG. The central role of the parietal lobe in consciousness. *Conscious. Cognit.* 2001; 10: 379-417.

[120] Taylor WD, Steffens DC, MacFall JR, et al.: White matter hyperintensity progression and late-life depression outcomes. *Arch. Gen. Psychiatry*. 2003;60:1090–6.

[121] Taylor WD, MacFall JR, Payne ME, et al.: Greater MRI lesion volumes in elderly depressed subjects than in control subjects. *Psychiatry Res. Neuroimaging.* 2005;139:1–7.

[122] Thomas AJ, O'Brien JT, Davis S, et al.: Ischemic basis for deep white matter hyperintensities in major depression: a neuropathological study. *Arch. Gen. Psychiatry.* 2002;59:785–92.

[123] Tupler LA, Krishnan KR, McDonald WM, et al.: Anatomic location and laterality of MRI signal hyperintensities in late-life depression. *J. Psychosom. Res.* 2002;53:665–76.

[124] Tupler LA, Krishnan KRR, McDonald WM, et al.: Anatomic location and laterality of MRI signal hyperintensities in late-life depression. *J. Psychosom. Res.* 2002;53:665–76.

[125] Van Praag HM. CSF 5-H1AA and suicide in non-depressed schizophrenics. *Lancet.* 1983; 2: 977-978.

[126] Videbech P: MRI findings in patients with affective disorder: a meta-analysis. *Acta Psychiatr. Scand.* 1997;96:157–68.

[127] Vinod KY, Hungund BL: Role of the endocannabinoid system in depression and suicide. *Trends Pharmacol. Sci.* 2006;27:539-45.

[128] Weissman MM, Bland RC, Canino GJ, et al.: Prevalence of suicide ideation and suicide attempts in nine countries. *Psychol. Med.* 1999;29:9-17.

[129] White matter. Retrieved on September 19 2008. http://en.wikipedia. org/wiki/ White_matter.

[130] Whitaker AH, Van Rossem R, Feldman JF, Schonfeld IS, Pinto-Martin JA, Tore C, Shaffer D, Paneth N. Psychiatric outcomes in low-birth-weight children at age 6 years: relation to neonatal cranial ultrasound abnormalities. *Arch. Gen. Psychiatry.* 1997; 54: 847-856.

[131] Whitman GT, DiPatre PL, Lopez IA, et al.: Neuropathology in older people with disequilibrium of unknown cause. *Neurology.* 1999;53:375-382.

[132] Whitman GT, Tang Y, Lin A, Baloh RW: A prospective study of cerebral white matter abnormalities in older people with gait dysfunction. *Neurology.* 2001:57:990-4.

[133] Wong TY, Klein R, Sharret AR, et al.: Cerebral white matter lesions, retinopathy and incidence of clinical stroke. *Jama.* 2002 288:67-74

[134] Yanai I, Fujkawa T, Horiguchi J, Jamawaki S, Touhouda Y. The 3-year course and outcome of patients with major depression and silent cerebral infarction. *J. Affect Disord.* 1998; 47: 25-30

[135] Ylikoski R, Ylikoski A, Raininko R, Keskivavra P, Sulkava R, Tilvis R, Erkinjuntti T. Cardiovacular diseases, health status, brai imaging findings and neuropsychological functioning in neurologically healthy elderly individuals. *Arch. Geront. Geriatr.* 2000; 30: 115-13

[136] Zanetti MV, Cordeiro Q, Busatto GF: Late onset bipolar disorder associated with white matter hyperintensities: a pathophysiological hypothesis. *Prog. Neuropsychopharmacol. Biol. Psychiatry.* 2007;31:551–6.

[137] Zanetti MV, Schaufelberger MS, de Castro CC, et al.: White-matter hyperintensities in first-episode psychosis. *Br. J. Psychiatry.* 2008;193:25–30.

In: Handbook on White Matter
Editors: T. B. Westland and R. N. Calton
ISBN: 978-1-60741-034-8

Chapter VIII

A Quantitative Study of the Pathological Changes in the Cortical White Matter in Variant Creutzfeldt-Jakob Disease (vCJD)

Richard A. Armstrong*
Vision Sciences, Aston University, Birmingham B4 7ET, UK

Abstract

The objective of this study was to determine the degree of white matter pathology in the cerebral cortex in cases of variant Creutzfeldt-Jakob disease (vCJD) and to study the relationships between the white matter and grey matter pathologies. Hence, the pathological changes in cortical white matter were studied in individual gyri of the frontal, parietal, occipital, and temporal cortex in eleven cases of vCJD. Vacuolation ('spongiform change'), deposition of the disease form of prion protein (PrP^{sc}) in the form of discrete PrP deposits, and gliosis were observed in the white matter of virtually all cortical regions studied. Mean density of the vacuoles in the white matter was greater in the parietal lobe compared with the frontal, occipital, and temporal lobes but there were fewer glial cells in the occipital lobe compared with the other cortical regions. In the white matter of the frontal cortex, vacuole density was negatively correlated with the density of both glial cell nuclei and the PrP deposits. In addition, the densities of glial cells and PrP deposits were positively correlated in the frontal and parietal cortex. In the white matter of the frontal cortex and inferior temporal gyrus, there was a negative correlation between the densities of the vacuoles and the number of surviving neurons in laminae V/VI of the adjacent grey matter. In addition, in the frontal cortex, vacuole density in the white matter was negatively correlated with the density of the diffuse PrP deposits in laminae II/III and V/VI of the adjacent grey matter. The densities of PrP deposits in the white matter of the frontal cortex were positively correlated with the

* Corresponding Author: Dr. R.A. Armstrong, Vision Sciences, Aston University, Birmingham, B4 7ET, UK. Tel 0121-359-3611, Fax 0121-333-4220, EMail: R.A.Armstrong@aston.ac.uk

density of the diffuse PrP deposits in laminae II/III and V/V1 and with the number of surviving neurons in laminae V/V1. The data suggest that in the white matter in vCJD, gliosis is associated with the development of PrP deposits while the appearance of the vacuolation is a later development. In addition, neuronal loss and PrP deposition in the lower cortical laminae of the grey matter may be a consequence of axonal degeneration within the white matter.

Keywords: Variant Creutzfeldt-Jakob disease (vCJD), white matter, cerebral cortex, vacuolation, cortico-cortical pathways

Introduction

A number of diseases have been described in animals and humans believed to be caused by proteinaceous infectious particles called prions (Prusiner, 1995) and collectively referred to as the ‘transmissible spongiform encephalopathies’ (TSEs). Prions differ significantly in behaviour from bacteria and viruses and are composed mainly of protein. Prion diseases include 'scrapie' in sheep, 'bovine spongiform encephalopathy' (BSE) in cattle, and Creutzfeldt-Jakob disease (CJD) in humans. These diseases are important because they can be transmitted between members of the same species and may also cross the species barrier and adapt to new hosts. Of particular concern, is whether a new form of CJD in humans, largely found in the United Kingdom (UK) and termed variant CJD (vCJD), can be acquired from cattle with BSE (Will et al., 1996; Ironside, 2000).

Prion Diseases

CJD itself is only one of a group of human diseases caused by prions. In addition, three other human prion diseases have been identified. First, the disease 'kuru' occurred in the past in the 'Fore highlanders', natives of Papua and New Guinea, and was probably transmitted as a consequence of ritual cannibalism. Second, 'fatal familial insomnia' (FFI) is a recently described genetic disorder that is characterised initially by sleep disturbance, insomnia, and agitation and later, by the development of hallucinations, stupor, and coma (Collins et al., 2001). Third, Gerstman-Straussler-Scheinker (GSS) disease is a rare genetic disorder first described in 1936 and characterised by ataxia, dementia, limb weakness, and speech problems (Collins et al., 2001).

Prions and Prion Disease

CJD was first described by Creutzfeldt and Jakob in the 1920s (Creutzfeldt, 1921; Jakob, 1921) and is the most important human form of prion disease. Patients develop dementia, which may be preceded by ataxia and loss of coordination, with death resulting in about 3-12 months after the onset of symptoms. The characteristic pathological signs of prion disease are observed in the grey matter of the brain including vacuolation (‘spongiform change’),

neuronal loss, the proliferation of astrocytes, and the deposition of prion protein (PrP) in the form of discreet deposits or plaques. PrP exists in two forms, viz., normal cellular PrP (PrP^c), which does not cause disease and a disease specific form of PrP (PrP^{sc}), the presence of which can induce prion disease (DeArmond and Prusiner, 1995). Within a species, these two forms of PrP are identical in amino acid composition but differ in molecular conformation and in the composition of the attached chains of carbohydrates. Normal PrP^c is believed to comprise four α–helices with virtually no β–sheets whereas PrP^{sc} displays an identical primary structure to PrP^c but differs in secondary and tertiary structure (Caughey, 2001). Hence, PrP^{sc} displays a four-stranded β–sheet configuration covered on one face by two α-helices. Prusiner (1995) found that transgenic mice reared without the gene for PrP^c could not be infected with the disease scrapie suggesting that PrP^c was required for the disease process to take place. Hence, it has been hypothesised that normal PrP^c is converted into pathogenic PrP^{sc} in the presence of PrP^c, the process being auto-catalytic and proceeding at an exponential rate within the brain. Conversion of PrP^c to PrP^{sc} may also be chaperone mediated (Stockel and Hartl, 2001) and a conserved sequence of PrP (residues 90-121) may be critical for PrP^{sc} generation (Stockel and Hartl, 2001). PrP^{sc}, due to the presence of β–sheets, has a greater tendency than PrP^c to form insoluble aggregates in brain tissue. Hence, the deposition of PrP^{sc} in the brain may result in the development of vacuolation and subsequently to the death of neurons. Within the nervous system, PrP^{sc} appears to target specific nerve cell populations and may spread through the brain via cerebral spinal fluid or by anatomical connections (Prusiner and DeArmond, 1994; Armstrong et al., 2000). No significant immune response has been detected in prion disease but complement proteins (C1q, C3b) have been found associated with PrP deposits and the membrane attack complex (MAC) in neurons (Kovacs et al., 2004).

Subtypes of CJD

There are several subtypes of CJD including those associated with genetic factors (familial or fCJD), those resulting from the transmission of PrP^{sc} (iatrogenic or iCJD) and those that occur sporadically within the population (sporadic or sCJD). About 10-15% of cases of CJD are genetic and this condition is inherited as an autosomal dominant gene. Point mutations of the coding region of the *PrP* gene on chromosome 20 have been identified in a number of these cases (Goldfarb et al., 1994). A small number of CJD cases can be traced to a transmissible cause. Possible sources of transmission include corneal transplant (Hogan and Cavanagh, 1995), the use of electrodes implanted in the brain, neurosurgery, dura mater grafts, and the use of growth hormone. In the latter case, the disease was acquired as a result of the use of growth hormone extracted from human pituitary glands and has largely been eliminated as a result of the use of genetically engineered growth hormone. About 85% of recorded cases of CJD are sporadic. The mean age of onset of sCJD is 60 years of age and its incidence is approximately 1/1,000,000. Two theories have been proposed to explain cases of sCJD. First, a mutation of the *PrP* gene could result in the formation of PrP^{sc} rather that PrP^c or second, PrP^c could be converted spontaneously to PrP^{sc}, the chance of both processes occurring increasing with age.

Variant CJD

The recent appearance of vCJD, which may be related to BSE, is causing considerable concern especially in the UK. The first cases of vCJD were recorded in 1995 and by 2008, the total number of deaths ascribed to the disease was 163 (National CJD Surveillance Unit data). The new variant of CJD differs significantly from previously described forms of the disease in having an earlier age of onset (mean 28 years) and a prolonged duration of illness (up to 2 years) (Will et al., 1996; Ironside, 2000). Presentation of the disease is largely psychiatric with patients exhibiting anxiety, depression, and behavioural changes. After a period of weeks or months, a cerebellar syndrome develops and the patient experiences problems in walking and with movement. Memory problems generally develop late in the clinical course and the patient ultimately becomes mute and unable to move. Myoclonus usually occurs at some stage in the disease in the majority of patients. In addition, the pathology of vCJD differs from other forms of the disease in the presence of widespread and concentrated deposits of PrP^{sc} throughout the brain in the form of 'florid plaques' (Grigoriev et al., 1999; Ironside, 2000; Ironside et al., 1996; McLean et al., 1998; Armstrong et al., 2003a). The PrP^{sc} characteristic of vCJD has a uniform glycotype (PrP^{sc}, Type 4) and is distinct from that observed in sCJD (Hill et al., 1999, Ironside et al., 2000).

White Matter Pathology in CJD

In addition to changes affecting the grey matter, pathological changes have also been observed in the white matter in CJD. Widespread white matter degeneration has been reported in the hippocampus of iatrogenic cases (Masullo and Machin, 1997) and in the 'panencephalic' variant of CJD (Carola et al., 1996). In addition, vacuolation may be observed in myelinated areas of many cases with typical secondary vacuoles and curled membranes in the axoplasm and myelin sheaths (Walis et al., 1997). Accompanying the vacuolation, a diffuse glial reaction may be present (Muhleisen et al., 1995). In a previous study of cases of sporadic CJD (sCJD) (Armstrong et al., 2002a), the development of large clusters of vacuoles and the proliferation of glial cells were observed in the white matter of cortical gyri but discrete PrP deposits were usually absent. In sCJD, the formation of clusters of vacuoles in the white matter may either precede or be a consequence of pathological changes within the grey matter (Armstrong et al., 2002a). The objectives of the present study were: 1) to quantify the pathological changes in the cortical white matter of various brain areas in vCJD, 2) to study the correlations between the pathological changes within the white matter, and 3) to test the hypothesis that the pathological changes in white matter are correlated with those in the adjacent grey matter.

Materials and Methods

Cases

Eleven cases of vCJD (details in table 1) were studied at the Department of Neuropathology, Institute of Psychiatry, King's College London, UK. Brain material was obtained from the National CJD Surveillance Unit, Western General Hospital, Edinburgh, UK. Informed consent was given for the removal of all brain tissue according to the 1964 Declaration of Helsinki (as modified Edinburgh 2000). All cases fulfilled the neuropathological diagnostic criteria for vCJD (Ironside et al., 2000). None of the cases had any of the known mutations of the *PrP* gene or family history of prion disease, and there was no evidence of the known types of iatrogenic aetiology. Anxiety and/or depression were early symptoms in six of the cases while significant short-term memory and gait problems were present in nine and eight cases respectively. Three cases had complained of insomnia and two patients had reported hallucinations during the course of the disease. Only one case had significant visual problems.

Table 1. Demographic data and general brain details of the variant Creutzfeldt-Jakob disease (vCJD) cases

Case	Sex	Age at onset (yrs)	Duration (yrs)	Brain weight (gm)	Brain Atrophy
A	F	39	2	586L	None
B	F	28	1	1375	None
C	F	28	1	NA	NA
D	M	19	1	NA	NA
E	M	30	1	699R	None
F	M	48	2	1470	None
G	F	34	1	810L	None
H	M	18	1	1434	None
I	M	24	1	NA	NA
J	F	21	2	1394	None
K	M	35	1	718R	None

Abbreviations: M = Male, F = Female, L = Left hemisphere only, R = Right hemisphere only, NA = Data not available.

Preparation of Material

Blocks of the frontal cortex (B8) at the level of the genu of the corpus callosum, parietal cortex (B7) at the level of the splenium of the corpus callosum, occipital cortex including the calcarine sulcus (B17), and temporal cortex at the level of the lateral geniculate body were taken from each brain. Within the temporal lobe, the inferior temporal gyrus (B22) and parahippocampal gyrus (B28) were studied. Tissue was fixed in 10% phosphate buffered formal-saline and embedded in paraffin wax. Immunohistochemistry (IHC) was carried out

on coronal 7μm sections using the monoclonal antibody 12F10 (dilution 1:250) that binds to residues 142-160 of human PrP downstream of the neurotoxic domain adjacent to helix region 2 (Krasemann et al., 1996) (kindly provided by Prof. G. Hunsmann, The German Primate Centre, Gottingen, Germany). Immunoreactivity was enhanced by formic acid (98% for 5 minutes) and autoclaving (121°C for 10 minutes) pretreatment. Sections were treated with Dako Biotinylated Rabbit anti-Mouse (RAM) (dilution 1:100) and Dako ABComplex HRP kit for 45 minutes (Amersham, UK). Diaminobenzidine tetrahydrochloride was used as the chromogen. Immunostained sections were counterstained with haematoxylin for 1 minute. Adjacent sections from each block were also routinely stained with haematoxylin and eosin (H/E).

Morphometric Methods

The degree of vacuolation and glial cell density were quantified in the H/E sections in a region of white matter at the base of the gyrus. Quantification was carried out across the gyrus perpendicular to the axons using 50 x 250 μm contiguous sample fields; the shorter, lower edge of the sample field being aligned with a guideline marked on the slide connecting the bases of the two adjacent sulci. All vacuoles greater than 5μm in diameter and glial cell nuclei were counted in each sample field. In addition, PrP deposition was quantified in the immunostained sections and the number of discrete deposits counted in each sample field. Two morphological types of PrP deposit are commonly observed in the grey matter in vCJD (Armstrong et al., 2003a,b). First, 'florid' plaques comprise a condensed core of PrP and are heavily stained with antibodies raised against PrP^{sc}. Second, 'diffuse' plaques (also known as 'fine feathery diffuse deposits' or 'fine diffuse plaques') are more lightly stained, irregular in shape, and lack a condensed PrP core.

Data Analysis

First, the densities of the vacuoles, glial cell nuclei, and PrP deposits were compared between brain regions using a two-way (cases x brain regions) analysis of variance (ANOVA). Subsequent comparison between group means was made using the Scheffé's *post-hoc* test. Second, within each gyrus the degree of correlation between the densities of the vacuoles, glial cell nuclei, and PrP deposits were tested using Pearson's correlation coefficient ('r'). Third, correlations between the densities of the pathological features in the cortical white matter and the densities of the vacuoles, surviving neurons, PrP deposits, and glial cell nuclei in the adjacent grey matter (Armstrong et al., 2003c) were tested for each brain region using Pearson's 'r'.

Pathological Changes within the White Matter

Clusters of vacuoles, accompanied by diffusely distributed glial cell nuclei were observed in the cortical white matter in the majority of gyri studied (figure 1). In addition, PrP deposits were observed within the white matter, the majority being of the condensed florid-type (figure 2), although a smaller number of more diffuse deposits were also present.

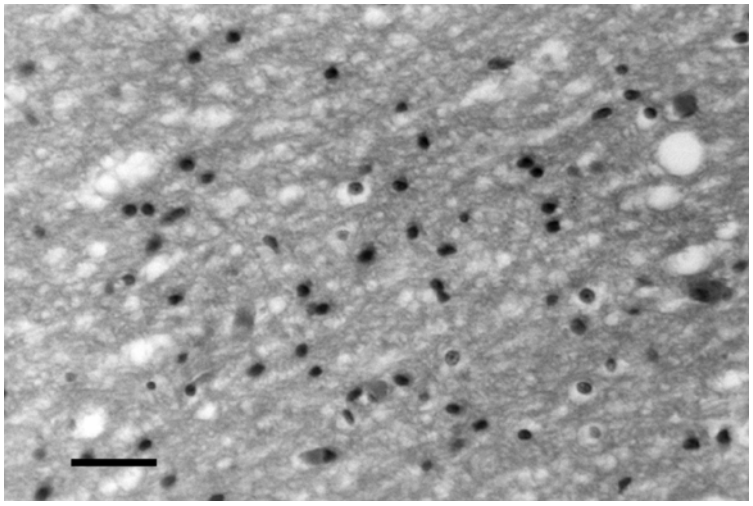

Figure 1. Vacuolation (light areas) and gliosis (darkly stained nuclei) within the white matter of the frontal lobe in a case of variant Creutzfeldt-Jakob disease (vCJD) (H/E stain, Magnification bar = 50 μm).

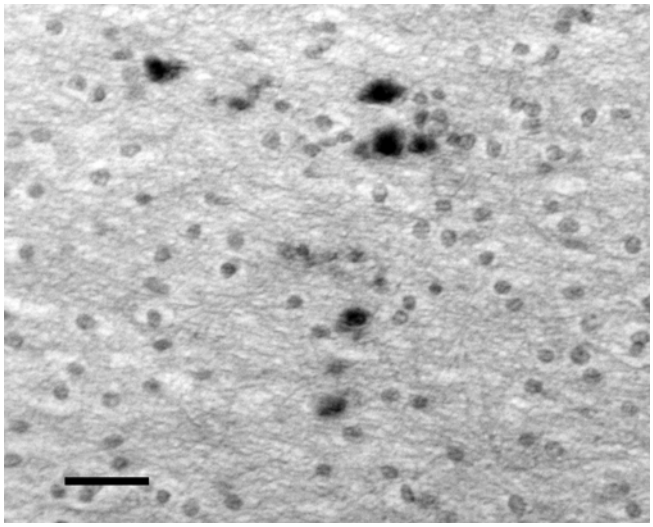

Figure 2. Prion protein deposits (dark stained patches) resembling florid plaques within the white matter of the frontal lobe in a case of variant Creutzfeldt-Jakob disease (vCJD) (12F10 antibody, haematoxylin counterstain, Magnification bar = 50 μm).

Pathological changes were evident in the cortical white matter of all cases of vCJD studied as previously reported in sCJD (Armstrong et al., 2002a). These changes included the development of large clusters of vacuoles and a diffuse glial cell reaction similar to sCJD. The distribution of the vacuoles and glial cells contrasts with that present in white matter of control brain, in which there are rows of tightly packed oligodendroglial nuclei between nerve fibre bundles surrounded by 'haloes' and small numbers of vacuoles (Armstrong et al., 2007). Small numbers of discrete PrP deposits were also present in the cortical white matter in vCJD whereas PrP immunoreactivity was usually absent in sCJD (Armstrong et al., 2002a). The majority of PrP deposits in the white matter morphologically resembled the florid-type plaques that are present in large numbers in the adjacent cortical grey matter (Armstrong et al., 2003b). PrP is normally regarded as a synaptic protein and deposits in the white matter may have originated from damaged axons or may have diffused from neurons located at the boundary between the white matter and the adjacent laminae VI of the grey matter.

Quantification of the Pathology

The mean densities of the pathological changes in the cortical white matter in each brain region are shown in figure 3. The mean density of the vacuoles in the white matter was significantly less in the parietal lobe compared with gyri of the frontal, occipital, and temporal lobes. Within the temporal lobe, the densities of the vacuoles were similar in the ITG and PHG. The density of the glial cell nuclei was significantly lower in the occipital cortex compared with the frontal, parietal, and temporal cortex. There were no statistically significant differences in PrP density between cases or brain regions, although the density of PrP deposits may be lower in the occipital cortex.

Correlations between the densities of the vacuoles, glial cell nuclei, and PrP deposits within the cortical white matter of each region are shown in table 2. In the frontal cortex, the density of the vacuoles was negatively correlated with that of the glial cell nuclei ($r = -0.68$, $P < 0.05$) and PrP deposits ($r = -0.80$, $P < 0.01$). In addition, in the frontal ($r = 0.66$, $P < 0.05$) and parietal cortices ($r = 0.65$, $P < 0.05$), the densities of the glial cells and PrP deposits were positively correlated.

Variations in the density of the pathological changes were evident in the white matter of the various regions, less vacuolation being observed in the parietal cortex and fewer glial cells in the occipital cortex. These gross variations in white matter pathology do not necessarily reflect the severity of pathological changes in adjacent grey matter, e.g., grey matter pathology is often most extensive in the occipital lobe in vCJD (Armstrong et al., 2002b) whereas the white matter pathology is less dense in this region. Within some gyri, the densities of the PrP deposits were positively correlated with the glial cell nuclei and negatively correlated with the density of the vacuoles. There are two possible hypotheses that could explain these results. First, vacuolation could be an early pathological change in the white matter but the vacuoles subsequently disappear before the development of PrP deposits and the proliferation of glial cells. Second, gliosis of white matter could be a response to the

appearance of the PrP deposits, the development of the vacuoles being a later feature, and the PrP deposits being subsequently cleared by glial cells.

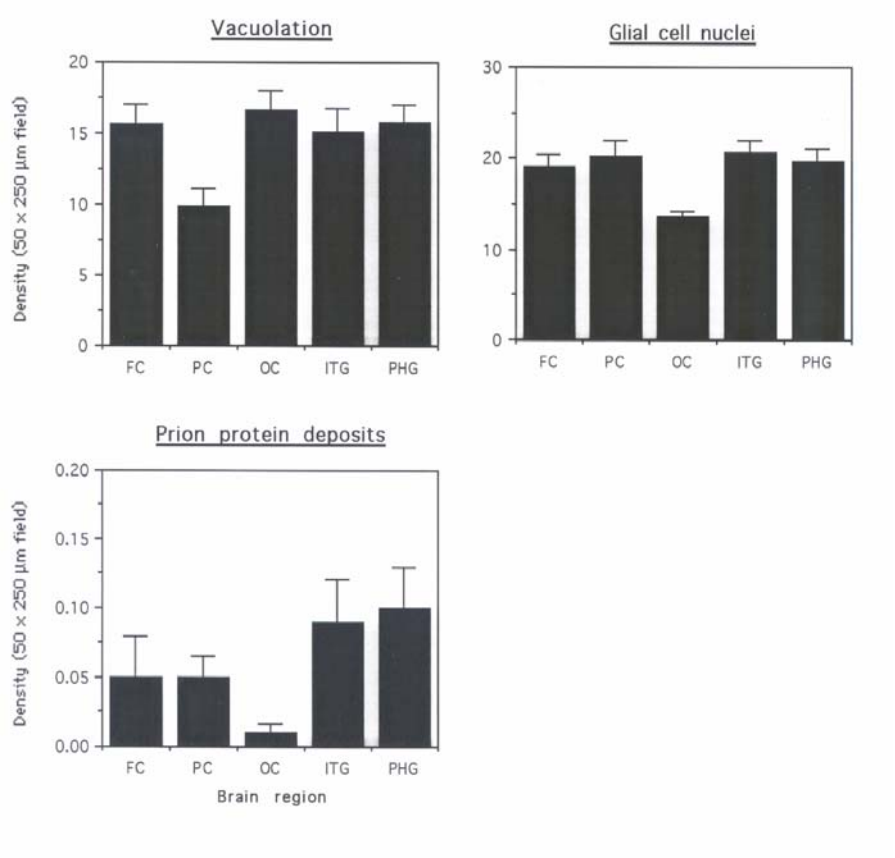

Figure 3. The densities of the vacuolation, glial cell nuclei and prion protein (PrP deposits) in 11 cases of variant Creutzfeldt-Jakob disease (vCJD). Analysis of variance: Vacuolation Between brain regions ($F = 6.38$, $P < 0.001$); Glial cells Between brain regions ($F = 5.94$, $P < 0.001$); PrP deposits Between brain regions ($F = 1.66$, $P > 0.05$).

Table 2. Correlations (Pearson's 'r') between the densities of the vacuoles, glial cell nuclei, and prion protein (PrP) deposits in the cortical white matter in cases of variant Creutzfeldt-Jakob disease (vCJD). (* P < 0.01, ** P < 0.01)

		Correlation	
Brain region	Vacuoles/Glia	Vacuoles/PrP	Glia/PrP
Frontal cortex	-0.68*	-0.80**	0.66*
Parietal cortex	-0.06	0.29	0.65*
Occipital cortex	-0.06	-0.02	-0.44
ITG	-0.28	-0.47	0.55
PHG	-0.40	0.33	-0.11

ITG = Inferior temporal gyrus, PHG = Parahippocampal gyrus.

Correlations between Grey and White Matter Pathology

Correlations between the densities of pathological features in white and grey matter are summarised in table 3. First, in the frontal cortex ($r = 0.79$, $P < 0.01$) and ITG ($r = -0.60$, $P < 0.05$), there was a negative correlation between the densities of the vacuoles in the white matter and the number of surviving neurons in lamina V/VI of the grey matter. Second, in the frontal cortex, the density of vacuoles in the white matter was negatively correlated with the density of the diffuse PrP deposits in both laminae II/III ($r = -0.69$, $P < 0.05$) and V/VI ($r = -0.70$, $P < 0.05$). Third, the density of glial cell nuclei in the white matter was positively correlated with the number of surviving neurons ($r = 0.67$, $P < 0.05$) and the diffuse PrP deposits ($r = 0.66$, $P < 0.05$) in laminae V/VI of the frontal cortex and negatively correlated with the diffuse ($r = -0.65$, $P < 0.05$) and florid PrP deposits ($r = -0.66$, $P < 0.05$) in laminae V/VI of the parietal cortex. Fourth, in the frontal cortex, the density of the PrP deposits in the white matter was positively correlated with the diffuse deposits in laminae II/III ($r = 0.80$, $P < 0.01$) and V/VI ($r = 0.76$, $P < 0.01$) and the number of surviving neurons ($r = 0.84$, $P < 0.01$).

Correlations were observed between the pathological features in the white matter with those of the adjacent grey matter. Degeneration of the white matter in vCJD could be a cause or a consequence of pathological changes affecting the adjacent grey matter (Armstrong et al., 2002a). First, in the frontal cortex, there was a negative correlation between the density of the vacuoles in the white matter and the number of surviving neurons in laminae V/VI of the corresponding grey matter. This correlation suggests a relationship between neuronal loss in the lower cortical laminae and the development of vacuolation within the adjacent white matter. Second, the density of vacuoles in the white matter was negatively correlated with the density of the diffuse PrP deposits in both laminae II/III and V/VI. This correlation could be a consequence of the fact that there was a negative correlation between the densities of the vacuoles and surviving neurons. Previous studies suggest that diffuse plaques are spatially correlated with neuronal cell bodies and represent an early stage in the degeneration of the cortex in vCJD (Armstrong et al., 2003b). In areas of cortex with extensive neuronal loss in the grey matter, there may be fewer diffuse PrP deposits as a consequence of the clearance by glial cells but a more extensive vacuolation in the white matter. Third, there is a complex relationship between gliosis in the white matter and the pathological changes in adjacent grey matter. Glial cell density in the white matter was positively correlated with the densities of the surviving neurons and of the diffuse PrP deposits in laminae V/VI of the frontal cortex but negatively correlated with the florid and diffuse PrP deposits in laminae V/VI in the parietal cortex. It is possible that white matter gliosis is a local response to pathological changes in the white matter and especially to the appearance of PrP deposits but may not be directly related to changes in the adjacent grey matter. Fourth, the density of PrP deposits in the white matter was positively correlated with the densities of the diffuse deposits in both laminae II/III and V/VI of the frontal cortex. This result supports the hypothesis that the appearance of PrP deposits in the white matter is related to their development in the grey matter. It is possible that PrP is mobilised within damaged neuronal systems and their processes and is transported along the axons, and that subsequently damage to these axons releases PrP into the white matter.

Table 3. Correlations (Pearson's 'r') between the densities of the pathological changes (Vac = vacuolation, PrP = Prion protein deposits) in the cortical white matter of various brain regions and those in laminae II/III and V/VI of the corresponding grey matter in cases of variant Creutzfeldt-Jakob disease (vCJD). (* P < 0.05)

		Grey matter pathology							
Region	White Matter pathology	Vac II/III	Vac V/VI	Neu II/III	Neu V/VI	PrPd II/III	PrPd V/VI	PrPf II/III	PrPf V/VI
FC	Vac	-0.20	-0.27	-0.20	-0.79*	-0.69*	-0.70*	-0.43	-0.27
	Glia	-0.19	-0.14	-0.20	0.67*	0.51	0.66*	0.17	0.09
	PrP	0.26	-0.06	0.17	0.84*	0.80*	0.76*	0.39	0.24
PC	Vac	-0.05	0.02	0.31	0.55	0.26	0.27	-0.13	0.22
	Glia	0.33	-0.02	0.05	0.06	-0.65*	-0.66*	-0.49	-0.61*
	PrP	0.27	0.13	0.46	0.46	-0.04	-0.04	-0.28	-0.11
OC	Vac	0.10	0.12	0.41	0.15	-0.30	-0.43	-0.15	-0.70*
	Glia	-0.15	-0.14	-0.16	-0.51	-0.49	-0.34	-0.39	-0.32
	PrP	-0.22	0.16	0.03	0.27	0.15	-0.04	0.19	0.02
ITG	Vac	-0.10	-0.05	-0.59	-0.62*	0.12	-0.26	0.01	0.18
	Glia	0.11	0.26	0.25	0.17	0.03	-0.03	0.22	0.15
	PrP	0.02	0.37	0.37	0.52	0.12	0.36	0.54	0.43
PHG	Vac	-0.45	-0.34	-0.41	-0.37	-0.02	-0.04	-0.08	-0.34
	Glia	-0.04	0.13	-0.25	0.58	-0.14	-0.13	0.14	0.29
	PrP	0.24	-0.52	-0.36	-0.33	-0.06	-0.25	0.40	0.05

Abbreviations: FC = Frontal cortex, PC = Parietal cortex, OC = Occipital cortex, ITG = Inferior temporal gyrus, PHG = Parahippocampal gyrus, Vac = Vacuolation, PrP, Prion protein deposits, PrPd = diffuse plaques, PrPf = florid plaques, Neu = Surviving neurons.

The Spread of the Pathology in vCJD

The data suggest significant pathological changes within the cortical white matter in cases in vCJD, viz., the formation of vacuoles, deposition of PrP, and the proliferation of glial cells. The development of white matter pathology appears to be closely linked to that of the corresponding grey matter and especially to pathological changes within laminae V/VI. Various hypotheses have been proposed to explain how PrP^{sc} spreads into the brain in vCJD (Brown 2001), e.g., direct neural transmission from the site of infection, replication of PrP^{Sc} in the spleen followed by neural entry through the spinal cord, infection of gut-associated lymphoid tissue with subsequent spread to the dorsal motor nucleus of the vagus nerve, and haematogenous spread. Neural entry is likely to affect the brain stem and midbrain before the cerebral cortex and hence, it is possible that the pathology in the cortical grey matter is a consequence of subcortical pathological changes affecting the white matter. Hence, vacuoles in the white matter could reflect degeneration of the ascending axons and subsequently of the cortico-cortical pathways. These changes may result in neuronal loss in laminae V/VI of the grey matter and to the appearance of PrP deposits. PrP deposition in the white matter may then be a result of the leakage of PrP from damaged axons while the proliferation of glial cells in the white matter could be a reaction to these changes.

Conclusion

In conclusion, there is significant pathology within the cortical white matter in cases of vCJD including the formation of vacuoles, deposition of PrP, and the proliferation of glial cells. The development of white matter pathology appears to be closely related to pathology in the corresponding grey matter and especially within laminae V/VI. The data suggest that white matter gliosis in vCJD is associated with the development of PrP^{sc} deposits while the appearance of the vacuolation is a later development. In addition, neuronal loss and PrP^{sc} deposition in the lower cortical laminae of the grey matter may be a consequence of axonal degeneration within the white matter.

Acknowledgments

The assistance of the National CJD Surveillance Unit, Western General Hospital, Edinburgh and the Brain Bank, Institute of Psychiatry, King's College London in supplying cases for this study and in preparation of tissue sections is gratefully acknowledged.

References

Armstrong RA, Cairns NJ, Lantos PL. The spatial pattern of the vacuolation in patients with sporadic Creutzfeldt-Jakob disease. *Neuroscience Letters,* 2000, 281, 187-190.

Armstrong RA, Lantos PL, Cairns NJ. Spatial patterns of the vacuolation in subcortical white matter in sporadic Creutzfeldt-Jakob disease (sCJD). *Clinical Neuropathology,* 2002a, 21, 284-288.

Armstrong RA, Cairns NJ, Ironside JW, Lantos PL Quantification of vacuolation, ('spongiform change'), surviving neurons and prion protein deposition in eleven cases of variant Creutzfeldt-Jakob disease. *Neuropathology and Applied Neurobiology,* 2002b, 28, 129-135.

Armstrong RA, Lantos PL, Ironside JW, Cairns NJ. Differences in the density and spatial distribution of florid and diffuse plaques in variant Creutzfeldt-Jakob disease (vCJD). *Clinical Neuropathology*, 2003a, 22, 209-214.

Armstrong RA, Cairns NJ, Ironside JW, Lantos PL. Florid prion protein (PrP) plaques in patients with variant Creutzfeldt-Jakob disease (vCJD) are spatially related to blood vessels. *Neuroscience Research Communications,* 2003b, 32, 29-36.

Armstrong RA, Cairns NJ, Lantos PL. A quantitative study of the pathological changes in white matter in multiple system atrophy. *Neuropathology* 2007, 27, 221-227.

Brown P. The pathogenesis of transmissible spongiform encephalopathy: routes to the brain and the erection of therapeutic barricades. *Cell and Molecular Life Science,* 2001, 58, 259-265.

Carola A, Pizzolato GP, Gailloud P, Macchi G, Fasel J, LeFloch J, Cardone F. A panencephalic type of Creutzfeldt-Jakob disease with selective lesions of the thalamic nuclei in two Swiss patients. *Clinical Neuropathology,* 1996, 15, 125-134.

Caughey B. Interactions between prion protein isoforms: the kiss of death? *Trends in Biochemical Science*, 2001, 26, 235-242.

Collins S, McLean CA, Masters CL. Gerstmann-Straussler-Scheinker syndrome, fatal familial insomnia and kuru: a review of these less common human transmissible spongiform encephalopathies. *Journal of Clinical Neuroscience,* 2001, 8, 387-397.

Creutzfeldt HG. Über eines eigenartige herd-formige Erkrankung des Zentralnervensystems. In: Nissl F, Alzheimer A, eds., Histologische und Histopathologische Arbeiten uber die Grosshirnrinde, Jena, Gustav Fisher, 1921, 1-48.

DeArmond SJ, Prusiner SB. Etiology and pathogenesis of prion disease. *American Journal of Pathology,* 1995, 146, 785-804.

Goldfarb LG, Brown P, Cervenakova L, Gajdusek DC. Genetic analysis of Creutzfeldt-Jakob disease and related disorders. *Philosophical Transactions of the Royal Society*, Series B, 1994, 343, 379-384.

Grigoriev V, Escarg-Haye F, Streichenberger N, Kopp N, Langeveld J, Brown P, Fournier JG. Submicroscopic immunodetection of prion protein in the brain of a patient with new variant Creutzfeldt-Jakob disease. *Neuroscience Letters,* 1999, 264, 57-60.

Hill AF, Butterworth RJ, Joiner S, Jackson G, Rossor MN, Thomas DJ, Frosh A, Tolley N, Bell JE, Spencer M, King A, Al-Sarraj S, Ironside JW, Lantos PL, Collinge J. Investigation of variant Creutzfeldt-Jakob disease and other human prion diseases with tonsil biopsy samples. *Lancet,* 1999, 353, 183-189.

Hogan RN, Cavanagh HD. Transplantation of corneal tissue from donors with disease of the central nervous system. *Cornea,* 1995, 14, 533-547.

Ironside JW. Pathology of variant Creutzfeldt-Jakob disease. *Archives of Virology* [Suppl], 2000, 16, 143-151.

Ironside JW, Sutherland K, Bell JE, McCardle L, Barrie C, Estebeiro K, Zeidler M, Will RG. A new variant of Creutzfeldt-Jakob disease: neuropathological and clinical features. *Cold Spring Harbour Symposium of Quantitative Biology*, 1996, LXI, 523-530.

Ironside JW, Head MW, Bell JE, McCardle L, Will RG. Laboratory diagnosis of variant Creutzfeldt-Jakob disease. *Histopathology*, 2000, 37, 1-9.

Jakob A. Über eigenartige Erkrankungen des Zentralnervensystems mit bemerkenswerten anatomischen Befunden (spastische Pseudosklerose-Encephalomyelopathic mit disseminierten Degenerationsherden). *Dtsch Z Nervenheilk,* 1921, 70, 132-146.

Kovacs GG, Gasque P, Strobel T, Lindeck-Pozza E, Strohschneider M, Ironside JW, Buddka H, Guentchev M. Complement activation in human prion disease. *Neurobiology of Disease*, 2004, 15, 21-28.

Krasemann S, Groschup MH, Harmeyer L, Hunsmann G, Bodemer W. Generation of monoclonal antibodies against human prion proteins in PrPO/O mice. *Molecular Medicine*, 1996, 2, 725-734.

Masullo C, Machin G. Resistance of the hippocampus in Creutzfeldt-Jakob disease. *Clinical Neuropathology,* 1997, 16, 37-44.

McLean CA, Ironside JW, Alpers MP, Brown PW, Cervenakova L, Anderson RMD, Masters CL. Comparative neuropathology of kuru with new variant of Creutzfeldt-Jakob disease: evidence for strain of agent predominating over genotype of host. *Brain Pathology*, 1998, 8, 429-437.

Muhleisen, H., Gehrmann, J. and Meyermann, R. 1995 Reactive microglia in Creutzfeldt-Jakob disease. *Neuropathology and Applied Neurobiology,* 1995, 21, 505-517

Prusiner SB. The prion diseases. *Scientific American*, 1995; 31-37.

Prusiner SB, DeArmond SJ. Prion diseases and neurodegeneration. *Annual Revue of Neuroscience,* 1994, 17, 311-339.

Stockel J, Hartl FU. Chaperonin-mediated *de novo* generation of prion protein aggregates. *Journal of Molecular Biology*, 2001, 313, 861-872.

Walis A, Liberski PP, Brown P, Gajdusek DC. Electron microscopic studies of the otic nerve in experimental scrapie and the panencephalopathic type of Creutzfeldt-Jakob disease. *Folia Neuropathologica* 1997, 35, 255-258

Will RG, Ironside JW, Zeidler M, Cousins SN, Estebeiro K, Alperovitch A, Poser S, Pocchiari M, Hofman A, Smith PG. A new variant of Creutzfeldt-Jakob disease in the United Kingdom. *Lancet* 1996, 347, 921-925.

In: Handbook on White Matter
Editors: T. B. Westland and R. N. Calton
ISBN: 978-1-60741-034-8

Chapter IX

Progressive Multifocal Leukoencephalopathy

Endre Pál*
Department of Neurology, University of Pécs, Hungary
H-7623 Pécs Rét u. 2, Hungary

Abstract

Progressive multifocal leukoencephalopathy (PML) is a rare demyelinating disease of the central nervous system. It is caused by opportunistic infection by the JC virus, a human polyomavirus. The primary infection is common and usually remains asymptomatic. The virus resides in the kidney in a latent form and can be reactivated when the immune system becomes compromised. B cells may transmit the virus to oligodendrocytes in the brain. Destruction of oligodendrocytes results in progressive and multifocal central nervous system symptoms and the outcome is usually fatal. PML has been increasingly detected in patients with AIDS and other secondary immunodeficiency conditions, and it might develop in exceptional cases with primary immunodeficiencies. Efficient therapies have not been established for patients with PML. Antiviral agents, highly active antiretroviral treatment in AIDS, and immunotherapies might be beneficial in acquired and iatrogenic immunodeficiency. The associated conditions, assumed pathomechanism, clinical and neuropathological features and therapeutic possibilities are summarized.

Introduction

Progressive multifocal leukoencephalopathy (PML) is a rare and devastating neurological complication of immunodeficiency of various origin usually results in death.

* endre.pal@aok.pte.hu; Tel: +36-72-535-900; Fax:+36-72-535-911

Impaired cellular immunity results in the reactivation of the opportunistic infective agent, JC virus (JCV) [Koralnik, 2006].

PML was first described in 1958 by Richardson and colleagues in two patients, one with leukemia and another with Hodgkin's disease [Aström et al., 1958]. Viral etiology was confirmed by electronmicroscopical (EM) examination, where virus particles were found in the nuclei of oligodendrocytes [Zu Rhein et al., 1965]. The JC virus was identified in 1971 and named after the patient's initials whose tissue was isolated it from [Padgett et al., 1971]. Official name, JCV MAD-1 was given in 1984 after its DNA was sequenced [Frisque et al, 1984].

Epidemiology

The disease was rare before the 1980s, Brooks and Walker found 230 previous publication of PML cases [Brooks et al., 1991]. After the worldwide AIDS epidemic the frequency remarkably increased. The estimated annual incidence in a Canadian study was 1:1.000.000 [Power et al., 1997]. Before AIDS, male:female ratio was 3:2. Since than the vast majority (89-100%) of published cases were male patients [Berger et al., 1997, Gillespie et al., 1991]. PML usually is associated with compromised cellular immunity due to innate or acquired immunodeficiency.

There are few reported PML cases due to inherited/primary immunodeficiencies, including ICF syndrome (immunodeficiency, centromeric instability of chromosomes 1,9,16 and facial dysmorphism), isolated CD4 deficiency, X-linked hyper-IgM syndrome (CD40L defect), common variable immunodeficiency, hyper-IgE, -IgM syndrome, Wiskott-Aldrich syndrome, adenosine deaminase deficiency and purin nucleoside phosphorylase deficiency [Haider et al., 2000, Colucci et al., 2004, Aschermann et al., 2007, Parvaneh et al., 2007].

Association of PML with acquired immunodeficiencies/immune suppression is much more frequent. Before 1984 four percent of the reported cases were attributed to AIDS [Brooks et al., 1984]. Recent publications showed that HIV-induced immune suppression currently accounts for 80-85% of PML cases [Manji et al., 2000, Tyler, 2003, Bore et al., 2008]. PML develops in 4-5% of AIDS patients according to clinical observations [Holman et al., 1991], but in large neuropathological series it was 7-9,8% in autopsied AIDS patients [Lang et al., 1989, Kuchelmeister et al., 1993].

The remaining 15-20% of patients suffers from immune suppression due to hematological malignancies (13%) (lymphoproliferative diseases, sarcoidosis), after kidney, heart and other organ transplantation (5%) and because of chronic autoimmune diseases (2%), such as systemic lupus erithematosus (SLE), scleroderma, dermatomyositis, polymyositis, Wegener granulomatosis, rheumatoid arthritis, Sjögren syndrome and mycosis fungoides [Koralnik et al., 1999, 2006, Pagnoux et al., 2003, Lee et al., 2007, Völker et al., 2007, Bore et al., 2008, De Raedt et al., 2008, Hayashi et al., 2008] (table 1).

Table 1. Diseases associated with PML

I. Hereditary immune deficiencies
1. ICF syndrome
2. Isolated CD4 deficiency
3. X-linked hyper-IgM syndrome (CD40L defect)
4. Common variable immunodeficiency
5. Hyper-IgE, -IgM syndrome
6. Wiskott-Aldrich syndrome
7. Adenosine deaminase deficiency
8. Purin nucleoside phosphorylase deficiency
II. Acquired immune deficiencies
1. HIV-induced immune suppression
2. Hematological malignancies
3. Lymphoproliferative diseases, sarcoidosis
4. Transplantation recipients
5. Chronic autoimmune diseases (SLE, scleroderma, dermatomyositis, polymyositis, Wegener granulomatosis, rheumatoid arthritis, Sjögren syndrome, mycosis fungoides)

In the last few years „new" and targeted immunemodulatory therapies were introduced for treatment of autoimmune diseases. Natalizumab is a humanized recombinant monoclonal antibody that binds to the $\alpha_4\beta_1$ integrin (very late activation antigen=VLA-4) and $\alpha_4\beta_7$ integrin and inhibits leukocyte trafficking into central nervous system [Stuve et al., 2007]. This drug has powerful anti-inflammatory effect and was proved to be effective in treatment of certain forms of multiple sclerosis and Crohn's disease. Unfortunately, in 3 of 3000 patients treated developed P+ML [Van Assche et al., 2005, Kleinschmidt-Demasters et al., 2005, Langer-Gould et al., 2005, Gold et al., 2007]. In the mechanism of natalizumab-induced PML the direct effect on bone marrow and in particular on B cells was suspected instead of generalized immune suppression. One believes that α_4 integrin blockade mobilizes immature, JCV-infected B cells from bone marrow and uncontrolled proliferation of virus leads to the development of PML [Ransohoff, 2005, 2007]. According to another hypothesis natalizumab can prevent migration of activated (JCV-specific) cytotoxic T lymphocytes at the sites of JCV latency, might have led virus activation [Pasquier et al., 2006]. These were based on those observation that JCV DNA load in blood was raised in a natalizumab treated patient, before appearance of PML [Van Assche et al., 2005].

JCV and Pathogenesis of Infection

JCV belongs to the polyomaviruses. Non-enveloped viruses belonging to this family have icosahedral capsid containing circular, double-stranded DNA. Polyomaviruses have been isolated from several species, but each virus has a very limited host-specificity, where

the virus can cause productive infection [Imperiale, 2001]. Mouse and simian polyomavirus (SV40) was first discovered in 1960s [Sweet et al., 1960], JCV (Type B Human Polyomavirus) and the other human polyomavirus, BKV (Type A Human Polyomavirus) were identified in 1971 from the brain of a patient suffered from PML, and in urine of a kidney allograft recipient, respectively [Sweet et al., 1960, Padgett et al., 1971, Gardner et al., 1971].

The above mentioned viruses are similar in size of DNA (approx. 5.2 Kb) and their genomic organization. The DNA contains two coding regions, the early and the late transcription unit. Transcription of both units is initiated from a common regulatory region. The early transcription proceeds in a counterclockwise direction resulting in two alternatively spliced transforming proteins, large T and small t antigens. The late transcription proceeds clockwise direction on the opposite strand of the DNA. This region encodes structural capsid proteins (VP1, VP2, VP3) and a regulatory factor, agnoprotein [Trowbridge et al., 1995].

The infection of host cells is initiated by binding of the virion to a receptor on the cell surface. SV40 binds to the major histocompatibility complex (MHC-I). In contrast, JCV binds to the 5HT2AR serotonin receptor on the surface of human glial cells [Norkin, 1999, Elphick et al., 2004]. Virus is taken up by endocytosis and transported to the nucleus. After the capsid proteins removed, early transcription unit is activated and mRNA of large T and small t antigens produced. Large T antigen (1) binds to the viral origin of DNA replication and promotes DNA synthesis, (2) stimulates progression of the cell cycle to S phase (3) stimulates transcription from the late promoter. The virus does not have own protein to DNA synthesis therefore uses the host's ones. Assembling the viral DNA and the capsid proteins the host cell produces intranuclear virions, which are released upon cell lysis [Cole, 1996]. JCV has a unique tropism for replication in glial cells, especially for oligodendrocytes (ODC). Replication of virus in target cells causes lysis of ODCs and leads to focal area of demyelination [Safak et al., 2003]. The virus can growth in human fetal glial cell culture and can replicate not only in ODCs but in astrocytes, as well [Major et al., 1989]. The explanation is that 5HT2AR receptor responsible for specific binding of JCV to host cell is present not only on ODCs, but on astrocytes, kidney epithelial cells and B cells also [Elphick et al., 2004].

Enzyme-linked immunosorbent assay (ELISA) testing has revealed specific antibodies for JCV in 85% of healthy adults [Weber et al., 1997, 2001]. The route of primary infection is not known but urine-oral infection is supposed. In healthy adults the virus does not cause illness, but intermittently appears in urine, for example in pregnancy. After the primary infection the virus remains latent in kidneys, lymphoid organs and bone marrow due to the immune surveillance by CD4+ and CD8+ T cells [Weber et al., 2001]. Interestingly, the genotype of latent and activated virus is different, the later contains tandem repeats in the transcription control region, and this tandem sequences are necessary to the ability to infect cells [Hou et al., 2006, Koralnik, 2006]. The mechanism of CNS infection is unresolved: the role of B cells suspected. It is possible that virus do not infect the lymphocytes, but binds to their surface and it is transported from blood stream to CNS like „Trojan horse" [Atwood et al., 1992, Dubois et al., 1997].

The above described latency/activation model is generally accepted, but it has not proved. Several details of pathomechanism remained unresolved: (1) the route and age of

infection (2) the initialization of rearrangement of virus regulatory region, (3) the time and route of brain infection.

Although the main target of JCV was thought to be ODCs, it might be possible that infection of astrocytes precedes and promotes the infection of ODCs [Mázló et al., 2001].

Impairment of supportive function of, or/and spreading the virus by astrocytes might be possible. This hypothesis based on the finding that astrocyte reactivation (astrogliotic clusters) is the very early histological sign before the evidence of demyelination [Aström et al., 1994].

It is possible that JCV reactivation involves transcription factors that respond to intracellular signaling pathways downstream of cytokines and other immunemodulators. The non-coding region contains a transcriptional regulatory element that contains a 23 base pair GGA/C rich sequence serving as a binding site of transcription factors. Recently a transcription factor, the early growth response-1 protein (Egr-1) was found to stimulate the transcription of JCV late promoter. The Egr-1 gene responds rapidly variety of extracellular stimuli including neurotransmitters, hormones, cytokines [Romagnoli et al., 2008].

The frequency of PML in HIV/AIDS is higher than that of any other immunosuppressive disorders relative to their frequency. Possible explanations might be as: (1) profound and long-lasting cellular immunosuppression in HIV infection, (2) facilitation of entry into the brain of JCV-infected B cells through HIV compromised blood-brain barrier, and upregulation of adhesion molecules on brain vascular endothel cells [Houff et al., 1990], (3) retroviral transregulating proteins might play a role in reactivation, such as the HIV-encoded Tat [Chowdhury et al., 1990].

Human Diseases Caused by Polyomaviruses

JCV having tropism to glial cells most commonly cause PML [Koralnik, 2006]. However, direct infection of cerebellar granule cells results in granule cell neuronopathy (GCN) [Koralnik et al., 2005 Hecht et al., 2007].

BKV is associated with hemorrhagic cystitis in bone marrow transplant recipients, ureteric stenosis and polyomavirus-associated nephropathy in renal transplant recipients [Trofe et al., 2004].

SV40 does not cause human disease, because its natural host is the rhesus monkey. Unfortunately millions of people had been exposed to SV40 during poliovirus vaccination in the 1950-1960s, because the monkey kidney cell culture used to maintain poliovirus was contaminated with SV40 [Cole, 1996]. Therefore seropositivity of SV40, BKV and JCV polyomaviruses was demonstrated in the adult population worldwide.

JCV and Tumors

It is well known that the polyomaviruses, SV40 and JCV have oncogenic potential in laboratory animals (hamsters, rat, owl- and squirrel monkeys). The first human case with tumor was reported by Richardson in a patient with PML. Further reports noted various brain

tumors, such as oligodendroglioma, oligoastrocytoma, medulloblastoma, glioblastoma multiforme, CNS lymphoma [White et al., 2005]. In few cases extracranial tumors were also associated with JCV positivity. Detection of JCV antigens and DNA became possible after improvement of molecular biological methods. De Valle reported that depending on tumor type, 57-83% of brain tumors were positive for JCV (DNA and largeT antigen) [Valle et al., 2001]. The molecular mechanism of oncogenesis resides in the ability of T antigen to interfere with the two tumor suppressor proteins, pRb (retinoblastoma family) and p53. Inactivation of these proteins results in promoting cell cycle to proliferation (from G0-G1 phase to S phase) and inhibition of apoptosis, respectively. Furthermore, t antigen augments viral DNA replication and promotes cell proliferation via inactivation PP2A, a negative regulator of growth-promoting protein kinases. The agnoprotein has also multiple site of action, including p21/WAF-1 and p53 [White et al., 2005]. In spite of the increasing number of reported cases, the evidence of human oncogenesis in astrocytomas or gliomas by JCV remains uncertain.

Clinical Presentation of PML

PML develops in patients with compromised cellular immunity of various origin.

There is no unique clinical picture. The course is rapidly progressive. It usually starts with unilateral complaints and neurological signs resembling to the parieto-occipital lesion: hemiparesis, hemianopia, ataxia [Berger et al., 1997]. In the HIV-associated cases fronto-parietal signs (hemiparesis, pyramidal signs, cognitive dysfunction) dominate and cerebellar signs are more frequent [Einsiedel et al., 1993]. Interestingly, headache was more commonly reported in HIV-associated series. Visual disturbances are frequent, including visual field loss, diplopia, but optic nerve disease does not occur in PML. Although spinal cord lesion rarely detected during autopsy, clinical myelopathy usually does not develop.

Unifocal disease occurred 60% of patients in a retrospective study of HIV-associated cases [Adcock et al., 1997]. Table 2 shows the most frequent neurological signs [Gillespie et al., 1991].

Table 2. Clinical presentation of PML

Hemiparesis	60-67%
Ataxia	26-43%
Mental disturbances	30-39%
Language disorders	31%
Visual alterations	30%
Headache	23%
Sensory loss	18%
Seizures	11%

[Modified from Adcock et al., 1997, and Gillespie et al., 1991].

The characteristic age of onset is 6th decade of non-AIDS cases and 3rd-4th decade of HIV-associated forms [Stoner et al., 1988, Giesen et al., 1997]. PML usually progresses to death within 3-6 months. However remission, prolonged survival, even recovery may occur [Berger et al., 1997, 1999, Gillespie et al., 1991]. Only a higher CD4 cell count of greater than 50/μl but no clinical signs were found to be associated with better survival. Neither pathological findings, nor treatment were prognostic value, although highly active antiretroviral therapy (HAART) improves survival [Adcock et al., 1997]. Recent molecular biological findings implicates that JCV DNA load in cerebrospinal fluid is a strong predictor of patients survival [Marzocchetti et al., 2007].

Diagnosis

After a suggestive clinical picture there are different methods to confirm the diagnosis.

First choice is brain imaging. Computer tomography sometimes reveals hypointense lesions of the affected white matter, but magnetic resonance imaging (MRI) is far more sensitive [Whiteman et al., 1993]. It usually shows multifocal, asymmetric lesions with high signal intensity on T2 and hypointensity on T1 weighted images, localized to the subcortical white matter, with no mass effect, without contrast enhancing and cortical atrophy. The grey/white matter border sometimes looks „scalloping" followed by subcortical edema. Later the lesions extend into the deep white matter as well and became confluent. The typical localization is parieto-occipital, but any part of the white matter can be involved, as well as brainstem and cerebellum [Guilleux et al., 1986]. Presence of mass effect is rare, but it is a negative prognostic factor [Post et al., 1989, Pal et al., 2007] (figure 1). Despite its name, the disease is not restricted to white matter, lesions occur in thalamus, in basal ganglia and in cortex, as well.

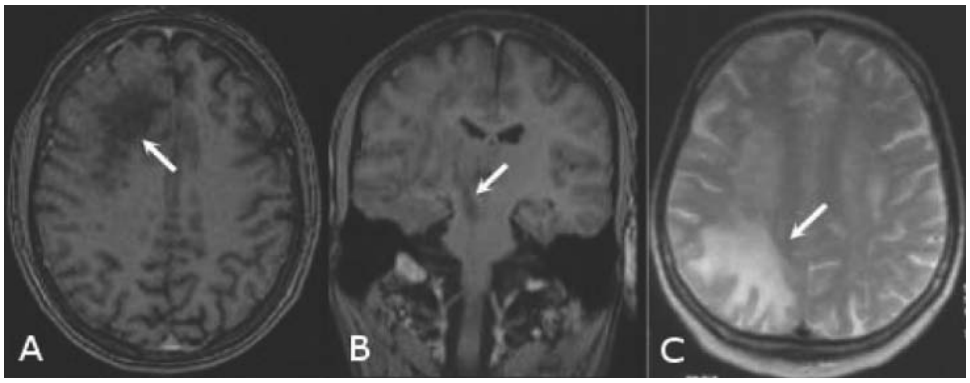

Figure 1. MRI alterations in PML brain; A: T1-weighted MRI showing fronto-parietal lesion with slight mass effect (arrow). B: T1-weighted image demonstrated right midbrain lesion (arrow). C: Confluent white-matter lesions on a T2-weighet image, involving both hemispheres, predominating on right side (arrow). Reprinted with modifications from *Clin Neurosci (Hungary)*, 2007 60, 263-268.

Concerning the multifocal white matter lesions, several other diseases must be excluded:

Other CNS infections (HIV encephalopathy), autoimmune diseases (e.g. multiple sclerosis, systemic lupus erythematosus), metabolic-, cerebrovascular diseases, primary cerebral lymphoma, leukodystrophy and toxic encephalopathies (table 3) [Pal et al., 2007]. The location of lesions (subcortical white matter), hypointensity on T1-weighted images, and the absence of contrast enhancement are important radiological markers of PML, because these differ from the majority of subacute progressive white matter diseases (especially in HIV: AIDS-dementia complex, viral/fungal encephalitis, CNS lymphoma) [Whiteman et al., 1993].

Table 3. Differential diagnosis of PML

Genetical:	Leukodystrophies (MLD, ALD, PMD)
Demyelinating diseases:	Multiple sclerosis, acute disseminated encephalomyelitis (ADEM)
CNS infections:	AIDS-dementia-complex, Neuroborreliosis, VZV-, CMV-encephalitis
Metabolic:	Hepatic encephalopathy, hypoxia, uremia, folsav-, B12-vitamin-deficiency
Cerebrovascular:	Binswanger's disease, hypertensive encephalopathy, amyloid angiopathy, CADASIL
Traumatic:	diffuse axonal lesion
Anti-neoplastic agents:	cytostatics
Immunosuppressive drugs:	interferon-alpha, cyclosporin, etc.
Drogs:	ethanol, toluen, cocain, heroin, etc.
Environmental:	carbone-monoxide, carbon-tetrachloride, arsene, etc.
Hydrocephalus:	normal-pressure hydrocephalus

Abbreviations: ALD: adrenoleukodystrophy; CADASIL: cerebral autosomal dominant arteriopathy with subcortical infarcts and leukoencephalopathy; CMV: cytomegalovirus, MLD: metachromatic leukodystrophy; PMD: Pelizaeus–Merzbacher disease; VZV: varicella-zoster virus.

Routine cerebrospinal fluid (CSF) tests are usually normal (no cellular reaction, normal, or slightly raised protein level, no oligoclonal bands were reported), but very helpful in excluding other diagnoses. Serological tests from blood are not useful, because the majority of adult population is seropositive. Detection of JCV-specific antibodies in CSF is not routinely used, but anti-VP-1 oligoclonal antibodies were found in 55% in a series [Sindic et al., 1997].

The best way to confirm the diagnosis is to detect JCV DNA in patient's CSF sample. Several methods were developed, including simple, or nested-PCR [Weber et al., 1996, 1997], competitive PCR [Drews et al., 2000] and quantitative, real time PCR (QR-PCR) [Bossolasco et al., 2005, Fink et al., 2006]. Seventy six percent sensitivity and 100% specificity of these methods was reported [Bossolasco et al., 2005, Mazorchetti et al., 2007]. Measuring JCV DNA load in cerebrospinal fluid gives possibility to follow up the efficacy of highly active anti-retroviral therapy (HAART) in AIDS patients [Mazorchetti et al., 2007].

Pathological Hallmarks

Brain biopsy and autopsy give the final chance to confirm the diagnosis.

Basic pathological findings in PML correspond to the ODC pathology. The virus has a tropism to ODCs and causes their lytic infection resulting in multifocal demyelination. Lesions develop anywhere in white matter, but usually are localized at the cortico-subcortical border. In early phase combined staining (e.g. luxol-fast blue or immunostaining) demonstrates focal absence of myelin sheaths with relative preservation of axons in the subcortical region. Decrease or complete absence of ODCs is usual in the centre of demyelination, while at the border, or in newly formed lesions infected ODCs appear with enlarged, basophilic nuclei corresponding to viral inclusions. Rarely inclusions present in the nuclei of enlarged astrocytes, but these usually do not occupy the whole nucleus. Virus infects both glial elements: in ODCs it causes lytic, in astrocytes abortive or transforming infection [Aström et al., 1994] . Immunohistochemistry (antibodies to JCV or SV40 T antigen, or VP1) or in situ hybridization to JCV DNA specifically visualizes JCV in nuclear inclusions of ODC, and in nucleus, or cytoplasm of astrocytes [Itoyama et al., 1982]. Infected ODCs showed both JCV DNA and late proteins, however in astrocytes capsid proteins were demonstrated less often [Aksamit et al., 1987]. Immunohistochemical methods demonstrated that apoptosis occurs in ODCs associated with demyelinated lesions, regardless of HIV positivity. Infected astrocytes are never undergo apoptosis. [Richardson-Burns et al., 2002]. Foamy macrophages and (peri) vascular inflammation usually is not present, but rarely occurs (figure 2). In the advanced lesions total loss of myelin and ODCs, proliferation of astrocytes and lipid-laden macrophages appear. In 80% of cases bizarre giant astrocytes can be seen. Axonal and neuronal changes (shrinkage or swelling) can be seen, as well.

In infected cells EM shows mainly round intranuclear virus particles 40-42.5 nm in diameter (fixed or not, respectively), and few filamentous forms 15-25 nm in with [Howatson et al., 1965] (figure 3). Ultrastructural studies demonstrated each phases of infection and virus assembly in ODCs and the presence of JCV in astrocytes as well. The attached viruses enter into host cell by endocytosis and are transported to nucleus via vacuoles and cisterns of granular endoplasmic reticulum. In the nucleus the host's cell cromatin changes to viral DNA, while viral proteins are produced in the cytoplasm. Virus assembly occurs int he nucleoplasm and viruses are released from the cell by cytolysis. In autopsy, or biopsy material plasma membrane and cytoplasmic organelles might be disintegrated, but nuclei filled with virus particles are usually preserved and let to identify viruses [Mázló et al., 1980, 1982, 1991, Pal et al., 2007]. Diagnostic criteria are shown in table 4. HIV-related and unrelated PML pathology is different. In HIV positive patients the involvement of basal ganglia (thalamus), cerebellar granular layer and spinal cord is more frequent, and mononuclear/macrophage infiltration is more pronounced, as well [Lang et al.,1989, Kuchelmeister et al., 1993].

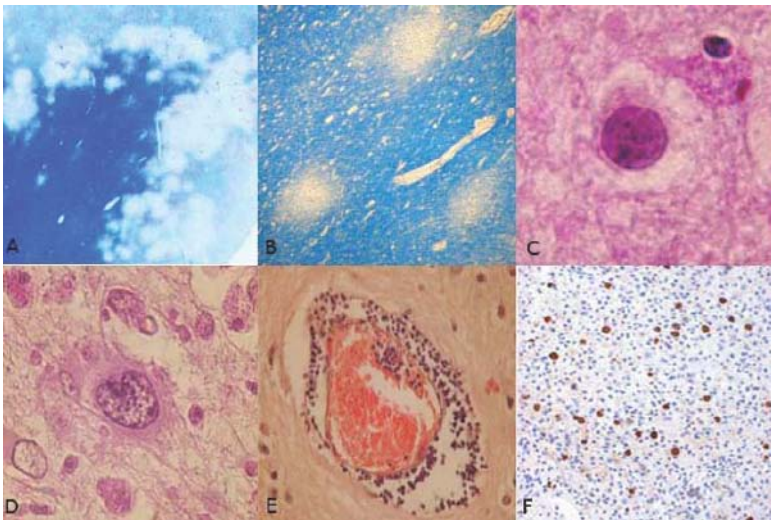

Figure 2. Light microscopic appearance of PML; A: patchy demyelinating lesions at the white-gray matter border. Luxol-fast blue (LFB). B: small demyelinating areas with higher magnification (LFB). C: ODC nuclear inclusion (HE). D: giant astrocyte (HE). E: mild vascular wall cellular reaction (HE), F: ODC nuclear inclusions (SV40 immunohistochemistry, courtesy of Professor Budka). Original magnification: A:10x , B:20x , C, D:100x , E:40x , F: 20x. Reprinted with modifications from *Clin Neurosci (Hungary)*, 2007 60, 263-268.

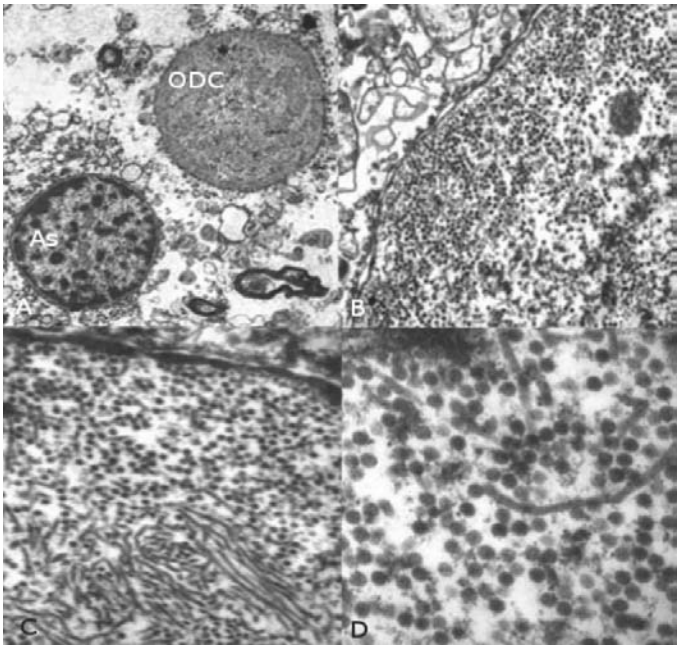

Figure 3. Ultrastructural features of PML; A: Nucleus of an infected ODC and astrocyte (As) in an autopsy specimen. B: Virus particles in an ODC nucleus. C and D: round and filamentous virus particles on high-power EM image. Original magnification: A: 5.000x, B: 20.000x, C: 40.000x, D: 75.000x . Reprinted with modifications from *Clin Neurosci (Hungary)*, 2007 60, 263-268.

Table 4. Diagnostic criteria of PML

• Hundreds of foci of demyelination from 0.1 to 1 cm in diameter, scattered the white matter with sparing axons
• Absence of ODCs in the central part of the lesions, presence of ODC nuclear inclusions at the margins
• Presence of bizarre giant astrocytes in chronic lesions (presents in 80%)

[Aström et al., 1958, Richardson et al., 1970, Mázló et al., 1991].

Therapy

Actually PML does not have effective therapy. In HIV-negative patients suspension of the immune suppressive therapy is recommended. In HIV-positive patients administration of highly active anti-retroviral therapy (HAART) was reported to be resulted in improvement and longer survival [Clifford et al., 1999].

Various antiviral treatments were studied. Cytosine arabinoside failed to demonstrate significant improvement, but might be effective in selected cases [Adcock et al., 1997, Hall et al., 1998].

Alpha-interferon treatment in the initial studies resulted in doubtful results, but open-labeled studies showed significantly longer survival (325 versus 175 days) and clinical improvement [Huang et al., 1998, Geschwind et al., 2001].

Cidofovir, a nucleoside analog, inhibitor of viral DNA polymerase licensed for treatment of cytalomegalovirus retinitis, resulted in improved neurological outcome, survival and more effective control of JCV replication in HIV-positive patients if it was added to HAART [De Luca et al., 2000]. Unfortunately, cidofovir alone was neither effective in HIV unrelated, nor HIV-associated PML [Houston et al., 2001, Mara et al., 2001].

Future Treatment Options

Recently was found that irisolidone, an isoflavone metabolite, significantly inhibited the JC virus expression in primary cultured human astrocytes and glial cell lines. Irisolidone treatment repressed Sp1 binding to Sp1-II site, which is important for the basal JC virus promoter activity [Kim et al., 2006].

Since 5HT2A serotonin receptor has been recently identified as a cellular receptor for JCV, using serotonin antagonists, including atypical antipsychotics are under consideration as therapeutic option for preventing spread of JCV. Focosi et al. reported clinical and virological response in a hematopoietic stem cell transplant recipient with PML who was treated with short-term, low-dose course of risperidon [Focosi et al., 2007].

Roscovitine, pharmacological cyclin-dependent kinase (cdk) inhibitor has antiviral activity against viruses. It was found that roscovitine significantly inhibited the viral production and cytopathic effects in a JCV-infected cell line. Roscovitine attenuated the

transcription, prevented viral replication via inhibiting phosphorylation of large T antigen [Orba et al., 2008].

Antisense oligodeoxynucleotide against SV40 large T antigen inhibited expression of the oncoprotein expression in SV40-transformed human fetal glial cells [Wang et al., 2004].

Conclusion

The discovery and investigation of polyomaviruses resulted in major progress in molecular biology and virology. However, several points of infection are not clear. The number of HIV-infected cases and the use of old and new immunosuppressive methods increases. Therefore, extensive further investigation is necessary to find new alternative therapies for PML that is currently lethal disease.

Acknowledgment

The author thanks to Mária Mázló MD. PhD. for reviewing the manuscript and her critical remarks and helpful advices.

References

Adcock, JE; Davies, MA; Turner J; Pell, M; Brew, BJ. Progressive multifocal leukoencephalopathy: a retrospective study of 30 cases. *J. Clin. Neurosci.* 1997 4, 463-468.

Aschermann, Z; Gomori E; Kovacs, GG; Pal, E; Simon, G; Komoly, S; Marodi, L; Illes, Z. X-linked hyper-IgM syndrome associated with a rapid course of multifocal leukoencephalopathy. *Arch. Neurol.* 2007 64, 273-276.

Aksamit, AJ; Major, EO; Ghatak, NR; Sidhu, GS; Parisi, JE; Guccion, JG. Diagnosis of progressive multifocal leukoencephalopathy by brain biopsy with biotin labeled DNA:DNA in situ hybridization. *J. Neuropathol. Exp. Neurol.* 1987 46, 556-566.

Aström, KE; Mancall, EL; Richardson, EP. Progressive multifocal leukoencephalopathy. *Brain.* 1958 81, 93-127.

Aström KE; Stoner GL. Early pathological changes in progressive multifocal leukoencephalopathy: a report of two asymptomatic cases occurring prior to the AIDS epidemic. *Acta Neuropathol.* 1994 88, 93-105.

Atwood, WJ; Amemiya, K; Traub, R; Harms, J; Major, EO. Interaction of the human polyomavirus, JCV, with human B lymphocytes. *Virology.* 1992 190, 716-723.

Berger, JR; Gallo, BV; Concha, M. Progressive multifocal leukoencephalopathy. In: Berger, JM; Levy RM, editors. *AIDS and the nervous system*. Philadelphia: Lippincott Raven Publishers; 1997; 569-594.

Berger, JR; Major, EO. Progressive multifocal leukoencephalopathy. *Semin. Neurol.* 1999 19, 193–200.

Boren, EJ; Cheema, GS; Naguwa, SM; Ansari, AA; Gershwin, ME. The emergence of progressive multifocal leukoencephalopathy (PML) in rheumatic diseases. *J. Autoimmunity.* 2008 30, 90-98.

Bossolasco, S; Calori, G; Moretti, F; Boschini, A; Bertelli, D; Mena, M; Gerevini, S; Bestetti, A; Pedale, R; Sala, S; Lazzarin, A; Cinque, P. Prognostic significance of JC virus DNA levels in cerebrospinal fluid of patients with HIV-associated progressive multifocal leukoencephalopathy. *Clin. Infect. Dis.* 2005 40, 738-44.

Brooks, BR; Walker, DL. Progressive multifocal leukoencephalopathy. *Neurol. Clin.* 1984 2, 299-313.

Clifford, DB; Yiannoutsos, C; Glicksman, M; Simpson, DM; Singer, EJ; Piliero, PJ; Marra, CM; Francis, GS; McArthur, JC; Tyler, KL; Tselis, AC; Hyslop, NE. HAART improves prognosis in HIV associated progressive multifocal leukoencephalopathy. *Neurology.* 1999 52, 623-625.

Cole, CN. Polyomavirinae: the viruses and their replication, In: Fields BN, Knipe DN, Howley PM, Editors. *Fundamental Virology, Third edition*. Philadelphia: Lippincott, Williams and Wilkins; 1996; 917–946.

Colucci, M; Cocitoa, LL; Capelloa, E; Mancardi, GL; Serrati, C; Cinque, P; Schenone, A. Progressive multifocal leukoencephalopathy in an adult patient with ICF syndrome. *J. Neurol. Sci.* 2004 217, 107-110.

Chowdhury, M; Taylor, JP; Tada, H; Rappaport, J; Wong-Staal, F; Amini, S; Khalili K. Regulation of the human neurotropic virus promoter by JCV-T antigen and HIV-1 tat protein. *Oncogene.* 1990 5, 1737-1742.

De Luca, A; Giancola, ML; Ammassari, A; Grisetti, S; Cingolani, A; Paglia, MG; Govoni, A; Murri, R; Testa, L; Monforte, AD; Antinori, A. Cidofovir added to HAART improves virological and clinical outcome in AIDS-associated progressive multifocal leukoencephalopathy. *AIDS*, 2000 14, F117–F121.

De Raedt, S; Lacor, P; Michotte, A; Flamez, A; Ebinger, G. Progressive multifocal leukoencephalopathy as first manifestation of sarcoidosis. *Clin. Neurol. Neurosurg.* 2008 110, 186-189.

Drews, K; Bashir, T; Dörries K. Quantification of human polyomavirus JC in brain tissue and cerebrospinal fluid of patients with progressive multifocal leukoencephalopathy by competitive PCR. *J. Virol. Methods.* 2000 84, 23–36.

Dubois, V; Dutrone, H; Lafon, ME; Poinsot, V; Pellegrin, JL; Ragnaud, JM; Ferrer, AM; Fleury, HJ. Latency and reactivation of JC virus in peripheral blood of human immunodeficiency virus type 1-infected patients. *J. Clin. Microbiol.* 1997 35, 2288-2292.

Du Pasquier, RA; Stein, MC; Lima, MA; Dang, X; Jean-Jacques, J; Yheng, Y; Letvin, NL; Koralnik, IJ. JC virus induces a vigorous CD83 cytotoxic T cell response in multiple sclerosis patients. *J. Neuroimmunol.* 2006 176, 181-186.

Einsiedel, RW; Fife, TD; Aksamit, AJ; Cornford, ME; Secor, DL; Tomiyasu, U. Progressive multifocal leukoencephalopathy in AIDS: a clinicopathological study and review of the literature. *J. Neurol.* 1993 240, 391-406.

Elphick, GF; Querbes, W; Jordan, JA; Gee, GV; Eash, S; Manley, K; Dugan, A; Stanifer, M; Bhatnagar, A; Kroeze, WK; Roth, BL; Atwood, WJ. The human polyomavirus, JCV, uses serotonin receptors to infect cells. *Science.* 2004 306, 1380–1383.

Fink, MCDS; Penalva de Oliveira, AC; Milagres, FAP; Vidal, JE; Picerno-Pouza, AF; Neto, AD; Pannuti, CS. JC virus DNA in cerebrospinal fluid samples from Brazilian AIDS patients with focal brain lesions without mass effect. *J. Infect.* 2006 52, 30-36.

Focosi, D; Fazzi, R; Montanaro, D; Emdin, M; Petrini, M. Progressive multifocal leukoencephalopathy in a haploidentical stem cell transplant recipient: a clinical, neuroradiological and virological response after treatment with risperidone. *Antivir. Res.* 2007 74, 156–158.

Frisque, RJ; Bream, GL; Cannella, MT. Human polyomavirus JC virus genome. *J. Virol.* 1984 51, 458-469.

Gardner, SD; Field, AM; Coleman, DV; Hulme, B. New human papovavirus (B.K.) isolated from urine after renal transplantation. *Lancet.* 1971 1, 1253– 1257.

Geschwind, MD; Skolasky, RI; Royal, WS; McArthur, JC. The relative contributions of HAART and alpha-interferon for therapy of progressive multifocal leukoencephalopathy in AIDS. *J. Neurovirol.* 2001 7, 353-357.

Giesen, HV; Neuen-Jacob, E; Dörries, K; Jablonowski, H; Roick, H; Arendt, G. Diagnostic criteria and clinical procedures in HIV-1 associated progressive multifocal leukoencephalopathy. *J. Neurol. Sci.* 1997 147, 63-72.

Gillespie, SM; Chang, Y; Lemp, G; Arthur, R; Buchbinder, S; Steimle, A; Baumgartner, J; Rando, T; Neal, D; Rutherford, G. Progressive multifocal leukoencephalopathy in persons infected with human immunodeficiency vírus, San Francisco 1981–1989. *Ann. Neurol.* 1991 30, 597-604.

Gold, R; Jawad, A; Miller, DH; Henderson, DC; Fassas, A; Fierz, W; Hartung, HP. Expert opinion: Guidelines for the use of natalizumab in multiple sclerosis patients previously treated with immunomodulating therapies. *J. Neuroimmunol.* 2007 187, 156-158.

Guilleux, M-H; Steiner, RE; Young, IR. MR imaging in progressive multifocal leukoencephalopathy. *Am. J. Neuroradiol.* 1986 7, 1033–1035.

Haider, S; Nafziger, D; Gutierrez, JA; Brar, I; Mateo, N; Fogle, J. Progressive multifocal leukoencephalopathy and idiopathic CD4+ lymphocytopenia: a case report and review of reported cases. *Clin. Infect. Dis.* 2000 31, E20-22.

Hall, CD; Dafni, U; Simpson, D; Clifford, D. Failure of citarabine in progressive multifocal leucoencephalopathy associated with human immunodeficiency virus infection. *N. Engl. J. Med.* 1998 338, 1345–1351.

Hayashi, Y; Kimura, A; Kato, S; Koumura, A; Sakurai, T; Tanaka, Y; Hozumi, I; Sunden, Y; Orba, Y; Sawa, H; Takahashi, H; Inuzuka, T. Progressive multifocal leukoencephalopathy and CD4-T-lymphocytopenia in a patient with Sjögren syndrome. *J. Neurol. Sci*. 2008 268, 195-198.

Hecht, J; Glenn, OA; Wara, DW; Wu, ZW. JC virus granule cell neuronopathy in a child with CD40 ligand deficiency. *Pediat. Neurol.* 2007 36, 186-189.

Holman, RC; Janssen, RS; Buehler, JW; Zelansky, MT; Hooper, WC. Epidemiology of progressive multifocal leukoencephalopathy in the United States: analysis of national mortality and AIDS surveillance data. *Neurology.* 1991 41, 1733-6.

Hou, J; Seth, P; Major, EO. JC virus can infect human immune and nervous system progenitor cells: implications for pathogenesis. *Adv. Exp. Med. Biol.* 2006 577, 266-273.

Houff, SA; Major, EO; Katy, DA; Kufta, CV; Sever, JL; Pittaluga, S; Roberts, JR; Gitt, J; Saini, N; Lux, W. Involvement of JC virus-infected mononuclear cells from the bone marrow and spleen in the pathogenesis of progressive multifocal leukoencephalopathy. *N. Engl. J. Med.* 1988 318, 301-305.

Houston, S; Roberts, N; Mashinter, L. Failure of cidofovir therapy in progressive multifocal leukoencephalopathy unrelated to human immunodeficiency virus. *Clin. Infect. Dis.* 2001 32, 150–152.

Howatson, AF; Nagai, M; Zu Rhein, GM. Polyoma-like virions in human demyelinating disease. *Can. Med. Assoc. J.* 1965 93, 379.

Huang, SS; Skolasky, GJ; Dal Pan, GJ; Royal, W3rd; McArthur, JC. Survival prolongation in HIV-associated progressive multifocal leukoencephalopathy treated with alpha-interferon: an observational study. *J. Neurovirol.* 1998 4, 324-332.

Imperiale, MJ. The human polyoma viruses: an overview, In: Khalili K, Stoner GL Editors. *Human Polyomaviruses: Molecular and Clinical Perspective*. New York: Wiley-Liss Inc; 2001; 53–71.

Itoyama, Y; Webster, HD; Sternberger, NH; Richardson, EP Jr; Walker, DL; Quarles, RH; Padgett, BL. Distribution of papovavirus, myelin-associated glycoprotein and myelin basic protein in progressive multifocal leukoencephalopathy lesions. *Ann. Neurol.* 1982 11, 396-407.

Kim, Sy; Kim, DH; Hyun, JW; Henson, JW; Kim, HS. Irisolidone, an isoflavone metabolite, represses JC virus gene expression via inhibition of Sp1 binding in human glial cells. *Biochem. Biophys. Res. Comm.* 2006 344, 3–8.

Kleinschmidt-Demasters, BK; Tyler, KL. Progressive multifocal leukoencephalopathy complicating treatment with natalizumab and interferon beta-1a for multiple sclerosis. *N. Engl. J. Med.* 2005 353, 369–374.

Koralnik, IJ. Progressive multifocal leukoencephalopathy revisited: has the disease outgrown its name? *Ann. Neurol.* 2006 60, 162-173.

Koralnik, IJ; Boden, D; Mai, VX; Lord, CI: Letvin, NL. JC virus DNA load in patients with and without progressive multifocal leukoencephalopathy. *Neurology.* 1999 52, 253-260.

Koralnik, IJ; Wuthrich, C; Dang, X; Rottnek, M; Gurtman, A; Simpson, D; Morgello, S. JC virus granule cell neuronopathy: A novel clinical syndrome distinct from progressive multifocal leukoencephalopathy. *Ann. Neurol.* 2005 57, 576-580.

Kuchelmeister, K; Gullotta, F; Bergman, M; Angeli, G; Masini, T. Progressive multifocal leukoencephalopathy (PML) in the acquired immunodeficiency syndrome (AIDS). A neuropathological study of 21 cases. *Pathol. Res. Pract.* 1993 189, 163-173.

Lang, W; Miklossy, J; Deruaz, JP; Pizzolato, GP; Probst, A; Schaffner, T; Gessaga, E; Kleihues, P. Neuropathology of the acquired immunodeficiency syndrome (AIDS): A report of 135 consecutive autopsy cases from Switzerland. *Acta Neuropathol.* 1989 77, 379-390.

Langer-Gould, A; Atlas, SW; Green, AJ; Bollen, AW; Pelletier, D. Progressive multifocal leukoencephalopathy in a patient treated with natalizumab. *N. Engl. J. Med.* 2005 353, 375–381.

Lee, J; Richardson, SK; Melhm, ER; Rook, AH; Kim, EJ. Progressive multifocal leukoencephalopathy from JC virus in a patient with advanced mycosis fungoides. *J. Am. Acad. Dermatol.* 2007 57, 893-895.

Major, EO; Vacante, DA. Human fetal astrocytes in culture support the growth of the neurotropic human polyomavirus, JCV. *J Neuropathol Exp Neurol*, 1989 48, 425– 436.

Manji, H; Miller, R. Progressive multifocal leukoencephalopathy: Progress in the AIDS era. *J. Neurol. Neurosurg. Psychiat.* 2000, 69, 569–571.

Marra, CM; Rajici, N; Barker, DE; Cohen, B; Clifford, D; and the ACTG 363 Team. Prospective pilot study of cidofovir for HIV-associated progressive multifocal leukoencephalopathy (PML). Proceeding of the 8th Conference on Retroviruses and Opportunistic Infections. Chicago, IL. 2001, 02.04-08.

Marzocchetti, A; Sanguinetti, M; Giambenedetto, SD; Cingolani, A; Fadda, G; Cauda, R; De Luca, A. Characterization of JC virus in cerebrospinal fluid from HIV-1 infected patients with progressive multifocal leukoencephalopathy: insights into viral pathogenesis and disease prognosis. *J. Neurovirol. 2007 13, 338-346*.

Mázló, M; Ressetar, HG; Stoner, GL. The neuropathology and pathogenesis of progressive multifocal leukoencephalopathy. In: Khalili K, Stoner GL editors. *Human Polyomaviruses, Molecular and Clinical Perspectives*. New York: Wiley-Liss Inc.; 2001; 257–335.

Mázló, M; Tariska I. Are astrocytes infected in progressive multifocal leukoencephalopathy (PML)? *Acta Neuropathol*, 1982 56, 46-51.

Mázló, M; Tariska I. Morphological demonstration of the first phase of polyomavirus replication in oligodendroglia cells of human brain in progressive multifocal leukoencephalopathy (PML). *Acta Neuropathol.* 1980 49, 133-143.

Norkin, LC. Simian virus 40 infection via MHC class I molecules and caveolae. *Immunol. Rev.* 1999 168, 13– 22.

Orba, Y; Sunden, Y; Suzuki, T; Nagashima, K; Kimura, T; Tanaka, S; Sawa, H. Pharmacological cdk inhibitor R-Roscovitine suppresses JC virus proliferation. *Virology.* 2008, 370, 173–183.

Padgett, BL; Walker, DL; ZuRhein, GM; Eckroade, RJ; Dessel BH. Cultivation of papova-like virus from human brain with progressive multifocal leukoencephalopathy. *Lancet.* 1971 1, 1257-1260.

Pagnoux, C; Hayem, G; Roux, F; Rouidi, SA; Palayyo, E; Henin, D; Meyer, O. JC virus leukoencephalopathy complicating Wegener's granulomatosis. *Joint Bone Spine.* 2003 70, 376-379.

Pal, E; Aschermann, Z; Gomori, E; Kovacs, GG: Simon, G: Marodi, L; Komoly, S; Illes, Z. Progresive multifocal leukoencephalopathy. *Clin Neurosci (Hungary)*, 2007 60, 263-268.

Parvaneh, N; Ashrafi, MR; Yeganeh, M; Pouladi, N; Sayarifar, F; Parvaneh, L. Progressive multifocal leukoencephalopathy in purin nucleoside phosphorylase deficiency. *Brain Dev.* 2007 29, 124-126.

Post, MJD; Yiannoutsos, C; Simpson, D. Progressive multifocal leukoencephalopathy in AIDS: are there any MR findings useful to patient management and predictive of patient survival? *Am. J. Neuroradiol.* 1989 20, 896–906.

Power, C; Del Bigio, MR; Halliday, W; Nath, A. Progressive multifocal leukoencephalopathy: Icidence and survival. *Journal of the Neurological Sciences*, 1997 150, S74-75.

Ransohoff, RM. „Thinking without thinking" about natalizumab and PML. *J. Neurol. Sci.* 2007 259, 50-52.

Ransohoff, RM. Natalizumab and PML. *Nat. Neurosci.* 2005 8,1275.

Richardson-Burns, SM; Kleinschmidt-DeMasters, BK; DeBiasi, RL; Tyler, KL. Progressive multifocal leukoencephalopathy and apoptosis of infected oligodendrocytes in the central nervous system of patients with and without AIDS. *Arch. Neurol.* 2002 59, 1930-1936.

Romagnoli, L; Sariyer, IK; Tung, J; Feliciano, M; Sawaya, BE; Valle, LD; Ferrante, P; Khalili, K; Safak, M; White, MK. Early growth response-1 protein is induced by JC virus infection and binds and regulates the JC virus promoter. *Virology.* 2008 3475, 331-341.

Safak, M; Khalili, K. An overview: human polyomavirus JC virus and its associated disorders. *J. NeuroVirol.* 2003 9, 3 – 9.

Sindic, CJM; Trebst, C; Van Antwerpen, MP; Fry, S; Enzensberger, W; Hunsmann, G; Lüke, W; Weber, T. Detection of CSF-specific oligoclonal antibodies to recombinant JC virus VP1 in patients with progressive multifocal leukoencephalopathy. *J. Neuroimmunol.* 1997 76, 100-104.

Stoner, GL; Walker, DL; Webster, HF. Age distribution of progressive multifocal leukoencephalopathy. *Acta Neurol. Scand.* 1988 78, 307-312.

Stuve, O; Bennett, JL. Pharmacological properties, toxicology and scientific rationale for the use of natalizumab (Tysabri) in inflammatory diseases. *CNS Drug Rev.* 2007 13, 79–95.

Sweet, BH; Hilleman, MR. The vacuolating virus, SV40. *Proc. Soc. Exp. Biol. Med.* 1960 105, 420–427.

Trofe, J; Gordon, J; Roy-Chaudhury, P; Koralnik, IJ; Atwood, WJ; Alloway, RR; Khalili, K; Woodle, ES. Polyomavirus nephropathy in kidney transplantation. *Prog. Transplant.* 2004 14, 130–140.

Trowbridge, PW; Frisque, RJ. Identification of three new JC virus proteins generated by alternative splicing of the early viral mRNA. *J. NeuroVirol.* 1995 1, 195–206.

Tyler, K. The uninvented guest. JC virus infection in neurons in PML. *Neurology.* 2003 61, 734–735.

Valle, LD; Gordon, J; Assimakopolou, M; Enam, S; Geddes, JF; Varakis, J; Katsesos, C; Croul, SE; Khalili, K. Detection of JC virus DNA sequences and expression of the viral regulatory protein, T-antigen, in tumors of the central nervous system, *Cancer Res.* 2001 61, 4287– 4293.

Van Assche, G; Van Ranst, M; Sciot, R; Dubois, B; Vermeire, S; Noman, M; Verbeeck, J; Geboes, K; Robberecht, W; Rutgeerts, P. Progressive multifocal leukoencephalopathy after natalizumab therapy for Crohn's disease. *N. Engl. J. Med.* 2005 353, 362–368.

Völker, HU; Kraft, K; Arnold, E; Steinhoff, S; Kolios, G; Sommer, S. Progressive multifocal leukoencephalopathy developing in advanced pulmonal sarcoidosis. *Clin. Neurol. Neurosurg.* 2007 109, 624-630.

Wang, M; Tsou, TH; Chen, LS; Ou, WC; Chen, PL; Chang, CF; Fung, CY; Chang, D. Inhibition of simian virus 40 large tumor antigen expression in human fetal glial cells by

an antisense oligodeoxynucleotide delivered by the JC virus-like particle. *Hum. Gene. Ther.* 2004 15, 1077-1090.

Weber, T; Frye, S; Bodemer, M; Otto, M; Luke, W. Clinical implications of nucleic acid amplification methods for the diagnosis of viral infections of the nervous system. *J. Neurovirol.* 1996 2, 175–190.

Weber, T; Klapper, PE; Cleator, GM; Bodemer, M; Luke, G; Knowles, W; Cinque, P; Van Loon, AM; Grandien, M; Hammarin, AL; Ciardi, M; BogdanovicG; the European Union Concerted Action on Viral Meningitis and Encephalitis. Polymerase chain reaction for detection of JC virus DNA in cerebrospinal fluid: a quality control study. *J. Virol. Methods.* 1997 69, 231–237.

Weber, T; Trebst, C; Frye, S; Cinque, P; Vago, L; Sindic, CJ; Schulz-Schaeffer, WJ; Kretzschmar, HA; Enzensberger, W; Hunsmann, G; Lüke, W. Analysis of the systemic and intrathecal humoral immune response in progressive multifocal leukoencephalopathy. *J. Infect. Dis.* 1997 176, 250-254.

Weber, T; Weber, F; Petry, H; Lüke, W. Immune response in progressive multifocal leukoencephalopathy: an overview. *J. Neurovirol.* 2001 7, 311-317.

White, MK; Gordon, J; Reiss, K; Valle, LD; Croul, S; Giordano, A; Darbinzan, A; Khalili, K. Human polyomaviruses and brain tumors. *Brain Res. Rev.* 2005 50, 69-85.

Whiteman, ML; Post, MJ; Berger, JR; Tate, LG; Bell, MD; Limonte, LP. Progressive multifocal leukoencephalopathy in 47 HIV-seropositive patients: Neuroimaging and clinical and pathologic correlation. *Radiology.* 1993 187, 233-240.

Zu Rhein, GM; Chou, S-M. Particles resembling papova viruses in human cerebral demyelinating disease. *Science.* 1965 148, 1477-1479.

In: Handbook on White Matter
Editors: T. B. Westland and R. N. Calton
ISBN: 978-1-60741-034-8

Chapter X

Remyelination Failure in Multiple Sclerosis and Vulnerability of Oligodendrocytes to Repeated Insults

Catherine Fressinaud*
Neurology Department, UPRES EA 3143,
University Hospital, Angers, France

Abstract

Oligodendrocytes (OL) synthesize myelin sheaths that insulate axons, forming the main components of the central nervous system (CNS) white matter. The considerable importance of this structure is well underlined by the fact that its lesions occuring during Multiple Sclerosis (MS) result often in patients severe disability. Permanent neurological deficit relies on axonal lesions that are associated with demyelination, and the remyelination process is impaired, for yet unknown reasons.

To get insight into these pathophysiological phenomenons we have analyzed the capability of OL to synthesize myelin in MS chronic lesions. A constant and pronounced decrease in the number of myelinated fibres per OL compared to the adjacent normal appearing white matter (NAWM) was observed (Fressinaud, 2007). This suggests that, at the cellular level, OL are incapable of synthesizing an appropriate number of myelin sheaths. Thus, restricted metabolic capacities of OL could result in their failure to remyelinate a sufficient number of damaged fibres, and might represent an important mechanism in MS, since, conversely, the number of OL is less constantly decreased.

This hypothesis was supported by two sets of experimental data in vivo, and in vitro. In vivo, rat corpus callosum demyelination by lysophosphatidyl choline (LPC) stereotaxic microinjection is followed by spontaneous remyelination, and this process is

* Correspondence to: Dr Catherine Fressinaud, Neurology Department, University Hospital, 4 rue Larrey, F49933 Angers Cedex 9, France; E-mail : Catherine.fressinaud@univ-angers.fr; Phone : 33 (0)2 41 35 46 13; Fax : 33 (0)2 41 35 35 94

significantly accelerated by treatment with either platelet-derived growth factor (PDGF) (Allamargot et al., 2001), or neurotrophin-3 (NT-3) (Jean et al., 2003). As expected, given the known proliferative effect of these growth factors on OL progenitors (Besnard et al., 1987; Barres et al., 1994), the number of OL increased by 20% in NT-3 remyelinated lesions compared to animals receiving LPC only, and, more interestingly, the number of myelinated fibres per cell increased far more, up to 100%, compared to spontaneous remyelination. Thus, these results strengthen the hypothesis that a more efficient remyelination relies not only on the availability of a sufficient pool of myelinating OL, but also, individually, on an increased capability of OL to synthesize myelin sheaths in large amounts, and that this ability too might be partly lost in MS.

Since MS often evolves on a remitting-relapsing pattern, the repetition of attacks could represent one of the main factors that account for the failure of OL to remyelinate adequately lesions; nevertheless, the consequences for OL of repeated insults were largely unknown. In order to mimic this schematically, we have constructed an in vitro paradigm in which OL from newborn rat brain, grown in pure cultures, were submitted to either a single exposure to LPC (2.10^{-5} M, 24 h) (Fressinaud and Vallat, 1994), or to several LPC exposures, although for shorter periods and at lower concentration ($0.5\ 10^{-5}$ M, 4 x 6 h). Indeed, OL were very susceptible to multiple attacks versus a single one (despite a similar total dose and duration of treatment), and in particular mature OL – which are the myelinating cells, and constitute the major part of the population of cells of the OL lineage in the adult CNS –. Mature OL might thus represent the principal target of relapses during MS (Fressinaud, 2005).

Taken together our results converge, and suggest that cells of the OL lineage are particularly vulnerable to multiple insults, which lead both to the death of numerous cells and to restricted capability to synthesize myelin by surviving OL. This defect could constitute one of the significant causes contributing to their failure to remyelinate axons in MS. Our data add to the accumulating scientific knowledge suggesting that early treatment and attempts to avoid relapses are needed for patients suffering from MS.

Keywords: Axon cytoskeleton; Growth factors; Multiple sclerosis; Myelin Basic Protein; Neurofilament; Oligodendrocyte; Remyelination.

Abbreviations

bFGF	basic fibroblast growth factor
CDM	chemically-defined medium
CNP	2',3'-cyclic nucleotide 3'-phosphodiesterase
CNS	central nervous system
GFAP	glial fibrillary acidic protein
LPC	lysophosphatidyl choline
MBP	myelin basic protein
MS	multiple sclerosis
NAWM	normal appearing white matter
NF	neurofilament proteins
NT-3	neurotrophin 3
OL	oligodendrocyte
PDGF	platelet-derived growth factor

PLP	myelin proteolipid
PNS	peripheral nervous system
WM	white matter

Introduction

Multiple sclerosis (MS) is one of the most frequent chronic and disabling neurological diseases in young adults (e. g. Kurtzke, 1991; Frohman, 2003; Debouverie et al., 2007; Hader and Yee, 2007). Its lesions primarily affect the white matter (WM) of the central nervous system (CNS) (review in Frohman et al., 2006), which consists mainly of axons wrapped up in myelin sheaths. The exceptionally high content in lipids (around 70%) of myelin, which is unique among cellular membranes (Norton and Cammer, 1984), gives to this structure its white colour. Astrocyte processes, forming finger-like extensions, contact axons at specific regions – the nodes of Ranvier – where myelin sheaths are interrupted (Reichenbach and Wolburg, 2005).

Myelin consists in the extension and periodic winding up around axons of cellular processes of specialized glial cells : the oligodendrocytes (OL) in the CNS, and the Schwann cells in the peripheral nervous system (PNS). Whereas Schwann cells myelinate only one segment of a single axon, OL are able to synthesize up to 50 internodes distributed on several axons (Butt, 2005). This corresponds to a huge volume of myelin (up to 150,000 μm^3), especially in proportion of OL cell body size (15-20 μm) (Raine, 1984). Myelin preserves axon integrity, and, by insulating axons, allows the saltatory conduction of nerve impulse. Only axons of large diameter are myelinated, and the saltatory conduction of action potentials considerably increases the velocity of neural conduction. This property is lost when myelin is damaged, and is restored after remyelination (review in Zhao et al., 2005). The WM of mammalian brain contains about 50-60% myelin on a dry weight basis, and myelin constitutes 35% of the dry weight of adult human brain (Norton and Cammer, 1984). It is noteworthy that myelinated fibre tracts in the CNS correspond to major neurological functions such as proprioception, voluntary movement, and connections between specialized cortical areas. Indeed, the crucial role of WM in CNS function is well illustrated by the fact that its volume increases even more than that of grey matter during species evolution, including human and non-human primates (e. g. Rilling and Insel, 1999). Thus, myelin and WM are an essential anatomical support of human physical and cognitive distinctive abilities.

Nevertheless, the regulation of myelination in the CNS is incompletely known, and relies on complex axon-OL interactions, including bidirectional trophic (Adlkofer et al., 1995) and regulatory interactions (review in Doyle and Colman, 1993; Bozzali and Wrabetz, 2004; Fields, 2004), as well as metabolic exchanges (Ledeen et al., 1992; Chakraborty et al., 2001). For example, axon-derived neuregulins (NRG) promote OL survival (Fernandez et al., 2000), regulate tau (Lopresti et al., 2001) or myelin basic protein (MBP) expression (Lai and Feng, 2004), and NRG-1 increases myelination (Taveggia et al., 2006). Since myelination depends on axon diameter, these interactions involve also neurofilaments (NF) (Hisanaga and Hirokawa, 1988 ; 1990), which modulate axon calibre (Friede and Bischhausen, 1982; deWaegh et al., 1992 ; Hsieh et al., 1994; Starr et al., 1996), and microtubules responsible for

axonal transport (Hirokawa, 1997). In the PNS, myelin-associated glycoprotein (MAG, review in Schachner and Bartsch, 2000) modulates axon radial growth through NFM phosphorylation (Cole et al., 1994; Rao et al., 2003), whereas in the CNS, OL regulate axon calibre growth independently of myelination (Sanchez et al., 1996).

Demyelination can result from a multitude of conditions affecting other components of the WM (namely blood vessels, axons, and astrocytes) or myelin per se; and in some instances, remyelination occurs (e. g. after cuprizone experimental intoxication, or following central pontine myelinolysis) (review in Raine, 1984). In rodents CNS a single demyelinating event induced by lysophosphatidyl choline (LPC) injection is followed by spontaneous and complete remyelination (e. g. Allamargot et al., 2001). During the course of MS, on the contrary, relapses occur and remyelination of lesions by OL is incomplete (review in Frohman et al., 2006). Moreover axonal lesions - either secondary to the inflammatory process, or to demyelination itself (review in Silber et Sharief, 1999) - associate with demyelination, and probably account for patients disability, and for atrophy of the CNS (Brück et al., 2002; Losseff et al., 1996), which are, at present, above therapeutic resources. The origin of the remyelination defect in MS is yet unknown, and four main factors might be involved in it, which relative share has to be determined. It might rely either on astrocytic gliosis (e. g. Prineas and McDonald, 1997), or on axon degeneration (Raine and Cross, 1989) and/or OL alterations (Lucchinetti et al., 1999). The coexistence of these parameters with inflammatory cells and molecules in the lesions renders the elucidation of their respective involvement in the persistency of lesions difficult.

In particular, some axonal proteins involved in myelination are altered in MS lesions : the expression of paranodin, which localizes to paranode when myelination begins, is repressed (Guennoc et al., 2001), and PSA-NCAM, which inhibits myelination, is expressed by some axons in plaques (Charles et al., 2002). Moreover, axon cytoskeleton alterations, especially abnormal phosphorylated forms of NF (e. g. Trapp et al., 1998 ; Chang et al., 2002), and decrease in NF and β tubulin expression (Fressinaud et al., 2005 ; Fressinaud and Sazdovitch, 2006) are present in MS lesions. Finally, as numerous OL at a premyelinating stage have been observed in contact with dystrophic axons, it has been hypothesized that axons might be unproper for remyelination (Chang et al., 2002). Indeed, the role of axon molecules in the regulation of myelination is largely unknown. Axon-OL interactions are subtle, and the integrity of both is required for proper CNS function, thus the putative consequences of these axon alterations on remyelination in MS have to be precised. Although OL are able to synthesize myelin-like membranes in vitro in the absence of neurons (e. g. Fressinaud et al., 1990, 1996), neurons in cocultures increase myelin messenger RNAs and proteins (Demerens et al., 1996; Macklin et al., 1986). Moreover, in rodents axotomy decreases the number of OL progenitors in the optic nerve (Barres and Raff, 1993), now numerous axon sections have been observed in MS lesions (Trapp et al., 1998). Thus, axon lesions could, at least partly, be involved in the remyelination defect during MS. Nevertheless, the number of OL in MS lesions does not correlate with axon loss (Lucchinetti et al., 1999; Fressinaud and Sazdovitch, 2006).

On the other hand, abnormalities in the OL population are frequently, although inconstantly, encountered in MS lesions. Mature OL and OL progenitors (Scolding et al., 1998; Chang et al., 2002) are either decreased, or not, even in the same patient and according

to authors (e.g. Rodriguez et al., 1993; Brück et al., 1994, 2002; Ozawa et al., 1994 ; Mews et al., 1998). Their density does not correlate with the intensity of inflammation (Lucchinetti et al., 1999), suggesting that it depends on other factors too. Since the expression of the anti-apoptotic protein bcl-2 by OL is associated with remyelination, it could thus contribute to the survival of some OL during MS (Kuhlmann et al., 1999). These discrepancies between OL alterations reported in MS have led some authors to describe several histological forms of the disease (e. g. Brück et al., 1994; Ozawa et al., 1994). In demyelinating active lesions, Lucchinetti et al. (2000) have described four different patterns, two suggestive of experimental autoimmune encephalitis (EAE), and two suggesting a primary (viral or toxic) lesion of OL.

Since these results hardly explain MS remyelination failure completely, we have approached this problematic with another angle. Indeed, myelination of CNS axons results from the synthesis of a great number of sheaths by each OL. Nevertheless, the capability of OL to synthesize myelin during MS is unknown. Moreover, although a relative plasticity of OL, which grow processes again and synthesize new myelin-like membranes after a single injury, has been reported in vitro (Fressinaud and Vallat, 1994; Knapp, 1997; Knapp and Adams, 2004), their fate after repeated insults was not known, whereas one of the main characteristics of MS is precisely the occurrence of relapses. So, we have analyzed by immunocytochemistry and morphometry the capacity of OL to remyelinate lesions in MS, and this has been studied also in experimental models in vitro (Fressinaud, 2005), and in vivo (Fressinaud, 2007). In MS we observed that, above the decrease in OL number in most of the lesions, the number of myelinated fibres per mature (MBP+) OL was more severely, and constantly, decreased in plaques compared to the normal appearing white matter (NAWM). Conversely, the ratio of myelinated fibres per cell was increased over the number of OL after LPC injection in rat corpus callosum, when remyelination was improved by neurotrophin 3 (NT-3) or platelet-derived growth factor (PDGF) treatment. This suggested that residual OL in MS have a decreased ability to synthesize new myelin membranes. We hypothesized that this defect might result from exhaustion of OL metabolic capacities after several relapses, since we have demonstrated that a single injury induced by LPC in myelinating OL cultures is followed by partial recovery (synthesis of new myelin-like membranes), which is improved by basic fibroblast growth factor (bFGF) (Fressinaud and Vallat, 1994) or PDGF (Fressinaud et al., 1996). This hypothesis was confirmed by the observation that repeated insults in vitro (using recurrent exposures of OL cultures to LPC) are deleterious for cells of the OL lineage, and especially mature OL (Fressinaud, 2005).

Oligodendrocytes and Remyelination in MS

We have analyzed 18 chronic lesions from brain autopsy of 6 patients (3 women, and 3 men, mean age : 54.5 ± 11.5 years) with histologically confirmed MS (Neuropathology Laboratory, Pr J.J. Hauw, University Hospital Pitié-Salpêtrière, Paris, France). Mean disease duration was 18.5 ± 6 years, EDSS score was > 8.5 in all cases, 5 patients had remitting-progressive (RP) forms, and one a primary progressive (PP) form (Fressinaud, 2007).

Serial sections (7 µm thick) from paraffin blocks were used for luxol-fast blue (LFB)-phloxin-hematein staining and immunohistochemistry. Chronic plaques were recognized by the absence of LFB-positive inclusions in macrophages (Giordana et al., 2002; Prineas and McDonald, 1997).

Axonal loss in plaques was semi-quantitatively estimated on LFB-stained sections, and, depending on the number of preserved fibres, expressed as mild (-25%), moderate (-50%), or severe (-100%, i.e. axon loss was virtually complete), compared to the adjacent normal appearing white matter (NAWM).

Immunocytochemistry on paraffin sections was performed for axon cytoskelon and OL, as well as for astrocytes. The cytoskeleton components were labelled with antibodies raised against each of the 3 neurofilament subunits (light, medium, and heavy chain : NFL, NFM, NFH) and β tubulin. Antibodies raised against myelin basic protein (MBP, Dako, Trappes, France), myelin proteolipid (PLP, gift of Dr E. Trifilieff (Trifilieff et al., 1986)), 2',3'-cyclic nucleotide 3'-phosphodiesterase (CNP, Sigma Immunochemicals, St Louis, MO), and glial fibrillary acidic protein (GFAP, Dako) were used to label myelin and OL (MBP, PLP, CNP), or astrocytes (GFAP), respectively. Procedures were performed as previously described with hematein counterstain (Jean et al., 2002; Jean and Fressinaud, 2003; Fressinaud et al., 2005).

Immunolabelled cells (OL and astrocytes), as well as the whole cell population (defined by nucleus staining with hematein), were counted in the totality of standardized microscopic fields, defined by an ocular morphometric grid, using a X 100 objective. Similarly the number of immunolabelled fibres for myelin antibodies, and the number of axons stained for antibodies to the cytoskeleton, were counted per optic field. All these measurements were performed in 5 optic fields within each of the lesions, and in 5 optic fields in the adjacent NAWM.

Results were first expressed as mean ± SD of counts per optic field within the lesion, or in the NAWM. To allow comparison between lesions counts were subsequently expressed as percentage of variation compared to the NAWM. Comparison of mean counting between plaques and NAWM employed Mann and Whitney's test.

Demyelination, decreased number of OL, and axon loss (figure 1) were the hallmarks of MS lesions ($p < 0.01$), in block (4*2) excepted in which the number of OL was modestly increased compared to the NAWM (non significant). Comparison of the number of OL expressing CNP, PLP, or MBP within one lesion did not reveal differences, indicating that most differentiated (CNP+) cells had acquired a mature, myelinating (MBP+), phenotype in the different lesions (Fressinaud and Sazdovitch, 2006).

Since the number of OL was generally reduced in MS lesions compared to the NAWM ($\alpha < 1\%$, Mann and Whitney's test), this result could account for the failure of remyelination in most of our cases, although not in all of them (block (4*2)). Indeed, neither the maturation characteristics, which appeared normal, nor the cell count of the OL population, could explain completely our observations. Therefore this prompted us to determine the ratio of the number of myelinated (MBP+) fibres to the number of myelinating (MBP+) OL within each optic field (figure 2), and to compare results between MS lesions and the adjacent NAWM.

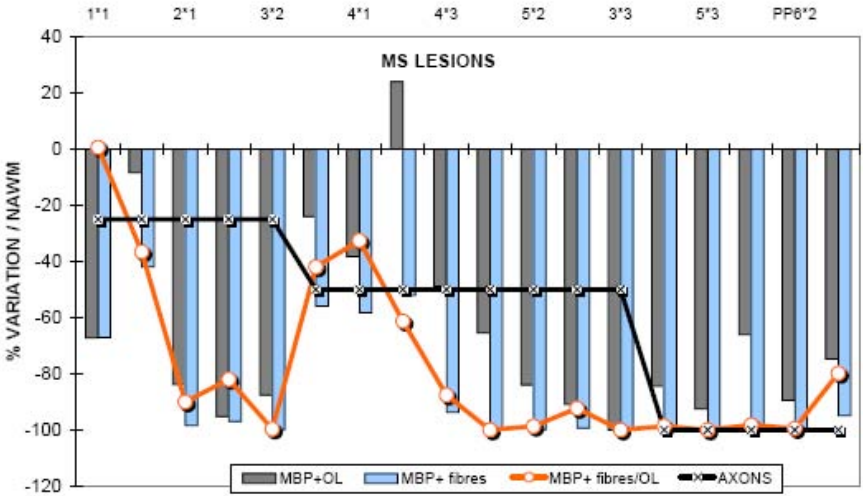

Figure 1. Results of immunocytochemistry using anti-myelin basic protein antibody for each of the 18 MS lesions analyzed (lesions by increasing order of axonal damage expressed semi-quantitatively as mild (25% axon loss), moderate (50% axon loss), or severe (nearly 100% axon loss)). Results are expressed as percentage of variation compared to the adjacent normal appearing white matter.

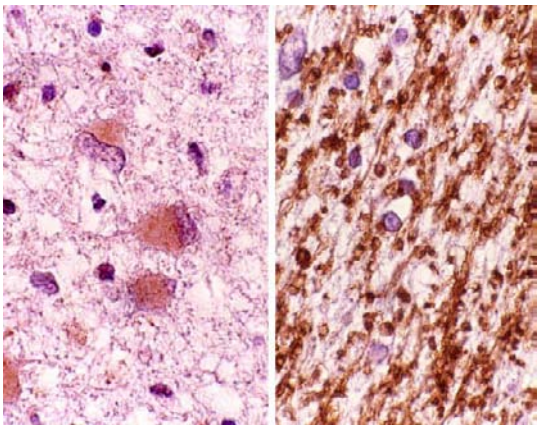

Figure 2. Immunocytochemistry using anti-myelin basic protein antibody (peroxydase, hematein counterstain) of one MS lesion (left), and the adjacent normal appearing white matter (right). Note MBP+ oligodendrocytes in the center of the lesion contrasting with complete demyelination, whereas numerous MBP+ fibres are present in the normal appearing white matter. Original magnification x 250.

This enabled us to establish that, in all lesions, the ratio of myelinated fibres to OL was decreased by 37 to 100% compared to the NAWM (figure 1). Moreover this ratio was decreased too in block (4*2), despite the increase in the number of MBP+ OL. The mean of this ratio was 6.7 myelinated fibres/OL in MS plaques versus 47 in the NAWM, respectively (figure 3A), corresponding to a decrease of 86% in lesions, whereas OL number and myelinated fibres number decreased in mean by 65 and 88%, respectively, compared to the NAWM. There was no correlation between MBP+ fibres/OL ratio and axon loss or axon cytoskeleton alterations (figure 1).

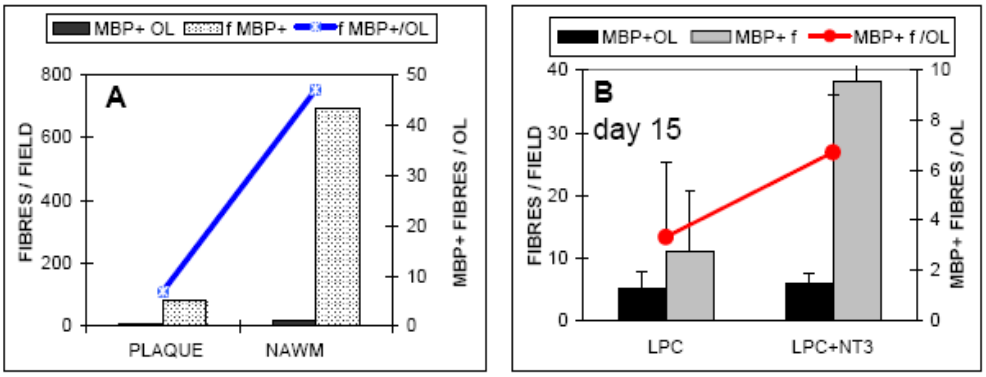

Figure 3. Results of immunocytochemistry using anti-myelin basic protein antibody in MS lesions (means of 18 lesions) compared to the normal appearing white matter (A), and in the center of the lesion where remyelination is in progress 15 days after lysophosphatidyl choline (LPC) injection in rat corpus callosum and their littermates treated with NT-3 (LPC + NT-3) (B). From Fressinaud C., Rev. Neurol. (Paris), 2007, 163 (4), 448-454. © Reprinted with permission of Elsevier Masson SAS, Ed.

Thus, incomplete remyelination of MS lesions in our cases was associated usually (17 lesions out of 18) with a decrease in the number of OL, as reported by numerous authors (e.g. Rodriguez et al., 1993; Brück et al., 1994, 2002; Ozawa et al., 1994 ; Mews et al., 1998). This decrease could thus explain in itself the paucity of remyelination in most of our patients. Nevertheless, as in one of our cases, normal or increased numbers of OL within plaques could also be observed in this disease, as it has been reported too by several authors (Scolding et al., 1998; Chang et al., 2002), suggesting that decreased OL number might not be the exclusive factor of this incomplete repair. Two other hypotheses might be proposed. Our results did not favour the hypothesis of a defective maturation of OL (Chang et al., 2002) per se, since we found that the number of differentiated (CNP+) OL was equivalent to that of mature (MBP+) OL in lesions. Rather, they revealed a constant and profound decrease in the number of myelinated fibre per OL in plaques, compared to the NAWM. On this point of view it is noteworthy to precise that our results for the NAWM are in the same range (around 50 fibre per OL) than that reported in the literature (e.g. Ludwin, 1997 ; Waxman and Bangalore, 2004). This suggested that residual OL in MS lesions might have reduced metabolic capabilities to synthesize myelin sheaths (Fressinaud, 2007), or, alternately, as proposed by other authors (Chang et al., 2002), that axons are unproper for remyelination. Indeed, the role of axonal modifications (Guennoc et al., 2001 ; Charles et al., 2002) have been suspected too. Nevertheless, as reported by Lucchinetti et al. (1999), we did not find any correlation between OL fate and axon alterations in our samples.

Therefore, to circumvent this problematic, and to rid of the putative involvement of axon alterations in this pathophysiological process, we have analyzed the myelination capability of OL in an experimental paradigm in which spontaneous remyelination occurs, and axon lesions are mild (i. e. without significant axon loss), in order to compare the fate of OL under basal remyelination conditions, and during enhanced remyelination.

Remyelination Capability of Oligodendrocytes Is Individually Increased when Remyelination Is Improved

A single microinjection of lysophosphatidylcholine (LPC) in rat corpus callosum is followed by spontaneous, and complete, remyelination (e. g. Allamargot et al., 2001), and this process is accelerated by the concomitant administration above the lesion of platelet-derived growth factor (PDGF) (Allamargot et al., 2001), or neurotrophin 3 (NT-3) (Jean et al., 2003). Moreover there is no significant axon loss in this model (Allamargot et al., 2001), and although axon alterations associate with demyelination (namely a decrease in NF and tubulin immunostaining), they improve when remyelination occurs (Jean et al., 2002). This offered us the opportunity to compare physiological, and efficient, remyelination under basal conditions, with enhanced remyelination, in the absence of major axonal lesions (contrary to the situation encountered in MS lesions).

For this purpose, adult male Wistar rats received under anesthesia 1 µl of 1 % LPC into the corpus callosum (stereotaxic coordinates : Bregma + 0,12 cm, lateral – 0,07 cm, meninx – 0,35 cm (Paxinos and Watson's atlas), and 1 µl of 10 mM acetic acid (meninx – 0,33 cm) (control group, n = 9). The treated groups (n = 9) received 1 µl of 1 % LPC, and 1 µg of NT-3 (Jean et al., 2003), or of PDGF (Allamargot et al., 2001), in 1 µl of 10 mM acetic acid (R and D Systems, Abingdon, UK). Animals were sacrificed under anaesthesia after 15 days, and brain hemispheres were embedded in paraffin for serial sections (5 µm) of the entire lesion. The volume of the lesion was calculated on luxol fast blue stained sections. Sections corresponding to the center of the lesion – which was only partly remyelinated at that period – were choosen for immunocytochemistry (see above) and counts of the number of remyelinated (MBP+) fibres and of MBP+ OL. Counts were performed in 4 optic fields in the center of the lesion, using a X 100 objective and a morphometric grid, and experiments were realised 3 times in triplicate (Fressinaud, 2007).

As previously reported, PDGF or NT-3 greatly reduced the volume of the lesion induced by LPC (by more than 55% on day 15) and increased significantly the number of OL compared to controls (Allamargot et al., 2001 ; Jean et al., 2003). Analysis of the most central part of the lesion 15 days after LPC injection revealed that remyelination was in progress in both treated and untreated animals (figure 4). Rather numerous MBP+ OL were observed in rats having received LPC only (figure 4A), but myelinated fibres were still relatively scarce compared to NT-3 treated animals (figure 4B). Indeed, in NT-3 treated animals cells and fibres counts showed an increase of 20% in the number of MBP+ OL (figure 3B), and an increase of 100% in the ratio of myelinated fibres per OL compared to controls (LPC only, $p < 0.05$). Similarly, transmission electron microscopy of ultrathin sections, revealed that remyelination 15 days after lesion was characterized in animals treated with PDGF by a pronounced increase in myelinated fibres, whereas the number of OL appeared more modestly increased compared to LPC controls (not shown) (Fressinaud, 2007).

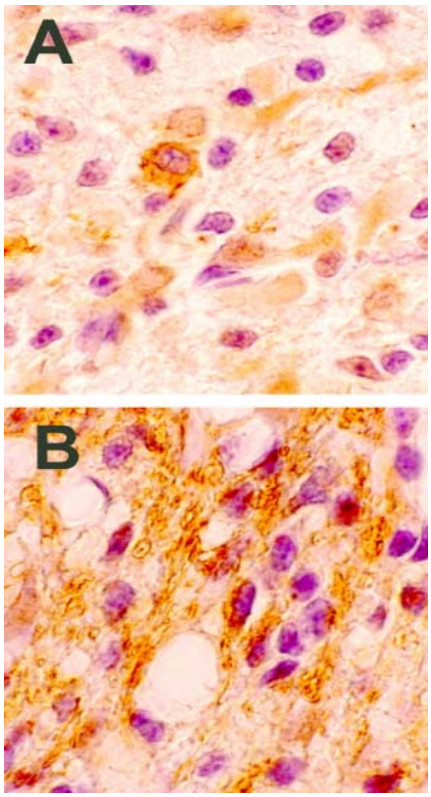

Figure 4. Immunocytochemistry using anti-myelin basic protein antibody (peroxydase, hematein counterstain) 15 days after lysophosphatidyl choline (LPC) microinjection in rat corpus callosum (LPC, A) and in its littermate treated with NT-3 (LPC + NT-3, B). In the center of the lesion where remyelination is in progress note MBP+ oligodendrocytes contrasting with few remyelinated fibres in (A), whereas numerous MBP+ fibres are present when remyelination is improved by NT-3 (B). Original magnification x 250.

Thus, enhanced remyelination in our model, which occurred in the absence of major axonal lesions, was associated with an increase in the number of OL, but above all, with a more pronounced increase in the ability of these cells to synthesize a great number of myelin sheaths (figure 3B). This appears reminiscent of the situation encountered in the NAWM of MS cases versus lesions (figure 3A), and suggests that remyelination failure in MS proceeds both from OL loss, and/or from altered capability of residual cells to remyelinate a sufficient number of axons.

Despite the observations of some OL survival, regrowth of processes, and synthesis of new myelin sheaths after a single demyelinating event in vitro or in vivo (e. g. Fressinaud and Vallat, 1994; Fressinaud et al., 1995; Knapp, 1997; Allamargot et al., 2001; Knapp and Adams, 2004), which supported the concept of OL plasticity, the consequences of repeated insults – which corresponds especially to the situation in relapsing-remitting MS - were unknown. In an attempt to answer this question we have determined the survival of OL, and their capability to synthesize myelin-like membranes after repeated toxic exposures in vitro.

Vulnerabilty of Oligodendrocytes to Multiple Insults In Vitro

The most frequent form of MS is the remitting-relapsing type, and we have hypothesized that the repetition of attacks might represent an important factor of the OL population depletion, as well as of the inability of surviving cells to synthesize myelin in sufficient amounts to remyelinate efficiently lesions. In particular, although in vivo OL progenitors might not be depleted by 2-3 episodes of toxic demyelination (Penderis et al., 2003), this does not provide conclusions about the fate of resident cells (i. e. mostly mature OL in the adult CNS). Since the effects of repeated insults on this cell population had not been reported, we have determined the consequences of multiple versus single demyelinating events by using exposure of rat pure OL cultures to LPC (Fressinaud and Vallat, 1994), as well as the putative pro-remyelinating effects of PDGF and of NT-3 in these conditions (Fressinaud, 2005).

Secondary pure OL cultures from newborn rat brain were grown on poly-L-lysine precoated glass coverslips in chemically-defined medium (CDM) composed of Dulbecco's modified Eagle's medium, supplemented with 50 U/ml penicillin, 50 µg/ml streptomycin, 4 g/l glucose, 5 µg/ml insulin, 10 µg/ml transferrin, 0.5 mg/ml bovine serum albumin, and 30 nM selenium. These cultures are at least 95% pure, and contain approximately 15% OL progenitors (A2B5+ cells), 85% differentiated OL (CNP+ cells), and 40% mature OL (MBP+ cells) after 2-4 days (e. g. Fressinaud et al., 1995), and OL synthesize myelin-like membranes (Fressinaud et al., 1990; 1996). Proliferation was assessed by bromodeoxyuridine (BrdU, 10 µg/ml) incorporation for 10 h.

Previous dose response curve experiments (Fressinaud and Vallat, 1994) had demonstrated that a single 24 h treatment with lysophosphatidyl choline (LPC, Sigma) induced around 60% cell loss at $2.\ 10^{-5}$ M concentration, whereas $0.5.\ 10^{-5}$ M LPC exposure for 6 h induced 20-25% cell loss each time it was administered. Exposure to 10^{-6} M LPC (24 h) had no effect on cell number, and concentrations above $5.\ 10^{-5}$ M induced nearly immediate complete cell death.

Thus, OL cultures were treated as follows (figure 5) : 1) untreated control : CDM alone; 2) single lysophosphatidyl choline (LPC, Sigma) exposure ($2.\ 10^{-5}$ M, 24 h) on day 4 of the subculture; 3) split LPC exposure ($0.5.\ 10^{-5}$ M, 6 h) on days 2, 3, 4, and 5 (total duration equal to single treatment); 4) multiple LPC exposures ($2.\ 10^{-5}$ M, 24 h) on days 2 and 4 of the subculture. After each exposure and LPC removal, dishes were rinsed with CDM, and cells were grown further in CDM alone, or supplemented with either PDGF (15 ng/ml/24 h (Fressinaud et al., 1996)) or NT-3 (5 ng/ml/48 h (Barres et al., 1994)), which were added immediately after LPC removal and rinsing, and until the next treatment (Fressinaud, 2005).

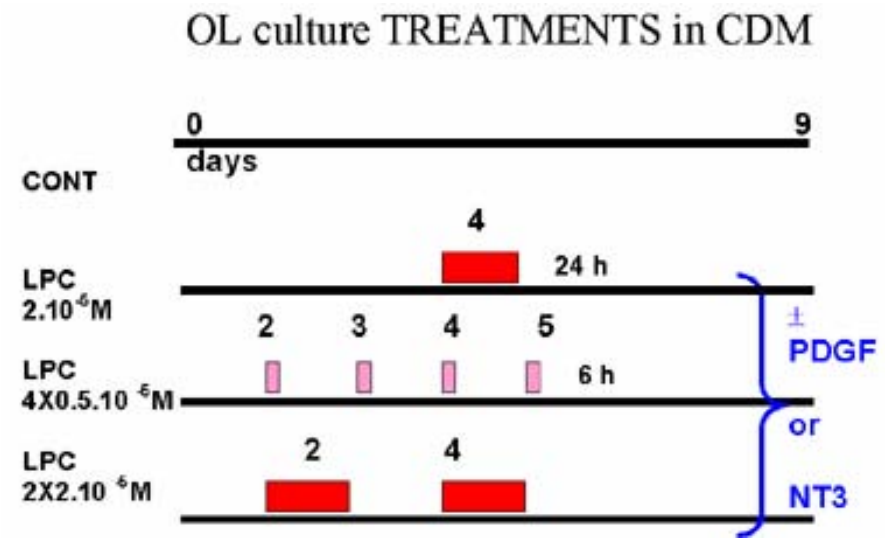

Figure 5. Schematic chart of the various types of LPC exposure used for newborn rat oligodendrocyte pure cultures grown in chemically-defined medium.

Experiments were run 3 times in triplicate for each of the treatments, and prolonged until day 6 or 9 of the subculture. Immunocytochemistry was performed as previously reported (Fressinaud, 2005). Cell counting of total cells, or of cells labelled with antibodies raised against BrdU, A2B5, CNP, or MBP, was performed on 10 optic fields distributed at random on coverslips. Results were averaged and compared with appropriate tests (Mann and Whitney's test, and Student's t test adapted to small samples).

As previously described (Fressinaud and Vallat, 1994; Fressinaud et al., 1996) a single LPC exposure (2. 10^{-5} M, 24 h) killed around 60 % of cells, compared to untreated controls (figures 6-7). The entire population of cells of the OL lineage was susceptible to LPC attack from progenitors (A2B5+ cells) to mature (MBP+) OL ($p < 0.01$, Student's t test). As it could have been expected, two LPC treatments (2. 10^{-5} M, 2 X 24 h) killed virtually all the cells of the OL lineage which number decreased by 96% on day 6, compared to controls. Recovery did not occur (98% cell loss on day 9, figures 6-7) ($p < 0.01$, Student's t test). Finally, total cells decreased by 92% on day 6 after split LPC exposure (0.5. 10^{-5} M, 4 X 6 h) ($p < 0.01$), and, again, there was no recovery. Thus, interestingly, split LPC treatment induced a more pronounced loss of cells than single LPC treatment, despite a far less concentration, and a total duration of OL exposure to LPC equal to the single treatment. Intermediate cell counts revealed that cell loss increased by steps of 20-25% after each administration of LPC compared to controls. As for single LPC exposure, the entire population of cells of the OL lineage (OL progenitors, differentiated OL, and mature OL) was affected by split LPC treatment. Thus, in cultures repeatedly exposed to LPC, few immature cells persisted, moreover mature OL did not survive : strikingly, MBP+ cells completely disappeared from cultures after split LPC exposure.

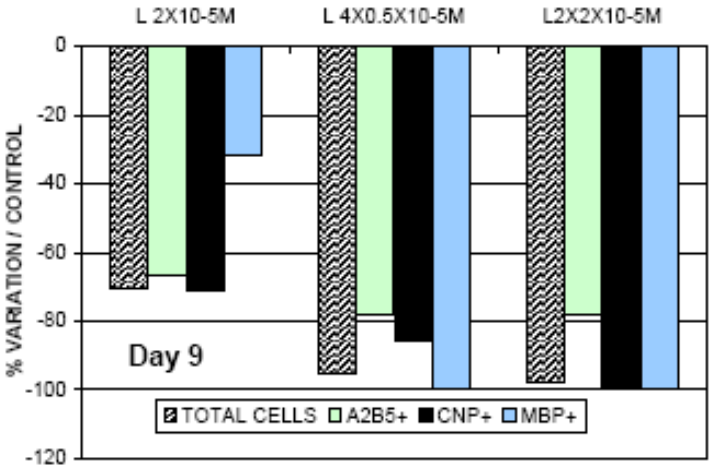

Figure 6. Effects of repeated lysophosphatidyl choline (LPC) exposures on oligodendrocyte number in vitro, compared to single LPC treatment. Results were recorded after 9 days in culture, and expressed as percentage variation compared to controls (untreated sister cell cultures). From Fressinaud C., Glia, 2005, 49 (4), 555-566. Copyright ©. Reprinted with permission of Wiley-Liss, Inc., a subsidiary of John Wiley and Sons, Inc.

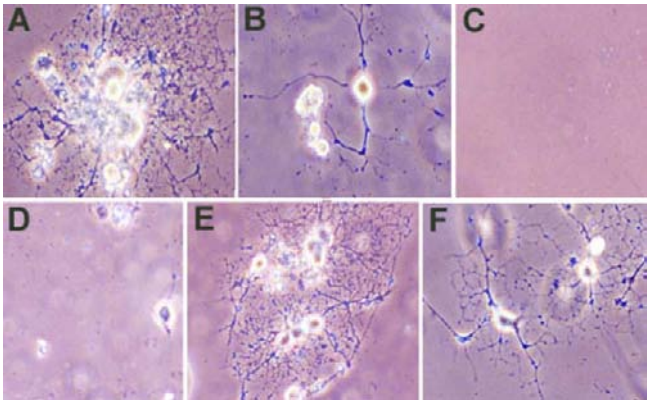

Figure 7. Phase contrast microphotographs of oligodendrocyte pure cultures after 9 days in chemically-defined medium. Cells were treated as follows : (A) untreated control; (B) single lysophosphatidyl choline (LPC) exposure (2. 10^{-5} M, 24 h) on day 4 of the subculture; (C) two LPC treatments (2. 10^{-5} M, 2 X 24 h); (D) split LPC exposure (0.5. 10^{-5} M, 6 h on day 2, 3, 4 and 5 (total duration equal to single treatment)); (E) split LPC exposure and PDGF (15 ng/ml/24 h); (F) split LPC exposure and NT-3 (5 ng/ml/48 h). Note the severe decrease in cell number in cultures submitted to multiple LPC exposures (C, D), and partial recovery after either growth factor treatment (E, F). Original magnification x 200. From Fressinaud C., Glia, 2005, 49 (4), 555-566. Copyright ©. Reprinted with permission of Wiley-Liss, Inc., a subsidiary of John Wiley and Sons, Inc.

Cell proliferation, assessed by nuclear BrdU labelling of A2B5+ OL progenitors (figure 8), was nearly abolished (> 85% decrease compared to untreated control) on day 6, whatever LPC treatment was administered ($p < 0.01$). This effect persisted on day 9, and proliferation was abolished in cultures submitted to multiple LPC exposures.

OL surviving repeated LPC exposures, showed profound morphological alterations compared to controls, with less numerous and shortened processes that were poorly branched. Moreover, membranes and myelin balls had disappeared (figure 7).

So, these results demonstrated the pronounced vulnerability of cells of the OL lineage to repeated - versus single - insults. They pointed also out to the special loss of mature OL in these conditions.

Growth factors alleviated these lesions : in all types of LPC toxicity induction, and at all times studied, PDGF, as well as NT-3, induced at least partial recovery (figures 7-9). Globally the effects of PDGF and NT-3 were in the same order of magnitude, and more pronounced (in percentage of appropriate controls) with multiple and split LPC exposures. On day 9 (figure 8) the increase in total cell number reached 150% (PDGF) to 268% (NT-3) compared to the single LPC treatment alone, and 900% (PDGF and NT-3) to up to 1050% (PDGF and NT-3) for split and multiple LPC treatments, respectively ($p < 0.01$). Nevertheless, it should be noticed that the effects of multiple or split LPC exposures were particularly drastic, and that total cell counts per optic field were very low even after growth factors treatments.

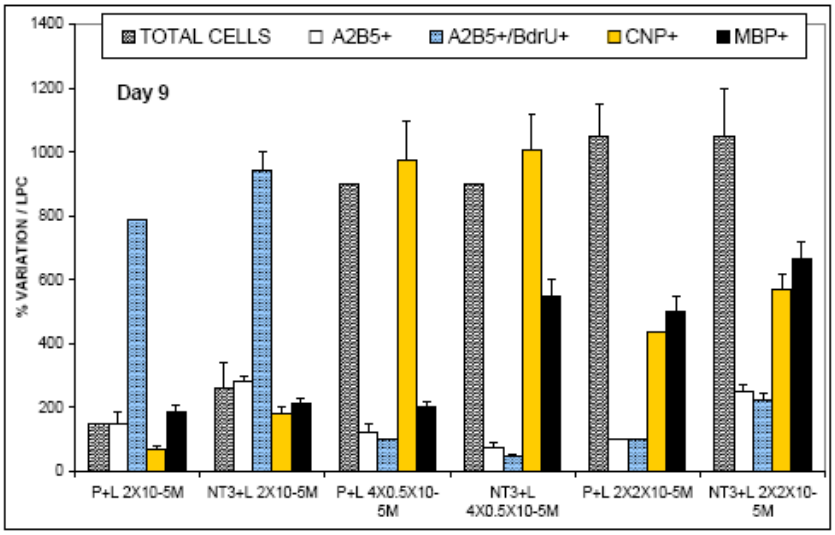

Figure 8. Results of immunocytochemistry in oligodendrocyte pure cultures after 9 days in chemically-defined medium. Cultures were submitted either to one (L2X) (2. 10^{-5} M, 24 h), or to two LPC treatments (L2X2) (2. 10^{-5} M, 2 X 24 h); or to split LPC exposure (L4X) (0.5. 10^{-5} M, 6 h on day 2, 3, 4 and 5), and grown further with PDGF (P+L) or NT-3 (NT3+L). Results are expressed in percentage of increase relative to respective controls (LPC without growth factors). From Fressinaud C., Glia, 2005, 49 (4), 555-566. Copyright ©. Reprinted with permission of Wiley-Liss, Inc., a subsidiary of John Wiley and Sons, Inc.

The increase in total cell number with either growth factor appeared largely due to enhanced OL progenitor proliferation (assessed by BrdU labelling of A2B5+ cells), which reached 422% (NT-3) to 556% (PDGF), respectively compared to split LPC exposure ($p < 0.01$) (figure 8).

Nevertheless, PDGF and NT-3 did not delay OL differentiation since they significantly increased all differentiation and maturation phenotypes of cells of the OL lineage, whatever LPC treatment was given (figure 8), and this was observed from day 6. Finally, on day 9, the effects of both growth factors consisted mainly in a dramatic increase in the number of MBP+ cells. This increase reached 200% (PDGF) and 550% (NT-3) compared to split LPC treatment alone. Analysis of the relative percentage of MBP+ cells (compared to the total number of cells observed by phase contrast microscopy) for one given treatment revealed that mature OL represented more than 25 to 30% of total cells in cultures treated with either PDGF or NT-3, whereas these cells were absent from cultures submitted only to split or multiple LPC exposures on day 9. In addition, in cultures exposed repeatedly to LPC, PDGF and NT-3 obviously resulted in an increase in the number of differentiated (CNP+) (figure 9) or mature (MBP+) OL, with a very complex morphology - as the untreated controls - characterized by numerous processes, and putative myelin balls suggestive of myelin-like membrane synthesis (figures 7E-F, 9).

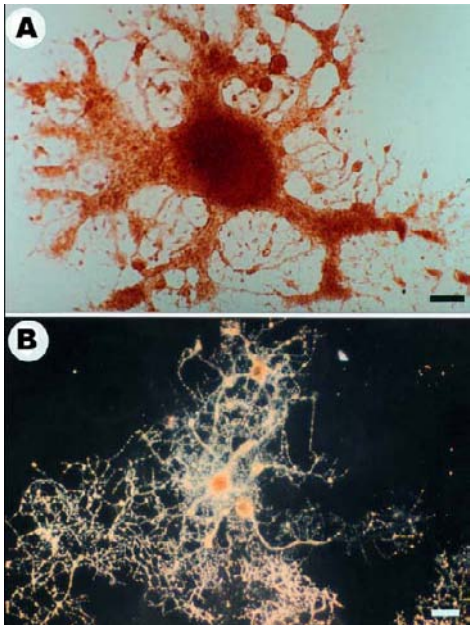

Figure 9. Microphotographs of immunocytochemistry with anti-CNP antibody (peroxydase staining, (B) dark field contrast) in oligodendrocyte pure cultures after 9 days. Cells were submitted to split LPC exposure followed by NT-3 treatment. Note putative myelin balls in (A), and numerous finally branched process in (B). Bar = 10 µm in (A), and 40µm in (B). From Fressinaud C., Glia, 2005, 49 (4), 555-566. Copyright ©. Reprinted with permission of Wiley-Liss, Inc., a subsidiary of John Wiley and Sons, Inc.

Thus our results demonstrate that cells of the OL lineage are particularly vulnerable to repeated insults, and that mature OL are drastically decreased after split and multiple LPC exposures, which induced more cell loss than a single one. The lack of spontaneous recovery suggests that OL plasticity - formerly observed in vitro (Fressinaud et al., 1996; Knapp, 1997) - is restricted, and insufficient to compensate the consequences of the repetition of attacks. Interestingly, PDGF, as well as NT-3, which pro-remyelinating effects have been

observed in vivo (Allamargot et al., 2001, Jean et al., 2003), induced at least partial recovery after several LPC exposures, and enhanced OL progenitor proliferation without delaying their differentiation. In cultures treated with either of these growth factors, mature OL represented 1/4 of cells, and extended numerous ramified processes with putative myelin balls, suggesting that maturation characteristics and myelination capabilities of cells had been, at least partly, restored too (Fressinaud, 2005).

So, these data are in agreement with our previous studies demonstrating that after a single demyelinating event in vivo NT-3- and PDGF-enhanced remyelination associates with increased number of mature OL, and increased number of myelinated fibres per OL. They suggest that the metabolic capabilities of OL to synthesize myelin might be rescued by some growth factors after repeated insults too. In addition, we have shown that mature OL in particular – which are the most abundant and myelinating cells in the adult CNS – are drastically lost in these conditions of repeated insults, and that surviving cells are unable to differentiate properly. The lack of mature OL, and of OL with a differentiated morphology after several LPC exposures in vitro is reminiscent of our observations in MS lesions : i. e. decreased number of MBP+ OL, and decreased ratio of myelinated fibre per cell. Although this experimental paradigm is remote from MS, it suggests that exhaustion of OL remyelinating capabilities might also occur following MS relapses.

Conclusion

Taken together our data suggest that defective remyelination during MS results not only from OL loss, but also from the occurrence, at the cellular level, of OL inability to synthesize new myelin sheaths in sufficient number, and that the repetition of relapses could account for this death of cells and loss of function. Conversely, there are less arguments suggesting that altered expression of neurofilaments (NF) by axons occurring during MS (Trapp et al., 1998, Fressinaud et al., 2005, Fressinaud and Sazdovitch, 2006) could be involved, since, experimentally, NF expression alterations are known to associate with a single demyelinating event, but without impairing spontaneous remyelination (Jean et al., 2002). Moreover, we have demonstrated that remyelination alleviates these lesions (Jean et al., 2002). Moreover, in NFH-lacZ transgenic mice, which lack axonal NF (Eyer and Peterson, 1994), CNS remyelination is not impaired, at least after a single LPC injection (Jean and Fressinaud, 2003), and proceeds as well as in wild-type mice, and with equivalent time schedules.

Finally our study reveals too that growth factors, such as PDGF and NT-3, which have known pro-remyelinating effects in vivo after a single demyelinating event, might also rescue cells of the OL lineage from repeated attacks as observed in vitro. The fact that, although they increase OL progenitor proliferation, they do not delay their maturation in our model, make them appear as potentially interesting agents on a therapeutic point of view in order to promote remyelination in MS and other demyelinating diseases.

The demonstration of the vulnerability of OL to repeated attacks, which are known to occur in MS, adds to growing scientific bases in favor of early treatment of the disease in order to prevent definitive OL and myelin alterations, which are deleterious for white matter and CNS proper functions.

Acknowledgments

This work was supported by a grant from the University Hospital of Angers (P.H.R.C. # 21-01).

References

Adlkofer K, Martini R, Aguzzi A, Zielasek J, Toyka KV, Suter U. (1995). Hypermyelination and demyelinating peripheral neuropathy in Pmp22-deficient mice. *Nat. Genet.* 11: 274-280.

Allamargot, C., Pouplard-Barthelaix, A., Fressinaud, C. (2001). A single intracerebral injection of platelet-derived growth factor (PDGF) accelerates the rate of remyelination in vivo. *Brain Res.* 918: 28-39.

Barres, B.A., Raff, M.C. (1993). Proliferation of oligodendrocyte precursor cells depends on electrical activity in axons. *Nature.* 361: 258-260.

Barres BA, Raff MC, Gaese F, Bartke I, Dechant G, Barde YA. (1994). A crucial role for neurotrophin-3 in oligodendrocyte development. *Nature.* 367: 371-375.

Bashir, K., Whitaker, J.N. (1999). Clinical and laboratory features of primary progressive and secondary progressive MS. *Neurology.* 53: 765-771.

Besnard F, Perraud F, Sensenbrenner M, Labourdette G. (1987). Platelet-derived growth factor is a mitogen for glial but not for neuronal rat brain cells in vitro. *Neurosci. Lett.* 73: 287-292.

Bitsch, A., Schuchardt, J., Bunkowski, S., Kuhlmann, T., Bruck, W. (2000). Acute axonal injury in multiple sclerosis. Correlation with demyelination and inflammation. *Brain.* 123: 1174-1183.

Bozzali M, Wrabetz L. (2004). Axonal signals and oligodendrocyte differentiation. *Neurochem. Res.* 29: 979-988.

Brück, W., Schmied, M., Suchanek, G., Brück, Y., Breitschopf, H., Poser, S., Piddlesden, S, Lassmann, H. (1994). Oligodendrocytes in the early course of multiple sclerosis. *Ann. Neurol*. 35: 65-73.

Brück, W., Lucchinetti, C., Lassmann, H. (2002). The pathology of primary progressive multiple sclerosis. *Mult. Scler.* 8: 93-97.

Butt AM (2005). Structure and function of oligodendrocytes. In : Neuroglia, Kettenmann H, Ransom BR eds, Oxford, NY, pp 36-47.

Chakraborty G, Mekala P, Yahya D, Wu G, Ledeen RW. (2001). Intraneuronal N-acetylaspartate supplies acetyl groups for myelin lipid synthesis: evidence for myelin-associated aspartoacylase. *J. Neurochem.* 78:736-745.

Chang, A., Tourtelotte, W.W., Rudick, R., Trapp, B.D. (2002). Premyelinating oligodendrocytes in chronic lesions of multiple sclerosis. *N. Engl. J. Med.* 346: 165-173.

Charles, P., Reynolds, R., Seilhean, D., Rougon, G., Aigrot, M.S., Neizgoda, A., Zalc, B., Lubetzki, C. (2002). Re-expression of PSA-NCAM by demyelinated axons : an inhibitor of remyelination in multiple sclerosis ? *Brain.* 125: 1972-1979.

Cole JS, Messing A, Trojanowski JQ, Lee VMY. (1994). Modulation of axon diameter and neurofilaments by hypomyelinating Schwann cells in transgenic mice. *J. Neurosci.* 14: 6956-6966.

Debouverie M, Pittion-Vouyovitch S, Louis S, Roedere T, Guillemin F (2007). Increasing incidence of multiple sclerosis among women in Lorraine, Eastern France. *Mult. Scler.* 13: 962-969.

Demerens, C., Stankoff, B., Anglade, P., Allinquant, B., Couraud, F., Zalc, B., Lubetzki, C. (1996). Induction of myelination in the central nervous system by electrical activity. *Proc. Natl. Acad. Sci. USA.* 93 : 9887-9892.

deWaegh SM, Lee VM, Brady ST. (1992). Local modulation of neurofilament phosphorylation, axonal caliber, and axonal transport by myelinating Schwann cells. *Cell.* 68: 451-463.

Doyle JP, Colman DR. (1993). Glial-neuron interactions and the regulation of myelin formation. *Curr. Opin. Cell Biol.* 5:779-785.

Eyer J, Peterson AC. (1994). Neurofilament deficient axons and perikaryal aggregates in viable transgenic mice expressing a neurofilament-beta- galactosidase fusion protein. *Neuron.* 12: 389-405.

Fernandez PA, Tang DG, Cheng L, Prochiantz A, Mudge AW, Raff MC. (2000). Evidence that axon-derived neuregulin promotes oligodendrocyte survival in the developing rat optic nerve. *Neuron.* 28: 81-90.

Fields RD. (2004). Volume transmission in activity-dependent regulation of myelinating glia. *Neurochem. Int.* 45: 503-509.

Fressinaud, C. (2005). Repeated injuries dramatically affect cells of the oligodendrocyte lineage : effects of PDGF and NT-3 in vitro. *Glia*. 49 : 555-566.

Fressinaud, C. (2007). Déficit oligodendrocytaire et insuffisance de la remyélinisation au cours de la SEP : Etude anatomoclinique et expérimentale comparative. *Rev. Neurol.* (Paris) 163: 448-454.

Fressinaud C, Vallat JM. (1994). Basic fibroblast growth factor improves recovery after chemically induced breakdown of myelin-like membranes in pure oligodendrocyte cultures. *J. Neurosci. Res.* 38: 202-213.

Fressinaud C, Sazdovitch V. (2006). Neurofilaments as the central core of Axonal Damage in Multiple Sclerosis. In : Multidrug resistance-associated proteins, C. V. Aiello (Ed), Nova Science Publishers (New York), 2006, chapter 6, pp. 137-157.

Fressinaud, C., Vallat, J.M., Rigaud, M., Cassagne, C., Labourdette, G., Sarlieve, L.L. (1990). Investigation of myelination in vitro: polar lipid content and fatty acid composition of myelinating oligodendrocytes in rat oligodendrocyte cultures. *Neurochem. Int.* 16: 27-39.

Fressinaud, C., Vallat, J.M., Labourdette, G. (1995). Basic fibroblast growth factor down-regulates myelin basic protein gene expression and alters myelin compaction of mature oligodendrocytes in vitro. *J. Neurosci. Res.* 40: 285-293.

Fressinaud, C., Vallat, J.M., Pouplard-Barthelaix, A. (1996). Platelet-derived growth factor partly prevents chemically induced oligodendrocyte death and improves myelin-like membranes repair in vitro. *Glia.* 16: 40-50.

Fressinaud, C., Jean, I., Dubas, F. (2005). Modifications des neurofilaments et des microtubules axonaux en fonction du mécanisme lésionnel : étude pathologique et expérimentale. *Rev. Neurol.* (Paris) 161: 55-60.

Friede RL, Bischhausen R. (1982). How are sheath dimensions affected by axon caliber and internode length? *Brain Res.* 235: 335-350.

Frohman EM (2003). Multiple sclerosis. *Med. Clin. North Am.* 87: 867-897, VIII-IX.

Frohman Em, Racke Mk, Raine CS. (2006). Multiple sclerosis – The plaque and its pathogenesis. *N. Engl. J. Med*. 354: 942-955.

Giordana, M.T., Richiardi, P., Trevisan, E., Boghi, A., Palmucci, L. (2002). Abnormal ubiquitination of axons in normally myelinated white matter in multiple sclerosis brain. *Neuropathol. Appl. Neurobiol.* 28: 35-41.

Guennoc, A.M., Stankoff, B., Barbin, G., Zalc, B., Lubetzki, C. (2001). Rôle de la paranodine dans la myélinisation du SNC. *Rev. Neurol.* (Paris) 157 suppl 3: 2S51, abstract F13.

Hader WJ, Yee IM. (2007). Incidence and prevalence of multiple sclerosis in Saskatoon, Saskatchewan. *Neurology*. 69: 1224-1229.

Hartung, H.P., Ritz, M.F., Steck, A.J. (1999). Eléments de neuro-immunologie. In: . Steck, A.J., coordinator, Bogousslavsky, J., Léger, J.M., Mas, J.L., (Eds), Affections démyélinisantes. Neuroimmunologie et clinique. Traité de neurologie. Doin, Rueil-Malmaison, pp. 35-60.

Hirokawa N. (1997). The mechanisms of fast and slow transport in neurons: identification and characterization of the new kinesin superfamily motors. *Curr. Opin. Neurobiol.* 7: 605-614.

Hisanaga S, Hirokawa N. (1988). Structure of the peripheral domains of neurofilaments revealed by low angle rotary shadowing. *J. Mol. Biol.* 202: 297-305.

Hisanaga S, Hirokawa N. (1990). Dephosphorylation-induced interactions of neurofilaments with microtubules. *J. Biol. Chem.* 265: 21852-21858.

Hoffman, P.N., Cleveland, D.W., Griffin, J.W., Landes, P.N., Cowan, N.J., Price, D.L. (1987). Neurofilament gene expression : a major determinant of axonal caliber. *Proc. Natl. Acad. Sci. USA* 84 : 3472-3476.

Hsieh S, Kidd G, Crawford T, Xu Z, Lin W, Trapp BD, Cleveland D, Griffin JW. (1994). Regional modulation of neurofilament organization by myelination in normal axons. *J. Neurosci.* 14: 6392-6401.

Jean, I., Allamargot, C., Barthelaix-Pouplard, A., Fressinaud, C. (2002). Axonal lesions and PDGF-enhanced remyelination in the rat corpus callosum after lysolecithin demyelination. *Neuroreport.* 13: 627-631.

Jean I, Fressinaud C. (2003). Spontaneous central nervous system remyelination is not altered in NFH-lacZ transgenic mice after chemical demyelination. *J. Neurosci. Res.* 73: 54-60.

Jean, I., Lavialle, C., Barthelaix-Pouplard, A., Fressinaud, C. (2003). Neurotrophin-3 specifically increases mature oligodendrocyte population and enhances remyelination after chemical demyelination of adult rat CNS. *Brain Res.* 972: 110-118.

Knapp PE. (1997). Injury stimulates outgrowth and motility of oligodendrocytes grown in vitro. *Exp. Cell Res.* 234: 7-17.

Knapp PE, Adams PH. (2004). Epidermal growth factor promotes oligodendrocyte process formation and regrowth after injury. *Exp. Cell Res.* 296: 135-144.

Kuhlmann T, Lucchinetti C, Zettl UK, Bitsch A, Lassmann H, Brück W (1999). Bcl-2-expressing oligodendrocytes in multiple sclerosis lesions. *Glia.* 28: 34-39.

Kurtzke JF. (1991). Multiple sclerosis : changing times. *Neuroepidemiology.* 10: 1-8.S

Lai C, Feng L. (2004). Implication of γ-secretase in neuregulin-induced maturation of oligodendrocytes. *BBRC.* 314: 535-542.

Lassmann, H. (2002). Mechanisms of demyelination and tissue destruction in multiple sclerosis. *Clin. Neurol. Neurosurg.* 104: 168-171.

Ledeen RW, Golly F, Haley JE. (1992). Axon-myelin transfer of phospholipids and phospholipid precursors. Labeling of myelin phosphoinositides through axonal transport. *Mol. Neurobiol.* 6: 179-90.

Lopresti P, Muma NA; de Vries GH. (2001). Neu differentiation factor regulates tau protein and mRNA in cultured neonatal oligodendrocytes. *Glia.* 35: 147-155.

Losseff, N.A., Webb, S.L., O'riordan, J.I., Page, R., Wang, L., Barker, G.J., Tofts, P.S., Mcdonald, W.I., Miller, D.H., Thompson, A.J. (1996). Spinal cord atrophy and disability in multiple sclerosis. A new reproductible and sensitive MRI method with potential to monitor disease progression. *Brain.* 119: 701-708.

Lucchinetti, C., Brück, W., Parisi, J., Scheithauer, B., Rodriguez, M., Lassmann, H., (1999). A quantitative analysis of oligodendrocytes in multiple sclerosis. A study of 113 cases. *Brain.* 122: 2279-2295.

Lucchinetti, C., Brück, W., Parisi, J., Scheithauer, B., Rodriguez, M., Lassmann, H. (2000). Heterogeneity of multiple sclerosis lesions: implications for the pathogenesis of demyelination. *Ann. Neurol.* 47: 707-717.

Ludwin SK. (1997). The pathobiology of the oligodendrocyte. *J. Neuropathol. Exp. Neuro.* 56: 111-124.

Macklin, W.B., Weill, C.L., Deininger, P.L. (1986). Expression of myelin proteolipid and myelin basic protein mRNAs in culture cells. *J. Neurosci. Res.* 16 : 203-217.

Mews, I., Bergmann, M., Bunkowski, S., Gulotta, F., Brück, W. (1998). Oligodendrocyte and axon pathology in clinically silent multiple sclerosis lesions. *Mult. Scler.* 4: 55-62.

Norton WT, Cammer W. (1984). Isolation and characterization of myelin. In : Myelin, Morel P., ed, Plenum Press, NY, London, pp. 147-195.

Ozawa, K., Suchanek, G., Breitschopf, H., Brück, W., Budka, H., Jellinger, K., Lassmann, H. (1994). Patterns of oligodendroglia pathology in multiple sclerosis. *Brain.* 117: 1311-1322.

Penderis J, Shields SA, Franklin RJM. (2003). Impaired remyelination and depletion of oligodendrocyte progenitors does not occur following repeated episodes of focal demyelination in the rat central nervous system. *Brain.* 126: 1382-1391.

Prineas, J.W., Mcdonald, W.I. (1997). Demyelinating diseases. In: Graham DI, Lantos PL. (Eds), *Greenfield's neuropathology,* Arnold, London, pp. 813-896.

Raine CS. (1984 a). Morphology of myelin and myelination. In : Myelin, Morel P., ed, Plenum Press, NY, London, pp. 1-50.

Raine CS. (1984 b). The neuropathology of myelin diseases. In : Myelin, Morel P., ed, Plenum Press, NY, London, pp. 259-310.

Raine, C.S., Cross , A.H. (1989). Axonal dystrophy as a consequence of long-term demyelination. *Lab. Invest.* 60: 714-725.

Rao MV, Campbell J, Yuan A, Kumar A, Gotow T, Uchiyania Y, Nixon RD. (2003). The neurofilament middle molecular mass subunit carboxyl-terminal tail domains is essentaial for the radial growth and cytoskeletal architecture of axons but not for regulating neurofilament transport rate. *J. Cell. Biol.* 163: 1021-1031.

Reichenbach A, Wolburg H (2005). Astrocytes and ependymal cells. In : Neuroglia, Kettenmann H, Ransom BR, eds, Oxford, NY, pp. 19-35.

Rilling JK, Insel TR (1999). The primate neocortex in comparative perspective using magnetic resonance imaging. *J. Human Evol.* 37: 1991-223.

Rodriguez, M., Scheithauer, B.W., Forbes, G., Kelly, P. (1993). Oligodendrocyte injury is an early event in lesions of multiple sclerosis. *Mayo Clin. Proc.* 68: 627-636.

Sanchez I, Hassinger L, Paskevich PA, Shine HD, Nixon RD. (1996). Oligodendroglia regulate the regional expansion of axon caliber and local accumulation of neurofilaments during development independently of myelin formation. *J. Neurosci.* 16: 5085-5105.

Schachner M, Bartsch U. (2000). Multiple functions of the myelin-associated glycoprotein MAG siglec-4a. in formation and maintenance of myelin. *Glia.* 29: 154-165.

Scolding, N., Franklin, R., Stevens, S., Heldin, C.H., Compston, A., Newcombe, J. (1998). Oligodendrocyte progenitors are present in the normal adult human CNS and in the lesions of multiple sclerosis. *Brain.* 121: 2221-2228.

Silber, E., Sharief, M.K. (1999). Axonal degeneration in the pathogenesis of multiple sclerosis. *J. Neurol. Sci.* 170: 11-18.

Starr R, Attema B, deVries G, Monteiro M. (1996). Neurofilament phosphorylation is modulated by myelination. *J. Neurosci. Res.* 44: 328-337.

Taveggia C, Zanazzi G, Petrylak A, Yano H, Rosenbluth J, Einheber S et al; (2005). Neuregulin-1 type III determines the ensheathment fate of axons. *Neuron.* 47: 631-694.

Trapp, B.D., Peterson, J., Ransohof, R.M., Rudick, R., Mörk, S., Bö, L. (1998). Axonal transection in the lesions of multiple sclerosis. *N. Engl. J. Med.* 338: 278-285.

Trifilieff E, Luu B, Nussbaum JL, Roussel G, Espinosa de los Monteros A, Sabatier JM, Van Rietschoten J. (1986). A specific immunological probe for the major myelin proteolipid. Confirmation of a deletion in DM-20. *FEBS Lett.* 198: 235-239.

Waxman SG, Bangalore L. (2004). Electrophysiologic consequences of myelination. In : Myelin biology and disorders, Lazzarini RA (Ed), Elsevier, Amsterdam, Vol. 1, pp. 117-141.

Zhao C, Fancy SPJ, Magy L, Urwin JE, Franklin RJM. (2005). Stem cells, progenitors and myelin repair. *J. Anat.* 207: 251-258.

In: Handbook on White Matter
Editors: T. B. Westland and R. N. Calton
ISBN: 978-1-60741-034-8

Chapter XI

Endoscopic Anatomy of the Thecal Sac Using a Flexible Steerable Endoscope

Jan Peter Warnke
Neurology Department, Paracelsus Clinic, Zwickau, Germany

Abstract

The use of minimal invasive methods and edoscopic procedures for diagnosis and treatment of certain pathologic entities involving the spina canal expands permanently. The sacral spinal canal as a place of such interventions is for a long time known. Thecaloscopy is the endoscopy of lumbar subarachnoid space performed through different approaches by using flexible endoscopes.

The subject of this study was the measurement of certain anatomic diameters in the sacral spinal canal by using the lubosacral MRI studies of 25 patients.

Introduction

The corpus callosum is the largest connective pathway in the human brain. It is a structure deep-seated in the longitudinal fissure, which connects the left and right cerebral hemispheres. It is the largest *white matter* structure in the brain, a wide flat bundle of axons beneath the cortex, consisting of 200-250 million *contralateral axonal* projections.

If we cut a brain in half down the middle, we would also cut through the fibers of the corpus callosum. When looking macroscopically at the middle side of one half of the brain, the corpus callosum looks like a cross-section of a mushroom cap at the center of the brain. In this view it forms three parts: the *anterior* part, which is called the genu (or "knee") the *posterior* portion called the *splenium* and the part between the two called the 'body.' The most anterior part is called the *rostrum.*

There is a topographic organization of callosal fibers, which represents the cortical regions that are connected. Fibers connecting frontal regions travel through the anterior

aspect of the corpus callosum, while fibers connecting occipital cortices travel through the posterior segment. Much of the inter-hemispheric communication in the brain is conducted across the corpus callosum. Each hemisphere of the brain is specialized to control movement and feeling in the opposite half of the body, and each hemisphere specializes in processing certain types of information (such as language or spatial patterns). Thus, to coordinate movement or to think about complex information, the hemispheres must communicate with each other. The corpus callosum is the main connector that allows that communication.

In a typical infant brain, the corpus callosum develops between 12 to 16 weeks after conception (near the end of the first trimester). While the entire structure develops prior to birth, the fibers of the corpus callosum continue to become more and more effective and efficient on into adolescence. By the time a child is approximately 12 years of age, the corpus callosum functions essentially as it will in adulthood, allowing rapid interaction between the two sides of the brain. From this age on (and typically earlier) the corpus callosum becomes increasingly functional in their typically developing peers.

There are disputed claims about the difference of the size of the human corpus callosum in men and women and about the relationship of any such differences to gender differences in human behaviour and cognition. There is scientific dispute not only about the implications of anatomical difference, but whether such a difference actually exists.

Because of the controversies and our interest on morphology and function of corpus callosum we started to study corpus callosum in cadaveric brains on magnetic resonance imaging examinations as well as special cases to understand better the role, the function and the morphology of this anatomical structure in brain.

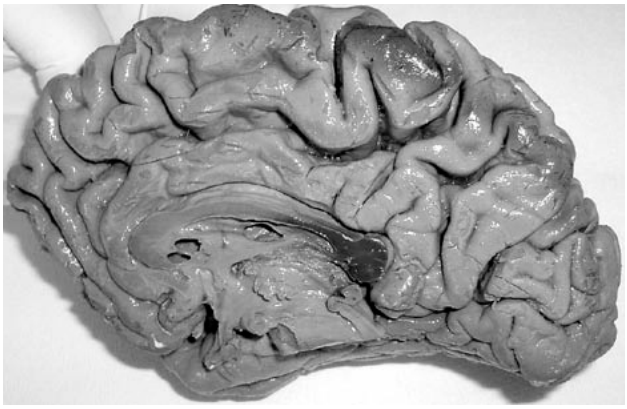

Figure 1.

First we conducted a study on post-mortem brains. The purpose of this study was to measure the longitudinal diameters of corpus callosum and its parts as well as the longitudinal and vertical diameters of the brain; in order to define the position of corpus callosum within the brain.

In this study, 42 formalin fixed brains, which were removed from cadavers (23 males, 19 females), aged 30-40 years, used. Brains were carefully cut in the mediosagittal plane (figure 1) and the medial surface of the brain hemispheres and then were printed on a transparent

sheet of paper. On these papers, the longitudinal diameters of every anatomical part of corpus callosum, the longitudinal and vertical diameters of brain hemispheres were measured.

The diameters measured (figure 2) were: the longitudinal (frontal to occipital pole-AB) and the vertical diameter (upper to lower surface-CD) of brain hemispheres, the distance of genu to frontal pole (AE), the distance of splenium to occipital pole (ZB), the longitudinal diameter of genu (EZ/3) and splenium (EZ/5), and the longitudinal diameter of CC (EZ).

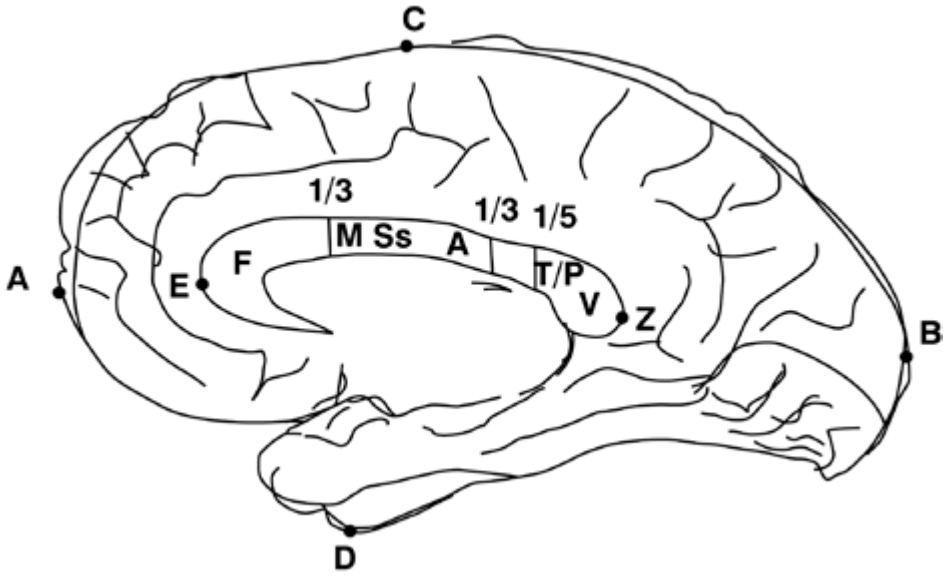

Figure 2.

Statistical analysis followed, which was performed by using the 2-tailed Pearson correlation test. The results from this study were the following: AB has a positive linear correlation with CD, AE, BZ and EZ. EZ has a positive linear correlation with AB and CD. The ratios EZ/AB=0.46, EZ/CD=0.85, EZ/AE=2.29 and EZ/ZB=1.42 represented stable analogies.

In all cadaveric brains we examined in this study, all the measurements were within certain limits; and the ratios between the diameters of CC and those of brain hemispheres were stable. This means that CC had a stable position in brain hemispheres, which was retained in every brain studied.

The longitudinal and vertical diameters of the brain had a positive linear association between each other, as did also the distances of CC from the frontal and occipital pole, which means that augmentation of one diameter was associated with the augmentation of the other in a parallel manner, so that the symmetrical size of the brain was retained.

Astonishing is the finding that the longitudinal diameter of the brain had the strongest correlation with the distance between the splenium to the occipital pole, which may present the importance of the visual cortices fiber distribution. The distance of the genu from the frontal pole had a positive linear correlation with the distance of splenium from the occipital pole, but both diameters had no relation with the longitudinal diameter of CC. These findings suggest that there is symmetry between all the diameters of brain hemispheres; although these

distances play a role in the maintenance of the symmetrical size of brain, they do not influence the position of CC. While analyzing the relationship between CC and longitudinal and vertical diameters of the brain simultaneously, we have found that only the longitudinal diameter of the brain had a statistically significant correlation with the longitudinal diameter of CC, while the vertical diameter of brain did not.

Anatomically, this finding means that the longitudinal diameter of brain interacts for the horizontal site of CC, whilst the vertical diameter is less important. Further the ratios EZ/AB = 0.47 and EZ/CD = 0.86 were found to be stable analogies in every individual that were studied. All these findings suggest that there is a quotation, symmetry and stable proportions in every studied brain. These should be taken into account as stable anatomical data before performing some neurosurgical procedures [1] so as undesired intervention dependent clinical outcomes could be avoided [2]. There is a positive correlation between the size of brain and respective size of CC, a finding which is consistent with the findings of the study of Estruch et al [3]; in which they studied CC atrophy among alcoholic patients with severe cortical damage, and imposed that the size of CC depends on the size of the brain. From the clinical point of view, all these findings (tables 1, 2) suggest that CC can be found in a certain place in brain hemispheres, depending on the size itself and that of the brain, a fact that is very important in callosotomy procedures for intractable epilepsy cases [4, 5].

Next step in our study was to measure the same parameters in MRI examinations to test if the same results could be extracted.

Table 1. Correlation-coefficient Spearman's rho (n=35) between the diameters measured-in cadavers

	CD	AE	BZ	EZ
AB	0.475**	0.769**	0.819**	0.402**
CD		0.336*	0.513**	0.371*
AE			0.499**	0.184
BZ				0.256

* Correlation is significant at the 0.05 level (2-tailed).
** Correlation is significant at the 0.01 level (2-tailed).

Table 2. Correlation between CC and both diameters of the brain in cadavers

Model	Unstandardized coefficients	Standardized coefficients		t	p
	B	Std. Error			
Constant	2.774	1.192		2.327	0.025
AB (cm)	0.214	0.084	0.403	2.559	0.014
CD (cm)	0.144	0.115	0.196	1.244	0.221

Dependent variable: EZ (cm).

The primary purposes of this study were to investigate the possible existence of sex- and age-related differences in 1) the various dimensions of the corpus callosum, and 2) its relative position within the brain. Magnetic resonance images (MRI) from 21 females and 14 males, ranging in age from 24 to 80, were reviewed (figure 3).

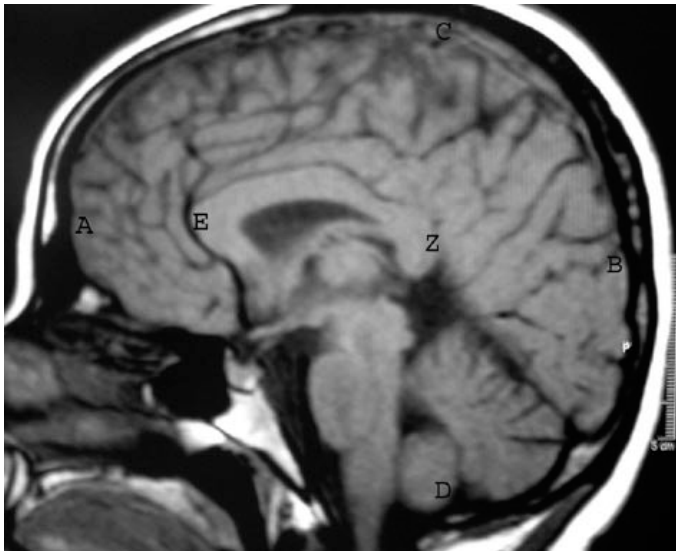

Figure 3.

Only MRI studies without any pathologic findings were included in analysis. The diameters measured were the same as in the previous study on cadavers and were the following: maximum longitudinal dimension (frontal to occipital pole-AB); maximum vertical dimension (upper to lower surface-CD); length of the genu (EZ/3); length of the splenium (EZ/5); and total longitudinal dimension of the corpus callosum (EZ). Callosal longitudinal dimensions were measured using the Witelson division method (figure 2), and were correlated with brain dimensions in the same living humans, in order tom examine for sex- and age-related differences.

To investigate age-related differences, we stratified the studied population into age subgroups (24-45, 46-65, 66-80). Statistical analysis involved Spearman correlations and Wilcoxon sign ranks tests. Across all subjects, there was minimal variability in the dimensions and relative dimensions of the corpus callosum. The longitudinal dimension of the genu (EZ/3) and total corpus callosum (EZ) were found to be larger in males, whereas the longitudinal dimension of the splenium (EZ/5) was larger in females. Females exhibited a smaller brain vertical dimension versus males. The ratios –EZ/AE and EZ/CD - were larger in females, but the dimensions EZ/3, EZ, and EZ/5 did not vary with gender. Corpus callosum dimensions were statistically less, by 3%, in those over age 45 versus those younger than 45. The corpus callosum's dimensions and position remain stable relative to surrounding brain, but some sex differences exist. Also, the brain and corpus callosum both appear to decrease in size in older individuals.

These data demonstrate that the longitudinal and vertical diameters of the brain and the distance of the corpus callosum from the frontal and occipital poles have a positive linear

association. However, there is no statistical relationship between the diameters of the brain with the longitudinal dimensions of the corpus callosum. This means that the various dimensions of the brain change in concert with each other, thereby maintaining brain symmetry; but they do not directly influence the position and dimensions of the corpus callosum. In other words, the corpus callosum adopts a certain position within the cerebral hemispheres, but its dimensions are not correlated with those of the brain. The fact that the values of EZ/AB and EZ/CD had a little variation between the subjects studied suggests further that there is symmetry in the distances between every part of the corpus callosum and every part of the brain (tables 3,4,5).

Table 3. Correlation-coefficient between the diameters measured-in MRIs Spearman's rho (n=35)

	CD	AE	BZ	EZ
AB	0.536**	0.464**	0.630**	0.090
CD		0.430*	0.291	0.094
AE			0.176	-0.233
BZ				-0.344*

* Correlation is significant at the 0.05 level (2-tailed).
** Correlation is significant at the 0.01 level (2-tailed).

Table 4. Group statistics-sex differences inMRI measurements

	Male (n=14) Mean (cm)	Female (n=21) Mean (cm)	p
AB	15.44 (±0.82)	15.14 (±0.80)	0.293
CD	13.36 (±0.65)	12.75 (±0.72)	0.016
EZ	7.02 (±0.58)	6.84 (±0.46)	0.305
EZ/3	2.15 (±0.40)	2.12 (±0.38)	0.819
EZ/5	0.72 (±0.19)	0.75 (±0.15)	0.594
AE	3.25 (±0.32)	3.10 (±0.33)	0.208
BZ	5.16 (±0.40)	5.15 (±0.55)	0.945
EZ/AB	0.45 (±0.04)	0.45 (±0.04)	0.874
EZ/CD	0.53 (±0.05)	0.54 (±0.46)	0.509
EZ/AE	2.18 (±0.28)	2.23 (±0.30)	0.624
EZ/BZ	1.37 (±0.15)	1.35 (±0.20)	0.742

Table 5. Group statistics-age differences in MRI measurements

	Ages 24-45 (n=11)	Ages 46-65 (n=13)	Ages 66-80 (n=11)	p
AB	15.12 (±0.66)	15.46 (±0.96)	15.15 (±0.77)	0.527
CD	12.84 (±0.70)	12.88 (±0.74)	13.28 (±0.78)	0.307
EZ	7.24 (±0.53)	6.63 (±0.37)	6.92 (±0.47)	0.011
EZ/3	2.23 (±0.51)	2.02 (±0.31)	2.16 (±0.30)	0.363
EZ/5	0.79 (±0.14)	0.73 (±0.21)	0.70 (±0.12)	0.432
AE	3.07 (±0.36)	3.16 (±0.28)	3.25 (±0.36)	0.449
BZ	4.97 (±0.36)	5.44 (±0.55)	5.01 (±0.40)	0.027
EZ/AB	0.48 (±0.03)	0.43 (±0.03)	0.46 (±0.04)	0.006
EZ/CD	0.56 (±0.03)	0.52 (±0.04)	0.52 (±0.05)	0.026
EZ/AE	2.38 (±0.26)	2.11 (±0.22)	2.16 (±0.32)	0.056
EZ/BZ	1.46 (±0.17)	1.23 (±0.15)	1.39 (±0.15)	0.003

Although there is no statistical correlation between corpus callosum and brain dimensions, we could observe from the measurements that there was a symmetry between corpus callosum and brain size, with stable proportions, in every studied individual, a finding which agrees with the conclusions of Estruch et al. [3], that corpus callosum size is proportionate to the size of the brain.

From the findings of our study, we conclude that brain size does not itself determine the size of the corpus callosum, but that the size of both may be influenced by a common growth mechanism, as shown by the existence of stable dimensional ratios. These findings agree with the findings of Bishop and Wahlsten [6], who further proposed that brain size and weight both are the sum of many components, whether they be viewed as anatomical regions or histological elements. However, that there is a statistical correlation says nothing about the reasons behind the correlation.

Our study indicates that there is no cause and effect relationship, but nonetheless there is some common developmental relationship between the corpus callosum and the brain, a finding that agrees with that of Kawamura et al [7], who, in a series of 23 patients, found that all callosal anomalies were accompanied by hemispheric ones. Although EZ, CD and AE are smaller in females, the ratios EZ/CD and EZ/AE are larger in females, in absolute numbers and not in a statistically significant way, a finding that may reflect another brain-volume arrangement in females.

There appears a statistically-significant reduction in corpus callosum size after the age of 45, a finding that agrees, in part, with the writings of Driesen and Raz [8], who concluded, based upon a meta-analysis of 26 studies, that corpus callosum area does decrease slightly with age. Decreasing callosal size in older patients should be expected, because of the generalized atrophy of cortical neurons that occurs with advancing age. Atrophy not only

causes a decrease in the amount of gray matter, but also a loss of white matter. This age-related decrease in neuronal size, number of myelinated fibers, and amount of myelination likely is responsible for the age-related decrease in size of the corpus callosum [9].

The next step in our thinking process and further study of corpus callosum was to compare the two methods, MRI and cadaveric measurements, in order to estimate which of the measured parameters were the same or different in both above mentioned studies and to estimate if the methods are statistical equivalent. Between both studies there was a statistical difference of $p<5\%$ for the following diameters: AB, CD, EZ/3, EZ5, EZ/CD. Between MRI and cadaveric measurements there was not found any statistically significant difference for the following diameters: EZ/AB, EZ/AE, EZ/BZ and AE. In both measurement methods the diameters which are significant, are the corpus callosum in comparison with the longitudinal diameters of the brain. In every studied method the longitudinal diameter of the brain and the longitudinal diameter of the corpus callosum are maintained. The quotations of these diameters are the most stable in all measurements by both methods and in relation to each other. That makes stronger the belief, resulted already from our previous studies, that there is no cause and effect relationship between brain and corpus callosum development, but may be there is some common developmental relationship between corpus callosum and brain. In conclusion the two methods are not statistically equivalent but they conduct in the same conclusions.

Except from these cases we tried to take some piece of information from two clinical cases, one with corpus callosum agenesis and one with corpus callosum lipoma. From both case studies we could draw conclusions for the function of corpus callosum.

In our clinical practice we studied a case of a 9-year-old female patient who underwent severe hypoxia during birth with concomitant agenesis of the corpus callosum and colpocephaly, without evidence of genetic transmission. Although the coexistence of all these pathological entities the clinical picture was that of mild mental retardation.

This 9-year old female patient had been admitted to the outpatient department of the pediatric “Agia Sofia” hospital initially, as a newborn, because of severe hypoxia due to persistent embryonic circulation (patent ductus arteriosus). She was born by caesarian section after 37 weeks of gestation because of cardiac arrhythmia in the fetus.

At the age of 3 years she had be presented to the same hospital, because of an episode of febrile tonic-clonic seizures. Tonic-clonic spasms were located mostly on the left side of her body, and were accompanied by visual fixation and spasms of the right side of her mouth of ten minutes duration, and by high temperature. She underwent brain CT which revealed agenesis of the corpus callosum and colpocephaly.

The recent clinical picture is that of a hyperactive girl, with normal somatometric parameters, mild mental retardation, inability to focus, satisfactory social communication and perception, speech disorder and epilepsy treated appropriately with anticonvulsive drug therapy.

The physical examination revealed no pathologic findings no altered pain perception or sensitivity. The head circumference measurement was normal and no spinal abnormalities were observed. The results of all laboratory and genetic tests were normal. Thoracic plain x-rays revealed no further pathological findings. Ocular examination showed no edema in the eye fundus. Brain CT scan revealed agenesis of the corpus callosum, pathologic dilatation of

the occipital horns of the lateral ventricles (colpocephaly) and dilatation of the cerebellospinal cisternae, without hemispheric hypoplasia. Gray matter was situated more medial than normal, relative to the position of the midline structures.

Agenesis of the corpus callosum (ACC) is a birth defect in which the corpus callosum is partially or completely absent. It occurs when the corpus callosum fails to develop normally, typically in utero, resulting in disconnected brain hemispheres. The development of the fibers which would otherwise form the corpus callosum become longitudinally orientated within each hemisphere and form structures called Probst Bundles.

ACC can occur as an isolated condition or in combination with other cerebral abnormalities, including Arnold-Chiari malformation, Dandy-Walker syndrome, Andermann syndrome, schizencephaly and holoprosencephaly. ACC can also be associated with malformations in other parts of the body, such as midline facial defects.

The effects of the disorder range from subtle or mild to severe, depending on associated brain abnormalities. Intelligence may be normal with mild compromise of skills requiring matching of visual patterns. But children with the most severe brain malformations appear to have developmental retardation, may have also intellectual retardation, seizures, hydrocephalus, and spasticity.

Prognosis depends on the extent and severity of malformations. ACC does not cause death in the majority of children. Mental retardation does not worsen. Although many children with the disorder have average intelligence and lead normal lives, neuropsychological testing reveals subtle differences in higher cortical function compared to individuals of the same age and education without ACC.

Corpus callosum is not the only connective path between the hemispheres of the brain, but it is by far the most important. Some much smaller connections are usually present in ACC. The anterior commissure is the largest and most useful of these other pathways. However, it only has about 50,000 nerve fibers, much less of the 200 million fibers included in the corpus callosum.

Callosal dysgenesis implies a malformation of the corpus callosum originating in the embryogenesis of the telencephalon. The term ‘dysgenesis (malformation)’ includes three distinct categories: agenesis (total abscence), hypogenesis (partial formation), and hypoplasia (underdevelopment). The basis of this distinction relies on considerations about neural tube closure, formation and maintenance of the massa commisuralis inductive plate, and migration of the neuronal elements of the cerebral cortex responsible for the projection of the corpus callosum commisural fibers. These processes are somewhat interdependent in their expression resulting in a mosaic of callosal and cortical gray matter arrangement and hemispheric clinicoradiologic manifestations [10].

In our case corpus callosum agenesis was not associated with other organ malformations, but was associated with colpocephaly and an enlarged cerebellospinal cistern (figure 4).

Colpocephaly has a typical association with learning disability, seizures, motor and visual abnormalities. There are only two literature reports of genetically-transmitted colpocephaly hypothesized in identical twins [11].

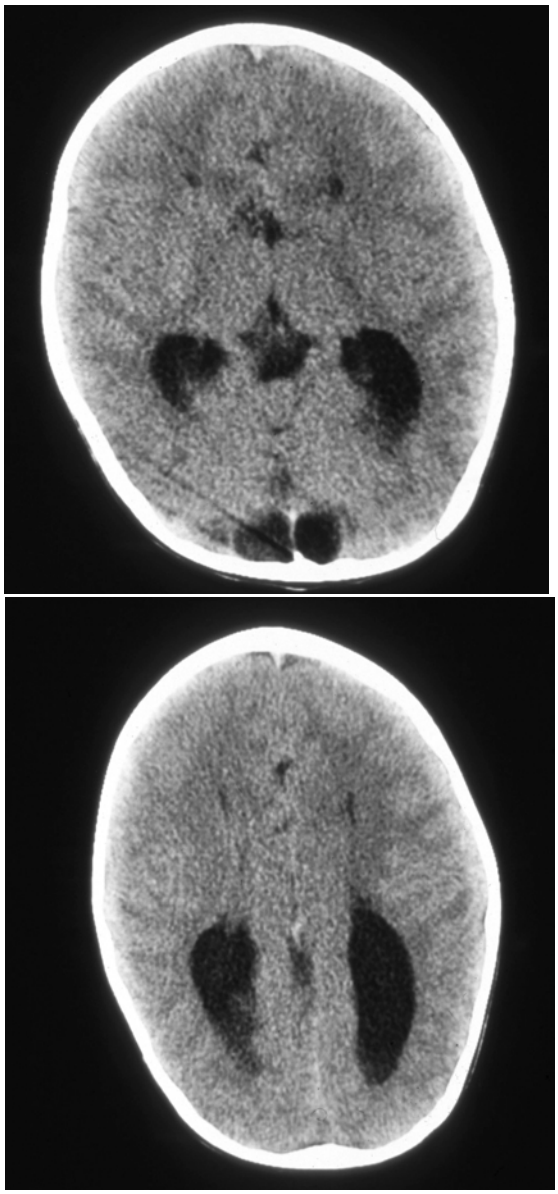

Figure 4. Agenesis of corpus callosum.

In our case there was not found evidence of genetic transmission, neither for the corpus callosum agenesis nor for colpocephaly. The child had no altered pain perception or sensitivity [12], no spinal dysraphism, no hemispheric abnormalities [13], and no abnormal head circumference [14]. Although all three pathological entities, corpus callosum agenesis, colpocephaly and brain hypoxia, have been associated with developmental delay, learning disability, seizures, and motor abnormalities, what is promising for this child is that she has not progressed over time. Furthermore, masses of gray matter on brain CT have adopted a more medial location relative to the midline structures (figures 5,6), a finding that probably

facilitates the development of extracallosal means of interhemispheric communication. Such reorganization of brain regions and interconnections already is demonstrated for the visual cortex in callosal agenesis and colpocephaly [15]. These findings may be correlated with the mild clinical picture this child. The clinical observation that the symptoms of interhemispheric disconnection are much less severe in total callosal agenesis than in partial callosal agenesis or even than what is observed after surgical section of the corpus callosum [16]. This may be of significant value in prenatal counseling.

A patient that we studied next was one with a corpus callosum lipoma.

We present a case of a rare tumor, an intracranial lipoma, diagnosed incidentally by computed tomography (CT) and magnetic resonance imaging (MRI). The lipoma was located in the midline, in the posterior part of the corpus callosum and was extending in the third ventricle. This case is reported now in order to state the incidental diagnosis of a corpus callosum lipoma extending in the third ventricle without any other callosal or cerebral anomaly. The increase use recently of advanced neuroradiological techniques such as CT and MRI for diagnosing general neurological symptoms such as memory disturbances and headaches has lead to increase incidental findings as in our case.

The patient was a 53-year-old man who was examined with brain CT and MRI because he had complained of very short duration memory loss attacks and mild morning frontal headaches. General physical findings were normal. On neurological examination he showed no neurological deficit. He had no past history of neurological symptoms. No particular problems were found in his family history. Plain radiographs of the skull were unremarkable.

Neuroimaging findings from CT and MRI studies indicated the presence of a mass under the splenium of the corpus callosum, which measured 1,3x1cm (figures 1, 2) and had the characteristic features of fatty tissue.

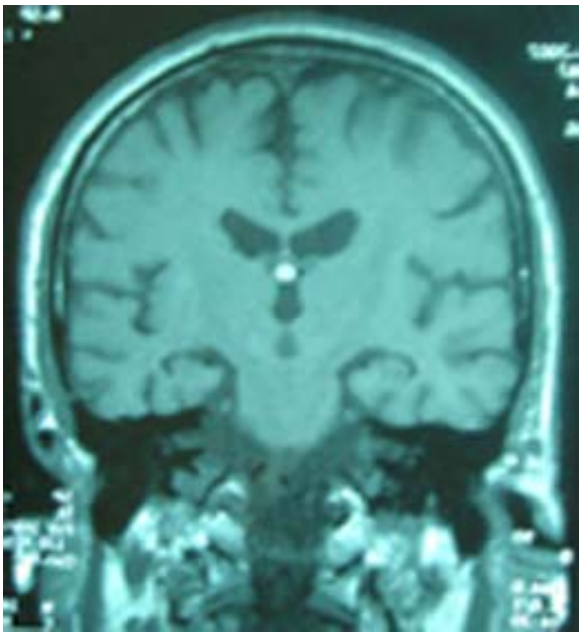

Figure 5.

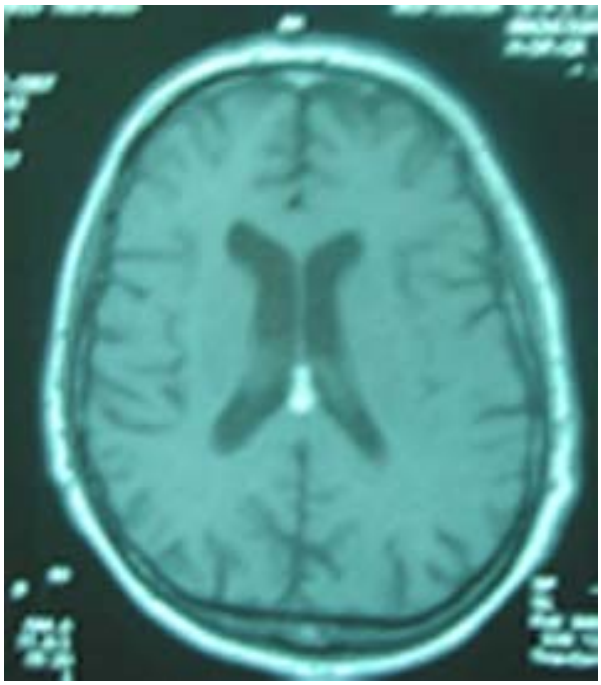

Figure 6.

The tentative diagnosis was lipoma. Conventional waking EEG was normal. Since there were no neurological problems, we advised a follow up to the patient. There was no change in the tumor size in two consecutive follow-ups of 6 months each, without epileptic seizures or neurological problems. Histological confirmation of the lesion was not obtained, since each neuroimaging technique used, offered the characteristic image of adipose tissue with a high degree of certainty.

Lipoma of the corpus callosum is a rare congenital condition. The pathogenesis of a pericallosal lipoma is considered to be the result of an abnormal resorption of the primitive meninges. Usually, this resorption occurs between the eighth and the 10th week of development. When the primitive meninge persists longer, instead of being resorbed, it differentiates into lipomatous tissue. Such lipoma may develop in all the cerebral cisternae, but they are much more frequent in the area of the corpus callosum where it interferes with its normal growth between the 11th and 20th weeks. Therefore, anomalies of the development of the corpus callosum (complete or partial agenesis, hypoplasia) almost always coexist. The degree of anomaly seems to be in relation with the size and location of the lipoma. It is often asymptomatic, but may present as epilepsy, hemiplegia, dementia, or headaches.

Intracranial lipoma is a rare congenital malformation and not true neoplasm that results from abnormal persistence and maldifferentiation of the meninx primitive, the mesenchymal precursos of lepotomeninges, during the development of the subarachnoid cisterns (17,18,19). It accounts for 0.1-0.5% of all primary brain tumors (20,21). Intracranial lipoma frequently develops in the supratentorial midline region, mostly in the corpus callosum (40-50%) and is associated with varying degrees of dysgenesis of corpus callosum (20,22). Other sites where they have been reported include the choroids plexus, the quadrigeminal,

interpendicular, ambient and cerebellopontine cisterns (22,23); as well as the spinal cord. It can be complicated with other malformations such as, encephalocele, agenesis of vermis, cranium bifidum and absence of septum pellucidum (24).

To see that a lipoma is entering the ventricular system is even rare. We describe this case of callosal lipoma extending in the third ventricle without agenesis of corpus callosum in order to denote that this rare finding was incidental.

Lipomas occur in most parts of the body but intracranial lipomas are extremely rare. Several hypotheses have been proposed for the aetiology of intracranial lipomas (25, 26). The most widely accepted explanation is that there is a true congenital or developmental disorder in the resorption of meninx primitiva, which persists and subsequently differentiates into fatty tissue. Meninx primitiva is the primitive meningeal tissue, which embryologically fills the potential subarachnoid cisterns and normally resorbes and in this way produces the subarachnoid spaces.

Although it is a separate entity, it is almost always associated with dysgenesis or agenesis of corpus callosum(50%), craniofacial anomalies and encephalocele. But, our case exhibited none of these anomalies.

Most patients with isolated intracranial lipomas are asymptomatic. The curvilinear calllosal lipomas are usually asymptomatic, whereas the tubulonodular lipomas commonly situated in the anterior or posterior callosum are more frequently symptomatic (27). Symptomatic intracranial lipomas are very rare, and symptoms differ according to the location of the lipoma (28). Epilepsy occurs in 30-50% of the cases, while hemiparesis, headache, psychic or mental retardation are common (20,21).

Intracranial lipomas are generally treated conservatively (29) for the symptoms they cause because surgical removal yields poor results with almost 50% mortality in the immediate postoperative period (30). They show little neoplastic proliferation and are too difficult to extirpate totally due to their deep location, vascularity and strong attachment to the surrounding structures (21, 31). The resection is indicated once there are manifestations of compression by the tumour and symptoms specific to lipoma. In the present case, the intracranial lipoma did not cause any manifestations of compression

Because asymptomatic lipomas can become symptomatic, follow-up of this tumour is essential (32). In our case, after one year follow up the patient became asymptomatic and is still alive. The symptoms were transitory and we consider that it is unlikely that they were caused by the callosal lipoma.

Prognosis depends mainly on the associated malformations and the symptoms a lipoma causes. The prognosis is very good for patients with isolated lipoma of the corpus callosum. If other anomalies are encountered, the prognosis is variable.

This incidental diagnosed intracranial lipoma was found because of the use of developed neuroimaging techniques for diagnosing the aetiology of headache and memory loss attacks.

Conclusions

By applying these ratios to radiological images of patients, the neurosurgeons would perform the targeted callosal procedures in a more precise way.

The anatomical parts of CC have a stable proportion to each other; and the position of CC within the brain is stable, mostly in its horizontal position. Brain retains its symmetry but does not influence the size and position of CC. Stable proportions, ratios and resulting analogies, when applied on MRI images, could facilitate the planning of callosal interventions for intractable epilepsy or other targeted neurosurgical procedures.

References

[1] Goncalves-Ferreira AJ, Herculano-Carvalho M, Melancia JP, Farias JP, Gomes L. Corpus callosum: Microsurgical anatomy and MRI. *Surg. Radiol. Anat.* 2001; 23: 409–414.

[2] Aboitiz F, Scheibel AB, Fisher RS, Zaidel E. Fiber composition of the human corpus callosum. *Brain Res.* 1992; 598: 143–153.

[3] Estruch R, Nicolas JM, Salamero M, Aragon C, Sacanella E, Fernandez-Sola J, Urbano-Marquez A. Atrophy of the corpus callosum in chronic alcoholism. *J. Neurol. Sci.* 1997; 146: 145–151.

[4] Cowell PE, Allen LS, Kertesz A, Zalatimo NS, Denenberg VH. Human corpus callosum: a stable mathematical model of regional neuroanatomy. *Brain Cogn.* 1994; 25: 52–66.

[5] Morino M, Shimizu H, Ohata K, Tanaka K, Hara M. Anatomical analysis of different hemispherotomy procedures based on dissection of cadaveric brains. *J. Neurosurg.* 2002; 97: 423–431.

[6] Bishop KM, Wahlsten D. Sex differences in the human corpus callosum: Myth or reality? *Neurosci. Biobehav. Rev.* 1997; 21: 581–601.

[7] Kawamura T, Nishio S, Morioka T, Fukui K. Callosal anomalies in patients with spinal dysraphism: correlation of clinical and neuroimaging features with hemispheric abnormalities. *Neurol. Res.* 2002; 24: 463–467.

[8] Driesen NR, Raz N. Sex-, age- and handedness-related differences in human corpus callosum observed in vivo. *Psychobiology.* 1995; 23: 240–247.

[9] Kertesz A, Polk M, Howell J, Black SE. Cerebral dominance, sex and callosal size in MRI. *Neurology.* 1987; 37: 1385-1388.

[10] Jinkins JR, Whitemore AR, Brandley WG MR imaging of callosal and corticocallosal dysgenesis *AJNR Am. J. Neuroradiol.* 1989 Mar-Apr; 10(2): 339-344

[11] Cerullo A, Marini C, Cevoli S, Carelli V, Montagna P, Tinuper P Colpocephaly in two siblings: further evidence of genetic transmission. *Dev. Med. Child. Neurol.* 2000 Apr; 42(4): 280-282

[12] Doherty D., Tu S., Schilmoeller K., Schilmoeller G. Health-related issues in ndividuals with agenesis of the corpus callosum Child: *Care, Health and Development,* Volume 32 Page 333-May 2006

[13] Kawamura T.; Nishio S.; Morioka T.; Fukui K. Callosal anomalies in patients with spinal dysraphism: Correlation of clinical and neuroimaging features with hemispheric abnormalities. *Neurological Research,* Volume 24, Number 5, July 2002, pp. 463-467(5)

[14] Chen Chih-Ping; LIN Shuan-Pei ; CHIU Nan-Chang ; Microcephaly with dysgenesis of corpus callosum and colpocephaly in the survivor after the first-trimester death of a monochorionic co- twin. *Prenatal diagnosis.* 2002, vol. 22, n°7, pp. 634-636

[15] Bittar RG, Ptito A, Dumoulin SO, Andermann F, Reutens DC. Reorganisation of the visual cortex in callosal agenesis and colpocephaly. *Journal of Clinical Neuroscience.* (2000) 7(1), 13-15

[16] Aglioti S, Beltramello A, Tassinari G, Berlucchi G Paradoxically greater interhemispheric transfer deficits in partial than complete callosal agenesis. *Neuropsychologia.* 1998 Oct; 36(10): 1015-24

[17] Fitoz S, Atasoy C, Erden I, Akyar S. Intracranial lipoma with extracranial extension through foramen ovale in a patient with encephalocraniocutaneous lipomatosis syndrome. *Neuroradiology*. 44:175-178, 2002

[18] Ichikawa T, Kumazaki T, Mizumura S, Kijima T, Motohashi S, Gocho G. Intracranial lipomas: demonstration by computed tomography and magnetic resonance imaging. *J. Nippon. Med. Sch.* 67:388-391, 2000

[19] Yilmaz N, Unal O, Kiymaz N, Yilmaz C, Edik O. Intracranial lipomas: a clinical study. *Clin. Neurol. Neurosurg*. 108:363-368, 2006.

[20] Donati F, Vassella F, Kaiser G, Blumberg A. Intracranial lipomas. *Neuropediatrics.* 23:32-38, 1992

[21] Eghwrudjakpor PO, Kurisaka M, Fukuoka M, Mori K. Intracranial lipomas: current perspectives in their diagnosis and treatment. *Br. J. Neurosurg*. 6:139-144, 1992

[22] Truwit CL, Barkovich AJ: Pathogenesis of intracranial lipoma: an MR study in 42 patients *AJR Am. J. Roentgenol.* 155: 855-865, 1990

[23] Kash F, Brown G, Smirniotopoulos JA, Boyer R, Osborn AG Intracranial lipomas: Pathology and imaging spectrum. *Int. J. Neuroradiol.* 1996; 2:109-116.

[24] Zettner A, Netsky M. Lipoma of the corpus callosum. *J. Neuropathol. Exp. Neurol.* 1960; 19: 305-319

[25] Sasahira M, Uchimura K, Okada A, Fujimoto T, Kawahara Y, Asakura T. Intracranial lipoma, with special reference to magnetic resonance imaging: a case report. CT Kenkyu. 11: 205-210, 1989

[26] Zee CS, McComb JG, Segall HD, Tsai FY, Stanley P. Lipomas of the corpus callosum associated with frontal dysraphism. *J. Comput. Assist. Tomogr.* 5: 201-205, 1981.

[27] Demaerel Ph., Van de Gaer Ph., Wilms, G., Baert A. L. Interhemispheric lipoma with variable callosal dysgenesis: relationship between embryology, morphology, and symptomatology. *European Radiology,* Volume 6, Number 6 , December 1996

[28] Kurt G, Dogulu F, Kaymaz M, Emmez H, Onk A, Baykaner MK. Hypothalamic lipoma adjacent to mamillary bodies. *Childs Nerv. Syst*. 18: 732-734, 2002

[29] Given CA, Fields TM, Pittman T. Interhemispheric lipoma connected to subcutaneous lipoma via lipomatous stalk. *Pediatr. Radiol.* 35:1110-1112, 2005.

[30] Yock DH. Choroid plexus lipomas associated with lipoma of the corpus callosum. *J. Comput. Assist. Tomogr*. 1980; 4: 78-82.

[31] Gerber SS, Plotkin R. Lipoma of the corpus callosum: case report. *J. Neurosurg.* 57: 281-285, 1982.

[32] Haga HJ, Thomassen E, Johannesen A, Krakens J. Neural compressive symptoms appearing during steroid treatment in a patient with intracranial lipoma. *Scand. J. Rheumatol.* 28:184-186, 1999.

In: Handbook on White Matter
Editors: T. B. Westland and R. N. Calton
ISBN: 978-1-60741-034-8

Chapter XII

White Matter Abnormalities in the Diabetic-Hypertensive Brain

***Natalia Rincon*[a] *and Cory Toth*[b]**
[a]University of Calgary,
[b]University of Calgary and Hotchkiss Brain Institute, Alberta, Canada

Abstract

White matter fills nearly half of the brain, but receives disproportionately less scientific attention when compared to grey matter. For the past century, neuroscientists have demonstrated little interest in white matter, thought to be simply insulation for the more important axonal pathways contained within. The importance of white matter in learning tasks, mastering and executing mental and physical activities, as well as perfecting mental and social skills has become clearer over the recent decades. Much of this realization has developed from the study of diseases predominantly affecting white matter, and therefore disrupting intraneural communication, such as with multiple sclerosis and the leukodystrophies.

Two diseases that have reached epidemic status—diabetes and hypertension—also contribute to white matter disease. The mechanisms by which these two common disorders affect white matter remain under study and may share commonalities but also disparities. Interestingly, the human condition of white matter abnormalities in patients with diabetes and/or hypertension can be modeled in rodents, with the hope that this will lead to future understanding and management.

Keywords: white matter abnormalities, diabetes mellitus, hypertension

Abbreviations

advanced glycation end products	AGEs
Alzheimer's disease	AD

apparent diffusion coefficient	ADC
computerized tomography	CT
cyclic AMP response element binding protein	CREB
diabetes mellitus	DM
diffusion tensor imaging	DTI
electrophoretic mobility shift assays	EMSA
fractional anisotropy	FA
glycogen synthase kinase 3β	GSK-3β
inhibitory subunit κB	IκB
magnetic resonance imaging	MRI
nuclear factor κB	NFκB
phosphoinositide 3-kinase	PI3K
receptor for advanced glycation end products	RAGE
soluble RAGE	sRAGE
spontaneously hypertensive rat	SHR
white matter abnormalities	WMA
Wistar–Kyoto	WKY
Zucker Diabetic Fat	ZDF

Role of Imaging

It was the introduction of computerized tomography (CT) scanning in the 1970s that first led to detection of cerebral white matter disease, followed by the subsequent and substantial introduction of magnetic resonance imaging (MRI) in the 1980s. These interventions led to the discovery of largely unexpected changes within the cerebral white matter for both asymptomatic and symptomatic individuals. Since that time, these changes have been described using numerous terms—white matter abnormalities (WMA), cerebral white matter changes, unidentified bright objects, or leukoaraiosis—to refer to all white matter changes visible on neuroimaging studies. For this work, we will refer to these changes as WMA.

WMA are frequently detected on T2-weighted MRI of the brain, especially in more senior adults. Partly due to their ubiquitous appearance in the elderly, there remains uncertainty concerning their clinical relevance. Up to 80 percent of MRI scans performed in persons older than 65 years have demonstrable WMA changes in their cerebral white matter (1). In this population, the presence of WMA was associated with increased relative risk for stroke and the presence of retinal microvascular abnormalities, first indicating their potential for pathogenic association. Women may have more subcortical WMA than men, particularly in frontal regions, and also more periventricular WMA, although no statistical significant difference has been shown (2).

However, the use of imaging to detect white matter signal abnormalities as a clinically relevant measure of white matter pathology remains controversial due to studies which have failed to demonstrate consequences upon clinical state (3, 4) Additionally, the use of white matter volume measures are limited due to the need to define regionally identifiable borders using morphometry landmarks, a particularly difficult task given the complex anatomy of

white matter and the limited information provided from a standard structural MR image. For this reason, other MR modalities have become important in the assessment of WMA. Diffusion tensor imaging (DTI) has been applied extensively to understand the regional basis of white matter in a variety of clinical conditions including the study of normal aging (5) (6) (7, 8). DTI is based upon the ability to measure characteristics of water diffusion, such as fractional anisotropy (FA), apparent diffusion coefficient (ADC) and diffusion direction (principle eigenvector). Water molecules more readily diffuse along the major axis of the fiber bundle rather than perpendicular to it (9), permitting the in vivo visualization of white matter tracts (10). The FA value depends upon the integrity of axons and their myelin sheaths, therefore degeneration of neural tracts can be detected by measurement of FA values (11). DTI uses both axial and radial components, which could provide selective information on axonal and myelin pathology (12).

Changes in diffusion measures have been demonstrated in white matter regions in patients with AD and in subjects with mild cognitive impairment (13). There have been differences in conclusions regarding white matter pathology in DTI studies, with some studies concluding that compromised myelin occurs (14) while others suggest a loss of axonal processes (15).

In patients with long-standing type 1 diabetes, DTI revealed reduced mean FA for white matter tracts including the posterior corona radiata and the optic radiation as compared to control subjects. In addition, reduced FA also correlated with duration of diabetes and an increased hemoglobin A1C, but not with episodes of severe hypoglycemia (16). In patients with untreated hypertension, impaired executive functioning and attention is related to DTI mean diffusivity values (17). Future studies utilizing DTI in patients with diabetes and hypertension, as well as studies of the rodent brain, are underway.

Clinical Role and Detection of General WMA

Although earlier papers did not find an association between WMA and cognitive decline, a more clear picture has emerged with positive association between the two (18, 19); (20) (21) (22). WMA presence has been associated with slowing of processing speed, psychomotor functioning, memory deficit, problems with executive function (23), and global functioning of cognition (24). In particular, the presence of WMA and periventricular leukomalacia have been associated with a decline in Wechsler Performance IQ scores, Block Design, Object Assembly, and Digit Symbol tests in older adults, with greater decline related to higher numbers of WMAs (25).

The degree of WMA present are associated with overall cognition, independent of childhood cognitive ability, for subjects aged 11–78 years (26). Hypertension may have accounted for at least a portion of WMA effects in this study across multiple age groups. In general, normal subjects do not appear to have cognitive testing abnormalities in the presence of leukoaraiosis (27) (28) (29) (30). However, when multivariate analysis is performed with controls for age, sex, educational level and presence of stroke on imaging, WMA identified during CT imaging correlate with lower neuropsychological scores in normal subjects (31). WMA-related cognitive deficits can be identified in functions such as memory and executive

functioning, and associated abnormalities in gait and balance dysfunction (24) (23, 32). White matter abnormalities disrupt prefrontal-subcortical loops involved in frontal lobe executive control (33). In addition, these WMA locations isolate structures within the grey matter, such as in the medial temporal lobe (34), contributing to cognitive dysfunction.

Although such clinical deficits can be detected, neuroimaging remains the most valuable tool for the detection of WMA, even in otherwise normal subjects. The added sensitivity that MRI provides has also identified more severe WMA in normal volunteer subjects to be related to a significant impairment in cognitive and neurobehavioral functioning when compared to those subjects without WMA (35) (36) (37). A threshold effect may exist for the volume of abnormal white matter before subtle but significant changes in cognition may be detected; in one MRI study, subjects with summation of WMA greater than 10 cm2 had impairment of attention, processing speed, and frontal lobe functioning (38). Therefore, even in subjects without diabetes or hypertension, WMA accumulation plays a role in cognitive decline.

In addition to cognitive changes as described, gait disturbance and susceptibility to falling has been associated with the presence of WMA, likely secondary to disruption of subcortical brain pathways. In elderly males, greater than median volumes for WMA lead to poor performance with standing balance tests, with an additive effect of ApoE ε4 positivity (39). Abnormal age-related decreases in white matter volume and age-independent increases in WMAs correlate with impairment of gait and balance in a mobility-impaired elderly group when compared with an age-controlled control group (40). As well, frequency of WMA also relate to the occurrence of falls in an elderly population (41).

Pediatric subjects are not immune to the potential clinical effects of WMA and related deficits in white matter volume. Children aged five years of age or younger who underwent MRI with demonstration of white matter changes were investigated for abnormalities in muscle tone and muscle stretch reflexes, and found to have increased tone and tendon reflexes in the presence of more MRI signal abnormalities (42). Thus, such WMA are related to the presence of spasticity (42). Other examination findings possibly found in young patients with WMA include positive extensor plantar reflexes and the presence of primitive reflexes, related to subcortical brain region legions. Other clinical signs predictive of the presence of periventricular WMA on MRI include abnormal three-step motor sequencing and horizontal extraocular tracking tests (43). Although such WMA changes would not be anticipated to be due to diabetes or hypertension in a pediatric population, identification of dysfunction related to WMA in children signifies that association of dysfunction with WMAs is largely a non-specific effect of multiple pathways.

Definition of Diabetes

Diabetes mellitus (referred to as diabetes) is of two types, both of which are characterized by abnormally high glycemic levels, or hyperglycemia. Type I diabetes develops as a result of T-cell mediated autoimmune attack upon insulin-producing pancreatic beta cells of the islets of Langerhans (44, 45), leading to decreased insulin production. The onset of Type I diabetes generally occurs during childhood, leading to the title of juvenile

diabetes, but type 1 diabetes may also affect adults. There are no known preventive measures against type I diabetes. The main treatment for Type I diabetes mellitus is replacement of insulin combined with careful monitoring of glycemic levels. Experimental therapies such as immunosuppression with monoclonal antibodies (46) and stem-cell based therapies (47) have not yet entered routine clinical practice.

Type II diabetes mellitus occurs due to insulin resistance or reduced insulin sensitivity. The cellular response to insulin is inappropriate, associated with elevated levels of insulin initially followed by reduced levels of insulin in later stages of the disease. Hyperglycemia is managed by a combination of diet, exercise, and pharmacotherapies which improve insulin sensitivity or reduce hepatic gluconeogenesis. The causes and associations of type II diabetes are complex and numerous. Chronic obesity leading to increased insulin resistance is the most common association, although co-occurrences with hypertension, elevated cholesterol, heredity, and aging also occur (48). Type II diabetes has a later onset in life than Type I diabetes, being most common in middle-later age adults. Unlike Type I diabetes, Type II diabetes may be overlooked for years due to insidious onset, absence of ketoacidosis and lack of visible symptoms, which can lead to long term severe complications after years of lack of recognition.

Definition of Hypertension

Hypertension is a chronic elevation in blood pressure, often idiopathic in nature. Hypertension is typically defined as a blood pressure greater than 140/90 mm Hg, but in the presence of diabetes, the threshold is lowered to 130/85. Chronic hypertension predisposes individuals to heart failure, cerebral stroke, myocardial infarction, and renal failure. As with type II diabetes, hypertension is often insidious as well, and is asymptomatic. There are several factors associated with development of hypertension including obesity, excessive alcohol consumption, a high sodium diet, familial tendencies, and aging.

Etiologies of WMA

Normal Subjects

Amongst otherwise “normal” elderly subjects, differences in cardiovascular risk factors over the course of 25 years of adult life appear to influence WMA. In particular, abnormalities in midlife glucose levels, high-density lipoprotein cholesterol, and systolic blood pressure are associated with differences in WMA volumes, which in turn are significantly associated with differences in performance on cognitive and physical function tests (49). Such results are suggestive that such cardiovascular risk factors are important upon cerebral function even in subjects felt to be “normal”. When both dizygotic and monozygotic male twins were investigated with MRI and neuropsychological testing, genetic influences also appeared to explain about two thirds of the variability in cognitive functioning and impaired performance in cognitive function (50).

"Normal" Elderly Subjects

Aging has a large effect on both the frequency and the severity of CT- and MRI-identifiable WMAs, and is likely an independent risk factor on its own. Additional risk factors identified in various multivariate analytical studies have included a history of stroke, male sex, hypertension, diabetes and heart disease (51). The presence of WMA within "normal" brains tends to occur in temporal and occipital areas, and is associated with greater age, hypertension, late-onset depressive disorder and perhaps poor global cognitive function (52). Even in high-functioning older adults without evidence of stroke or dementia, gait abnormalities such as slowed speed, shortened stride and greater support time have a positive association with presence of WMA on MRI (53). Accumulation of these lesions can be observed using sequential MRI scans, which have demonstrated a five-fold acceleration in the accumulative volume of WMAs in mobility-impaired subjects (54). In addition to the presence of WMAs, longitudinal analysis in elderly subjects without dementia has determined that other brain MRI abnormalities occur and progress, such as ventricular enlargement and subclinical small brain infarcts. These changes are likely to also contribute to poor motor performance and faster gait speed decline over time, (55) and are difficult to separate from WMA in many studies of elderly subjects.

Alzheimer's Disease

In a population of Alzheimer's Disease (AD) patients, brain atrophy may remain the most important factor for cognitive outcome, but presence of WMA relate to impaired short-term memory/language, reduced mental flexibility or poor short-term and working memory depending upon their physical location (56). Recently referred to as "Type III diabetes" due to abnormal level of insulin and its receptor machinery, (57) the brain in AD can also be subjected to the presence of WMA. It has been speculated that such findings may be associated with presence of cerebral congophilic angiopathy (58, 59), but this remains unclear. In particular, older AD patients have greater levels of periventricular, lobar white matter and basal ganglia WMA on MRI when compared to a control group, whereas younger-onset AD patients do not have similar WMA changes present. (60). WMA in AD patients have preferential involvement of the frontal lobes (61), associated with a general decline in cognition. However, in age controlled non-demented subjects, such decline is not evident (62). In AD patients, such WMA can also be associated with urinary bladder incontinence, presence of grasp reflex and abnormal motor examinations (63).

Even in AD patients, vascular risk factors contribute to risk of WMA development. The elevation of homocysteine is another vascular risk factor for WMA presence on CT scanning (64), particularly over deep white matter regions. Hypertension, along with elevations in pulse pressure, also correlate with presence of WMA in AD patients (65). Finally, patients with diagnoses of both type 2 diabetes and AD have greater cortical atrophy identified on MRI when compared to patients with AD alone. Even though infarcts are more common in Alzheimer's patients with type 2 diabetes, ischemic disease could not be used to explain the

identified increase in atrophy, suggesting that non-vascular mechanisms are contributing to increased cortical atrophy associated with diabetes (66).

Pathologically, up to 60% of AD patients demonstrate demyelination in addition to axonal and oligodendroglial loss with accompanying gliosis in deep white matter, separate from more commonly described gray matter changes (67) (68-70). Such white matter changes in the AD brain may also occur in the absence of documented vascular disease (71). It is possible that age-related myelin breakdown and vulnerable oligodendrocytes may play a role in the development of AD with or without the presence of hypertension and/or diabetes (72). In patients with AD in whom WMA could be detected during life have a substantial loss of oligodendrocytes when compared with age-matched controls (73). This loss may occur independently of the severity of cortical involvement from AD (67, 73). In fact, [7] A. Brun and E. Englund, A white matter disorder in dementia of the Alzheimer type: a pathoanatomical study, *Ann Neurol 19* (1986), pp. 253–262. Full Text via CrossRef | View Record in Scopus | Cited By in Scopus (341) quantitative presence of WMA in AD patients appears to be greatest in frontal white matter, in contrast to localization of more typical cortical AD pathology in the posterior portions of the brain (74).

Diabetes

Diabetes has been associated with the presence of both cerebral atrophy and WMA. Even in patients not diagnosed with diabetes, elevated glycated hemoglobin levels, such as found in patients with diabetes or impaired glucose tolerance, are associated with MRI-identified WMA in non-demented elderly patients (75). Diabetic subjects possess significantly more deep WMA, with or without hypertension, when compared to non-diabetic subjects undergoing MRI (76). Not only is type II diabetes associated with deep WMAs, but it is also associated with both cortical and subcortical atrophy and impaired cognitive performance (attention and executive function, information-processing speed, and memory) (77).

The most common locations for diabetes-associated WMA are in the caudate and putaminal nuclei, internal capsule, thalamus, dentate nucleus, supratentorial white matter, and brainstem (78). Diabetic-associated WMA are also a risk factor for stroke, cognitive deficits such as memory and executive functioning, and abnormalities in gait and balance dysfunction (79) (80). In the diabetic brain, periventricular brain regions are predominantly affected with increased T2-weighted MRI signals, speculated to be due to changes in periventricular fluid dynamics with a disrupted subependymal lining (81). There are no well-founded clinical hypotheses regarding the development of diabetes-associated WMA, but rodent models (below) have provided some insight.

Hypertension

Hypertension is commonly associated with presence of WMA, whether they are demonstrated in patients with co-existing stroke, transient ischemic attack or vascular dementia, or in asymptomatic control subjects. In addition, the presence of WMA on CT is

strongly associated with presence of lacunar infarcts and intracerebral hemorrhage (82, 83), both of which occur in the presence of hypertension. Patients with hypertension have more WMA than non-hypertensive controls or hypertensive patients in whom blood pressure was controlled with antihypertensives (84).

When AD patients receiving MRI are subsequently examined for hypertension, the presence of WMA is predictive for those subjects to be later discovered to have hypertension (85). To increase the complexity, genetic factors may play a role, as the presence of a positive family history of stroke or hypertension in first degree relatives is also significantly associated with the presence of WMA in AD patients (86). As with diabetes, there are no substantiated hypotheses regarding hypertension-mediated WMA development, but animal models have provided some initial insight (below).

Pathogenesis

Initially postulated to result from changes in periventricular fluid dynamics, (24, 87) (23) vascular border zone hypoperfusion or subclinical ischemia (88-90), neuronal loss and axonal degeneration (23, 24, 87, 91) or abnormalities in the blood-brain barrier and cerebrospinal fluid dynamics (23, 24, 87-91), there has been no defined single cause for WMA in the human brain. Although WMA in the human thalamus and basal ganglia have been hypothesized to represent ischemia or perivascular spaces, pathological changes within such regions containing WMA demonstrate regions of myelin pallor with a relative loss of axons, myelinated fibers, and oligodendrocytes (23, 24, 74, 87-89, 92-97). Overall, there are scarce pathological studies of the human brain to adequately determine the pathogenesis of human WMA.

Toth et al. have described an animal model of diabetes with cerebral abnormalities (98) where cognitive decline, cerebral atrophy, and WMA were identified. In a type I diabetic model induced by streptozotocin injection to diminish pancreatic production of insulin, such diabetic brain changes were associated with a striking upregulation of the Receptor for Advanced Glycation End Products (AGEs), named RAGE (see below) (99). Although AGEs are toxic on their own, their interaction with RAGE activates several important signaling pathways detrimental in the diabetic brain. Interestingly, diabetic RAGE null mice are protected from cerebral atrophy and WMA when compared to wildtype diabetic mice Figure 1. Although many hypotheses regarding WMA centre around vascular changes, pathological changes in both wildtype and RAGE null diabetic mice are not associated with vascular endothelial changes (98), raising new questions regarding the non-vascular etiology of WMA in the experimental diabetic brain.

One potential pathophysiological mechanism for WMA is loss of oligodendrocyte function. Recent post-mortem data (100-104) and *in vitro* (105) demonstrate that myelin loss and oligodendrocyte degeneration may be important features in AD and in brains subjected to diabetes and/or hypertension. It is known that apoptotic pathways are active in neurons of the AD brain (106), and oligodendrocytes may also degenerate via apoptosis, but comparably little is known about their plight in either AD or diabetes/hypertension.

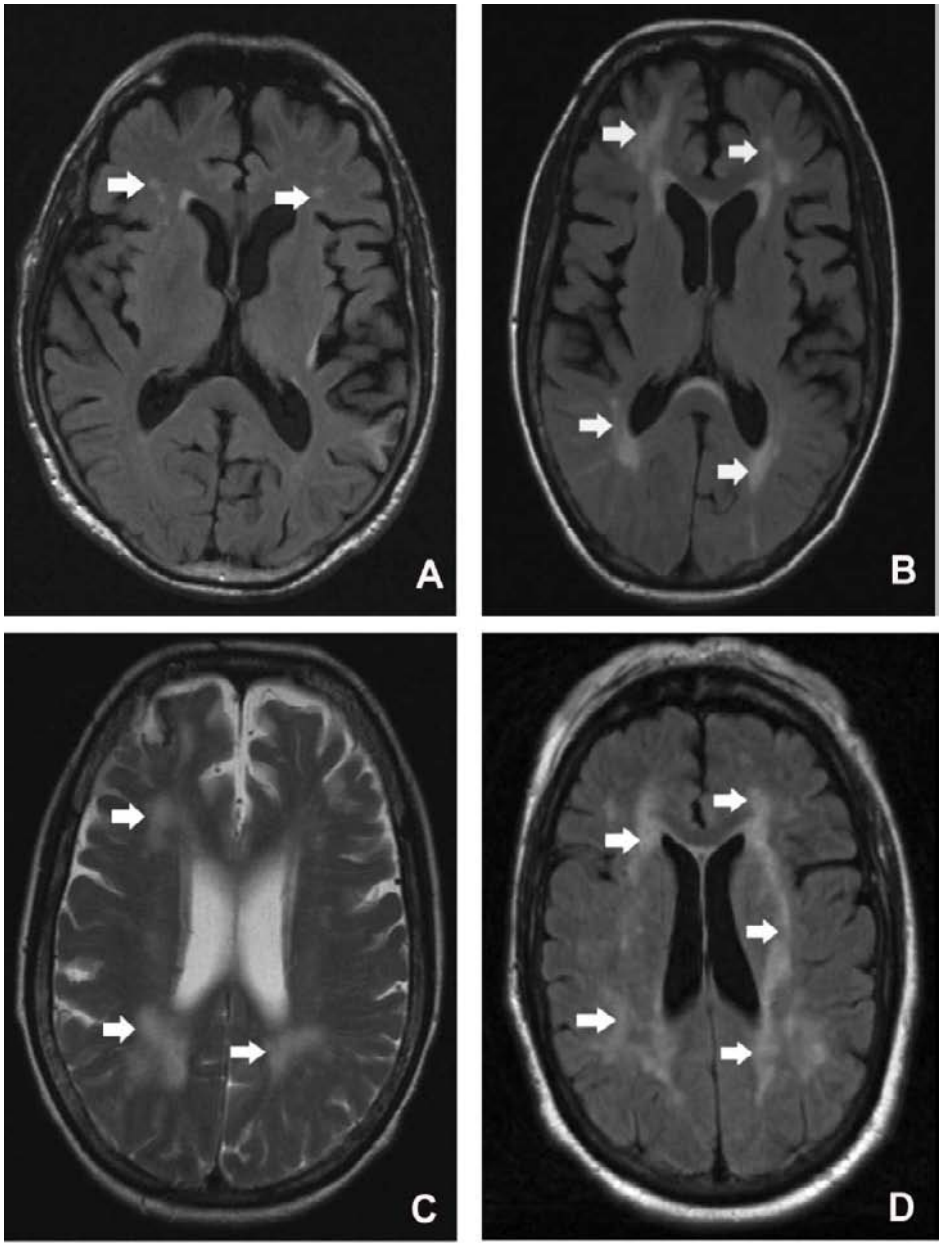

Figure 1. LAIR and T2 MRIs demonstrating white matter abnormalities in patients with diabetes and hypertension. Subfigure A demonstrates a FLAIR MRI with mild but detectable white matter abnormalities over periventricular locations as well the right anteroinferior corona radiata (arrows) in the brain of a patient with poorly controlled hypertension and gait abnormality. The middle image (B) illustrates more easily detected WMA using FLAIR MRI technique in a patient with poorly managed diabetes mellitus and cognitive decline. While C demonstrates the T2 MRI findings in a patient with poorly managed diabetes mellitus combined with hypertension presenting with cognitive decline, subfigure D demonstrates the same brain using FLAIR technique with abnormalities more easily detected.

Oxidative stress contributes to primary rat oligodendrocytes degeneration *in vitro* (107). Within oligodendrocytes, H_2O_2 induces fragmentation of DNA, loss of expression of myelin-specific genes, increased expression of the *bcl-2* anti-apoptotic gene, and nuclear condensation and chromatin margination, all features consistent with apoptosis (108). Oxidative damage to mitochondrial DNA (109) may occur as well, in relationship to Aβ protein (105). The induction of the redox-sensitive transcription factors, nuclear factor (NF) κB and activator protein (AP)-1 also play an important role (105, 108). When such mitochondrial pathways are stressed, cytochrome *c* release occurs, followed by its binding to cytoplasmic apoptosis protease activating factor-1 (Apaf-1), which subsequently leads to recruitment and activation of pro-caspase 9 (110, 111). Activated caspase 9 then cleaves and activates caspase 3, which is the best-established apoptosis-associated caspase. The presence of activated caspase 3 in oligodendrocytes in human post-mortem brains exposed to AD or diabetes/hypertension has not yet been established, although this process occurs in neurons of the AD brain (112).

As oligodendrocytes degenerate, iron is released which may promote maturation of oligodendrocyte precursor cells, which may possibly replace lost cells (74). Iron loss from dysfunctional oligodendrocytes (113, 114) may accelerate neuronal production of reactive oxygen species, which may lead to accumulation of amyloid plaques and tangles in the AD brain (115-117). Agents maintaining mitochondrial function may be promising as potential therapies, including Vitamin E and the iron chelator, deferoxamine (108).

Diabetes and the Experimental Brain

Models of long-term experimental diabetes have also demonstrated changes analogous to the human condition, with development of brain atrophy, WMA, and cognitive decline including slowed memory processing. We have used models of type I and type II diabetes in rodent models to assist in determining the pathogenesis of diabetes-mediated WMA. In addition, we have recently studied rodent models of hypertension as well.

The streptozotocin mouse model is analogous to type I diabetes due to destruction of the pancreatic β islet cells. One important mechanism for the development of brain atrophy and WMA in these mice is the presence of deposited Advanced Glycation End Products (AGEs) and their interaction with their receptor (RAGE). Chronic hyperglycemia stimulates the formation of these unstable, reactive AGEs via the Maillard reaction between carbohydrates and biological molecules such as free amino acids or proteins, generated with glycation, or as an end product of lipid oxidation (118). AGEs are toxic and are formed in excess during aging, diabetes mellitus and renal failure (118). RAGE is a multi-ligand member of the immunoglobulin superfamily of receptors. It contains an extracellular region with one V-type and two C-type immunoglobulin domains, a hydrophobic transmembrane domain and a highly charged short cytosolic tail, essential for intracellular signaling (118) (Figure 2) Under normal physiological conditions, RAGE expression is ubiquitous, but under hyperglycemic conditions, such as in diabetes mellitus, AGEs accumulate along with the subsequent propagation of RAGE. Glucose levels are increased up to thirty-fold within the hippocampus of diabetic rats, contributing to AGE accumulation in the diabetic brain (119). Ligation of

AGEs to RAGE results in cell activation leading to increased expression of extracellular cytokines, formation of reactive oxygen species (120, 121), and activation of key cell signaling pathways including the activation of nuclear factor-κB (NFκB) (98, 122).

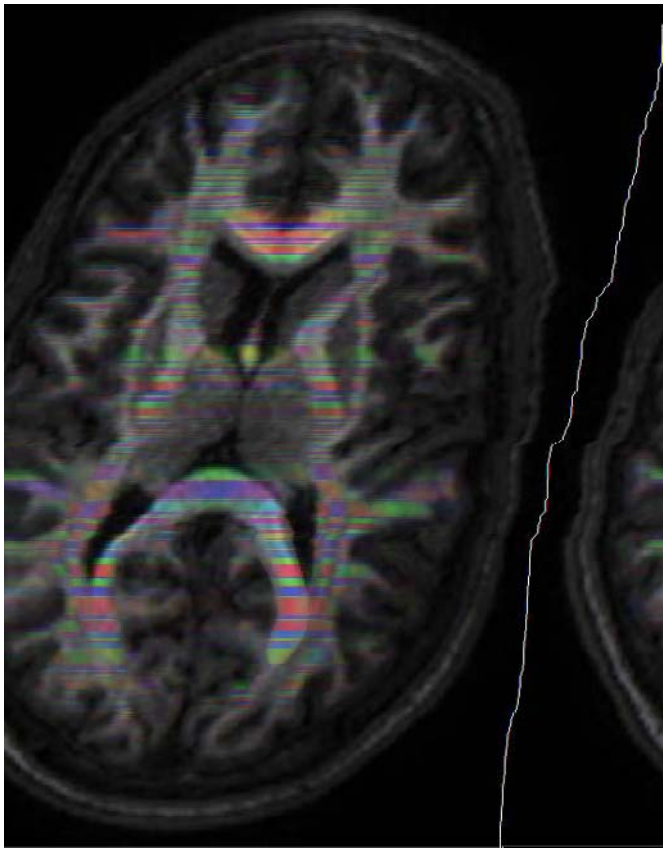

Figure 2. Diffusion tensor imaging (DRI) using MRI showing the distribution of white matter pathways in a normal subject's brain. In this image, red color indicates those white matter pathways travelling left to right, blue superior to inferior, and green anterior to posterior. Such imaging techniques will be important in the future detection of white matter abnormalities.

During the latter portion of 8 months of diabetes, diabetic mice demonstrate cognitive deficits in visuospatial and procedural tasks (98, 123, 124) (Figure 3). Concurrent development of brain atrophy and WMA identified with both MRI T2 and magnetization transfer (MT) imaging as well as with structural examination of myelination occurs (98, 124). Abnormally high RAGE expression has been detected in grey matter areas including hippocampus, and cortex, but also in white matter regions such as corpus callosum and internal capsule in diabetic mice. Higher RAGE expression is identified amongst neuronal and glial cells including astrocytes, oligondendrocytes and microglia. Transgenic RAGE null mice are phenotypically normal, but diabetic RAGE null mice demonstrate protection against brain atrophy and development of WMA (98). In data not yet published, cognitive decline is also limited in RAGE null diabetic mice when compared to wild-type diabetic mice.

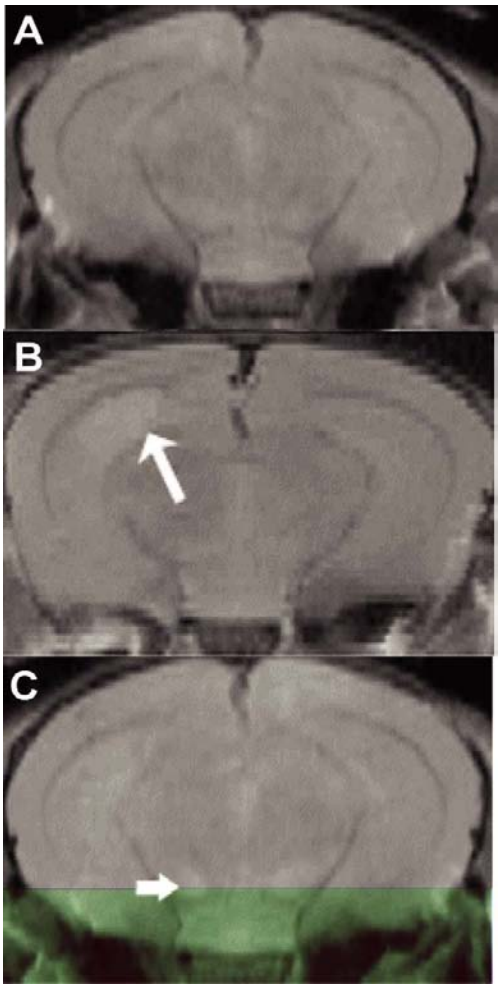

Figure 3. Two MRI images of the mouse brain, either not exposed to diabetes (A) or exposed to long-term diabetes (B, C). Hyperintensity of numerous brain regions, both grey matter (hippocampus, arrow in B), or white matter in nature (cerebral peduncle, arrow in C) can be identified after exposure to long term uncontrolled diabetes.

One of the most important outcomes of up-regulation of RAGE presence is the heightened activity of nuclear factor κB (NFκB), a transcription factor made up of several subunits, of which p50 and p65 are the most prominent. During basal conditions, NFκB exists in an inactive state in the cytoplasm of cellular components held together by an inhibitory subunit IκB. In the case where RAGE is ligated by AGE, IκB will no longer inhibit NFκB and as a result, the subunits of NFκB are translocated to the nucleus where it will bind to functional NFκB binding sites within the RAGE promoter regions—this ligation is critical for expression of RAGE in pathological processes (125) (Figure 4). Electrophoretic mobility shift assays (EMSA) from data in progress have shown upregulation of NFκB-DNA interactions in the brain of RAGE null diabetic mice. This upregulation may play a role in the loss of oligodendrocytes in the diabetic brain over time.

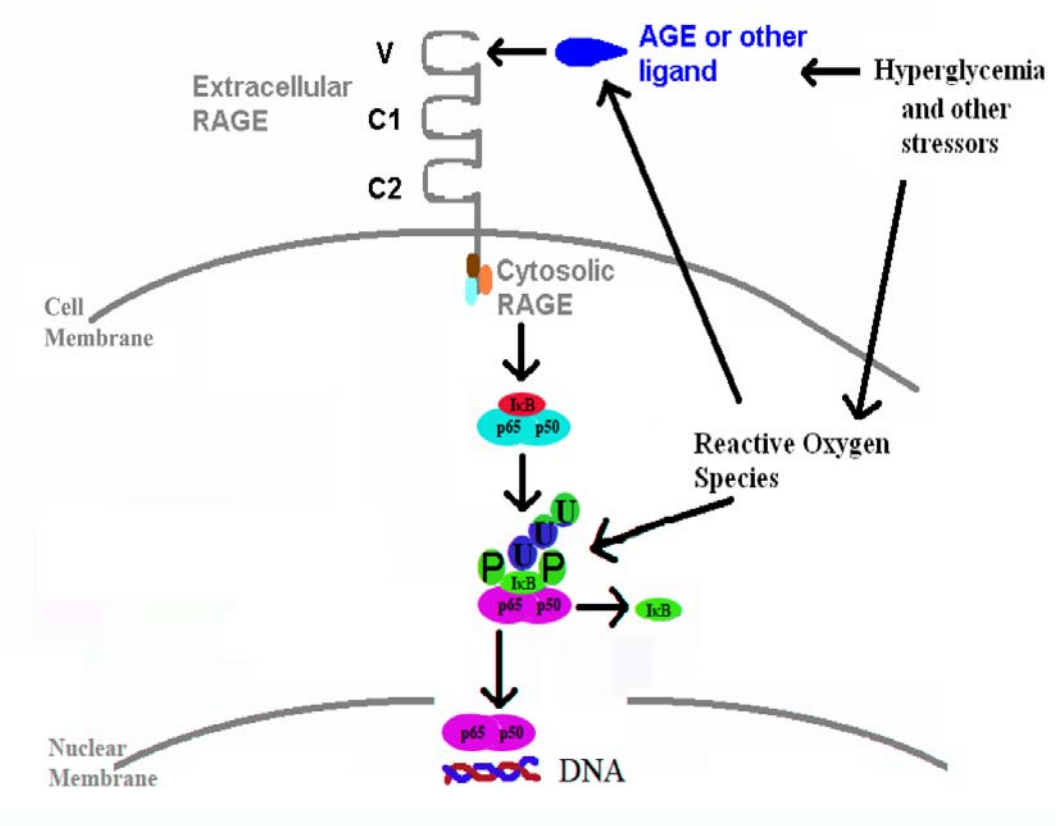

Figure 4. The Advanced Glycation End Product (AGE) pathway and its receptor RAGE. The ligation of AGEs, or other RAGE ligands to RAGE initiates a number of cascades, including the NFκB pathway. Once RAGE is activated, phosphorylation followed by ubiquitination of IκB, and its subsequent release from the NF□B complex and then degradation by proteosomes. This leads to the activation of NFκB, leading to the nuclear translocation of NFκB subunits p65 and p50, with subsequent modification of deoxyribonucleic acid transcription. This process of NFkB activation can also be stimulated by other processes, including reactive oxygen species overabundance and other hyperglycemia-mediated pathways occurring in diabetes.

Recent studies not yet published have examined the systemic delivery of soluble RAGE (sRAGE), which acts as a competitive decoy by binding RAGE ligands, thereby preventing ligation of RAGE and subsequent activation of RAGE-mediated pathways. sRAGE lacks the intracellular domain that RAGE contains, permitting it to be able to move freely through the blood binding the toxic AGE ligands. Mice treated with systemic sRAGE are subject to decreased activation of NFκB (both p50 and p65) suggesting that sRAGE may protect against cellular RAGE activity and its downstream changes in the diabetic brain. Administration of sRAGE to wild type diabetic mice has also protected against cognitive decline when compared to wild-type diabetic mice. In addition, sRAGE administration to diabetic wild-type mice incompletely protected against brain atrophy and WMA development (unpublished data) when compared to placebo-treated wild-type diabetic mice. Future studies targeting the RAGE pathway may be viable treatment possibilities for diabetic human patients at risk for brain pathology.

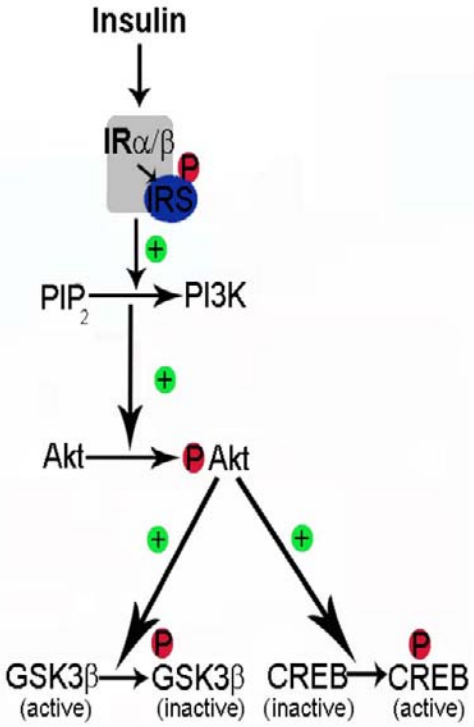

Figure 5.The insulin receptor pathway may also play a critical role in the development of diabetes-mediated white matter abnormalities. The ligation of insulin to insulin receptor α/βinitiates a number of cascades, including the phosphoinositide 3-kinase (PI3K)/Akt pathway. This system is a cascade of phosphatases, which initiates with phosphorylation of PI3K, and its subsequent phosphorylation of Akt. Then, pAkt leads to inactivation of glycogen synthase kinase 3β (GSK-3β) and activation of the transcription factor cyclic AMP response element binding protein (CREB), both of which may play critical roles in the functioning of neurons and glia in the diabetic brain. Our published work has determined that replacement of insulin within the brain restores the lack of activation of CREB and partially reverses the detrimental activation of GSK-3β in association with partial protection against development of brain atrophy and white matter abnormalities in the experimental murine brain.

Another factor in development of changes in the diabetic brain is insulin deficiency present in type I diabetes. Delivery of systemic and, more so, intranasal insulin protects against the development of cerebral atrophy, WMA and cognitive decline in work completed by our group (124) (Figure 5). In particular, intranasal insulin provided this protection without modifying systemic glycemia levels (124). The diabetic brain is subject to deficiencies in the insulin receptor-mediated pathways, particularly the phosphoinositide 3-kinase (PI3K)/Akt pathway. Insulin delivery to the brain restored PI3K/Akt signaling, leading to activation of the transcription factor cyclic AMP response element binding protein (CREB) and inhibition of glycogen synthase kinase 3β (GSK-3β), both of which may be important in neuronal and oligodendroglial functioning (124).

A rat model of type II diabetes, the Zucker Diabetic Fat (ZDF) rat has also demonstrated the presence of brain atrophy and WMA when compared to a control ZDF Lean littermate (data in progress). ZDF rats are also subjected to increased levels of RAGE, suggesting a common pathway as identified in the rodent models of type I diabetes. Studies in progress will determine the impact of type II diabetes upon the cognition of the ZDF rat over time. Along with streptozotocin-injected rats mimicking type I diabetes, white matter regions in rat brains have fewer oligodendrocytes with more marked expression of NFκB within remaining oligodendrocytes (data in submission).

Oligodendrocytes from the diabetic brain express higher levels of NFκB both *in vivo* and *in vitro* (data in submission). When harvested after 3 months of diabetes, oligodendrocytes express greater levels of RAGE and NFκB, suggesting that they are also targets of systemic diabetes. Such greater expression of NFκB may result from greater expression of RAGE upstream, although this is yet to be determined.

Hypertension and the Experimental Brain

A model for human hypertension is the Spontaneously Hypertensive Rat (SHR), which offers several similarities to patients with essential hypertension; they are normotensive early in life and gradually developing stable hypertension over the first 2–4 months of life. When SHR brains are compared to brains of Wistar–Kyoto (WKY) rats, the normotensive corresponding strain for SHR, greater morphological differences are apparent (126-128). Hypertension alone contributes to loss of hippocampal volume, along with neuronal loss and astroglial reaction in 4-6 month old SHR compared to species matched littermates (129, 130). After only 6 months of age, SHR demonstrate evidence of hypertensive brain damage, such as cytoskeletal breakdown, astrogliosis, and hippocampal atrophy (129, 131). Over time, the SHR performs inferiorly on a variety of memory-related tasks, including conditioned avoidance (132-134) and forms of spatial learning tasks (135-140).

In recently completed studies in our laboratory, the SHR rat is subject to a mild degree of whole brain atrophy when compared to the non-hypertensive WKY control rat (data in submission). SHR rats also have mild hippocampus and corpus callosum atrophy after months of sustained hypertension. Changes in MRI T2 and MT imaging were also present in SHR rats, albeit milder than in diabetic rat cohort groups (data in submission), with correlation with mild loss of myelin after examination of Luxol Fast Blue and myelin basic protein immunohistochemistry assessments of white matter. These changes are more subtle than in diabetic rat cohorts, as SHR rats are not subjected to loss of oligodendrocytes (data in submission) when compared to age-matched diabetic rats

Finally, a new rat model, the ZSF-1 rat, has been developed by the breeding of ZDF and SHR rats, providing a model of combined diabetes and hypertension. After prolonged exposure to diabetes and hypertension, the ZSF-1 brain is subjected to brain atrophy and WMA, although changes present are not greater than in the ZDF rat (data in submission). As with the ZDF rat, however, there is a loss of oligodendrocytes present in white matter regions. The lack of additive effect in the ZSF-1 rat may suggest a threshold for the effects of diabetes and hypertension upon white matter structures. Additional vascular changes in ZSF-

1 and SHR rats may contribute to susceptibility to vascular ischemia, but more work will be required to determine if this is associated with WMA development (data in submission).

Conclusions

The development of WMA in the human diabetic/hypertensive brain, first discovered essentially serendipitously with neuroimaging, has led to further evidence and concepts regarding human cognitive ability. It has become clear over time that WMA contribute to cognitive deficit and decline, even amongst diseases where grey matter pathology is already present. New animal models of the diabetic/hypertensive brain have revealed pathological disturbances of white matter resulting from oligodendrocyte dysfunction and loss. Although mechanisms for these disturbances remain unclear in the hypertensive brain, new pathological associations of RAGE pathway activation and insulin deficiency within the targeted cerebrum play a role in the development of WMA and brain atrophy. Ongoing studies hope to determine the potential for therapeutic intervention in humans exposed to diabetes and hypertension with the expectation of prevention of the measurable changes of WMA, brain atrophy, and cognitive decline.

Acknowledgments

The authors would like to acknowledge the Juvenile Diabetes Research Foundation and the Alberta Heritage Foundation for Medical Research whose funding made this work possible.

References

[1] Wong TY, Klein R, Sharrett AR, Couper DJ, Klein BE, Liao DP, et al. Cerebral white matter lesions, retinopathy, and incident clinical stroke. *JAMA2002* Jul 3;288(1):67-74.

[2] de Leeuw FE, de Groot JC, Achten E, Oudkerk M, Ramos LM, Heijboer R, et al. Prevalence of cerebral white matter lesions in elderly people: a population based magnetic resonance imaging study. The Rotterdam Scan Study. *J Neurol Neurosurg Psychiatry*2001 Jan;70(1):9-14.

[3] Mungas D, Harvey D, Reed BR, Jagust WJ, DeCarli C, Beckett L, et al. Longitudinal volumetric MRI change and rate of cognitive decline. *Neurology2005* Aug 23;65(4):565-71.

[4] Schmidt R, Schmidt H, Kapeller P, Enzinger C, Ropele S, Saurugg R, et al. The natural course of MRI white matter hyperintensities. *J Neurol Sci*2002 Nov 15;203-204:253-7.

[5] Moseley M. Diffusion tensor imaging and aging—a review. *NMR Biomed2002* Nov-Dec;15(7-8):553-60.

[6] Pfefferbaum A, Adalsteinsson E, Sullivan EV. Frontal circuitry degradation marks healthy adult aging: Evidence from diffusion tensor imaging. *Neuroimage2005* Jul 1;26(3):891-9.

[7] Sullivan EV, Adalsteinsson E, Pfefferbaum A. Selective age-related degradation of anterior callosal fiber bundles quantified in vivo with fiber tracking. *Cereb Cortex*2006 Jul;16(7):1030-9.

[8] Sullivan EV, Pfefferbaum A. Diffusion tensor imaging and aging. *Neurosci Biobehav Rev*2006;30(6):749-61.

[9] Moseley ME, Cohen Y, Kucharczyk J, Mintorovitch J, Asgari HS, Wendland MF, et al. Diffusion-weighted MR imaging of anisotropic water diffusion in cat central nervous system. *Radiology1990* Aug;176(2):439-45.

[10] Le Bihan D. Looking into the functional architecture of the brain with diffusion MRI. *Nat Rev Neurosci*2003 Jun;4(6):469-80.

[11] Gupta RK, Saksena S, Hasan KM, Agarwal A, Haris M, Pandey CM, et al. Focal Wallerian degeneration of the corpus callosum in large middle cerebral artery stroke: serial diffusion tensor imaging. *J Magn Reson Imaging*2006 Sep;24(3):549-55.

[12] Budde MD, Kim JH, Liang HF, Schmidt RE, Russell JH, Cross AH, et al. Toward accurate diagnosis of white matter pathology using diffusion tensor imaging. *Magn Reson Med*2007 Apr;57(4):688-95.

[13] Rose SE, McMahon KL, Janke AL, O'Dowd B, de Zubicaray G, Strudwick MW, et al. Diffusion indices on magnetic resonance imaging and neuropsychological performance in amnestic mild cognitive impairment. *J Neurol Neurosurg Psychiatry*2006 Oct;77(10):1122-8.

[14] Choi SJ, Lim KO, Monteiro I, Reisberg B. Diffusion tensor imaging of frontal white matter microstructure in early Alzheimer's disease: a preliminary study. *J Geriatr Psychiatry Neurol*2005 Mar;18(1):12-9.

[15] Huang J, Friedland RP, Auchus AP. Diffusion tensor imaging of normal-appearing white matter in mild cognitive impairment and early Alzheimer disease: preliminary evidence of axonal degeneration in the temporal lobe. *AJNR Am J Neuroradiol*2007 Nov-Dec;28(10):1943-8.

[16] Kodl CT, Franc DT, Rao JP, Anderson FS, Thomas W, Mueller BA, et al. Diffusion tensor imaging identifies deficits in white matter microstructure in subjects with type 1 diabetes that correlate with reduced neurocognitive function. *Diabetes2008* Nov;57(11):3083-9.

[17] Hannesdottir K, Nitkunan A, Charlton RA, Barrick TR, Macgregor GA, Markus HS. Cognitive impairment and white matter damage in hypertension: a pilot study. *Acta Neurol Scand2008* Sep 15.

[18] Gupta SR, Naheedy MH, Young JC, Ghobrial M, Rubino FA, Hindo W. Periventricular white matter changes and dementia. Clinical, neuropsychological, radiological, and pathological correlation. *Arch Neurol1988* Jun;45(6):637-41.

[19] Snowdon DA, Kemper SJ, Mortimer JA, Greiner LH, Wekstein DR, Markesbery WR. Linguistic ability in early life and cognitive function and Alzheimer's disease in late life. Findings from the Nun Study. *JAMA1996* Feb 21;275(7):528-32.

[20] Kitagaki H, Mori E, Hirono N, Ikejiri Y, Ishii K, Imamura T, et al. Alteration of white matter MR signal intensity in frontotemporal dementia. *AJNR Am J Neuroradiol1997* Feb;18(2):367-78.

[21] Kuller LH, Shemanski L, Manolio T, Haan M, Fried L, Bryan N, et al. Relationship between ApoE, MRI findings, and cognitive function in the Cardiovascular Health Study. *Stroke1998* Feb;29(2):388-98.

[22] Wolf H, Ecke GM, Bettin S, Dietrich J, Gertz HJ. Do white matter changes contribute to the subsequent development of dementia in patients with mild cognitive impairment? A longitudinal study. *Int J Geriatr Psychiatry2000* Sep;15(9):803-12.

[23] Gunning-Dixon FM, Raz N. The cognitive correlates of white matter abnormalities in normal aging: a quantitative review. *Neuropsychology2000* Apr;14(2):224-32.

[24] de Groot JC, de Leeuw FE, Oudkerk M, van GJ, Hofman A, Jolles J, et al. Cerebral white matter lesions and cognitive function: the Rotterdam Scan Study. *Annals of Neurology2000;*47(2):145-51.

[25] Garde E, Mortensen EL, Krabbe K, Rostrup E, Larsson HB. Relation between age-related decline in intelligence and cerebral white-matter hyperintensities in healthy octogenarians: a longitudinal study. *Lancet2000* Aug 19;356(9230):628-34.

[26] Deary IJ, Leaper SA, Murray AD, Staff RT, Whalley LJ. Cerebral white matter abnormalities and lifetime cognitive change: a 67-year follow-up of the Scottish Mental Survey of 1932. *Psychol Aging2003* Mar;18(1):140-8.

[27] Masdeu JC, Wolfson L, Lantos G, Tobin JN, Grober E, Whipple R, et al. Brain white-matter changes in the elderly prone to falling. *Arch Neurol1989* Dec;46(12):1292-6.

[28] Rao SM, Mittenberg W, Bernardin L, Haughton V, Leo GJ. Neuropsychological test findings in subjects with leukoaraiosis. *Arch Neurol1989* Jan;46(1):40-4.

[29] Mirsen TR, Lee DH, Wong CJ, Diaz JF, Fox AJ, Hachinski VC, et al. Clinical correlates of white-matter changes on magnetic resonance imaging scans of the brain. *Arch Neurol1991* Oct;48(10):1015-21.

[30] Fukui T, Sugita K, Sato Y, Takeuchi T, Tsukagoshi H. Cognitive functions in subjects with incidental cerebral hyperintensities. *Eur Neurol1994*;34(5):272-6.

[31] Steingart A, Hachinski VC, Lau C, Fox AJ, Diaz F, Cape R, et al. Cognitive and neurologic findings in subjects with diffuse white matter lucencies on computed tomographic scan (leuko-araiosis). *Arch Neurol1987* Jan;44(1):32-5.

[32] Vermeer SE, Prins ND, den Heijer T, Hofman A, Koudstaal PJ, Breteler MM. Silent brain infarcts and the risk of dementia and cognitive decline. *New England Journal of Medicine2003*;348(13):1215-22.

[33] Whitman GT, Tang Y, Lin A, Baloh RW. A prospective study of cerebral white matter abnormalities in older people with gait dysfunction. *Neurology2001*;57(6):990-4.

[34] Salat DH, Tuch DS, van der Kouwe AJ, Greve DN, Pappu V, Lee SY, et al. White matter pathology isolates the hippocampal formation in Alzheimer's disease. *Neurobiol Aging2008* May 2.

[35] Matsubayashi K, Shimada K, Kawamoto A, Ozawa T. Incidental brain lesions on magnetic resonance imaging and neurobehavioral functions in the apparently healthy elderly. *Stroke1992* Feb;23(2):175-80.

[36] Breteler MM, van Amerongen NM, van Swieten JC, Claus JJ, Grobbee DE, van Gijn J, et al. Cognitive correlates of ventricular enlargement and cerebral white matter lesions on magnetic resonance imaging. The Rotterdam Study. *Stroke1994* Jun;25(6):1109-15.

[37] Breteler MM, van Swieten JC, Bots ML, Grobbee DE, Claus JJ, van den Hout JH, et al. Cerebral white matter lesions, vascular risk factors, and cognitive function in a population-based study: the Rotterdam Study. *Neurology1994* Jul;44(7):1246-52.

[38] Boone KB, Miller BL, Lesser IM, Mehringer CM, Hill-Gutierrez E, Goldberg MA, et al. Neuropsychological correlates of white-matter lesions in healthy elderly subjects. A threshold effect. *Archives of Neurology1992*;49(5):549-54.

[39] Carmelli D, DeCarli C, Swan GE, Kelly-Hayes M, Wolf PA, Reed T, et al. The joint effect of apolipoprotein E epsilon4 and MRI findings on lower-extremity function and decline in cognitive function. *J Gerontol A Biol Sci Med* Sci2000 Feb;55(2):M103-9.

[40] Guttmann CR, Benson R, Warfield SK, Wei X, Anderson MC, Hall CB, et al. White matter abnormalities in mobility-impaired older persons. *Neurology2000* Mar 28;54(6):1277-83.

[41] Kerber KA, Enrietto JA, Jacobson KM, Baloh RW. Disequilibrium in older people: a prospective study. *Neurology1998* Aug;51(2):574-80.

[42] Lasbury N, Garg B, Edwards-Brown M, Cowan LD, Dimassi H, Bodensteiner JB. Clinical correlates of white-matter abnormalities on head magnetic resonance imaging. *J Child Neurol2001* Sep;16(9):668-72.

[43] Bae CJ, Pincus JH. Neurologic signs predict periventricular white matter lesions on MRI. *Can J Neurol Sci2004* May;31(2):242-7.

[44] Rother KI. Diabetes treatment--bridging the divide. *N Engl J Med2007* Apr 12;356(15):1499-501.

[45] Rosenbloom AL. The variable but inevitable loss of beta cells in overt type 1 diabetes. *Pediatr Diabetes2003* Mar;4(1):1-3.

[46] Herold KC, Hagopian W, Auger JA, Poumian-Ruiz E, Taylor L, Donaldson D, et al. Anti-CD3 monoclonal antibody in new-onset type 1 diabetes mellitus. *N Engl J Med2002* May 30;346(22):1692-8.

[47] Voltarelli JC, Couri CE, Stracieri AB, Oliveira MC, Moraes DA, Pieroni F, et al. Autologous nonmyeloablative hematopoietic stem cell transplantation in newly diagnosed type 1 diabetes mellitus. *JAMA2007* Apr 11;297(14):1568-76.

[48] Rosenbloom AL. Obesity, Insulin Resistance, beta-Cell Autoimmunity, and the Changing Clinical Epidemiology of Childhood Diabetes. *Diabetes Care2003* Oct;26(10):2954-6.

[49] DeCarli C, Miller BL, Swan GE, Reed T, Wolf PA, Garner J, et al. Predictors of brain morphology for the men of the NHLBI twin study. *Stroke1999*;30(3):529-36.

[50] Carmelli D, Reed T, DeCarli C. A bivariate genetic analysis of cerebral white matter hyperintensities and cognitive performance in elderly male twins. *Neurobiol Aging2002* May-Jun;23(3):413-20.

[51] van der Flier WM, van Straaten EC, Barkhof F, Ferro JM, Pantoni L, Basile AM, et al. Medial temporal lobe atrophy and white matter hyperintensities are associated with mild cognitive deficits in non-disabled elderly people: the LADIS study. *J Neurol Neurosurg Psychiatry2005* Nov;76(11):1497-500.

[52] Artero S, Tiemeier H, Prins ND, Sabatier R, Breteler MM, Ritchie K. Neuroanatomical localisation and clinical correlates of white matter lesions in the elderly. *J Neurol Neurosurg Psychiatry2004* Sep;75(9):1304-8.

[53] Rosano C, Brach J, Longstreth Jr WT, Newman AB. Quantitative measures of gait characteristics indicate prevalence of underlying subclinical structural brain abnormalities in high-functioning older adults. *Neuroepidemiology2006*;26(1):52-60.

[54] Wolfson L, Wei X, Hall CB, Panzer V, Wakefield D, Benson RR, et al. Accrual of MRI white matter abnormalities in elderly with normal and impaired mobility. *J Neurol Sci2005* May 15;232(1-2):23-7.

[55] Rosano C, Kuller LH, Chung H, Arnold AM, Longstreth WT, Jr., Newman AB. Subclinical brain magnetic resonance imaging abnormalities predict physical functional decline in high-functioning older adults. *J Am Geriatr* Soc2005 Apr;53(4):649-54.

[56] Swartz RH, Stuss DT, Gao F, Black SE. Independent cognitive effects of atrophy and diffuse subcortical and thalamico-cortical cerebrovascular disease in dementia. *Stroke2008* Mar;39(3):822-30.

[57] Rivera EJ, Goldin A, Fulmer N, Tavares R, Wands JR, de la Monte SM. Insulin and insulin-like growth factor expression and function deteriorate with progression of Alzheimer's disease: link to brain reductions in acetylcholine. *J Alzheimers Dis2005* Dec;8(3):247-68.

[58] Gray F, Dubas F, Roullet E, Escourolle R. Leukoencephalopathy in diffuse hemorrhagic cerebral amyloid angiopathy. *Ann Neurol1985* Jul;18(1):54-9.

[59] Janota I, Mirsen TR, Hachinski VC, Lee DH, Merskey H. Neuropathologic correlates of leuko-araiosis. *Arch Neurol1989* Oct;46(10):1124-8.

[60] Scheltens P, Barkhof F, Valk J, Algra PR, van der Hoop RG, Nauta J, et al. White matter lesions on magnetic resonance imaging in clinically diagnosed Alzheimer's disease. Evidence for heterogeneity. *Brain1992* Jun;115 (Pt 3):735-48.

[61] Capizzano AA, Acion L, Bekinschtein T, Furman M, Gomila H, Martinez A, et al. White matter hyperintensities are significantly associated with cortical atrophy in Alzheimer's disease. *J Neurol Neurosurg Psychiatry2004* Jun;75(6):822-7.

[62] Burns JM, Church JA, Johnson DK, Xiong C, Marcus D, Fotenos AF, et al. White matter lesions are prevalent but differentially related with cognition in aging and early Alzheimer disease. *Arch Neurol2005* Dec;62(12):1870-6.

[63] Hirono N, Kitagaki H, Kazui H, Hashimoto M, Mori E. Impact of white matter changes on clinical manifestation of Alzheimer's disease: A quantitative study. *Stroke2000* Sep;31(9):2182-8.

[64] Hogervorst E, Ribeiro HM, Molyneux A, Budge M, Smith AD. Plasma homocysteine levels, cerebrovascular risk factors, and cerebral white matter changes (leukoaraiosis) in patients with Alzheimer disease. *Arch Neurol2002* May;59(5):787-93.

[65] Lee AY, Jeong SH, Choi BH, Sohn EH, Chui H. Pulse pressure correlates with leukoaraiosis in Alzheimer disease. *Arch Gerontol Geriatr2006* Mar-Apr;42(2):157-66.

[66] Biessels GJ, De Leeuw FE, Lindeboom J, Barkhof F, Scheltens P. Increased cortical atrophy in patients with Alzheimer's disease and type 2 diabetes mellitus. *J Neurol Neurosurg Psychiatry2006* Mar;77(3):304-7.

[67] Brun A, Englund E. A white matter disorder in dementia of the alzheimer type: a pathoanatomical study. *Annals of Neurology1986*;19:253-.

[68] Englund E, Brun A. White matter changes in dementia of Alzheimer's type: the difference in vulnerability between cell compartments. *Histopathology1990* May;16(5):433-9.

[69] Englund E, Brun A, Alling C. White matter changes in dementia of Alzheimer's type. Biochemical and neuropathological correlates. *Brain1988* Dec;111 (Pt 6):1425-39.

[70] Hyman BT, Van Hoesen GW, Kromer LJ, Damasio AR. Perforant pathway changes and the memory impairment of Alzheimer's disease. Ann Neurol1986 Oct;20(4):472-81.

[71] Sjobeck M, Haglund M, Englund E. White matter mapping in Alzheimer's disease: A neuropathological study. *Neurobiol Aging2006* May;27(5):673-80.

[72] Whitman GT, Cotman CW. Oligodendrocyte degeneration in AD. *Neurobiol Aging2004* Jan;25(1):33-6.

[73] Sjobeck M, Englund E. Glial levels determine severity of white matter disease in Alzheimer's disease: a neuropathological study of glial changes. *Neuropathol Appl Neurobiol2003* Apr;29(2):159-69.

[74] Bartzokis G. Age-related myelin breakdown: a developmental model of cognitive decline and Alzheimer's disease. *NeurobiolAging2004*;25(1):5-18.

[75] Murray AD, Staff RT, Shenkin SD, Deary IJ, Starr JM, Whalley LJ. Brain white matter hyperintensities: relative importance of vascular risk factors in nondemented elderly people. *Radiology2005*;237(1):251-7.

[76] van Harten B, Oosterman JM, Potter van Loon BJ, Scheltens P, Weinstein HC. Brain lesions on MRI in elderly patients with type 2 diabetes mellitus. *EurNeurol2007*;57(2):70-4.

[77] Manschot SM, Brands AM, van der GJ, Kessels RP, Algra A, Kappelle LJ, et al. Brain magnetic resonance imaging correlates of impaired cognition in patients with type 2 diabetes. *Diabetes2006*;55(4):1106-13.

[78] Schmidt R, Launer LJ, Nilsson LG, Pajak A, Sans S, Berger K, et al. Magnetic resonance imaging of the brain in diabetes: the Cardiovascular Determinants of Dementia (CASCADE) Study. *Diabetes2004*;53(3):687-92.

[79] Awad N, Gagnon M, Messier C. The relationship between impaired glucose tolerance, type 2 diabetes, and cognitive function. *Journal of Clinical and Experimental Neuropsychology2004;*26(8):1044-80.

[80] Korf ES, White LR, Scheltens P, Launer LJ. Brain aging in very old men with type 2 diabetes: *the Honolulu-Asia Aging Study. Diabetes Care2006* Oct;29(10):2268-74.

[81] Harris GD, Lohr JW, Fiordalisi I, Acara M. Brain osmoregulation during extreme and moderate dehydration in a rat model of severe DKA. *Life Sciences1993*;53(3):185-91.

[82] Inzitari D, Mascalchi M. Leuko-araiosis: a reappraisal. I. CT studies. *Ital J Neurol Sci1990* Jun;11(3):241-8.

[83] Cadelo M, Inzitari D, Pracucci G, Mascalchi M. Predictors of leukoaraiosis in elderly neurological patients. . *Cerebrovasc Dis 1991*;1:345-51.

[84] Dufouil C, de Kersaint-Gilly A, Besancon V, Levy C, Auffray E, Brunnereau L, et al. Longitudinal study of blood pressure and white matter hyperintensities: the EVA MRI Cohort. *Neurology2001*;56(7):921-6.

[85] De Leeuw FE, Barkhof F, Scheltens P. Alzheimer's disease--one clinical syndrome, two radiological expressions: a study on blood pressure. *J Neurol Neurosurg Psychiatry2004* Sep;75(9):1270-4.

[86] Reed T, Kirkwood SC, DeCarli C, Swan GE, Miller BL, Wolf PA, et al. Relationship of family history scores for stroke and hypertension to quantitative measures of white-matter hyperintensities and stroke volume in elderly males. *Neuroepidemiology2000* Mar-Apr;19(2):76-86.

[87] Vermeer SE, Hollander M, van Dijk EJ, Hofman A, Koudstaal PJ, Breteler MM. Silent brain infarcts and white matter lesions increase stroke risk in the general population: the Rotterdam Scan Study. *Stroke2003*;34(5):1126-9.

[88] Fazekas F, Schmidt R, Scheltens P. Pathophysiologic mechanisms in the development of age-related white matter changes of the brain. *DementGeriatrCogn Disord1998;*9 Suppl 1:2-5.

[89] Pantoni L, Inzitari D, Pracucci G, Lolli F, Giordano G, Bracco L, et al. Cerebrospinal fluid proteins in patients with leucoaraiosis: possible abnormalities in blood-brain barrier function. *Journal of the Neurological Sciences1993;*115(2):125-31.

[90] Yoshiura T, Higano S, Rubio A, Shrier DA, Kwok WE, Iwanaga S, et al. Heschl and superior temporal gyri: low signal intensity of the cortex on T2-weighted MR images of the normal brain. *Radiology2000*;214(1):217-21.

[91] Ball MJ. "Leukoaraiosis" explained. Lancet1989;1(8638):612-3.

[92] Knopman D, Boland LL, Mosley T, Howard G, Liao D, Szklo M, et al. Cardiovascular risk factors and cognitive decline in middle-aged adults. *Neurology2001*;56(1):42-8.

[93] Bartzokis G, Cummings JL, Sultzer D, Henderson VW, Nuechterlein KH, Mintz J. White matter structural integrity in healthy aging adults and patients with Alzheimer disease: a magnetic resonance imaging study. Archives of *Neurology2003*;60(3):393-8.

[94] Takao M, Koto A, Tanahashi N, Fukuuchi Y, Takagi M, Morinaga S. Pathologic findings of silent, small hyperintense foci in the basal ganglia and thalamus on MRI. *Neurology1999*;52(3):666-8.

[95] Takao M, Koto A, Tanahashi N, Fukuuchi Y, Takagi M, Morinaga S. Pathologic findings of silent hyperintense white matter lesions on MRI. *Journal of the Neurological Sciences1999*;167(2):127-31.

[96] Schmidt R, Fazekas F, Kleinert G, Offenbacher H, Gindl K, Payer F, et al. Magnetic resonance imaging signal hyperintensities in the deep and subcortical white matter. A comparative study between stroke patients and normal volunteers. *Archives of Neurology1992*;49(8):825-7.

[97] Braffman BH, Zimmerman RA, Trojanowski JQ, Gonatas NK, Hickey WF, Schlaepfer WW. Brain MR: pathologic correlation with gross and histopathology. 1. Lacunar infarction and Virchow-Robin spaces. *AJR AmJRoentgenol1988*;151(3):551-8.

[98] Toth C, Schmidt AM, Tuor UI, Francis G, Foniok T, Brussee V, et al. Diabetes, leukoencephalopathy and rage. *Neurobiol Dis2006* Aug;23(2):445-61.

[99] Schmidt AM, Hori O, Chen JX, Li JF, Crandall J, Zhang J, et al. Advanced glycation endproducts interacting with their endothelial receptor induce expression of vascular cell adhesion molecule-1 (VCAM-1) in cultured human endothelial cells and in mice. A potential mechanism for the accelerated vasculopathy of diabetes. *JClinInvest1995*;96(3):1395-403.

[100] Braak H, Braak E. Development of Alzheimer-related neurofibrillary changes in the neocortex inversely recapitulates cortical myelogenesis. Acta Neuropathol1996 Aug;92(2):197-201.

[101] Kobayashi K, Hayashi M, Nakano H, Fukutani Y, Sasaki K, Shimazaki M, et al. Apoptosis of astrocytes with enhanced lysosomal activity and oligodendrocytes in white matter lesions in Alzheimer's disease. *Neuropathol Appl Neurobiol2002* Jun;28(3):238-51.

[102] Lassmann H, Bancher C, Breitschopf H, Wegiel J, Bobinski M, Jellinger K, et al. Cell death in Alzheimer's disease evaluated by DNA fragmentation in situ. *Acta Neuropathol1995*;89(1):35-41.

[103] Roher AE, Weiss N, Kokjohn TA, Kuo YM, Kalback W, Anthony J, et al. Increased A beta peptides and reduced cholesterol and myelin proteins characterize white matter degeneration in Alzheimer's disease. *Biochemistry2002* Sep 17;41(37):11080-90.

[104] Vlkolinsky R, Cairns N, Fountoulakis M, Lubec G. Decreased brain levels of 2',3'-cyclic nucleotide-3'-phosphodiesterase in Down syndrome and Alzheimer's disease. *Neurobiol Aging2001* Jul-Aug;22(4):547-53.

[105] Xu J, Chen S, Ahmed SH, Chen H, Ku G, Goldberg MP, et al. Amyloid-beta peptides are cytotoxic to oligodendrocytes. *J Neurosci2001* Jan 1;21(1):RC118.

[106] Marx J. Neuroscience. New leads on the 'how' of Alzheimer's. *Science2001* Sep 21;293(5538):2192-4.

[107] Laszkiewicz I, Mouzannar R, Wiggins RC, Konat GW. Delayed oligodendrocyte degeneration induced by brief exposure to hydrogen peroxide. *Journal of Neuroscience Research1999*;55(3):303-10.

[108] Vollgraf U, Wegner M, Richter-Landsberg C. Activation of AP-1 and nuclear factor-kappaB transcription factors is involved in hydrogen peroxide-induced apoptotic cell death of oligodendrocytes. *J Neurochem1999* Dec;73(6):2501-9.

[109] Bozner P, Grishko V, LeDoux SP, Wilson GL, Chyan YC, Pappolla MA. The amyloid beta protein induces oxidative damage of mitochondrial DNA. *J Neuropathol Exp Neurol1997* Dec;56(12):1356-62.

[110] Li P, Nijhawan D, Budihardjo I, Srinivasula SM, Ahmad M, Alnemri ES, et al. Cytochrome c and dATP-dependent formation of Apaf-1/caspase-9 complex initiates an apoptotic protease cascade. *Cell1997* Nov 14;91(4):479-89.

[111] Wilson MR. Apoptotic signal transduction: emerging pathways. *Biochem Cell Biol1998*;76(4):573-82.

[112] Svennerholm L, Vanier MT, Jungbjer B. Changes in fatty acid composition of human brain myelin lipids during maturation. *J Neurochem1978* Jun;30(6):1383-90.

[113] Bondy SC, Guo-Ross SX, Truong AT. Promotion of transition metal-induced reactive oxygen species formation by beta-amyloid. *Brain Res1998* Jul 13;799(1):91-6.

[114] Iwamoto N, Nishiyama E, Ohwada J, Arai H. Distribution of amyloid deposits in the cerebral white matter of the Alzheimer's disease brain: relationship to blood vessels. *Acta Neuropathol1997* Apr;93(4):334-40.

[115] Markesbery WR, Carney JM. Oxidative alterations in Alzheimer's disease. *Brain Pathol1999* Jan;9(1):133-46.

[116] Hensley K, Carney JM, Mattson MP, Aksenova M, Harris M, Wu JF, et al. A model for beta-amyloid aggregation and neurotoxicity based on free radical generation by the peptide: relevance to Alzheimer disease. *Proc Natl Acad Sci U S A1994* Apr 12;91(8):3270-4.

[117] Varadarajan S, Kanski J, Aksenova M, Lauderback C, Butterfield DA. Different mechanisms of oxidative stress and neurotoxicity for Alzheimer's A beta(1--42) and A beta(25--35). *J Am Chem Soc2001* Jun 20;123(24):5625-31.

[118] Wautier MP, Chappey O, Corda S, Stern DM, Schmidt AM, Wautier JL. Activation of NADPH oxidase by AGE links oxidant stress to altered gene expression via RAGE. *AmJPhysiol EndocrinolMetab2001*;280(5):E685-E94.

[119] van der GM, Janssen SW, van Asten JJ, Hermus AR, Sweep CG, Pikkemaat JA, et al. Metabolic profile of the hippocampus of Zucker Diabetic Fatty rats assessed by in vivo 1H magnetic resonance spectroscopy. NMR in *Biomedicine2004*;17(6):405-10.

[120] Yan SD, Schmidt AM, Anderson GM, Zhang J, Brett J, Zou YS, et al. Enhanced cellular oxidant stress by the interaction of advanced glycation end products with their receptors/binding proteins. *Journal of Biological Chemistry1994*;269(13):9889-97.

[121] Schmidt AM, Hasu M, Popov D, Zhang JH, Chen J, Yan SD, et al. Receptor for advanced glycation end products (AGEs) has a central role in vessel wall interactions and gene activation in response to circulating AGE proteins. *ProcNatlAcadSciUSA1994*;91(19):8807-11.

[122] Toth C, Rong LL, Yang C, Martinez J, Song F, Ramji N, et al. Receptor for advanced glycation end products (RAGEs) and experimental diabetic neuropathy. *Diabetes2008*;57(4):1002-17.

[123] Francis G, Martinez J, Liu W, Nguyen T, Ayer A, Fine J, et al. Intranasal Insulin Ameliorates Experimental Diabetic Neuropathy. *Diabetes2009* Jan 9.

[124] Francis GJ, Martinez JA, Liu WQ, Xu K, Ayer A, Fine J, et al. Intranasal insulin prevents cognitive decline, cerebral atrophy and white matter changes in murine type I diabetic encephalopathy. *Brain2008* Dec;131(Pt 12):3311-34.

[125] Li J, Schmidt AM. Characterization and functional analysis of the promoter of RAGE, the receptor for advanced glycation end products. *Journal of Biological Chemistry1997*;272(26):16498-506.

[126] Lehr RP, Jr., Browning RA, Myers JH. Gross morphological brain differences between Wistar-Kyoto and spontaneously hypertensive rats. *Clinical and Experimental Hypertension1980*;2(1):123-7.

[127] Nelson DO, Boulant JA. Altered CNS neuroanatomical organization of spontaneously hypertensive (SHR) rats. *Brain Research1981;*226(1-2):119-30.

[128] Tajima A, Hans FJ, Livingstone D, Wei L, Finnegan W, DeMaro J, et al. Smaller local brain volumes and cerebral atrophy in spontaneously hypertensive rats. *Hypertension1993*;21(1):105-11.

[129] Sabbatini M, Strocchi P, Vitaioli L, Amenta F. The hippocampus in spontaneously hypertensive rats: a quantitative microanatomical study. *Neuroscience2000*;100(2):251-8.

[130] Sabbatini M, Mignini F, Venarucci D, Vega JA, Amenta F. Effect of nicardipine treatment on the expression of neurofilament 200 KDa immunoreactivity in the brain of spontaneously hypertensive rats. Clinical and Experimental *Hypertension2001*;23(1-2):127-41.

[131] Sabbatini M, Catalani A, Consoli C, Marletta N, Tomassoni D, Avola R. The hippocampus in spontaneously hypertensive rats: an animal model of vascular dementia? *Mechanisms of Ageing and Development2002*;123(5):547-59.

[132] Knardahl S, Karlsen K. Passive-avoidance behavior of spontaneously hypertensive rats. *Behavioral and Neural Biology1984*;42(1):9-22.

[133] Sutterer JR, DeVito WJ, Rykaszewski I. Developmental aspects of 2-way shuttlebox avoidance in the spontaneously hypertensive and normotensive rat. *Developmental Psychobiology1981*;14(5):405-14.

[134] Sutterer JR, Perry J, DeVito W. Two-way shuttle box and lever-press avoidance in the spontaneously hypertensive and normotensive rat. *JComp Physiol Psychol1980*; 94(1):155-63.

[135] Mori S, Kato M, Fujishima M. Impaired maze learning and cerebral glucose utilization in aged hypertensive rats. *Hypertension1995*;25(4 Pt 1):545-53.

[136] Nakamura-Palacios EM, Caldas CK, Fiorini A, Chagas KD, Chagas KN, Vasquez EC. Deficits of spatial learning and working memory in spontaneously hypertensive rats. *Behavioural Brain Research1996*;74(1-2):217-27.

[137] Wyss JM, Fisk G, van GT. Impaired learning and memory in mature spontaneously hypertensive rats. *Brain Research1992*;592(1-2):135-40.

[138] Gattu M, Terry AV, Jr., Pauly JR, Buccafusco JJ. Cognitive impairment in spontaneously hypertensive rats: role of central nicotinic receptors. Part II. *Brain Research1997;*771(1):104-14.

[139] Gattu M, Pauly JR, Boss KL, Summers JB, Buccafusco JJ. Cognitive impairment in spontaneously hypertensive rats: role of central nicotinic receptors. I. *Brain Research1997*;771(1):89-103.

[140] Terry AV, Jr., Hernandez CM, Buccafusco JJ, Gattu M. Deficits in spatial learning and nicotinic-acetylcholine receptors in older, spontaneously hypertensive rats. *Neuroscience2000*;101(2):357-68.

In: Handbook on White Matter
Editors: T. B. Westland and R. N. Calton
ISBN: 978-1-60741-034-8

Chapter XIII

Brain Tissue Segmentation Based on Multi-Channel Diffusion Tensor Imaging Data

Tianming Liu[1] and Stephen T.C. Wong[2]
[1] Department of Computer Science and Bioimaging Research Center, The University of Georgia, Athens, GA;
[2] The Center for Biotechnology and Informatics, The Methodist Hospital Research Institute, Weill Medical College of Cornell University, Houston, TX

1. Introduction

Brain tissue segmentation has important applications in studying the structure and function of the brain. A number of methods based on structural MRI data have been proposed for the segmentation problem (Zhang et al., 2001; Wells et al., 1996; Pham et al., 1999; Dale et al., 1999). In this chapter, we present a robust method for automated brain tissue segmentation based on the multiple-channel fusion in DTI (diffusion tensor imaging) space. Our method can be employed to define accurate tissue maps when dealing with fused structural and diffusion MRI data. This enables us to study the gray matter diffusivity in neurodegenerative and neurological diseases (Liu et al., 2005a; Liu et al., 2005b, Liu et al., 2006). When fusing structural and diffusion information, the imperfect alignment of structural MRI data, e.g., SPGR (Spoiled Gradient Echo) image, with DTI data results in the problem of heterogeneous voxels when the anatomic information in the structural data is applied to the DTI data. Under the problem of heterogeneous voxels, the measurements of the GM (Gray Matter) diffusivity based on the anatomic information in the SPGR image may fail to reveal the real diffusion in the GM (Liu et al., 2006). Specifically, following non-rigid co-registration using the UCLA AIR tools (Woods et al., 1998), the GM boundaries of SPGR image are crossing CSF of ADC image. Consequently, the GM voxels in the SPGR image correspond to CSF (Cerebrospinal Fluid) voxels in the ADC (Apparent Diffusion Coefficient) image. Such a problem can occur for a variety of reasons, including geometric distortion in

DTI imaging (Jezzard et al., 1995), partial volume effect (Helenius et al.,2002; Gonza´lez Ballester et al.,2002), reslicing and interpolation of DTI data, and errors in co-registration.

2. Method

2.1. Background

Diffusion-weighted imaging (DWI) and DTI permit in-vivo measures of the diffusion of water molecules in living tissues (Le Bihan, 1991). The diffusion of water molecules are typically represented by unrestricted Brownian motion, a particular tissue structure can preferentially restrict the molecular motion, which leads to anisotropic diffusion that is measured by DWI and DTI (Le Bihan D 1991; Bammer, 2003). As an approximation, the measured diffusion can be modeled as an anisotropic Gaussian, parameterized by the diffusion tensor in each voxel (Basser et al., 1994), in order to create a 3D field of diffusion tensors. Diffusion tensor measurements provide a rich data set from which a measure of diffusion anisotropy can be obtained in various ways through the application of mathematical formulas and recalculation of the underlying eigen values (Bammer, 2003; Moseley et al., 1990; Le Bihan D et al., 2001; Basser et al., 2002). The ADC, $\lambda 1$, $\lambda 2$, and $\lambda 3$ channels are well suited for the measuring of overall diffusivity, while anisotropy can be represented by FA, RA, or VR (Sundgren et al., 2004). In Sundgren et al., 2004, it was reported that, the diffusivity values of the CSF are more than double the values of GM and WM (White Matter). This is because water diffusion in CSF is much less restricted than those in the GM and WM tissues (Johanna et al., 2002). Therefore, we can use these four channels of images to segment CSF from non-CSF tissues. Also, since highly directional white matter structures have much larger fractional anisotropy values, the FA (Fractional Anisotropy), RA (Relative Anisotropy), and VR(Volume Ratio) images can be used to separate WM from non-WM tissues. Since all these images intrinsically share the same DTI space, the CSF/non-CSF and WM/non-WM images can be combined into a complete CSF/GM/WM segmentation map in the DTI space without the need of any registration.

2.2. Overview

Our computational framework for brain tissue segmentation based on DTI data consists of six steps, as summarized in figure 1. The first step consists of pre-processing to perform eddy current correction through the use of FSL FDT tools (http://www.fmrib.ox.ac.uk/fsl/fdt/index.html), tensor calculation, and channel image generation using DTIStudio (http://cmrm.med.jhmi.edu/DTIuser/DTIuser.asp). As a result, seven channels are obtained: ADC, $\lambda 1$, $\lambda 2$, $\lambda 3$, FA, RA, and VR. To reduce noise, we smoothen these seven channels through an edge preserving anisotropic diffusion filter (Perona et al., 1990). The second step consists of segmenting the brain into CSF and non-CSF compartments by utilizing the tissue contrasts existing in the first four channels, i.e., ADC, $\lambda 1$, $\lambda 2$, and $\lambda 3$. The third step consists of segmenting the brain into WM and non-WM

compartments using the last three channels, i.e., FA, RA and VR, separately. To generate the final CSF and non-CSF map, the fourth step employs the STAPLE algorithm (Warfield et al., 2004) to fuse the tissue segmentation results of the first four channels (ADC, λ1, λ2, λ3). The WM and non-WM map is generated in the fifth step. And the final step consists of combining both CSF/non-CSF and WM/non-WM maps to obtain a complete tissue map detailing the CSF, WM, and GM segments.

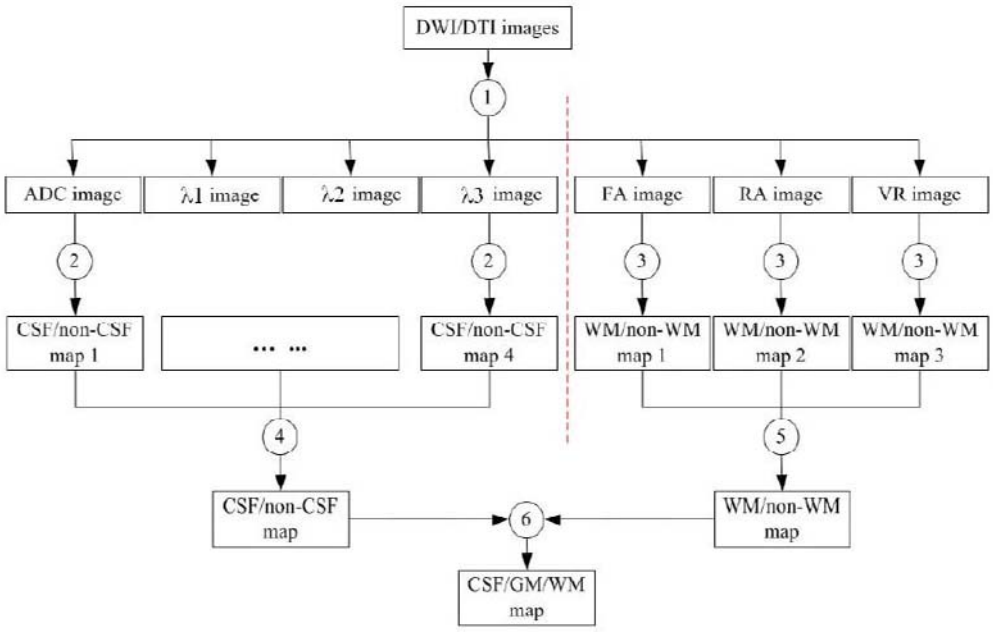

Figure 1. An illustration of the computational framework of brain tissue segmentation based on DWI/DTI data. There are six steps: (1) Pre-processing; (2) CSF/non-CSF segmentation; (3) WM/non-WM segmentation; (4) multi-channel fusion to obtain CSF/non-CSF map; (5) multi-channel fusion to obtain WM/non-WM map; and (6) combining the CSF/non-CSF and WM/non-WM maps into a complete CSF/WM/GM tissue segmentation.

2.3. Tissue Segmentation Based on DTI Data

2.3.1. HMRF-EM Tissue Segmentation

In each individual channel outlined above, the brain is classified into two classes: either CSF and non-CSF, or WM and non-WM, depending on the channel. The Expectation-Maximization (EM) algorithm in combination with a Hidden Markov Random Field (HMRF) model is used for the two-class tissue segmentation (Zhang et al., 2001; Liu et al., 2005a; Liu et al., 2006). The EM model fitting and the MRF Iterated Conditional Modes (ICM) labeling in the HMRF-EM segmentation both require the selection of an initial parameter set (Zhang et al., 2001). In the literature, the k-means clustering has been widely used for automated selection of initial centroids (Zhang et al., 2001; Pham et al., 1999). We use this method for the initial estimation.

2.3.2. Multi-Channel Fusion

2.3.2.1. Motivation

The application of the HMRF-EM segmentation method to different channels, such as ADC and eigenvalues results in a discrepancy in the segmentation results. Figure 2 provides an example, where the distribution of the ADC values in entire brain along with the segmented CSF of ADC channel and the λ3 channel are presented. The figure indicates that there are no clear boundaries between different tissues in the ADC distribution of the whole brain (shown in red). Also the CSF segmentation results of ADC channel (shown in green) and λ3 channel (shown in blue) are quite different. From this, we postulate that segmentations from multiple channels provide richer information, and an optimal combination of these results will be more desirable.

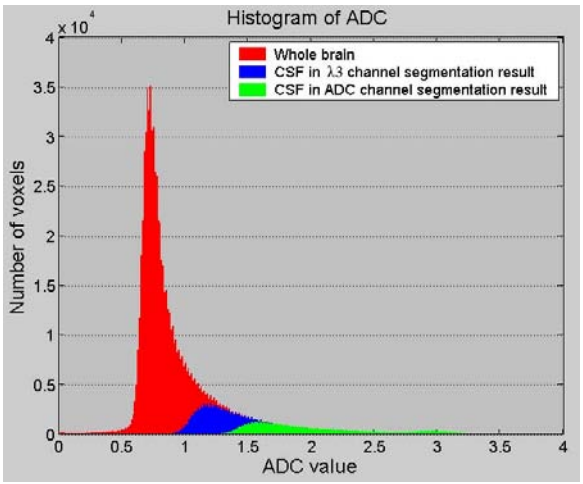

Figure 2. The distribution of the ADC values in the whole brain and in the CSF of single channel segmentation result using ADC and λ3 channels separately. ADC scale is 10^{-3} mm^2/sec.

Due to the difficulty of obtaining or estimating a known true segmentation for real data, the performance of the segmentation from any given channel is difficult to quantify, and each channel could not be assumed to contribute equally to the combined segmentation result. To deal with this problem, we make use of the Expectation-Maximization algorithm for Simultaneous Truth and Performance Level Estimation (STAPLE) algorithm proposed in (Warfield et al., 2004). The algorithm considers a collection of segmentations and, for each segmentation, computes a probabilistic estimate of the true segmentation and a measure of the performance level represented by that segmentation. It then proceeds to estimate the optimal combination of the segmentations in order to obtain a probabilistic estimate of the true segmentation. This is done by weighting each segmentation according to its estimated performance level while employing a prior model for the spatial distribution of structures being segmented and spatial homogeneity constraints. Since we consider seven two-class tissue segmentation maps, the goal of our multi-channel fusion is to combine the seven binary segmentation maps to construct an improved overall segmentation map and to characterize the segmentation performance level of every channel, simultaneously.

2.3.2.2. Fusion of CSF/Non-CSF Segmentations Using STAPLE

As outlined above, there are four binary segmentation maps (CSF/non-CSF) associated with four channels (ADC, λ1, λ2, λ3). Let X be the random field defined in the whole volume of N voxels, and x_i denote the configuration of each voxel i. We have

$$X = \{x_i = (x_{i1}, x_{i2}, x_{i3}, x_{i4}) \,|\, x_{ij} \in \{0,1\}, i = 1, \cdots, N, j = 1, \cdots 4\} \tag{1}$$

where 0 and 1 represent the CSF and non-CSF two tissue types. Let Y be the true segmentation map. The segmentation performance of every channel is characterized by sensitivity and specificity. Sensitivity is the relative frequency of $x_{ij} = 1$ when $Y_i = 1$. We define $p = (p_1, p_2, p_3, p_4)^T$ as a column vector, whose i-th element is the sensitivity parameter for the segmentation on the i-th channel. Similarly, specificity is the relative frequency of $x_{ij} = 0$ when $Y_i = 0$ for which we define the column vector of specificity values $q = (q_1, q_2, q_3, q_4)^T$ for the four channels considered (Warfield *et al*., 2004).

We then apply the STAPLE algorithm to estimate the true map via the maximum a posteriori (MAP) method. Specifically, we seek a map Y^*, which is an estimate of the true map Y, according to the MAP criterion :

$$Y^* = \arg\max_{Y \in \Omega}(f(X|Y,p,q)f(Y)) = \arg\max_{Y \in \Omega}(\prod_i [\prod_j f(X_{ij} \,|\, Y_i, p_j, q_j)] f(Y_i)) \tag{2}$$

where $f(Y_i)$ is the prior probability of Y_i, and a voxel-wise independence assumption has been made here. Next, assuming that the channels are mutually independent, the performance level parameter, which maximizes the complete data (X,Y) log likelihood function, is given by:

$$(p_j, q_j) = \arg\max_{p_j, q_j} \ln f(X_j, Y \,|\, p_j, q_j) \tag{3}$$

To estimate the solution of Equation (3), an EM algorithm is used. The iteration of the EM algorithm will be performed as:

$$p_j^{(k)} = \frac{\sum_{i:X_{ij}=1} W_i^{(k-1)}}{\sum_i W_i^{(k-1)}} \tag{4}$$

$$q_j^{(k)} = \frac{\sum_{i:X_{ij}=0} (1 - W_i^{(k-1)})}{\sum_i (1 - W_i^{(k-1)})} \tag{5}$$

In equation (4) and (5), $w_i^{(k-1)}$ indicates the probability of the true segmentation at voxel i being equal to one :

$$W_i^{(k-1)} \equiv f(Y_i = 1 \mid X_i, p^{(k-1)}, q^{(k-1)}) = \frac{m_i^{(k-1)}}{m_i^{(k-1)} + n_i^{(k-1)}} \tag{6}$$

where $m_i^{(k-1)} = f(Y_i = 1) \prod_{j:X_{ij}=1} p_j^{(k-1)} \prod_{j:X_{ij}=0} (1 - p_j^{(k-1)})$,

and $n_i^{(k-1)} = f(Y_i = 0) \prod_{j:X_{ij}=0} q_j^{(k-1)} \prod_{j:X_{ij}=1} (1 - q_j^{(k-1)}))$

Since the true segmentation is a binary random variable, the posterior probability $f(Y_i = 0 \mid X_i, p^{(k-1)}, q^{(k-1)})$ is equal to $1 - W_i^{(k-1)}$. According to Eq. (2), the fusion model can be set as:

$$Y_i = \begin{cases} 0 & if \quad W_i < 0.5 \\ 1 & if \quad W_i \geq 0.5 \end{cases} \tag{7}$$

In summary, there are two steps in STAPLE for multiple-channel fusion. At each iteration, the first step entails the estimation of the conditional probability of the true segmentation given the segmentation maps of four channels and previous performance parameter estimates. In the second step, estimation values of the performance parameters are updated. More details concerning implementation of the iterative algorithm can be founded in (Warfield *et al*., 2004). The fusion result is finally obtained through Eq. (7).

2.3.2.3. Fusion of WM/Non-WM Segmentations

First, the three channels of FA, RA, and VR images are separately segmented into WM/non-WM tissue maps using the HMRF-EM method described in subsection 2.3.1. Then, the three tissue segmentation maps are fused into a complete WM/non-WM tissue map by using the STAPLE algorithm described in subsection 2.3.2.2. As a result, the FA, RA and VR channels provide an independent segmentation of the brain tissues into the WM and non-WM compartments.

3. Experimental Results

3.1. Datasets

We have applied our tissue segmentation and multiple-channel fusion method to ten SPGR and DTI datasets. For the SPGR imaging settings, a 1.5 Tesla GE Echospeed system was used with coronal series of contiguous spoiled gradient images. The voxel dimensions in

this case are equal to: 0.9375 x 0.9375 x 1.5 mm. For the DTI settings, a 1.5 Tesla GE Echospeed system was used with the following settings. Sequence: maximum gradient amplitudes: 40 mT/M; rectangular FOV: 220 x 165 mm; 4 mm slice thickness; 1 mm inter-slice distance; TE: 70 ms; TR: 2500 ms; b-value: 1000 s/mm^2. DWI images along six non-collinear directions were collected. More details about our imaging settings can be found in (Kubicki *et al*., 2005).

The SPGR data and DTI datasets have been processed using the pre-processing methods as described in (Liu et al., 2006). In particular, the SPGR image has been co-registered with the DTI images using the non-rigid registration method in the UCLA AIR package (Woods et al., 1998).

3.2. Experiment 1

In the fusion of CSF/non-CSF segmentation maps, the initial values $(p_j^{(0)}, q_j^{(0)})$ for four channels are set to (0.45, 0.98), (0.55, 0.98), (0.55, 0.98), and (0.55, 0.98) respectively, according to the volume overlaps of the segmentation maps between the SPGR image and DTI image (Liu et al., 2006). The prior probability of $f(Y_i)$ is available in the single channel segmentation using HMRF-EM (Zhang *et al*., 2001). In this experiment, we average the probability maps of the four channel segmentations with equal weight to obtain $f(Y_i)$.

Table 1. Multiple-channel fusion result

SPGR		CSF (%)	GM (%)	WM (%)	O_j (%)	A_j (%)	p_j, q_j (%)
		19.7	41.0	39.3			
DWI/DTI		CSF(%)	Non-CSF(%)				
*	ADC	11.7	88.3		45.2	74.4	50.4, 99.9
	λ1	18.2	81.8		56.3	96.0	67.1, 99.6
	λ2	15.5	84.5		54.3	88.0	65.6, 99.9
	λ3	22.2	77.8		60.7	94.0	96.1, 99.9
#	*Y*	21.4	78.6		70.5	95.8	
DWI/DTI		WM(%)	Non-WM(%)				
*	FA	67.6	32.4		90.1	73.5	100, 93.4
	RA	62.3	37.5		87.4	77.4	100, 93.9
	VR	58.6	41.4		85.2	80.3	100, 94.3
#	*Y*	49.5	50.5		86.3	88.5	

"*" marks the single channel segmentation result, and "#" marks the fusion result. The third and fourth columns show the volume percentages of each tissue types in SPGR space or DWI/DTI space. The fifth column shows the volume overlap (O_j), which is determined as the tissue volume overlap ratio of each DWI/DTI channel against the corresponding tissue type in SPGR image. The sixth column shows volume agreement (A_j , please refer to Liu *et*

al., 2006 for the definition of volume agreement). The seventh column shows the segmentation performance level of every single channel.

As an example, table 1 provides the results for a randomly selected case. It is clear from the results that the CSF and non-CSF segmentation results from the four channels are quite different, e.g., the CSF volume percentages vary from 11.7% to 22.2% while the CSF percentage on SPGR data is 19.7%. The CSF percentage obtained by multi-channel fusion is 21.4%, which is very close to that of SPGR segmentation result. Considering that tissue segmentation based on SPGR image is relatively accurate, these results indicate the relatively good performance of the proposed tissue segmentation method.

For the fusion of WM and non-WM segmentations, the WM percentages obtained by different channels are also quite different, ranging from 58.6% to 67.6%. Similarly, the multi-channel fusion renders closer result (49.5 %) to SPGR segmentation result (39.3 %). It should be noted that there are relatively large gaps between the fusion result and SPGR segmentation result. However, using the multiple-channel fusion method, these gaps can be improved.

The results in this section support our point in subsection 2.3.2 that the single channel segmentation is less reliable, and that an optimal combination of multiple channels, e.g., using the STAPLE algorithm, provides improved performance.

3.3. Experiment 2

This experiment provides an example of evaluation by visual inspection. As shown in figure 3, it is difficult to obtain an ideal tissue segmentation result by using only one channel in DTI space. For example, in the segmentation of CSF/non-CSF (figure 3(a)), the CSF volume agreement (please refer to Liu et al. 2006 for the definition of volume agreement) with that of SPGR segmentation for the ADC channel is 74.4%. Using our multi-channel fusion method, the CSF volume agreement increases to 95.8%. Another example is that in the segmentation of WM and non-WM regions (figure 3(b)), the WM volume agreement of the FA channel with that of SPGR segmentation is 73.5%. On the other hand, our multi-channel fusion method increases the agreement to 88.5%.

In general, the multi-channel fusion method based on DTI data obtains visually reasonable tissue segmentation result, compared to the tissue segmentation results based on SPGR data (figure 3). This supports our claim about the advantage of multi-channel fusion introduced in subsection 2.3.2. Our experimental result shows that it is possible to obtain a reasonably good tissue segmentation map by combining the multiple-channel segmentation results based on the DTI data only.

To compare the proposed multiple-channel fusion method with the simple voting method, figure 3a shows the voting result of ADC, $\lambda 1$, $\lambda 2$, and $\lambda 3$, as an example. The CSF volume percentage of the segmentation result by voting is 13.5%, which is far away from the SPGR segmentation result (19.7%). However, the multi-channel fusion method obtains more consistent segmentation result, compared to the SPGR channel segmentation.

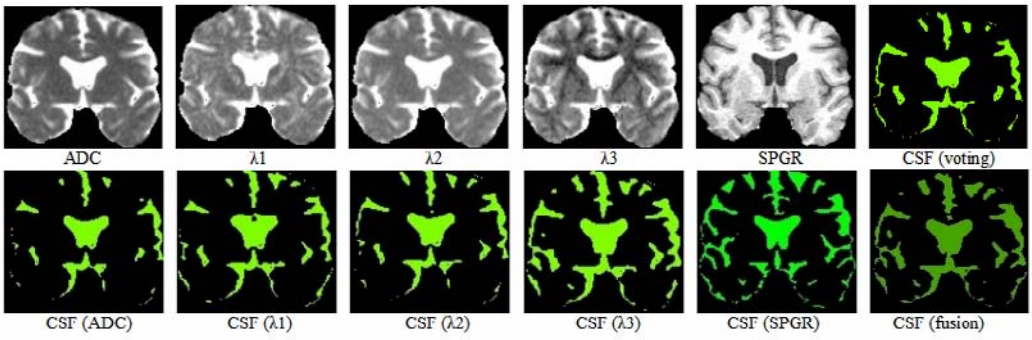

(a)

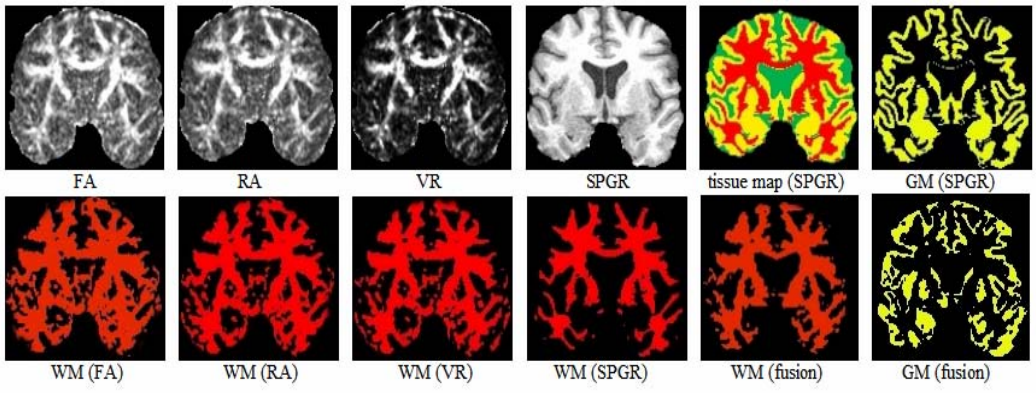

(b)

Figure 3. Multi-channel data fusion. (a) CSF tissue maps obtained by different methods. The left five columns are results by single channel segmentation. The right top is the segmentation by simple voting strategy. The right bottom is the result by 7-channel fusion. (b) WM and GM tissue maps obtained by different methods. The left four columns are results by single channel segmentation. The right two bottom columns are result obtained by 7-channel fusion.

3.4. Experiment 3

We evaluated the tissue segmentation method based on DTI data for ten cases. Figure 4 shows the volume overlaps and agreements between DTI segmentation and SPGR segmentation for these ten cases (please refer to Liu *et al*., 2006 for the definitions of volume overlap and volume agreement).

Note in figure 4(a) that the volume overlaps for the different channels are quite discrepant, with different cases having different channels that yield the highest level of overlap. For example, in the first case, the λ3 channel has the highest overlap, whereas in the second case, the λ2 channel has the highest overlap. This clearly elucidates the value of the multiple-channel fusion method in estimating the performance levels of different channels and in obtaining the final segmentation result based on more reliable channels. In general, the

fusion result of tissue segmentation has the highest volume overlap averaged over the ten cases, as shown in figure 4(a). The mean value and the stand deviation of overlaps for four individual channel segmentations and the fusion result are 0.44 ± 0.08, 0.48 ± 0.13, 0.60 ± 0.08, 0.57 ± 0.07 and 0.63 ± 0.04 respectively. This partly shows that the fusion strategy generates more desirable tissue segmentation results than a single channel based on DTI data, considering that tissue segmentation based on SPGR image can serve as a comparison target.

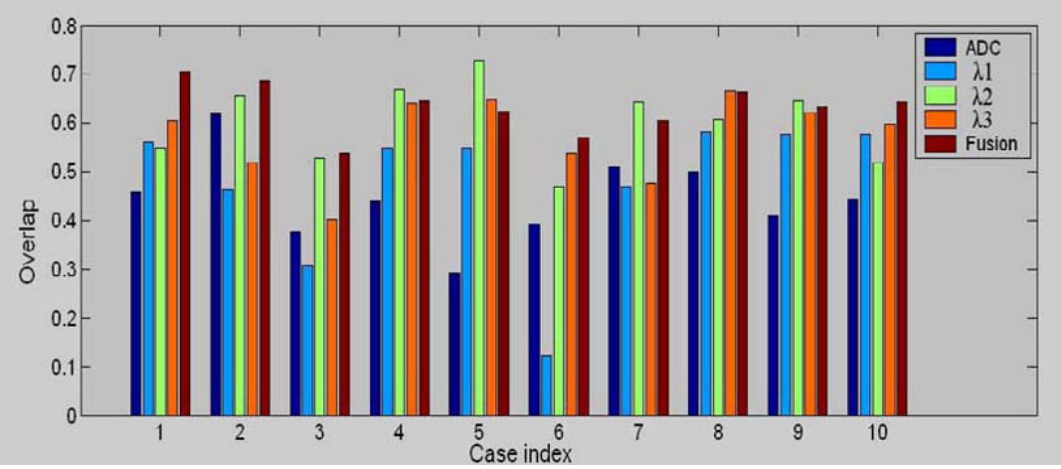

(a)

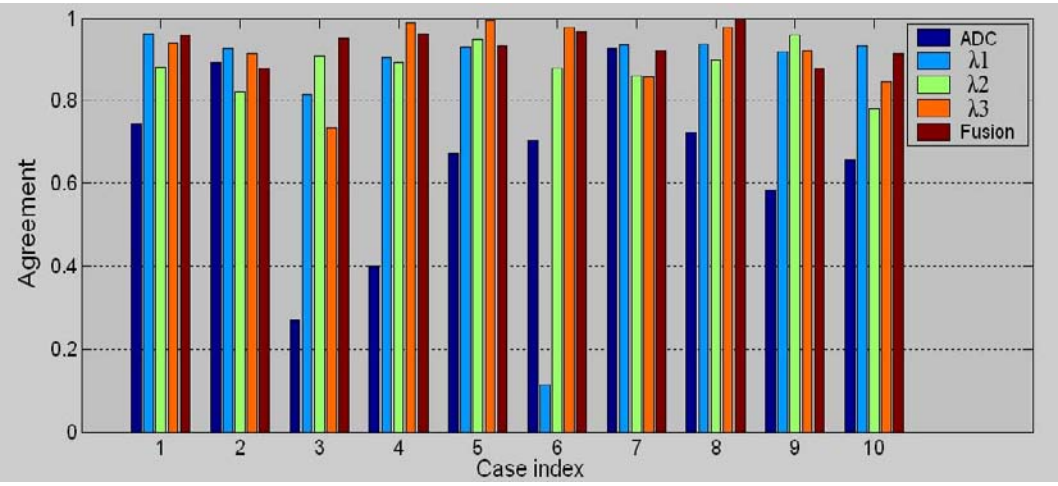

(b)

Figure 4. Evaluation of the tissue segmentation method. (a) Volume overlap for individual channel segmentation result and that for fusion result. The average overlaps of four single channel segmentations and the fusion result are 0.44 ± 0.08, 0.48 ± 0.13, 0.60 ± 0.08, 0.57 ± 0.07 and 0.63 ± 0.04 respectively. (b) Volume agreement for individual channel segmentation result and that for fusion result. The average agreements of four single channel segmentation results and the fusion result are 0.66 ± 0.18, 0.84 ± 0.23, 0.88 ± 0.05, 0.92 ± 0.08 and 0.94 ± 0.04 respectively.

The results of volume agreement for these ten cases are shown in figure 4(b). We see that the channels with maximum volume agreement vary with each case (see figure 4(b)). This again emphasizes the importance of the multiple-channel fusion method in differentiating the performance levels of different channels. Figure 4(b) shows that the multiple-channel fusion result has the highest volume agreement averaged over the ten cases. On average, the mean values and the stand deviations of agreements for four individual channel segmentation results and the fusion result are 0.66 ± 0.18, 0.84 ± 0.23, 0.88 ± 0.05, 0.92 ± 0.08 and 0.94 ± 0.04 respectively.

3.5. Experiment 4

The previous experiments show that the multi-channel fusion algorithm has better results from only one channel. To demonstrate how the different channels affect the results of multi-channel fusion segmentation, we evaluated the contribution from different channels by measuring the change of the posterior probability (reference to Equation 6) between W_i and W_{ij}, where W_i is the posterior probability got from all channel according to Equation 6, and W_{ij} is also the posterior probability got from all channel except channel j.

We can define the change weight as following:

$$CW_j = \frac{\sum_i \left| W_{ij} - W_i \right|}{\sum_j \sum_i \left| W_{ij} - W_i \right|} \tag{8}$$

Where j indicates the channel we use for the multi-channel fusion, and i indicates the voxels of the image volume. According to Equation (8), channel with high change weight(CW) indicates high contribution, because the posterior probability varies greatly without this channel, whereas channel with low change weight indicates low contribution, because the posterior probability varies little with or without this channel.

We conducted this experiment over the ten cases. Figure 5 shows the change weight for four channels (ADC, λ1, λ2, λ3). The average change weight of posterior probability for the four channels are 0.17 ± 0.07, 0.20 ± 0.04, 0.43 ± 0.08 and 0.19 ± 0.10 respectively. Based on the result in figure 5, it is apparent that the channel λ2 has a larger contribution to the fusion procedure in most cases. Nevertheless, the other three channels also have import contributions to the segmentation result.

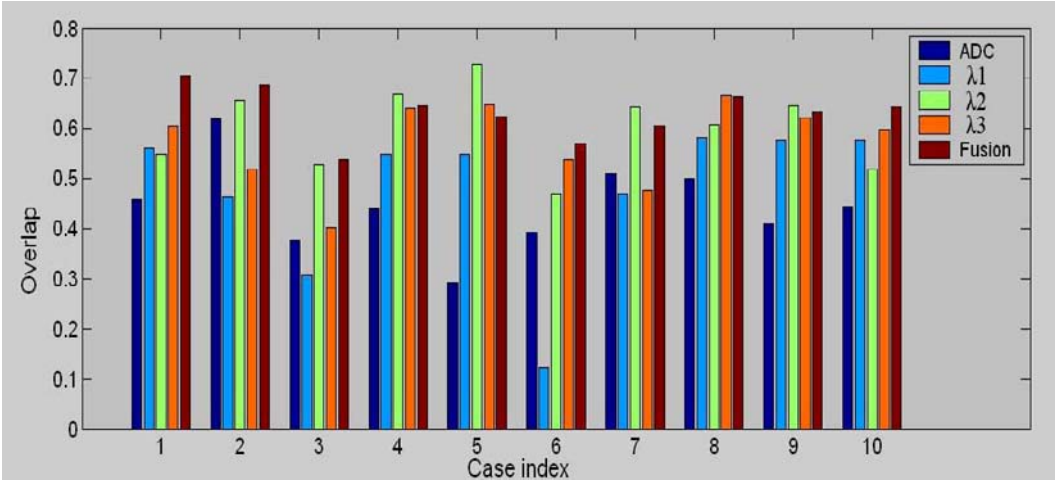

(a)

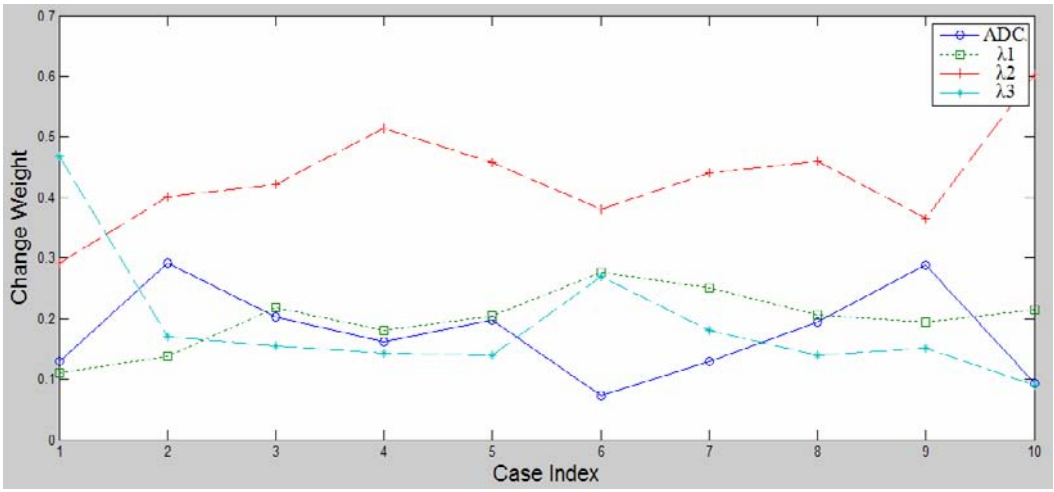

(b)

Figure 5. Change weight of posterior probability of four channels (ADC, λ1, λ2, λ3) for CSF segmentation over ten cases. The average change weight of posterior probability for the four channels are 0.17±0.07, 0.20±0.04, 0.43±0.08 and 0.19±0.10 respectively.

3.6. Experiment 5

In this section, we compare the proposed multiple-channel fusion method with our previous method of using two only, e.g., ADC and FA channels (Liu *et al*., 2006), as well as with the multi-spectral segmentation algorithm in the FSL MFAST (Zhang *et al*., 2001). It is noted that when performing the multi-spectral segmentation, we used all of the seven channels. To quantify the comparison, table 2 shows the volume overlaps (O_j) and volume agreements (A_j) between the segmentation maps using different algorithms with that

obtained by the SPGR segmentation map. It is apparent that the results using the ADC and FA channels have much lower CSF overlaps and agreements than the multi-spectral segmentation algorithm and the proposed multiple-channel fusion method. It is noted that the volume overlaps and agreements of CSF are much lower than the results in (Liu *et al*., 2006), because the SPGR segmentation result was used to guide the segmentation of CSF in (Liu *et al*., 2006), but not used in this work. Since low volume overlap and agreement in CSF would cause severe problems of heterogeneous voxels in measurement of gray matter properties, the result in table 2 verifies that the proposed multiple-channel fusion method is much more preferred than the tissue segmentation method based on only two channels.

For the multi-spectral segmentation algorithm, though its performance in CSF volume overlap and agreement is comparable to the proposed multiple-channel fusion method (table 2), its performances in GM and WM volume overlaps and agreements are poor (table 2). The reason might be the proposed multiple-channel fusion method exploits the STAPLE algorithm to estimate the optimal combination of the segmentations in seven different channels, while the multi-spectral segmentation algorithm does not.

Table 2. Volume overlap (O_j) and volume agreement (A_j) with different algorithms

	WM		GM		CSF	
	O_j (%)	A_j (%)	O_j (%)	A_j (%)	O_j (%)	A_j (%)
ADC+FA	0.83	0.84	0.56	0.94	0.28	0.56
Multi-spectral	0.46	0.74	0.43	0.84	0.80	0.57
Multi-channel	0.68	0.89	0.64	0.85	0.63	0.94

The result is averaged over ten cases. The third, fourth and fifth rows show the volume overlaps and volume agreements of the segmentation results using the ADC+FA channel, using the FSL MFAST multi-spectral segmentation algorithm and using the proposed multi-channel fusion algorithm respectively.

As an example, figure 6 shows the segmentation results using the segmentation method based on the two channels of ADC and FA, the segmentation result using the FSL MFAST multi-spectral segmentation method, and the segmentation result using the proposed multi-channel fusion method and the SPGR segmentation result. Clearly, the proposed multiple-channel fusion method generates closer segmentation result with SPGR segmentation result than the other two methods.

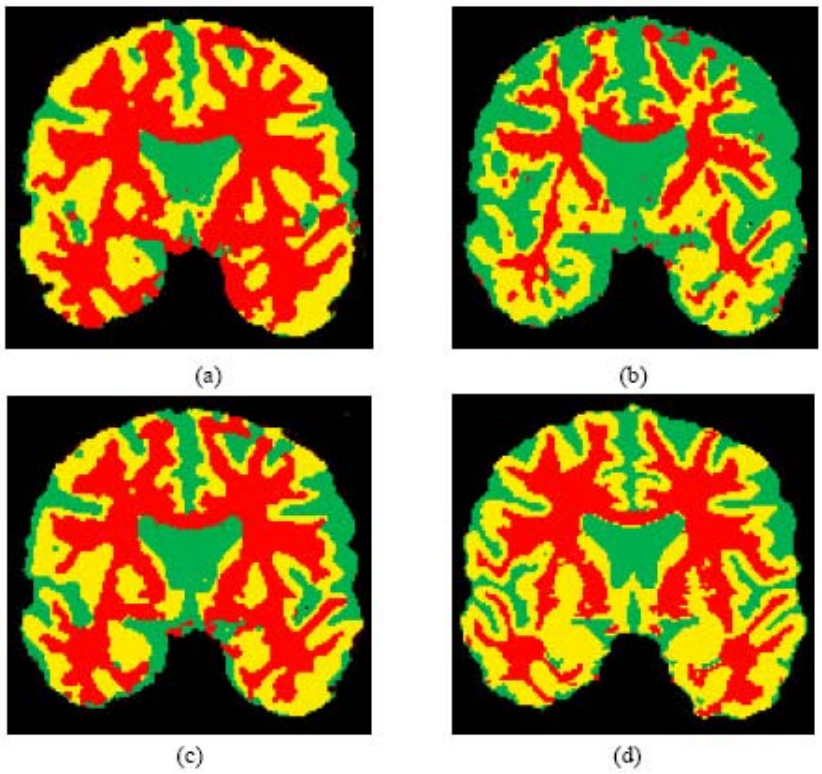

Figure 6. (a) Tissue segmentation map using ADC and FA channels. (b) Tissue segmentation map using FSL MFAST multi-spectral segmentation algorithm. (c) Tissue segmentation map using multiple-channel fusion algorithm. (d) Tissue segmentation map using SPGR image.

3.7. Application: Alternative Brain Tissue Segmentation Method

Tissue segmentation based on structural data, e.g., T2-weighted image, sometimes can produce undesirable segmentation result. For example, tissue segmentation using T2-weighted image cannot accurately distinguish putamen and thalamus, as shown in figure 7(b), whilst tissue segmentation based on DTI data can achieve better results, as shown in figure 7(e) (The data is provided by Dr. Susumu Mori of the Johns Hopkins Univ. Details about imaging settings are referred to http://cmrm.med.jhmi.edu/). White arrows point to putamen and thalamus areas where tissue segmentation in DTI space has better results than that based on T2-weighted image. Therefore, in the absence of structure data or in the case where desirable segmentation result from structure data cannot be obtained, tissue segmentation based on DTI data via the multiple-channel fusion method provides an alternative means to obtain tissue maps of the brain.

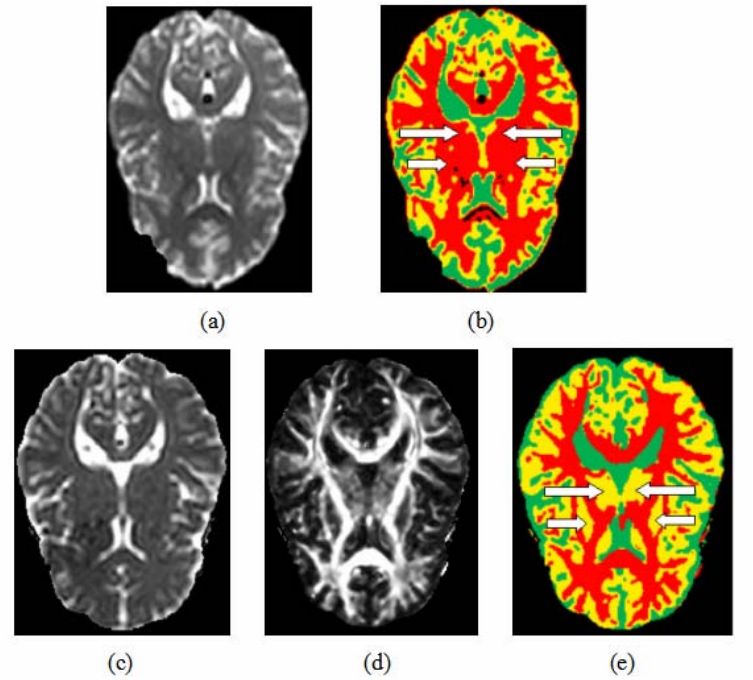

Figure 7. Tissue segmentation using T2-weighted image and DTI images (seven channels). (a) T2-weighted image. (b) Tissue segmentation using T2 image. (c). ADC image. (d). FA image. (e). Tissue segmentation map through multichannel fusion. White arrows point to areas where tissue segmentation in DWI/DTI space has better results than that in T2-weighted image.

4. Discussion and Conclusion

We have demonstrated that the brain tissue segmentation based only on single channel in DTI space produces less reliable result, and that the multiple-channel fusion method presented in this chapter can substantially improve the segmentation. There are two important aspects to the final segmentation results: (1) the performance of individual channel segmentation, and (2) the assessment of individual channel segmentation and fusion of them. A variety of issues are related to the first aspect, including the performance of individual channel segmentation, e.g., DTI data quality and the segmentation method used. In the future, we will test our multiple-channel fusion method on datasets with various image resolutions and qualities. In addition, we will test different tissue segmentation methods, e.g., the methods in (Wells *et al*., 1996; Pham *et al*., 1999; Dale *et al*., 1999), for individual channel segmentation and investigate how different segmentation methods affect the final result.

The second issue is addressed by the published STAPLE algorithm, which identifies the performance levels of different segmentation maps and estimates an optimal combination of the segmentation. This is fundamentally different from the voting rule (Warfield *et al*., 2004). In this work, we used one fixed set of overlaps (please refer to subsection 3.2) for the initialization of $(p_j^{(0)}, q_j^{(0)})$. In our future work, we will investigate how the initialization of

$(p_j^{(0)}, q_j^{(0)})$ will influence the final multi-channel fusion results, and how to achieve desirable initializations.

In this work, we use seven channels that are the most frequently used in the DWI/DTI image analysis, as we believe these channels provide complementary important information, e.g., the λ1, λ2, and λ3 channels describe the diffusion of three orthogonal directions separately. However, how many channels, or what combination of these channels, is adequate to obtain a satisfactory brain tissue segmentation result would need further investigation. A related issue is that the original STAPLE algorithm assumes that different channels are mutually independent. However, this is not the case in the application of DTI based tissue segmentation since certain channels are derived from other channels. Therefore, how the degree of mutual independence between channels influence the segmentation result by the STAPLE based fusion method needs further investigation. Another interesting issue to be investigated is how the inclusion of channels that are not intrinsically within the same space as DTI, e.g., T1 or T2 weighted channel, into the STAPLE fusion procedure will influence the final multi-channel fusion result.

In the absence of digital DTI phantoms, currently, we evaluate the proposed tissue segmentation method by measuring the volume agreement and volume overlap between the segmentation results in DWI/DTI space and that in SPGR space. A similar assumption made here as that in Liu *et al.*, 2006 is that the SPGR image provides relatively reliable tissue contrast and segmentation. However, it is noted that SPGR images do not have ideal tissue contrast, and cannot serve as a gold standard. Voxel-based comparison using the volume overlap measure might be inaccurate given the possible mis-alignment between the DTI image and SPGR image caused by a variety of reasons such as the geometric distortion in DTI imaging, the partial volume effect, the reslicing and interpolation of DTI data, and the co-registration error. In the future, evaluation and validation studies could be performed based on comparison of the automated segmentation result with those obtained by expert manual segmentation results.

In summary, we presented a brain tissue segmentation method based on DTI data. This method fuses seven two-class segmentation maps, generated by utilizing the tissue contrast exiting in the corresponding single channel, to obtain a complete brain tissue segmentation map using the STAPLE algorithm. The tissue segmentation results for ten test cases show that the single channel segmentation in DTI space is less reliable, and an optimal combination of seven selected channels produces significantly improved results. The STAPLE algorithm also plays a key role in computing the probabilistic estimate of the true segmentation and a measure of the performance level represented by each segmentation.

Acknowledgment

This research was done and funded by a research grant to STCW by Harvard Center for Neurodegeneration and Repair, Harvard Medical School (HMS), when both authors were affiliated with HMS. Parts of public DTI and SPGR datasets from NIH funded NAMIC provided by the Laboratory of Neuroscience, Department of Psychiatry, Boston VA Healthcare System and Harvard Medical School. We want to express our thanks to Dr.

Susumu Mori for sharing the DTIStudio software and DTI datasets, to STAPLE authors and ITK for sharing the STAPLE filter, to FSL developers, and to Hai Li of the Center for Biotechnology and Informatics at The Methodist Hospital Research Institute for helping prepare some of the figures presented in this chapter.

References

[Basser, 1994] Basser PJ, Mattiello J, LeBihan D,1994. Estimation of the effective self-diffusion tensor from the NMR spin echo. *J. Magn. Reson,* 103:247-254.

[Basser, 2002]Basser PJ, Jones DK, 2002. Diffusion tensor MRI: theory, experimental design and data analysis-a technical review. *NMR Biomed.* 14:456-467.

[Bammer, 2003] Bammer R, 2003. Basic principles of diffusion-weighted imaging. *Eur. J. Radiol.* 45: 169-184.

[Dale, 1999] Dale, A.M., Fischl, Bruce, Sereno, M.I.,1999. Cortical Surface-Based Analysis I: Segmentation and Surface Reconstruction. *NeuroImage.* 9(2):179-194.

[Johanna, 2002]Johanna Helenius, Lauri Soinne et al, 2002. Diffusion-Weighted MR imaging in normal human brains in various age groups. *AJNR,* 23: 194-199;

[Kubicki 2005] Kubicki M, Park H, Westin CF, Nestor PG, Mulkern RV, Maier SE, Niznikiewicz M, Connor EE, Levitt JJ, Frumin M, Kikinis R, Jolesz FA, McCarley RW, Shenton ME. DTI and MTR abnormalities in schizophrenia: analysis of white matter integrity, *Neuroimage.* 2005 Jul 15; 26(4):1109-18.

[Le Bihan D,1991] Le Bihan D, 1991. Molecular diffusion nuclear magnetic resonance imaging. *Magn. Reson.* Q 7: 1-30.

[Le Bihan D, 2001]Le Bihan D, Mangin JF, Poupon C et al., 2001. Diffusion tensor imaging: concepts and applications. *Magn. Reson. Imaging.* 13: 534-546.

[Li, 2001] Li S. Z., 2001. Markov random field modeling in image analysis, Springer-Verlag, New York

[Liu, 2005a]Liu T., Young GS, Chen NK, Huang L, Wong STC, 2005. 76-space analysis of gray matter diffusivity: methods and application, *MICCAI* 2005, *Palm Springs,* California.

[Liu, 2004] Liu T., Shen D., Davatzikos C., 2004. Deformable registration of cortical structures via hybrid volumetric and surface warping. *NeuroImage,* 22(4): 1790-1801.

[Liu, 2006] Liu T, Young G, Huang L, Chen NK, Wong STC. 76-Space analysis of grey matter diffusivity: Methods and applications. *NeuroImage.* 2006 May 15;31(1):51-65.

[Moseley, 1990] Moseley ME, Kucharczyk J, Mintorovitch J, et al.,1990. Diffusion-weighted MR imaging of acuter stroke: correlation with T2-weighted and magnetic susceptibility-enhanced MR imaging in cats. *AJNR.* 11:423-429.

[Perona, 1990] Perona P, Malik J, 1990. Scale-space and edge detection using anisotropic diffusion. *IEEE Transactions on Pattern Analysis Machine Intelligence,* 12:629-639.

[Pham, 1999] Pham D. L. and Prince J. L., 1999. Adaptive fuzzy segmentation of magnetic resonance images. *IEEE Trans. Med. Imag.* 18(9):737-52.

[Sundgren, 2004] Sundgren P. C. , Dong1 Q. , Gómez-Hassan1 D. , Mukherji1 S. K. , Maly1 P., Welsh1 R., 2004. Diffusion tensor imaging of the brain: review of clinical applications. *Neuroradiology*. 46(5): 339-350.

[Warfield, 2004]Warfield S.K, Zou K.H *et al*., 2004. Simultaneous truth and performance level estimation (STAPLE): an algorithm for the validation of image segmentation. *IEEE Trans. Med. Imag.* 23:903-921.

[Wells, 1996] Wells W. M., Grimson E. L., Kikinis R., Jolesz F. A., 1996. Adaptive segmentation of MRI data. *IEEE Trans. Med. Imag.* 15:429–442.

[Woods, 1998] Woods R. P., Grafton S. T., Watson J. D. G., Sicotte N. L., Mazziotta J. C., 1998. Automated image registration: II. Intersubject validation of linear and nonlinear models. *Journal of Computer Assisted Tomography.* 22:153-165.

[Zhang, 2001] Zhang Y., Brady M., Smith S., 2001. Segmentation of brain MR images through a hidden Markov random field model and the expectation-maximization algorithm. *IEEE Trans. Med. Imag.* 20(1): 45-57.

In: Handbook on White Matter
Editors: T. B. Westland and R. N. Calton
ISBN: 978-1-60741-034-8

Chapter XIV

Three-Dimensional Microstructural Analysis of Human Brain Tissue by Using Synchrotron Radiation Microtomographs

Ryuta Mizutani*[*a], Akihisa Takeuchi[b], Kentaro Uesugi[b], Susumu Takekoshi[c], R. Yoshiyuki Osamura[c] and Yoshio Suzuki[b]

[a] Department of Applied Biochemistry, School of Engineering,
Tokai University, Kitakaname 1117, Hiratsuka, Kanagawa 259-1292, Japan
[b] Research and Utilization Division, JASRI/SPring-8,
Kouto 1-1-1, Sayo, Hyogo 679-5198, Japan
[c] Department of Pathology, Tokai University School of Medicine,
Shimokasuya 143, Isehara, Kanagawa 259-1193, Japan

Abstract

Recent application of synchrotron radiation to high-resolution computed tomography has resolved three-dimensional structures at micrometer to submicrometer resolution, although little is known about the microstructure of soft tissues including white matter of human brain. This is because soft tissues are composed of light elements that give little contrast in a hard x-ray transmission image. In clinical diagnosis, luminal structures of a living body are visualized by using x-ray contrast media. These contrast media contain high atomic-number elements that absorb x-rays efficiently. We have recently shown that the neuronal structure of human brain can be visualized by contrasting neurons using the metal impregnation method. Here, we report x-ray microtomographic studies of human cerebral cortex stained with high atomic-number elements. Staining protocols were developed to visualize the three-dimensional microstructure of white and gray matter of human brain tissues. Methods for embedding and mounting soft tissues for the microtomographic analysis are also described. The obtained three-dimensional images

* Corresponding author: ryuta@tokai-u.jp
Abbreviations: CT, computed tomography; high-Z, high atomic number.

revealed the microstructures of white and gray matter, which are responsible for human brain functions.

Introduction

The three-dimensional structure of the central nervous system (CNS) is composed of a huge number of neural cells and extracellular matrices, which are responsible for the cerebral function. The functional mechanism of the brain can be revealed by visualizing these constituents forming the neuronal networks. Confocal optical microscopy is the primary method for visualizing three-dimensional structures of biological systems [1]. However, absorbance at emission or excitation wavelengths interferes with the detection of fluorescence elicited from the internal architecture. Thus, confocal microscopy is mainly used for imaging sectioned samples labeled with highly selective probes. Reconstruction of the entire three-dimensional structure from such sectioned samples entails defining the precise spatial relationships of each image. Optical computed tomography and ultramicroscopy have recently been applied to the three-dimensional analysis of biological tissues [2,3], although the internal structure of opaque or chromatic samples cannot be observed using visible light. While magnetic resonance imaging provides a non-invasive mapping of neural activity [4], cellular structures are not visualized because of the limited spatial resolution.

In contrast, the transparency of biological tissue to hard x-rays enables radiographic analysis of the internal microstructure. However, soft tissues are composed of light elements, which produce little contrast in a hard x-ray transmission image. The contrast can be enhanced by using soft x-rays, but these are significantly absorbed even by water and air, so analysis has consequently been performed using thin samples. The application of phase contrast techniques for developing interferometric images has been reported [5-7]. An interferometric image of soft tissue gives the distribution of electron densities, while the image contrast has no inherent relationship with the biological functions or cellular organization. Therefore, the three-dimensional structure of soft tissues should be visualized by contrasting each biological constituent.

In clinical diagnosis, luminal structures of a living body are visualized by using x-ray contrast media. These contrast media contain high atomic-number (high-Z) elements, such as barium or iodine, that absorb x-rays efficiently. We have recently shown that the neuronal structure of the *Drosophila* larvae CNS can be visualized by contrasting every neuron with the metal impregnation method [8,9]. This microcontrasting method allowed the visualization of cellular and subcellular structures of human brain [10,11]. Element-specific structural analysis has also been achieved by using x-ray absorption edges of the contrasting elements [12].

Recent application of synchrotron radiation to computed microtomography (micro CT) has resolved three-dimensional structures at micrometer to submicrometer scales [13-16]. In conjunction with the metal microcontrasting, micro-CT analysis has revealed the three-dimensional structure of the fruit fly CNS [9,12], human cerebral cortex [10,11], human capillary vessels [10,11], zebrafish body [11], and fruit fly body [11].

The microcontrasting CT analysis can be applied to any biological tissues. A number of metal impregnation methods have been developed for the radiographic observation of biological tissues [8-12]. Here, we report micro-CT analysis of the three-dimensional microstructure of human cerebral cortex using the impregnation methods.

Tissue Staining

For the microcontrasting visualization of tissue structures, samples should be stained with elements in the 5th or 6th row of the periodic table. The high electron density given by these high-Z elements can be visualized as x-ray absorption contrasts in radiographs. While Golgi staining gives sufficient contrast with the 5th-row element silver, most of the following staining methods use 6th-row elements because the visualization of microstructure can be achieved only with the highly localized density of electrons.

Absorption contrast in tomograms is expressed by the linear absorption coefficient. The coefficients at 12.000 keV (corresponding to an x-ray wavelength of 1.0332 Å) are 3477 cm^{-1} for gold and 777 cm^{-1} for silver. To visualize the structure with 5 cm^{-1} contrast, the sample should be stained with gold metal particles at a density of 0.14%(v/v) or silver at the higher density of 0.64%(v/v). It has been reported that gold-impregnated tissue appropriate for micro-CT analysis exhibited a gold density of 0.24%(v/v) [9].

The x-ray absorption spectrum of each element shows stepwise edges that originate from the energy levels of electron orbitals. The linear absorption coefficient exhibits a maximum at the wavelength corresponding to the edge top of the absorption spectrum. The x-ray wavelengths available from synchrotron radiation sources vary depending on the radiation facilities and beamline optics, but typically they are in the energy range from 5 to 30 keV. Therefore, elements showing absorption edges in this range, such as the 6th-row elements gold, platinum, mercury, and osmium, can be used for effective visualization of microstructural components.

Element-specific visualization has been performed using x-ray absorption edges [11,12]. Each element was visualized as a difference absorption-coefficient image by subtracting the three-dimensional distribution of linear absorption coefficients at the edge bottom of the x-ray absorption spectra from those at the edge top. Although the element-specific images are not shown in this chapter, the staining methods described below can also be used for specific visualization.

Tissue Samples

Frontal cortex of normal brain tissue (44 years old, male) was dissected at autopsy and fixed with 10% formaldehyde for 7 days. Anatomical analysis found no abnormality in the brain tissue. The tissue sample was further dissected into tissue blocks and subjected to staining procedures. Human samples were obtained with consent, using protocols approved by the Clinical Research Review Board of Tokai University Hospital.

Golgi Impregnation

Golgi silver impregnation [17] is a conventional staining method for the optical observation of neural cells. While this method uses dichromate and silver ions as stain dyes, electron densities given by silver should provide the major contribution for the x-ray absorption. While only a limited population of neurons is stained with this method, the mechanism of selective staining has not been revealed clearly.

Tissue blocks with dimensions of about 5 mm × 5 mm × 10 mm were subjected to Golgi impregnation as described previously [10]. The tissues were washed for 5 min in a solution containing 25 mg/mL potassium dichromate and 4% formaldehyde and then incubated at 25°C for 7 days in a solution containing 25 mg/mL potassium dichromate. After being blotted with filter paper, the tissues were further incubated at 25°C for 48 hr in 7.5 mg/mL silver nitrate. Residual silver nitrate was washed away with water. These steps were repeated three times.

Bodian Impregnation

Reduced-silver Bodian impregnation is another conventional procedure used for the optical observation of neural tissues [18]. This method stains argyrophil neuropils with silver ions. The stained image is then enhanced with gold particles, which can be visualized in the x-ray image. It has been reported that tissue treated with the following procedure was stained with gold metal particles but not with silver ones [9].

Tissue samples with typical dimensions of 0.5 mm × 0.5 mm × 2.5 mm were prepared from the fixed tissue block. These samples were progressively dehydrated in 70%, 80%, 90%, 95%, and 100% ethanol. Defatting was performed by immersing these tissues sequentially in acetone for 24 hr and xylene for 24 hr. After being washed with ethanol, the tissues were progressively rehydrated in 90% and 70% ethanol and then in distilled water. These rehydrated tissues were subjected to modified reduced-silver staining, as described previously [9,11]. The impregnation was performed for 15 hr at 37°C using 0.4 mg/mL silver nitrate solution containing 7.5 mg/mL pyridine and 50 mM sodium borate (pH 8.4). The silver impregnation can also be performed using 10 mg/mL silver protein (Merck, NJ) solution. The samples were then developed for 10 min at 30°C in a solution containing 10 mg/mL hydroquinone and 100 mg/mL sodium sulfite. After being washed with distilled water twice, the samples were immersed sequentially in 5 mg/mL hydrogen tetrachloroaurate containing 0.5% Triton-X100 (MP Biomedicals, OH) for 50 min, 20 mg/mL oxalic acid for 30 min, and 50 mg/mL sodium thiosulfate for 5 min, with washes in distilled water between immersions. The aurate deposition can be enhanced by the irradiation of 350- or 940-nm light. Finally, the samples were washed with distilled water.

Osmification

Osmium fixation is a widely used method mainly for electron microscopic analysis. There has been discussion of phospholipids in plasma membranes being stained by osmification. Tissue cubes of about 1 mm were treated with 10 mg/mL osmium tetroxide solution for 4 hr. The stained tissues were washed with distilled water and further dissected into 0.5-mm cubes.

Mercury Fixative Staining

B-5 fixative containing mercuric chloride has been used for tissue fixation. Mercury localization in the fixed tissue can be visualized by x-ray analysis. Tissue samples were immersed in fixative containing 50 mg/mL mercuric chloride, 12.5 mg/mL sodium acetate, and 4% formaldehyde for 4 hr at 25°C. The stained tissue was then washed with distilled water.

Reticulin Silver Impregnation

Reticular fiber can be visualized by reticulin silver impregnation. Tissue samples with typical dimensions of 0.5 mm × 0.5 mm × 2.5 mm were prepared from the fixed tissue block and defatted as described in the Bodian impregnation procedure. The tissue was then treated with 5 mg/mL potassium permanganate for 10 min, 20 mg/mL oxalic acid for 10 min, and 20 mg/mL ferric ammonium sulfate for 3 min, with washes in distilled water between immersions. The obtained tissue was washed with distilled water five times. Ammoniacal silver solution was prepared by adding 28% aqueous ammonia to a mixture of 10 mL of 100 mg/mL silver nitrate and 0.88 mL of 1.0 M sodium hydroxide, until brown precipitates in the silver solution dissolved. The tissue was incubated in a ten-fold diluted solution of this ammoniacal silver for 25 min in the dark and washed with 95% ethanol. The stained tissue was treated with a solution containing 0.4 mg/mL ferric ammonium sulfate and 0.4% formaldehyde for 10 min. After being washed with distilled water five times, the samples were immersed sequentially in 10 mg/mL hydrogen tetrachloroaurate for 150 min, 20 mg/mL oxalic acid for 10 min, and 50 mg/mL sodium thiosulfate for 5 min, with washes in distilled water between immersions.

Immunogold Staining

Immunological staining is rather difficult for block tissues. Although it has been reported that the permeability of antibodies can be improved by heat treatment [19], the brain tissue used in the present study showed insufficient contrast for visualizing the three-dimensional structure. Therefore, the nerve tissue of *Drosophila* larvae was used as test samples for the immunological visualization. Wild-type *D. melanogaster* Canton-S larvae were raised on

standard cornmeal-molasses fly food and kept at 20°C. The CNSs of third instar larvae were dissected and fixed overnight at 4°C in 4% formaldehyde. After being washed three times with a phosphate buffered saline (PBS: 10 mM sodium phosphate and 0.15 M sodium chloride, pH 7.4) containing 0.5% Triton-X100, the CNSs were incubated with 5% goat serum in PBS-Triton for 1 hr at 25°C. The tissues were incubated overnight at 4°C with mouse monoclonal antibody BP102 against *Drosophila* axon (Abcam, UK) diluted 1/1000 in the 5% serum PBS-Triton solution. After three rinses with PBS, the tissues were stained overnight at 4°C with 5-nm gold-conjugate of anti-mouse IgG (MP Biomedicals) diluted 1/10 in a 5% serum PBS solution. The stained tissues were rinsed three times with PBS, and then postfixed for 30 min at 25°C with 4% formaldehyde in PBS. After one 5-min rinse in PBS and five in distilled water, the tissues were subjected to silver impregnation as counter staining. The impregnation was performed for 40 hr at 37°C using 0.4 mg/mL silver nitrate solution containing 7.5 mg/mL pyridine and 50 mM sodium borate (pH 8.4). The CNS samples were then developed for 10 min at 25°C in a solution containing 10 mg/mL hydroquinone and 100 mg/mL sodium sulfite. These stained tissues were used for tomographic analysis without the aurate treatment.

Microtomographic Analysis

The x-ray dose of synchrotron radiation is much higher than that of laboratory x-ray tubes. Undulator light sources, such as BL20XU beamline of SPring-8 [20], have achieved an x-ray flux of over 10^{14} photons per second. Assuming that the photon flux density is 10^{12} photons/s/mm^2 at the sample position and the sample absorption coefficient is 1 mm^{-1}, the irradiation energy density is approximately 2×10^{-3} J/s/mm^2. The major effect of this high x-ray dose on post-mortem tissues is thermal influence causing structural changes. Therefore, tissue samples should be embedded in rigid resin, as described below.

The embedded tissue should be firmly mounted on the goniometer of the microtomograph because sample drift causes distortion in tomograms. Three-dimensional structural analysis is then performed by recording two-dimensional images of a sample by rotating the sample itself. According to sampling theorem, the presampling resolution can be retrieved from data sampled at a rate corresponding to twice the resolution spacing. Therefore, images for tomographic analysis are acquired with a pixel width of less than half the spatial resolution of the two-dimensional image.

These two-dimensional radiographs should be acquired by taking a sufficient step of $R\Delta\theta$ in the circumferential direction, where R denotes the distance from the rotation axis and $\Delta\theta$ the rotation angle per frame. If the detector pixel width is 2000, the distance R is 1000 pixels. Although each pixel in the reconstructed tomogram can be resolved by taking an $R\Delta\theta$ step of less than 1, a small step makes the data acquisition longer. Long data acquisition increases the possibility of sample drift, leading to unresolved sample images. Therefore, in this study, the $\Delta\theta$ step was set to 0.00175 radian or 0.10°, giving $R\Delta\theta$ of 1.75. Because two-dimensional images in the range from 0° to 180° should be taken for the tomographic reconstruction, a total of 1800 frames were acquired to determine one three-dimensional image.

By using each raster strip from these two-dimensional radiographs, we reconstructed a tomographic slice by the convolution back-projection method [21]. This reconstruction calculation was repeated for each tomographic slice, giving the entire three-dimensional structure. The obtained three-dimensional images were used for the analysis of cellular and subcellular structures of brain tissue.

Tissue Embedding

The stained tissues were sequentially dehydrated in 30%, 50%, 70%, and 90% ethanol, and then immersed in ethanol for 24 hr and *n*-butylglycidyl ether for 16 hr at room temperature. These dehydrated tissues were incubated in Petropoxy 154 epoxy resin (Burnham Petrographics, ID) at 4°C for 24 hr. The epoxy resin should be degassed in vacuum before use. If glycidyl ether was still observed as an upper layer of the resin solution, the tissues were placed into a new resin solution and incubated for an additional 24 hr at 4°C. Block samples larger than the width of the viewing field were dissected with razor blades in this step.

For the tomographs with a viewing field width of 1 mm, the tissue samples were embedded in a glass capillary [10]. Capillaries made of quartz, borosilicate, and soda glass (W. Müller Glas, Germany) have been used for x-ray diffraction experiments. Borosilicate capillaries with an outer diameter of 0.3–1.0 mm are appropriate for microtomographic analysis because borosilicate glass exhibits low x-ray absorption.

A setup for capillary embedding is shown in figure 1a. First, the capillary was filled with epoxy resin using a 1-mL syringe, as shown in figure 1b. After the top of the resin reached the funnel end of the capillary, the stopcock was open to air and the capillary was removed (figure 1c). The stained sample was placed at the funnel end of the capillary by using tweezers or needles (figure 1d). The capillary was again connected to the syringe while the stopcock was still kept open to air. Then the stopcock was turned to form a pass-through between the capillary and syringe. The sample in the resin was moved using the syringe into the capillary (figure 1e). After the sample was moved to the appropriate position, the stopcock was closed to fix the sample position (figure 1f). The sample position should be adjusted to about 20 mm from the capillary end in the case of the microtomographs at SPring-8. The capillary was cut with a diamond cutter and inserted in a short piece of silicone tubing (figure 1f–g). This tubing avoids contact between capillary ends and surroundings, and thus prevents resin leakage from the capillary ends by surface tension. These capillaries were placed in a polypropylene case and incubated at 90°C for 16 hr to rigidify the epoxy resin.

The larger samples with widths of 2–5 mm were embedded in resin pellets [10]. Silicone rubber tubing with an inside diameter of 3–5 mm and length of about 10–15 mm was attached to a flat surface of a polypropylene case by using the epoxy resin (figure 2a). This resin works as a bottom cap for the tubing. The tubing should be almost perpendicular to the polypropylene surface because the sample rotation axis is set perpendicular to the sample end surface. The tubing was incubated at 110°C for 2 hr to rigidify the resin cap. After the polypropylene case was cooled, the tubing was filled with resin by using a micropipette (figure 2b), and the sample was placed in this tubing (figure 2c). The sample tubing was

incubated again at 90°C for 16 hr to rigidify the resin, and finally the silicone tubing was removed (figure 2d).

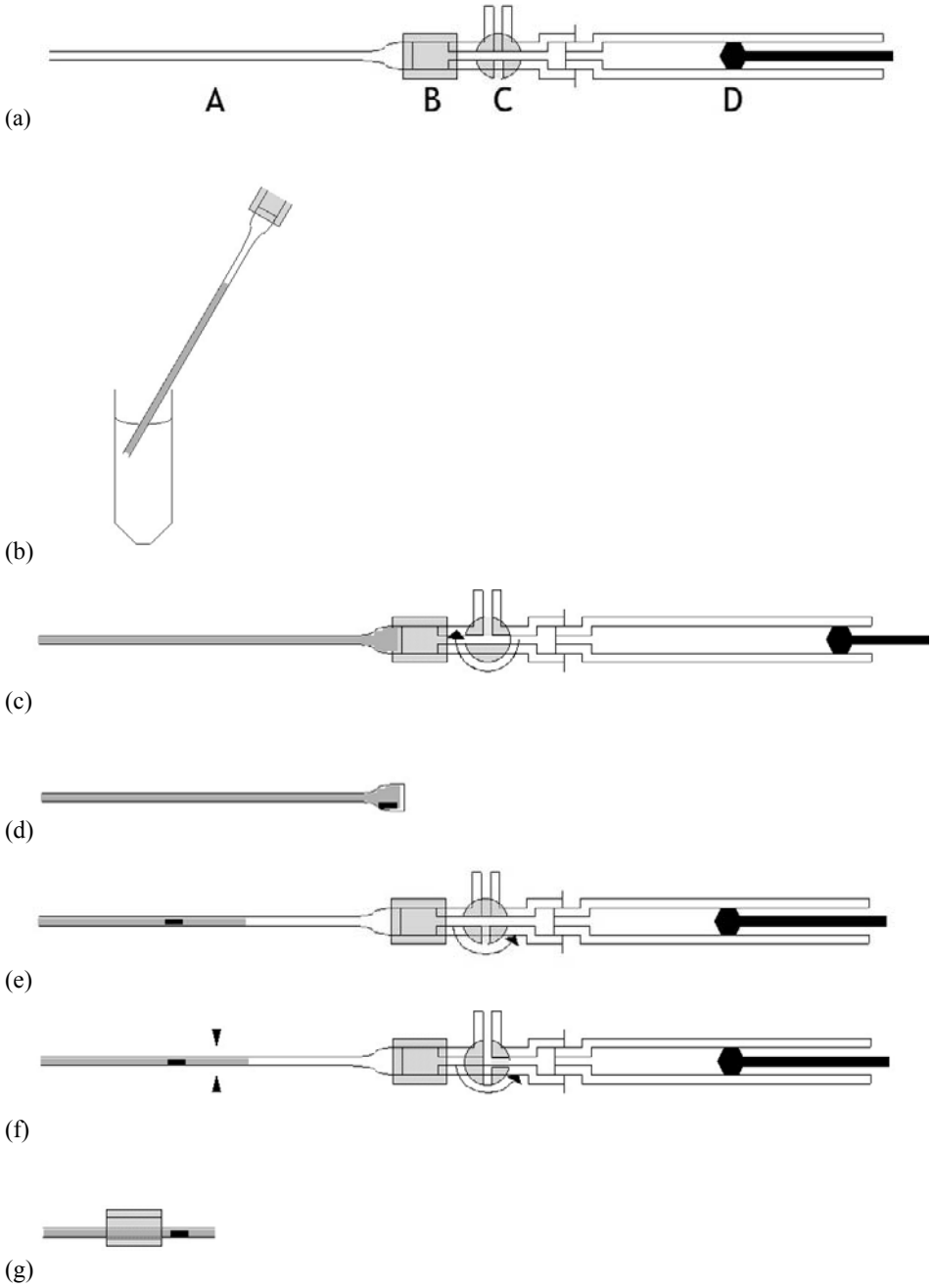

Figure 1. Capillary embedding. (a) Setup for capillary embedding. A, borosilicate capillary. B, tygon tubing. C, 3-way stopcock. D, syringe. (b) Fill the capillary with epoxy resin. (c) Open stopcock to remove capillary. (d) Place sample at the funnel end. (e) After connecting the capillary with the syringe, turn stopcock to move sample. (f) Close stopcock to fix the sample position and cut capillary. (g) Place capillary in short silicone tubing to avoid contact during rigidification at 90°C for 16 hr.

Loop embedding is another method for embedding a sample with dimensions of 0.2–1.5 mm [9]. The nylon loops used in protein cryocrystallography [22] can be used for tissue embedding. We used 0.4–0.5-mm diameter loops made of 20-µm diameter nylon fiber attached to a stainless steel pin (CryoLoops, Hampton Research, CA). First, the steel pin was cut at the 18-mm position and attached to a cryotube (CrystalCap, Hampton Research) using epoxy glue (figure 3a). The cryotube can be used for handling and keeping the loop sample (figure 3b). Then the tissue in a resin drop was placed on a stereomicroscope. Because most stained tissues are heavier than resin, the tissue should be moved to the drop surface by resin flows made by the loop. The tissue brought to the drop surface can be picked up with the loop (figures 3c, 3d). Excess resin attached on the sample loop was removed by streaking the loop on a flat surface of the resin drop container. These handling steps were performed under stereomicroscope observation. Then the loop was covered with a cryotube and incubated at 90°C for 16 hr. Resin rigidification should be confirmed by touching the resin surface with a needle because the heat conduction through the cryotube, steel pin, and nylon fiber largely depends on the sample setup.

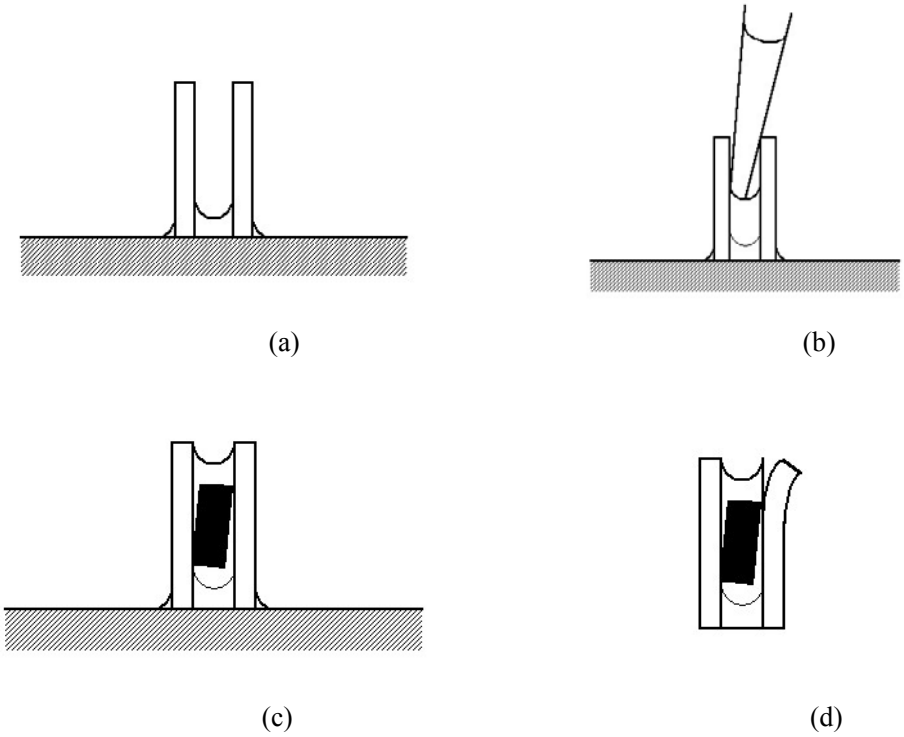

Figure 2. Pellet embedding. (a) Silicone tubing attached to a flat surface of a polypropylene case by using the epoxy resin. Incubate at 110°C for 2 hr to rigidify. (b) After cooling, fill the tubing with resin by using a micropipette. (c) Place sample in the tubing and incubate at 90°C for 16 hr to rigidify. (d) Remove silicone tubing.

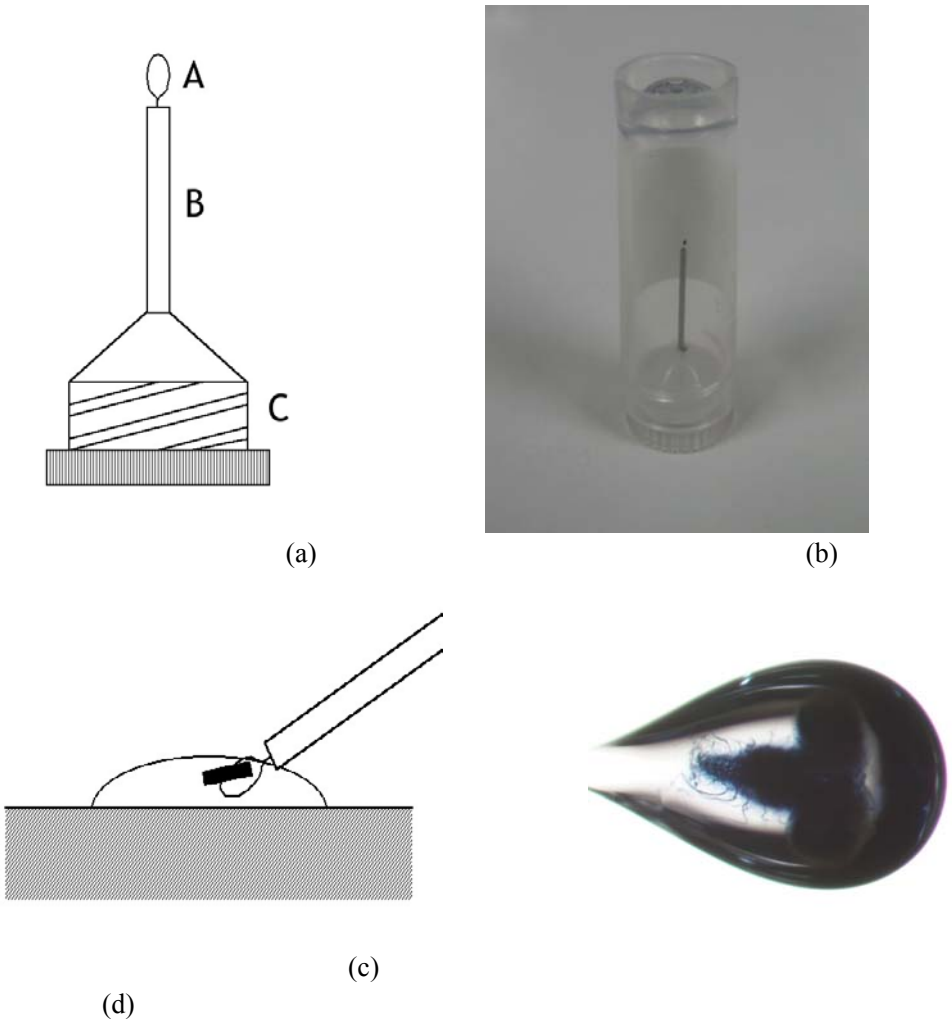

Figure 3. Loop embedding. (a) Setup of a loop with a cryotube. A, nylon loop. B, stainless steel pin. C, cryotube cap. (b) The tube can be used as a container. (c) Sample pickup. (d) Loop-embedded sample.

Sample Mount

The tissue samples were mounted by using brass fittings specially designed for the microtomographic analysis (figure 4a–c). Their bottom base has a diameter of 10 mm and height of 10–20 mm, which is suitable for the goniometer head of the microtomograph at SPring-8. The upper-half columns of the fittings were designed to suit the glass capillary, loop, and resin pellet samples.

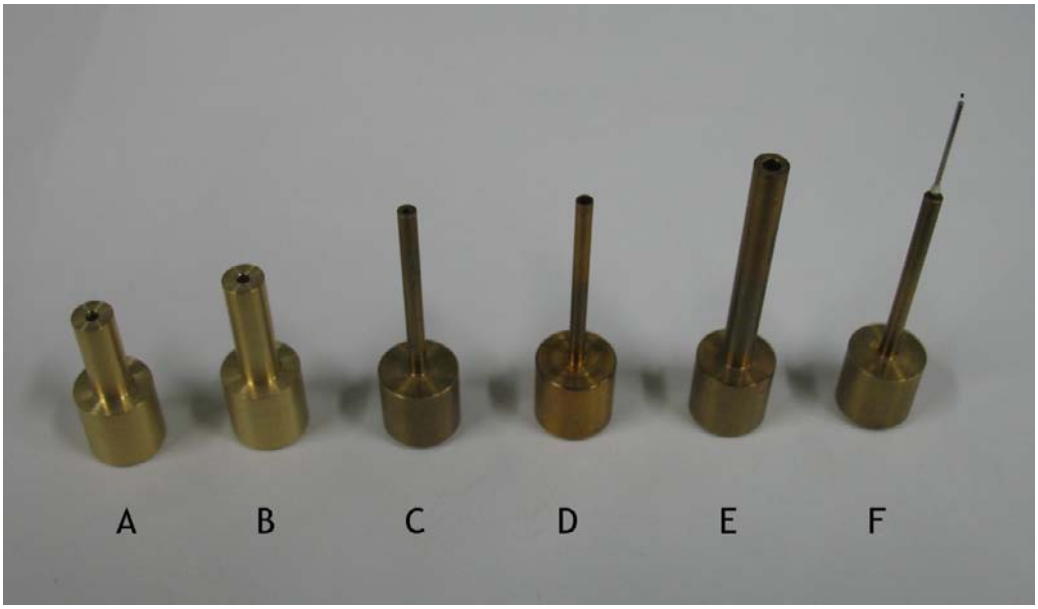

(a)

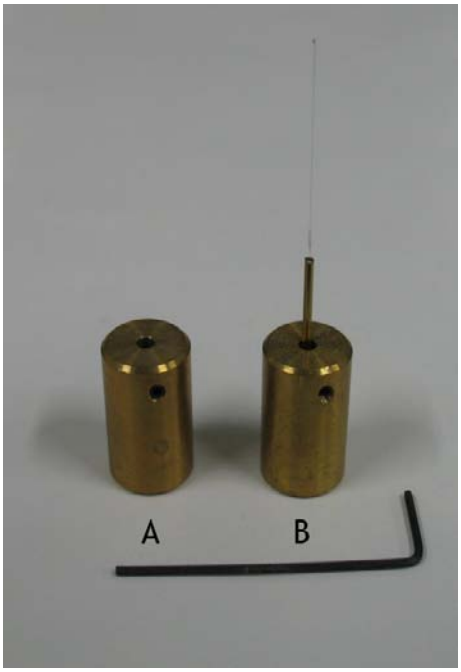

(b)

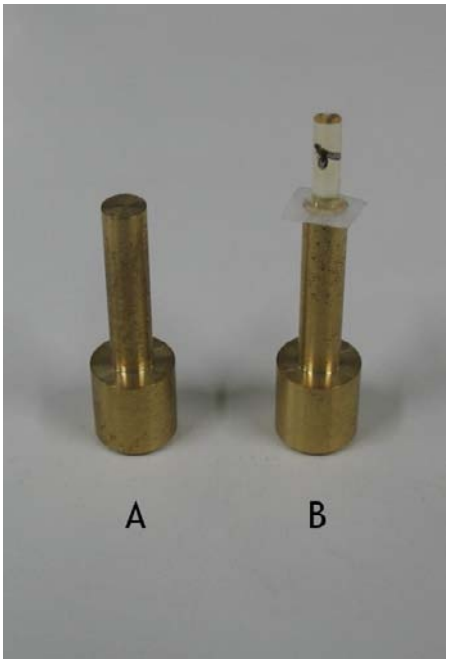

(c)

Figure 4. (Continues)

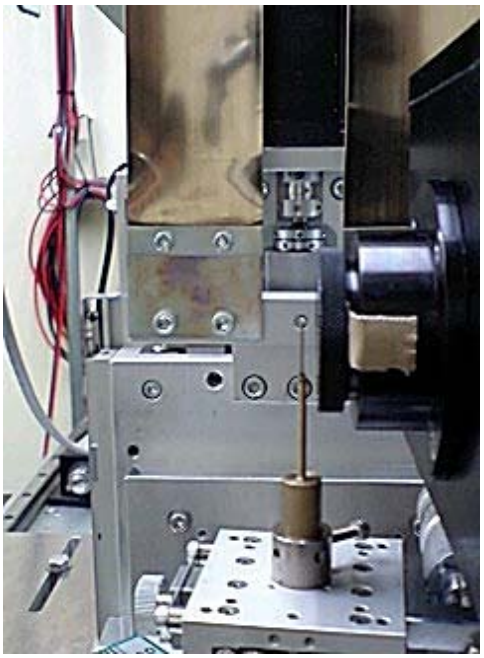

(d)

Figure 4. Brass fittings for micro-CT analysis. (a) A, fitting with upper column 5 mm in diameter × 12 mm in height with a 1.5-mmϕ hole. B, 5 mm in diameter × 15 mm in height with 1.5-mmϕ hole. C, 2 mm in diameter × 25 mm in height with 1.0-mmϕ hole. D, 2 mm in diameter × 25 mm in height with 1.5-mmϕ hole. E, 4 mm in diameter × 30 mm in height with 2.0-mmϕ hole. F, loop-embedded sample with fitting C. (b) A, fitting 10 mm in diameter × 17 mm in height with a 2.0-mmϕ hole. B, 0.4-mm capillary sample sleeved with brass tubing 15 mm in length × 1.0 mm outside diameter × 0.6 mm inside diameter is fixed with a set screw. (c) A, fitting with upper column 5 mm in diameter × 20 mm in height with flat end. B, pellet sample was attached to the flat end with adhesive tape. (d) Thin upper columns of fittings allowed the sample and imaging detector to be arranged in close proximity. This fitting has a taller base with a height of 20 mm.

The glass capillary samples and pin-hold loop samples were held with compound clay (Hampton Research) in a hole in the upper column of the fitting. The clay was rigid enough for radiographs to be taken during data acquisition. The thin upper column with a diameter of 2–5 mm and height of 12–30 mm allows the sample and image detector to be arranged in close proximity (figure 4d) to avoid image interference caused by phase contrast effects. Because the capillary has a diameter of 0.3–1.0 mm, the upper end of the fittings has a hole with a diameter of 1–2 mm and depth of 5 mm. Capillaries thinner than 0.5 mm in diameter were sleeved with brass tubing attached with epoxy glue. These brass sleeves can be fixed onto the fittings using set screws (figure 4b).

The pellet samples were mounted on the flat end of the brass fitting (figure 4c) using double-sided tape (NW-R15, Nichiban, Japan). The spatial resolution of the tomograph used for the pellet samples was evaluated to be 6–7 μm as described below. Therefore, sample drift was negligible even for mounting by adhesive tape.

Micro CT

The capillary and loop samples were mainly analyzed at the BL20XU beamline [20] of SPring-8 (Hyogo, Japan). Transmission radiographs were recorded with a CCD-based x-ray imaging detector (AA50 and C4880-41S, Hamamatsu Photonics, Japan) using monochromatic x-rays (CCD: charge-coupled device). The field of view and effective pixel size of the image detector were 1.00 mm × 0.65 mm and 0.50 μm × 0.50 μm, respectively. These pixel sizes were calibrated by moving samples with the goniometer stage. A total of 1800 images were acquired with a rotation step of 0.10° and exposure time of 300 ms. The spatial resolution of the three-dimensional structure was estimated to be 1.0 μm. It took about 35 min to acquire one dataset, though the imaging time can be shortened by reducing the viewing field or the number of radiographs if the faster acquisition is required.

The resin pellet samples were analyzed at the BL20B2 beamline [23] of SPring-8. Transmission radiographs were recorded using a CCD-based x-ray imaging detector (AA40P and C4880-41S, Hamamatsu Photonics) and monochromatic x-rays. The field of view and effective pixel size of the detector were 5.5 mm × 3.6 mm and 2.75 μm × 2.75 μm, respectively. Each image was acquired with a rotation step of 0.10° and exposure time of 600 ms. The resolution limits were evaluated to be 6.1 μm along the sample rotation axis and 7.4 μm perpendicular to the axis [24]. It took about 90 min to acquire one dataset.

Three-Dimensional Structural Analysis

The convolution back projection method using a Chesler-type filter was used for tomographic reconstruction [21]. The reconstruction calculation of 1312 tomograms of 2000 × 2000 pixels took about 3 hr on a Windows PC equipped with the Core 2 Duo processor operating at 2.1 GHz. Tomographic reconstruction with improved spatial resolution can be achieved by real-space interpolation [24] using the reconstruction program RecView available from http://www.el.u-tokai.ac.jp/ryuta/. The protocol for the tomographic reconstruction using this program is described in the Appendix.

Since the viewing field of micro-CT analysis is limited to a cylindrical region determined from the detector viewing field, data sets of samples longer than the height of the viewing field were taken in multiple batches. Each data set was recorded by displacing the sample along the sample rotation axis. The obtained radiographs were subjected to reconstruction calculation. To determine the positional relationship of the reconstructed structures, we superposed the ends of the three-dimensional structures by minimizing the root-mean-square difference in voxel density using the program RMSD [25]. The whole image was built up by stacking these data sets. Then, if necessary, voxels corresponding to the capillary glass wall were removed for easier recognition of the three-dimensional structure of the tissue sample using the program suite SLICE [25]. Volume-rendered figures of the obtained three-dimensional structures were produced using the program VG Studio MAX (Volume Graphics, Germany).

Results

Golgi Impregnation

Reconstructed images revealed the three-dimensional structure of frontal cortex of human brain. The three-dimensional structure of brain tissue consisting of gray and white matter is shown in figure 5a. Tissue components stained with the metal dye were obviously distinguished from the unstained surroundings. Luminal networks are seen in the middle part corresponding to white matter. These structures were assigned as blood vessels. The cut end of a stained capillary vessel has been observed at the sample surface [10]. Gray matter is seen in the upper-left and lower-right layers. These regions indicate an anatomical hallmark characterized by localization of dense granules. These granules can be assigned as somas of pyramidal cells.

Histologically, neurons of gray matter of frontal cortex are arranged into six layers, called the molecular layer (layer I), external granular layer (II), external pyramidal layer (III), internal granular layer (IV), internal pyramidal layer (V), and multiform layer (VI). The layer structure has been observed as a three-dimensional structure by micro-CT analysis [10]. The external and internal pyramidal layers are characterized by pyramidal neurons. A high-resolution three-dimensional image of pyramidal cells in the internal pyramidal layer is shown in figure 5b. Axons and dendrites arising from somas were visualized as a network structure. Spherical structures can be seen in the interior of somas, indicating that micro-CT analysis can reveal the intracellular microstructure. These microstructures have been assigned as cellular nuclei [10]. The surroundings of the nuclei were stained deeper than the cytoplasm, while the nuclei themselves displaced the stain dye and appeared as negatively stained images.

The blood vessel network in white matter was traced to analyze the capillary structure responsible for maintaining the brain function. A skeletonized model of capillary vessels in white matter is shown in figure 5c. Vessels with a diameter of approximately 6–8 μm form a network structure to cover the whole tissue. These skeletonized models were built by using the program RefineView (available from http://www.el.u-tokai.ac.jp/ryuta/). The protocols for building skeletonized models in the tomographic images are described in the Appendix. The capillary vessel structure was extracted with this program and used for replicating the three-dimensional structure by rapid prototyping (figure 5d) [11]. This result indicated that the microtomographic structure of soft tissues can be used as a three-dimensional template for the artificial fabrication of biological architectures.

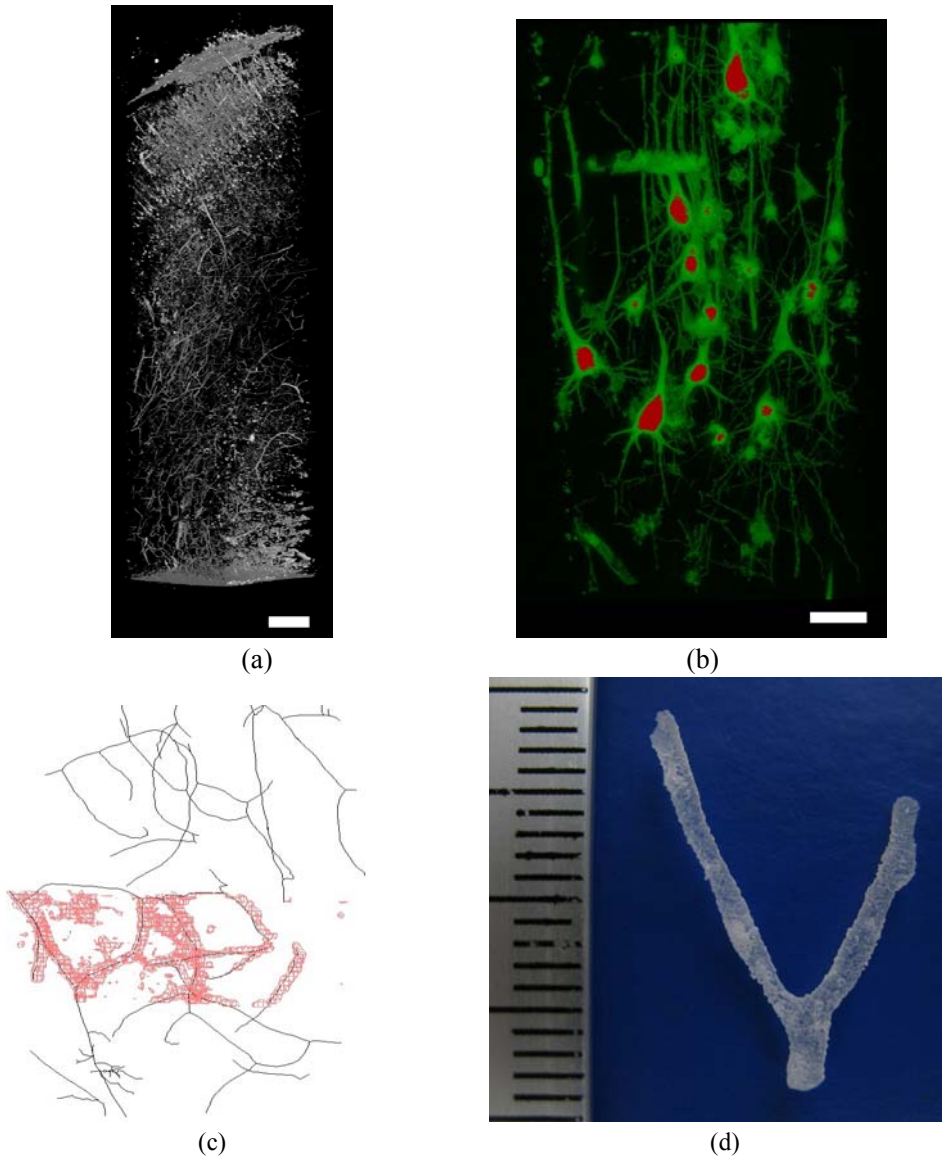

Figure 5. Three-dimensional structures of human frontal cortex stained by Golgi impregnation. The brain surface is to the top. (a) Overall structure. Micro-CT analysis was performed at BL20B2 using 12.000-keV x-rays. Capillary vessel networks are observed in white matter located in the middle of the sample. Gray matter is in the upper-left and lower-right layers. CT densities are rendered by the scatter HQ algorithm at a linear absorption coefficient of 11.0 cm^{-1}. Scale bar: 500 μm. (b) Pyramidal neurons in the internal pyramidal layer. Micro-CT analysis was performed at BL20XU using 12.000-keV x-rays. CT densities were rendered by the maximum projection method. Linear absorption coefficients from 0 to 142 cm^{-1} are colored in green, and those over 142 cm^{-1} in red. Scale bar: 50 μm. (c) Capillary vessel model produced using the program RefineView. The skeletonized models are drawn in black. Linear absorption coefficients of 310 × 370 × 125 μm region corresponding to white matter are shown in red as a cage representation. The absorption coefficients are contoured at 5 times the standard deviation in this region with 5-μm grids. (d) A 200-fold magnified model of a capillary vessel fabricated by rapid prototyping. A continuous density of the capillary vessel showing linear absorption coefficients greater than 17.6 cm^{-1} was used for prototyping.

Bodian Impregnation

While Golgi impregnation visualizes a limited number of neural cells, Bodian impregnation visualizes every neuron by staining neuropils. The three-dimensional structure of white matter of human frontal cortex is shown in figure 6. Spherical densities along with network structures can be seen over the entire tissue image. These spherical densities should be cellular nuclei of smaller neural cells. Granules with higher densities were observed within these spherical structures, suggesting that the nucleolus can be visualized by this method.

Bodian impregnation has been used for staining sectioned samples. The surfaces of the tissue sample can be easily stained, although visualization of the inner structure of a block sample is rather difficult. The permeation of metal dyes in Bodian impregnation can be improved by using detergents with dyes and by defatting sample tissues.

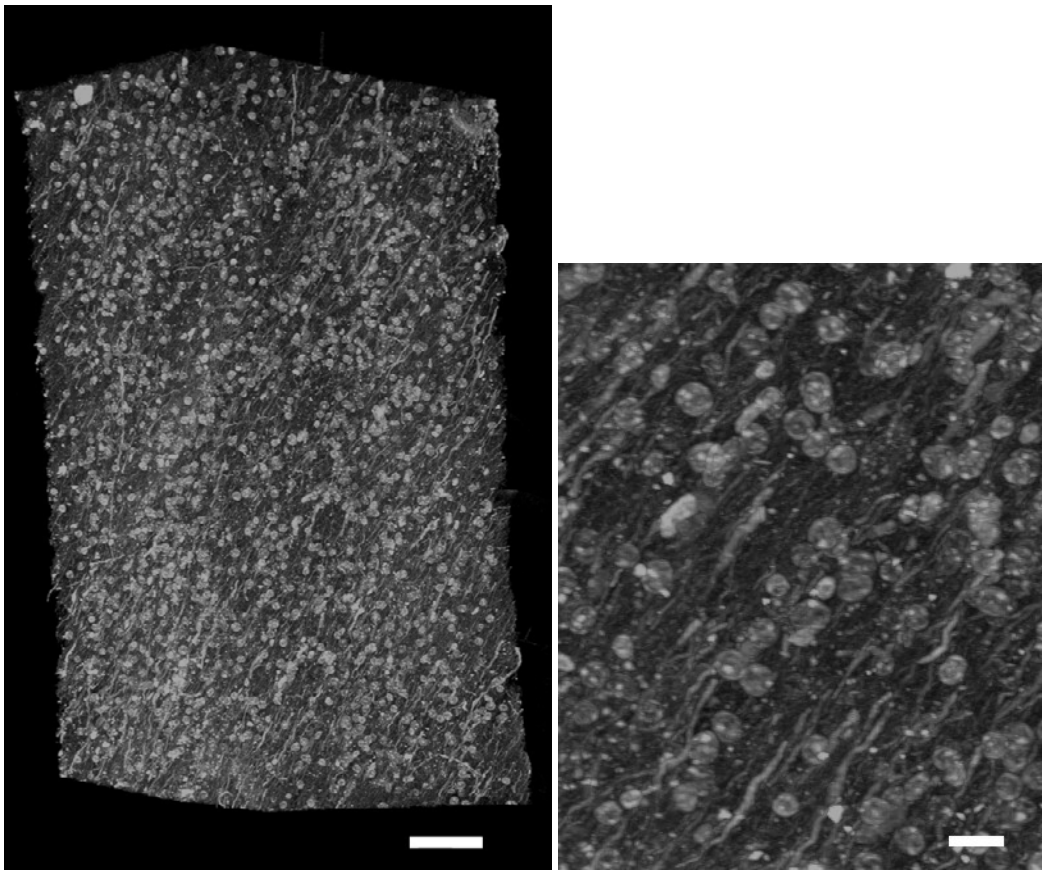

(a) (b)

Figure 6. Three-dimensional structures of white matter of human frontal cortex stained by Bodian impregnation. Micro-CT analysis was performed at BL20XU using 12.000-keV x-rays. The brain surface is to the top. (a) Overall structure. Cellular nuclei along with neuropils were visualized. CT densities are rendered by the maximum projection method from linear absorption coefficients of 14.1 to 32.9 cm^{-1}. Scale bar: 50 μm. (b) Magnified image. High-density granules were seen in spherical structures. CT densities are rendered by the maximum projection method from linear absorption coefficients of 14.1 to 40.0 cm^{-1}. Scale bar: 10 μm.

Osmification

Osmification gave uniformly stained images even for the block sample. The three-dimensional structure of a loop-embedded sample of white matter of human frontal cortex is shown in figure 7. Fibriform structures can be observed in white matter, indicating that the directions of nerve fibers can be visualized. Because the tissue entrails were stained uniformly by the osmification, the image contrast is rather low compared with other staining methods. For this reason, the osmified tissue gave an obscure image. However, osmification can be applied to tissue samples in which the entire structure should be visualized because uniform staining of the overall tissue is also essential for tomographic visualization.

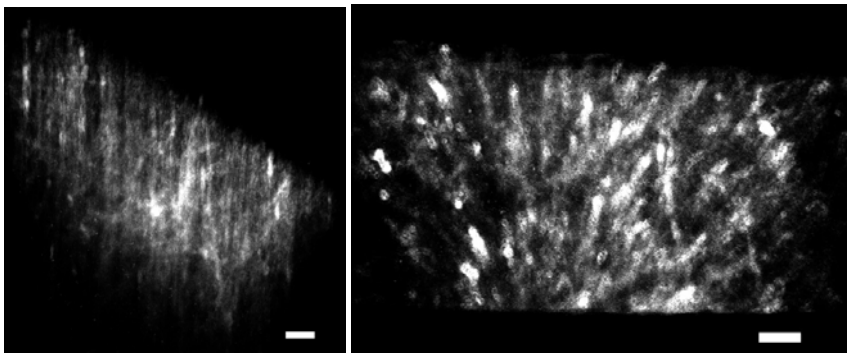

(a) (b)

Figure 7. Three-dimensional structure of white matter of human frontal cortex stained by osmification. Micro-CT analysis was performed at BL20XU using 12.000-keV x-rays. CT densities were rendered using the sum-along-ray algorithm from linear absorption coefficients of 25.2 to 34.0 cm^{-1}. Scale bar: 50 μm. (a) Side view. (b) Top view.

Mercury Fixative Staining

B-5 fixative has been used for tissue sample fixation. However, the three-dimensional micro-localization of mercury in the fixed tissue structure has not been visualized. The three-dimensional structure of a sample stained with B-5 fixative is shown in figure 8. The high-density granules were distributed in the entire tissue structure. These granules were asymmetrically located in the lower half of the sample corresponding to white matter. Because mercury was the only high-Z element used in the sample preparation, the granular density should originate from x-ray absorption of mercury. Although the granular density was not assigned to a particular histological structure, this method can be used for visualizing the microstructure of soft tissues.

Reticulin Silver Impregnation

Reticulin silver impregnation visualizes reticular fiber structures. The three-dimensional structure of human frontal cortex stained by reticulin impregnation is shown in figure 9. The fibriform structures were observed over the entire image. A large luminal structure in the

upper half of the tissue probably corresponds to connective tissues surrounding the capillary vessel. Therefore, the x-ray image reflects silver depositions at collagen fibers in the connective tissue.

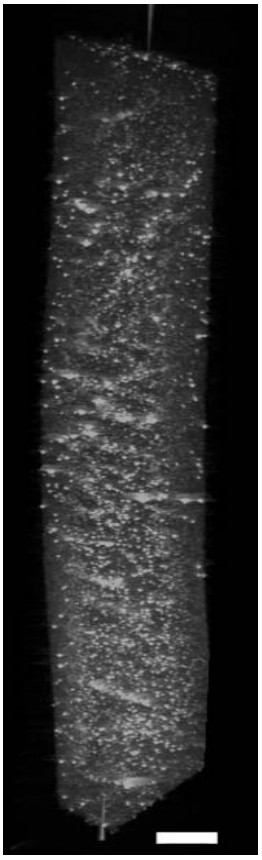

Figure 8 (left).
Three-dimensional structure of human frontal cortex stained with B-5 fixative. Micro-CT analysis was performed at BL20B2 using 12.400-keV x-rays. The brain surface is to the top. High-density granules are asymmetrically located in the lower half of the sample corresponding to white matter. CT densities are rendered by the maximum projection method from linear absorption coefficients of 2.0 to 20.0 cm^{-1}. Scale bar: 100 μm.

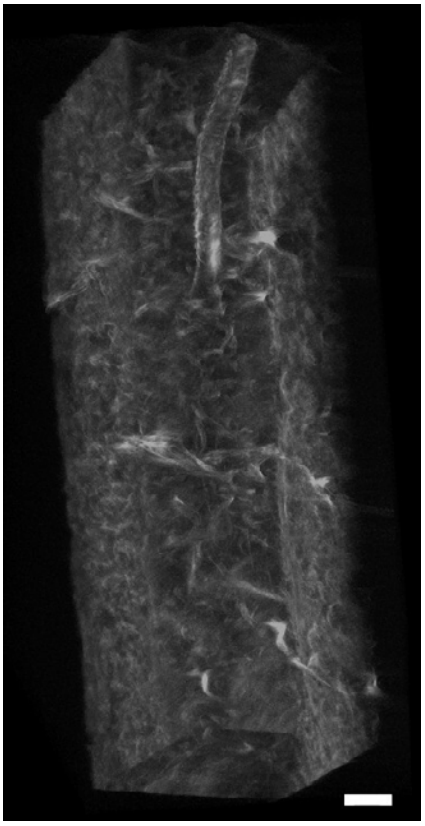

Figure 9 (right).
Three-dimensional structure of human frontal cortex stained with reticulin silver impregnation. Micro-CT analysis was performed at BL20XU using 12.000-keV x-rays. A large luminal structure is seen in the upper half of the tissue. Streaks are due to sample drift. CT densities are rendered by the maximum projection method from linear absorption coefficients of 5.1 to 50.0 cm^{-1}. Scale bar: 50 μm.

Immunogold Staining

Selective staining using neuronal marker antibodies has been reported for histological analysis [e.g., 19]. Gold and other metal/antibody conjugates have been used as electron-dense markers, especially in electron microscopic imaging [e.g., 26]. We have recently reported colloidal gold staining of the *Drosophila* adult CNS for micro-CT analysis [12].

In this study, we stained the *Drosophila* larvae CNS with anti-axon monoclonal antibody. The three-dimensional structures of the nerve tissue stained with immunogold conjugates are shown in figure 10. The image stained with the anti-axon antibody showed the structure of the optic lobe in the supraesophageal ganglions, while the image stained without this primary antibody gave negligible density in the optic lobe. These results indicated the possibilities of applying immunological staining to three-dimensional micro-CT analysis of soft tissues.

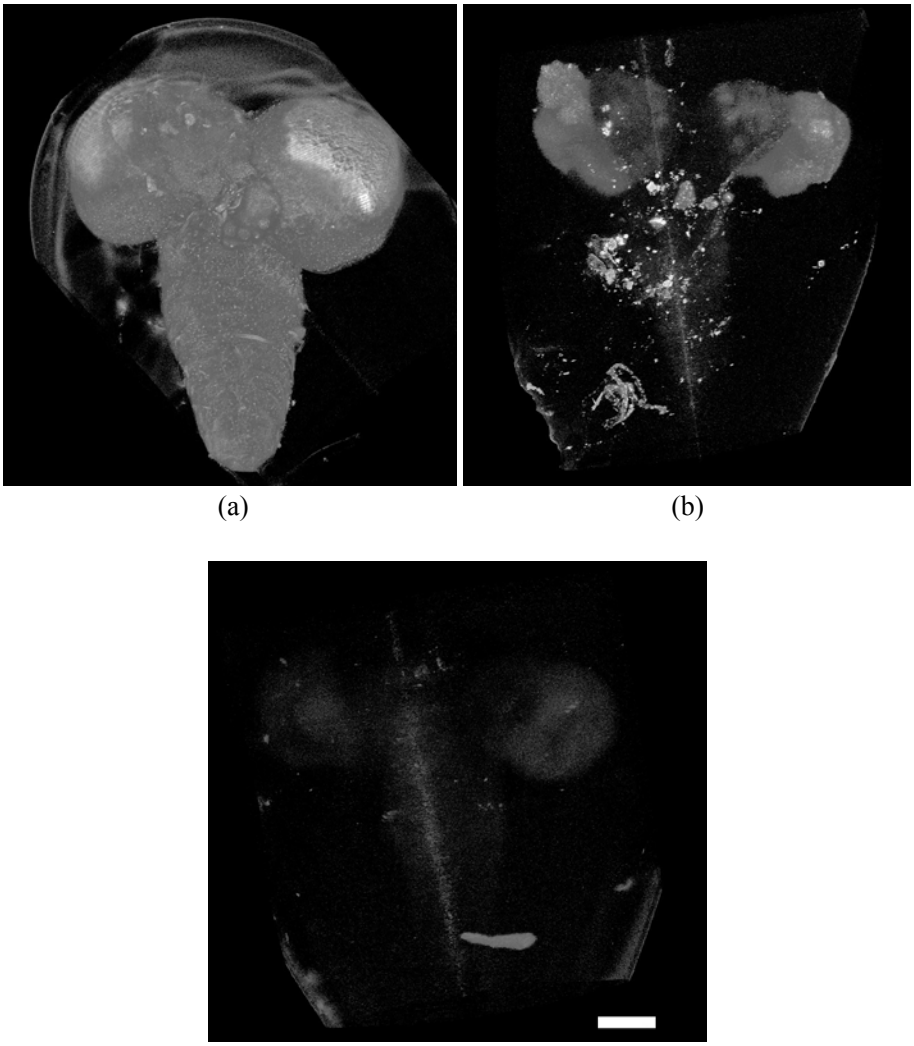

(a) (b)

(c)

Figure 10. Dorsal view of three-dimensional structures of *Drosophila* larvae CNS. Micro-CT analysis was performed at BL20XU using 12.000-keV x-rays. CT densities were rendered by the scatter HQ algorithm from linear absorption coefficients of 7.1 to 30.0 cm^{-1}. Scale bar: 50 μm. (a) CNS stained by Bodian impregnation visualizing the entire tissue structure consisting of left and right hemispheres of supraesophageal ganglions and ventral nerve cord. (b) CNS stained with monoclonal antibody BP102 against *Drosophila* axon. Densities of antibody-gold conjugates are located at optic lobes of the left and right supraesophageal ganglions. (c) CNS stained without the BP102 primary antibody.

Discussion

Microstructures of biological tissues have generally been characterized from thin histological slices. The mechanical stress introduced by microtomy procedures results in physical distortion of the microstructure, making it difficult to reconstruct the precise three-dimensional structure from slice images. Therefore, optical sectioning microscopy including confocal microscopy has been used for visualizing three-dimensional structures of biological systems. However, because of absorption and refraction effects arising from interference by the sample itself, the observation depth is typically limited to 100 μm. This causes difficulties in three-dimensional reconstruction of the entire image of a thick sample. Thus, optical sectioning microscopy is mainly used for imaging sectioned samples labeled with highly selective probes.

In contrast, the transparency of biological tissue to hard x-rays enables micro-CT analysis of the entire sample structure. The main advantages of such microcontrasting CT analysis compared with conventional histology are the three-dimensional character of the obtained structure and the exclusion of artificial deformation originating from microtomy procedures. The microcontrasting CT analysis performed in this study revealed the three-dimensional microarchitecture of human brain composed of a huge number of cellular and intracellular constituents, which are responsible for the cerebral function.

The viewing field and spatial resolution of the micro-CT analysis can be varied depending on the pixel size, image dimensions, and x-ray optics. Although the spatial resolution of the structure reconstructed from projection images obtained at BL20XU has been estimated to be 1.0 μm [15], application of zone plate optics [16] would enable structure determination at a higher resolution. We have reported a radiographic analysis of nerve tissue at 160-nm resolution [9] visualizing the neuronal structures. Microcontrasting tomographic analysis at this higher resolution would enable functional analysis of biological tissues from the three-dimensional cellular and subcellular structures.

The three-dimensional microstructures can be utilized in histological diagnosis. At present, two-dimensional optical images are the primary information for the diagnosis. Such histological images provide hardly any information about the three-dimensional nature of clinical samples. It is fundamentally difficult to comprehend the three-dimensional structures of clinical samples from only two-dimensional images. The results presented in this chapter indicate that the three-dimensional structures of soft tissues can be visualized as cellular and subcellular structures by microcontrasting. Therefore, micro-CT analysis of clinical samples contrasted with high-Z elements provides novel pathological information that has not been visualized in two-dimensional images. Although the present analyses were performed on post-mortem tissue, biopsy samples of any organ could be subjected to microcontrasting CT analysis. The three-dimensional structure of such a sample gives the entire image of the tissue, from which any arbitrary two-dimensional sections could be generated.

The neuronal network visualized in the three-dimensional structure is essential for cerebral functions. Analysis of the entire network leads to the revealing of the functional mechanism of the brain. The brain model should be built up as a circuit to reveal its functions, so it is essential to trace neuronal tracts in order to understand the functional mechanism of the brain. The skeletonization technique applied to the structural analysis of

the capillary vessel structures facilitates tracing the neuronal tracts in the three-dimensional microstructure of brain.

Microtomography in the future

Along with the microcontrasting techniques, micro-CT analysis sheds light on the underlying structural basis of biological functions. We have reported that the microtomographic structure of soft tissues can be used as a three-dimensional template for the artificial fabrication of a biological architecture [11]. Furthermore, it has been proposed that bioprinting techniques could be used to fabricate biomimetic structures [27]. Therefore, microtomographic analysis can provide the three-dimensional microstructural basis that allows the reproduction of biological tissues and organs.

Three-dimensional microtomographic analysis of every constituent in a biological object enables computerization of the entire biological entity. The computerized data of any biological entity can be sent by electronic transmission or saved in data storage for a long period of time. If the three-dimensional regeneration of a biological entity from computerized data is realized further in the future, then the transmission of biological objects beyond time and space can be accomplished. Therefore, the microtomographic analysis could be used as a basic technology related to a time machine or a teleportation mechanism like in the spaceship Enterprise. It goes without saying that there is much concern over the ethical problems of such devices.

Conclusion

High-Z element microcontrasting in conjunction with micro-CT analysis can be applied to any biological tissues. The results in this chapter indicate that the conventional metal staining methods facilitate three-dimensional x-ray visualization of soft tissue structures. The three-dimensional structures revealed by microtomographic analysis have a much broader range of applications, including histological analysis, three-dimensional diagnosis, functional study of nerve circuitry, and three-dimensional tissue engineering.

Acknowledgments

We thank Noboru Kawabe, Teaching and Research Support Center, Tokai University School of Medicine, for immunological staining. We also thank Kiyoshi Hiraga, Technical Service Coordination Office, Tokai University, for preparing brass fittings. The synchrotron radiation experiments were performed at SPring-8 with the approval of the Japan Synchrotron Radiation Research Institute (JASRI) (proposal nos. 2006B1716, 2007A1844, 2007A2072, 2007B1102, 2007B1894, 2008A1190, and 2008B1261).

References

[1] Conchello, J.-A. and Lichtman, J.W. (2005). Optical sectioning microscopy. *Nat. Methods, 2,* 920-931.

[2] Alanentalo, T., Asayesh, A., Morrison, H., Lorén, C.E., Holmberg, D., Sharpe, J. and Ahlgren, U. (2007). Tomographic molecular imaging and 3D quantification within adult mouse organs. *Nat. Methods, 4,* 31-33.

[3] Dodt, H.-U., Leischner, U., Schierloh, A., Jährling, N., Mauch, C.P., Deininger, K., Deussing, J.M., Eder, M., Zieglgänsberger, W. and Becker, K. (2007). Ultramicroscopy: three-dimensional visualization of neuronal networks in the whole mouse brain. *Nat. Methods, 4,* 331-336.

[4] Yu, X., Wadghiri, Y.Z., Sanes, D.H. and Turnbull, D.H. (2005). In vivo auditory brain mapping in mice with Mn-enhanced MRI. *Nat. Neurosci., 8,* 961-968.

[5] Snigirev, A., Snigireva, I., Kohn, V., Kuznetsov, S. and Schelokov, I. (1995). On the possibilities of x-ray phase contrast microimaging by coherent high-energy synchrotron radiation. *Rev. Sci. Instrum., 66,* 5486-5492.

[6] Momose, A., Takeda, T., Itai, Y. and Hirano, K. (1996). Phase-contrast X-ray computed tomography for observing biological soft tissues. *Nat. Medicine, 2,* 473-475.

[7] Wilkins, S.W., Gureyev, T.E., Gao, D., Pogany, A. and Stevenson, A.W. (1996). Phase-contrast imaging using polychromatic hard X-rays. *Nature, 384,* 335-338.

[8] Mizutani, R., Hara, T., Takeuchi, A., Uesugi, K. and Suzuki, Y. (2006). Microtomographic analysis of *Drosophila* brain. *The Fifth East Asian Biophysics Symposium: Abstracts*, (p. S388). Okinawa, Japan.

[9] Mizutani, R., Takeuchi, A., Hara, T., Uesugi, K. and Suzuki, Y. (2007). Computed tomography imaging of the neuronal structure of *Drosophila* brain. *J. Synchrotron Radiat., 14*, 282-287.

[10] Mizutani, R., Takeuchi, A., Uesugi, K., Ohyama, M., Takekoshi, S., Osamura, R.Y. and Suzuki, Y. (2008). Three-dimensional microtomographic imaging of human brain cortex. *Brain Res., 1199*, 53-61.

[11] Mizutani, R., Takeuchi, A., Uesugi, K., Takekoshi, S., Osamura, R.Y. and Suzuki, Y. (2008). X-ray microtomogaphic imaging of three-dimensional structure of soft tissues. *Tissue Eng. Part C, 14,* 359-363.

[12] Mizutani, R., Takeuchi, A., Akamatsu, G., Uesugi, K. and Suzuki, Y. (2008). Element-specific microtomographic imaging of *Drosophila* brain stained with high-Z probes. *J Synchrotron Radiat., 15*, 374-377.

[13] Bonse, U., Busch, F., Gunnewig, O., Beckmann, F., Pahl, R., Delling, G., Hahn, M. and Graeff, W. (1994). 3D computed X-ray tomography of human cancellous bone at 8 microns spatial and 10^{-4} energy resolution. *Bone Miner., 25,* 25-38.

[14] Salome, M., Peyrin, F., Cloetens, P., Odet, C., Laval-Jeantet, A.M., Baruchel, J. and Spanne, P. (1999). A synchrotron radiation microtomography system for the analysis of trabecular bone samples. *Med. Phys., 26,* 2194-2204.

[15] Uesugi, K., Suzuki, Y., Yagi, N., Tsuchiyama, A. and Nakano, T. (2001). Development of high spatial resolution X-ray CT system at BL47XU in SPring-8. *Nucl. Instrum. and Meth., A467-468,* 853-856.

[16] Takeuchi, A., Uesugi, K., Takano, H. and Suzuki, Y. (2002). Submicrometer-resolution three-dimensional imaging with hard x-ray imaging microtomography. *Rev. Sci. Instrum., 73,* 4246-4249.

[17] Valverde, F. (1970). The Golgi method. In W.J.H. Nauta and S.O.E. Ebbesson (Eds.), Contemporary Research Methods in Neuroanatomy (pp. 12-31). New York, Springer-Verlag.

[18] Tyrer, N. M., Shepherd, D. and Williams, D. W. (2000). Methods for imaging labeled neurons together with neuropil features in *Drosophila*. *J. Histochem. Cytochem., 48,* 1575-1581.

[19] Evers, P. and Uylings, H.B.M. (1997). An optimal antigen retrieval method suitable for different antibodies on human brain tissue stored for several years in formaldehyde fixative. *J. Neurosci. Methods, 72,* 197-207.

[20] Suzuki, Y., Uesugi, K., Takimoto, N., Fukui, T., Aoyama, K., Takeuchi, A., Takano, H., Yagi, N., Mochizuki, T., Goto, S., Takeshita, K., Takahashi, S., Ohashi, H., Furukawa, Y., Ohata, T., Matsushita, T., Ishizawa, Y., Yamazaki, H., Yabashi, M., Tanaka, T., Kitamura, H. and Ishikawa, T. (2004). Construction and commissioning of a 248 m-long beamline with x-ray undulator light source. *AIP Conf. Proc., 705,* 344-347.

[21] Huesman, R.H., Gullberg, G.T., Greenberg, W.L. and Budinger, T.F. (1977). RECLBL library users manual: Donner algorithms for reconstruction tomography. Lawrence Berkeley Laboratory, University of California.

[22] Teng, T.-Y. (1990). Mounting of crystals for macromolecular crystallography in a free-standing thin film. *J. Appl. Cryst., 23,* 387-391.

[23] Goto, S., Takeshita, K., Suzuki, Y., Ohashi, H., Asano, Y., Kimura, H., Matsushita, T., Yagi, N., Isshiki, M., Yamazaki, H., Yoneda, Y., Umetani, K. and Ishikawa, T. (2001). Construction and commissioning of a 215-m-long beamline at SPring-8. *Nucl. Instrum. and Meth., A467-468,* 682-685.

[24] Mizutani, R., Takeuchi, A., Uesugi, K. and Suzuki, Y. (2008). Evaluation of the improved three-dimensional resolution of a synchrotron radiation computed tomograph by using a micro-fabricated test pattern. *J. Synchrotron Radiat., 15*, 648-654.

[25] Nakano, T., Tsuchiyama, A., Uesugi, K., Uesugi, M. and Shinohara, K. (2008). The 3D Image Processing Tools SLICE. Hyogo, Japan: Japan Synchrotron Radiation Research Institute.

[26] Zuber, C., Fan, J., Guhl, B. and Roth, J. (2005). Applications of immunogold labeling in ultrastructural pathology. *Ultrastruct. Pathol., 29,* 319-330.

[27] Campbell, P.G. and Weiss, L.E. (2007). Tissue engineering with the aid of inkjet printers. *Expert Opin. Biol. Ther., 7,* 1123-1127.

Appendix

Tomographic Reconstruction

Here, we describe the tomographic reconstruction procedure using the program RecView (http://www.el.u-tokai.ac.jp/ryuta/). Tomographic reconstruction can also be performed using the standard program suite provided at http://www-bl20.spring8.or.jp/xct/index.html.

RecView is freely available for all researchers. The executable downloaded as an archive file can be placed in any folder on a PC. This program is designed for use with x-ray images obtained at the BL20B2, BL20XU, and BL47XU beamlines of SPring-8 and cannot be applied to data obtained from other tomographs at present.

The first step of tomographic reconstruction is to determine the coordinates of the sample rotation axis in radiographs. Although the rotation axis is aligned along the vertical axis of two-dimensional images, precise coordinates of the axis should be determined both at the top and bottom of the two-dimensional image. Then tomograms are reconstructed by batch execution. The obtained tomograms can be trimmed and compressed into 8-bit TIFF format. These tomographic reconstruction are performed by the following steps:

1. Run RecView (figure A1).

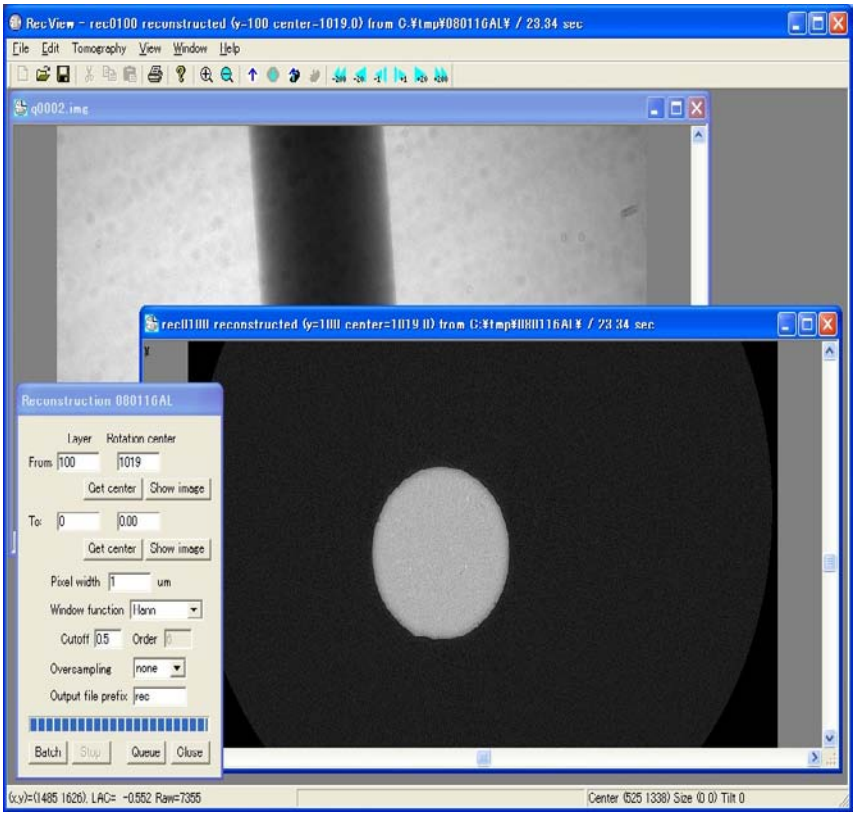

Figure A1. RecView window.

2. Open 'conv.bat' file in the data folder using the 'File - Prepare files' menu. This function renames radiograph files and prepares reference images.
3. Open one of the raw image files of the sample in ITEX format, such as q0002.img.
4. Open the 'Tomography - Reconstruction' dialog (figure A2) from the menu bar.

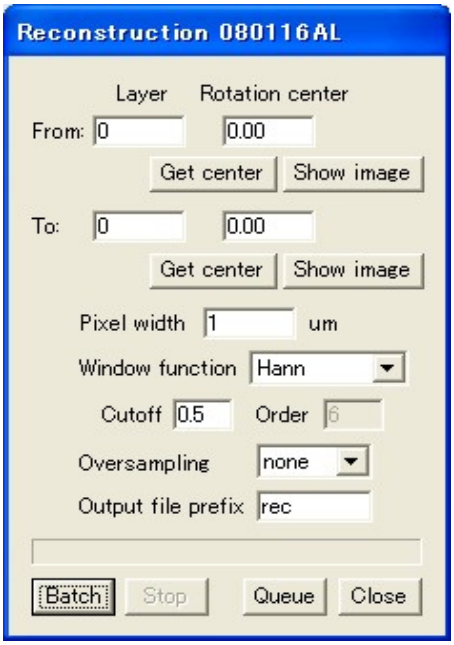

Figure A2. 'Tomography - Reconstruction' dialog.

5. Open 'conv.bat' file in the data folder using the 'File - Prepare files' menu. This function renames radiograph files and prepares reference images.
6. Open one of the raw image files of the sample in ITEX format, such as q0002.img.
7. Open the 'Tomography - Reconstruction' dialog (figure A2) from the menu bar.
8. Input the upper end of the sample in the 'Layer' box in the 'From' section. Although the sample image should be observed in this 'Layer' position only to determine the rotation axis, the 'Layer' value can be changed later to accommodate the whole sample.
9. Set an appropriate value in the 'Pixel width' box.
10. (Optional) The default window function [21] can be customized. The resolution can be improved by 'Oversampling' [24], though the reconstructed tomogram becomes larger by a factor of the square of the oversampling. The name of the output file can also be changed.
11. Click the button 'Get center' to perform an automatic search for the rotation axis. The resulting coordinates are shown in the 'Rotation center' box.
12. Invoke tomographic reconstruction with the 'Show image' button. This takes a little time—several seconds to a few minutes—depending on the image width, number of images, and PC specifications.

13. If the obtained tomogram has an overhang, as seen in figure A3, increase the axis coordinate and go back to step 9. If there is a reverse overhang, decrease the coordinate and go back to step 9.

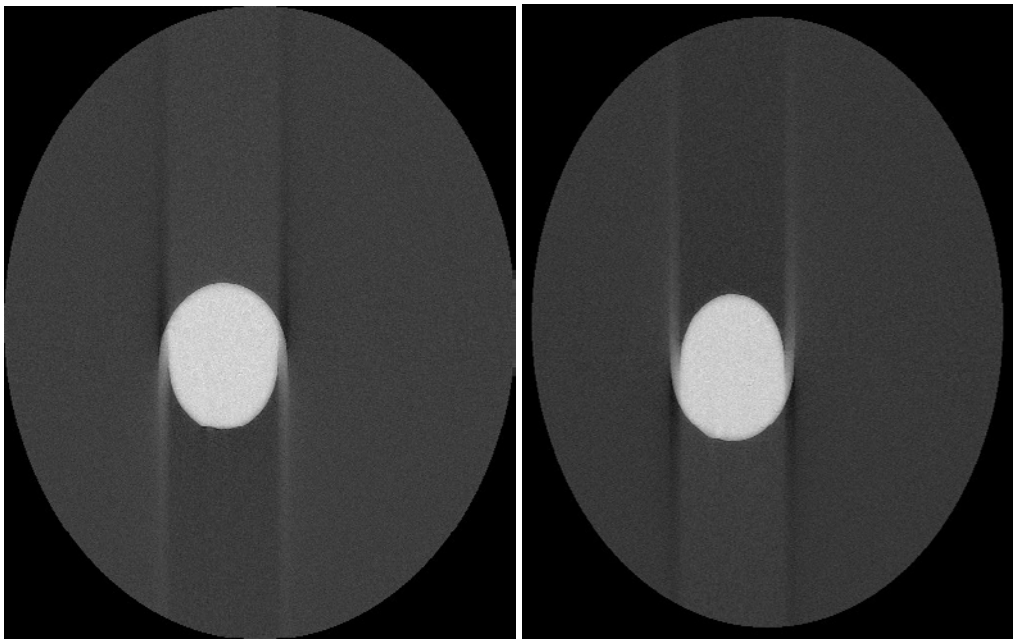

(a) (b)

Figure A3. Examples of reconstructed tomograms. If the tomogram has an overhang, as shown in panel (a), the coordinate of the rotation center axis should be increased. If it has a reverse overhang (b), the axis coordinate should be decreased.

14. After fixing the overhangs near the upper end of the sample, repeat steps 8–10 for the lower end of the sample as well by using the 'To' section.
15. The reconstruction calculation will be repeated from the upper layer to the lower layer. To ensure the sample image does not overrun this layer range, set it to allow for reconstruction of the whole sample image.
16. The 'Batch' button invokes batch calculation over the layer range. This takes from a few to several dozen hours depending on the image width, number of layers, and PC specifications.
17. To compress tomograms by converting them into 8-bit TIFF format, click the tomogram to select it and open the 'Tomography - Histogram=>8bitTIF' dialog (figure A4) from the menu.

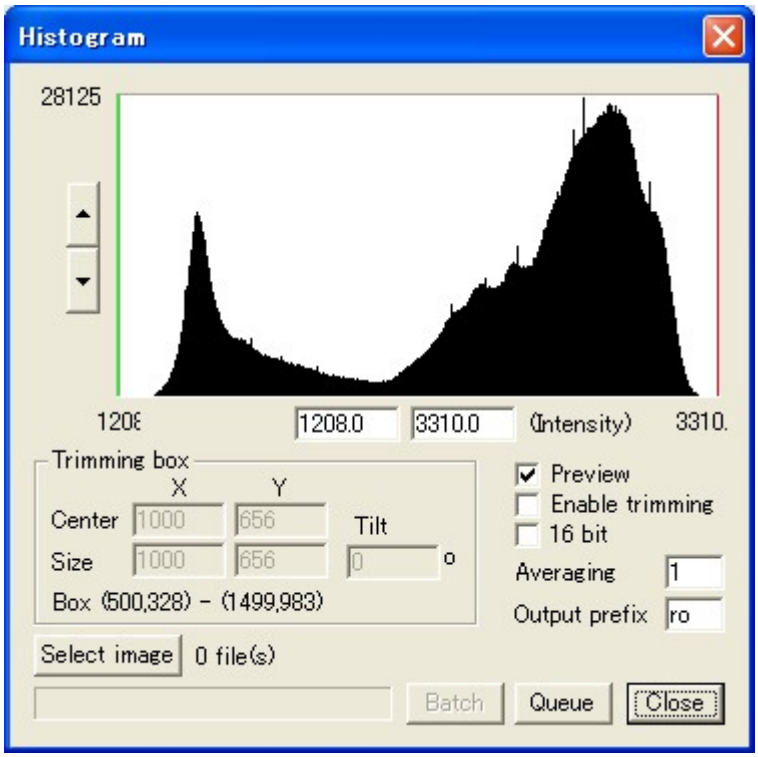

Figure A4. 'Tomography - Histogram=>8bitTIF' dialog.

18. (Optional) Check the box 'Enable trimming' to trim tomograms. Edit the 'Trimming box' values to set the X and Y center coordinates and sizes. A green box will be displayed in the tomogram window to indicate the region that will be saved in the file.
19. Set the highest and lowest thresholds for the 8-bit conversion by using edit boxes under the histogram or by moving green and red lines in the histogram.
20. Click the 'Select image' button and select tomogram files to be converted into 8-bit TIFF format.
21. The 'Batch' button invokes batch conversion. This takes a few minutes to several hours.

The resultant 8-bit TIFF tomograms can be used for three-dimensional rendering by using commercially available programs, or for model building by using the program RefineView described below.

Skeletonized Model Building in the Three-Dimensional Density Distribution

In this study, a skeletonized model was built in the Golgi impregnated image. With this skeletonization procedure, three-dimensional distributions of linear absorption coefficients that describe a huge number of cellular and extracellular constituents can be simplified.

The skeletonization was performed using the program RefineView (available from http://www.el.u-tokai.ac.jp/ryuta/). This program can be applied to any stack of three-dimensional images in 8-bit TIFF or BMP format. A license should be obtained if the program is used for profit but is not required for non-profit use. The program can be installed using the installation package that contains the RefineView executable along with parameter files. A warning window will be displayed upon installation because this package is built without any official certification. Because this program is still under development, there some functions may have been added, deleted or disabled.

After the images have been loaded, the density map can be displayed as a cage representation that illustrates the three-dimensional density distribution. Skeletonized models can be built using manual or automatic tracing functions along with manual intervention. The procedure for building the model is briefly described below:

1. Run RefineView (figure A5).

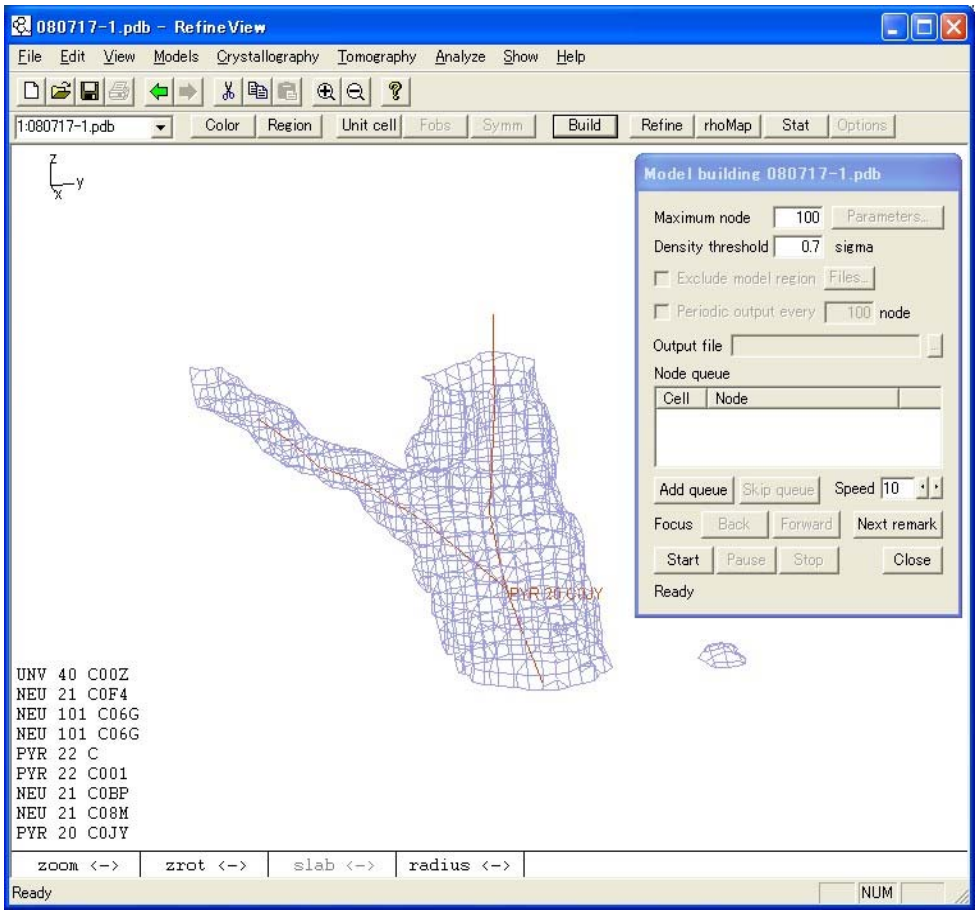

Figure A5. RefineView window.

2. If models have already been built, open the model coordinate file. If not, open a new model.
3. Open the 'Tomography - Load slices' dialog (figure A6) from the menu.
4. Click the 'Files' button to browse and select images for model building.
5. Enter the pixel width in the 'Pixel size' box.

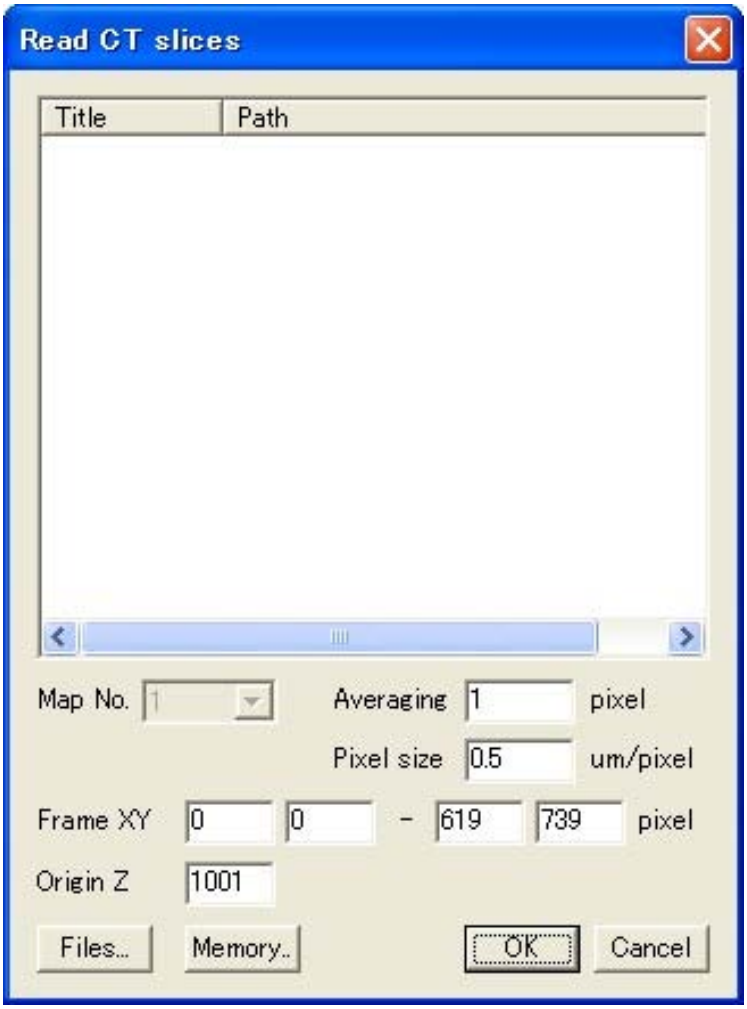

Figure A6. 'Tomography - Load slices' dialog.

6. (Optional) The memory size required for loading image can be reduced by 'Averaging' pixels or by limiting the 'Frame' to be loaded.
7. Load images by clicking the 'OK' button. This takes a few minutes.

8. Open the 'Tomography - Rho Map' dialog (figure A7) from the menu.

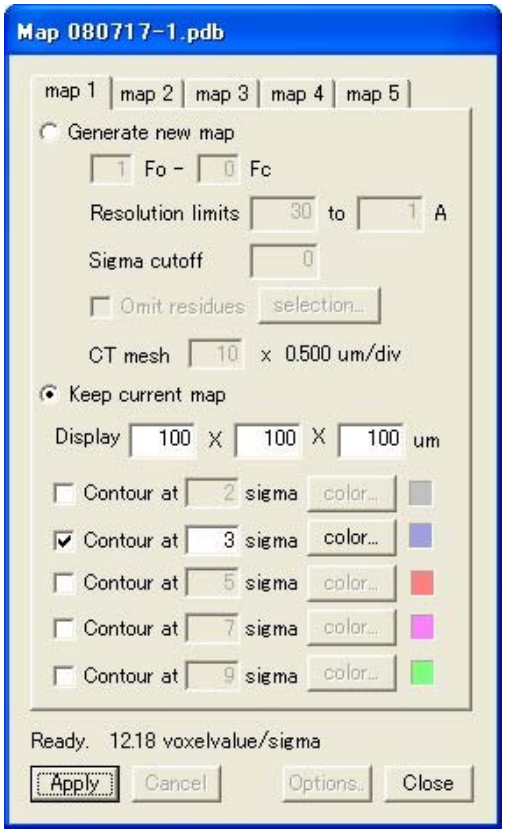

Figure A7. 'Tomography - Rho Map' dialog.

9. Select 'Generate new map' and enter an averaging factor (*e.g.,* 10) in the 'CT mesh' box. This averaging factor is just for displaying and not applied for image storage. Check one of the contours and set the contour level as 3 to 5 sigma. The entire densities can be displayed by taking the large 'Display' dimensions. The 'Apply' button updates the map. This takes from a few seconds to several minutes.
10. (Optional) A mini map may be seen in the upper-left corner of the window. The mini map is useful for finding where you are on the display, but CPU intensive. This function can be enabled or disabled from the 'Show - Mini map' menu.
11. (Optional) If the models have already been built, right-click the node of interest to open a pop-up menu and select the 'Focus' to move the display location. The display can also be moved from the 'View - Focus' menu.
12. Right-click to open a pop-up menu at the electron density to be treated and select the 'Focus'. The center of the display will move to the clicked position.
13. In the 'Tomography - Rho Map' dialog, select 'Generate new map' again and reduce the value in the 'CT mesh' box. 'Display' dimensions should also be reduced because it takes a lot of CPU time to draw maps with fine meshes. The 'Apply' button updates the map. Repeat steps 12–13 to find the region where models should be built.

14. To add a new model, select 'Add node' from the right-click menu to open the 'Add atom' dialog (figure A8). Turn on 'New residue' to add a new model. If the target density can be assigned to a particular biological object, 'Residue type' can be selected. Then click OK.

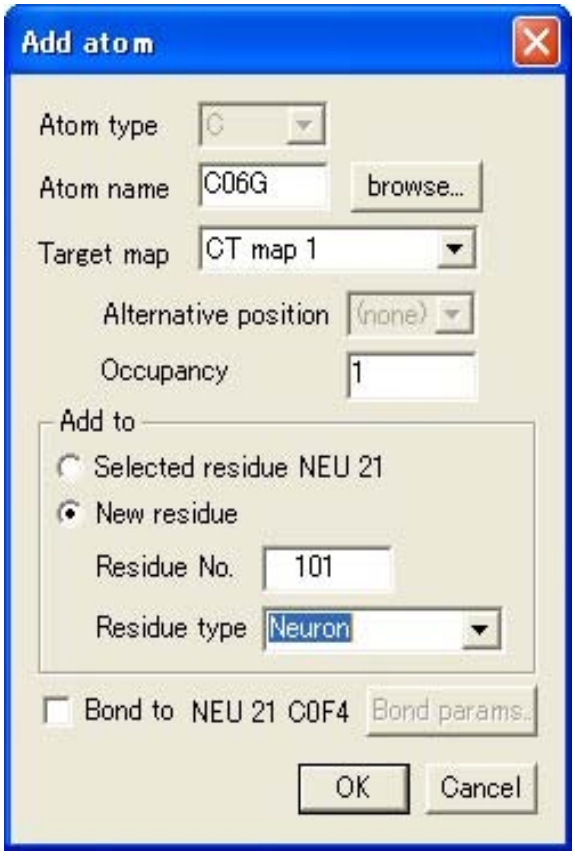

Figure A8. 'Add atom' dialog.

15. A node will be modeled at the position right-clicked and displayed in the window. Double click the modeled node to select it.
16. A skeletonized model can be built manually by the right-click menu 'Chain' to trace along the CT density.

The model coordinates can be saved from the 'File - Save' menu. Furthermore, many other functions are implemented including automatic tracing that can be performed by using the 'Tomography - Build model' dialog.

In: Handbook on White Matter
Editors: T. B. Westland and R. N. Calton
ISBN: 978-1-60741-034-8

Chapter XV

Origin and Function of Amoeboid Microgliai Cells in the Periventricular White Matter in the Developing Brain

C. Kaur [*] ***and E.A. Ling***
Department of Anatomy, Yong Loo Lin School of Medicine,
National University of Singapore, Singapore

Abstract

Microglial cells are mononuclear phagocytes present ubiquitously in the developing brain. In the white matter, they first appear as round cells called the ameboid microglia which differentiate into ramified forms with maturation. The amoeboid microglial cells (AMC) are present in large numbers in the periventricular white matter (peripheral to the lateral ventricles) in the developing brain where they are known to exert other functions besides their primary phagocytic function. Although various theories have been proposed regarding the origin of these cells such as mesodermal, neuroectodermal and monocytic, their origin is still a matter of debate. The macrophagic nature of these cells has been demonstrated by different methods such as electron microscopy and immunohistochemistry. Expression of major histocompatibility complex class I and II antigens on them, induced by lipopolysaccharide or interferon-γ, supports their involvement in immune functions. They are also known to release cytokines and chemokines such as tumor-necrosis factor-α, interleukin-1β and monocyte chemoattractant protein-1 in inflammatory and hypoxic-ischemic injuries which may contribute to death of immature oligodendrocytes in such conditions. Recent investigations have reported that AMC also express potassium channels (Kv1.2) and release glutamate, nitric oxide and reactive oxygen species under hypoxic conditions. This chapter will review the origin and function of AMC in the periventricular white matter in the developing brain under normal conditions and the role of these cells in hypoxic/ischemic conditions.

[*] Corresponding author: E-mail : ***antkaurc@nus.edu.sg***; Fax: 65-67787643; Phone: 65-65163209

Abbreviations

AMC: amoeboid microglial cells
CNS: central nervous system
CR3: complement type 3 receptors
IGF-1: insulin-like growth factor-1
IL-1: interleukin-1
iNOS: inducible nitric oxide synthase
MCP-1: monocyte chemoattractant protein-1
MHC: major histocompatibility
NO: nitric oxide
Sdc-2: syndecan-2
TGF-β1: transforming growth factor-β1
TβRI: TGF-β receptor I
TβRII: TGF-β receptor II
TNF-α: tumour necrosis factor-α
TNFR1: TNF receptor 1
TNFR2: TNF receptor 2

Introduction

Amoeboid microglia cells (AMC) are one of the glial cell types in the developing central nervous system (CNS) having immunocompetent and phagocytic properties. Many theories on their origin have been proposed since the identification of microglia by del Rio-Hortega (1932). Three hypotheses have been put forward in relation to origin of microglia i.e. (1) mesodermal, (2) neuroectodermal, and (3) monocytic. They display surface receptors and antigens similar to macrophages at other sites. AMC are present transiently till 10-14 days of age whence all of them transform into the adult ramified microglial cells. The microglial cells, considered as resting or dormant cells, are activated in response to many CNS insults and are capable of transforming into the amoeboid form and releasing cytotoxic substances such as free radicals and proinflammatory cytokines. Activation of microglia has been associated with neuronal and glial cell degeneration in neurodegenerative disorders of the CNS such as Alzheimer's disease, Parkinson's disease, multiple sclerosis and stroke.

Localization of Amoeboid Microglial Cells

AMC are widely distributed in the brain during fetal and early postnatal development. They are present in large numbers in the periventricular white matter either singly or in clusters (Figure 1). Other areas in which AMC are preponderant include the cavum septum pellucidum and the subependymal cysts closely associated with the third and fourth ventricles and the cerebral aqueduct (Figure 1). They may be spatially associated with neurons, blood vessels or dispersed freely in different regions of the brain. AMC, known to be active

macrophages, play an important role in the defense of the neural parenchyma removing cellular debris during normal development as well as in pathological conditions. Besides their scavenging function, AMC may also exert a cytotoxic effect through secretion of toxic factors such as nitric oxide (NO). Recent studies in our laboratory have greatly amplified the functional roles of these cells during development other than their primary role in phagocytosis.

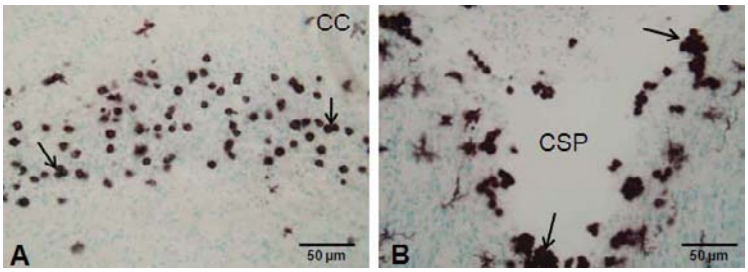

Figure 1. AMC in the periventricular white matter (A) in a 2 days old rat are distributed either singly or in clusters (arrows). In the cavum septum pellucidum (CSP), majority of the cells are present in clusters (arrows). Sections are stained with the OX-42 antibody, a specific microglial marker.

Features of Amoeboid Microglial Cells

The AMC in the white matter in the developing brain are mostly round cells with some of them showing fine cytoplasmic processes projecting from the cell surface (Figures 2 and 3). At the ultrastructural level, the cells show a round or indented nucleus, with margination of chromatin masses. The cytoplasm is abundant and contains a variable number of membrane bound dense granules, a well-developed Golgi apparatus, vacuoles and cisternae of rough endoplasmic reticulum (Figure 2). Under the scanning electron microscope, the cell surface shows blebs and pseudopodia (Figure 3).

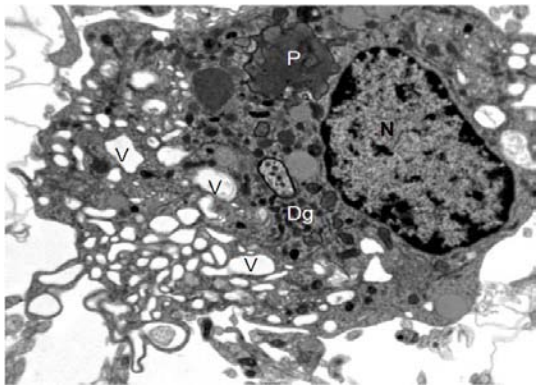

Figure 2. An AMC in the periventricular white matter of a 3 days old rat shows an eccentrically placed nucleus (N). The cytoplasm contains dense granules (Dg), vacuoles (V) and phagosomes (P).

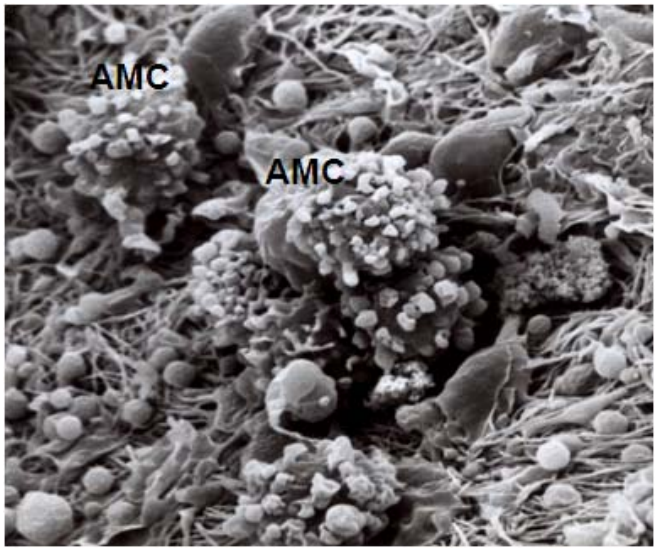

Figure 3. Scanning electron micrograph of AMC located in the subependymal cyst associated with the fourth ventricle. The surface of the cells shows a large number of protrusions or blebs.

Origin of Amoeboid Microglial Cells

Three hypotheses have been put forward in relation to origin of microglia: (1) mesodermal, (2) neuroectodermal, and (3) monocytic.

Mesodermal Origin

Hematopoietic cell-derived precursors such as macrophages invading the immature CNS from the meninges, through the immature blood vessels or from the ventricles have been proposed as precursors of microglia. The concept of a mesodermal origin of microglia was first postulated by del Rio-Hortega (1932) and later supported by many investigators (Penfield, 1932; Kershman, 1939; Dougherty, 1944; Cammermeyer, 1970; Boya et al, 1979). Different sources of mesodermal cells such as the embryonic mesenchymal cells or the primitive or fetal macrophages of the yolk sac have been reported to give rise to microglia.

The seminal study by del Rio-Hortega (1919) reported that a concentration of pial elements called “fountains of microglia” occurred at three specific sites (superior tela choroidea, pia covering the cerebral peduncles and inferior tela choroidea) on the brain surface. The cells from these sources or “fountains” then invaded the brain, transformed into round cells called ‘AMC’ which spread throughout the brain and eventually settled as the ramified microglia. Migration of pial cells from the brain surface to give rise to microglia was confirmed by Penfield (1932). Kershman (1939) reported that microglia in human embryos and fetuses originated from cells invading the CNS from meninges and blood vessels. Another suggestion was that the mesenchymal cells entered the nervous tissue by way of the

ventricles in addition to those from the brain surface and transformed into microglia (Schmidt, 1973). Studies using cytochemical and silver impregnation methods showed that microglia originated from cells in the meninges which infiltrated the superficial layers of the nervous tissues or spread along the blood vessels and invaded the nervous parenchyma in newborn rats (Boya et al*,* 1979). Further support to the mesodermal origin of microglial cells came from histochemical studies using the lectin Ricinus communis agglutinin and isolectin Griffonia simplicifolia (Boya et al, 1987, 1991). In other experimental models such as avian embryos, it was reported that invasion of the CNS by macrophages from the pial surface and their proliferation generated all the microglia (Kurz and Christ, 1998).

Besides the above, it has been suggested that the adult microglial cell population is derived from some precursor cells in the yolk sac which colonize the brain rudiment during early developmental stages (Alliot et al, 1999) and appear in the brain parenchyma before the circulation is established (Cuadros et al, 1993). Microglial precursors originating from different mesodermal sources have been reported to dependent on the embryonic age (Dalmau et al, 1997). A developmental window (latter half of the first trimester and throughout the early part of second trimester in humans, and between embryonic days 10–19 (E10–E19) in rodents) has been proposed by many investigatiors during which microglial progenitors populate the nervous system (Jeetle et al, 2002; Corbisiero et al, 2003; Rezaie et al, 2005; Chan et al, 2007).

Neuroectodermal Origin

A neuroectodermal lineage for the microglial cells has been suggested by many authors (Rydberg, 1932; Caley and Maxwell, 1968; Lewis 1968; Blakemore, 1969; Matsuyama et al, 1973; Paterson et al, 1973; Ling and Tan, 1974; Ling, 1976). Glioblasts originating from the neuroectoderm were thought to be the precursors of microglia (Paterson *et al.,* 1973; Fujita and Kitamura, 1975; Fujita *et al.,* 1981; Kitamura et al, 1984) and this was further supported by the presence microglial cells within the germinal matrix during development (Hutchins *et al,* 1990). However, it has also been suggested that microglial cells within the neuroepithelium were cells which traversed the neuroepithelial layer from the cerebral ventricles (Cuadros *et al* 1994).

Labeling of microglial cells with markers of neuroepithelial cells such as lipocortin-1 (McKanna, 1993a, b; Fedoroff et al, 1997) provided strong support for the neuroectodermal origin of microglia. Immunohistochemical studies using antibodies that labeled microglial cells as well as astroglia or oligodendroglia also favoured the neuroectodermal orgin (Fedoroff et al, 1997; Dickson and Mattiace, 1989; Wolzwijk 1995). Non-radioactive *in situ* hybridization and immunoperoxidase techniques (de Groot et al, 1992) have demonstrated that the majority of the resting (ramified) microglial cells in the mouse brain were of neuroectodermal origin. *In vitro* investigations have also favoured the neuroectodermal origin based on generation of the microglial cells in cultures of embryonic neuroepithelium (Hao et al, 1991; Richardson et al, 1993; Papavasiliou et al, 1996).

Monocytic Origin

The monocytic origin of microglia was proposed by Santha and Juba (1933) and Juba (1934) and later supported by others (Ling and Tan, 1974; Imamoto and Leblond, 1978). Imamoto and Leblond (1978) demonstrated the labeling of nascent forms of microglia, called the AMC, with ^{3}H thymidine in their radioautography study and concluded that these cells were derived through various stages of transition from monocytes. With further development, the AMC are transformed into ramified microglia (Ling et al, 1980; Imamoto et al, 1982). The entry of monocytes into the developing brain to become AMC has been demonstrated by using colloidal carbon particles and histochemical localization of various enzymes present in the monocytes and their derivative macrophages including non-specific esterase, 5'-nucleotidase, thiamine pyrophosphatase and nucleotide phosphatase (Ling, 1979; Ling *et al.,* 1980; Ling et al, 1982; Murabe and Sano, 1983; Kaur et al, 1984; Kaur et al, 1987). With monoclonal antibodies directed against monocytes or mononuclear phagocytes, the monocytic nature of microglia was greatly amplified over the past many years. The first immunohistochemical study was by Perry et al. (1985) in which the labeling of AMC and microglial cells with the macrophage-specific antigen F4/80 in the developing and adult mouse brain was demonstrated convincingly. Since F4/80 positive cells were closely related to the blood vessels prior to the appearance of microglia, the above-mentioned authors suggested that microglial cells had originated from monocytes. Since monocyte-derived tissues macrophages at other sites are known to express complement type 3 (CR3) receptors (Robinson et al, 1986), the demonstration of the presence of these receptors on the AMC in the postnatal rat brain (Ling et al, 1990) lent further support to their monocytic origin. In rodents (Imamura et al, 1990; Gehrmann and Kreutzberg, 1991) and humans (Penfold et al, 1991; Paulus et al, 1992), various monoclonal antibodies which are known to label monocytes or cells of the mononuclear phagocyte system in the peripheral organs have also been shown to label microglia. An antibody, QH1, was shown to label both microglia and hemopoetic cells in the quail thus strengthening the monocytic lineage of the cells (Cuadros et al, 1993).

Besides using specific antibodies as markers, lectin has also been used to label microglia in human embryos and fetuses (Andjelkovic et al, 1998). It was suggested that there might exist two subpopulations of microglial cells each of which may have different origins, i.e. one set being derived from the monocytes and the other from the primitive macrophages from the yolk sac.

Indirect evidence of monocytic origin of microglia was provided by observations that cortisone (Ling, 1982) or dexamethasone (Kaur et al, 1994) administered intraperitoneally into postnatal rats led to a reduction in the number of AMC in the corpus callosum. Since cortisone and dexamethasone are known to suppress the production of blood monocytes (Russo-Marie, 1992), it was concluded that the reduction in AMC numbers could be due to suppression of monocyte numbers and their release from the bone marrow into circulation and, hence, their entry into the brain (Kaur et al, 1994).

Functions of Amoeboid Microglia

The phagocytic nature of the AMC in the developing brain has been established by many studies (Thomas, 1992; Ling and Wong, 1993). Besides phagocytosis, the cells have other functional roles such as antigen presentation, sequestration of iron, release of NO and growth factors under normal and pathological conditions of the brain.

Phagocytosis

The phagocytic nature of the AMC has been demonstrated by several methods such as electron microscopy, localization of hydrolytic enzymes, immunohistochemical methods and use of carbon particles and tracers injected intravenously or intraperitoneally.

The AMC share many ultrastructural features of macrophages derived from monocytes in the peripheral tissues. In the normal developing brain, they were often found to be phagocytosing degenerating axons and cells (Kaur et al, 1985). Their macrophagic nature was further evidenced by their engagement in phagocytosis of apoptotic or necrotic cells (Figure 4) and degenerating axons in hypoxic injury to the developing brain (Li et al, 1997; Kaur and You, 2000; Kaur et al, 2006a).

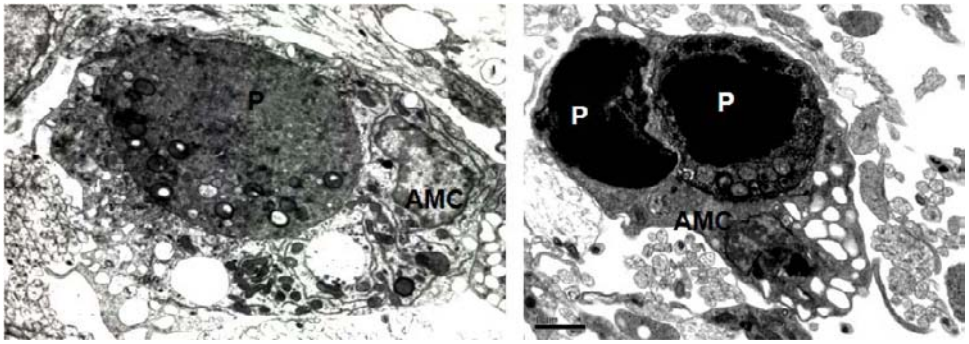

Figure 4. AMC in the periventricular white matter of a 3 days old rat, which had been subjected to hypoxia, showing internalized phagosomes (P) which appear to be derived from dead cells.

In experimental studies in which *Escherichia coli* (*E. coli*) was injected intracerebrally into the neonatal brain, the bacteria were readily phagocytosed by AMC in less than 3 h of the injection (Kaur et al, 2004).

Additional evidence of the phagocytic nature of AMC comes from the detection of hydrolytic enzymes including acid phosphatase, aryl phosphatase, non-specific esterase and 5'- nucleotidase in them (Ling, 1977; Ling et al, 1982; Kaur et al, 1984). The high contents of these hydrolytic enzymes in the AMC, as in macrophages at other sites, suggested that these cells are active macrophages.

The macrophagic nature of the AMC is further evidenced by their labeling with tracers such as rhodamine isothiocyanate and horseradish peroxidase (HRP) following intraperitoneal or intravenous administration (Kaur et al, 1986; Xu et al, 1993). This suggests that exogenous substances introduced in circulation can leak through the immature blood

brain barrier into the brain tissue where they may be phagocytosed by the AMC. It has also been shown that another tracer, biotinylated dextran, when injected in various areas of the brain far removed from the periventricular white matter also resulted in the labeling of the AMC (Earle and Mitrofanis, 1997). It was concluded that AMC ingested the tracer which diffused slowly through the extracellular spaces from the injection site. Injection of HRP in the lumbosacral region of the spinal cord also resulted in labeling of the AMC in the corpus callosum (Leong et al, 1983). The results suggested an ascending diffusion of the injected HRP in the spinal cord via the wide interstitial spaces to reach the cerebrum where it was engulfed by the AMC.

Further support to the macrophagic nature of the AMC was lent by the expression of ED1 antigens and CR3 receptors on these cells (Dijkstra et al, 1985; Ling et al, 1990). ED1 antigens and CR3 receptors are expressed by cells of monocyte/macrophage lineage (Newman et al, 1980; Beller et al, 1982; Abrahamson and Fearon, 1983; Wright et al, 1983) and are known to be involved in endocytosis (Ling et al, 1990)

Antigen Presentation

AMC constitutively express major histocompatibility (MHC) class I antigens (Ling et al, 1991). However, they do not express MHC class II antigens under normal conditions. MHC class II expression, on the other hand, is induced under pathological and experimental conditions when the cells are challenged with lipopolysaccharide (LPS) (Xu and Ling, 1994a), interferon-γ (IFN- γ) (Xu and Ling, 1994b) or *E.coli* (Kaur et al, 2004).

Iron Sequestration

AMC express transferrin receptors (Kaur and Ling, 1995) which facilitate the acquisition of iron needed for various functions of the cells, and to sequester iron for storage in pathological conditions when there is excessive influx of iron into the brain (Kaur and Ling, 1999)

Growth Factor Related Functions

Insulin-Like Growth Factors

Insulin-like growth factor-1 (IGF-1) is required by developing neurons for their optimal proliferation, differentiation, and survival. IGF-1 also promotes proliferation of oligodendrocytes as well as myelin synthesis in the developing brain. We have reported recently that AMC express IGF-1 and IGF-2 (Kaur et al, 2006b) and it was suggested that this may be linked to the state of cell activation. IGF-1 has been shown to enhance phagocytic activity of neutrophils *in vitro* when they were challenged with *E. coli* (Balteskard et al, 1998) and is known to increase the phagocytic capacity of peritoneal macrophages (Inoue et al, 1995). Besides modulating the phagocytic activity of AMC, as mentioned above,

IGF-1 has been considered as an important factor for oligodendrocyte proliferation and survival as well as myelination (Dubois-Dalcq and Murray, 2000; Guan et al, 2001). Although the exact function of IGF-2 in the developing brain is not clear, it may play a role in myelination (Logan et al, 1994; Walter et al, 1999) or in the phagocytic activity of AMC. IGF-1 may also be related to antigen presenting function of AMC as it is known to modulate cellular immune functions of neutrophils and macrophages (Auernhammer and Strasburger, 1995).

Transforming Growth Factor-β1

Transforming growth factor-βl (TGF-β1), a prototype of multifunctional growth factors generally considered as an anti-inflammatory cytokine, is normally present at low levels in the brain but is rapidly upregulated after injury (Lu et al., 2005). TGF-β1 exerts its functions through two serine/ threonine kinase receptors, termed type I and type II receptors (TβRI and TβRII) and is involved in the modulation of cell growth, differentiation, angiogenesis, immune function, extracellular matrix production and hematopoiesis (Flanders et al, 1998). We have recently reported that TGF-β1, TβRI and TβRII are expressed constituitively by the AMC in the periventricular white matter of neonatal rats. The expression of TGF-β1 and its receptors in the AMC was upregulated markedly after a hypoxic exposure suggesting that it may help to autoregulate microglial activation in adverse conditions via its receptors (Li et al, 2008).

Nitric Oxide Related Functions

NO production in macrophages has been described to have protective or destructive functions. Sustained production of NO endows macrophages with cytotoxic activity against viruses, bacteria and fungi (MacMicking et al, 1997). On the other hand, NO has suppressive effects on lymphocyte proliferation and causes damage to other normal host cells (MacMicking et al, 1997) which can be deleterious. AMC are known to express inducible nitric oxide synthase (iNOS) under pathological conditions such as a hypoxic injury (Kaur and You, 2000; Kaur et al, 2006a). It has been reported that activated AMC cells in the white matter may contribute to perinatal brain injury through noxious substances such as NO which is highly damaging to the oligodendrocytes (Merrill et al, 1993).

Inflammatory Response

The production of inflammatory cytokines such as interleukin-1 (IL-1) and tumour necrosis factor-α (TNF- α) is known to increase in the developing brain under pathological conditions. AMC play an important role in the development of an inflammatory response in the developing brain (Chew et al, 2006). They are thought to cause damage to axons and the developing oligodendrocytes by releasing IL-1 and TNF- α in many pathological conditions such as hypoxic-ischemic conditions and have been shown to express both TNFR1 and TNFR2 receptors (Dopp et al, 1997). Aberrant TNF-α /TNFR1 signaling in the CNS can have

a potentially major role in the CNS pathologies in which oligodendrocyte death and demyelination is a primary pathological feature (Akassoglou et al, 2003). We have recently reported that TNF-α produced by AMC in hypoxic conditions induces oligodendrocyte apoptosis via TNFR1 (Deng et al, 2008). IL-1β produced by AMC in hypoxic conditions may delay the white matter development and recovery in hypoxic conditions by inhibiting oligodendrocyte progenitor proliferation through its receptor IL-1R1 (Deng et al, 2008). Besides their inflammatory actions cytokines IL-1β and TNF-α may also be involved in transcriptional activation of iNOS gene (Lopez-Figueroa et al, 2000; Kadhim et al, 2006). AMC also express monocyte chemoattractant protein-1 (MCP-1), a member of β-chemokine subfamily, and its receptor CCR2. Along with this, expression of the chemokine receptor CCR5 has also been reported on the AMC until 2 weeks of age (Cowell et al, 2002; 2006). MCP-1, CCR2 and CCR5 may be involved in microglial recruitment and activation during brain development and after neonatal brain injury such as hypoxic-ischemic injury of the periventricular white matter.

Our recent study has shown the expression of heparan sulphate proteoglycan, syndecan-2 (Sdc-2) in the AMC and its upregulation by hypoxia (Kaur et al, 2008). Sdc-2 has been reported to play a role in cytokine/chemokine signaling (Halden et al., 2004). Our study suggested a proinflammatory role of Sdc-2 in the developing brain in response to hypoxic injury as it induced increased release of cytokines and chemokines.

The AMC cells also express Kv1.2, a Shaker-like voltage-gated potassium channel (Li et al, 2008). Increased expression of Kv1.2 in activated microglia induced by stimulation with ATP, hypoxia and lipopolysaccaride is linked to neuroinflammation through increasing the expression of IL-1β and TNF-α by these cells (Li et al, 2008). The cells also express Notch-1 receptor and Notch-1 signaling in them has been suggested to modulate the expression of proinflammatory cytokines (Cao et al, 2008).

Fate of Amoeboid Microglial Cells

The population of AMC in the periventricular white matter does not remain static but diminishes with age (Ling and Tan, 1974; Imamoto and Leblond, 1978) suggesting that the cells have degenerated, emigrated or transformed into other cell types. The pioneering study by del Rio-Hortega (1932) had put forth the idea that AMC transformed into ramified microglial cells with advancing age. This view was later shared by many authors (Penfiled, 1932; Kershman, 1939; Ling and Tan, 1974). Several methods such as electron microscopy, enzyme histochemistry and immunohistochemistry have been used to trace the fate of the AMC. Thus by electron microscopy in a rat animal model, the AMC were shown to undergo sequential changes with increasing age (Kaur et al, 1985). In early postnatal rats, the cells were round but undergo transformation assuming an oval cell body with concomitant reduction in cytoplasm between 7 and 10 days of age. By 12 days, the cytoplasm was further attenuated with decreased number of dense granules and vacuoles. The nucleus was also oval or angular with dense chromatin masses. In more mature rats at 15-20 days of age, all cells became elongated with branching processes and were intercalated in the narrow spaces between the closely packed axons (Figure 5). There was a steady decline in the amount of

cytoplasm from the 5th postnatal day onwards so that only one-sixth of the original cytoplasm was retained around 20 days of age. Isolated profiles of rough endoplasmic reticulum were present in the cytoplasm which was devoid of vacuoles at this stage. The sequential ultrastructural changes followed by lectin electron microscopy strongly supported the hypothesis of the transformation of the AMC into ramified microglia (Kaur and Ling, 1991; Wu et al, 1994). Further support was gained by the observation that as the population of AMC declines, the number of ramified microglial cells increased concomitantly.

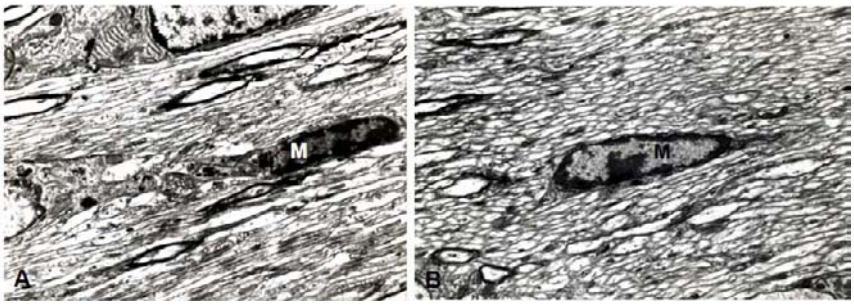

Figure 5. Microglial cells (M) in the periventricular white matter of a 15 (A) and 20 (B) days old rat are elongated and contain flattened nuclei and very little cytoplasm.

The transformation of the AMC into ramified microglia was also evidenced by the localization of various hydrolytic enzymes i.e. non- specific esterase, aryl sulphatase, acid phosphatase and thiamine pyrophosphatase in round AMC cells in 1-5 and oval cells in 7-10 days old rats (Ling, 1977; Ling et al, 1982; Kaur et al, 1984,1986). At 12-15 days of age, the cells which were ramified exhibited very weak reaction for these enzymes. The transformation of the AMC into ramified microglia was strongly supported by the expression of CR3 receptors labeled by the antibody OX 42 (Ling et al, 1990) in these cells as well as the ramified microglia (Figure 6).

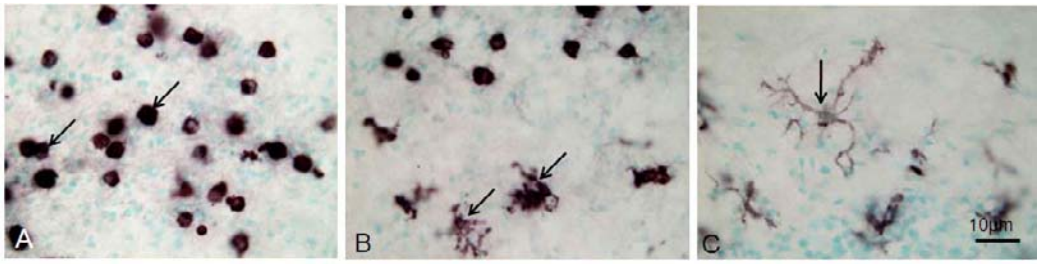

Figure 6. OX 42 positive AMC (arrows) in the periventricular white matter show gradual transformation from a round form in 3 days old rat (A) to a ramified form in 10 days old rat (C). Round and ramified AMC (arrows) are seen in the periventricular white matter of a 7 days old rat (B).

The transformation of AMC into ramified microglia appears to be a regressive phenomenon. In the early postnatal period they are active macrophages removing the debris of degenerating cells and axons (Ling, 1976; Innocenti et al, 1983a, b). At this stage the cells are endowed with various hydrolytic enzymes. The content of these enzymes gradually diminishes with the transformation of the cells into ramified microglia considered to be in a

resting or dormant form. Ramified microglial cells become activated in pathological conditions of the CNS and revert to their amoeboid form.

The origin and fate of AMC is depicted in figure below (Figure 7).

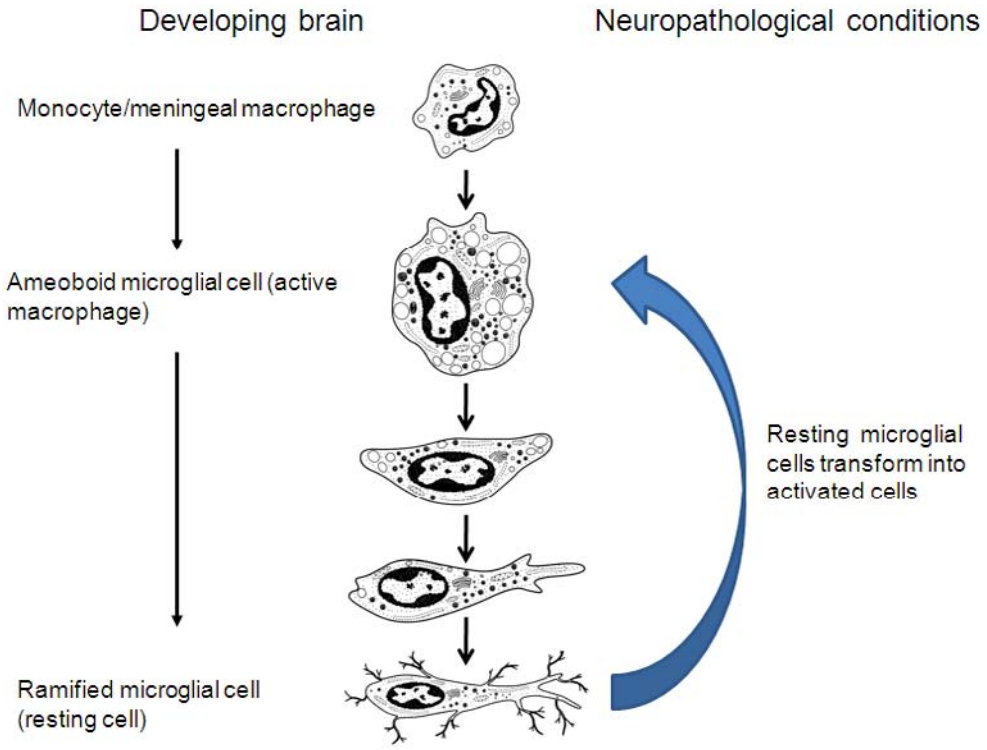

Figure 7. A semi-schematic digram depicting the development of AMC from monocytes/macrophages and their transformation into ramified microglial cells in the normal brain. In pathological conditions, the ramified microglial cells change their external morphology to an amoeboid form indicating their activated state.

Conclusion

Although various theories have been proposed regarding the origin of AMC such as mesodermal, neuroectodermal and monocytic, their origin remains a debated issue. Early investigations on AMC had focused on their primary role i.e. phagocytosis in the developing brain. Over the past 15 years, a battery of investigative tools has added a new dimension on the roles of these cells in the developing brain and in pathological conditions. Indeed, recent demonstration of expression of a plethora of molecules and growth factors in these cells points towards their multiple functional roles such as cytokine and chemokine release, iron sequestration and modulation of proliferation and development of other cells in the developing brain.

Acknowledgments

This work was supported by a research grant (R-181-000-098-112) from the National University of Singapore. The help provided by Dr Viswanathan Sivakumar in the preparation of this chapter is gratefully acknowledged.

References

[1] Abrahamson, D.R. and Fearon, D.T. (1983). Endocytosis of the C3b receptor of complement within coated pits in human polymorphonuclear leukocytes and monocytes. *Lab. Invest.,* 48, 162-168.

[2] Akassoglou, K., Douni, E., Bauer J, Lassmann, H., Kollias, G. and Probert, L. (2003). Exclusive tumor necrosis factor (TNF) signaling by the p75TNF receptor triggers inflammatory ischemia in the CNS of transgenic mice. *Proc. Natl. Acad. Sci. U S A.*, 100, 709-714.

[3] Alliot, F., Godin, I. and Pessac, B. (1999). Microglia derive from progenitors, originating from the yolk sac, and which proliferate in the brain. *Dev. Brain Res.,* 117, 145-152.

[4] Andjelkovic, A.V., Nikolic, B., Pachter, J.S. and Zecevic N. (1998). Macrophages/microglial cells in human central nervous system during development: an immunohistochemical study. *Brain Res.,* 814, 13-25.

[5] Auernhammer, C.J. and Strasburger, C.J. (1995). Effects of growth hormone and insulin-like growth factor I on the immune system. *Eur. J. Endocrinol.,* 133, 635-645.

[6] Balteskard, L., Unneberg, K., Halvorsen, D., Hansen, J.B. and Revhaug, A. (1998). Effects of insulin-like growth factor 1 on neutrophil and monocyte functions in normal and septic states. *J. Parenter Enteral. Nutr.,* 22, 127-135.

[7] Beller, D.I., Springer, T.A. and Schreiber, R.D. (1982). Anti-Mac-1 selectively inhibits the mouse and human type three complement receptor. *J. Exp. Med.,* 156, 1000-1009.

[8] Blakemore, W.F. (1969). The ultrastructure of the subependymal plate in the rat. *J. Anat.,* 104, 423-433.

[9] Boya, J., Calvo, J. and Prado, A. (1979). The origin of microglial cells. *J. Anat.,* 129, 177-186.

[10] Boya, J., Carbonell, A.L., Calvo, J. and Borregon, A. (1987). Ultrastructural study on the origin of rat microglia cells. *Acta Anat.,* 130, 329-335.

[11] Boya, J., Calvo, J.L., Carbonell, A.L. and Borregon, A. (1991). A lectin histochemistry study on the development of rat microglial cells. *J. Anat.,* 175, 229-236.

[12] Caley, D.W. and Maxwell, D.S. (1968). An electron microscopic study of the neuroglia during postnatal development of the rat cerebrum. *J. Comp. Neurol.,* 133, 45-70.

[13] Cammermeyer, J. (1970). The life history of the microglial cell: a light microscopic study. *Neurosci. Res.,* 3, 43-129.

[14] Cao, Q., Lu, J., Kaur, C., Sivakumar, V., Li, F., Cheah, P.S., Dheen, S.T. and Ling, E.A. (2008). Expression of Notch-1 receptor and its ligands Jagged-1 and Delta-1 in amoeboid microglia in postnatal rat brain and murine BV-2 cells. *Glia.* 56,1224-1237.

[15] Chan, W.Y., Kohsaka, S. and Rezaie, P. (2007). The origin and cell lineage of microglia: new concepts. *Brain Res. Rev.,* 53, 344-354.

[16] Chew, L.J., Takanohashi, A. and Bel, M. (2006). Microglia and inflammation: impact on developmental brain injuries. *Ment. Retard. Dev. Disabil. Res Rev.,* 12, 105-112.

[17] Corbisiero, V., Hagger, G., Topps, S., Kohsaka, S., Imai, Y., Male, D. and Rezaie, P. (2003). Colonization of the developing mouse brain by microglial progenitors. *Neuroembryology*. 2, 181–182.

[18] Cowell, R.M., Xu, H., Galasso, J.M. and Silverstein, F.S. (2002). Hypoxic-ischemic injury induces macrophage inflammatory protein-1alpha expression in immature rat brain. *Stroke.* 33, 795-801.

[19] Cowell, R.M., Xu, H., Parent, J.M. and Silverstein, F.S. (2006). Microglial expression of chemokine receptor CCR5 during rat forebrain development and after perinatal hypoxia-ischemia. *J. Neuroimmunol.,* 173, 155-165.

[20] Cuadros, M.A., Martin, C., Coltey, P., Almendros, A. and Navascues J. (1993). First appearance, distribution and origin of macrophages in the early development of the avian central nervous system. *J. Comp. Neurol.,* 330, 113-129.

[21] Cuadros, M.A., Moujahid, A., Quesada, A. and Navascues, J. (1994). Development of microglia in the quail optic tectum. *J. Comp. Neurol.,* 348, 207-224.

[22] Dalmau, I., Vela, J.M., Gonzalez, B. and Castellano, B. (1997). Expression of LFA-1alpha and ICAM-1 in the developing rat brain: a potential mechanism for the recruitment of microglial cell precursors. *Dev. Brain Res.,* 103, 163-170.

[23] de Groot, C.J., Huppes, W., Sminia, T., Kraal, G. and Dijkstra, C.D. (1992). Determination of the origin and nature of brain macrophages and microglial cells in mouse central nervous system, using non-radioactive in situ hybridization and immunoperoxidase techniques. *Glia.* 6, 301-309.

[24] del Rio-Hortega, P. (1919). El “tercer elemento” de los centros nerviosus. *Bol. Soc. Esp. Biol.,* 9, 69-120.

[25] del Rio-Hortega P. (1932). Microglia . In: *Cytology and Cellular Pathology of the Nervous System,* Vol.2, pp 483-534. Ed. W. Penfield. PaulB. Hoeber, New York.

[26] Deng, Y.Y., Lu, J., Sivakumar, V., Ling, E.A. and Kaur, C. (2008). Amoeboid microglia in the periventricular white matter induces oligodendrocyte damage through expression of proinflammatory cytokines via MAP kinase signaling pathway in hypoxic neonatal rats. *Brain Pathology.* 18, 387-400.

[27] Dickson, D.W. and Mattiace, L.A. (1989). Astrocytes and microglia in human brain share an epitope recognized by a B-lymphocyte-specific monoclonal antibody (LN-1). *Am. J. Pathol.,* 135, 135-147.

[28] Dijkstra, C.D., Dopp, E.A., Joling, P. and Kraal, G. (1985). The heterogeneity of mononuclear phagocytes in lymphoid organs: distinct macrophage subpopulations in rat recognized by monoclonal antibodies ED1, ED2 and ED3. *Adv. Exp. Med. Biol.,* 186, 409-419.

[29] Dopp, J.M., Mackenzie-Graham, A., Otero, G.C. and Merrill, J.E. (1997). Differential expression, cytokine modulation, and specific functions of type-1 and type-2 tumor necrosis factor receptors in rat glia. *J. Neuroimmunol.,* 75, 104-112.

[30] Dougherty, T.F. (1944). Studies on the cytogenesis of microglia and their relation to the cells of the reticulo-endothelial system. *Am. J. Anat.,* 74, 61-95.

[31] Dubois-Dalcq, M. and Murray, K. (2000). Why are growth factors important in oligodendrocyte physiology? *Pathol. Biol. (Paris)*., 48, 80-86.

[32] Earle, K.L. and Mitrofanis, J. 91997). Identification of transient microglial cell colonies in the forebrain white matter of developing rats. *J. Comp. Neurol.,* 1997; 387, 371-384.

[33] Fedoroff, S., Zhai, R. and Novak, J.P. (1997). Microglia and astroglia have a common progenitor cell. *J. Neurosci. Res.,* 50, 477-486.

[34] Flanders, K.C., Ren, R.F. and Lippa, C.F. (1998) Transforming growth factor-βs in neurodegenerative disease. *Prog. Neurobiol.,* 54, 71–85.

[35] Fujita, S. and Kitamura, T. (1975). Origin of brain macrophages and the nature of the so-called microglia. *Acta Neuropathol. Suppl. (Berl).,* 6, 291-296.

[36] Fujita, S., Tsuchihashi, Y. and Kitamura, T. (1981). Origin, morphology and function of the microglia. *Prog. Clin. Biol. Res.,* 59, 141-169.

[37] Gehrmann, J. and Kreutzberg, G.W. (1991). Characterisation of two new monoclonal antibodies directed against rat microglia. *J. Comp. Neurol.,* 313, 409-430.

[38] Guan, J., Bennet, L., George, S., Wu, D., Waldvogel, H.J., Gluckman, P.D., Faull, R.L., Crosier, P.S., Gunn, A.J. Insulin-like growth factor-1 reduces postischemic white matter injury in fetal sheep. *J. Cereb. Blood Flow Metab.,* 21, 493-502.

[39] Halden, Y., Rek, A., Atzenhofer, W., Szilak, L., Wabnig, A. and Kungl, A.J. (2004). Interleukin-8 binds to syndecan-2 on human endothelial cells. *Biochem. J.,* 377, 533-538.

[40] Hao, C., Richardson, A. and Fedoroff, S. (1991). Macrophage-like cells originate from neuroepithelium in culture: characterization and properties of the macrophage-like cells. *Int. J. Dev. Neurosci.,* 9, 1-14.

[41] Hutchins, K.D., Dickson, D.W., Rashbaum, W.K. and Lyman, W.D. (1990). Localization of morphologically distinct microglial populations in the developing human fetal brain: implications for ontogeny. *Dev. Brain Res.,* 55, 95-102.

[42] Imamoto, K. and Leblond, C.P. (1978). Radioautographic investigation of gliogenesis in the corpus callosum of young rats. II. Origin of microglial cells. *J. Comp. Neurol.,* 180, 139-163.

[43] Imamoto, K., Fujiwara, R., Nagai, T. and Maeda, T. (1982). Distribution and fate of macrophagic ameboid cells in the rat brain. *Arch. Histol. Jpn.,* 45, 505-518.

[44] Imamura, K., Ito, M., Suzumura, A., Asai. J. and Takahashi, A. (1990). Generation and characterization of monoclonal antibodies against rat microglia and ontogenic distribution of positive cells. *Lab. Invest.,* 63, 853-861.

[45] Innocenti, G.M., Koppel, H. and Clarke, S. (1983a). Transitory macrophages in the white matter of the developing visual cortex. I. Light and electron microscopic characteristics and distribution. *Brain Res.,* 313, 39-53.

[46] Innocenti, G.M., Clarke, S. and Koppel, H. (1983b). Transitory macrophages in the white matter of the developing visual cortex. II. Development and relations with axonal pathways. *Brain Res.,* 313, 55-66.

[47] Inoue. T., Saito, H., Fukushima, R., Inaba, T., Lin, M.T., Fukatsu, K. and Muto, T. (1995). Growth hormone and insulinlike growth factor I enhance host defense in a murine sepsis model. *Arch. Surg.,* 130, 1115-1122.

[48] Juba, A. (1934). Untersuchungen uber die entwicklung der Hortegaschen mikroglia des menschen. *Arch. Psychiat. Nervenkr.,* 101, 577-592.

[49] Jeetle, J., Hagger, G., Topps, S., Male, D. and Rezaie, P. (2002). Microglia in the CD11b knockout mouse. *Neuroembryology.* 1, 191.

[50] Kadhim, H., Khalifa, M., Deltenre, P., Casimir, G. and Sebire, G. Molecular mechanisms of cell death in Periventricular leukomalacia. *Neurology.* 67, 293-299.

[51] Kaur, C., Ling, E.A. and Wong, W.C. (1984). Cytochemical localisation of 5'-nucleotidase in amoeboid microglial cells in postnatal rats. *J. Anat.,* 139, 1-7.

[52] Kaur, C., Ling, E.A. and Wong, W.C. (1985). Transformation of amoeboid microglial cells into microglia in the corpus callosum of the postnatal rat brain. An electron microscopical study. *Arch. Histol. Jpn.,* 48, 17-25.

[53] Kaur, C., Ling, E.A. and Wong, W.C. (1986). Labelling of amoeboid microglial cells in rats of various ages following an intravenous injection of horseradish peroxidase. *Acta Anat. (Basel).,* 125, 132-137.

[54] Kaur, C., Ling, E.A. and Wong, W.C. (1987). Localisation of thiamine pyrophosphatase in the amoeboid microglial cells in the brain of postnatal rats. *J. Anat.,* 152, 13-22.

[55] Kaur, C. and Ling EA. (1991). Study of the transformation of amoeboid microglial cells into microglia labelled with the isolectin Griffonia simplicifolia in postnatal rat. *Acta Anat.,* 142,118-125.

[56] Kaur, C., Wu, C.H., Wen, C.Y. and Ling, E.A. (1994). The effects of subcutaneous injections of glucocorticoids on amoeboid microglia in postnatal rats. *Arch. Histol. Cytol.,* 57, 449-459.

[57] Kaur, C. and Ling, E.A. (1995). Transient expression of transferrin receptors and localisation of iron in amoeboid microglia in postnatal rats. *J. Anat.,* 186, 165-173.

[58] Kaur, C. and Ling, E.A. (1999). Increased expression of transferrin receptors and iron in amoeboid microglial cells in postnatal rats following an exposure to hypoxia. *Neurosci. Lett.,* 26, 183-186.

[59] Kaur, C. and You, Y. (2000). Ultrastructure and function of the amoeboid microglial cells in the periventricular white matter in postnatal rat brain following a hypoxic exposure. *Neurosci. Lett.,* 290, 17-20.

[60] Kaur, C., Too, H.F. and Ling, E.A. (2004). Phagocytosis of Escherichia coli by amoeboid microglial cells in the developing brain. *Acta Neuropathol. (Berl).,* 107, 204-208.

[61] Kaur, C., Sivakumar, V., Ang, L.S. and Sundaresan, A. (2006a). Hypoxic damage to the periventricular white matter in neonatal brain: role of vascular endothelial growth factor, nitric oxide and excitotoxicity. *J. Neurochem.,* 98, 1200-1216.

[62] Kaur, C., Sivakumar, V., Dheen, S.T. and Ling, E.A. (2006b). Insulin-like growth factor I and II expression and modulation in amoeboid microglial cells by lipopolysaccharide and retinoic acid. *Neuroscience.* 138, 1233-1244.

[63] Kaur, C., Sivakumar, V., Yip, G.W. and Ling, E.A. (2008). Expression of Syndecan-2 in the amoeboid microglial cells and its involvement in inflammation in the hypoxic developing brain. *Glia.* (in press).

[64] Kershman, J. (1939). Genesis of microglia in the human brain. *Arch. Neurol. Psychiatr.,* 41, 24-50.

[65] Kitamura, T., Miyake, T. and Fujita S. (1984). Genesis of resting microglia in the gray matter of mouse hippocampus. *J. Comp. Neurol.,* 226, 421-433.

[66] Kurz, H. and Christ, B. (1998). Embryonic CNS macrophages and microglia do not stem from circulating, but from extravascular precursors. *Glia.* 22, 98-102.

[67] Leong, S.K., Shieh, J.Y., Ling, E.A. and Wong, W.C. (1983). Labelling of amoeboid microglial cells in the supraventricular corpus callosum following the application of horseradish peroxidase in the cerebrum and spinal cord in rats. *J. Anat.,* 136, 367-377.

[68] Lewis, P.D. (1968). The fate of the subependymal cell in the adult rat brain, with a note on the origin of microglia. *Brain.* 91, 721-736.

[69] Li, Y.B., Kaur, C. and Ling, E.A. (1997). Labeling of amoeboid microglial cells and intraventricular macrophages in fetal rats following a maternal injection of a fluorescent dye. *Neurosci. Res.,* 28, 119-125.

[70] Li, F., Lu, J., Wu, C.Y., Kaur, C., Sivakumar, V., Sun, J., Li, S. and Ling E.A. (2008). Expression of Kv1.2 in microglia and its putative roles in modulating production of proinflammatory cytokines and reactive oxygen species. *J. Neurochem.,* (in press).

[71] Ling, E.A. and Tan, C.K. (1974). Amoeboid microglial cells in the corpus callosum of neonatal rats. *Arch. Histol. Jpn.,* 36, 265-280.

[72] Ling, E.A. (1976) Some aspects of amoeboid microglia in the corpus callosum and neighbouring regions of neonatal rats. *J. Anat.,* 121, 29-45.

[73] Ling, EA. (1977). Light and electron microscopic demonstration of some lysosomal enzymes in the amoeboid microglia in neonatal rat brain. *J. Anat.,* 123, 637-648.

[74] Ling, E.A. (1979). Transformation of monocytes into amoeboid microglia in the corpus callosum of postnatal rats, as shown by labelling monocytes by carbon particles. *J. Anat.,* 128, 847-858.

[75] Ling, E.A., Penney, D. and Leblond, C.P. (1980). Use of carbon labeling to demonstrate the role of blood monocytes as precursors of the 'ameboid cells' present in the corpus callosum of postnatal rats. *J. Comp. Neurol.,* 193, 631-657.

[76] Ling, E.A. (1982). Influence of cortisone on amoeboid microglia and microglial cells in the corpus callosum in postnatal rats. *J. Anat.,* 134, 705-717.

[77] Ling, E.A., Kaur, C. and Wong, W.C. (1982). Light and electron microscopic demonstration of non-specific esterase in amoeboid microglial cells in the corpus callosum in postnatal rats: a cytochemical link to monocytes. *J. Anat.,* 135, 385-394.

[78] Ling, E.A., Kaur, C., Yick, T.Y. and Wong, W.C. (1990). Immunocytochemical localization of CR3 complement receptors with OX-42 in amoeboid microglia in postnatal rats. *Anat. Embryol. (Berl).,* 182, 481-486.

[79] Ling, E.A., Kaur, C. and Wong, W.C. (1991). Expression of major histocompatibility complex and leukocyte common antigens in amoeboid microglia in postnatal rats. *J. Anat.,* 177, 117-126.

[80] Ling, E.A. and Wong, W.C. (1993). The origin and nature of ramified and amoeboid microglia: a historical review and current concepts. *Glia.* 7, 9-18.

[81] Logan. A., Gonzalez. A.M., Hill, D.J., Berry, M., Gregson, N.A. and Baird, A. (1994). Coordinated pattern of expression and localization of insulin-like growth factor-II (IGF-II) and IGF-binding protein-2 in the adult rat brain. *Endocrinology.* 135, 2255-2264.

[82] Lopez-Figueroa, M.O., Day, H.E., Lee, S., Rivier, C., Akil, H. and Watson, S.J. (2000). Temporal and anatomical distribution of nitric oxide synthase mRNA expression and nitric oxide production during central nervous system inflammation. *Brain Res.,* 852, 239-246.

[83] Lu, Y.Z., Lin, C.H., Cheng, F.C. and Hsueh, C.M. (2005). Molecular mechanisms responsible for microglia-derived protection of Sprague–Dawley rat brain cells during in vitro ischemia. *Neurosci. Lett*., 373, 159–164.

[84] MacMicking, J., Xie, Q.W. and Nathan, C. (1997). Nitric oxide and macrophage function. *Annu. Rev. Immunol.,* 15, 323-350.

[85] Matsuyama, H., Komatsu, N. and Senda, R. (1973). Electron microscopic studies on the developing telencephalic wall of the rat fetus. *Okajimas Folia Anat. Jpn.,* 50, 273-293.

[86] McKanna, J.A. (1993a). Primitive glial compartments in the floor plate of mammalian embryos: distinct progenitors of adult astrocytes and microglia support the notoplate hypothesis. *Perspect. Dev. Neurobiol.,* 1, 245-255.

[87] McKanna, J.A. (1993b). Lipocortin 1 immunoreactivity identifies microglia in adult rat brain. *J.Neurosci. Res.,* 36, 491-500.

[88] Merrill, J.E., Ignarro, L.J., Sherman, M.P., Melinek, J. and Lane, T.E. (1993). Microglial cell cytotoxicity of oligodendrocytes is mediated through nitric oxide. *J. Immunol.,* 151, 2132-2141.

[89] Murabe, Y. and Sano, Y. (1983). Morphological studies on neuroglia. VII. Distribution of "brain macrophages" in brains of neonatal and adult rats, as determined by means of immunohistochemistry. *Cell Tissue Res.,* 229, 85-95.

[90] Newman, S.L., Musson, R.A. and Henson, P.M. (1980). Development of functional complement receptors during in vitro maturation of human monocytes into macrophages. *J. Immunol.,* 125, 2236-2244.

[91] Papavasiliou, A.K., Mehler, M.F., Dobrenis, K., Marmur, R., Mabie, P.C. and Kessler, J.A. (1996). Microglial lineage species are expressed in mammalian epidermal growth factor-generated embryonic neurospheres. *J. Neurosci. Res.,* 46, 49-57.

[92] Paterson, J.A., Privat, A., Ling, E.A. and Leblond, C.P. (1973). Investigation of glial cells in semithin sections. 3. Transformation of subependymal cells into glial cells, as shown by radioautography after ^{3}H-thymidine injection into the lateral ventricle of the brain of young rats. *J. Comp. Neurol.,* 149, 83-102.

[93] Paulus, W., Roggendorf, W. and Kirchner, T. (1992). Ki-M1P as a marker for microglia and brain macrophages in routinely processed human tissues. *Acta Neuropathol.,* 84, 538-544.

[94] Penfield, W. (1932). Neuroglia and microglia. The interstitial tissue of the central nervous system. In *Special Cytology*, (E.V. Cowdry, ed.), 2nd ed., Vol. III. Hoeber, New York.

[95] Penfold, P.L., Madigan, M.C. and Provis, J.M. (1991). Antibodies to human leucocyte antigens indicate subpopulations of microglia in human retina. *Vis. Neurosci.,* 7, 383-388.

[96] Perry, V.H., Hume, D.A. and Gordon, S. (1985). Immunohistochemical localization of macrophages and microglia in the adult and developing mouse brain. *Neuroscience.* 15, 313-326.

[97] Rezaie, P., Dean, A., Male, D., Ulfig, N. (2005). Microglia in the cerebral wall of the human telencephalon at second trimester. *Cereb. Cortex.,* 15, 938-949.

[98] Richardson, A., Hao, C. and Fedoroff, S. (1993). Microglia progenitor cells: a subpopulation in cultures of mouse neopallial astroglia. *Glia.* 7, 25-33.

[99] Robinson, A.P., White, T.M. and Mason, D.W. (1986). Macrophage heterogeneity in the rat as delineated by two monoclonal antibodies MRC OX-41and MRC OX-42, the latter recognizing complement receptor type 3. *Immunology.* 57, 239-247.

[100] Russo-Marie, F. Macrophages and the glucocorticoids. *J. Neuroimmunol.,* 40: 281-286.

[101] Rydberg, E. (1932). Cerebral injury in newborn children consequent on birth trauma, with an inquiry into the normal and pathological anatomy of the neuroglia. *Acta Pathol. Microbiol. Scand.,* 10, 1-247.

[102] Santha, K. and Juba, A. (1933). Weitre untersuchungen uber entwicklung der Hortegaschen mikroglia. *Arch. Psychiat. Nervenkr.,* 98, 598-613.

[103] Schmidt, D. (1973). Glycoprotein containing amoeboid cells in the chicken's embryonic brain. A light and electron microscopical investigation of the reserve volume during brain development. *Z. Anat. Entwicklungsgesch.,* 142, 341-358.

[104] Thomas, W.E. (1992). Brain macrophages: evaluation of microglia and their functions. *Brain Res. Brain Res. Rev.,* 17, 61-74.

[105] Walter, H.J., Berry, M., Hill, D.J., Cwyfan-Hughes, S., Holly, J.M. and Logan, A. (1999). Distinct sites of insulin-like growth factor (IGF)-II expression and localization in lesioned rat brain: possible roles of IGF binding proteins (IGFBPs) in the mediation of IGF-II activity. *Endocrinology.* 140, 520-532.

[106] Wolswijk, G. (1995). Strongly GD3+ cells in the developing and adult rat cerebellum belong to the microglial lineage rather than to the oligodendrocyte lineage. *Glia.* 13, 13-26.

[107] Wright, S.D., Rao, P.E., Van Voorhis, W.C., Craigmyle, L.S., Iida, K., Talle, M.A., Westberg, E.F., Goldstein, G. and Silverstein, S.C. (1983). Identification of the C3bi receptor of human monocytes and macrophages by using monoclonal antibodies. *Proc. Natl. Acad. Sci. U S A.,* 80, 5699-5703.

[108] Wu, C.H., Wen, C.Y., Shieh, J.Y. and Ling, E.A. (1994). Down-regulation of membrane glycoprotein in amoeboid microglia transforming into ramified microglia in postnatal rat brain. *J. Neurocytol.,* 23, 258-269.

[109] Xu, J., Kaur, C. and Ling, E.A. (1993). Variation with age in the labelling of amoeboid microglial cells in rats following intraperitoneal or intravenous injection of a fluorescent dye. *J. Anat.,* 182, 55-63.

[110] Xu, J. and Ling, E.A. (1994a). Upregulation and induction of major histocompatibility complex class I and II antigens on microglial cells in early postnatal rat brain following

intraperitoneal injections of recombinant interferon-gamma. *Neuroscience.* 60, 959-967.

[111] Xu, J. and Ling, E.A. (1994b). Upregulation and induction of surface antigens with special reference to MHC class II expression in microglia in postnatal rat brain following intravenous or intraperitoneal injections of lipopolysaccharide. *J. Anat.,* 184 285-296.

In: Handbook on White Matter
Editors: T. B. Westland and R. N. Calton
ISBN: 978-1-60741-034-8

Chapter XVI

Diffusion Tensor Imaging is More Sensitive than Conventional Magnetic Resonance Imaging in Demonstrating White Matter Abnormalities in Susac's Syndrome

Ilka Kleffner*[*1], Michael Deppe[†1], Siawoosh Mohammadi[1], Philip Van Damme[2], Stefan Sunaert[3], Wolfram Schwindt[4], Jens Sommer[1], Peter Young[1] and E.B. Ringelstein[1]

[1] Department of Neurology, University of Muenster, Albert-Schweitzer-Str. 33, 48129 Muenster, Germany
[2] Department of Neurology, Catholic University of Leuven, Herestraat 49, 3000; Leuven, Belgium
[3] Department of Radiology, Catholic University of Leuven, Herestraat 49, 3000; Belgium
[4] Department of Clinical Radiology, University of Muenster, Albert-Schweitzer-Str. 33, 48129 Muenster, Germany

Abstract

Objective: Susac's syndrome is characterized by the triad of hearing loss, branch retinal artery occlusions, and encephalopathy with predominantly cognitive and psychiatric symptoms. Focal ischemic lesions in the corpus callosum detectable by conventional magnetic resonance imaging (MRI) are a characteristic feature of Susac's syndrome. They do not, however, fully explain the type and severity of the neuropsychological deficits. In this study, we tested the hypothesis that widespread tissue

[*] Corresponding author: Dr. med. Ilka Kleffner; Department of Neurology; University of Muenster; Albert-Schweitzer-Str. 33; 48129 Muenster; Germany; phone office: +49-(0)251-8348222; e-mail: kleffnil@uni-muenster.de
[†] The authors Ilka Kleffner and Michael Deppe contributed equally to this study.

damage of otherwise normal-appearing white matter (NAWM) can be detected in Susac's syndrome when using diffusion tensor imaging (DTI).

Methods: Three-dimensional fractional anisotropy (FA) maps were calculated from DTI data of five patients with Susac's syndrome and a group of 63 matched healthy controls.

Results: Voxel-based statistics of spatially normalized FA maps revealed highly significant widespread impairment of fiber integrity in all patients. Lesions were particularly located in the genu of the corpus callosum and in the frontotemporal connecting fascicles. Patients showed specifically reduced mean FA values in the region of interest outlining the genu. This was true even if the genu was not focally affected on conventional MRI.

Interpretation: We conclude that DTI is much more sensitive than conventional MRI in demonstrating WM abnormalities in Susac's syndrome. FA reductions in NAWM of the genu of the corpus callosum seem to be disease-specific. Psychiatric symptoms and cognitive deficits of these patients are most likely caused by the disruption of the anatomical connectivity of the frontal lobes.

Introduction

Susac's syndrome is a rare disease in young adults. It has first been described by Susac in 1979 (Susac et al. 1979). The original description pinpoints the three leading symptoms to be visual field defects, sensorineural hearing loss and encephalopathy. About 150 cases of Susac's syndrome have been described in the literature so far. Mostly young women between the ages of 20 and 40 years are affected (O'Halloran et al. 1998; Plummer et al. 2005). Recent publications indicate that Susac's syndrome is much more common than previously thought (Petty et al. 1998).

The diagnosis is based on the findings during ophthalmological examination, audiometry, magnetic resonance imaging (MRI), and a characteristic history. As a correlative of small peripheral visual field defects, branch retinal artery occlusions (BRAO), poststenotic retinal vessel leakage, hyperfluorescence of retinal arterial wall plaques, and retrograde vessel filling can be detected by fluorescence angiography (Gass et al. 1986; Notis et al. 1995; Saw et al. 2000; Egan et al. 2003). Otological findings reveal sensorineural, asymmetric pancochlear hypoacusis, mostly for lower frequencies (Ayache et al. 2000; Gross et al. 2004), often accompanied by tinnitus. Magnetic resonance imaging (MRI) shows typical small, multifocal hyperintense lesions in the periventricular white matter and the corpus callosum on T2-weighted, diffusion-weighted (DWI) and fluid attenuated inversion recovery (FLAIR) images. In the acute and subacute phase, these lesions show contrast enhancement in some cases (Susac et al. 2003; White et al. 2004; Do et al. 2004; Kleffner et al. 2006), but not in all.

Prodromal migrainous headache is also a common feature associated with Susac's syndrome (Susac 1994; Kleffner et al. 2006).

The major manifestation of encephalopathy are acute symptomatic psychosis, severe behavioural abnormalities and cognitive deficits (Susac et al. 1979; Susac 1994; Susac 2004). The severity and type of these deficits can hardly be explained by the small focal callosal lesions often seen on T2-weighted and FLAIR MRI and considered pathognomonic for the

disease (Susac et al. 2003; White et al. 2004; Do et al. 2004; Ringelstein and Knecht 2006). Particularly the severity of the psychotic symptoms would suggest a much more extended structural disintegration of the cerebral tissue as opposed to the small lesions mentioned above (Kleffner et al. 2008). In this study, we tested the hypothesis that widespread tissue damage of the otherwise normal-appearing white matter (NAWM) can be detected in Susac's syndrome when using diffusion tensor imaging (DTI). DTI is a non-invasive MRI technique for the measurement of the diffusibility of water molecules within cerebral tissue. In coherent white matter tracts, diffusion is restricted perpendicular to the direction of the fibers dictated by normal anatomy of neuronal structures, i.e. membranes of axons, Schwann cells, and myelin sheaths that act as barriers to crosssectional but facilitate longitudinal diffusion. Any lesion of these structures results in an increasing mean water diffusibility, and a decreased directionality of the diffusion, measured by the fractional anisotropy (FA) (Basser and Jones 2002; Le Bihan 2003). Previous DTI studies in cerebral autosomal dominant arteriopathy with subcortical infarcts and leukoencephalopathy (CADASIL) (O'Sullivan et al. 2004a), cocaine and alcohol abuse (Moeller et al. 2005; Pfefferbaum et al. 2006), degenerative cerebral small vessel disease (O'Sullivan et al. 2004b), epilepsy (Deppe et al. 2008; Anneken et al. 2008), mild cognitive impairmentand dementia (Fellgiebel et al. 2006), and schizophrenia (Foong et al. 2000; Burns et al. 2003) have all confirmed that DTI is an appropriate tool to detect macro- and microstructural impairment of fiber integrity. We hypothesised that the neuropsychological symptoms in Susac's syndome detected by DTI correlate well with these fiber aberrations.

Methods

We investigated five patients with proven Susac's syndrome. The severity and type of their encephalopathic symptoms varied from mild cognitive impairment to severe acute psychosis (table 1). Diagnosis of Susac's syndrome was proven by the documentation of branch retinal artery occlusions, sensorineural hearing loss, encephalopathy and the characteristic snowball-like hyperintense lesions of the corpus callosum on DWI. Regional white matter integrity was assessed by whole brain FA maps (Deppe et al. 2007).

Table 1. Neuropsychological deficits in five patients with Susac's syndrome.

	Neuropsychological symptoms
Patient 1	severe cognitive deficits (dyscalculia, impaired verbal and numerical memory, strongly impaired alertness, reduced motivation, and impaired cognitive flexibility) hallucinations, paranoia, disorientation
Patient 2	severe cognitive deficits, reduced short-term memory, emotional indifference, loss of motivation and concentration, amnesic aphasia, fatigue
Patient 3	normal results in neuropsychological testing (considering the academical grade of the patient, higher levels would have been expected.)
Patient 4	mildly impaired short-term memory
Patient 5	memory loss, disorientation, memory deficits, dyscalculia, dysgraphia, motor aphasia

Data of the five individual patients were statistically compared with a group of 63 age- and gender-matched healthy controls on a voxel-by-voxel basis and by regions-of-interest (ROI). T1-weighted MRI was used to compare white matter (WM) and grey matter (GM) volumes in patients with Susac's syndrome, and in controls. The degree and location of structural brain lesions were correlated to the patients' symptoms.

Patients

Patient 1

A 17-year-old girl developed migrainous headache, cognitive deficits, hallucinations, paranoia, disorientation, vertigo, nausea, impaired vision and paresthesia. She was treated by high-dose corticosteroids and recovered completely. Within two months, she presented twice with hearing loss, tinnitus and dysarthric speech. Treatment with corticosteroids and pentoxiphylline lead to partial recovery. Neurological findings during the last episode were the following: generalized hyperreflexia, mild gait ataxia, asymmetric hypoacusis, dysarthria, and cognitive impairment. Neuropsychological testing revealed dyscalculia, impaired verbal and numerical memory, strongly impaired alertness, reduced motivation, and impaired cognitive flexibility. MRI showed multifocal, snowball-like, small hyperintense lesions in the corpus callosum and the periventricular WM (figure 1A). Typical abnormalities in audiometry, presenting as a sensorineural, low-frequency hearing loss, retinal fluorescein angiography, slowing electroencephalography (EEG) and cerebrospinal fluid (CSF) confirmed the diagnosis of Susac's syndrome and excluded other disease entities. Her visual, auditory, motor and sensory evoked responses were normal. We initiated a secondary prophylactic therapy with nimodipine 3x30 mg/d and aspirin 100 mg/d. Over a periode of 18 months, no further episode had occurred so far (Kleffner et al. 2006).

Patient 2

A 26-year-old woman presented with paresthesia and numbness of her left arm and leg. She also complained of temporal headache, nausea and vomiting, as well as impaired vision on her left eye. She was disoriented, suffered from fatigue and had severe disturbances of concentration and short-term memory.

She was admitted to a psychiatric hospital with symptoms of an acute psychosis. A cerebral vasculitis was assumed. She recovered partially after treatment with prednisolone. Predominantly the psychiatric symptoms ceased under this therapy. Two months later, she developed tinnitus and impaired hearing of her left ear. Treatment with pentoxiphylline led to a normaliziation of tinnitus and hearing loss.

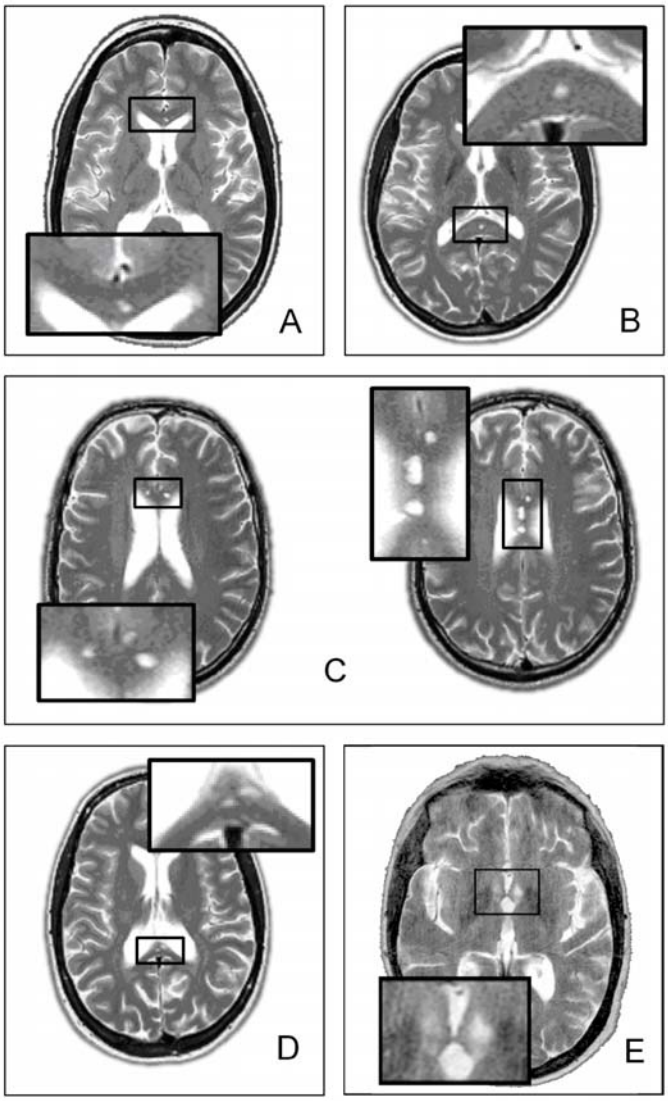

Figure 1. MRI findings in five patients with Susac's syndrome. Note the snowball-like lesions of the corpus callosum (inserts).

Clinical findings revealed peripheral scotoma, hypoacusis of her left ear and a mild left hemiparesis. Neuropsychological testing showed severe cognitive deficits, reduced short-term memory, emotional indifference, loss of motivation and concentration, and anomia. Laboratory serum examination revealed mildly elevated IgA and IgG levels for Yersinia species and complement C3. In the CSF, high protein levels were found (1230 mg/l), mild pleocytosis (5 lymphocytes/mm³) and a severe blood-CSF barrier disturbance. EEG showed bilateral, predominantly frontal intermittent rhythmic delta activity (FIRDA). Visual, auditory, motor and sensory evoked responses were normal.

MRI showed multifocal, small hyperintense white matter lesions up to 12 mm in diameter in the cerebellum and the para- and supraventricular WM on T2-weighted images.

One of the lesions showed contrast enhancement indicating an active lesion (figure 1B). Audiometry revealed mild asymmetric bilateral sensorineural cochlear hypoacusis. Her retinal fluorescein angiography revealed a BRAO in her left eye with multiple collaterals, hyperfluorescence and peripheral telangiectasia.

She was treated with a combination therapy recommended in the literature (Wildemann et al. 1996) and consisting of azathioprin (125 mg/d), aspirin (100 mg/d), and nimodipine (3x30 mg/d). Oral contraception was replaced by a contraceptive vaginal ring. The clinical course remained stable, but the patient still suffers from severe cognitive deficits and intermittent headache.

Patient 3

A 25-year-old man presented with migrainous headache which did not respond to any treatment. It ceased spontaneously after two months. One year later, he suffered from sudden hearing loss on his left ear and vertigo. The hearing loss was successfully treated with pentoxiphylline and betahistin. Vertigo persisted despite treatment with corticosteroids. Four months later, he presented with tinnitus and vertigo, and two months thereafter with visual field defects.

Clinical findings were the following: reduced blood pressure of 90/60 mmHg, spotty visual field defects, blurred sight, mild nystagmus, left facial palsy, and a mild subclinical right hemiparesis. Neuropsychological testing was normal for his age-group, but considering his academical grade, higher levels would have been expected. Laboratory serum examination revealed an elevated thyroid stimulating hormone level of 2,9 µU/ml due to a former thyreoiditis. CSF protein level was 281 mg/l, and 1 lymphocyte/mm³ was found. EEG showed bilateral frontotemporal slowing presenting mainly as theta activity without signs of epileptic discharges. Peaks III-V of his auditory evoked responses were reduced on the right, while being normal on the left. Visual, motor and sensory evoked responses were normal.

Multifocal, small hyperintense lesions without contrast enhancement were seen on MRI in the genu and the splenium of the corpus callosum, as well as in the periventricular WM (figure 1C). Audiometry revealed bilateral sensorineural pancochlear hypoacusis. The retinal fluorescein angiography revealed bilateral multifocal BRAO with hyperfluorescent retinal arterial wall plaques, collateralization, poststenotic vessel leakage and exsudation, predominantly in the right eye.

Currently, he is treated with a secondary prophylactic therapy with aspirin and has not developed any new symptoms so far.

Patient 4

A 25-year-old woman presented with sudden hearing loss and tinnitus of her right ear. She improved partially on an oral therapy with prednisolone. Two years later, she developed periauricular numbness and paresthesia of her right auricle. After another year, a scotoma appeared in her right visual field, followed by another one in her left visual field one month

later. For three times she noticed gait ataxia of several hours duration. For five years, she had suffered from bifrontal migrainous headache.

On clinical examination, severe hypoacusis of her right ear, spotty visual field defects and gait ataxia on the right were found. Laboratory findings, visual, motor and sensory evoked responses, EEG, echocardiogram and ultrasound examination of her intracranial and extracranial arteries were normal. CSF examination revealed 2 lymphocytes/mm³ and a protein level of 210 mg/l. Three oligoclonal immunoglobulin bands were detected identical in the CSF and the serum. Neuropsychological testing revealed mildly impaired short-term memory.

Her ophthalmological findings were as follows: narrowing of retinal arteries, telangiectasis, and subtotal branch retinal artery occlusions in the periphery. MRI studies showed several hyperintense lesions in the corpus callosum with a diameter of up to 2 mm on T2-weighted and FLAIR images, but no contrast enhancement on T1-weighted images (figure 1D). Currently, she is treated with aspirin and nimodipin. Oral contraception was replaced by an intrauterine device. So far, she did not develop any new symptoms.

Patient 5

A 38-year old woman developed a right central facial palsy and fever that ceased spontaneously. Half a year later, she developed a second right facial palsy, accompanied by headaches and paresthesia of the arms. She was reffered to the hospital one month later because of progressing gait disturbance and a weakness of her right hand, memory loss and other cognitive deficits. Treatment with aciclovir and corticosteroids was not successful. Another three months later, a treatment with intravenous corticosteroids and cyclophosphamide was successfully administered.

On examination, the patient showed disorientation, memory deficits, dyscalculia, dysgraphia, motor aphasia, anisocoria, saccadic eye movements, a right motor deficit, spasticity and hyperreflexia and bilateral flexor plantar responses. Laboratory tests were unremarkable. CSF protein level was 105,2 mg/l. MRI showed multiple small white matter lesions in the corpus callosum, in the periventricular region, the pons, the left pedicle and in the basal ganglia (figure 1E). A brain biopsy showed gliosis and some inflammatory cells, but no hints on a vasculitis. EEG showed bilateral slowing. In the left eye, fluorescence angiography revealed a BRAO. There was no hearing loss, and the hearing tests and brain stem auditory evoked responses were normal. A progressive improvement occurred with a continuated therapy with oral corticosteroids.

In all patients, the diagnosis was based on the typical clinical triad of branch retinal artery occlusions, asymmetric sensorineural cochlear hypoacusis, and encephalopathy, including multifocal, hyperintense WM lesions detected by MRI. General diseases, such as infections and autoimmune diseases, or inflammatory diseases of the CNS, were excluded. Acute treatment and secondary prophylactic therapy were based on the published recommendation (Wildemann et al. 1996; Papo et al. 1998). Oral contraception was replaced because of the reported enhanced coagulation in some patients with Susac's syndrome (Notis et al. 1995; Barker et al. 1999).

MRI Data Acquisition

All five patients, as well as the 63 age-matched healthy control subjects (33 male, 30 female, mean age 27.9 years (males 28.3 years, females 27.4 years, range 21 - 41 years), underwent DTI to investigate quantitative structural differences of the WM integrity, high resolution (0.5 mm x 0.5 mm x 0.5 mm) structural T1-weighted imaging for brain volumetry, as well as T2-weighted, and FLAIR imaging. All subjects gave written informed consent prior to the examinations. For DTI we employed echo planar imaging (EPI) at 3 Tesla (20 diffusion directions, 36 slices, slice thickness 3.6 mm, matrix 128 x 128, in-plane resolution 1.8 mm x 1.8 mm) according to Jones et al. (Jones et al. 1999).

MRI Data Analysis

After correction for eddy currents with the aid of in-house software, the EPI images were spatially normalized to the Montreal Neurological Institute (MNI) coordinate system (Chau and McIntosh 2005) following the steps suggested by Büchel et. al. (Buchel et al. 2004). All time consuming calculations like eddy currents correction and normalizations, were carried out on a 64-bit 64-processor parallel computer (Sun Microsystems, Inc., Palo Alto). The diffusion tensor and FA field maps of all participants were calculated from the spatially normalized images using in-house software written by the authors S.M. and M.D.. In a second step, all individual FA images were normalized to a grand average FA template image also corresponding to the MNI coordinate space. Fiber direction maps were calculated on the basis of the largest eigenvector. Voxel-by-voxel FA differences between patients and controls were evaluated using statistical parametric mapping (SPM2, two-sample t-test, $P < 0.001$, uncorrected; min. cluster size 10 voxels). Details about SPM2 can be found at www.fil.ion.ucl.ac.uk/spm/. For the voxel-by-voxel statistics, the FA images were smoothed by a 4 mm isotropic Gaussian kernel. To assess the specificity of regional FA alterations, we further defined three regions of interest: (1) a global region covering the major part of the brain's WM (so called "ROI-global"), (2) a subregion covering the genu of the corpus callosum ("ROI-genu") and (3) a subregion corresponding to the splenium of the corpus callosum ("ROI-splenium"). The spatial extent of the three ROIs is illustrated in figure 2. Mean FA values of all three ROIs were calculated for all patients and controls. Group differences of ROI-specific mean FA values between patients and controls were statistically evaluated by analysis of covariance (ANCOVA), modeling the factor age as co-variable to account for a potential age dependency of the FA.

Brain tissue volume was estimated with SIENAX (Smith et al. 2001; Smith et al. 2002), distributed as part of the "FSL neuroimaging tool suite" (Smith et al. 2004). After brain extraction from the individual whole-head input data (Smith 2002), the brain images were affine-registered to the MNI152 space (Jenkinson and Smith 2001; Jenkinson et al. 2002). Tissue-type segmentation with partial volume estimation was carried out (Zhang et al. 2001) in order to calculate total volume of brain tissue (including separate estimates of volumes of GM, WM, peripheral GM and ventricular CSF). WM and GM volumes were corrected, i.e.

normalized, for subject head size. Differences between patients and control subjects of all tissue types were analyzed by Student's t-test for independent samples.

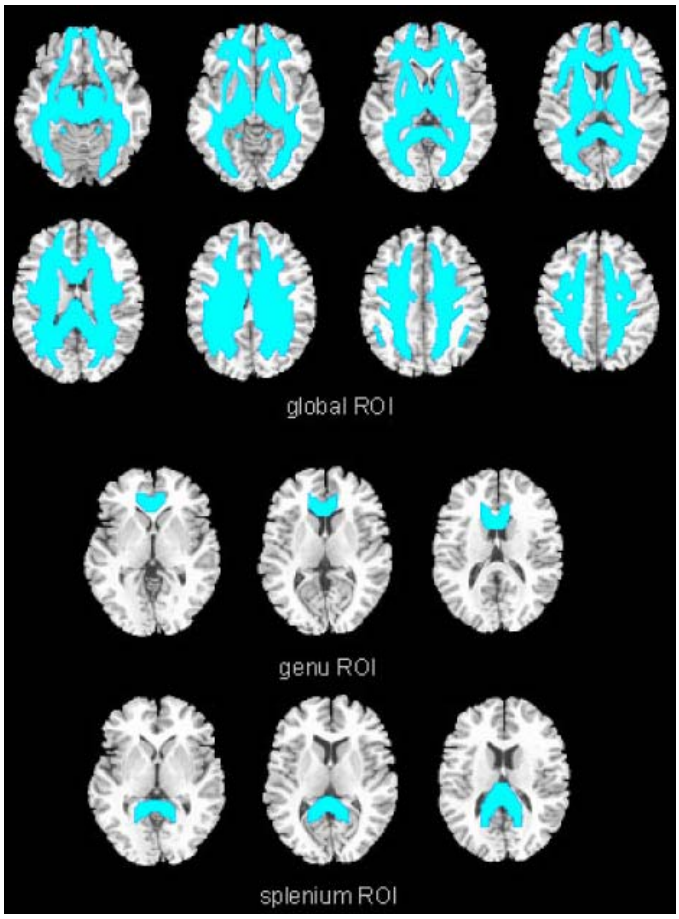

Figure 2. Definition of three regions of interest, a global region covering the major part of the brain's WM (so called "ROI-global"), (2) a subregion covering the genu of the corpus callosum ("ROI-genu") and (3) a subregion corresponding to the splenium of the corpus callosum ("ROI-splenium").

Results

The statistical volumetric evaluation of CSF, WM, and GM showed no significant quantitative differences between control subjects and patients indicating that Susac's syndrome does not reduce overall WM or GM volumes (figure 3, table 2). The only significant difference between absolute GM volume of patients versus controls (table 2, 7th row) was presumably due to a significant difference in head size between both groups ($P<0.05$), because no significant difference was seen any more after normalization for that latter parameter. In particular, we found no systematic overall deviations of WM volumes of the patients versus controls irrespective of whether these volumes were corrected for head size or not (see also figure 3, table 2).

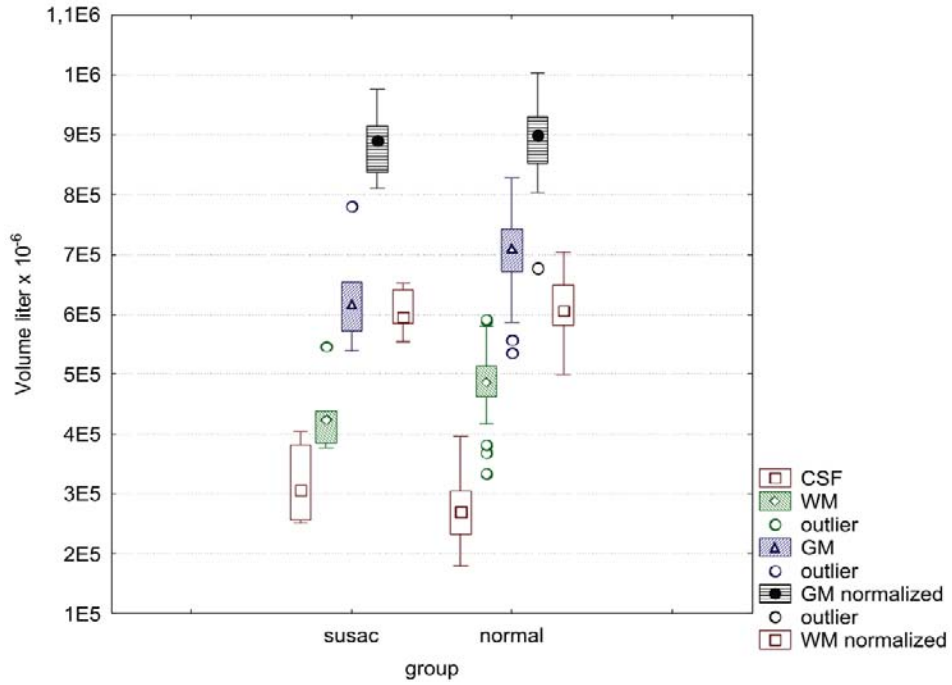

Figure 3. Statistical volumetric evaluation of CSF, WM, and GM showing no significant quantitative differences between control subjects and patients. Red, cerebrospinal fluid; green, white matter; blue, grey matter; black, normalized grey matter; dark red, normalized white matter; whiskers, standard deviation.

Table 2. Comparison between patients and controls of mean FA values of 3 ROIs and CSF, WM, and GM tissue volumes. WM and GM volumes are given in absolute and normalized size

	Mean of Susac patients	Mean of control group	P 2-sample t-test	STD of Susac patients	STD of control group
FA by DTI					
ROI-global (mean FA)	0.301	0.358	P < 0.000001	0.031	0.015
ROI-genu (mean FA)	0.279	0.422	P < 0.000001	0.040	0.043
ROI-splenium (mean FA)	0.329	0.462	P < 0.000001	0.066	0.040
tissue volumes by MRI					
brain size (liter)	1,491	1,505	P = 0.70	0.103	0.102
CSF (liter)	0.320	0.273	P = 0.07	0.070	0.053
normalized GM (liter)	0.885	0.892	P = 0.82	0.065	0.061
Normalized WM (liter)	0.606	0.613	P = 0.76	0.041	0.049

In contrast to the volumetric tissue analysis, DTI revealed severe widespread disruption of fiber integrity in all patients unexceptionally. Comparing the mean FA values of ROI-global, we found a significantly reduced overall FA in Susac's syndrome compared to controls (table 2, 1st row). Significant reductions of the patients' FA were also found by means of voxel-by-voxel statistics in the corpus callosum, predominantly in the genu and in

prefrontal areas. Systematically increased FA values could not at all be observed in the patients. The FA reductions within the prefrontal areas and the genu of the corpus callosum were not only statistically significant in the group analysis (i.e. voxel-by-voxel statistics), but were also present in all five patients within the ROI-genu and ROI-splenium if compared to the normal ranges for FA values (table 2, figure 5, figure 6B, figure 6C). In figure 4 fiber-direction-resolved and color-coded FA maps are compared for each of the patients with an illustrative healthy control subject selected from the control group. The selection criteria for this control subject were representative mean FA values (here: ROI-global=0.360, ROI-genu=0.416, ROI-splenium=0.469). For comparison, mean FA values and corresponding standard deviations for the normal group are given in table 2 (row 1-3). The ANCOVA, which also accounted for age, revealed that patients with Susac's syndrome showed highly significant reductions of FA in all three ROIs (ROI-global $p < 0.000001$, ROI-genu $p < 0.000002$, ROI-splenium $p < 0.000001$). Figure 5 illustrates the distribution of the mean FA values calculated for the three ROIs in patients and normal controls. Figure 6A, figure 6B, and figure 6C show the mean FA of each ROI for all patients and control subjects in dependence of their age. No significant effects of age or gender on the mean FA values of the ROIs were found in the control group by ANCOVA (age) and 2-sample t-test for independent samples (gender). None of the 63 control subjects showed an FA value in her or his ROI-genu that was as low as seen in any of the five patients with Susac's syndrome (figure 6B). An approximately 25 % FA reduction in the genu seems to be specific for Susac's syndrome (FA ROI-genu = 0.296 +/- 0.019) in comparison to healthy controls (FA ROI-genu = 0.418 +/- 0.015). This finding is interesting in so far as patients 2 and 4 show no obvious snowball-like or other lesion in the genu on T2 or FLAIR images (figure 1B and 1D). By contrast, patient 2 shows an obvious lesion in the splenium on T2 weighed images (figure 1B) but no FA reduction in the immediately adjacent callosal fibers (figure 4, column 3, lower panel). This discrepancy highlights the independency of the macroscopic WM lesions visible on T2-weighted images from the lesions indicated by FA reduction.

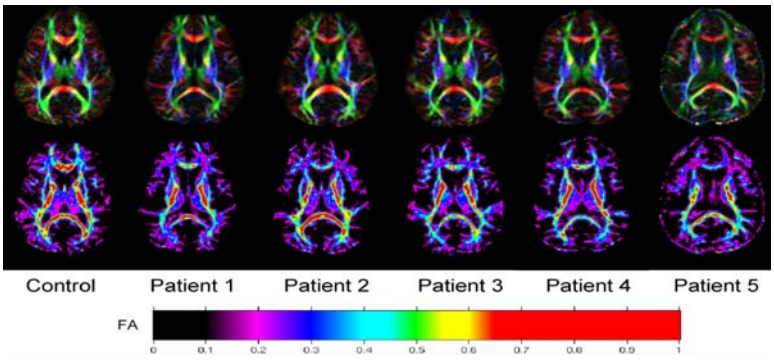

Figure 4. Fiber-direction-resolved (upper row) and color-coded FA maps compared for each of the patients with an illustrative healthy control subject selected from the control group
Fiber directions red, left – right; green, anterior – posterior; blue, inferior – superior.

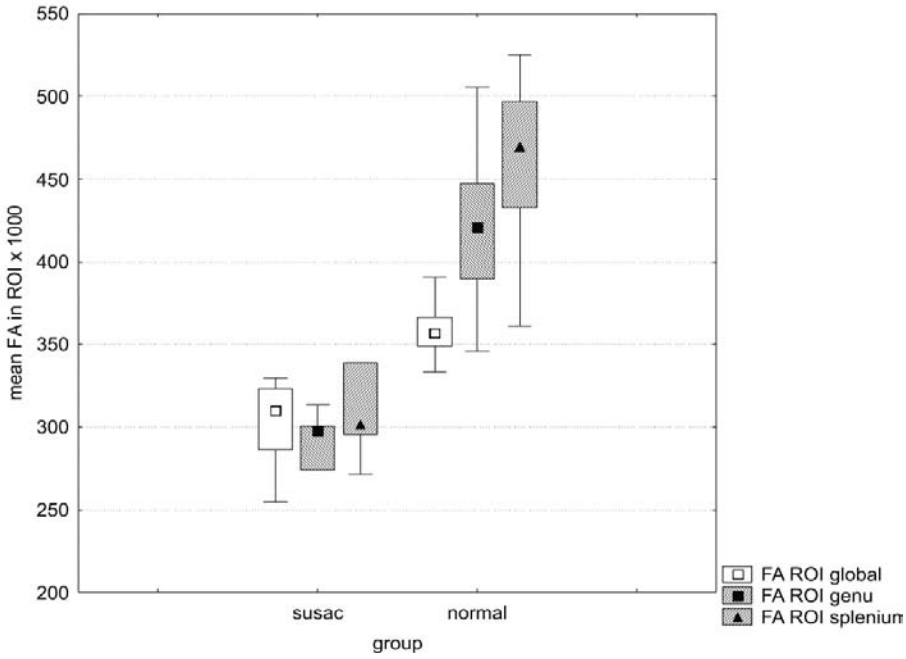

Figure 5. Distribution of the mean FA values calculated for the three ROIs in patients and normal controls. Boxes and whiskers represent FA quartiles and distribution ranges, respectively.

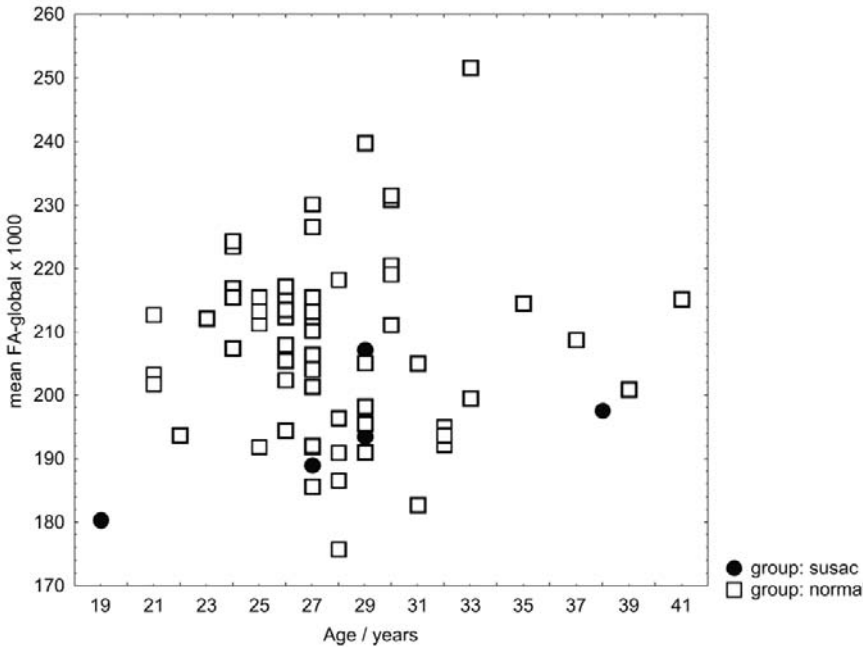

(a)

Figure 6. (Continues)

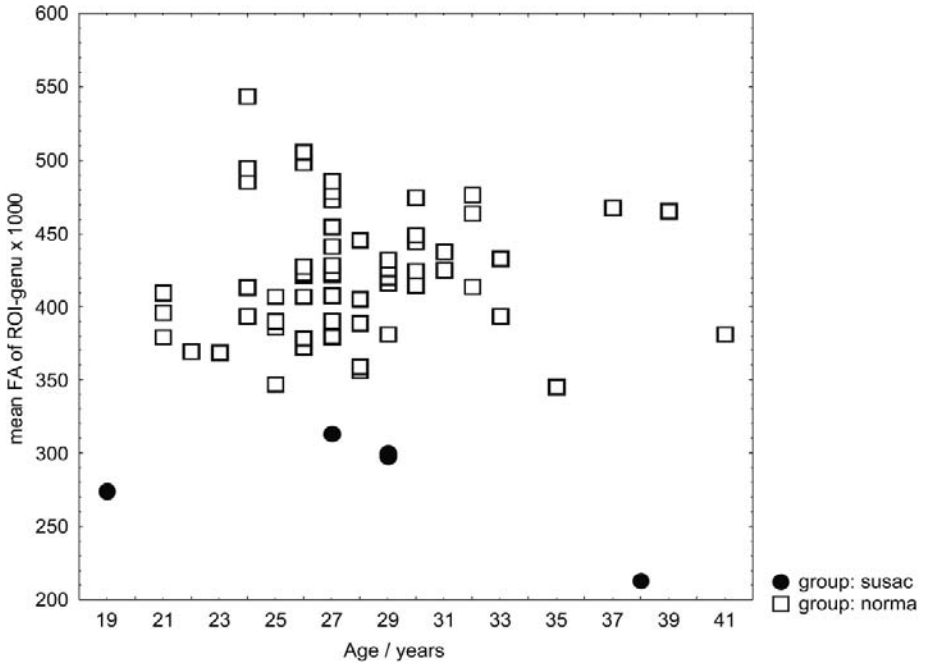

(b)

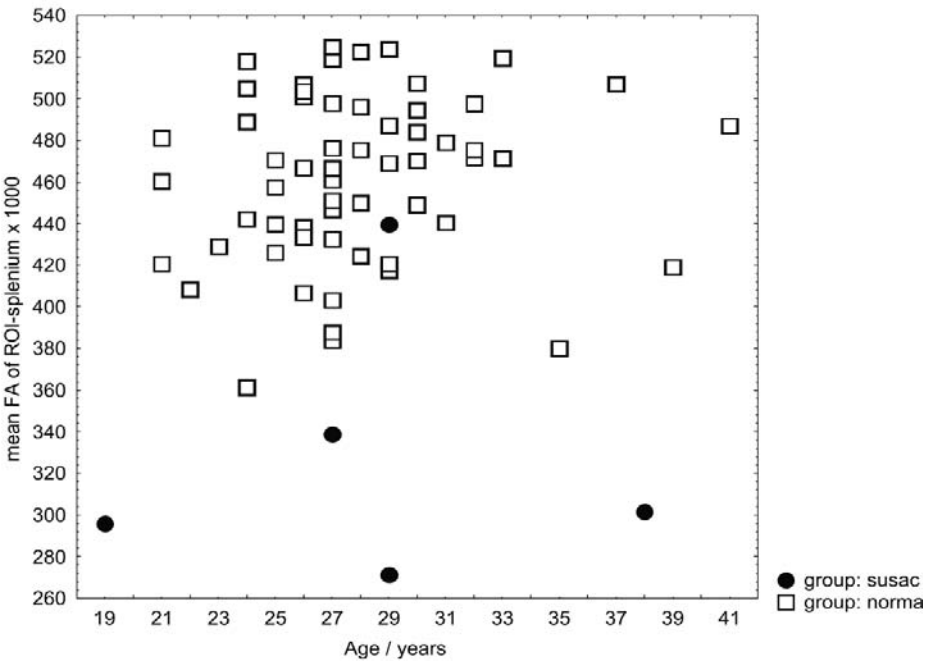

©

Figure 6. Mean FA of each ROI for all patients and control subjects in dependence of their age. a; ROI-global; b, ROI-genu; c, ROI-splenium.

Discussion

Susac's syndrome is defined by the occurrence of the typical triad of BRAO, hearing loss and encephalopathy. Symptoms often do not coincide, but occur one after another, with weeks to years between the onset of the first symptom and the completion of the triad. This episodic course of the disease often leads to misdiagnosis. We describe five patients with Susac's syndrome who were investigated by DTI for their major brain fiber tract integrity. When doing this, characteristic and widespread disruption of fiber integrity was identified in NAWM.

Acute psychosis, behavioural changes, cognitive deficits and personality changes were the initial findings in two of the five patients, while the other three had only mild cognitive impairment at the onset of the syndrome (table 1). Migrainous headache was reported by four of the five patients. Up to now, the severity of these behavioural changes could not be explained by the small WM lesions seen on DWI, although the site of these lesions is typical for Susac's syndrome (Xu et al. 2004; White et al. 2004; Do et al. 2004; Ringelstein and Knecht 2006). Here we provide evidence that DTI is much more sensitive to damage of fiber integrity in NAWM, particularly if located in the corpus callosum and the frontal cortex. As neuropsychological changes and exogenic psychosis have been shown to be associated with lesions in certain white matter tracts (Walterfang et al. 2005; Walterfang et al. 2006), cognitive deficits and psychosis of patients with Susac's syndrome could well be attributed to these fiber tract abnormalities detected by DTI. As recently shown for diseases affecting the white matter, i.e. multiple sclerosis, systemic lupus erythematodes, metachromatic leukodystrophy and other leukodystrophies, structural disconnectivity in frontosubcortical, frontotemporal and interhemispherical callosal connections may result in psychosis and neuropsychological changes (Walterfang et al. 2005). For example, DTI in patients with schizophrenia showed reduced FA values in the left uncinate fascicle and left arcuate fascicle, indicating that failure of integrity of frontotemporal and frontoparietal white matter tracts is relevant for the development of psychotic symptoms (Burns et al. 2003; Kubicki et al. 2005). Interestingly, the FA values were reduced in the splenium, but not the genu of the corpus callosum in schizophrenic patients (Foong et al. 2000).

In our study, the corpus callosum, especially the genu, was mainly affected by fiber disruption indicated by an approximately 25 % FA reduction, and this damage appeared characteristic for patients with Susac's syndrome. The extent of neuropsychological symptoms did not, however, correlate directly with the damage of the corpus callosum. Two of the patients suffered from an acute, self-limiting paranoid-hallucinatory psychosis and mild cognitive impairment and one from severe neuropsychological deficits but no psychosis, while two patients only suffered from mild cognitive impairment without psychosis. Recent DTI studies showed disruption of fiber integrity in the corpus callosum in patients with cocaine and alcohol abuse (Moeller et al. 2005; Pfefferbaum et al. 2006). In cocaine abuse, this damage of the corpus callosum is thought to be the consequence of damages in the prefrontal cortex, and has been related to increased impulsivity and reduced discriminability as a sign of cognitive decline in these addicts (Moeller et al. 2005).

Migrainous headache was found in all patients with Susac's syndrome. The prevalence of WM lesions in patients with migrainous headache is higher than in the normal population

(Gladstone and Dodick 2005). Protein elevation and mild pleocytosis in the CSF suggest a mild involvement of the small meningeal arteries in the disease.

The paucitiy of psychosis in multiple sclerosis and other demyelinating diseases may be related to the maturity of CNS structures affected, causing psychosis only when critical circuits are affected. Myelination begins prenatally in the CNS and continues postnatally. In adolescence, prefrontal and hippocampal connections achieve full myelination, the intracortical connections are the latest ones to become myelinated (Graaf-Peters and Hadders-Algra 2006). As patients with Susac's syndrome get affected mainly in their early adulthood, expansion and development of white matter tracts in some regions of the CNS might not yet be completed, and these structures may be more vulnerable than those of completely mature brains. The severe onset of the psychotic symptoms is well correlated with the extent of the impairment of fiber integrity, although the evolution of the fiber disruptions in NAWM is not fully understood. For further investigations it will be useful to apply DTI repetitively over the course of the disease in order to address the question how the affected brain responds to the vascular tissue injury and whether functional cortical reorganization phenomena could be detected in Susac's syndrom.

From a clinical point of view, we summarize that DTI qualifies as a new auxiliary technique to strengthen the diagnosis of Susac's syndrome in uncertain cases. It might serve as a sensitive clinical tool to differentiate between Susac's syndrome and other psychotic or WM diseases. Susac's syndrome causes widespread tissue damage in the NAWM of the brain not yet demonstrated before. The extent and severity of this damage correlates much better with the clinical encephalopathic symptoms than the extent of focal pathology revealed by conventional MRI. Lesions detected by conventional MRI must be regarded as just the tip of the iceberg underlying the pathology of Susac's syndrome.

Acknowledgments

We are grateful to Dr. rer. nat. Harald Kugel for implementation of the DTI sequences on the MR scanner.

This work was supported by the Transregional Collaborative Research Centre SFB/TR 3 Project A08 of the Deutsche Forschungsgemeinschaft (DFG), by grants of the Stiftung Neuromedizin Medical Foundation, Germany, and the Innovative Medizinische Forschung (IMF), Universitiy of Münster (DE510405).

References

Anneken K, Evers S, Mohammadi S, Schwindt W, Deppe M. 2008. Transient lesion in the splenium related to antiepileptic drug: *Case report and new pathophysiological insights. Seizure.*

Ayache D, Plouin-Gaudon I, Bakouche P, Elbaz P, Gout O. 2000. Microangiopathy of the inner ear, retina, and brain (Susac syndrome): report of a case. *Arch. Otolaryngol. Head Neck Surg.* 126: 82-84.

Barker RA, Anderson JR, Meyer P, Dick DJ, Scolding NJ. 1999. Microangiopathy of the brain and retina with hearing loss in a 50 year old woman: extending the spectrum of Susac's syndrome. *J. Neurol. Neurosurg. Psychiatry.* 66: 641-643.

Basser PJ, Jones DK. 2002. Diffusion-tensor MRI: theory, experimental design and data analysis - a technical review. *NMR Biomed.* 15: 456-467.

Buchel C, Raedler T, Sommer M, Sach M, Weiller C, Koch MA. 2004. White matter asymmetry in the human brain: a diffusion tensor MRI study. *Cereb. Cortex.* 14: 945-951.

Burns J, Job D, Bastin ME, Whalley H, Macgillivray T, Johnstone EC, Lawrie SM. 2003. Structural disconnectivity in schizophrenia: a diffusion tensor magnetic resonance imaging study. *Br. J. Psychiatry.* 182: 439-443.

Chau W, McIntosh AR. 2005. The Talairach coordinate of a point in the MNI space: how to interpret it. *Neuroimage.* 25: 408-416.

Deppe M, Duning T, Mohammadi S, Schwindt W, Kugel H, Knecht S, Ringelstein EB. 2007. Diffusion-Tensor Imaging at 3 T: Detection of White Matter Alterations in Neurological Patients on the Basis of Normal Values. *Invest. Radiol.* 42: 338-345.

Deppe M, Kellinghaus Ch, Duning T, Möddel G, Mohammadi S, Deppe K, Schiffbauer H, Kugel H, Keller S, Ringelstein EB, Knecht S. 2008. Nerve fiber impairment of anterior thalamocortical circuity in juvenile myoclonic epilepsy. *Neurology.* 71: 1981-1985

Do TH, Fisch C, Evoy F. 2004. Susac syndrome: report of four cases and review of the literature. *AJNR Am. J. Neuroradiol.* 25: 382-388.

Egan RA, Ha NT, Gass JD, Rizzo JF, III, Tivnan J, Susac JO. 2003. Retinal arterial wall plaques in Susac syndrome. *Am. J. Ophthalmol.* 135: 483-486.

Fellgiebel A, Dellani PR, Greverus D, Scheurich A, Stoeter P, Muller MJ. 2006. Predicting conversion to dementia in mild cognitive impairment by volumetric and diffusivity measurements of the hippocampus. *Psychiatry Res.* 146: 283-287.

Foong J, Maier M, Clark CA, Barker GJ, Miller DH, Ron MA. 2000. Neuropathological abnormalities of the corpus callosum in schizophrenia: a diffusion tensor imaging study. *J. Neurol. Neurosurg. Psychiatry.* 68: 242-244.

Gass JD, Tiedeman J, Thomas MA. 1986. Idiopathic recurrent branch retinal arterial occlusion. *Ophthalmology.* 93: 1148-1157.

Gladstone JP, Dodick DW. 2005. Migraine and cerebral white matter lesions: when to suspect cerebral autosomal dominant arteriopathy with subcortical infarcts and leukoencephalopathy (CADASIL). *Neurologist.* 11: 19-29.

Graaf-Peters VB, Hadders-Algra M. 2006. Ontogeny of the human central nervous system: what is happening when? *Early Hum. Dev.* 82: 257-266.

Gross M, Banin E, Eliashar R, Ben Hur T. 2004. Susac syndrome. *Otol. Neurotol.* 25: 470-473.

Jenkinson M, Bannister P, Brady M, Smith S. 2002. Improved optimization for the robust and accurate linear registration and motion correction of brain images. *Neuroimage.* 17: 825-841.

Jenkinson M, Smith S. 2001. A global optimisation method for robust affine registration of brain images. *Med. Image Anal.* 5: 143-156.

Jones DK, Horsfield MA, Simmons A. 1999. Optimal strategies for measuring diffusion in anisotropic systems by magnetic resonance imaging. *Magn. Reson. Med.* 42: 515-525.

Kleffner I, Deppe M, Mohammadi S, Schiffbauer H, Stupp N, Lohmann H, Young P, Ringelstein EB. 2008. Diffusion tensor imaging demonstrates fiber impairment in Susac syndrome. *Neurology*. 70: 1867-1869.

Kleffner I, Ringelstein EB, Stupp N, Niederstadt TU, Young P. 2006. Neurological picture. Susac's syndrome: effective combination of immunosuppression and antiplatelet treatment. *J. Neurol. Neurosurg. Psychiatry.* 77: 1335.

Kubicki M, McCarley R, Westin CF, Park HJ, Maier S, Kikinis R, Jolesz FA, Shenton ME. 2005. A review of diffusion tensor imaging studies in schizophrenia. *J. Psychiatr. Res.* 41: 15-30.

Le Bihan D. 2003. Looking into the functional architecture of the brain with diffusion MRI. *Nat. Rev. Neurosci.* 4: 469-480.

Moeller FG, Hasan KM, Steinberg JL, Kramer LA, Dougherty DM, Santos RM, Valdes I, Swann AC, Barratt ES, Narayana PA. 2005. Reduced anterior corpus callosum white matter integrity is related to increased impulsivity and reduced discriminability in cocaine-dependent subjects: diffusion tensor imaging. *Neuropsychopharmacology*. 30: 610-617.

Notis CM, Kitei RA, Cafferty MS, Odel JG, Mitchell JP. 1995. Microangiopathy of brain, retina, and inner ear. *J. Neuroophthalmol*. 15: 1-8.

O'Halloran HS, Pearson PA, Lee WB, Susac JO, Berger JR. 1998. Microangiopathy of the brain, retina, and cochlea (Susac syndrome). A report of five cases and a review of the literature. *Ophthalmology.* 105: 1038-1044.

O'Sullivan M, Morris RG, Huckstep B, Jones DK, Williams SC, Markus HS. 2004a. Diffusion tensor MRI correlates with executive dysfunction in patients with ischaemic leukoaraiosis. *J. Neurol. Neurosurg. Psychiatry*. 75: 441-447.

O'Sullivan M, Singhal S, Charlton R, Markus HS. 2004b. Diffusion tensor imaging of thalamus correlates with cognition in CADASIL without dementia. *Neurology.* 62: 702-707.

Papo T, Biousse V, Lehoang P, Fardeau C, N'Guyen N, Huong DL, Aumaitre O, Bousser MG, Godeau P, Piette JC. 1998. Susac syndrome. *Medicine.* (Baltimore) 77: 3-11.

Petty GW, Engel AG, Younge BR, Duffy J, Yanagihara T, Lucchinetti CF, Bartleson JD, Parisi JE, Kasperbauer JL, Rodriguez M. 1998. *Retinocochleocerebral vasculopathy. Medicine. (*Baltimore) 77: 12-40.

Pfefferbaum A, Adalsteinsson E, Sullivan EV. 2006. Dysmorphology and microstructural degradation of the corpus callosum: Interaction of age and alcoholism. *Neurobiol. Aging.* 27: 994-1009.

Plummer C, Rattray K, Donnan GA, Basilli S. 2005. An unusual disease presenting at an unusual age: Susac's syndrome. *J. Clin. Neurosci*. 12: 99-100.

Ringelstein EB, Knecht S. 2006. Cerebral small vessel diseases: manifestations in young women. *Curr. Opin. Neurol.* 19: 55-62.

Saw VP, Canty PA, Green CM, Briggs RJ, Cremer PD, Harrisberg B, McCluskey P, O'Day J, Paine M, Wakefield D, Watson JD. 2000. Susac syndrome: microangiopathy of the retina, cochlea and brain. *Clin. Experiment. Ophthalmol.* 28: 373-381.

Smith SM. 2002. Fast robust automated brain extraction. Hum.Brain Mapp. 17: 143-155.

Smith SM, De Stefano N, Jenkinson M, Matthews PM. 2001. Normalized accurate measurement of longitudinal brain change. *J. Comput. Assist. Tomogr.* 25: 466-475.

Smith SM, Jenkinson M, Woolrich MW, Beckmann CF, Behrens TE, Johansen-Berg H, Bannister PR, De Luca M, Drobnjak I, Flitney DE, Niazy RK, Saunders J, Vickers J, Zhang Y, De Stefano N, Brady JM, Matthews PM. 2004. Advances in functional and structural MR image analysis and implementation as FSL. *Neuroimage.* 23 Suppl 1: S208-S219.

Smith SM, Zhang Y, Jenkinson M, Chen J, Matthews PM, Federico A, De Stefano N. 2002. Accurate, robust, and automated longitudinal and cross-sectional brain change analysis. *Neuroimage.* 17: 479-489.

Susac JO. 1994. Susac's syndrome: the triad of microangiopathy of the brain and retina with hearing loss in young women. *Neurology.* 44: 591-593.

Susac JO. 2004. Susac's syndrome. *AJNR Am. J. Neuroradiol.* 25: 351-352.

Susac JO, Hardman JM, Selhorst JB. 1979. Microangiopathy of the brain and retina. *Neurology.* 29: 313-316.

Susac JO, Murtagh FR, Egan RA, Berger JR, Bakshi R, Lincoff N, Gean AD, Galetta SL, Fox RJ, Costello FE, Lee AG, Clark J, Layzer RB, Daroff RB. 2003. MRI findings in Susac's syndrome. *Neurology.* 61: 1783-1787.

Walterfang M, Wood SJ, Velakoulis D, Copolov D, Pantelis C. 2005. Diseases of white matter and schizophrenia-like psychosis. *Aust. N. Z. J. Psychiatry.* 39: 746-756.

Walterfang M, Wood SJ, Velakoulis D, Pantelis C. 2006. Neuropathological, neurogenetic and neuroimaging evidence for white matter pathology in schizophrenia. *Neurosci. Biobehav. Rev.* 30: 918-948.

White ML, Zhang Y, Smoker WR. 2004. Evolution of lesions in Susac syndrome at serial MR imaging with diffusion-weighted imaging and apparent diffusion coefficient values. *AJNR Am. J. Neuroradiol.* 25: 706-713.

Wildemann B, Schulin C, Storch-Hagenlocher B, Hacke W, Dithmar S, Kirchhof K, Jansen O, Breitbart A. 1996. Susac's syndrome: improvement with combined antiplatelet and calcium antagonist therapy. *Stroke,* 27: 149-151.

Xu MS, Tan CB, Umapathi T, Lim CC. 2004. Susac syndrome: serial diffusion-weighted MR imaging. *Magn. Reson. Imaging.* 22: 1295-1298.

Zhang Y, Brady M, Smith S. 2001. Segmentation of brain MR images through a hidden Markov random field model and the expectation-maximization algorithm. *IEEE Trans. Med. Imaging.* 20: 45-57.

In: Handbook on White Matter
Editors: T. B. Westland and R. N. Calton
ISBN: 978-1-60741-034-8

Chapter XVII

Organisation of the Node of Ranvier in Myelinated Central Axons

James J.P. Alix
Academic Foundation Programme, Department of Medicine,
Imperial College, London, UK

Abstract

The organisation of the myelinated central axon into discrete domains is key to the function of the central nervous system. While most of the axolemma is covered by lipid rich myelin, areas known as nodes of Ranvier are exposed to the extracellular space. These specialised regions are enriched with the Na^+ channels responsible for action potential conduction, which, due to the low capacitance of the internodal myelin sheath, can travel with remarkable speed along even the smallest of myelinated axons. Restricting current flow in this way also lessens the metabolic burden of electrical activity, permitting the development of extensive white matter tracts. Recent work has identified numerous other proteins present at nodes and adjacent areas. These include, for example, the scaffolding proteins $ankyrin_G$ and $^{\beta}$IV spectrin at the node and members of contactin associated protein family in the paranodal and juxtaparanodal regions. The exact mechanisms by which such proteins are recruited to the appropriate axonal domains remain elusive, although myelinating oligodendroglia appear to play an important role. This review will describe what is currently known about the organisation of Ranvier's node and the myelinated central axon.

Introduction

The ability of neurons to communicate in a rapid and efficient manner is integral to the function of the nervous system. As evolution gradually increased the complexity of life the need for rapid impulse conduction between neurons became more and more important. One means to speed up the electrical signals, known as action potentials, through which neural

cells communicate is to increase the size of the axon along which the impulse travels. A fine example of this is the squid giant axon, which reaches a diameter of approximately 1 mm, a size that permitted the landmark experiments describing the ionic basis of the action potential [1]. However, the increase in size necessary to significantly increase conduction velocity is substantial and comes with a high metabolic cost. To circumvent this problem nature modified the organisation of axons, wrapping in them almost entirely in a high resistance, low capacitance fatty coat - the myelin sheath. Small portions of the axolemma, known as nodes of Ranvier, are not wrapped in myelin and are to be found at regular intervals measuring approximately 100 times the diameter of the axon.

Nodes of Ranvier are enriched with Na^+ channels (Na_Vs), through which depolarising current flows; this provides a boost to the current travelling down the myelinated internode by passive means. Without this the amplitude of the current would decay below that required to bring voltage gated ion channels to threshold, which would result in conduction block. Organising the axon in this way speeds up action potential conduction, since conduction velocity is inversely proportional to the product of axoplasmic resistance (R_a) and membrane capacitance (C_m) per unit length (F/cm). The act of myelination reduces capacitance by increasing the distance between the intra-axonal and extracellular compartments and thus for a given diameter, or R_a, conduction velocity is improved. Additionally, the resistance of the myelin sheath limits current decay and so increases what is known as the length constant, defined as the distance over which the current decays to 37% of its initial value. This leads to a local circuit that spreads further, and hence more quickly, down the axon. When arriving at the node the action potential slows due to the high capacitance of the bare axolemma, which, in the minds eye, causes the action potential to jump from one node to another. It is for this reason that action potential conduction in myelinated axons is known as saltatory conduction, from the Latin *saltare*, meaning to jump. For completeness it should also be noted that simply increasing axon diameter also improves conduction speed; however, since membrane capacitance is actually increased, as a result of the larger axolemmal area, R_aC_m is reduced by a lesser degree.

Such modifications also mean that more rapid conduction velocities are achieved at a fraction of the metabolic cost. This is because the perturbations of ionic homeostasis caused, for example, by the rapid flow of Na^+ ions from the extracellular space and into the axoplasm, are restricted to a smaller volume of the axon and hence restored with the expenditure of far less energy. The organisation of the central myelinated axon in this way has received a great deal of attention, not least because loss of this structure underlies the clinical deficits observed in demyelinating diseases, such as multiple sclerosis. Studies have now determined that the myelinated central axon consists of four domains: the node of Ranvier, the paranode, the juxtaparanode and the internode (figure 1). This chapter focuses on the composition of each domain, the function of the constituent proteins and the factors that control their localisation.

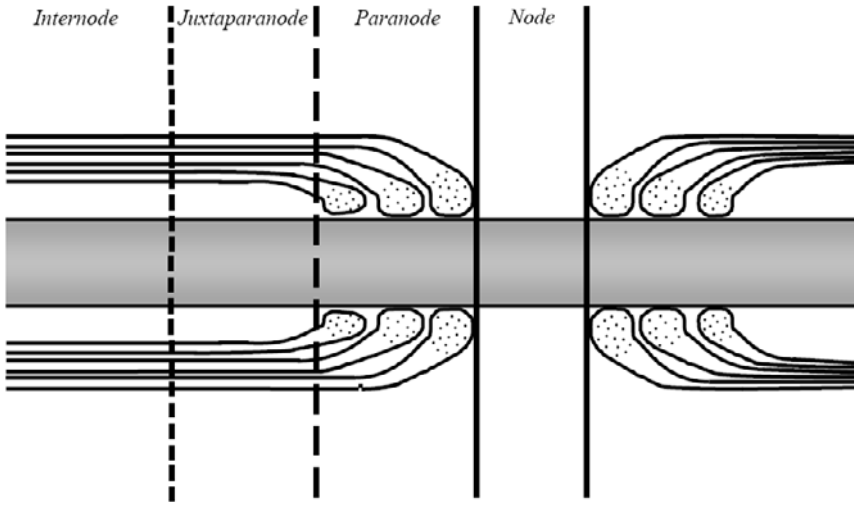

Figure 1. Organisation of the myelinated central axon.

The myelinated central axon is organised into four discrete domains. The node of Ranvier is the portion of the axolemma exposed to the extracellular surface and is abutted by the paranodes. Here pockets of cytoplasm, known as paranodal end loops, open out from the compact myelin and closely associate with the axolemma. Adjacent to the paranode is the juxtaparanode, which in turn becomes the internodal region, where compact myelin forms a high resistance, low capacitance barrier to current flow.

Composition of the Node of Ranvier

At the node of Ranvier Na_Vs are clustered at high density (>1200 μm^2) and provide the inward current necessary for saltatory conduction [2]. There are 9 genes encoding the different subtypes of Na_Vs ($Na_V1.1$-1.9) and it is $Na_V1.6$ that is found at the "mature" node of Ranvier [3, 4]. However, at the earliest stages of axon development, prior to myelination and node formation, only the $Na_V1.2$ subtype is present in the axolemma, where it is expressed diffusely along the axons length at a low density of approximately ~2/μm^2 [5, 6]. During this time action potential conduction, which is essential for the refinement of synaptic connections, is achieved via the flow of local circuits. This is possible since the input resistance (R_{in}) of the small axon cylinder is high and, as $\Delta V = I \times R_{in}$ (where ΔV = change in membrane potential, I = current), the relatively small current flow may still permit depolarisation of the membrane to threshold.

As development proceeds nodal proteins begin to cluster and the complex programme of myelination begins. This leads to the re-distribution of $Na_V1.2$ type channels already present in the axolemma to nodal sites [6, 7]. Gradually these channels are replaced by $Na_V1.6$, although the reasons for this change are not clear; one possibility is that $Na_V1.6$ channels may permit higher firing rates [8]. The mechanism underlying the switch in Na_V isoform expression appears to be the physical act of myelination since *shiverer* mice, which do not form compact myelin, continue to express $Na_V1.2$ with little $Na_V1.6$ seen at nodes in adult animals [6]. By way of contrast, the localisation of $Na_V1.2$ to immature nodes is not

dependent upon myelination and may be induced *in vitro* using oligodendrocyte conditioned media [7, 9]. The exact nature of the signals responsible for the aggregation of Na_Vs at nodes remain unknown. Present data would suggest that Na_Vs are recruited to other nodal proteins, such as the scaffolding protein $ankyrin_G$ (see below), as these proteins cluster at nodal sites prior to the arrival of Na_Vs and their deletion/mutation impairs Na_V recruitment.

The expression and stabilisation of the Na_V complex at the nodal membrane may be achieved through the Na_V β subunit, which contains an immunoglobulin domain known to interact with other nodal and paranodal proteins. These include the cell adhesion molecule neurofascin 186 (Nf186), contactin and the extracellular matrix proteins tenascin –R and –C, which may play a part in preventing the node being covered by myelin [10-13]. The absence of just one of these proteins significantly impairs Na_V aggregation, for example, analysis of neurofascin null mice reveals a significant decrease in the number of Na_V clusters in the ventral funiculus of the cervical spinal cord [14]. That some clusters were observed indicates that, in the absence of neurofascins, Na_Vs are still delivered to specific sites along the axon. However, the dramatic decrease in Na_V clusters, along with those of other nodal proteins such as $ankyrin_G$ and $^{\beta}$IV spectrin, suggests an important role for neurofascins in anchoring such proteins in place.

Other membranous proteins at the node include the Na^+/K^+ adenosine triphosphatase which is responsible for maintaining ionic homeostasis, the Na^+-Ca^{2+} exchange protein which is involved in Ca^{2+} homeostasis and a Na^+-dependent glutamate transporter known as excitatory amino acid transporter 1 (EAAC1 or EAAT3) [15]. In addition, the K^+ channels $K_v3.1b$ and KCNQ2 are also present, and all of these proteins may interact with the scaffolding protein $ankyrin_G$ [16-18]. Early investigations into the K^+ currents present in myelinated axons observed only a minimal voltage dependant K^+ response at the mammalian node of Ranvier and the function of these channels remains controversial [19-22]. It appears that they may play some role in membrane repolarisation, given the ability of the K^+ channel blocker 4-aminopyridine (4-AP) to broaden the action potential of myelinated CNS fibres [23-26]. However, the K^+ channel subtype(s) responsible for this effect is still unknown as 4-AP has an identical effect in $K_v3.1b$ deficient mice when compared to wild-type controls, and KCNQ2 mediates a slowly activating K^+ conductance that is insensitive to 4-AP [16, 17].

In addition to membrane bound proteins, several scaffolding proteins are present at the node, which, in recent years, have been shown to be integral to both the formation and stabilisation of the nodal superstructure. Ankyrins are widely expressed scaffolding proteins that link a broad range of proteins to the cytoskeleton via spectrins. The members of the family localised to the node of Ranvier are the 480 and 270 kilodalton (kDa) splice variants of the $ankyrin_G$ gene [27]. $Ankyrin_G$ aggregates early during axon development, for example, clusters have been observed using standard immunofluorescence at post-natal day 7 (P7) in the rat optic nerve (RON), and the protein is thought to be involved in the recruitment and retention of Na_Vs by linking them to the underlying cytoskeleton [28-31]. Interestingly, immunostaining initially extends into the paranodal region, indicating a refinement of the nodal structure occurs, an observation that would be consistent with the idea that myelinating processes push nodal proteins into place [28, 29]. Na_Vs appear to undergo a similar spatial refinement, first appearing at P9 in the RON in broad aggregations [29].

At the node, ankyrin$_G$ is linked to the cytoskeleton by $^{\beta}$IV spectrin; alternative splicing generates six isoforms of this protein ($^{\beta}$IVΣ1- $^{\beta}$IVΣ6) with $^{\beta}$IVΣ1 and $^{\beta}$IVΣ6 present at nodes of Ranvier [32, 33]. Data from $^{\beta}$IV spectrin knockout mice show a reduction in both Na_Vs and ankyrin$_G$ at the axon initial segment, while disrupted CNS nodal integrity has been reported qv^{3J} "quivering" mice, whose $^{\beta}$IV spectrin proteins lack domains thought to be involved in protein-protein and protein-lipid interactions [32-34]. Electron microscope and immunohistochemical studies on optic nerves from these mice revealed nodes that were longer and broader than those observed in wild-type controls [34]. Lacas-Gervais et al. (2004) reported similar findings in $^{\beta}$IVΣ1 -/- mice, indicating that this isoform is important in maintaining the nodal domain [35]. Recent evidence has also emerged for the role of $^{\alpha}$II spectrin at nascent nodes [36]. Using zebrafish, expression of $^{\alpha}$II spectrin along axons was enriched at both nodes and paranodes in embryos and larvae, and restricted to paranodes and the internode in adult animals; the latter being consistent with previous reports in mice [36, 37]. Mutation of $^{\alpha}$II spectrin resulted in a reduction in the number of Na_V clusters and disrupted node morphology indicating a role for the protein in node formation, perhaps achieved through an interaction with $^{\beta}$IV spectrin, prior to its dissipation from the nodal domain [36].

Central nodes of Ranvier are also contacted by glial processes in many instances. Fibrous astrocytes present in WM have been shown to send out processes that contact nodes of Ranvier and may participate in the uptake of K^+ released during action potentials [38, 39]. Astrocytes present in WM are known to react to other substances released by axons, namely glutamate and adenosine triphosphate (ATP), and astrocyte responses to the latter may influence myelination [40-42]. Cells expressing the NG2 chondroitin sulphate proteoglycan, termed NG2-positive glia, also contact nodes of Ranvier [43, 44]. During development (and also following demyelination) these cells may become myelinating oligodendrocytes and so are often described as oligodendrocyte precursor cells (OPCs), however, there is evidence to suggest that not all NG2-positive cells in mature WM are OPCs, leading some to regard them as a distinct cell type [45-47]. Regardless of this, their close association with nodes in mature WM tracts makes them well suited to respond to changes in tissue integrity. Indeed, in response to injury NG2-positive glia are capable not only of producing new oligodendrocytes, but also of becoming reactive and thus contributing to the glial scar that attempts to separate healthy tissue from damaged tissue [48].

Formation of the Node of Ranvier

Studies designed to ascertain which nodal protein clusters first, and hence is likely used to aid recruitment of other nodal members, suggest that ankyrin$_G$ marks the point at which nodes first develop [28, 49]. At P9 in the RON approximately 62% of ankyrin$_G$ clusters overlap with $^{\beta}$IV spectrin, while $^{\beta}$IV spectrin clusters are not observed independently of ankyrin$_G$ [28]. Similarly, qv^{3J} mice do not cluster $^{\beta}$IV spectrin but broad clusters of ankyrin$_G$ are present at elongated nodes, indicating that $^{\beta}$IV spectrin is not required for the appropriate targeting of ankyrin$_G$, but is important in stabilising the nodal superstructure [49]. In addition, deletion of the spectrin repeat 15 domain of $^{\beta}$IV spectrin, through which it interacts with

ankyrin$_G$, prevents its aggregation at the axon initial segment (AIS) and node of Ranvier [49]. Thus, present data indicate that, of the membrane bound proteins present at the mature node of Ranvier, ankyrin$_G$ is the central organizer. However, it remains unclear as to how ankyrin$_G$ is directed to the nodal site.

As described above early nodal markers undergo spatial refinement and, interestingly, cluster after the aggregation of paranodal proteins (see next section), observations that led researchers in the field to suggest that the clustering of nodal proteins was dependent on paranodal axo-glial contact [6, 29, 50]. It was speculated that the paranodal contacts formed at this early stage of development act as a rake, or molecular sieve, pushing larger Na$_V$s closer together while allowing smaller proteins, such as K^+ channels, through [50]. These conclusions were based on the observations that paranodal protein contactin associated protein(red)-1 (CASPR-1; see next section) aggregates first on the axolemma in association with myelinating oligodendrocyte processes, and that early Na$_V$ clusters were found adjacent to myelinating processes. [29]. In addition, studies using the hypomyelinating *shiverer* mouse, demonstrated a reduced number of Na$_V$ clusters throughout development [29].

However, evidence is accumulating against this model, the first of which was provided by Dupree et al. (1999). In this study the authors reported that mice unable to synthesise galactolipids (an important constituent of myelin) had disrupted paranodal interactions but did not display marked changes in nodal protein aggregation [51]. Similarly, Jenkins and Bennett (2002) reported that, in the dysmyelinating *jimpy* mouse, the absence of intact paranodal contacts did not prevent clustering of Na$_V$, ankyrin$_G$ or $^{\beta}$IV spectrin, although their number was reduced. Similar observations were also made in *myelin deficient* rats, in which dysmyelination is associated with oligodendrocyte death [52]. Disruptions to the axonal partners of the paranode also fail to completely abolish nodal aggregations, since Na$_V$ clustering is observed in mice lacking the paranodal protein CASPR-1 [53]. Conceptually, it is also difficult to explain how oligodendrocytes would control the precise spacing of nodes of Ranvier on axons when they often myelinate axons of different diameters, and hence with different internodal lengths. Similarly, the initial presence of anchoring proteins at developing nodes would appear to suggest that the nodal protein complex forms at a fixed site, subject only to minor spatial changes.

In spite of these reports it does appear that myelinating oligodendrocytes are crucial in the induction of protein localisation at the node, albeit in a contact independent manner. For example, Mathis et al. demonstrated that selective postnatal death of oligodendrocytes prevented the formation of both Na$_V$ and ankyrin$_G$ clusters [54]. Similarly, Kaplan et al. (1997) reported clustering of Na$_V$ and ankyrin$_G$ induced by a soluble factor released by oligodendrocytes, this time in an *in vitro* model of myelination, although the identity of this protein is remains unknown [9]. Interestingly, in this study nodal aggregations were formed at regularly spaced intervals, implying that the location of nodes is determined by the axon, with paranodal proteins and glia subsequently moving into place.

Recently, we have reported the requirement of functional axonal P/Q-type VGCCs in the formation of the node [55]. Clusters of these channels were observed on the axolemma of pre-myelinated axons at sites where nodes later form, but dispersed once nodal proteins began to accumulate. Interestingly, mutations affecting P/Q-type VGCCs led to the mis-localisation of NaVs, $^{\beta}$IV spectrin and CASPR-1, as well as the formation of nodes with

abnormal morphology at the ultrastructural level. This study also noted an association between VGCCs and the machinery of vesicle fusion, for example SNAP-25, suggesting that these channels might participate in axo-glial communication. In support of this Ca^{2+}-mediated, activity dependent signalling has been demonstrated in unmyelinated preparations [56, 57]. However, signals generated in this manner cannot be entirely dedicated to node formation, since they persist in unmyelinated axons in mixed tracts and so may play different roles at different stages of development, perhaps even contacting different cell types. It is also worth considering that the local elevations in intra-axonal Ca^{2+} concentration produced by propagated action potentials, might contribute directly to the accumulation of nodal proteins via intra-axonal signalling.

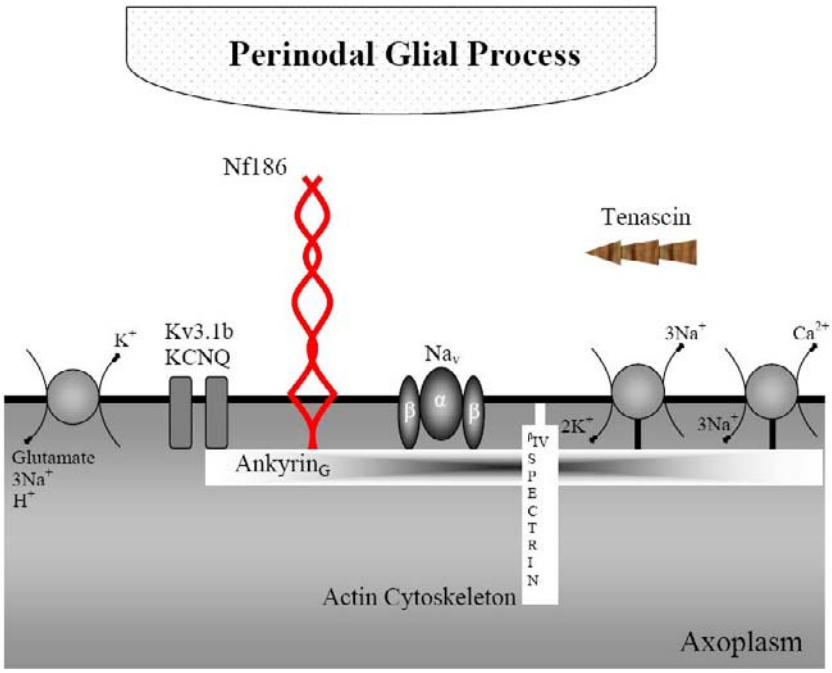

Figure 2. Composition of the node of Ranvier. At the node the adapter protein $ankyrin_G$ links numerous axolemmal proteins to the cytoskeleton via $^{\beta}$IV spectrin.

The Paranode

The paranodal domains are highly specialised regions that flank both sides of the node, forming a junction between the spiraling paranodal end loops of the myelinating oligodendrocyte and the axolemma. On the axolemmal side several proteins may be found, the first of which to be discovered were CASPR-1 (also known as paranodin) and contctin [58-61]. Interestingly, the expression of both proteins is required for the targeting and/or retention of the other. For example, CASPR-1 remains in the cell body in contactin-null mice, while contactin is undetectable in CASPR-1 knockout mice [53, 62]. Both of these studies

reported an increased gap between the axolemma and myelinating process at the ultrastructural level, the loss of the transverse bands formed between the end loops and axon, plus often everted paranodal loops [53, 62]. These observations are likely to be the consequences of the lost interaction between the CASPR-1/contactin complex and the glial cell adhesion molecule neurofascin 156 (Nf156), the expression of which is reduced in the absence of the axonal heterodimer [53, 62]. The finer details of this association remain to be elucidated though as Gollan et al. (2003) reported that CASPR-1 inhibits the interaction of contactin and Nf156 [63]. That, in some instances, paranodal loops still appear to attach to the axon without the CASPR-1/contactin complex, suggests that there are further members of the paranodal axo-glial junction not yet discovered.

Protein 4.1B, a member of the 4.1 protein family which binds to spectrins, is also found at the paranode and interacts with CASPR-1 [64, 65]. Through binding to the intracellular domain of CASPR-1, 4.1B appears to stabilise the CASPR-1/contactin complex, as contactin has no similar means to anchor itself to the underlying cytoskeleton. The interaction with the cytoskeleton appears to be mediated by the $^{\alpha}$II and $^{\beta}$II members of the spectrin family [37]. In the same study ankyrin$_B$ was also found at the paranode but, as it did not co-precipitate with paranodal markers, a question mark remains as to its function. The underlying network of axoplasmic proteins is important in retention of the CASPR-1/contactin complex, since absence of the cytoplasmic tail of CASPR-1 results in loss of the complex from the paranode, despite correct targeting [64].

Formation and Function of the Paranode

Analysis of dysmyelinating mutants indicates that axo-glial contact regulates the accumulation of proteins is this region [28, 51, 52, 54]. For example, the *jimpy* mouse completely lacks CASPR-1 immunoreactivity, while galactolipid-deficient mice, that on ultrastructural examination lack transverse bands and have everted paranodal end loops (common features of all mutants with disrupted paranodal contacts), have CASPR-1 immunofluorescence distributed long internodal segments [28, 51]. Temporally the membrane bound components of the paranode cluster first, with CASPR-1 immunoreactivity first observed at P7 in the RON [29]. Axoplasmic scaffolding proteins move into place thereafter with protein 4.1B and $^{\beta}$II spectrin noted at P11 in the same preparation [37]. This is a logical sequence of events given that it is likely that the membranous paranodal proteins are required to move along the axolemma in search of nodal sites, a task that would be far more difficult if anchoring proteins were already in place [14].

These studies, combined with CASPR-1 and contactin knockout models, have allowed suggestions as to the function of the paranodal junction to be made. In the absence of competent paranodal junctions, K^+ channels usually restricted to the juxtaparanode (see later) are found in the paranodal region [51, 53, 62, 66]. Thus, the paranodal junction plays an important role in restricting K^+ channels to the juxtaparanodal compartment. In addition, the loss of nodal protein clusters over time is also reported in these models, indicating that while axoglial contact might not coordinate the focal accumulation of these proteins, it is important in the maintenance of the nodal domain [66-70]. Interestingly, the presence of K_v1.1 and

$K_v1.2$ channels in the paranodal region has been reported in human and rat spinal cord, particularly in the dorsal and lateral columns [71]. It remains unclear as to how these channels are localised to the paranode as their presence does not fit with the hypothesis that axo-glial interactions restrict K^+ channel expression to the juxtaparanode.

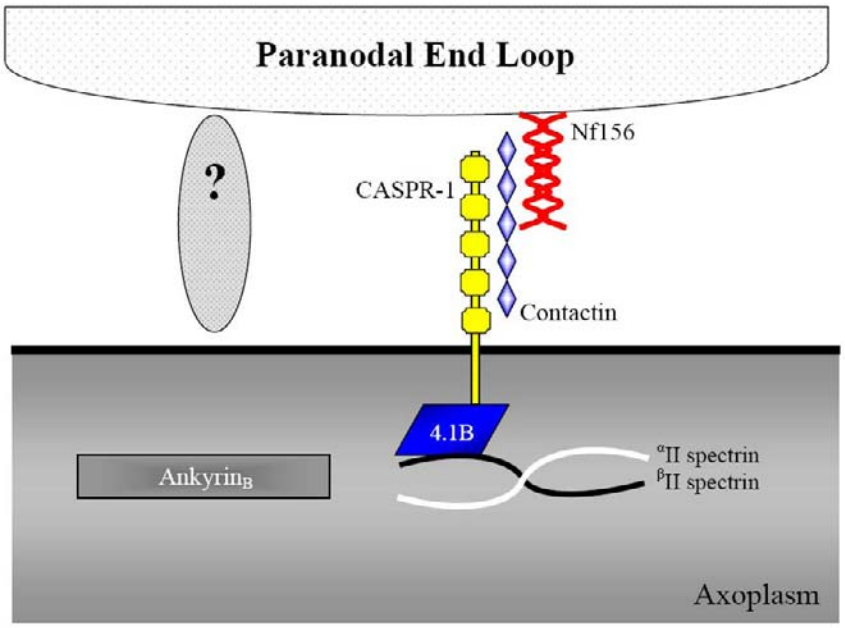

Figure 3. The paranodal region.

The CASPR-1/contactin complex interacts with Nf156 and is anchored to the underlying cytoskeleton through a CASPR-1 mediated interaction with protein 4.1B. AnkyrinB is also present at the paranode, although its function is presently unknown. Given the ability of the paranodal junction to form in the absence of the CASPR-1/contactin complex it is likely that other, as yet unidentified molecules contribute to the domain.

The Juxtaparanode: Form and Function

Within the juxtaparanode are located the delayed rectifier K^+ channels $K_v1.1$, $K_v1.2$ and $K_v1.6$ and an associated Kcβ2 subunit [25, 72, 73]. These channels appear to be associated with contactin associated protein(red)-2 (CASPR-2) which is specifically enriched in this region, although the mechanism through which this association is achieved remains elusive [74]. Transient axonal glycoprotein-1 (Tag1), a cell adhesion molecule related to contactin, is also found at the juxtaparanode and has been shown to bind with CASPR-2 [75, 76]. The absence of either protein decreases the density of K^+ channels at the juxtaparanode, observations in keeping with other data concerning the recruitment of axonal ion channels [76, 77]. Surprisingly, Tag1 is present on both the glial and axonal membrane and, while its function requires further investigation, a Tag1/CASPR-2 complex may form on the axolemma and bind to glial Tag1, helping stabilise the region and polarise K^+ channel

distribution [75]. Ogawa et al. (2006) reported the presence of protein 4.1B, $^{\alpha}$II spectrin and $^{\beta}$II spectrin in the juxtaparanodal region and these proteins may also contribute to juxtaparanodal stability via 4.1B, which interacts with CASPR-2 [37, 65]. The inner oligodendroglial membrane also contains connexin 29, which forms hemichannels similar to those that allow communication throughout the astrocyte syncytium; in this instance they may permit the flow of K^+ ions away from the axolemma [78].

Localisation of K^+ channels in the juxtaparanode appears to depend on the presence of myelinating oligodendroglia, since little K^+ channel immunoreactivity is seen in the optic nerve of the *shiverer* mouse [25]. Similar conclusions were also drawn by other studies in which axo-glial integrity was disrupted [51-54, 66]. The timing of the arrival of K^+ channels to their correct position appears to lag behind that of Na_Vs, with immunoreactivity first noted at P14 in the RON [25]. At this time $K_v1.2$ is observed as a faint band in the juxtaparanodal region and only 10% of Na_V clusters are associated with K^+ channel labelling [25]. At two months of age all nodal regions in the RON can be characterised by a focal Na_V cluster, bordered by a pair of CASPR-1 positive paranodes and associated juxtaparanodal $K_v1.2$ staining [25, 29].

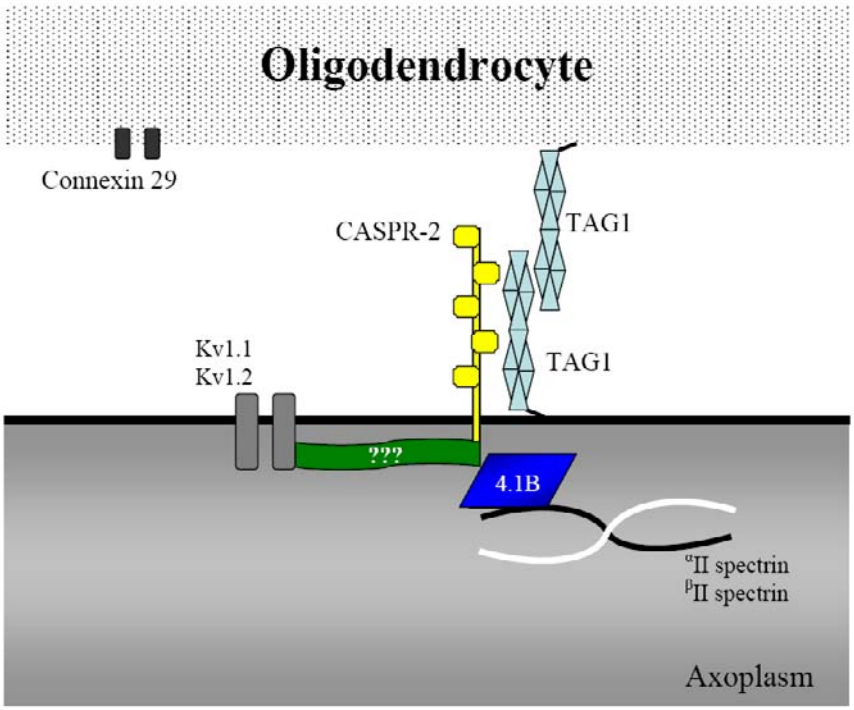

Figure 4. Organisation of the juxtaparanodal region.

K^+ channels are thought to associate, via an unknown protein, with the CASPR-2/TAG1 complex. The CASPR-2/TAG1 complex may then provide a link to the underlying cytoskeleton for both K^+ channels and the overlying glial membrane via protein 4.1B. Connexin 29 on the glial membrane could form functional hemichannels.

The role of juxtaparanodal K^+ channels appears unclear as they are likely to be somewhat electrically isolated from the changes in membrane potential that occur at the node. Potential roles include the prevention of ectopic firing, maintenance of the resting membrane potential of the region and/or some part in intercellular signaling, rather than repolarisation of the axolemma, the role they undertake in unmyelinated axons [19, 26, 79, 80]. With regard to repolarisation of the myelinated axon, it has been proposed that a rapid return to the resting membrane potential is achieved through a rapidly inactivating Na^+ current and a capacitative current flowing between the internodal and nodal membranes [81]. Several studies have demonstrated the presence of a K^+ current sensitive to 4-AP (which blocks rapidly activating K^+ channels) in myelinated axons [23, 24, 26, 82]. However, the contribution of this current to the recorded waveform diminishes as development proceeds, consistent with the original assertions that K^+ channels play a minimal role in action potential repolarisation in myelinated axons

The Internode

The internode of the central myelinated axon is a relatively barren domain. Early reports on the expression of Na_Vs in myelinated axons reported a Na_V density of $<25/\mu m^2$ [83]. In contrast to the PNS where CASPR-1, CASPR-2, contactin and K^+ channels are found, the internode of the central axons appears to only contain trace amounts of CASPR-1 [84, 85].

Summary

The organisation of the node of Ranvier is essential to the function of WM tracts and hence the CNS. Beginning as little more than a bare extension of the parent soma, the myelinated central axon gradually achieves a highly organised form that is reliant on the proper targeting and retention of numerous proteins. High densities of Na_Vs are present in the exposed membrane of the node, linked to the underlying cytoskeleton by a number of proteins that are also likely to be responsible for Na_V localisation. At the adjacent paranodal and juxtaparanodal regions a no less intricate arrangement of proteins is present. These regions not only ensure the stable association of the myelinating oligodendrocyte with its partner axon, but also guarantee the stability of the node. Although the mechanisms underlying the formation of these polarised domains are not completely understood, a clear appreciation of the inter-cellular interactions necessary to achieve rapid and reliable saltatory conduction is palpable within the literature. Understanding how the myelinated central axon achieves its mature phenotype represents a formidable scientific challenge, one that is sure to provide surprises and exciting new developments in the near future.

References

[1] Hodgkin AL, Huxley AF. A quantitative description of membrane current and its application to conduction and excitation in nerve. *J. Physiol.* 1952;117(4):500-44.

[2] Ritchie JM, Rogart RB. Density of sodium channels in mammalian myelinated nerve fibers and nature of the axonal membrane under the myelin sheath. *Proc. Natl. Acad. Sci. U. S. A.* 1977;74(1):211-5.

[3] Goldin AL, Barchi RL, Caldwell JH, Hofmann F, Howe JR, Hunter JC, et al. Nomenclature of voltage-gated sodium channels. *Neuron.* 2000;28(2):365-8.

[4] Caldwell JH, Schaller KL, Lasher RS, Peles E, Levinson SR. Sodium channel Na(v)1.6 is localized at nodes of ranvier, dendrites, and synapses. *Proc. Natl. Acad. Sci. U. S. A.* 2000;97(10):5616-20.

[5] Waxman SG, Black JA, Kocsis JD, Ritchie JM. Low density of sodium channels supports action potential conduction in axons of neonatal rat optic nerve. *Proc. Natl. Acad. Sci. U. S. A.* 1989;86(4):1406-10.

[6] Boiko T, Rasband MN, Levinson SR, Caldwell JH, Mandel G, Trimmer JS, et al. Compact myelin dictates the differential targeting of two sodium channel isoforms in the same axon. *Neuron.* 2001;30(1):91-104.

[7] Kaplan MR, Cho MH, Ullian EM, Isom LL, Levinson SR, Barres BA. Differential control of clustering of the sodium channels Na(v)1.2 and Na(v)1.6 at developing CNS nodes of Ranvier. *Neuron.* 2001;30(1):105-19.

[8] Rush AM, Dib-Hajj SD, Waxman SG. Electrophysiological properties of two axonal sodium channels, Nav1.2 and Nav1.6, expressed in mouse spinal sensory neurones. *J. Physiol.* 2005;564(Pt 3):803-15.

[9] Kaplan MR, Meyer-Franke A, Lambert S, Bennett V, Duncan ID, Levinson SR, et al. Induction of sodium channel clustering by oligodendrocytes. *Nature.* 1997;386(6626):724-8.

[10] Ratcliffe CF, Westenbroek RE, Curtis R, Catterall WA. Sodium channel beta1 and beta3 subunits associate with neurofascin through their extracellular immunoglobulin-like domain. *J. Cell. Biol.* 2001;154(2):427-34.

[11] Chen C, Westenbroek RE, Xu X, Edwards CA, Sorenson DR, Chen Y, et al. Mice lacking sodium channel beta1 subunits display defects in neuronal excitability, sodium channel expression, and nodal architecture. *J. Neurosci.* 2004;24(16):4030-42.

[12] Srinivasan J, Schachner M, Catterall WA. Interaction of voltage-gated sodium channels with the extracellular matrix molecules tenascin-C and tenascin-R. *Proc. Natl. Acad. Sci. U. S. A.* 1998;95(26):15753-7.

[13] Kazarinova-Noyes K, Malhotra JD, McEwen DP, Mattei LN, Berglund EO, Ranscht B, et al. Contactin associates with Na+ channels and increases their functional expression. *J. Neurosci.* 2001;21(19):7517-25.

[14] Zonta B, Tait S, Melrose S, Anderson H, Harroch S, Higginson J, et al. Glial and neuronal isoforms of Neurofascin have distinct roles in the assembly of nodes of Ranvier in the central nervous system. *J. Cell Biol*. 2008;181(7):1169-77.

[15] Arranz AM, Hussein A, Alix JJ, Perez-Cerda F, Allcock N, Matute C, et al. Functional glutamate transport in rodent optic nerve axons and glia. *Glia*. 2008;56(12):1353-67.

[16] Devaux J, Alcaraz G, Grinspan J, Bennett V, Joho R, Crest M, et al. Kv3.1b is a novel component of CNS nodes. *J. Neurosci.* 2003;23(11):4509-18.

[17] Devaux JJ, Kleopa KA, Cooper EC, Scherer SS. KCNQ2 is a nodal K+ channel. *J. Neurosci.* 2004;24(5):1236-44.

[18] Bennett V, Baines AJ. Spectrin and ankyrin-based pathways: metazoan inventions for integrating cells into tissues. *Physiol. Rev.* 2001;81(3):1353-92.

[19] Chiu SY, Ritchie JM. Evidence for the presence of potassium channels in the paranodal region of acutely demyelinated mammalian single nerve fibres. *J. Physiol.* 1981;313:415-37.

[20] Chiu SY, Ritchie JM. Potassium channels in nodal and internodal axonal membrane of mammalian myelinated fibres. *Nature.* 1980;284(5752):170-1.

[21] Kocsis JD, Waxman SG. Absence of potassium conductance in central myelinated axons. *Nature.* 1980;287(5780):348-9.

[22] Brismar T. Potential clamp analysis of membrane currents in rat myelinated nerve fibres. *J. Physiol.* 1980;298:171-84.

[23] Gordon TR, Kocsis JD, Waxman SG. Evidence for the presence of two types of potassium channels in the rat optic nerve. *Brain Res.* 1988;447(1):1-9.

[24] Brown AM, Westenbroek RE, Catterall WA, Ransom BR. Axonal L-type Ca2+ channels and anoxic injury in rat CNS white matter. *J. Neurophysiol.* 2001;85(2):900-11.

[25] Rasband MN, Trimmer JS, Peles E, Levinson SR, Shrager P. K+ channel distribution and clustering in developing and hypomyelinated axons of the optic nerve. *J. Neurocytol.* 1999a;28(4-5):319-31.

[26] Devaux J, Gola M, Jacquet G, Crest M. Effects of K+ channel blockers on developing rat myelinated CNS axons: identification of four types of K+ channels. *J. Neurophysiol.* 2002;87(3):1376-85.

[27] Kordeli E, Lambert S, Bennett V. AnkyrinG. A new ankyrin gene with neural-specific isoforms localized at the axonal initial segment and node of Ranvier. *J. Biol. Chem.* 1995;270(5):2352-9.

[28] Jenkins SM, Bennett V. Developing nodes of Ranvier are defined by ankyrin-G clustering and are independent of paranodal axoglial adhesion. *Proc. Natl. Acad. Sci. U. S. A*. 2002;99(4):2303-8.

[29] Rasband MN, Peles E, Trimmer JS, Levinson SR, Lux SE, Shrager P. Dependence of nodal sodium channel clustering on paranodal axoglial contact in the developing CNS. *J. Neurosci.* 1999b;19(17):7516-28.

[30] Garrido JJ, Giraud P, Carlier E, Fernandes F, Moussif A, Fache MP, et al. A targeting motif involved in sodium channel clustering at the axonal initial segment. *Science*. 2003;300(5628):2091-4.

[31] Lambert S, Davis JQ, Bennett V. Morphogenesis of the node of Ranvier: co-clusters of ankyrin and ankyrin-binding integral proteins define early developmental intermediates. *J. Neurosci.* 1997;17(18):7025-36.

[32] Komada M, Soriano P. [Beta]IV-spectrin regulates sodium channel clustering through ankyrin-G at axon initial segments and nodes of Ranvier. *J. Cell. Biol.* 2002;156(2):337-48.

[33] Berghs S, Aggujaro D, Dirkx R, Jr., Maksimova E, Stabach P, Hermel JM, et al. betaIV spectrin, a new spectrin localized at axon initial segments and nodes of ranvier in the central and peripheral nervous system. *J. Cell. Biol.* 2000;151(5):985-1002.

[34] Yang Y, Lacas-Gervais S, Morest DK, Solimena M, Rasband MN. BetaIV spectrins are essential for membrane stability and the molecular organization of nodes of Ranvier. *J. Neurosci.* 2004;24(33):7230-40.

[35] Lacas-Gervais S, Guo J, Strenzke N, Scarfone E, Kolpe M, Jahkel M, et al. BetaIVSigma1 spectrin stabilizes the nodes of Ranvier and axon initial segments. *J. Cell. Biol.* 2004;166(7):983-90.

[36] Voas MG, Lyons DA, Naylor SG, Arana N, Rasband MN, Talbot WS. alphaII-spectrin is essential for assembly of the nodes of Ranvier in myelinated axons. *Curr. Biol.* 2007;17(6):562-8.

[37] Ogawa Y, Schafer DP, Horresh I, Bar V, Hales K, Yang Y, et al. Spectrins and ankyrinB constitute a specialized paranodal cytoskeleton. *J. Neurosci.* 2006;26(19):5230-9.

[38] Butt AM, Duncan A, Berry M. Astrocyte associations with nodes of Ranvier: ultrastructural analysis of HRP-filled astrocytes in the mouse optic nerve. *J. Neurocytol*. 1994;23(8):486-99.

[39] Butt AM, Ransom BR. Morphology of astrocytes and oligodendrocytes during development in the intact rat optic nerve. *J. Comp. Neurol.* 1993;338(1):141-58.

[40] Ishibashi T, Dakin KA, Stevens B, Lee PR, Kozlov SV, Stewart CL, et al. Astrocytes promote myelination in response to electrical impulses. *Neuron*. 2006;49(6):823-32.

[41] Kriegler S, Chiu SY. Calcium signaling of glial cells along mammalian axons. *J. Neurosci.* 1993;13(10):4229-45.

[42] Butt AM, Pugh M, Hubbard P, James G. Functions of optic nerve glia: axoglial signalling in physiology and pathology. *Eye.* 2004;18(11):1110-21.

[43] Butt A, Kirvell S, Ibrahim M. 20: NG2 glia (oligodendrocyte progenitor cells) and sodium channel clustering at developing nodes of Ranvier in the rat brain. *J. Anat.* 2002;200(2):206.

[44] Butt AM, Duncan A, Hornby MF, Kirvell SL, Hunter A, Levine JM, et al. Cells expressing the NG2 antigen contact nodes of Ranvier in adult CNS white matter. *Glia.* 1999;26(1):84-91.

[45] Polito A, Reynolds R. NG2-expressing cells as oligodendrocyte progenitors in the normal and demyelinated adult central nervous system. *J. Anat.* 2005;207(6):707-16.

[46] Butt AM, Hamilton N, Hubbard P, Pugh M, Ibrahim M. Synantocytes: the fifth element. *J. Anat.* 2005;207(6):695-706.

[47] Nishiyama A, Watanabe M, Yang Z, Bu J. Identity, distribution, and development of polydendrocytes: NG2-expressing glial cells. *J. Neurocytol.* 2002;31(6-7):437-55.

[48] Butt AM, Kiff J, Hubbard P, Berry M. Synantocytes: new functions for novel NG2 expressing glia. *J. Neurocytol.* 2002;31(6-7):551-65.

[49] Yang Y, Ogawa Y, Hedstrom KL, Rasband MN. {beta}IV spectrin is recruited to axon initial segments and nodes of Ranvier by ankyrinG. *J. Cell. Biol.* 2007;176(4):509-19.

[50] Pedraza L, Huang JK, Colman DR. Organizing principles of the axoglial apparatus. *Neuron.* 2001;30(2):335-44.

[51] Dupree JL, Girault JA, Popko B. Axo-glial interactions regulate the localization of axonal paranodal proteins. *J. Cell. Biol.* 1999;147(6):1145-52.

[52] Arroyo EJ, Xu T, Grinspan J, Lambert S, Levinson SR, Brophy PJ, et al. Genetic dysmyelination alters the molecular architecture of the nodal region. *J. Neurosci.* 2002;22(5):1726-37.

[53] Bhat MA, Rios JC, Lu Y, Garcia-Fresco GP, Ching W, St Martin M, et al. Axon-glia interactions and the domain organization of myelinated axons requires neurexin IV/Caspr/Paranodin. *Neuron.* 2001;30(2):369-83.

[54] Mathis C, Denisenko-Nehrbass N, Girault JA, Borrelli E. Essential role of oligodendrocytes in the formation and maintenance of central nervous system nodal regions. *Development.* 2001;128(23):4881-90.

[55] Alix JJ, Dolphin AC, Fern R. Vesicular apparatus, including functional calcium channels, are present in developing rodent optic nerve axons and are required for normal node of Ranvier formation. *J. Physiol.* 2008;586(17):4069-89.

[56] Ziskin JL, Nishiyama A, Rubio M, Fukaya M, Bergles DE. Vesicular release of glutamate from unmyelinated axons in white matter. *Nat. Neurosci.* 2007;10(3):321-30.

[57] Kukley M, Capetillo-Zarate E, Dietrich D. Vesicular glutamate release from axons in white matter. *Nat. Neurosci.* 2007;10(3):311-20.

[58] Einheber S, Zanazzi G, Ching W, Scherer S, Milner TA, Peles E, et al. The axonal membrane protein Caspr, a homologue of neurexin IV, is a component of the septate-like paranodal junctions that assemble during myelination. *J. Cell. Biol.* 1997;139(6):1495-506.

[59] Rios JC, Melendez-Vasquez CV, Einheber S, Lustig M, Grumet M, Hemperly J, et al. Contactin-associated protein (Caspr) and contactin form a complex that is targeted to the paranodal junctions during myelination. *J. Neurosci.* 2000;20(22):8354-64.

[60] Menegoz M, Gaspar P, Le Bert M, Galvez T, Burgaya F, Palfrey C, et al. Paranodin, a glycoprotein of neuronal paranodal membranes. *Neuron.* 1997;19(2):319-31.

[61] Peles E, Nativ M, Lustig M, Grumet M, Schilling J, Martinez R, et al. Identification of a novel contactin-associated transmembrane receptor with multiple domains implicated in protein-protein interactions. *Embo. J.* 1997;16(5):978-88.

[62] Boyle ME, Berglund EO, Murai KK, Weber L, Peles E, Ranscht B. Contactin orchestrates assembly of the septate-like junctions at the paranode in myelinated peripheral nerve. *Neuron.* 2001;30(2):385-97.

[63] Gollan L, Salomon D, Salzer JL, Peles E. Caspr regulates the processing of contactin and inhibits its binding to neurofascin. *J. Cell Biol.* 2003;163(6):1213-8.

[64] Gollan L, Sabanay H, Poliak S, Berglund EO, Ranscht B, Peles E. Retention of a cell adhesion complex at the paranodal junction requires the cytoplasmic region of Caspr. *J. Cell. Biol.* 2002;157(7):1247-56.

[65] Denisenko-Nehrbass N, Oguievetskaia K, Goutebroze L, Galvez T, Yamakawa H, Ohara O, et al. Protein 4.1B associates with both Caspr/paranodin and Caspr2 at paranodes and juxtaparanodes of myelinated fibres. *Eur. J. Neurosci.* 2003;17(2):411-6.

[66] Ishibashi T, Dupree JL, Ikenaka K, Hirahara Y, Honke K, Peles E, et al. A myelin galactolipid, sulfatide, is essential for maintenance of ion channels on myelinated axon but not essential for initial cluster formation. *J. Neurosci.* 2002;22(15):6507-14.

[67] Rios JC, Rubin M, St Martin M, Downey RT, Einheber S, Rosenbluth J, et al. Paranodal interactions regulate expression of sodium channel subtypes and provide a diffusion barrier for the node of Ranvier. *J. Neurosci.* 2003;23(18):7001-11.

[68] Rosenbluth J, Dupree JL, Popko B. Nodal sodium channel domain integrity depends on the conformation of the paranodal junction, not on the presence of transverse bands. *Glia.* 2003;41(3):318-25.

[69] Dupree JL, Mason JL, Marcus JR, Stull M, Levinson R, Matsushima GK, et al. Oligodendrocytes assist in the maintenance of sodium channel clusters independent of the myelin sheath. *Neuron. Glia Biol.* 2005;1:1-14.

[70] Rasband MN, Kagawa T, Park EW, Ikenaka K, Trimmer JS. Dysregulation of axonal sodium channel isoforms after adult-onset chronic demyelination. *J. Neurosci. Res.* 2003;73(4):465-70.

[71] Rasband MN, Trimmer JS. Subunit composition and novel localization of K+ channels in spinal cord. *J. Comp. Neurol.* 2001;429(1):166-76.

[72] Wang H, Kunkel DD, Martin TM, Schwartzkroin PA, Tempel BL. Heteromultimeric K+ channels in terminal and juxtaparanodal regions of neurons. *Nature.* 1993;365(6441):75-9.

[73] Rhodes KJ, Strassle BW, Monaghan MM, Bekele-Arcuri Z, Matos MF, Trimmer JS. Association and colocalization of the Kvbeta1 and Kvbeta2 beta-subunits with Kv1 alpha-subunits in mammalian brain K+ channel complexes. *J. Neurosci.* 1997;17(21):8246-58.

[74] Rasband MN, Park EW, Zhen D, Arbuckle MI, Poliak S, Peles E, et al. Clustering of neuronal potassium channels is independent of their interaction with PSD-95. *J. Cell. Biol.* 2002;159(4):663-72.

[75] Traka M, Dupree JL, Popko B, Karagogeos D. The neuronal adhesion protein TAG-1 is expressed by Schwann cells and oligodendrocytes and is localized to the juxtaparanodal region of myelinated fibers. *J. Neurosci.* 2002;22(8):3016-24.

[76] Traka M, Goutebroze L, Denisenko N, Bessa M, Nifli A, Havaki S, et al. Association of TAG-1 with Caspr2 is essential for the molecular organization of juxtaparanodal regions of myelinated fibers. *J. Cell. Biol.* 2003;162(6):1161-72.

[77] Poliak S, Salomon D, Elhanany H, Sabanay H, Kiernan B, Pevny L, et al. Juxtaparanodal clustering of Shaker-like K+ channels in myelinated axons depends on Caspr2 and TAG-1. *J. Cell Biol.* 2003;162(6):1149-60.

[78] Altevogt BM, Kleopa KA, Postma FR, Scherer SS, Paul DL. Connexin29 is uniquely distributed within myelinating glial cells of the central and peripheral nervous systems. *J. Neurosci.* 2002;22(15):6458-70.

[79] Rasband MN, Shrager P. Ion channel sequestration in central nervous system axons. *J. Physiol.* 2000;525 Pt 1:63-73.

[80] Poliak S, Peles E. The local differentiation of myelinated axons at nodes of Ranvier. *Nat. Rev. Neurosci.* 2003;4(12):968-80.

[81] Barrett EF, Barrett JN. Intracellular recording from vertebrate myelinated axons: mechanism of the depolarizing afterpotential. *J. Physi*ol. 1982;323:117-44.

[82] Foster RE, Connors BW, Waxman SG. Rat optic nerve: electrophysiological, pharmacological and anatomical studies during development. *Brain Res.* 1982;255(3):371-86.

[83] Waxman SG, Ritchie JM. Molecular dissection of the myelinated axon. *Ann. Neurol.* 1993;33(2):121-36.

[84] Arroyo EJ, Xu T, Poliak S, Watson M, Peles E, Scherer SS. Internodal specializations of myelinated axons in the central nervous system. *Cell Tissue Res.* 2001;305(1):53-66.

[85] Stolinski C, Breathnach AS, Thomas PK, Gabriel G, King RH. Distribution of particle aggregates in the internodal axolemma and adaxonal Schwann cell membrane of rodent peripheral nerve. *J. Neurol. Sci.* 1985;67(2):213-22.

In: Handbook on White Matter
Editors: T. B. Westland and R. N. Calton
ISBN: 978-1-60741-034-8

Chapter XVIII

Organizing Principles of Projections of the Long Descending Reticulospinal Pathways and Their Targets' Spinal Commissural Neurons: With Special Reference to the Locomotor Function

***Kiyoji Matsuyama*[*1,2,3] *and Kaoru Takakusaki*[4]**
[1] Department of Occupational Therapy, Sapporo Medical University School of Health Sciences, Department of [2] Neuropsychiatry and [3] System Neuroscience, Sapporo Medical University School of Medicine, South-1, West-17, Chuo-ku, Sapporo 060-8556, Japan
[4] Department of Physiology, Asahikawa Medical College School of Medicine, Midorigaoka Higashi 2-1, Asahikawa 078-8510, Japan

Abstract

The neural control of locomotion in vertebrates involves continuous interactions between various kinds of neural subsystems which are widely distributed throughout the central nervous system. Among these subsystems, the long descending reticulospinal pathways and their targets' spinal lamina VIII commissural neurons with axons projecting across the midline to the contralateral side form a continuous, anatomical system that is involved in the generation and coordination of left-right reciprocal and bilateral locomotor activities. To advance understanding of locomotor roles of this brainstem-spinal cord system, we performed a series of neural tracing studies using anterograde neural tracers to characterize the axonal morphology of reticulospinal neurons and lamina VIII commissural neurons in the cat, with the goal of revealing some

[*] Corresponding should be addressed to Dr. Kiyoji Matsuyama. Department of Occupational Therapy, Sapporo Medical University School of Health Sciences, South-1, West-17, Chuo-ku, Sapporo 060-8556, Japan. Tel.: +81-11-611-2111 (ext. 2880); Fax: +81-11-611-2155 ; E-mail: matsuk@sapmed.ac.jp

of the organizing principles of their projections along their rostrocaudal extent in the spinal cord, including: the number and frequency of their axon collaterals in the white matter, the patterns of their collateral arborizations in the gray matter, and the relationships between locations of the parent axons and their collateral termination areas. The reticulospinal pathways are morphologically heterogeneous, being composed of various types of in-parallel-descending axons, each of which has a commonality of the pattern of collateral termination along its rostrocaudal extent in the spinal cord. Commissural neurons can be classified into two major groups on the basis of their projections, viz. those that project primarily to laminae VIII-VII and those that project to the motor nuclei in lamina IX. These suggest that the reticulospinal pathways and their targets' commissural neurons as a whole comprise varying types of functional subunits, which may serve as the flexible optimal neural substrate essential for the generation and coordination of the bilateral locomotor rhythm in self-induced, goal-directed locomotion.

Keywords: spinal cord, brainstem, reticular formation, reticulospinal pathway, commissural neurons, locomotion, central pattern generator.

Introduction

Locomotion is characterized by its highly automatized, rhythmic movements with widespread synergy of the whole body including all limbs and trunk (Bernstein, 1967). The neural control of locomotion in vertebrates involves continuous interactions between various kinds of neural subsystems which are widely distributed throughout the central nervous system (Grillner, 1985; Mori et al., 1992). Since locomotor acts belong to the category of extremely ancient movements, and they are phylogenetically older than the cortical hemispheres (Bernstein, 1967), the subcortical areas including the basal ganglia, cerebellum, brainstem and spinal cord are fundamental for the locomotor function. Among these areas, the brainstem and spinal cord are essential for the generation and regulation of basic locomotor patterns, e.g. rhythmic extension-flexion movements of each limb and reciprocal left-right interlimb coordination during locomotion (for review: Orlovsky et al., 1999).

In mammals, the long descending reticulospinal pathways, which originate primarily in the medial two-thirds of the reticular formation at the pontomedullary brainstem (Brodal, 1981), are the main descending routes for conveying locomotor command signals from supraspinal centers to the spinal cord in which neural circuits for generating locomotor patterns, viz. the spinal central pattern generators for locomotion (CPGs) are located (Grillner, 1985; Armstrong, 1986; Jordan, 1991; Mori et al., 1992, 2000). They descend throughout the full length of the spinal neuraxis, and terminate primarily in the internuncial layer of the ventral horn, that is, the lamina VIII of Rexed (1952) and the adjoining part of lamina VII, at all levels of the spinal cord, where several different types of propriospinal neurons including interneurons are distributed (Basbaum et al., 1978; Holstege and Kuypers, 1982; Peterson, 1984; Matsuyama et al., 1988, 1997, 1999a-b; Mitani et al., 1988; Jankowska, 1992). Laminae VIII-VII interneurons and ascending tract neurons in the cat lumbar spinal cord are excited monosynaptically by reticulospinal axons (Skinner and Remmel, 1978; Davies and Edgley, 1994; Jankowska et al., 2003; Matsuyama et al., 2004b;

Takakusaki et al., 2003). They are also rhythmically active during the generation of locomotor rhythm (see also review: Orlovsky et al., 1999).

Among the neurons in lamina VIII and the adjacent lamina VII in the cat lumbar spinal cord, ~85% were reported to be commissural neurons (CNs) with axons projecting across the midline to the contralateral side (Scheibel and Scheibel, 1969). In vitro studies of the organization and morphology of laminae VIII-VII CNs in the lumbar spinal cord of fetal or neonatal rats and mice have suggested that lumbar CNs play an important role in the generation and coordination of bilateral locomotor rhythms (Kjaerulff and Kiehn, 1996, 1997; Eide et al., 1999; Antonio-Green et al., 2002; Butt et al., 2002; Nakayama et al., 2002; Stokke et al., 2002; Birinyi et al., 2003; Butt and Kiehn, 2003; Kullander et al., 2003). Many lumbar CNs in the developing spinal cord are rhythmically active during locomotor-like activity and are considered to be fundamental components of CPGs (Butt et al., 2002; Butt and Kiehn, 2003).

Lumbar lamina VIII CNs in adult cats have also been reported to exhibit locomotor-related rhythmic activity during the generation of fictive locomotor rhythm (Huang et al., 2000; Matsuyama et al., 2004b), and a large part of them receive excitatory monosynaptic inputs from reticulospinal pathways (Jankowska et al., 2003; Matsuyama et al., 2004b). Therefore, these indicate that the reticulospinal pathways and their targets' lamina VIII CNs are not only anatomically continuous but also functionally coupled. To advance understanding of locomotor roles of such tightly coupled, reticulospinal-spinal CN systems, it is important to characterize the axonal morphology of reticulospinal neurons and lamina VIII CNs in the spinal cord, because function of each neuron highly depends on its axonal projection pattern. For this reason, we have performed a series of neural tracing studies using anterograde neural tracers, including *Phaseolus vulgaris*-leucoagglutinin (PHA-L) and biotinylated-dextran amine (BDA), both of which could label axons and their collateral branches over long distances in the cat spinal cord (Matsuyama et al., 1997, 1999b, 2006; Reiner et al., 2000). The goals of these studies were to reveal some of the organizing principles of their projections along their rostrocaudal extent in the spinal cord, including: the number and frequency of their axon collaterals in the white matter, the patterns of their collateral arborizations in the gray matter, and the relationships between locations of the parent axons and their collateral termination areas.

In this review, we will provide information on: the gross projection patterns of the long descending reticulospinal pathways and their axonal morphology; the axonal morphology and physiology of lumbar lamina VIII CNs. We will then discuss the possible functional role of the reticulospinal-spinal CN system in the control of locomotion.

1. The Long Descending Reticulospinal Pathways

The reticulospinal pathways originate primarily from the medial two-thirds of the pontomedullary reticular formation (PMRF), and they exhibit extensive projections in the spinal cord along their descending courses (see review: Holstege and Kuyper, 1981; Peterson, 1984). Based on the level of the axonal descents within the spinal cord, Peterson et al. (1984) classified the reticulospinal neurons into four groups: N cells, C cells, T cells and L cells, of

which axons extend as far as the upper cervical, upper thoracic, lower thoracic and lumbosacral cord levels, respectively, although distributions of these types of cells are intermingled within the PMRF. Among these groups, the long descending reticulospinal neurons (L cells) are thought to play an important role in the control of widespread coordinative motor activities of the whole body, such as orienting, postural and locomotor movements (Peterson, 1984; Drew et al., 1986; Drew and Rossignol, 1990).

According to Brodal (1981), the PMRF can be subdivided into four major nuclei according to their cytoarchitecture and location in the brainstem: the nuclei reticularis pontis oralis (NRPo) and caudalis (NRPc) in the pons, and the nuclei reticularis gigantocellularis (NRGc) and magnocellularis (NRMc) in the medulla. In the NRPo, NRPc and NRGc, large-sized cells with a diameter of ~50 μm are richly distributed, while the NRMc lacks such large cells. In sharp contrast to such clear anatomical subdivisions, the PMRF is organized in a loose topographical fashion in relation to limb-trunk motor outputs, with a large overlap in the representation, and no clear segregation as usually seen in the cerebral cortex (Peterson, 1984; Drew and Rossignol, 1990). Since motor functions of the PMRF are highly related to its descending projections in the spinal cord, we have performed a series of PHA-L tracing studies to reveal characteristics of the projection patterns of the long descending reticulospinal pathways arising from the PMRF in the cat (Matsuyama et al., 1988, 1997, 1999a-b).

1.1. Gross Projection Patterns

The results of our PHA-L tracing studies demonstrated the following characteristics of projections of the reticulospinal pathways originating from the pontine and medullary reticular formation (figure 1). As described previously (Holstege and Kuypers, 1982), PHA-L-labeled reticulospinal axons from the pontine reticular nuclei (NRPo and NRPc) descend purely ipsilaterally, while those from the medullary reticular nuclei (NRGc and NRMc) descend almost evenly bilaterally (Matsuyama et al., 1988, 1997, 1999a-b). Axons that descend contralaterally cross the midline at the medullary level (see schemes in figure 1B-C). Reflecting rich distributions of large-size cells in the NRPo, NRPc and NRGc, the reticulospinal pathways from these nuclei are composed of mainly thick axons (diameter 3-10 μm at the cervical cord) descending in the ventral (VF) and ventrolateral funiculi (VLF). These axons project fine collateral fibers mainly in the ventromedial part of the ventral horn, such as laminae VIII and adjacent lamina VII and additionally axial motor nuclei (medial lamina IX), at all levels of the spinal cord (figure 1A-B). The reticulospinal pathway from the NRMc that lacks large cells is composed of mainly thin axons (diameter < 3 μm at the cervical cord) descending widely in the white matter including the VF, VLF and additionally the dorsolateral funiculus (DLF) (Matsuyama et al., 1999a). These axons project widely in the gray matter, including laminae VIII-VII and axial motor nuclei, and additionally limb motor nuclei (lateral lamina IX) (figure 1C).

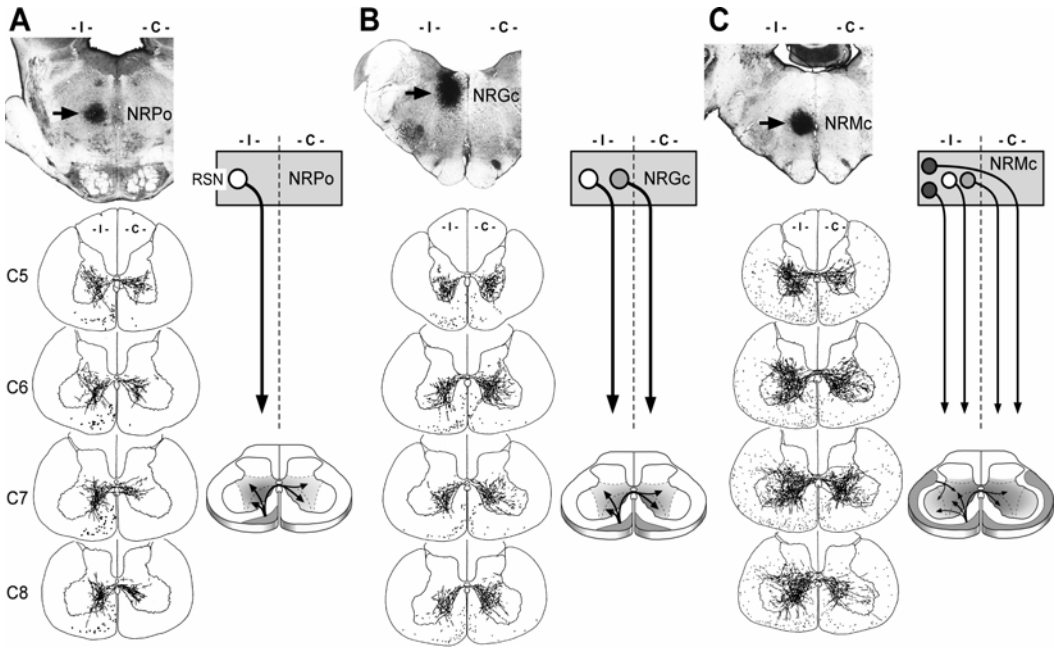

Figure 1. Characteristics of gross projection patterns of the reticulospinal pathways arising from the medial pontomedullary reticular formation (PMRF): the nucleus reticularis pontis oralis (NRPo) in the pons (A), the nuclei reticularis gigantocellularis (NRGc) (B) and magnocellularis (NRMc) (C) in the medulla of cats. In photographs in A-C, dark areas indicated by thick arrows show PHA-L injection areas in the NRPo, NRGc and NRMc. In each cat, 0.3-0.4 μl of 5% PHA-L solution was injected. Locations of PHA-L labeled reticulospinal axons descending in the white matter and distributions of their collateral fibers in the gray matter in the cervical cord at segment C5-C8 are plotted on a drawing of a representative transverse section of each segment. In the right columns in A-C, 3 major components of reticulospinal projections are schematically illustrated (see text in detail). A downward arrow with a white or gray circle indicates the first or second component descending in the ventral and ventrolateral funiculi purely ipsilaterally or contralaterally, respectively. Downward arrows with dark circles shown in C indicate the third components descending in the dorsolateral funiculus ipsilaterally and contralaterally. In the bottom drawings on the right in A-C, hatched areas in the white matter and gray-colored areas in the gray matter represent distribution areas of reticulospinal axons and their main termination areas, respectively. Thin arrows show directions of collateral fibers from stem axons. Thin arrows in the contralateral side in B-C are not shown to avoid making the figures much complicated. Abbreviations: C, contralateral side; I, ipsilateral side; RSN, reticulospinal neuron. Figure 1A and B were modified from Matsuyama et al. (1997) and (1988), respectively.

From the above characteristics of descending routes and projection areas in the spinal cord, we can assume that the reticulospinal pathways from the PMRF consist of 3 major descending components as follows (figure 1). The first component commonly originates from all reticular nuclei in the PMRF and descends in the ipsilateral VF and VLF (see cells indicated by white circles in figure 1A-C). The second one originates from the NRGc and NRMc, and descends in the contralateral VF and VLF after crossing the midline in the brainstem (see gray circles in figure 1B-C). These two components project primarily to laminae VIII-VII and axial motor nuclei mainly on the side where their axons descend and some additionally on the other side. The third component, which originates only from the

NRMc, descends in the DLF ipsilaterally and contralaterally, and project to the ventrolateral part of the ventral horn including limb motor nuclei (see dark circles in figure 1C). Therefore, as summarized on the schemes in figure 1, the pontine reticulospinal pathways from the NRPo and NRPc are composed of only the first component. The medullary reticulospinal pathway from the NRGc is composed of the first and second components, and the pathway from the NRMc is composed of all components. The differences in the compositions of the descending components strongly suggest that each reticulospinal pathway arising from the NRPo-NRPc, NRGc and NRMc has its own specific motor function although the representations of limb-trunk motor outputs of these reticular nuclei are largely overlapped with no clear segregation (Peterson, 1984; Drew and Rossignol, 1990).

1.2. Morphology of Individual Reticulospinal Axons

To advance understanding of the contribution of the long descending reticulospinal pathways in the control of locomotion, we wanted to further detail the morphology of reticulospinal axons along their descent in the spinal cord, especially their projection patterns including the number and frequency of their axon collaterals and the patterns of their collateral arborization. For this purpose, from serial transverse sections of the spinal cord, we traced trajectories of PHA-L labeled axons in continuity in the white matter at the cervicothoracic and lumbosacral spinal cord levels, and then characterized intricate details of their collateral arborization along their descending courses (Matsuyama et al., 1997, 1999b). In these studies, we restricted our attention to the pontine reticulospinal axons because they project purely ipsilaterally and thus can be traced serially with the certainty that all of the terminations found arise from a single parent axon descending on the ipsilateral side.

A. Collateralization Pattern

As shown in photographs in figure 2A, reticulospinal axons decrease their diameters as they descend caudally giving off multiple axon collaterals along their courses in the white matter. We counted the number and exit levels of axon collaterals arising from individual axons, of which trajectories were traced in continuity in the cervical and lumbar enlargements. These axons gave off 2-3 or 1-2 axon collaterals/segment in the cervical and lumbar enlargements, respectively (see also figure 2B). The mean intercollateral distances between exit levels of two neighboring axon collaterals arising from identical stem axons are ~5 mm in both enlargements. Although preliminary, we also found that reticulospinal axons give off 1 or less axon collateral/segment in the thoracic cord level, i.e. the mean intercollateral distance corresponding to more than 10 mm.

Therefore, as illustrated in figure 2C, we can assume that the long descending reticulospinal axons give off multiple axon collaterals along the full length of the spinal cord, but the frequency of collateralization along the rostrocaudal extent would be uneven, i.e. densely in the cervical and lumbar enlargements but sparsely in the thoracic cord. Considering that the motor nuclei innervating forelimb and hindlimb muscles are located in the cervical and lumbar enlargements, the dense collateralization in both enlargements would be rational to exert extensive controls on the limbs simultaneously. Such control pattern

might be necessitated in case of widespread synergistic movements of all limbs during locomotion. Similar uneven collateralization patterns along the rostrocaudal extent of the spinal cord are also found in the long descending lateral vestibulospinal axons arising from the Deiters nucleus in the cat (Kuze et al., 1999).

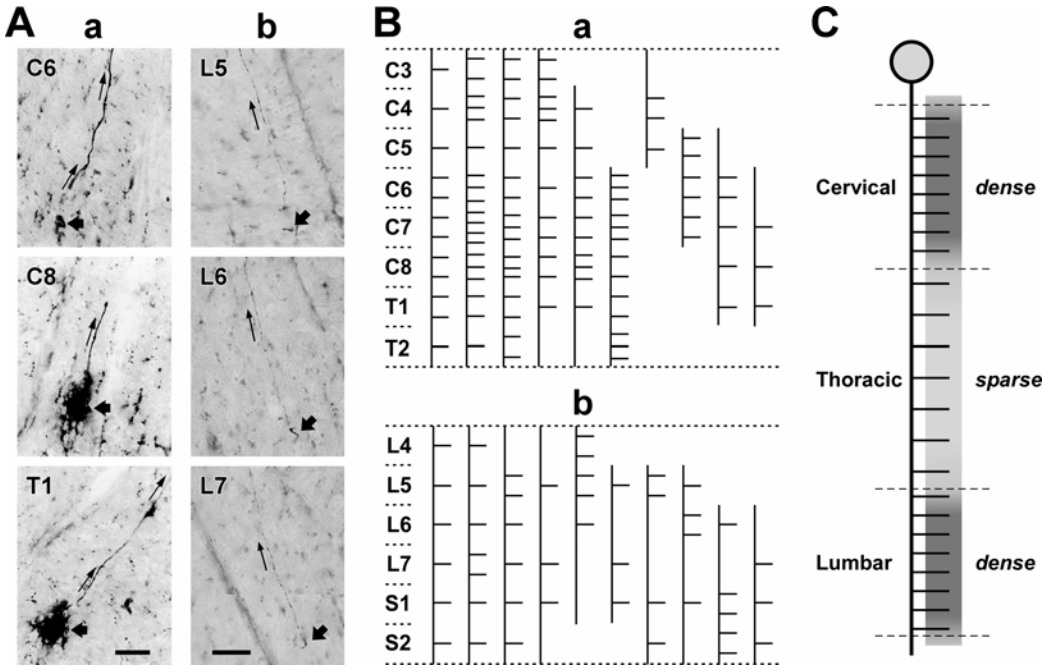

Figure 2. Collateralization pattern of individual pontine reticulospinal axons along their descent in the spinal cord. A: Photomicrographs of axon collaterals arising from two individual axons of which trajectories were traced in continuity in the cervical (a) and lumbar (b) enlargements. Thick arrows indicate locations of stem axons, and thin arrows indicate directions of axon collaterals projecting dorsally to the ventral horn. In a, dark staining areas around stem axons at C8 and T1 are leakage areas of PHA-L tracer. Scale bar = 50 μm. B: Diagrammatic representation of the collateralization patterns of single reticulospinal axons of which trajectories were traced continuously in the cervicothoracic cord level at C3-T2 (a) and lumbosacral cord level at L4-S2 (b). Key: solid vertical lines, extent that stem axons were traced; horizontal short bars, exit levels of axon collaterals. In a and b, collateralization patterns of a total of 10 identified axons are illustrated. C: Putative collateralization pattern of a representative long descending reticulospinal axon along the full length of the spinal cord. Note that the axon gives off multiple axon collaterals densely in the cervical and lumbar enlargements and sparsely in the thoracic cord. A grey circle on the top represents the soma of the neuron. Figure 2A and B were modified from Matsuyama et al. (1997, 1999b).

B. Collateral Arborization Pattern

To characterize the collateral arborization pattern of reticulospinal axons along their descent, we reconstructed intricate details of fiber branching of axon collaterals arising from individual axons at multiple segments. In keeping with the gross projection patterns, the axon collaterals that we reconstructed terminated primarily in lamina VIII and adjacent lamina VII. However, as shown in figure 3A-B, the main termination areas of each axon along the rostrocaudal extent was different from one stem axon to another. This indicates that the

reticulospinal pathway is morphologically a heterogeneous, parallel descending pathway composed of various types of axons with different projection patterns. This further indicates that the reticulospinal pathway is organized in a functionally, heterogeneous system composed of varying types of neuronal elements with different function. In fact, reticulospinal neurons are subdivided into several groups according to their discharge patterns during locomotion, e.g. EMG-related, locomotor-rhythm-related, unrelated, tonic, silent (Drew et al., 1986; Matsuyama and Drew, 2000; Prentice and Drew, 2001).

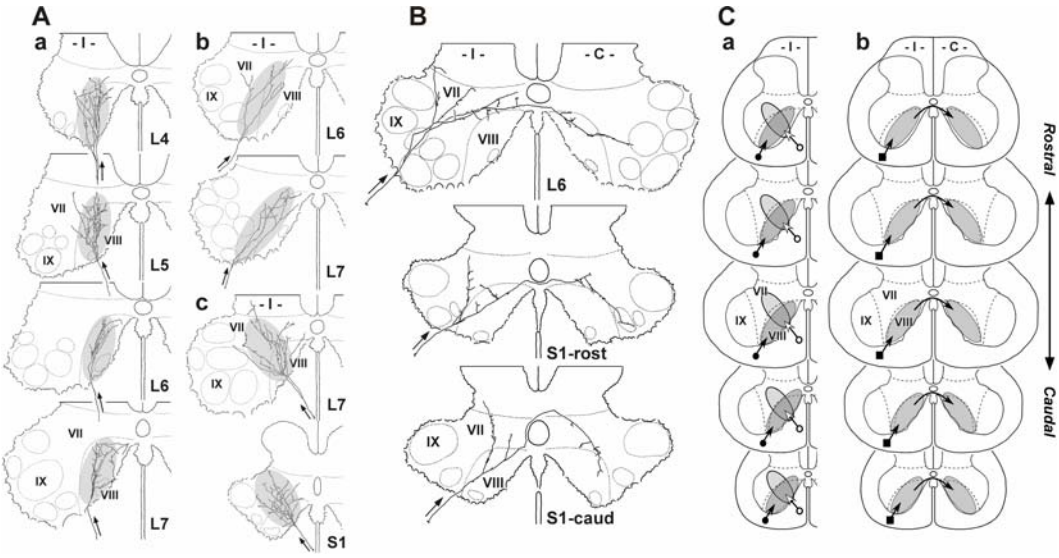

Figure 3. Multi-segmental innervation patterns of individual pontine reticulospinal axons in the lumbar enlargement. A: Three representative axons (a, b, c) innervating only unilaterally (ipsilaterally). Note that all axon collaterals arising from a given axon commonly project to similar regions (gray colored areas) in the gray matter at different segments. B: A representative axon innervating bilaterally. All axon collaterals project to the contralateral gray matter in addition to the ipsilateral side. C: Schematic representations of multi-segmental innervation patterns of individual reticulospinal axons. Two axons, of which locations in the white matter are indicated by dark and open circles in a, project only unilaterally at all levels of the spinal cord along their descent, while one axon indicated by dark squares in b project bilaterally. In A and C, gray and hatched areas represent common termination areas of axon collaterals arising from each individual axon. Thin arrows indicate directions of axon collaterals. Figure 3A and B were modified from Matsuyama et al. (1999b).

Despite such a high degree of morphological heterogeneity, there are three organizing principles related to the collateral termination pattern of individual reticulospinal axons. First, each axon collateral arborizes in a limited rostrocaudal region with a thickness of < 1 mm. Since the mean intercollateral intervals of reticulospinal axons are ~5 mm, the termination field of each axon collateral does not overlap with that of sibling axon collaterals. Second, axon collaterals arising from ~80% of reticulospinal axons that we identified innervate only the unilateral gray matter, ipsilateral to their stem axons (see figure 3A), whereas those from the remaining axons (~20%) innervate the bilateral gray matter (see figure 3B). Third, the termination areas of axon collaterals from a given reticulospinal axon are similar at each

segmental level along the course of that axon, and different from one stem axon to another (see figure 3C). Such commonality of the pattern of collateral termination along the rostrocaudal extent of parent axons is found throughout the cervical and lumbar enlargements. We therefore propose that a single reticulospinal neuron innervates a large number of interneurons at multiple segments throughout the full length of the spinal cord, and of more functional importance, a single reticulospinal neuron may activate interneurons at similar locations at different levels of the spinal cord.

2. Lumbar Commissural Neurons

A wide variety of propriospinal neurons including interneurons involved in motor functions are distributed in the internuncial layer of the ventral horn along the spinal neuraxis. These can be classified into several groups according to the characteristics of their morphology and physiology (for review: Scheibel and Scheibel, 1969; Jankowska, 1992). Among them, CNs with axons projecting across the midline to the contralateral side are distributed mainly in the medial part of the ventral horn, i.e., lamina VIII and adjacent lamina VII (Cajal, 1909; Scheibel and Scheibel, 1969; Matsushita, 1970; Harrison et al., 1986; Stokke et al., 2002; Nissen et al., 2005), where the long descending reticulospinal pathways primarily terminate. To understand the functional roles of CNs in the left-right coordination of bilateral limbs during locomotion, it is essential to know their projection patterns. These have been analyzed in detail extensively in developing rodents (Silos-Santiago and Snider, 1992; Eide et al., 1999; Stokke et al., 2002; Birinyi et al., 2003; Kadison and Kaprielian, 2004). These studies have shown that the axons of developing CNs project extensively to the contralateral spinal cord at the same level as their somata, as well as over long and short distances caudally and/or rostrally (Eide et al., 1999; Stokke et al., 2002; Kadison and Kaprielian, 2004), and terminate in the internuncial layer, the motor nuclei, or both (Birinyi et al., 2003).

To detail the morphology of lumbar lamina VIII CNs in adult cats, especially that of the full rostrocaudal extent of their axons in the lumbosacral cord, we performed an anterograde neural tracing study utilizing a tracer BDA (Matsuyama et al., 2006). We made localized injections of a small volume (5-10 nl) of 20% BDA solution into lamina VIII and adjacent lamina VII in the middle lumbar enlargement, where the motor nuclei innervating hindlimb muscles are mostly located (VanderHorst and Holstege, 1997). Then, we attempted to reconstruct the full morphology of BDA-labeled CN axons whose cell bodies were located in and around the injection areas.

2.1. Gross Projection Pattern of Lumbar CNs in The Lumbosacral Spinal Cord

In an anterograde degeneration study, Rustioni et al. (1971) demonstrated that propriospinal neurons with uncrossed axons that travel in the VF and lateral funiculus (LF) project to the intermediate zone (including laminae VIII-VII) and lamina IX. These

projections are most pronounced at the level of the lesion in the white matter but extended rostrally and caudally, with diminishing density, into adjoining segments. Moreover, the foci of the projections in the intermediate zone are similar at all levels above and below the lesion. This is similar to the projection patterns of CN axons demonstrated in our BDA tracing study (Matsuyama et al., 2006).

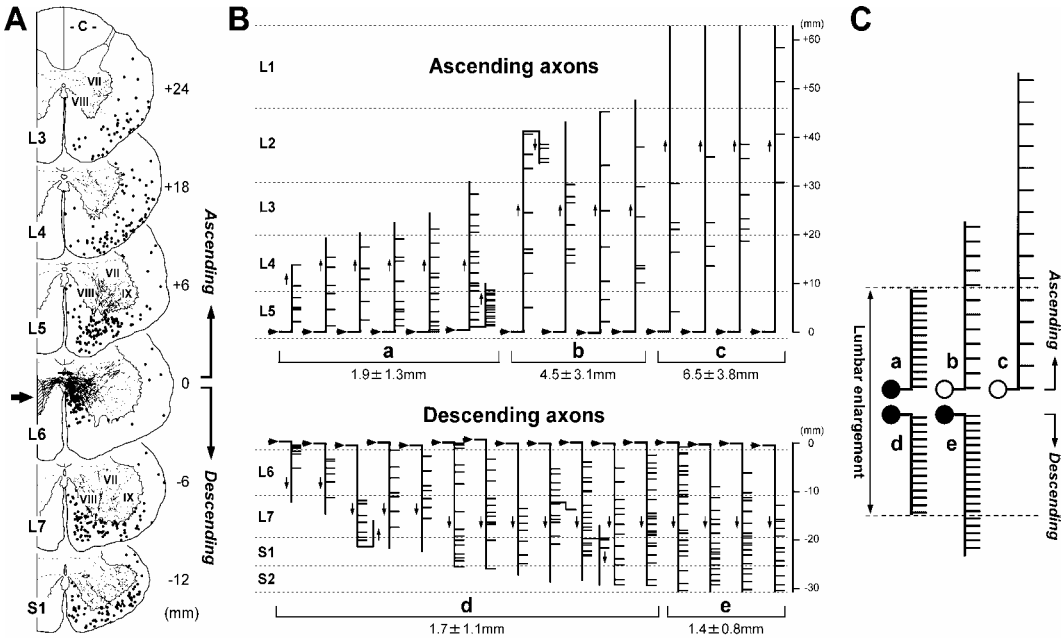

Figure 4. Intraspinal projection patterns of lumbar lamina VIII commissural neurons (CNs) in the lumbosacral spinal cord. A: Rostrocaudal distribution of BDA-labeled CN axons following the injection into lamina VIII at L6 segment. Dots in the white matter indicate the location of labeled CN axons, and the thin lines indicate labeled collateral branches. The thick arrow indicates the injection area at the rostral L6. Digits beside the drawings: 0 = BDA injection level; all other positive and negative numbers indicate the number of mm either rostral or caudal to the injection site, respectively. B: Diagrammatic representation of the collateralization patterns of single lumbar CN axons ascending rostrally and descending caudally. The trajectories of these axons were fully and continuously traced from the injection site to 16-63 mm rostrally or 12-31 mm caudally in the lumbosacral cord at L1-S2 that we explored. Identified CN axons are subdivided into 5 groups according to their directions and rostrocaudal distances that they travel: a, ascending < 30 mm; b, ascending 30-60 mm; c, ascending beyond the lumbar level (> 60 mm); d, descending < 30 mm; e, descending > 30 mm. The mean intercollateral distance of each group is calculated and shown in the bottom. The ordinates on the right indicate the distance (mm) from the center of the injection site. Key: solid vertical lines, extent that stem axons were traced; horizontal short bars, exit levels of axon collaterals; thick transverse arrows, levels at which axons crossed the midline; thin vertical arrows, axonal directions; thin broken horizontal lines, rostral and caudal borders of each segment; gray bars, rostrocaudal extent of BDA diffusion. C: Schematic drawings representing typical collateralization patterns of 5 groups of lumbar CN axons. Drawings a-e correspond to groups a-e in B, respectively. Note that the short ascending (a) and descending (d, e) CN groups show the dense collateralization, but long ascending groups (b, c) show the sparse collateralization. The area highlighted by dark gray shows that the lumbar enlargement receives CN projections much abundantly. Figure 4A and B were modified from Matsuyama et al. (2006).

As shown in figure 4A, at the BDA injection level, labeled CN axons formed a thick fibers' bundle and crossed the midline through the ventral white commissure to the dorsal portion of the contralateral VF (Matsuyama et al., 2006). After entering the opposite side, most of the labeled axons ran ventrally at first, and then ascended rostrally or descended caudally throughout the lumbosacral cord at L1-S2 segments that we explored. The majority of these axons ascended or descended through the VF within L1-S2 segments, but some shifted laterally to the LF as they traveled rostrally or caudally (see figure 4A). Ascending and descending CN axons commonly gave off a large number of axon collaterals. As in the study of Rustioni et al. (1971), collateral fibers of CN axons on the contralateral side were distributed to laminae VIII-VII and lamina IX, and the fiber density in laminae VIII-VII was highest at the injection level and diminished at more caudal and rostral levels.

It is well established that uncrossed propriospinal axons in different parts of the white matter project preferentially to different parts of the gray matter (for review, Kuypers, 1981). Thus, axons in the VF project primarily to laminae VIII-VII and axial motor nuclei, whereas those in the LF project primarily to laminae V-VII and the fore- or hindlimb motor nuclei. In our BDA tracing study, similar differences are found between CN axons that travel in the VF compared to those in the LF, suggesting that the lumbar CNs are varied in type and have different projection patterns according to locations of their courses in the white matter.

2. 2. Morphological Characteristics of Short and Long Projecting CN Axons

Propriospinal neurons are subdivided into long, intermediate, and short propriospinal neurons on the basis of the length of their axons (Kuypers, 1981). Long propriospinal neurons project throughout the length of the spinal cord, while the others project over a distance of a few segments, primarily within one of the enlargements. Among the latter are cells with axons that arborize within either the same or a few neighboring segments; these are more commonly referred to as segmental interneurons (Jankowska, 1992).

A. Rostrocaudal Extent

As shown in figure 4B, most CN axons identified in our BDA study have short rostral and/or caudal projections within the lumbosacral cord. The majority of them have a rostrocaudal extent of < ~30 mm, corresponding to the length of < ~3 segments in the lumbosacral cord (see a, d in figure 4B). These indicate that most of the lumbar laminae VIII CNs in the adult cat can be classified as short propriospinal neurons similar to those described in the neonatal preparation (Eide et al., 1999). Some of our identified CN axons projected rostrally beyond the lumbar level (c in figure 4B). These neurons might correspond to long propriospinal neurons or to ascending tract neurons (Maunz et al., 1978; Matsushita et al., 1979; Kuypers, 1981; Craig et al., 1989).

B. Collateralization Pattern

Most of the short axons had a small caliber, which diminished rapidly along their course. These axons commonly gave off many axon collaterals along the rostrocaudal extent in the lumbosacral enlargement with the mean intercollateral distance of < 2 mm (see a, d, e in

figure 4B-C). This dense collateralization of lumbar CNs will be well suited for intra- or inter-segmental integration and for the coordination of the activity of neurons located within the lumbosacral enlargement. Such CNs may help to generate synergistic movements around a single or a few joints of the contralateral hindlimb.

In contrast, the long ascending CN axons (c in figure 4B-C) had larger diameters, which remained relatively uniform along their course. These axons gave off only 4-6 collaterals from L1-L5 at mean intercollateral distances of ~6.5 mm, almost similar to those described in the long descending reticulo- and vestibulospinal axons (Kuze et al., 1999; Matsuyama et al., 1997, 1999b). Thus, assuming that long propriospinal or ascending tract lumbar CNs project to the cervical and lumbar enlargements, the divergent coordination imposed by the branching of such CNs is likely to be related to wider motor synergies, such as those underlying the interlimb coordination of the forelimbs and hindlimbs associated with postural adjustments and locomotion (Matsumoto et al., 1976; Antonio-Green et al., 2002; Juvin et al., 2005).

2.3. Collateral Arborization Patterns of Single Lumbar CN Axons

Although the details of the collateral branching patterns of single CN axons identified in our BDA study differ from axon to axon, there are two organizing principles related to their patterns. First, as shown in figures 5 and 6, most or all of the collateral branches of each individual CN axon projected to similar regions along its course at the lumbosacral level, e.g., with preferential projections to either the ventral or the medial aspects of laminae VIII-VII, or to the axial or the hindlimb motor nuclei. This uniformity in the collateral termination pattern was independent of axonal length and direction. Next, the termination areas of the axon collaterals in the gray matter were highly related to the course of their parent axons in the white matter. Two thirds of our identified axons traveled in the VF along their full extent in the white mater (see an example in figure 5A). Most of them had axons collaterals projecting primarily to laminae VIII-VII or a few axons had collaterals projecting to the axial motor nuclei within lamina VIII. In contrast, one third of the identified axons shifted laterally to the LF as they traveled rostrally or caudally in the white matter, and the majority had collaterals projecting preferentially to the hindlimb motor nuclei (see an example in figure 6A). Accordingly, most of lumbar lamina VIII CN axons that we identified fall into two distinct groups, i.e., axons traveling in the VF and projecting primarily to laminae VIII-VII (~60%; see figure 5B), and axons traveling in the LF and projecting preferentially to the hindlimb motor nuclei (~20%; figure 6B).

The above uniformity in the collateral termination patterns of single CN axons along the rostrocaudal extent suggest that the specific morphology of each axon develops in a manner that is dictated by its prospective function. Considering that most CN axons identified in our BDA study are of the segmental or short propriospinal type and they project densely to the opposite laminae VIII at and around the same segmental level as their somata (Matsuyama et al., 2006), it can be assumed that lumbar lamina VIII CNs on the left and right sides are mutually connected at the same segmental level (figure 5C). Such mutual CN-CN connections might form basic neural circuits that participate in coordinating activities of the

bilateral spinal cord. This neural action would be essential for generating the left-right alternation of bilateral limbs during locomotion.

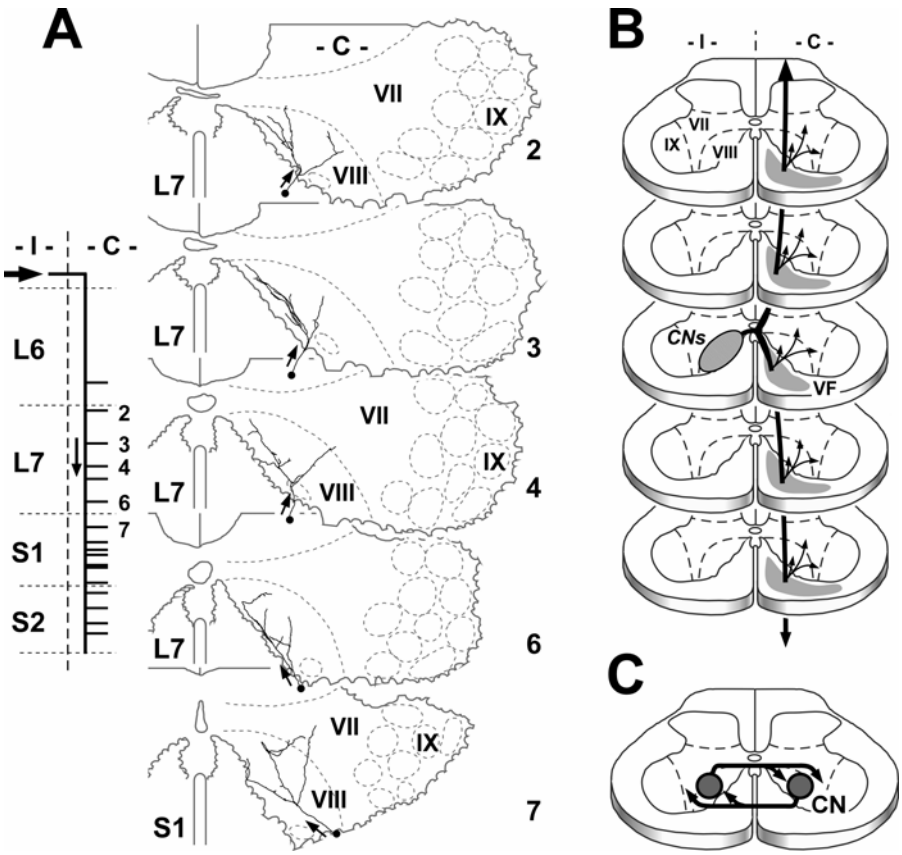

Figure 5. Collateral arborization patterns of lumbar lamina VIII CN axons with preferential projections to the opposite lamina VIII. A: One representative example of this CN group. On the drawings, the reconstructed arborization patterns of 5 axon collaterals are illustrated by thin black lines. Dots indicate the locations of the parent axons from which the axon collaterals originate, and small arrows indicate the directions of the collaterals. The inset on the left represents the collateralization patterns of the axons. The vertical broken line indicates the midline of the spinal cord; the other symbols are defined in the legend of figure 4. The numbers beside the short horizontal bars in the inset indicate the number of axon collaterals for each arborization pattern illustrated on the drawings. Note that this CN axon descends in the ventral funiculus along the full extent, giving of multiple axon collaterals that project preferentially to the opposite lamina VIII. B: Schematic drawings summarizing axonal projections of this CN group. A hatched area in the gray matter indicates lamina VIII where CN somata are located, and gray areas in the white matter indicate locations of ascending or descending CN axons. Thick arrows indicate directions of parent CN axons, and thin arrows indicate their collateral projections. Note that CN axons travel rostrally or caudally in the contralateral ventral funiculus, projecting collateral fibers primarily to lamina VIII. C: Putative mutual connections between left and right CNs located at the same segmental level (see text in detail). The above indicators and other explanations also apply to figure 6. Figure 5A was modified from Matsuyama et al. (2006).

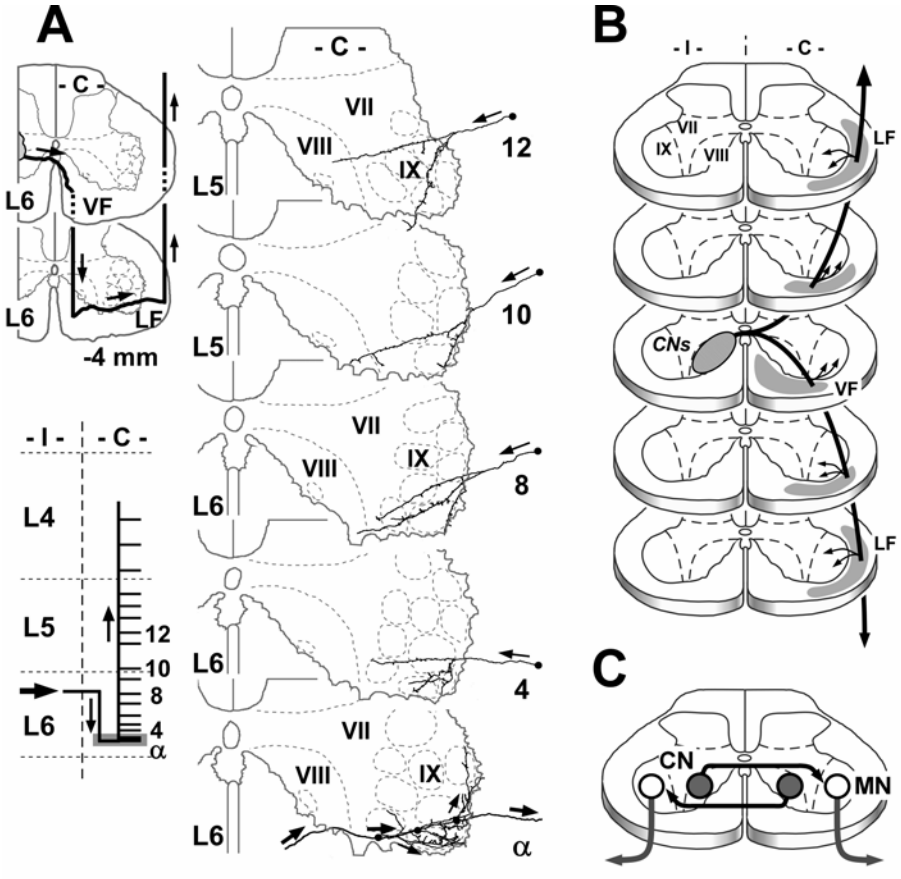

Figure 6. Collateral arborization patterns of lumbar lamina VIII CN axons with preferential projections to the opposite hindlimb motor nuclei. A: One representative example of this CN group. Note that this CN axon shifts laterally shortly after descending in the ventral funiculus (VF) and then ascends in the lateral funiculus (LF), giving of multiple axon collaterals that project preferentially to the opposite lamina IX where hindlimb motor nuclei are located. B: Schematic drawings summarizing axonal projections of this CN group. The drawings represent that CN axons shift laterally as they travel rostrally or caudally on the contralateral side, and project to the hindlimb motor nuclei along their courses. C: Putative neural connections between CNs and opposite hindlimb motoneurons (MN) (see text in detail). Figure 6A was modified from Matsuyama et al. (2006).

3. Locomotor-Related Activities of Lumbar Lamina VIII CNs

We have examined discharge characteristics of lumbar CNs with excitatory reticulospinal inputs during the generation of fictive locomotor rhythm, together with their axonal morphology (Matsuyama et al., 2004b). For these purposes, we utilized an intra-axonal recording technique combined with an intra-axonal injection of a tracer, neurobiotin (see figure 7A). This technique allowed us to obtain both physiological and morphological characteristics for each lumbar CN. The somata of neurobiotin-visualized CNs with

excitatory reticulospinal inputs were located mainly in lamina VIII and additionally in laminae VII-VI in the lumbar enlargement. This finding is in keeping with previous works showing that many laminae VIII-VI neurons in the cat lumbar spinal cord are excited monosynaptically from the reticulospinal pathways (Skinner and Remmel, 1978; Davies and Edgley, 1994; Jankowska et al., 2003; Takakusaki et al., 2003).

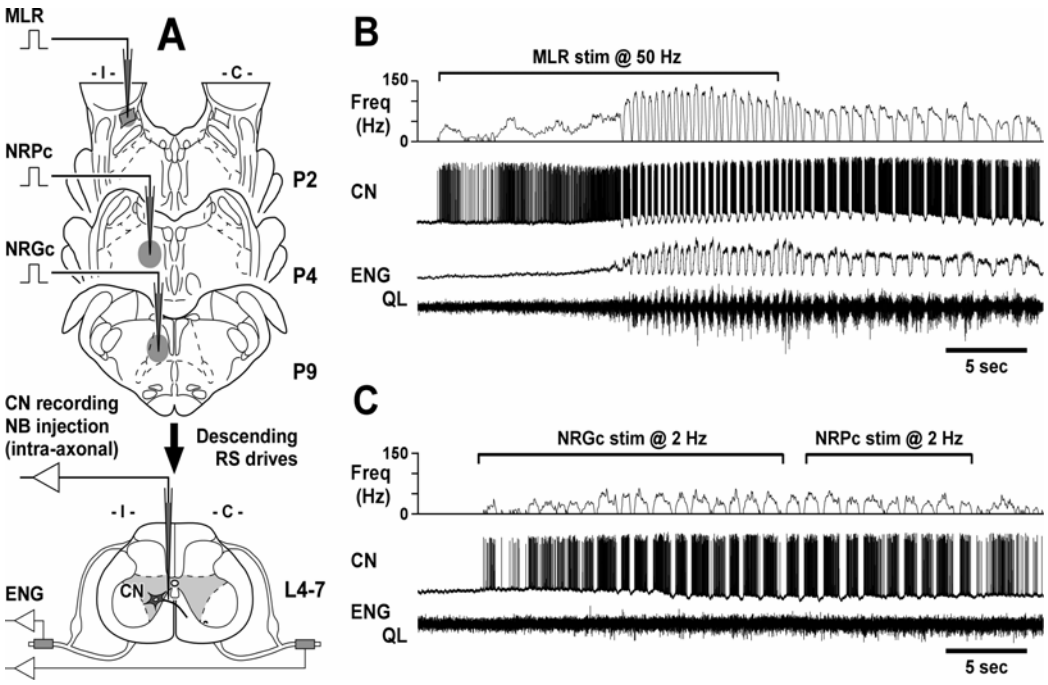

Figure 7. Locomotor-related rhythmic discharges of a lumbar lamina VIII CN receiving excitatory monosynaptic inputs from the reticulospinal pathways. A: Recording setup. Intraaxonal recordings were made from stem axons of lumbar lamina VIII CNs in a decerebrate, paralyzed cat. The microelectrode was positioned in the ventral funiculus at L4-7 segments. CN responses were determined as monosynaptic if CNs were excited orthodromically at a latency of < 1 ms from timing of segmental arrival (the first positive peak) of the descending volley following NRGc and/or NRPc stimulation (2 Hz, 100 μA pulses). To evoke fictive locomotion, the mesencephalic locomotor region (MLR) was stimulated at 50 Hz with an intensity of < 110 μA. After recording neuronal activities, to visualize the morphology of identified CNs, a neural tracer, neurobiotin (NB) was injected iontophoretically into the axon through the recoding micropipette. P2, P4, P9 = Posterior 2, 4, 9 mm of Horsley-Clarke coordinates (Berman, 1968). See Matsuyama et al (2004b) in detail. B: CN spike discharge and electroneurogram (ENG) activity of left quadriceps nerve (QL) during fictive locomotion evoked by 50 Hz electrical stimulation (100 μA pulses) of the MLR. Uppermost line, duration of electrical stimulation. Upper two panels, mean discharge frequency (upper histogram) and original neuronal records (lower trace). Lower two panels, integrated (upper trace) and raw (lower trace) ENG activity of the quadriceps nerves (QL) on the left, ipsilateral to the side of the CN soma. Note that the spike discharge is in-phase with that of the QL nerve. C: CN spike discharge evoked by 2 Hz stimulation to the NRPc and NRGc (100 μA pulses). Note that the spike discharge was modulated rhythmically at ~1 Hz, whereas rhythmic ENG activity was not observed. Figure 7B-C was modified from Matsuyama et al. (2004b).

Among the lumbar CNs that we recorded (Matsuyama et al., 2004b), most of lamina VIII CNs with monosynaptic reticulospinal inputs exhibited rhythmic firings during fictive locomotion evoked by stimulation to the mesencephalic locomotor region, with one peak per locomotor cycle (see figure 7B), thus indicating that these CNs are highly involved in the locomotor function. Furthermore, as shown in figure 7C, some lamina VIII CNs responded with rhythmic discharges to tonic descending reticulospinal drives that were subthreshold for locomotion. Therefore, as described in lumbar CNs in the developing spinal cord (Butt et al., 2002; Butt and Kiehn, 2003), these lamina VIII CNs in the adult cat lumbar spinal cord could be considered as primary components of the spinal central pattern generator for locomotion and well be directly involved in the initiation of locomotor rhythmogenesis.

Conclusion

Functional Implications of the Reticulospinal-Spinal CN System in the Control of Locomotion

It has been well established that the reticulospinal pathways are all-encompassing descending pathways, which mediate locomotor command signals to spinal interneuronal circuits from various higher locomotor centers including the cerebellar, mesencephalic and subthalamic locomotor regions (Grillner, 1985; Mori et al., 1992, 2000). The reticulospinal systems have also been suggested to play an important role in a number of additional motor behaviors, including orienting and postural movements (Peterson, 1984; Drew et al., 1986; Mori et al., 1992). These motor behaviors commonly require the simultaneously coordination of activity in the head and limbs and between different limbs. A large part of this coordinative activity is thought to be “hardwired” and mediated, in part, by the diffuse pattern of projection of individual reticulospinal axons (Kuypers, 1981; Peterson, 1984).

Considering that a large part of lamina VIII CNs receive monosynaptic reticulospinal excitation (Jankowska et al., 2003; Krutki et al., 2003; Matsuyama et al., 2004b) and assuming that such CNs are distributed at all levels of the spinal cord, the long descending reticulospinal pathways can be suggested to control and coordinate the activities of mutual CN-CN circuits which are widely located at all levels of the spinal neuraxis (figure 8). Such an arrangement of the reticulospinal-spinal CN system is appropriate for facilitating the smooth elaboration of the widespread motor synergy during locomotion, including rhythmic interlimb and limb-trunk coordinating activities.

Furthermore, since ~20% of our identified CNs projected predominantly to the hindlimb motor nuclei along their rostrocaudal extent (Matsuyama et al., 2006), it can be thought that these CNs operate as last order interneurons which directly excite or inhibit contralateral motoneurons (see figure 6C). In fact, lumbar lamina VIII CNs mediate crossed disynaptic excitatory or inhibitory actions from the reticulospinal and vestibulospinal pathways on contralateral hindlimb motoneurons (Bannatyne et al., 2003; Jankowska et al., 2003; Krutki et al., 2003). Since a number of supraspinal neuronal systems, including those activated by pyramidal tract neurons in the primary motor cortex and fastigial neurons in the cerebellum may activate lamina VIII CNs via either reticulospinal or vestibulospinal neurons (Homma et

al., 1995; Matsuyama and Drew, 1997; Edgley et al., 2004; Matsuyama and Jankowska, 2004; Matsuyama et al., 2004a), it is suggested that these CNs contribute to synergistic movements of the contralateral hindlimb initiated by various descending motor commands, in addition to crossed reflex actions that accompany the flexion reflex evoked by peripheral inputs from proprioceptors (Harrison et al., 1986; Edgley et al., 2003; Jankowska et al., 2005). Taken together, the reticulospinal-spinal CN system as a whole may serve as the flexible optimal neural substrate essential for the generation and coordination of the reciprocal bilateral locomotor rhythm and may also help to elaborate and refine locomotor patterns in self-induced, goal-directed locomotion.

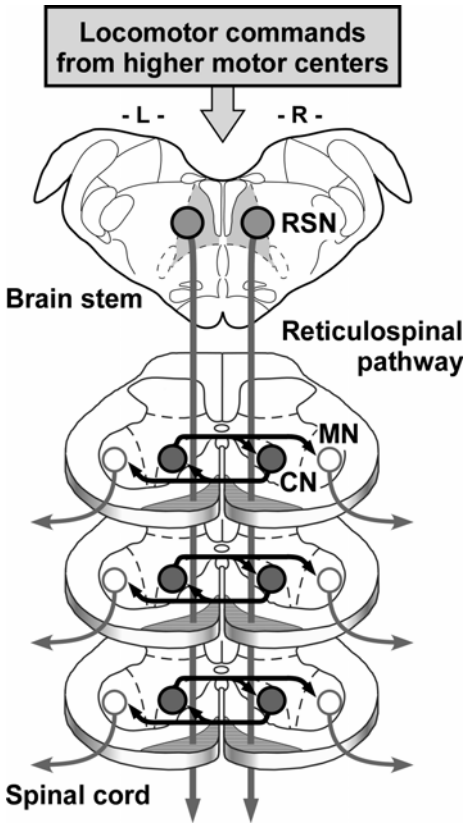

Figure 8. Schematic drawings of the putative neural circuits representing the reticulospinal-spinal CN system (see text in detail). On the drawings of the spinal cord, mutual CN-CN connections shown in figure 5C and CN-motoneuronal connections shown in figure 6C are combined.

Acknowledgment

The studies introduced into this chapter (Matsuyama et al., 1997, 1999a-b, 2004b, 2006) were supported by Grants in Aid for Scientific Research from the Ministry of Education, Culture, Sports, Science and Technology of Japan to K.M.

References

Antonio-Green, D.M., Cheng, J. and Magnuson, D.S.K. (2002) Neurons labeled from locomotor-related ventrolateral funiculus stimulus sites in the neonatal rat spinal cord. *J. Comp. Neurol.,* 442:226-238.

Armstrong, D.M. (1986) Supraspinal contributions to the initiation and control of locomotion in the cat. *Prog. Neurobiol.,* 26:273-361.

Bannatyne, B.A., Edgley, S.A., Hammar, I., Jankowska, E. and Maxwell, D.J. (2003) Networks of inhibitory and excitatory commissural interneurons mediating crossed reticulospinal actions. *Eur. J. Neurosci.,* 18:2273-2284.

Basbaum, A.I., Clanton, C.H. and Fields, H.L. (1978) Three bulbospinal pathways from the rostral medulla of the cat: an autoradiographic study of pain modulating systems. *J. Comp. Neurol.*, 178:209-224.

Berman, A.L. (1968) The Brain Stem of the Cat: A Cytoarchitectonic Atlas with Stereotaxic Coordinates. Madison: University of Wisconsin Press.

Bernstein, N. (1967) The Co-ordination and Regulation of Movements. Oxford: Pergamon Press.

Birinyi, A., Viszokay, K., Weber, I., Kiehn, O. and Antal, M. (2003) Synaptic targets of commissural interneurons in the lumbar spinal cord of neonatal rats. *J. Comp. Neurol*., 461:429-440.

Brodal, A. (1981) Neurological Anatomy: In Relation to Clinical Medicine (3rd edition). New York: Oxford University Press.

Butt, S.J.B., Harris-Warrick, R.M. and Kiehn, O. (2002) Firing properties of identified interneuron population in the mammalian hindlimb central pattern generator. *J. Neurosci.,* 22:9961-9971.

Butt, S.J.B. and Kiehn, O. (2003) Functional identification of interneurons responsible for left-right coordination of hindlimbs in mammals. *Neuron,* 38:953-963.

Cajal, S.R. (1909) Histologie du systeme nerveux de l'homme et des vertrbres, Vol.1, Paris: Maloine.

Craig, A.D. Jr., Linington, A.J. and Kniffki, K.D. (1989) Cells of origin of spinothalamic tract projections to the medial and lateral thalamus in the cat. *J. Comp. Neurol.,* 289:568-85.

Davies, H.E. and Edgley, S.A. (1994) Inputs to group II-activated midlumbar interneurones from descending motor pathways in the cat. *J. Physiol.,* 479:463-473.

Drew, T., Dubuc, R. and Rossignol, S. (1986) Discharge pattern of reticulospinal and other reticular neurons in chronic, unrestrained cats walking on a treadmill. *J. Neurophysiol.,* 55:375-401.

Drew, T. and Rossignol, S. (1990) Functional organization within the medullary reticular formation of intact unanesthetized cat. I. movements evoked by microstimulation. *J. Neurophysiol.*, 64:767-781.

Edgley, S.A., Jankowska, E. and Hammar, I. (2004) Ipsilateral actions of feline corticospinal tract neurons on limb motoneurons. *J. Neurosci.,* 24:7804-7813.

Edgley, S.A., Jankowska, E., Krutki, P. and Hammar, I. (2003) Both dorsal horn and lamina VIII interneurones contribute to crossed reflexes from feline group II muscle afferents. *J. Physiol.* 552:961-974.

Eide, A-L., Glover, J., Kjaerulff, O. and Kiehn, O. (1999) Characterization of commissural interneurons in the lumbar region of the neonatal rat spinal cord. *J. Comp. Neurol.,* 403:332-345.

Grillner, S. (1985) Neurobiological bases of rhythmic motor acts in vertebrates. *Science,* 228:143-149.

Harrison, P.J., Jankowska, E. and Zytnicki, D. (1986) Lamina VIII interneurons interposed in cross reflex pathways in the cat. *J. Physiol.,* 371:147-166.

Holstege, G. and Kuypers, H.G.J.M. (1982) The anatomy of brain stem pathways to the spinal cord in cat. A labelled amino acid tracing study. *Prog. Brain Res.,* 57: 145-175.

Homma, Y., Nonaka, S., Matsuyama, K. and Mori, S. (1995) Fastigiofugal projection to the brainstem nuclei in the cat: an anterograde PHA-L tracing study. *Neurosci. Res.,* 23:89-102.

Huang, A., Noga, B.R., Carr, P.A., Fedirchuk, B. and Jordan, L.M. (2000) Spinal cholinergic neurons activated during locomotion: localization and electrophysiological characterization. *J. Neurophysiol.,* 83:3537-3547.

Jankowska, E. (1992) Interneurnal relay in spinal pathways from proprioceptors. *Prog. Neurobiol.,* 38:335-378.

Jankowska, E., Hammar, I., Slawinska, U., Maleszak, K. and Edgley, S.A. (2003) Neuronal basis of crossed actions from the reticular formation on feline hindlimb motoneurons. *J. Neurosci.,* 23:1867-1878.

Jankowska, E., Krutki, P. and Matsuyama, K. (2005) Relative contribution of Ia inhibitory interneurones to inhibition of feline contralateral motoneurones evoked via commissural interneurones. *J. Physiol.*, 568:617-628.

Jordan, L.M. (1991) Brainstem and spinal cord mechanisms for the initiation of locomotion. In M. Shimamura, S. Grillner, and V.R. Edgerton (Eds.), Neurobiological Basis of Human Locomotion (pp. 3-20). Tokyo: Japan Scientific Societies Press.

Juvin, L., Simmers, J. and Morin, D. (2005) Propriospinal circuitry underlying interlimb coordination in mammalian quadrupedal locomotion. *J. Neurosci.,* 25:6025-6035.

Kadison, S.R. and Kaprielian, Z. (2004) Diversity of contralateral commissural projections in the embryonic rodent spinal cord. *J. Comp. Neurol.,* 472:411-422.

Kjaerulff, O. and Kiehn, O. (1996) Distribution of networks generating and coordinating locomotor activity in the neonatal rat spinal cord in vitro: a lesion study. *J. Neurosci.,* 15:5777-5794.

Kjaerulff, O. and Kiehn, O. (1997) Crossed rhythmic synaptic input to motoneurons during selective activation of the contralateral spinal locomotor network. *J. Neurosci.,* 17:9433-9447.

Krutki, P., Jankowska, E. and Edgley, S.A. (2003) Are crossed actions of reticulospinal and vestibulospinal neurons on feline motoneurons mediated by the same or separate commissural neurons? *J. Neurosci.,* 23:8041-8050.

Kullander, K., Butt, S.J.B., Lebret, J.M., Lundfald, L., Restrepo, C.E., Rydstrom, A., Klein, R. and Kiehn, O. (2003) Role of EphA4 and EphrinB3 in local neuronal circuits that control walking. *Science,* 229:1889-1892.

Kuypers, H.G.J.M. (1981) Anatomy of descending pathways. In V.B. Brooks (Ed.), Handbook of Physiology, Section 1: The Nervous System, Vol.II, Motor Control, Part 1 (pp.597-666). Bethesda: American Physiological Society.

Kuze, B., Matsuyama, K., Matsui, T., Miyata, H. and Mori, S. (1999) Segment-specific branching patterns of single vestibulospinal tract axons arising from the lateral vestibular nucleus in the cat: a PHA-L tracing study. *J. Comp. Neurol.,* 414:80-96.

Matsumoto, A., Aoki, M. and Mori, S. (1976) Ascending long spinal actions on forelimb motoneurons in the acute spinal cat. *Exp. Brain Res.,* 24:509-521.

Matsushita, M. (1970) The axonal pathways of spinal neurons in the cat. *J. Comp. Neurol.,* 138:391-418.

Matsushita, M., Hosoya, Y. and Ikeda, M. (1979) Anatomical organization of the spinocerebellar system in the cat, as studied by retrograde transport of horseradish peroxidase. *J. Comp. Neurol.,* 184:81-106.

Matsuyama, K. and Drew, T. (1997) Organization of the projections from the pericruciate cortex to the pontomedullary brainstem of the cat: a study using the anterograde tracer Phaseolus vulgaris-leucoagglutinin. J. *Comp. Neurol.,* 389:617-641.

Matsuyama, K. and Drew, T. (2000) Vestibulospinal and reticulospinal neuronal activity during locomotion in the intact cat: I. Walking on a level surface. *J. Neurophysiol.,* 84:2237-2256.

Matsuyama, K., Drew, T., Mori, F. and Mori, S. (1999a) The cortico-reticulo-spinal system: organization of the corticoreticular projection and fine architecture of the reticulospinal pathway in the cat. In G.N. Gantchev, S. Mori, and J. Massion (Eds.), *Motor Control Today and Tomorrow* (pp. 45-56). Sofia: Academic Publishing House "Prof. M. Drinov".

Matsuyama, K. and Jankowska, E. (2004) Coupling between feline cerebellum (fastigial neurons) and motoneurons innervating hindlimb muscles. *J. Neurophysiol.,* 91:1183-1192.

Matsuyama, K., Kobayashi, S. and Aoki, M. (2006) Projection patterns of lamina VIII commissural neurons in the lumbar spinal cord of the adult cat: an anterograde neural tracing study. *Neuroscience,* 140:203-218.

Matsuyama, K., Mori, F., Kuze, B. and Mori, S. (1999b) Morphology of single pontine reticulospinal axons in the lumbar enlargement of the cat: a study using the anterograde tracer PHA-L. *J. Comp. Neurol.,* 410:413-430.

Matsuyama, K., Mori, F., Nakajima, K., Drew, T., Aoki, M. and Mori, S. (2004a) Locomotor role of the corticoreticular-reticulospinal-spinal interneuronal system. *Prog. Brain Res.,* 143:239-249.

Matsuyama, K., Nakajima, K., Mori, F., Aoki, M. and Mori, S. (2004b) Lumbar commissural interneurons with reticulospinal inputs in the cat: morphology and discharge patterns during fictive locomotion. *J. Comp. Neurol.,* 474:546-561.

Matsuyama, K., Ohta, Y. and Mori, S. (1988) Ascending and descending projections of the nucleus reticularis gigantocellularis in the cat demonstrated by the anterograde neural tracer, Phaseolus vulgaris leucoagglutinin (PHA-L). *Brain Res.,* 460:124-141.

Matsuyama, K., Takakusaki, K., Nakajima, K. and Mori, S. (1997) Multi-segmental innervation of single pontine reticulospinal axons in the cervico-thoracic region of the cat: anterograde PHA-L tracing study. J. *Comp. Neurol.,* 377: 234-250.

Maunz, R.A., Pitts, N.G. and Peterson, B.W. (1978) Cat spinoreticular neurons: locations, responses and changes in responses during repetitive stimulation. *Brain Res.,* 148:365-379.

Mitani, A., Ito, K., Mitani, Y. and McCarley, R.W. (1988) Descending projections from the gigantocellular tegmental field in the cat: cells of origin and their brainstem and spinal cord trajectories. *J. Comp. Neurol.,* 268:546-566.

Mori, S., Matsui, T., Mori, F., Nakajima, K. and Matsuyama, K. (2000) Instigation and control of treadmill locomotion in high decerebrate cats by stimulation of the hook bundle of Russell in the cerebellum. *Can. J. Physiol. Pharmacol.,* 78:945-957.

Mori, S., Matsuyama, K., Kohyama, J., Kobayashi, Y. and Takakusaki, K. (1992) Neuronal constituents of postural and locomotor control systems and their interactions in cats. *Brain and Development,* 14 (Supple):S109-120.

Nakayama, K., Nishimaru, H. and Kudo, N. (2002) Basis of changes in left-right coordination of rhythmic motor activity during development in the rat spinal cord. *J. Neurosci.,* 22:10388-10398.

Nissen, U.V., Mochida, H. and Glover, J.G. (2005) Development of projection-specific interneurons and projection neurons in the embryonic mouse and rat spinal cord. *J. Comp. Neurol.,* 483:30-47.

Orlovsky, G.N., Deliagina, T.G. and Grillner S. (1999) *Neuronal Control of Locomotion: From Mollusc to Man*. New York: Oxford University Press.

Peterson, B.W. (1984) The reticulospinal system and its role in the control of movement. In C.D. Barnes (Ed), *Brainstem Control of Spinal Cord Function* (pp. 27-86). London: Academic Press.

Prentice, S.D. and Drew, T. (2001) Contribution of the reticulospinal system to the postural adjustments occurring during voluntary gait modifications. J. *Neurophysiol.,* 85:679-698.

Reiner, A., Veenman, C.L., Medina, L., Jiao, Y., Del Mar, N. and Honig, M.G. (2000) Pathway tracing using biotinylated dextran amines. *J. Neurosci. Methods,* 103:23-37.

Rexed, B. (1952) The cytoarchitectonic organization of the spinal cord in the cat. *J. Comp. Neurol.* 96:415-496.

Rustioni, A., Kuypers, H.G. and Holstege, G. (1971) Propriospinal projections from the ventral and lateral funiculi to the motoneurons in the lumbosacral cord of the cat. *Brain Res.,* 34:255-275.

Scheibel, M. E. and Scheibel, A.B. (1969) A structural analysis of spinal interneurons and Renshaw cells. In M.A.B. Brazier (Ed.), *The Interneuron*. (pp. 159-208). Los Angeles: University of California Press.

Silos-Santiago, I. and Snider, W.D. (1992) Development of commissural neurons in the embryonic rat spinal cord. *J. Comp. Neurol.,* 325:514-526.

Skinner, R.D. and Remmel, RS. (1978) Monosynaptic inputs to lumbar interneurons from the lateral vestibulospinal tract and the medial longitudinal fasciculus. *Neurosci. Lett.,* 10:259-264.

Stokke, M.F., Nissen, U.V., Glover, J.C. and Kiehn, O. (2002) Projection patterns of commissural interneurons in the lumbar spinal cord of the neonatal rat. *J. Comp. Neurol.,* 447:349-359.

Takakusaki, K., Kohyama, J. and Matsuyama, K. (2003) Medullary reticulospinal tract mediating a generalized motor inhibition in cats: III. Functional organization of spinal interneurons in the lower lumbar segments. *Neuroscience,* 121:731-746.

VanderHorst, V.G.J.M. and Holstege, G. (1997) Organization of lumbosacral motoneuronal cell groups innervating hindlimb, pelvic floor, and axial muscles in the cat. *J. Comp. Neurol.,* 382:46-76.

Commentaries

In: Handbook on White Matter
Editors: T. B. Westland and R. N. Calton
ISBN: 978-1-60741-034-8

Short Communication

Diffusion Tensor MRI Data Acquisition Methods for White Matter and Clinical Applications: Non Echo-Planar Imaging

Masaaki Hori
Department of Radiology, Toho University, 6-11-1 Omori-Nishi, Ota, Tokyo, Japan

Abstract

Among several techniques, single-shot echo-planar imaging has been a standard technique for diffusion-tensor MR imaging (DTI) of white matter because of its rapid acquisition time and high signal to noise ratio. However, inherent artifacts and distortions due to susceptibility often prevent the demonstration of normal structures and pathological changes in some situations.

Recently some studies have reported that line scan and single-shot fast spin-echo (ssfse) techniques (non echo-planar imaging techniques) have been used for DTI and their advantages. The line scan, simple spin-echo based one, can have benefits for brain stem and spinal cord imaging because of insensitivity of magnetic field inhomogeneity. Ssfse technique also avoids the artifacts and is useful for the region with geometric distortion (i.e., temporal lobe, metals after neurosurgical operation). However, these non echo-planar techniques have some disadvantages and therefore, are not commonly used in many institutions.

In this chapter, we review and illustrate the merits and limitations of non echo-planar imaging techniques for the DTI. Moreover, we discuss the current role and feasibility of the DTI for white matter studies in brain and spinal cord, i.e. quantitative analysis of apparent diffusion coefficient in patients with cervical myelopathy, including results from our experiments and clinical data.

1. Introduction

MR imaging has been an important tool for evaluating white matter in the brain and spinal cord. Recently, diffusion tensor MR imaging (DTI) has an emerging technique and provide several information of white matter structure and pathological changes, which conventional MR images (e.g., T1-weighted or T2-Weighted imaging) have not showed [1]. Quantitative measurements of DTI, apparent diffusion coefficient (ADC) and fractional anisotropy (FA) are the only information DTI provide (figure 1). For example, normal-appearing white matter in the brain and spinal cord in patients with relapsing-remitting multiple sclerosis demonstrate DTI changes and the measurements are useful in detecting occult pathologic changes, predicting clinical course, and monitoring disease progression and therapeutic effect [2].

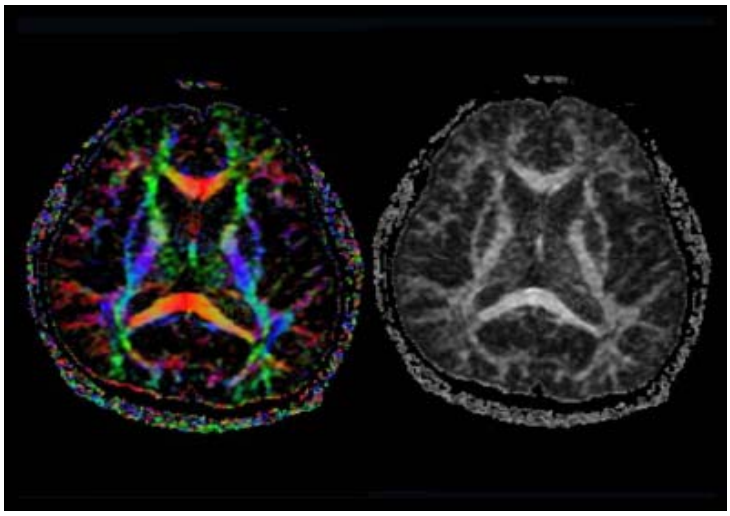

Figure 1. Color and gray-scaled FA map of normal brain. In the color map, blue denoted superior and inferior, green donates anterior and posterior, and red denotes right and left directions.

Another approach to demonstration of the results from DTI data, three-dimensional (3D) white matter tractography was introduced (figure 2). In fact, 3D tractography is visually comprehensive image and is in good agreement with postmortem studies previously reported [1, 3]

Many MR imaging techniques for DTI data acquisition have been introduced. Among several imaging techniques for DTI, single-shot echo-planar imaging (EPI) has been a standard technique for diffusion-tensor MR imaging (DTI) of white matter because of its rapid acquisition time and high signal to noise ratio in many clinical situations and researches. However, EPI's inherent artifacts and distortions due to susceptibility often prevent the demonstration of normal structures (figure 3) and pathological changes in some situations.

Recently some studies have reported that line scan [4-11] and single-shot fast spin-echo (ssfse) techniques [12-17] have been used for DTI and their advantages as non echo-planar imaging techniques. The line scan, simple spin-echo based one, can have benefits for brain

stem and spinal cord imaging because of insensitivity of magnetic field inhomogeneity. Ssfse technique also avoids the artifacts and is useful for the region with geometric distortion (i.e., temporal lobe, metals after neurosurgical operation). However, these non echo-planar techniques have some disadvantages and therefore, are not commonly used in many institutions.

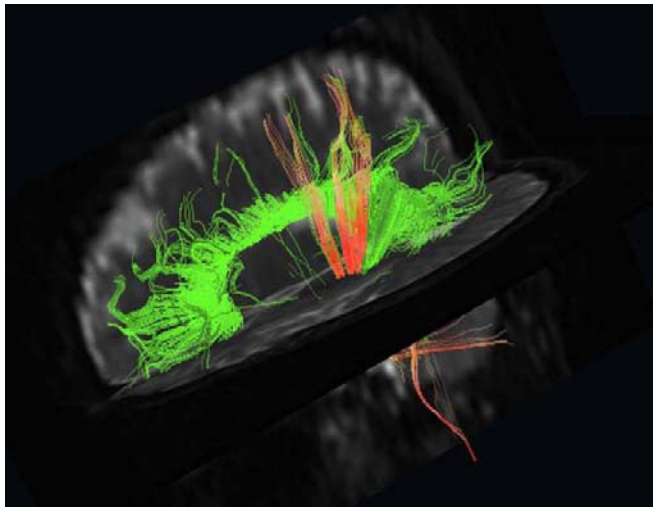

Figure 2. Three-dimensional fiber-tracking of the normal brain. The white matter fibers include cortico-spinal tracts (orange lines) and corpus callosum fibers (green lines).

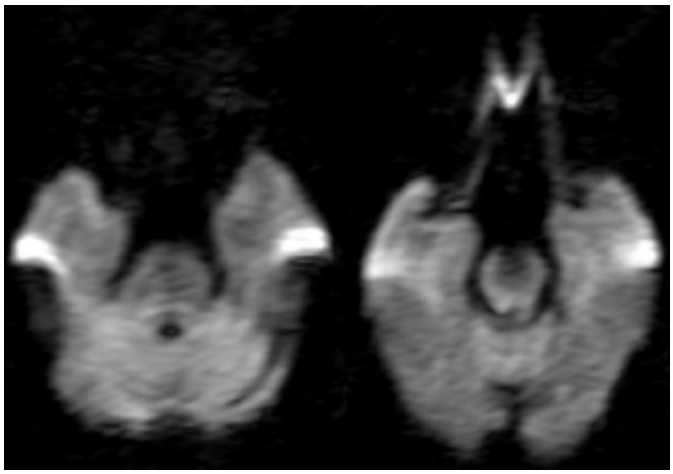

Figure 3. Severe image distortions and high-signal artifacts are seen in the frontal skull base and bilateral middle fossa on EPI based diffusion-weighted images.

In this chapter, we review and illustrate the merits and limitations of non echo-planar imaging techniques for the DTI. Moreover, we discuss the current role and feasibility of the DTI for white matter studies in brain and spinal cord

2. Line Scan Technique

Line scan diffusion-weighted imaging (LSDWI) is based on a simple spin-echo sequence [4]. A complete image of line scan data is acquired after each radio-frequency excitation and LSDWI is based on the sequential acquisition of parallel columns lying in the image plane. The sequential collection of the line data in independent single-shot acquisitions makes the sequence largely insensitive to bulk motion artifacts because no phase encoding is used. The data with motion makes no image and results in a dark line in the complete image.

The feasibility of this technique with three different diffusion directions on 1.5 T and 0.5 T clinical MR imagers was investigated in previous studies. Moreover, in vivo line scan diffusion tensor imaging (LSDTI) has demonstrated its potential clinical value.

The merits of this technique are insensitivity of magnetic field inhomogeneity, more accurate and precise for measurements and no requirement of high-slew rate gradient hardware.

The former merit is the most important character of this technique and is advantages for brain stem, spinal cord imaging and post neurosurgical imaging over EPI. One representative case is shown in figure 4. As in this figure, LSDTI has the potential to demonstrate the lesions which EPI technique is unable to characterize because of distortion and degraded image quality.

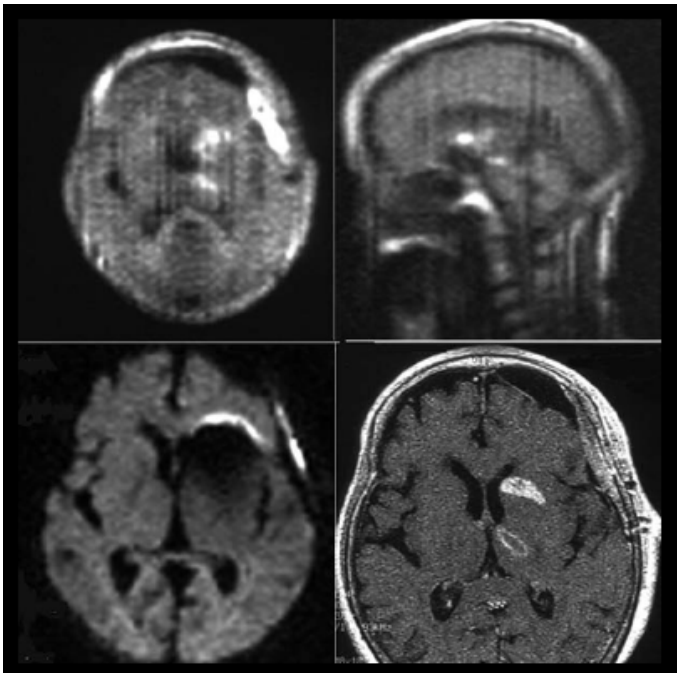

Figure 4. A patients with cerebral aneurysm, after surgical operation. Abnormal high signals indicating acute infarctions are clearly seen in the left basal ganglia and thalamus on line scan DWI (upper row). The lesions were not able to be identified because of severe artifact due to metal clip. Post-contrast T1-weighted image show the lesions as abnormal enhanced area.

For example, imaging of the spine and its pathologies is still a challenging because of difficult magnetic environment and inherent physiological motion. Several methods except LSDTI were introduced spinal cord diffusion imaging and diffusion tensor imaging in vivo [18-30] and LSDTI is another solution. Mamata et al. [8] examined 79 patients with cervical myelopathy and 11 normal volunteers for the assessments of ADC and FA values using LSDTI in sagittal sections. ADC increases and FA decreases with age in the normal spinal cord. Elevated ADC and reduced FA were measured in the spinal cord of spondylosis cases with clinical symptoms of myelopathy. The results of our study [10] at 0.2 T MR imager showed good agreement with these results. We included 14 patients with cervical myelopathy at early clinical stage. The ADC value in patients who presenting some clinical symptom but no abnormal signal on conventional images increased (P _ .001, Mann-Whitney U-test) and the FA decreased (P _ 0.24) on average, compared to normal. spinal cord. therefore, LSDT images at low field strength may be a sensitive method for evaluating the structural characteristics of spinal cord pathology in vivo (figure 5). As described above, LSDTI is an excellent method for spinal cord DTI.

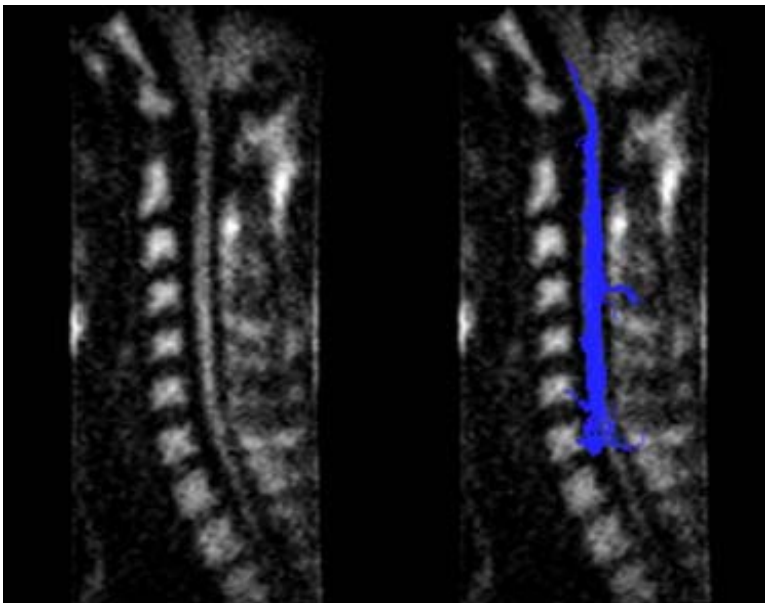

Figure 5. Isotropic DWI and three-dimensional fiber-tracking of the normal spinal cord based on LSDTI at 0.2 Tesla MR imager. Straight running white matter fibers of the spinal cord were demonstrated as blue lines.

The second merit may be related to the first merit. Kubicki et al. [31] compared between EPI and LSDTI and there was a significant difference among two methods in FA for the corpus callosum and the right uncinate fasciculus when intersession reproducibility for one subject was evaluated. Moreover, errors associated with each FA measure were larger for EPI than for LSDTI. Therefore, Kubicki et al. [32] used LSDTI to investigate the myelin and axonal alterations of the white matter in patients with schizophrenia, in comparison with normal subjects. In results, FA was decreased in schizophrenia in the following brain regions: the fornix, the corpus callosum, bilaterally in the cingulum bundle, bilaterally in the superior

occipito-frontal fasciculus, bilaterally in the internal capsule, in the right inferior occipito-frontal fasciculus and the left arcuate fasciculus. We guess that this study is reasonable because susceptibility artifacts may present more commonly in the temporal lobe in particular on EPI diffusion tensor images.

The last merit enabled that LSDTI can be implemented at low magnetic fields and now LSDWI employing six diffusion directions is available on 0.2 Tesla clinical MR imagers, and diffusion tensor (DT) images can be realized even on a low-magnetic-field clinical MR imager (figure 6). In our study [33], The ADCs and FAs of white matter in the brain at 0.2T MR imager show the appropriate values, in comparison with values obtained at high field strength in previous studies. Sequence parameters of this study were as follows: TR/TE = 380/116 msec, matrix _=128 _ 64 (frequency _column), bandwidth =3.92 kHz, FOV = 300 _ 150 mm (rectangular FOV), slice thickness/gap =6/0 mm, and *b*-value = 0 and 700 seconds/mm2 with the maximum *b*-value applied in six directions and the total scan time was 52 minutes 30 seconds for 18 slices with full-tensor images covering the whole brain.

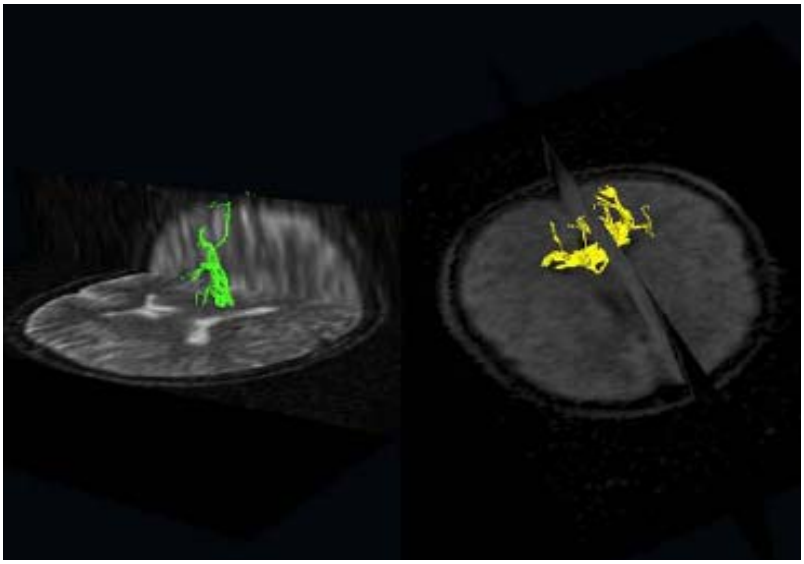

Figure 6. Three-dimensional fiber-tracking of the normal brain based on LSDTI at 0.2 Tesla MR imager. The white matter fibers include cortico-spinal tracts (green lines) and corpus callosum fibers (yellow lines).

Therefore, if time is not constrained, DTI at low field strength may be feasible for clinical use to estimate the white matter of brain with limited coverage, which often may be sufficient. Moreover, cost savings can be achieved on a 0.2 T MR imager, which means that DTI can be used more widely for clinical applications, in the developing countries and regions in particular and it has some social significance.

The disadvantage of this technique is time consuming for data acquisition because of simple spin-echo based one.

$$\text{Data acquisition time} = TR \cdot N_{ln} \cdot N_{ex}$$

Where TR is repetition time, N_{ln} is Number of line steps, and N_{ex} is number of excitations. For example, the parameters in our spinal cord study were as follows: TR=380 ms, N=64 and N=1. Therefore, scan time for one slice was 380x64x1x7 (the maximum b value applied in different six directions and one b=0 image), results in about 170 sec. For clinical routine whole brain diffusion tensor imaging data acquisition, using LSDTI is impractical idea.

Moreover, LSDTI often suffer from patients' motion artifact because of its long acquisition time, for spinal cord imaging in particular. Therefore, it should be used with motion-correction techniques in order to reduce artifacts. Our study [34] at 1.5 Tesla MR imager including five healthy volunteers in the comparison study with LSDTI with or without with echocardiogram (ECG). LSDTI images with ECG-gated technique were all superior to those without ECG–gating in imaging quality. The mean LSDTI durations were approximately12 minutes without ECG-gated technique and 14 minutes with it, depending on the patients' heart rate. Mean extended time for LSDTI with ECG-gating was approximately two minutes, which were permissible for clinical use. (Sequence parameters of this study is as follows: TR/ TE =800 without ECG gating, approximately 1200 with ECG gating/80 ms, matrix 128×64 (256×256 reconstructed), bandwidth = 3.92 kHz, FOV = 240×120 mm, slice thickness/gap=3/0 mm and b value of 0 and 700 s/mm2 with the maximum b value applied in six directions ((1,1,0), (0,1,1), (1,0,1), (0,1,–1), (1,–1,0), (–1,0,1))

In fact, the results of our clinical feasibility study [34] including eighteen patients with cervical spinal cord disorders (ten men and eight women, mean age 46 years, 11 with spondylotic myelopathy, three with syringomyelia, two with spinal AVM, one with spinal cavernous angioma and one with multiple sclerosis) after conventional MR examination showed usefulness of its qualitative and quantitative estimation. In examples form our clinical data, the ADC value of spinal cord in patients with cervical spondylotic myelopathy increased ($P<.001$, Mann-Whitney U-test) and FA decreased on average, compared with those in normal volunteers. This result was in agreement with previous reports. Moreover, FA and ADC values are similar to those of CSF at syrinx level in patients with asymptomatic syringomyelia (figure 7). A low signal line on the FA map may indicate a tear of the white matter fiber in the patient with spinal AVM who presented motor weakness and sensory loss at C5 and distant level. FA and ADC map in the patient with asymptomatic spinal cavernous angioma was demonstrated normally (figure 8). Therefore, these results showed that tractography reflected the conditions of the cervical spinal cord essentially although the results of tractography could not be pathologically correlated. Conventional T1- or T2-weighted images were sometimes inconsistent with clinical symptoms. For example, it is difficult to predict whether a small hemorrhagic lesion in the spinal cord causes a neurological abnormality or not on conventional MR images. However, in this feasibility study, continuous fibers or normal ADC/FA measurements were demonstrated in asymptomatic patients, even abnormal pathological changes seen on conventional MR images. Therefore, DTI has potential to reflect the neurological condition in patients more accurately than conventional MR images and add some essential information. Clinical correlation and long-term follow up in larger numbers of patients will be desired.

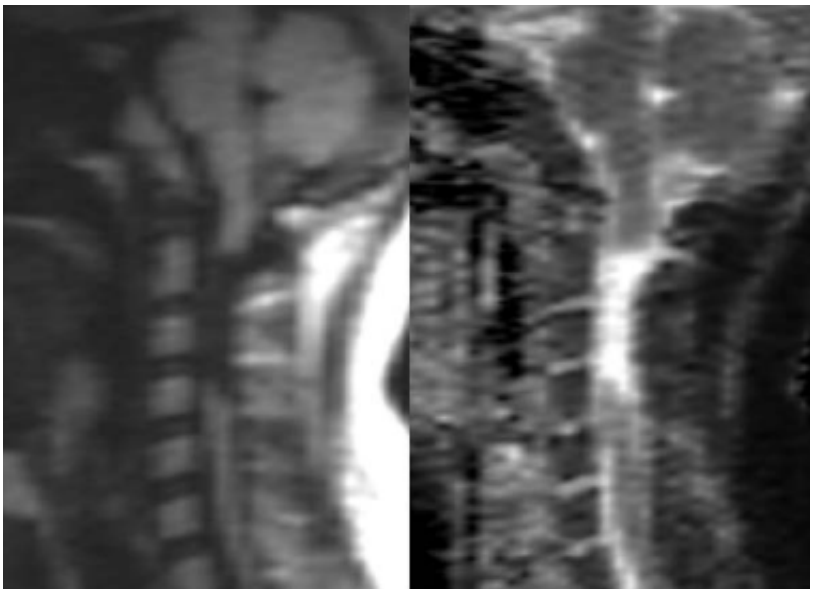

a

b

Figure 7. A, isotropic DWI and corresponding ADC map of cervical spine in a patient with syringomyelia. B, T1-weighted spin-echo image in sagittal view.

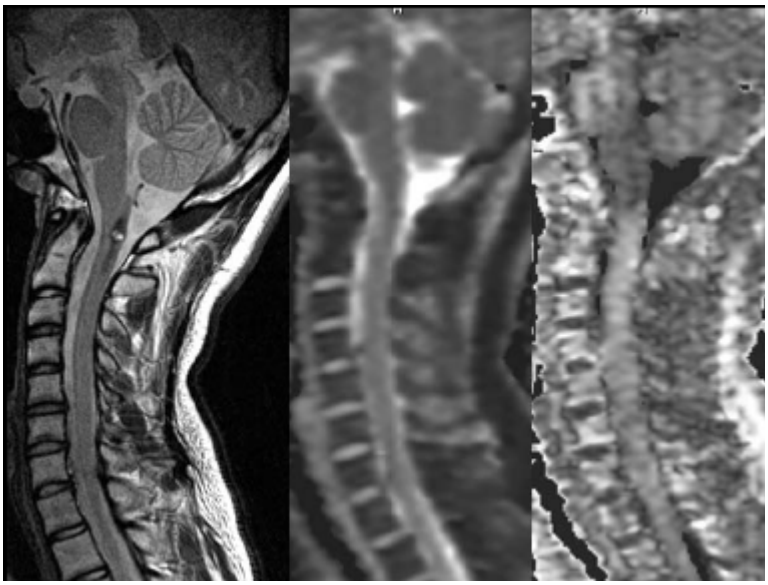

Figure 8. A patient with asymptomatic spinal cavernous angioma. High signal dot surrounded abnormal low intensity indicating old hematoma is seen on T2-weighetd image. There is no abnormal changes in the corresponding ADC and FA map.

3. SSFSE Technique

EPI utilizes gradient re-phasing, which results in spatial distortions from magnetic susceptibility effects, especially near air and bone interfaces. Another method for DTI, single-shot fast spin-echo (SSFSE)-based MR technique, has been introduced in some reports [12, 13, 16]. The advantages of this technique over EPI diffusion-weighted imaging are reduced image distortions and signal loss resulting from tissue susceptibility differences (e.g., bone and brain) (figure 9). Therefore, SSFSE may offer significant advantages for evaluating the cervical spine [14, 15], where large susceptibility and main magnetic field inhomogeneity- induced artifacts are commonly seen in SS-EPI data.

Xu D. et al. [16] investigated and reported the use of a single-shot fast spin-echo-based sequence to perform diffusion tensor imaging with improved anatomic fidelity through the entire brain and the cervical spine at 1.5T and 3 T MR imagers. The mean diffusion measurements obtained with the SSFSE acquisition were not statistically different ($p > 0.05$) from EPI-based acquisitions. Compared to routine T(2)-weighted MR images, the DTI-EPI sequence showed up to 20% in elongation of the brain in the anterior-posterior direction on a sagittal image due to magnetic susceptibility distortions, whereas in the DTI-SSFSE, the image distortions were negligible. They concluded diffusion tensor SSFSE method was also able to assess diffusion abnormalities in a brain stem hemorrhage, unaffected by the spatial distortions that limited conventional EPI acquisition.

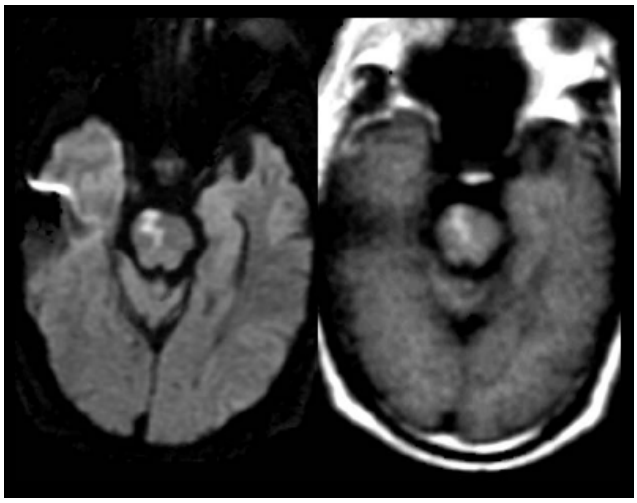

Figure 9. Abnormal linear high signal are seen on both EPI-based and ssfse-based DWIs. High signal artifact near the right temporal lobe is shown on EPI-based image only.

Moreover, the advantage of this technique over LSDTI is short acquisition times and free from patients' motion artifacts.

Disadvantages of this technique are T2 burring effect and low signal-to-noise ratio, compared with EPI. It is well known that T2 blurring effects are generally known with SSFSE acquisitions with long echo train lengths, tissues with short T2 times in particular. This is mainly depend on that usually the first echoes are collected close to the center of the k space, while late echoes are collected at the periphery affecting the spatial resolution. Low signal-to-noise ratio is also expected for tissues with short T2 times and SSFSE acquisitions with long echo trains due to signal decay.

Therefore, the diffusion tensor images based on SSFSE are often vague and show the structures less clearly than EPI-based images on clinical 1.5 Tesla MR scanner, as shown in figure 10.

Figure 10. Isotropic DWI of normal cervical spine based on ssfse-DTI data.

As expected, SSFSE suffers reduced SNR and increased blurring compared with EPI, the effects on the processed mean diffusivity, FA, or reconstructed fiber tracts had not been investigated in comparison with EPI technique.

We compared mean diffusivity maps, fractional anisotropy (FA) maps, and three-dimensional white-matter tractography between the SSFSE diffusion-tensor MRI technique and the more common EPI method [35].

A total of 30 patients (20 men and 10 women, mean age 59.4 years) with neurological disease participated in this study. Various pathological conditions of the patients included in this study: primary brain tumors [n=10; malignant lymphoma (n=6), glioblastoma (n=2), astrocytoma (n= 2)], acute infarction (n=14), intracranial hemorrhage (n=4) and hypoxic encephalitis (n=2). Diagnoses were made by brain biopsy (primary brain tumors) or by clinical history, presentation, and/or follow-up imaging studies.

All MR imaging was performed on a 1.5-Tesla MR imager with a birdcage head coil. After conventional T2- and T1- weighted scan in axial plane, SSFSE-DTI and EPI-DTI were performed. In this study, imaging parameters of SSFSE-DTI were as follows: TR/ TE=20,000/73 ms, matrix 128×128, bandwidth= 32 kHz, FOV=260×260 mm, slice thickness/ gap=5/0 mm, slice number=30, and b value of 0 and 1,000 s/mm2 with the maximum b value applied in 13 directions. Imaging parameters of EPI-DTI were as follows: TR/ TE=10,000/70 ms, bandwidth=116 kHz with the maximum b value applied in 15 directions. FOV, spatial resolution, slice thickness, slice gap, slice number and b value of EPI-DTI were the same as SSFSE-DTI. Total scan time was 4 min and 43 s for SSFSE-DTI and 3 min for EPI-DTI. (The parameters of SSFSE-DTI did not completely agree with those of EPI-DTI because of technical and clinical limitations.) And these parameters were suggestive and leave rooms for improvement.

All diffusion tensor images were routinely processed, that is, transferred to an independent workstation and calculated mean diffusivity maps. Moreover, FA maps on gray-scaled and three-dimensional tract projections of two major white-matter fibers, including the cortico-spinal tracts and corpus callosum fibers, were obtained by using dTV 1.5 software (Image Computing and Analysis Laboratory, Tokyo, Japan.) [3].

All SSFSE-DTI image data was each compared with the corresponding EPI-DTI image data using two qualitative criteria, conspicuousness of lesions and presence of distortion artifacts on mean diffusivity maps and diffusion tensor images (gray-scaled).

As results, conspicuousness of lesions on diffusion tensor images was comparable and distortion artifacts were higher on EPI images on the mean scale. In particular, SSFSE-DTI was the preferred method in patients who had undergone some neurosurgical procedures and had lesions in the brain stem and posterior fossa because there were fewer artifacts and less distortion in the images (figure 11).

As shown in figure 12, there were fewer visible white-matter tract fibers in SSFSE-based images. And as shown in this study, fiber tracking results from the SSFSE data were inferior to those of the SS-EPI data. Reasons for this poor performance are likely related to the intrinsically lower signal-to-noise ratio and increased blurring present in the SSFSE data, as noted in the past studies. This may be partially addressed through the use of custom multi-channel RF coils (as shown by Xu et al. [16]). However, the blurring effect is more difficult

to correct and lead to errors in the calculated principle diffusion direction as it affects adjacent and next to pixels or voxels.

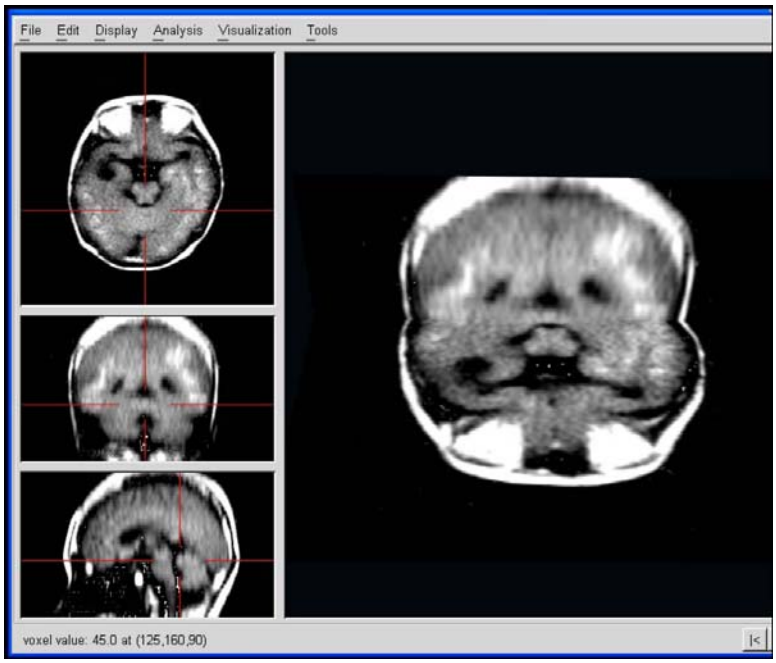

a

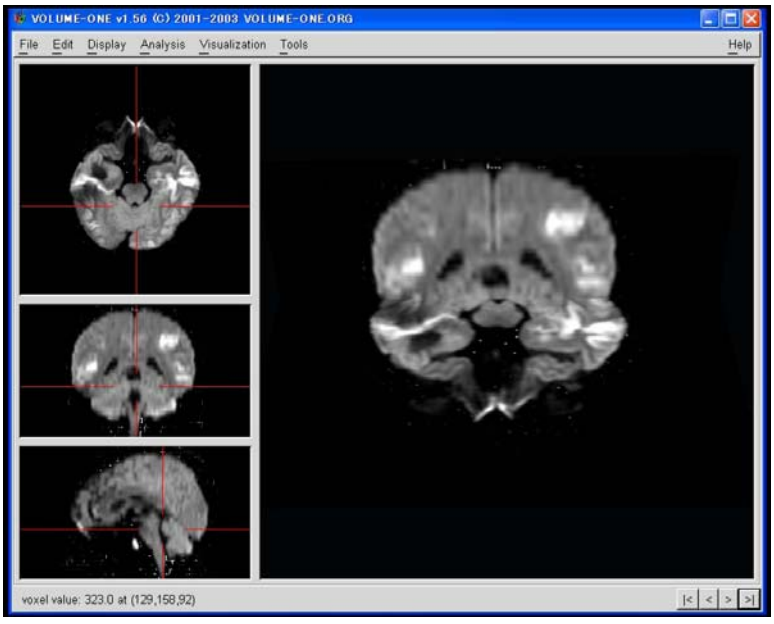

b

Figure 11. A, abnormal high signals are widely shown in bilateral cerebral white matter on isotropic DWIs based on ssfse-DTI data. B, in addition to A, there are some abnormal high signals near the frontal and temporal skull bases indicating artifacts.

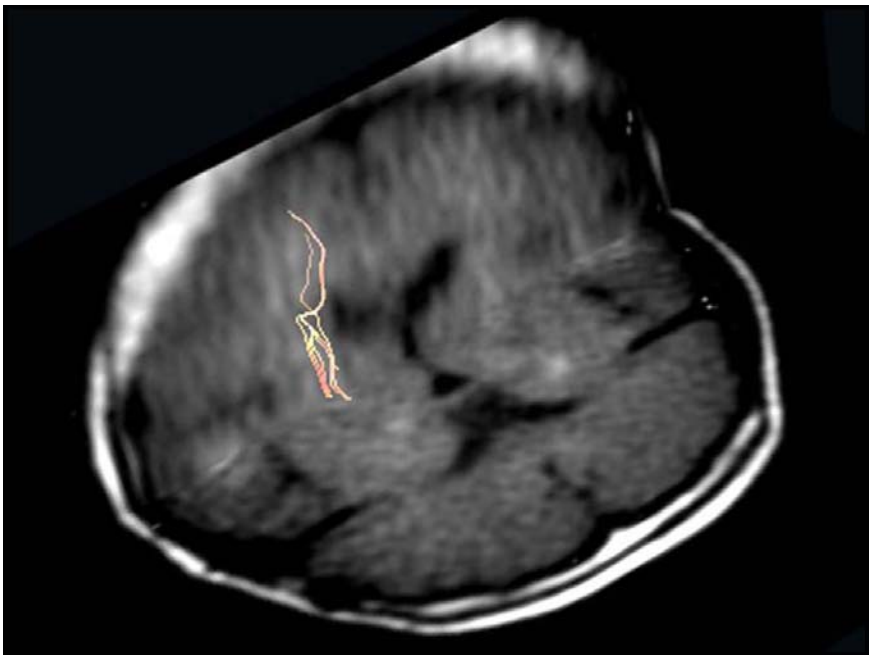

Figure 12. Only a few cortico-spinal white matter fibers are seen on SSFSE-DTI.

We can form some hypotheses. SSFSE-DTI with higher field magnet (3T or over) may improve results because of increased signal-to-noise ratio. Moreover, EPI would suffer more severe artifacts on 3T MR imager due to B0 static field inhomogeneity.

Further investigation is needed before the SSFSE based DTI can become valuable tool in evaluation of the brain. Quantitative assessment and sequence optimization are desirable in particular.

Besides the limitation of the MR imaging sequence, some more advanced MR imaging techniques, such as EPI with parallel imaging, non-CPMG SSFSE-DTI and PROPELLER-DTI [36-38], have been proposed to acquire diffusion tensor images with higher image quality. In near future, comparison between these methods may lead to different answers to the problem, including alternative methods of non-EPI sequence.

References

[1] Wakana S, Jiang H, Nagae-Poetscher LM, van Zijl PC, Mori S (2004) Fiber tract-based atlas of human white matter anatomy. *Radiology. 230*, 77–87

[2] Hesseltine SM, Law M, Babb J, Rad M, Lopez S, Ge Y, Johnson G, Grossman RI (2006) Diffusion tensor imaging in multiple sclerosis: assessment of regional differences in the axial plane within normal-appearing cervical spinal cord. *AJNR Am. J. Neuroradiol. 27*, 1189-93.

[3] Kunimatsu A, Aoki S, Masutani Y, Abe O, Mori H, Ohtomo K (2003) Threedimensional white matter tractography by diffusion tensor imaging in ischaemic stroke involving the corticospinal tract. *Neuroradiology. 45*, 532–535.

[4] Gudbjartsson H, Maier SE, Mulkern RV et al. (1996). Line scan diffusion imaging. *Magn. Reson. Med. 36*, 509-519.

[5] Robertson RL. Maier SE. Mulkern RV et al. (2000) MR line-scan diffusion imaging of the spinal cord in children. *Am. J. Neuroradiol. 21*, 1344-1348.

[6] Murphy BP, Zientara GP, Huppi PS et al. (2001). Line scan diffusion tensor MRI of the cervical spinal cord in preterm infants. *J. Magn. Reson. Imaging. 13*, 949-953.

[7] Hori M, Okubo T, Aoki S, et al. (2002). Line scan diffusion weighted imaging (LSDI) on 0.2 Tesla MRI of the normal cervical cord in vivo: preliminary study. *Nippon. Igaku. Hoshasen Gakkai. Zasshi. 62*, 221-223.

[8] Mamata H, Jolesz FA, Maier SE. (2005). Apparent diffusion coefficient and fractional anisotropy in spinal cord: Age and cervical spondylosis-related changes. *J. Magn. Reson. Imaging. 13*, 115-119.

[9] Maier SE, Mamata H. (2005). Diffusion tensor imaging of the spinal cord. *Ann. N. Y. Acad. Sci. 1064*, 50-60.

[10] Hori M, Okubo T, Aoki S et al. (2006). Line scan diffusion tensor MRI at low magnetic field strength: feasibility study of cervical spondylotic myelopathy in an early clinical stage. *J. Magn. Reson. Imaging. 23*, 183-188.

[11] Mamata H, De Girolami U, Hoge WS et al. (2006). Collateral nerve fibers in human spinal cord: visualization with magnetic resonance diffusion tensor imaging. *Neuroimage. 31*, 24-30.

[12] Bastin ME, Le Roux P. (2002). On the application of a non-CPMG single-shot fast spin-echo sequence to diffusion tensor MRI of the human brain. *Magn. Reson. Med. 48*, 6–14.

[13] Lovblad KO, Jakob PM, Chen Q et al. (1998). Turbo spin-echo diffusion weighted MR of ischemic stroke. *AJNR Am. J. Neuroradiol. 19*, 201–208.

[14] Fujikawa A, Tsuchiya K, Koppera P, Aoki C, Hachiya J. (2003). Case report: spinal cord infarction demonstrated on diffusion-weighted MR imaging with a single-shot fast spin-echo sequence. *J. Comput. Assist. Tomogr. 27*,415–419.

[15] Tsuchiya K, Katase S, Fujikawa A, Hachiya J, Kanazawa H, Yodo K. (2003). Diffusion-weighted MRI of the cervical spinal cord using a single-shot fast spin-echo technique: findings in normal subjects and in myelomalacia. *Neuroradiology. 45*,90–94

[16] Xu D, Henry RG, Mukherjee P et al. (2004). Single-shot fast spin-echo diffusion tensor imaging of the brain and spine with head and phased array coils at 1.5 T and 3.0 T. *Magn. Reson. Imaging. 22*, 751–759.

[17] Carballido-Gamio J, Xu D, Newitt D, Han ET, Vigneron DB, Majumdar S. (2007). Single-shot fast spin-echo diffusion tensor imaging of the lumbar spine at 1.5 and 3 T. *Magn. Reson. Imaging. 25(5)*, 665-70.

[18] Holder CA, Muthupillai R, Mukundan S Jr. et al. (2000). Diffusion- weighted MR imaging of the normal human spinal cord in vivo. *Am J Neuroradiol*, *21*, 1799-1806.

[19] Ries M, Jones RA, Dousset V et al. (2000). Diffusion tensor MRI of the spinal cord. *Magn. Reson. Med. 44*, 884-892.

[20] Clark CA, Barker GJ, Tofts PS. (1999). Magnetic resonance diffusion imaging of the human cervical spinal cord in vivo. *Magn. Reson. Med. 41*, 1269-1973.

[21] Bammer R, Fazekas F, Augustin M, et al. (2000). Diffusion-weighted MR imaging of the spinal cord. *Am. J. Neuroradiol. 21*, 587-591.

[22] Demir A, Ries M, Moonen CT, et al. (2003). Diffusion-weighted MR imaging with apparent diffusion coefficient and apparent diffusion tensor maps in cervical spondylotic myelopathy. *Radiology. 229*, 37-43.

[23] Clark CA, Werring DJ, Miller DH. (2000). Diffusion imaging of the spinal cord in vivo: estimation of the principal diffusivities and application to multiple sclerosis. *Magn. Reson. Med. 43*, 133-138.

[24] Castillo M, Arbelaez A, Fisher LL et al. (1999). Diffusion weighted imaging in patients with cervical spondylosis. *Int. J. Neuroradiol.* 5, 79-85.

[25] Ducreux D, Lepeintre JF, Fillard P et al. (2006). MR diffusion tensor imaging and fiber tracking in 5 spinal cord astrocytomas. *Am. J. Neuroradiol. 27*, 214-216.

[26] Facon D, Ozanne A, Fillard P et al. (2005). MR diffusion tensor imaging and fiber tracking in spinal cord compression. *Am. J. Neuroradiol. 26*, 1587-1594.

[27] Spengos K, Tsivgoulis G, Toulas P et al. (2006). Spinal cord stroke in a ballet dancer. *J. Neurol. Sci. 244*, 159-161.

[28] Schwartz ED, Duda J, Shumsky JS et al. (2005). Spinal cord diffusion tensor imaging and fiber tracking can identify white matter tract disruption and glial scar orientation following lateral funiculotomy. *Am. J. Neuroradiol. 26*, 1587-1594.

[29] Wheeler-Kingshott CA, Hickman SJ, Parker GJ et al. (2002). Investigating cervical spinal cord structure using axial diffusion tensor imaging. *Neuroimage. 16*, 93-102.

[30] Tsuchiya K, Fujikawa A, Suzuki Y. (2005). Diffusion tractography of the cervical spinal cord by using parallel imaging. *Am. J. Neuroradiol. 26*, 398-400.

[31] Kubicki M, Maier SE, Westin CF, et al. (2004). Comparison of single-shot echo-planar and line scan protocols for diffusion tensor imaging. *Acad. Radiol. 11(2)*, 224-232.

[32] Kubicki M, Park H, Westin CF, et al. (2005). DTI and MTR abnormalities in schizophrenia: analysis of white matter integrity. *Neuroimage. 26(4)*, 1109-1118.

[33] Hori M, Aoki S, Okubo T, Ishigame K, Kumagai H, Araki T. (2005). Line-scan diffusion tensor MR imaging at 0.2 T: feasibility study. *J. Magn. Reson. Imaging. 22(6)*, 794-798.

[34] Hori M, Ishigame K, Aoki S, Kumagai H, Araki T. (2007). Diffusion Tensor Imaging and 3D Tractography of the Cervical Spinal Cord Using the ECG-Gated Line-scan Technique. A Feasibility Study. *The Neuroradiology Journal. 20*, 574-579.

[35] Hori M, Ishigame K, Shiraga N, Kumagai H, Aoki S, Araki T. (2008). Mean diffusivity, fractional anisotropy maps, and three-dimensional white-matter tractography by diffusion tensor imaging. Comparison between single-shot fast spin-echo and single-shot echo-planar sequences at 1.5 Tesla. *Eur. Radiol. 18(4)*, 830-834.

[36] Cheryauka AB, Lee JN, Samsonov AA, Defrise M, Gullberg GT. (2004). MRI diffusion tensor reconstruction with PROPELLER data acquisition. *Magn. Reson. Imaging. 22*, 139–148

[37] Wang FN, Huang TY, Lin FH et al. (2005). PROPELLER EPI: an MRI technique suitable for diffusion tensor imaging at high field strength with reduced geometric distortions. *Magn. Reson. Med. 54*,1232–1240

[38] Kabasawa H, Masutani Y, Aoki S, Abe O, Masumoto T, Hayashi N, Ohtomo K. (2007). 3T PROPELLER diffusion tensor fiber tractography: a feasibility study for cranial nerve fiber tracking. *Radiat. Med. 25(9*), 462-6.

In: Handbook on White Matter
Editors: T. B. Westland and R. N. Calton
ISBN: 978-1-60741-034-8

Commentary

The Dimensions of the Sacral Spinal Canal in Thecaloscopy. A Morphometric MRI Study

***S. Mourgela*[*1], *A. Sakellaropoulos*[2], *S. Anagnostopoulou*[3] *and J.P.Warnke*[4]**

[1] Neurosurgical Department, "Agios Savas" Anticancer Institute, Athens, Greece
[2] Division of PCCM, Endoscopy and Sleep Medicine, Athens, Greece
[3] Department of Anatomy, Medical School, University of Athens, Greece
[4] Neurosurgical Department, Paracelsus Clinic, Zwickau, Germany

Abstract

The use of minimal invasive methods and endoscopic procedures for diagnosis and treatment of certain pathologic entities involving the spinal canal expands permanently. The sacral spinal canal as a place of such interventions is for a long time known. Thecaloscopy is the endoscopy of lumbar subarachnoid space performed through different approaches by using flexible endoscopes.

The subject of this study was the measurement of certain anatomic diameters in the sacral spinal canal by using the lumbosacral MRI studies of 25 patients with unclear pain symptoms, in order to estimate, from the pure anatomic point of view, the capability to perform thecaloscopy in this anatomical region.

Since now anatomic morphometric data of the sacral region were delivered only from the cadaver specimens' sectioning performed in anatomic institutes during the 60's and 70's years.

The parameters measured were: 1. the inclination of the lumbosacral angle, 2. the duralsack's end, 3. the length of all the sacral spinal processes 4. The length of the sacral spinal canal in its centre and 5. The width of the sacral hiatus.

[*] Correspondance: S. Mourgela, M.D. Neurosurgeon; Vikatou 12 str. 11524 Athens, Greece; E-mail: sofiamou@otenet.gr

The results of the measurements were in detail presented and an evaluation of them concerning the applicability of flexible endoscopes in the sacral spinal canal was performed.

It was proven that the duralsack's end in 40% of the patients at the middle of the S2 vertebral body lies, an anatomical position, which through the sacral hiatus easy to access is. The length under the sacral spinal processes is smaller than the length of the sacral spinal canal in its centre, a fact that makes the manipulation of a flexible endoscope easier, if someone works straight under the spinal processes and has a smaller distance to run. Through the sacral hiatus the introduction of the flexible endoscope is by many patients possible because of its adequate width.

Keywords: sacrum-diameters-morphology-endoscopy-thecaloscopy.

Introduction

Two thirds of the adult population is at least once in their life affected by back pain. This pain, as is usually described by the patients, stands in closer sense for complaints of the lower lumbar spine and/or of the lumbosacral transition [1]. Back complaints, mainly in the form of lumboischialgic pain, have themselves since the 20's years turned to be the most expensive musculosceletal diseases in the industrialized countries [2]. Therefore is the scientific interest in further diagnostics and therapy of these patients large. This corresponds particularly in patients, who revealed no pathological findings in the conventional diagnostic studies. New diagnostic and therapeutic methods were become necessary and minimal invasive neurosurgical procedures have been developed, in order to face this problem, such as neuroendoscopy and thecaloscopy [3,4,5,6].

Thecaloscopy is the endoscopy of lumbar subarachnoid space performed through different approaches in the lumbosacral spinal canal by using flexible endoscopes.

For thecaloscopy there are many approach possibilities available, such as translumbar (L3-L4 level) and transsacral (S1-S2 level or through the sacral hiatus) [6,7,8].

The knowledge of the morphometric anatomic dimensions of this region is a precondition for the atraumatic use of flexible endoscopes. Furthermore, by using MRI studies the determination of age- and sex-specific mean anatomic morphometric values of the sacral spinal canal is possible without the use of cadaver measurements. The measurement values, which originated in the past years particularly from the sectioning of cadavers, were representing actually only one age group, these beyond of 7th decade of life.

The goal of this study was to prove that transsacral endoscopy, from the pure anatomic site of view, is possible.

Material and Methods

During the time period between 1/1/03 to 31/12/03 in the Neurosurgical Department of the Paracelsus Clinic (Zwickau, Germany) 25 patients with non-specific back pain were examined in a prospective study by means of lumbosacral MRI studies. The study included

10 females and 15 males. The mean age was 53.36 years. The male mean age with standard error was 53.13+/-15.64 and the female 53.7+/-18.27. The confidence limits for the males were 45.21-61.05 and for the females 42.4-65.0.

By using MRI studies, the following parameters were determined:

1. The inclination of the lumbosacral angle
2. The end of the dural sack referred to the bony structures
3. The length of all sacral spinal processes
4. The length of the sacral spinal canal in its centre and
5. The width of the sacral hiatus (sketch 1).

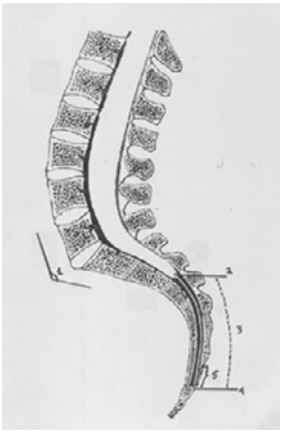

Sketch 1. The anatomic measurements performed.

The measurements of the digitized MRI studies were performed by using the Dicom Program. All the measurements were accomplished in mm. The projection of the end of the dural sack referred to the bony structures took place with an approximation of 0, 50 or 100, for the craniocaudal expansion of one given vertebral body. A duralsack's end of S2/50 means that the end of the duralsack, at the middle of the S2 vertebral body lies. The statistic analysis performed using the program SPSS 10.0 for Windows. Due to the small sample and to the fact that the variables weren't following the normal distribution, the non-parametric statistics were used to find out if any difference existed or not. The statistical significant level for the tests was p=0,05. The results of the measurements are presented in table 1.

Table 1. Descriptive for all parameters (n=25)

	Mean *(Std.Dev)*	Range (min-max)
AGE	53,36 *(16,37)*	(17 - 78)
LUMBO-SACRAL ANGLE	141,20 *(11,21)*	(115 – 165)
LENGTH SACRAL SPINAL PROCESSES	79,45 *(14,32)*	(58,59 – 116,62)
LENGTH SACRAL SPINAL CANAL	59,03 *(15,31)*	(38,38 – 104,36)
WIDTH SACRAL HIATUS	22,12 *(4,48)*	(13,85 – 32,21)

Results

The 60% of the patients were males and the 40% females. The 44% of the patients were in the age between 46-60 years. The mean value of the lumbosacral angle was 141.2 degrees and for the 40% of the patients this angle ranged between 136-140 degrees. The end of the duralsack was located for 10 patients in the middle of S2 vertebral body (40%) and for 7 patients at the level of the inferior end plate of the S2 vertebra (28%). The length of the sacral spinal canal in its centre for 12 patients ranged between 71-90mm (48%) and for 7 patients between 50-70mm (28%). The length of all the sacral spinal processes ranged for 10 patients between 51-65mm and for 8 patients between 35-50mm. The width of the sacral hiatus was 21,92±5mm for the males and 22,42±3,81mm for the females.

The statistic analysis (Mann-Whitney test) has proved that there is no statistically significant difference between both sexes for the lumbosacral angle's inclination (p=0,367) and for the width of the sacral hiatus (p=0,80) (table 2). Further analysis (Wilcoxon Signed Ranks Test) has shown that the length of altogether the sacral spinal processes smaller than the length of the sacral spinal canal in its centre is. (table 3)

Table 2.

	Male (n=15)	Female (n=10)	
	Mean *(Std.Dev)*	Mean *(Std.Dev)*	p
LUMBO-SACRAL ANGLE	142,67 *(12,08)*	139,00 *(9,94)*	0,367
WIDTH SACRAL HIATUS	21,92 *(5,00)*	22,43 *(3,81)*	0,567

Table 3.

	Mean *(Std.Dev)*	Range (min-max)
LENGTH SACRAL SPINAL PROCESSES	79,45 *(14,32)*	(58,59 – 116,62)
LENGTH SACRAL SPINAL CANAL	59,03 *(15,31)*	(38,38 – 104,36)
Paired differences	20,42 *(9,50)*†	(16,50 – 24,34)

† $p < 0,001$.

Discussion

Back pain is for patients, physicians and social insurance companies a very important issue. Many and different diagnostic and therapeutic procedures have been developed in the latter twenty years. Great interest lies in minimal invasive methods and particularly in endoscopic procedures, which include extradural and intradural exploration techniques [3,6].

The lumbosacral angle is considered as a theoretical reason for back pain symptomatology. In this study the lumbosacral angle was measured for another reason: the anatomical possibility for transsacral endoscopy through the sacral hiatus to prove. From our study we could state that the prevalence age for back pain, in the age group between 45 and 60 years stands, although these pain by young persons or by adults is also reported. This

result agrees with the study of R. Bratton [9]. This is also the age group, in which the cumulative effects of the spinal column movements present and pain symptoms begin.

For the transhiatal approach the length of all sacral spinal processes, the duralsack's end and the width of the sacral hiatus are important. The length under the sacral spinal processes smaller than this of the centre of the sacral spinal canal is. Thus, when someone the endoscope directly under the sacral spinal processes employs, can it further higher manipulate and the duralsack meet and dot, without the entire width of the sacral spinal canal to use. A mean difference of 20mm between the length of the sacral spinal canal in its centre and the length under the sacral spinal processes is important, because the "feeling" of the surgeon and the navigation of the endoscope is better, if the distance to run is smaller. In 68% of the patients the dural sac ends at the level of S2 vertebra. The distance from the sacral hiatus to the duralsack's end, ranges from 35 to 95mm, and is smaller than in cases where the dural sac at a higher level ends. Finally, the width of the sacral hiatus is large enough in both sexes for the passage of the flexible endoscope. The lumbosacral angle is simple to pass, because no smaller than 125° and no larger than 165° is. From this study we conclude that in most cases transsacral endoscopy is possible to perform since many of every individual anatomy permits it.

Conclusions

The endoscope can through the sacral hiatus over a length ranging between 35-95mm in the sacral spinal canal, be introduced. The lumbosacral angle is simple to pass, because no smaller than 125° and no larger than 165° is. No further means needs to be undertaken during thecaloscopy, since no statistically significant difference between sexes for the measured diameters exist.

References

[1] Bigos S.J. Industrial low back pain-Risk factors In : Wiesel, S.W., Weistein, J.N., Herkowitz, H., Bell, G. (Hrsg.): *The lumbar spine,* Vol. 2. Saunders, Philadelphia, 1996, S. 1065-1074

[2] Quinet R.J., Hadler N.M., 1979. Diagnosis and treatment of backache. *Semin. Arthritis Rheum.* 1979, 8, 261-287

[3] Heavner J.F., Cholkhavatia, S., and Kizelshteyn, G. Percutaneous evaluation of the epidural and subarachnoid space with flexible endoscope. *Reg. Anesth.:* 1991, 15 S1: 85

[4] Sabreski L.R., Kitahata L.M. Direct visualization of the lumbosacral epidural space through the sacral hiatus. *Anest. Anal.:* 1995, 60: 839-840

[5] 5. Warnke J.P., Köppert H., Bensch-Schreiter B,. Dzelzitis J., Tschabitscher M. Thecaloscopy Part III: First Clinical Application. *Minim. Invas. Neurosurg.;* 2003, 46: 94-99.

[6] Mourgela S., Anagnostopoulou S., Warnke J.P, Spanos A. Thecaloscopy through sacral bone approaches, cadavers study: further anatomic landmarks. *Minim Invasive Neurosurg.* 2006, 49(1): 30-3

[7] Warnke J.P., Tschabitscher M., Nobles A. Thecaloscopy Part I. The endoscopy of the lumbar subarachnoid space. Historical review and own cadaver studies. Minim. Invas. *Neurosurg.:* 2001, 42: 61-64

[8] Warnke J.P., Mourgela S., Tschabitscher M., Dzelzitis J. Thecaloscopy Part II: Anatomical Landmarks. *Minim. Invas. Neurosurg;* 2001, 44:181-185

[9] Bratton R. Assessment and management of acute low back pain. *American family Physician:* 1999, vol. 60/No 8/, 15/11

Index

A

B

C

D

E

F

G

H

I

J

K

L

M

N

O

P

Q

R

S

T

U

V

W

X

Y

Z